JPL Publication **02-25**

Chemical Kinetics and Photochemical Data for Use in Atmospheric Studies

Evaluation Number 14

NASA Panel for Data Evaluation:

S. P. Sander
R. R. Friedl
Jet Propulsion Laboratory
Pasadena, California

A. R. Ravishankara
NOAA Environmental
Research Laboratory
Boulder, Colorado

D. M. Golden
Stanford University
Stanford, California

C. E. Kolb
Aerodyne Research, Inc.
Billerica, Massachusetts

M. J. Kurylo
R. E. Huie
V. L. Orkin
National Institute of Standards and Technology
Gaithersburg, Maryland

M. J. Molina
Massachusetts Institute of Technology
Cambridge, Massachusetts

G. K. Moortgat
Max-Planck Institute for Chemistry
Mainz, Germany

B. J.Finlayson-Pitts
University of California, Irvine
Irvine, California

National Aeronautics and Space Administration

Jet Propulsion Laboratory
California Institute of Technology
Pasadena, California

February 1, 2003

The research described in this publication was carried out by the Jet Propulsion Laboratory, California Institute of Technology, under a contract with the National Aeronautics and Space Administration.

Reference herein to any specific commercial product, process, or service by trade name, trademark, manufacturer, or otherwise, does not constitute or imply its endorsement by the United States Government or the Jet Propulsion Laboratory, California Institute of Technology

ABSTRACT

This is the fourteenth in a series of evaluated sets of rate constants and photochemical cross sections compiled by the NASA Panel for Data Evaluation.

The data are used primarily to model stratospheric and upper tropospheric processes, with particular emphasis on the ozone layer and its possible perturbation by anthropogenic and natural phenomena.

Copies of this evaluation are available in electronic form and may be printed from the following Internet URL:

http://jpldataeval.jpl.nasa.gov/

TABLE OF CONTENTS

INTRODUCTION viii
- I.1 Basis of the Recommendations ... ix
- I.2 Scope of the Evaluation ... ix
- I.3 Format of the Evaluation ... x
- I.4 Computer Access ... x
- I.5 Data Formats ... x
- I.6 Units ... x
- I.7 Noteworthy Changes in This Evaluation ... x
- I.8 Acknowledgements ... xiii
- I.9 References ... xiii

SECTION 1. BIMOLECULAR REACTIONS 1-1
- 1.1 Introduction ... 1-1
- 1.2 Uncertainty Estimates ... 1-2
- 1.3 Notes to Table 1 ... 1-31
- 1.4 References ... 1-93

SECTION 2. TERMOLECULAR REACTIONS 2-1
- 2.1 Introduction ... 2-1
- 2.2 Low–Pressure-Limiting Rate Constant, $k_o^x(T)$ ... 2-1
- 2.3 Temperature Dependence of Low–Pressure Limiting Rate Constants: T^n ... 2-2
- 2.4 High-Pressure-Limit Rate Constants, $k_\infty(T)$ ... 2-2
- 2.5 Temperature Dependence of High-Pressure-Limiting Rate Constants: T^m ... 2-3
- 2.6 Uncertainty Estimates ... 2-3
- 2.7 Notes to Table 2 ... 2-8
- 2.8 References ... 2-16

SECTION 3. EQUILIBRIUM CONSTANTS 3-1
- 3.1 Format ... 3-1
- 3.2 Definitions ... 3-1
- 3.3 Notes to Table 3 ... 3-3
- 3.4 References ... 3-5

SECTION 4. PHOTOCHEMICAL DATA 4-1
- 4.1 Format and Error Estimates ... 4-3
- 4.2 Halocarbon Absorption Cross Sections and Quantum Yields ... 4-3
- 4.3 References ... 4-102

SECTION 5. HETEROGENEOUS CHEMISTRY ... 5-1
- 5.1 Introduction ... 5-1
- 5.2 Surface Types—Acid/Water, Liquids, and Solids ... 5-2
- 5.3 Surface Types—Soot and Alumina ... 5-2
- 5.4 Surface Composition and Morphology ... 5-3
- 5.5 Surface Porosity ... 5-4
- 5.6 Temperature Dependences of Parameters ... 5-4
- 5.7 Solubility Limitations ... 5-4
- 5.8 Data Organization ... 5-4
- 5.9 Parameter Definitions ... 5-5
- 5.10 Mass Accommodation Coefficients for Surfaces Other Than Soot ... 5-8
- 5.11 Notes to Table 5-1 ... 5-9
- 5.12 Gas/Surface Reaction Probabilities for Surfaces Other Than Soot ... 5-16
- 5.13 Notes to Table 5-2 ... 5-19

5.14 Soot Surface Uptake Coefficients 5-32
5.15 Notes to Table 5-3 5-32
5.16 Henry's Law Constants for Pure Water 5-35
5.17 Notes to Table 5-4 5-36
5.18 Henry's Law Constants for Acids 5-40
5.19 Notes to Table 5-5 5-40
5.20 References 5-44

APPENDIX A. THERMODYNAMIC PARAMETERS A-1
A.1 Gas-phase entropy and enthalpy values A-1
A.1 References A-8

TABLES

Table I-1. Editions of this Publication viii
Table I-2. Panel Members and their Major Responsibilities for the Current Evaluation viii

Table 1-1. Rate Constants for Second-Order Reactions 1-5

Table 2–1. Rate Constants for Termolecular Reactions 2-4

Table 3-1. Equilibrium Constants 3-2

Table 4-1. Photochemical Reactions 4-4
Table 4-2. Combined Uncertainties for Cross Sections and Quantum Yields 4-6
Table 4-3. Absorption Cross Sections of O_2 Between 205 and 240 nm 4-7
Table 4-4. Absorption Cross Sections of O_3 at 273 K 4-8
Table 4-5. Parameters for the Calculation of $O(^1D)$ Quantum Yields 4-9
Table 4-6. Absorption Cross Sections of HO_2 4-10
Table 4-7. Absorption Cross Sections of H_2O Vapor 4-11
Table 4-8. Absorption Cross Sections of H_2O_2 Vapor 4-11
Table 4-9. Mathematical Expression for Absorption Cross Sections of H_2O_2 as a Function of Temperature 4-12
Table 4-10. Absorption Cross Sections of NO_2 4-13
Table 4-11. Quantum Yields for NO_2 Photolysis 4-14
Table 4-12. Absorption Cross Sections of NO_3 at 298 K 4-16
Table 4-13. Mathematical Expression for Absorption Cross Sections of N_2O as a Function of Temperature* 4-16
Table 4-14. Absorption Cross Sections of N_2O at 298 K 4-17
Table 4-15. Absorption Cross Sections of N_2O_5 4-18
Table 4-16. Absorption Cross Sections of HONO 4-19
Table 4-17. Absorption Cross Sections and Temperature Coefficients of HNO_3 Vapor 4-20
Table 4-18. Absorption Cross Sections of HO_2NO_2 Vapor 4-20
Table 4-19. Absorption Cross Sections and Quantum Yields for Photolysis of CH_2O 4-21
Table 4-20. Absorption Cross Sections of CH_3O_2, $C_2H_5O_2$, and $CH_3C(O)O_2$ 4-22
Table 4-21. Absorption Cross Sections of CH_3OOH 4-23
Table 4-22. Absorption Cross Sections of PAN 4-25
Table 4-23. Absorption Cross Sections of FNO 4-26
Table 4-24. Absorption Cross Sections of CCl_2O, CClFO, and CF_2O at 298 K 4-27
Table 4-25. Absorption Cross Sections of Cl_2 4-28
Table 4-26. Absorption Cross Sections of ClOO 4-29
Table 4-27. Absorption Cross Sections of OClO at the Band Peaks 4-30
Table 4-28. Absorption Cross Sections of Cl_2O 4-32
Table 4-29. Absorption Cross Sections of ClOOCl at 200–250 K 4-33
Table 4-30. Absorption Cross Sections of Cl_2O_3 4-34
Table 4-31. Absorption Cross Sections of Cl_2O_4 4-34
Table 4-32. Absorption Cross Sections of Cl_2O_6 4-34

Table 4-33. Absorption Cross Sections of HCl Vapor 4-35
Table 4-34. Absorption Cross Sections of HOCl 4-36
Table 4-35. Absorption Cross Sections of ClNO 4-37
Table 4-36. Absorption Cross Sections of $ClNO_2$ 4-37
Table 4-37. Absorption Cross Sections of ClONO at 231 K 4-38
Table 4-38. Absorption Cross Sections of $ClONO_2$ 4-39
Table 4-39. Absorption Cross Sections of CCl_4 at 295–298 K 4-41
Table 4-40. Absorption Cross Sections of CH_3OCl 4-42
Table 4-41. Absorption Cross Sections of $CHCl_3$ at 295–298 K 4-43
Table 4-42. Absorption Cross Sections of CH_2Cl_2 at 295–298 K 4-44
Table 4-43. Absorption Cross Sections of CH_3Cl at 295–298 K 4-46
Table 4-44. Absorption Cross Sections of CH_3CCl_3 at 295–298 K 4-47
Table 4-45. Absorption Cross Sections of CH_3CH_2Cl at 298 K 4-47
Table 4-46. Absorption Cross Sections of $CH_3CHClCH_3$ at 295 K 4-48
Table 4-47. Absorption Cross Sections of $CFCl_3$ at 295–298 K 4-49
Table 4-48. Absorption Cross Sections of CF_2Cl_2 at 295–298 K 4-50
Table 4-49. Absorption Cross Sections of CF_3Cl at 295 K 4-51
Table 4-50. Absorption Cross Sections of $CF_2ClCFCl_2$ at 295–298 K 4-52
Table 4-51. Absorption Cross Sections of CF_2ClCF_2Cl at 295 K 4-53
Table 4-52. Absorption Cross Sections of CF_3CF_2Cl at 295–298 K 4-53
Table 4-53. Absorption Cross Sections of $CHFCl_2$ at 295–298 K 4-54
Table 4-54. Absorption Cross Sections of CHF_2Cl at 295–298 K 4-55
Table 4–55. Absorption Cross Sections of CH_2FCl at 298 K 4-55
Table 4-56. Absorption Cross Sections of CF_3CHCl_2 at 295 K 4-56
Table 4-57. Absorption Cross Sections of CF_3CHFCl at 295 K 4-57
Table 4-58. Absorption Cross Sections of CF_3CH_2Cl at 298 K 4-58
Table 4-59. Absorption Cross Sections of CH_3CFCl_2 at 295–298 K 4-59
Table 4–60. Absorption Cross Sections of CH_3CF_2Cl at 295–298 K 4-60
Table 4-61. Absorption Cross Sections of $CF_3CF_2CHCl_2$ and CF_2ClCF_2CFCl at 298 K 4-61
Table 4-62. Absorption Cross Sections at the Peak of Various Bands in the A ← X Spectrum of BrO 4-62
Table 4-63. Absorption Cross Sections of BrO 4-62
Table 4-64. Absorption Cross Sections of HOBr 4-65
Table 4-65. Absorption Cross Sections of $BrONO_2$ at 298 K 4-66
Table 4-66. Absorption Cross Sections of BrCl at 298 K 4-67
Table 4-67. Absorption Cross Sections of CH_3Br at 295–296 K 4-69
Table 4-68. Absorption Cross Sections of CH_2Br_2 at 295–298 K 4-70
Table 4-69. Absorption Cross Sections of $CHBr_3$ at 295–296 K 4-71
Table 4-70. Absorption Cross Sections of CH_2BrCH_2Br at 295 K 4-72
Table 4-71. Absorption Cross Sections of C_2H_5Br at 295 K 4-72
Table 4-72. Absorption Cross Sections of CH_2ClBr at 295 K 4-73
Table 4-73. Absorption Cross Sections of $CHClBr_2$ at 296 K 4-74
Table 4-74. Absorption Cross Sections of $CHCl_2Br$ at 298 K 4-75
Table 4-75. Absorption Cross Sections of CCl_3Br at 298 K 4-75
Table 4-76. Absorption Cross Sections of CHF_2Br at 298 K 4-76
Table 4-77. Absorption Cross Sections of CF_2Br_2 at 295–296 K 4-78
Table 4-78. Absorption Cross Sections of CF_2ClBr at 295–298 K 4-80
Table 4-79. Absorption Cross Sections of CF_3Br at 295–298 K 4-82
Table 4-80. Absorption Cross Sections of CF_3CH_2Br at 295 K 4-82
Table 4-81. Absorption Cross Sections of $CF_3CHClBr$ at 295–298 K 4-84
Table 4-82. Absorption Cross Sections of CF_3CHFBr at 295 K 4-84
Table 4-83. Absorption Cross Sections of CF_2BrCF_2Br at 296 K 4-86
Table 4-84. Absorption Cross Sections of CF_3CF_2Br at 298 K 4-87
Table 4-85. Absorption Cross Sections of CH_3I at 296–298 K and Temperature Coefficients 4-88
Table 4-86. Absorption Cross Sections of CH_2I_2 at 298 K 4-89
Table 4-87. Absorption Cross Sections of C_2H_5I at 298 K and Temperature Coefficients 4-90
Table 4-88. Absorption Cross Sections of CH_3CHI_2 at 298 K 4-91

Table 4-89. Absorption Cross Sections of C_3H_7I at 298 K and Temperature Coefficients 4-92
Table 4-90. Absorption Cross Sections of $(CH_3)_3CI$ at 298 K..... 4-93
Table 4-91. Absorption Cross Sections of CF_3I at 295–300 K..... 4-95
Table 4-92. Absorption Cross Sections of CF_2I_2 at 294 K 4-96
Table 4-93. Absorption Cross Sections of C_2F_5I at 323 K 4-96
Table 4-94. Absorption Cross Sections of 1-C_3F_7I at 295–298 K 4-97
Table 4-95. Absorption Cross Sections of CH_2ICl at 298 K and Temperature Coefficients 4-98
Table 4-96. Absorption Cross Sections of CH_2BrI at 298 K and Temperature Coefficients..... 4-99
Table 4-97. Absorption Cross Sections of OCS 4-100
Table 4-98. Absorption Cross Sections of NaCl Vapor at 300 K 4-101

Table 5-1. Mass Accommodation Coefficients (α) for Surfaces Other Than Soot. 5-8
Table 5-2. Gas/Surface Reaction Probabilities (γ) for Surfaces Other Than Soot. 5-16
Table 5-3. Soot Surface Uptake Coefficients. 5-32
Table 5-4. Henry's Law Constants for Pure Water. 5-35
Table 5-5. Henry's Law Constants for Acids 5-40

Table A-1. Gas-phase entropy and enthalpy values for selected species at 298.15 K and 100 kPa.....A-1

FIGURES

Figure 1-1. Symmetric and Asymmetric Error Limits.....1-3

Figure 4-1. Absorption Spectrum of NO_3 4-15
Figure 4-2. Absorption Spectrum of ClO 4-29
Figure 4-3. Absorption Spectrum of OClO 4-31
Figure 4-4. Absorption Spectrum of BrO 4-63

Figure 5-1. Recommended reactive uptake coefficients as a function of temperature for key stratospheric heterogeneous processes on sulfuric acid aerosols..... 5-7

INTRODUCTION

This compilation of kinetic and photochemical data is an update to the 13th evaluation prepared by the NASA Panel for Data Evaluation. The Panel was established in 1977 by the NASA Upper Atmosphere Research Program Office for the purpose of providing a critical tabulation of the latest kinetic and photochemical data for use by modelers in computer simulations of stratospheric chemistry. Table I-1 lists this publication's editions:

Table I-1. Editions of this Publication

	Edition	Reference
1	NASA RP 1010, Chapter 1	(Hudson [1])
2	JPL Publication 79-27	(DeMore et al. [12])
3	NASA RP 1049, Chapter 1	(Hudson and Reed [2])
4	JPL Publication 81-3	(DeMore et al. [10])
5	JPL Publication 82-57	(DeMore et al. [8])
6	JPL Publication 83-62	(DeMore et al. [9])
7	JPL Publication 85-37	(DeMore et al. [3])
8	JPL Publication 87-41	(DeMore et al. [4])
9	JPL Publication 90-1	(DeMore et al. [5])
10	JPL Publication 92-20	(DeMore et al. [6])
11	JPL Publication 94-26	(DeMore et al. [7])
12	JPL Publication 97-4	(DeMore et al. [11])
13	JPL Publication 00-3	(Sander et al. [14])
14	JPL Publication 02-25	(Sander et al. [13])

In addition to the current edition, several of the previous editions are available for download from the website.

Panel members, and their major responsibilities for the current evaluation are listed in Table I-2.

Table I-2. Panel Members and their Major Responsibilities for the Current Evaluation

Panel Members	Responsibility
S. P. Sander, Chairman	Editorial Review, publication, website
M. J. Kurylo V. L. Orkin	OH reactions with halocarbons
D. M. Golden	Three-body reactions, equilibrium constants
R. E. Huie	Aqueous chemistry, thermodynamics
B. J. Finlayson-Pitts C. E. Kolb M. J. Molina	Heterogeneous chemistry
R. R. Friedl A. R. Ravishankara	Upper Troposphere/Lower Stratosphere gas-phase chemistry
G. K. Moortgat	Photochemistry

As shown above, each Panel member concentrates his efforts on a given area or type of data. Nevertheless, the Panel's final recommendations represent a consensus of the entire Panel. Each member reviews the basis for all recommendations, and is cognizant of the final decision in every case.

Communications regarding particular reactions may be addressed to the appropriate panel member:

S. P. Sander
R. R. Friedl
Jet Propulsion Laboratory
M/S 183-901
4800 Oak Grove Drive
Pasadena, CA 91109
stanley.sander@jpl.nasa.gov
randall.friedl@jpl.nasa.gov

D. M. Golden
Department of Mechanical Engineering
Stanford University
Bldg 520
Stanford, CA 94305
david.golden@stanford.edu

R. E. Huie
M. J. Kurylo
V. L. Orkin
National Institute of Standards and Technology
Physical and Chemical Properties Division
Gaithersburg, MD 20899
robert.huie@nist.gov
michael.kurylo@nist.gov
vladimir.orkin@nist.gov

A. R. Ravishankara
NOAA-ERL, R/E/AL2
325 Broadway
Boulder, CO 80303
ravi@al.noaa.gov

C. E. Kolb
Aerodyne Research Inc.
45 Manning Rd.
Billerica, MA 01821
kolb@aerodyne.com

M. J. Molina
Department of Earth, Atmospheric, and Planetary Sciences
and Department of Chemistry
Massachusetts Institute of Technology
Cambridge, MA 02139
mmolina@mit.edu

G. K. Moortgat
Max-Planck-Institut für Chemie
Atmospheric Chemistry Division
Postfach 3060
55020 Mainz
Germany
moo@mpch-mainz.mpg.de

B. J. Finlayson-Pitts
Department of Chemistry
University of California, Irvine
516 Rowland Hall
Irvine, CA 92697-2025
bjfinlay@uci.edu

I.1 Basis of the Recommendations

The recommended rate data and cross sections are based on laboratory measurements. In order to provide recommendations that are as up-to-date as possible, preprints and written private communications are accepted, but only when it is expected that they will appear as published journal articles. Under no circumstances are rate constants adjusted to fit observations of atmospheric concentrations. The Panel considers the question of consistency of data with expectations based on the theory of reaction kinetics, and when a discrepancy appears to exist this fact is pointed out in the accompanying note. The major use of theoretical extrapolation of data is in connection with three-body reactions, in which the required pressure or temperature dependence is sometimes unavailable from laboratory measurements, and can be estimated by use of appropriate theoretical treatment. In the case of important rate constants for which no experimental data are available, the panel may provide estimates of rate constant parameters based on analogy to similar reactions for which data are available.

I.2 Scope of the Evaluation

In the past (releases 1-12 of this evaluation) it has been the practice of the Panel to reevaluate the entire set of reactions with individual Panel members taking responsibility for specific chemical families or processes. In recent years, the upper troposphere and lower stratosphere (UT/LS) have become the primary areas of focus for model calculations and atmospheric measurements related to studies of ozone depletion and climate change. Because the UT/LS is a region of relatively high chemical and dynamical complexity, a different approach has been adopted for future releases of the evaluation. Specifically, the entire reaction set of the data evaluation will no longer be re-evaluated for each release. Instead, specific subsets will be chosen for re-evaluation, with several Panel members working to develop recommendations for a given area. This approach will make it possible to treat each subset in

greater depth, and to expand the scope of the evaluation to new areas. It is the aim of the Panel to consider the entire set of kinetics, photochemical and thermodynamic parameters every three review cycles. Each release of the evaluation will contain not only the new evaluations, but also recommendations for every process that has been considered in the past. In this way, the tables for each release will constitute a complete set of recommendations.

It is recognized that important new laboratory data may be published that lie outside the specific subset chosen for re-evaluation. In order to ensure that these important data receive prompt consideration, each evaluation will also have a "special topics" category. Feedback from the atmospheric modeling community is solicited in the selection of reactions for this category.

For the current evaluation, the specific subsets include the following:

- Hydrocarbon chemistry of the upper troposphere (C3 hydrocarbons and below).
- Reactions of OH and Cl with halocarbon species.
- Photochemistry of halocarbon species.
- Heterogeneous processes on liquid sulfuric acid and soot surfaces
- Thermodynamic parameters (entropy and enthalpy of formation)
- The special topics category includes the following reactions: $O_3 + h\nu$, $O + O_2 + M$, $OH + O_3$, $HO_2 + O_3$, $OH + NO_2 + M$, $HO_2 + NO_2 + M$, $OH + HNO_3$, $OH + ClO$, $HO_2 + ClO$ and $ClO + ClO + M$.

I.3 Format of the Evaluation

Changes or additions to the tables of data are indicated by shading. A new entry is completely shaded, whereas a changed entry is shaded only where it has changed. In some cases only the note has been changed, in which case the corresponding note number in the table is shaded.

I.4 Computer Access

This document is available online in the form of individual chapters and as a complete document in Adobe PDF (Portable Data File) format. Files may be downloaded from http://jpldataeval.jpl.nasa.gov/. This document is not available in printed form from JPL.

Individuals who wish to receive notice when the web page is revised should submit email addresses in the appropriate reply box on the web page.

For more information, contact Stanley Sander (Stanley.Sander@jpl.nasa.gov).

I.5 Data Formats

In Table 1 (Rate Constants for Bimolecular Reactions) the reactions are grouped into the classes O_x, HO_x, NO_x, Organic Compounds, FO_x, ClO_x, BrO_x, IO_x, SO_x and Metal Reactions. The data in Table 2 (Rate Constants for Association Reactions) are presented in the same order as the bimolecular reactions. The presentation of photochemical cross section data follows the same sequence.

I.6 Units

The rate constants are given in units of concentration expressed as molecules per cubic centimeter and time in seconds. Thus, for first-, second-, and third-order reactions the units of k are s^{-1}, cm^3 $molecule^{-1}$ s^{-1}, and cm^6 $molecule^{-2}$ s^{-1}, respectively. Cross sections are expressed as cm^2 $molecule^{-1}$, base e.

I.7 Noteworthy Changes in This Evaluation

I.7.1 Bimolecular Reactions

I.7.1.1 Hydrocarbon Reactions Important in the Upper Troposphere

Atmospheric observations suggest that photochemistry in the upper troposphere has a much greater global significance than previously believed. The production of O_3 in this region is significant and is controlled by interaction of the HO_x and NO_x radical families. Increasingly, it has been recognized that organic compounds (e.g. ketones, aldehydes, peroxides, and acids) play an important role in supplying HO_x to the upper troposphere. NO_x sources in this region are numerous and long-lived reservoir species such as peroxyacyl nitrates (e.g. PAN) and peroxynitric acid (PNA) serve to redistribute NO_x globally.

In addition, there is renewed interest in the role of convective activity in lifting short-lived hydrocarbons and halocarbon species to levels near the tropopause. If the convection does not directly penetrate the stratosphere, the reactive organics and organo-halogens are likely to react in the upper troposphere. This would be a mechanism for the transport of aldehydes and peroxides noted above. In case of the organo-halogen compounds, releasing degradation products and/or chlorine and bromine radicals in the upper troposphere can be significant. The subsequent fate of the degradation products, especially whether they survive long enough to be transported from the upper troposphere into the stratosphere to affect the halogen budget, is an important open question.

In this update we have considered a set of reactions of importance in upper tropospheric HO_x, NO_x and shortlived halocarbon chemistry. The set includes reactions of OH and Cl with selected alkyl peroxides, organic acids, alkyl and acyl nitrates, aldehydes, and alcohols. It also includes reactions of Cl with various alkylhalides.

We have also updated kinetics parameters for a number of alkylperoxy self- and cross-reactions of importance in upper tropospheric HO_x chemistry. The reactions of peroxy radicals have been studied in the laboratory for many years. However, there are some key difficulties associated with such studies. First, many of the peroxy radicals of interest to the atmosphere are radical-radical reactions that are inherently difficult to study in isolation. For example, many of the reactions of peroxy radicals cannot be carried out under pseudo-first order conditions. Second, many peroxy radical reactions produce reactive products that unavoidably lead to further reactions with the species being monitored. Third, most peroxy radicals do not fluoresce and none have been observed via a fluorescence technique. They also have weak, unstructured absorption spectra in the ultraviolet, which often overlap with those of other peroxy radicals. Therefore, a sensitiveity and selectiveity method for the detection of peroxy radicals is missing. Lastly, in general, peroxy radical reactions often have more than one set of products.

Previously, it was not always possible to perform a critical analysis using a self-consistent data base because (a) all the information about the experiments was not available, (b) it required re-analysis of previous data in light of new information such as absorption cross sections and product yields, and (c) the knowledge of the interfering reactions and their rates was also uncertain. Therefore, a panel of scientists who have worked with the peroxy radicals of interest to the atmosphere and whose data usually form the basis of recommendations was assembled as a part of the SPARC-IGAC initiative. This panel critically reevaluated the existing data, discarded some, and modified others to arrive at a self-consistent evaluation of the rate coefficients and product yields in the reactions of RO_2 radicals. This effort resulted in a paper that was published in the Journal of Geophysical Research [15]. The current recommendation uses these evaluated data.

Our consideration of upper tropospheric reactions has resulted in the addition of 18 new reactions, most of which involve reactions of Cl with alkyl nitrates, alkyl halides and organic peroxides and acids. Changes to the existing reactions mainly represent small refinements of the Arrhenius parameters and tightening of the uncertainty limits. One significant change involves the OH + acetone reaction rate coefficient which may exhibit curved Arrhenius behavior.

I.7.1.2 OH + Halocarbon Reactions

A comprehensive review of the reactions of industrial and naturally occurring halocarbons with the hydroxyl radical (OH) was conducted for this evaluation. In doing so, attempts were made to understand and reconcile apparent differences between the results of absolute and relative rate measurements for some of the reactions. Relative rate constants were “renormalized” using the revised recommendations for the reference reactions. Thus, the re-evaluation procedure was an iterative one, since relative rate studies themselves were often included as the basis for the rate constant recommendations of these very reference reactions. The recommendations were then checked for self-consistency by seeing whether ratios of the recommended rate constants were in agreement with published relative rate measurements.

In some cases, disparities may seem to exist. However, it should be recognized that the focus of this re-evaluation was the generation of recommended rate constants over the temperature range of atmospheric importance (i.e., below 300 K). Many of the latest (or relatively recent) absolute rate studies have focused on this region but often extend to temperatures greater than 300 K Relative rate investigations, on the other hand, have been conducted predominantly above room temperature, with only limited extension below 300 K. This can lead to difficulties in evaluating the studies since many of the OH + halocarbon reactions exhibit pronounced Arrhenius curvature. This curvature has several possible causes including multiple reaction pathways (different types of abstractable H atoms), multiple reactant conformers (whose populations and reactivity differ with temperature), and tunneling. Of course, convincing evidence had to exist that such Arrhenius behavior was indeed real and not an artifact of the experimental procedure. For example, one of the common reasons for experimentally observed non-Arrhenius behavior is the

presence of highly reactive impurities in the samples used in the absolute measurements. However, most recent absolute studies have involved thorough reactant sample purification and analysis and curvature in the Arrhenius plot is not likely due to such impurities. Thus, in the presence of real Arrhenius curvature, a rate constant expression derived predominantly from absolute rate constant measurements conducted below room temperature may not be appropriate for normalizing relative rate constant measurements conducted above room temperature. More detail about these issues may be found in the notes for the reactions of OH with HFC-152a and HFC-152 (reactions E7 and E8, respectively).

For some reactions in this section, there have been significant revisions in the recommendations as a result of new and improved studies. For other reactions, only minor changes from earlier recommendations have been made. Nevertheless, in all cases, such changes were made so that the complete set of recommendations is completely current with the published literature and is self-consistent. Finally, several new reactions have been included and the rate constant uncertainty factors (f and g) have been carefully reviewed in an attempt to narrow the range of rate constant uncertainties for modeling purposes. Previous uncertainty limits were overly conservative in some cases. In the present evaluation, the 2σ confidence limits derived from these factors were visually inspected together with the complete experimental database for consistency.

I.7.1.3 Absorption Cross Sections and Quantum Yields

The database for the evaluation of the absorption cross sections and quantum yields has been expanded considerably for all the halocarbon compounds. Whereas the previous evaluation JPL 97-4 reported only the absorption cross sections of a limited number of selected halocarbons, the present evaluation includes now a comprehensive review of most halocarbons of atmospheric relevance investigated in recent years.

The newly evaluated halocarbons are listed in Table 4. This list includes new entries for C_1 to C_4 chloroalkanes, C_1 to C_2 chlorofluoroalkanes (CFCs) and C_1 to C_3 hydrochlorofluorocarbons (HCFCs). For these species the database was expanded from 14 to 26 compounds. Moreover, the database for the brominated hydro- and mixed halocarbons, including halons, was increased from 6 to 18 compounds. Finally, a large range of iodine-containing compounds (total 32) has now been implemented in the present evaluation.

Also new in this section is the incorporation of temperature-dependence data, including the parameters used to express the temperature variation of the absorption cross sections by a polynomial expansion formula. These expressions will allow the calculation of absorption cross sections in a wide range of stratospheric temperatures. Finally, quantum yield data have also been updated for many species.

I.7.2 Heterogeneous Processes

New and/or updated evaluations in this document have focused on uptake measurements on binary liquid sulfuric acid/water solutions, supplemented in a few cases by data on ternary liquid sulfuric acid/nitric acid/water solutions, on water ice, and on “soot” (see definitions in the section on heterogeneous chemistry). No updates on solid acid/ice compositions are presented in this document, although evaluations for key nitrogen oxide sequestration and/or halogen activation reactions on nitric acid trihydrate (NAT) surfaces were recently re-evaluated and presented in JPL 00-3 [14]. Uptake data on alumina, salt and aqueous salt solutions have not been updated since JPL 97-4 [11]. Henry’s law solubility data for reactive upper tropospheric/stratospheric species in binary liquid sulfuric acid/water, and, where available, in ternary liquid sulfuric acid/nitric acid/water solutions have also been updated and a much more extensive compilation of Henry’s law parameters for pure water has been added.

I.7.3 Thermodynamic Parameters

The table in Appendix 1 contains selected entropy and enthalpy of formation values at 298 K for a number of atmospheric species. As much as possible, the values were taken from primary evaluations, that is, evaluations that develop a recommended value from the original studies. Otherwise, the values were selected from the original literature, which is referenced in the table. Often, the enthalpy of formation and the entropy values are taken from different sources, usually due to a more recent value for the enthalpy of formation. The cited error limits are from the original references and therefore reflect widely varying criteria. Some enthalpy values were corrected slightly to reflect the value of a reference compound selected for this table; these are indicated. Values that are calculated or estimated are also indicated in the table.

I.8 Acknowledgements

The Panel wishes to acknowledge Hannelore Keller-Rudek for her assistance preparing the evaluation of the photochemistry section and efforts updating the database on absorption spectra of atmospheric relevant compounds.

The new and updated evaluations presented in this heterogeneous chemistry section were prepared by B.J. Finlayson-Pitts, R.E. Huie, C.E. Kolb and M.J. Molina. They would like to acknowledge valuable technical and editorial assistance from L.R. Williams, Q. Shi, L.T. Molina and D.M. Smith. They would also like to thank the members of the international heterogeneous research communities who provided copies of their reprints, preprints and written summaries of recent results from their laboratories.We gratefully acknowledge the critical reading of this evaluation by Drs. W. B. DeMore and R. F. Hampson. We also appreciate the expert editorial assistance and website suppport provided by T. Wilson and L. Palkovic of the Jet Propulsion Laboratory. The typing skills of X. Sabounchi are also gratefully acknowledged.

I.9 References

1. Chlorofluoromethanes and the Stratosphere. In *NASA Reference Publication 1010*; Hudson, R. D., Ed.; NASA: Washington, D.C, 1977.
2. The Stratosphere: Present and Future. In *NASA Reference Publication 1049*; Hudson, R. D., Reed, E. I., Eds.; NASA: Washington, D.C, 1979.
3. DeMore, W. B., D. M. Golden, R. F. Hampson, C. J. Howard, M. J. Kurylo, J. J. Margitan, M. J. Molina, A. R. Ravishankara and R. T. Watson "Chemical Kinetics and Photochemical Data for Use in Stratospheric Modeling, Evaluation Number 7," JPL Publication 85-37, Jet Propulsion Laboratory, California Institute of Technology, Pasadena CA, 1985.
4. DeMore, W. B., D. M. Golden, R. F. Hampson, C. J. Howard, M. J. Kurylo, M. J. Molina, A. R. Ravishankara and S. P. Sander "Chemical Kinetics and Photochemical Data for Use in Stratospheric Modeling, Evaluation Number 8," JPL Publication 87-41, Jet Propulsion Laboratory, California Institute of Technology, Pasadena CA, 1987.
5. DeMore, W. B., D. M. Golden, R. F. Hampson, C. J. Howard, M. J. Kurylo, M. J. Molina, A. R. Ravishankara and S. P. Sander "Chemical Kinetics and Photochemical Data for Use in Stratospheric Modeling, Evaluation Number 9," JPL Publication 90-1, Jet Propulsion Laboratory, California Institute of Technology, Pasadena CA, 1990.
6. DeMore, W. B., D. M. Golden, R. F. Hampson, C. J. Howard, M. J. Kurylo, M. J. Molina, A. R. Ravishankara and S. P. Sander "Chemical Kinetics and Photochemical Data for Use in Stratospheric Modeling, Evaluation Number 10," JPL Publication 92-20, Jet Propulsion Laboratory, California Institute of Technology, Pasadena, CA, 1992.
7. DeMore, W. B., D. M. Golden, R. F. Hampson, C. J. Howard, M. J. Kurylo, M. J. Molina, A. R. Ravishankara and S. P. Sander "Chemical Kinetics and Photochemical Data for Use in Stratospheric Modeling, Evaluation Number 11," JPL Publication 94-26, Jet Propulsion Laboratory, California Institute of Technology, Pasadena, CA, 1994.
8. DeMore, W. B., D. M. Golden, R. F. Hampson, C. J. Howard, M. J. Kurylo, M. J. Molina, A. R. Ravishankara and R. T. Watson "Chemical Kinetics and Photochemical Data for Use in Stratospheric Modeling, Evaluation Number 5," JPL Publication 82-57, Jet Propulsion Laboratory, California Institute of Technology, Pasadena CA, 1982.
9. DeMore, W. B., D. M. Golden, R. F. Hampson, C. J. Howard, M. J. Kurylo, M. J. Molina, A. R. Ravishankara and R. T. Watson "Chemical Kinetics and Photochemical Data for Use in Stratospheric Modeling, Evaluation Number 6," JPL Publication 83-62, Jet Propulsion Laboratory, California Institute of Technology, Pasadena CA, 1983.
10. DeMore, W. B., D. M. Golden, R. F. Hampson, M. J. Kurylo, J. J. Margitan, M. J. Molina, L. J. Stief and R. T. Watson "Chemical Kinetics and Photochemical Data for Use in Stratospheric Modeling, Evaluation Number 4," JPL Publication 81-3, Jet Propulsion Laboratory, California Institute of Technology, Pasadena CA, 1981.
11. DeMore, W. B., S. P. Sander, D. M. Golden, R. F. Hampson, M. J. Kurylo, C. J. Howard, A. R. Ravishankara, C. E. Kolb and M. J. Molina "Chemical Kinetics and Photochemical Data for Use in Stratospheric Modeling, Evaluation Number 12," JPL Publication 97-4, Jet Propulsion Laboratory, California Institute of Technology, Pasadena, CA, 1997.

12. DeMore, W. B., L. J. Stief, F. Kaufman, D. M. Golden, R. F. Hampson, M. J. Kurylo, J. J. Margitan, M. J. Molina and R. T. Watson "Chemical Kinetics and Photochemical Data for Use in Stratospheric Modeling, Evaluation Number 2," JPL Publication 79-27, Jet Propulsion Laboratory, California Institute of Technology, Pasadena, CA, 1979.
13. Sander, S. P., B. J. Finlayson-Pitts, R. R. Friedl, D. M. Golden, R. E. Huie, C. E. Kolb, M. J. Kurylo, M. J. Molina, G. K. Moortgat, V. L. Orkin and A. R. Ravishankara "Chemical Kinetics and Photochemical Data for Use in Atmospheric Studies, Evaluation Number 14," JPL Publication 02-25, Jet Propulsion Laboratory, Pasadena, 2002.
14. Sander, S. P., R. R. Friedl, W. B. DeMore, D. M. Golden, M. J. Kurylo, R. F. Hampson, R. E. Huie, G. K. Moortgat, A. R. Ravishankara, C. E. Kolb and M. J. Molina "Chemical Kinetics and Photochemical Data for Use in Stratospheric Modeling, Evaluation Number 13," JPL Publication 00-3, Jet Propulsion Laboratory, California Institute of Technology, Pasadena, CA, 2000.
15. Tyndall, G. S., R. A. Cox, C. Granier, R. Lesclaux, G. K. Moortgat, M. J. Pilling, A. R. Ravishankara and T. J. Wallington, 2001, J. Geophys. Res., **106**, 12157-12182.

SECTION 1. BIMOLECULAR REACTIONS

Table of Contents

SECTION 1. BIMOLECULAR REACTIONS 1-1
1.1 Introduction 1-1
1.2 Uncertainty Estimates 1-2
1.3 Notes to Table 1 1-31
1.4 References 1-94

Tables

Table 1-1. Rate Constants for Second-Order Reactions 1-5

Figures

Figure 1-1. Symmetric and Asymmetric Error Limits 1-3

1.1 Introduction

In Table 1 (Rate Constants for Second-Order Reactions) the reactions are grouped into the classes O_x, $O(^1D)$, Singlet O_2, HO_x, NO_x, Organic Compounds, FO_x, ClO_x, BrO_x, IO_x, SO_x and Metals. Some of the reactions in Table 1-1 are actually more complex than simple two-body reactions. To explain the pressure and temperature dependences occasionally seen in reactions of this type, it is necessary to consider the bimolecular class of reactions in terms of two subcategories, direct (concerted) and indirect (nonconcerted) reactions.

A direct or concerted bimolecular reaction is one in which the reactants A and B proceed to products C and D without the intermediate formation of an AB adduct that has appreciable bonding, i.e., there is no bound intermediate; only the transition state $(AB)^{\neq}$ lies between reactants and products.

$$A + B \rightarrow (AB)^{\neq} \rightarrow C + D$$

The reaction of OH with CH_4 forming $H_2O + CH_3$ is an example of a reaction of this class.

Very useful correlations between the expected structure of the transition state $[AB]^{\neq}$ and the A-Factor of the reaction rate constant can be made, especially in reactions that are constrained to follow a well-defined approach of the two reactants in order to minimize energy requirements in the making and breaking of bonds. The rate constants for these reactions are well represented by the Arrhenius expression $k = A \exp(-E/RT)$ in the 200–300 K temperature range. These rate constants are not pressure dependent.

The indirect or nonconcerted class of bimolecular reactions is characterized by a more complex reaction path involving a potential well between reactants and products, leading to a bound adduct (or reaction complex) formed between the reactants A and B:

$$A + B \leftrightarrow [AB]^* \rightarrow C + D$$

The intermediate $[AB]^*$ is different from the transition state $[AB]^{\neq}$, in that it is a bound molecule which can, in principle, be isolated. (Of course, transition states are involved in all of the above reactions, both forward and backward, but are not explicitly shown.) An example of this reaction type is ClO + NO, which normally produces $Cl + NO_2$. Reactions of the nonconcerted type can have a more complex temperature dependence and can exhibit a pressure dependence if the lifetime of $[AB]^*$ is comparable to the rate of collisional deactivation of $[AB]^*$. This arises because the relative rate at which $[AB]^*$ goes to products C + D vs. reactants A + B is a sensitive function of its excitation energy. Thus, in reactions of this type, the distinction between the bimolecular and termolecular classification becomes less meaningful, and it is especially necessary to study such reactions under the temperature and pressure conditions in which they are to be used in model calculation, or, alternatively, to develop a reliable theoretical basis for extrapolation of data.

The rate constant tabulation for second-order reactions (Table 1-1) is given in Arrhenius form:

$$k(T) = A \exp((-E/R)(1/T))$$

and contains the following information:

1. Reaction stoichiometry and products (if known). The pressure dependences are included, where appropriate.
2. Arrhenius A-factor.
3. Temperature dependence and associated uncertainty ("activation temperature" E/R±g).
4. Rate constant at 298 K.
5. Uncertainty factor at 298 K.
6. Note giving basis of recommendation and any other pertinent information.

1.2 Uncertainty Estimates

For bimolecular rate constants in Table 1-1, an estimate of the uncertainty at any given temperature, f(T), may be obtained from the following expression:

$$f(T)=f(298\ K)\exp\left|g\left(\frac{1}{T}-\frac{1}{298}\right)\right|$$

Note that the exponent is an absolute value. An upper or lower bound (corresponding approximately to one standard deviation) of the rate constant at any temperature T can be obtained by multiplying or dividing the recommended value of the rate constant at that temperature by the factor f(T). The quantity f(298 K) is the uncertainty in the rate constant at T = 298 K. The quantity g has been defined in this evaluation for use with f(298 K) in the above expression to obtain the rate constant uncertainty at different temperatures. It should not be interpreted as the uncertainty in the Arrhenius activation temperature (E/R). Both uncertainty factors, f(298 K) and g, do not necessarily result from a rigorous statistical analysis of the available data. Rather, they are chosen by the evaluators to construct the appropriate uncertainty factor, f(T), shown above.

This approach is based on the fact that rate constants are almost always known with minimum uncertainty at room temperature. The overall uncertainty normally increases at other temperatures, because there are usually fewer data at other temperatures. In addition, data obtained at temperatures far distant from 298 K may be less accurate than at room temperature due to various experimental difficulties.

The uncertainty represented by f(T) is normally symmetric; i.e., the rate constant may be greater than or less than the recommended value, k(T), by the factor f(T). In a few cases in Table 1-1 asymmetric uncertainties are given in the temperature coefficient. For these cases, the factors by which a rate constant is to be multiplied or divided to obtain, respectively, the upper and lower limits are not equal, except at 298 K where the factor is simply f(298 K). Explicit equations are given below for the case where g is given as (g +a, –b):

For T > 298 K, multiply by the factor

$$f(298)e^{\left[a\left(\frac{1}{298}-\frac{1}{T}\right)\right]}$$

and divide by the factor

$$f(298)e^{\left[b\left(\frac{1}{298}-\frac{1}{T}\right)\right]}$$

For T < 298 K, multiply by the factor

$$f(298)e^{\left[b\left(\frac{1}{T}-\frac{1}{298}\right)\right]}$$

and divide by the factor

$$f(298)e^{\left[a\left(\frac{1}{T}-\frac{1}{298}\right)\right]}$$

Examples of symmetric and asymmetric error limits are shown in Figure 1-1.

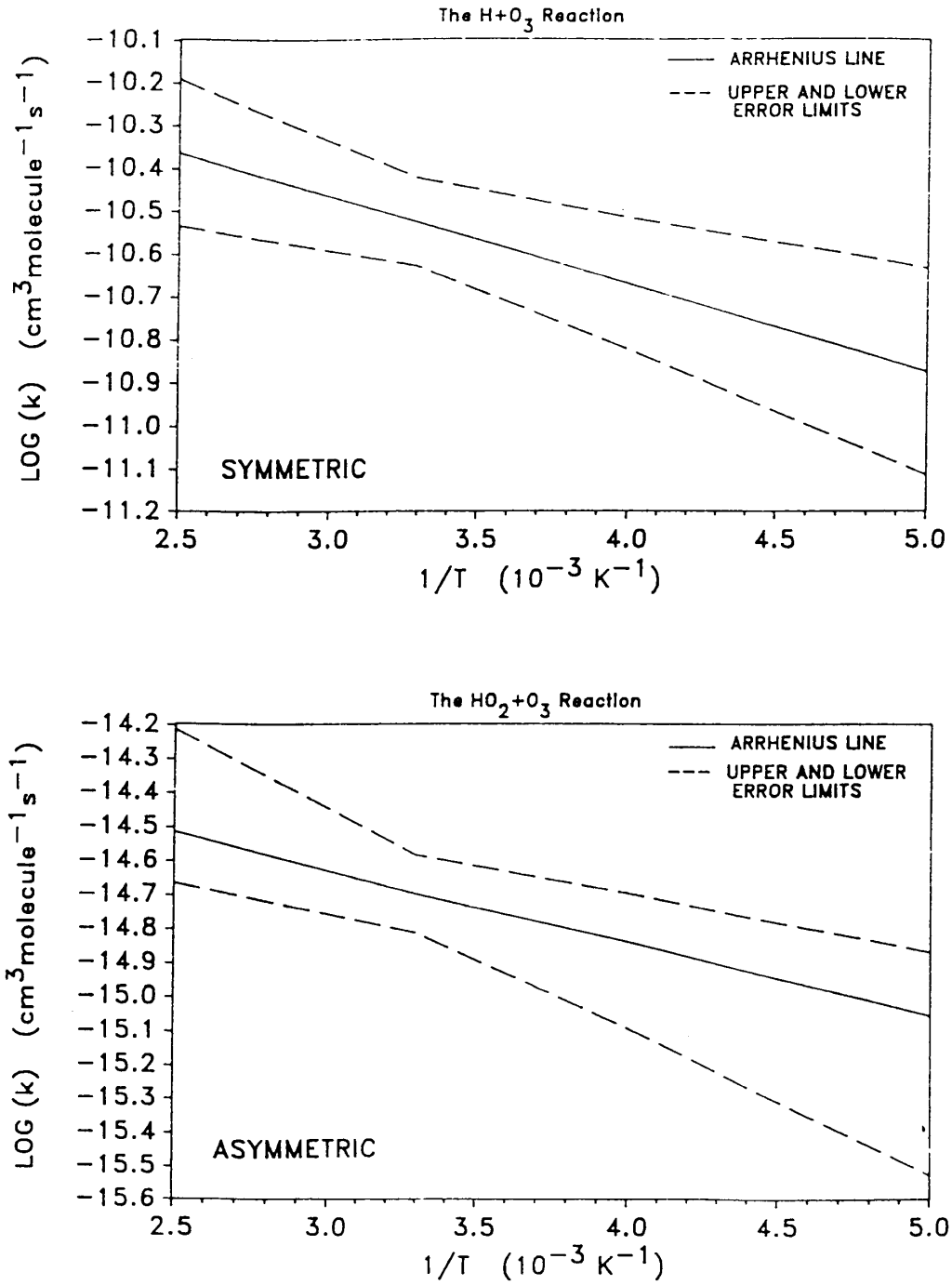

Figure 1-1. Symmetric and Asymmetric Error Limits

The assigned uncertainties represent the subjective judgment of the Panel. They are not determined by a rigorous, statistical analysis of the database, which generally is too limited to permit such an analysis. Rather, the uncertainties are based on knowledge of the techniques, the difficulties of the experiments, and the potential for systematic errors.

There is obviously no way to quantify these "unknown" errors. The spread in results among different techniques for a given reaction may provide some basis for an uncertainty, but the possibility of the same, or compensating, systematic errors in all the studies must be recognized.

Furthermore, the probability distribution may not follow the normal Gaussian form. For measurements subject to large systematic errors, the true rate constant may be much further from the recommended value than would be expected based on a Gaussian distribution with the stated uncertainty. As an example, in the past the recommended rate constants for the reactions HO_2 + NO and Cl + $ClONO_2$ changed by factors of 30–50. These changes could not have been allowed for with any reasonable values of σ in a Gaussian distribution.

Table 1-1. Rate Constants for Second-Order Reactions

Reaction	A-Factor[a]	E/R	k(298 K)[a]	f(298 K)[b]	g	Notes
O_x Reactions						
$O + O_2 \xrightarrow{M} O_3$	(See Table 2-1)					
$O + O_3 \rightarrow O_2 + O_2$	8.0×10^{-12}	2060	8.0×10^{-15}	1.15	250	A1
$O(^1D)$ Reactions						
$O(^1D) + O_2 \rightarrow O + O_2$	3.2×10^{-11}	–70	4.0×10^{-11}	1.2	100	A2, A3
$O(^1D) + O_3 \rightarrow O_2 + O_2$	1.2×10^{-10}	0	1.2×10^{-10}	1.3	100	A2, A4
$\rightarrow O_2 + O + O$	1.2×10^{-10}	0	1.2×10^{-10}	1.3	100	A2, A4
$O(^1D) + H_2 \rightarrow OH + H$	1.1×10^{-10}	0	1.1×10^{-10}	1.1	100	A2, A5
$O(^1D) + H_2O \rightarrow OH + OH$	2.2×10^{-10}	0	2.2×10^{-10}	1.2	100	A2, A6
$O(^1D) + N_2 \rightarrow O + N_2$	1.8×10^{-11}	–110	2.6×10^{-11}	1.2	100	A2
$O(^1D) + N_2 \xrightarrow{M} N_2O$	(See Table 2-1)					
$O(^1D) + N_2O \rightarrow N_2 + O_2$	4.9×10^{-11}	0	4.9×10^{-11}	1.3	100	A2, A7
$\rightarrow NO + NO$	6.7×10^{-11}	0	6.7×10^{-11}	1.3	100	A2, A7
$O(^1D) + NH_3 \rightarrow OH + NH_2$	2.5×10^{-10}	0	2.5×10^{-10}	1.3	100	A2, A8
$O(^1D) + CO_2 \rightarrow O + CO_2$	7.4×10^{-11}	–120	1.1×10^{-10}	1.2	100	A2
$O(^1D) + CH_4 \rightarrow$ products	1.5×10^{-10}	0	1.5×10^{-10}	1.2	100	A2, A9
$O(^1D) + HCl \rightarrow$ products	1.5×10^{-10}	0	1.5×10^{-10}	1.2	100	A10
$O(^1D) + HF \rightarrow OH + F$	1.4×10^{-10}	0	1.4×10^{-10}	2.0	100	A11
$O(^1D) + HBr \rightarrow$ products	1.5×10^{-10}	0	1.5×10^{-10}	2.0	100	A12
$O(^1D) + Cl_2 \rightarrow$ products	2.8×10^{-10}	0	2.8×10^{-10}	2.0	100	A13
$O(^1D) + CCl_2O \rightarrow$ products	3.6×10^{-10}	0	3.6×10^{-10}	2.0	100	A2, A14
$O(^1D) + CClFO \rightarrow$ products	1.9×10^{-10}	0	1.9×10^{-10}	2.0	100	A2, A14
$O(^1D) + CF_2O \rightarrow$ products	7.4×10^{-11}	0	7.4×10^{-11}	2.0	100	A2, A14
$O(^1D) + CCl_4 \rightarrow$ products (CFC-10)	3.3×10^{-10}	0	3.3×10^{-10}	1.2	100	A2, A15

Reaction	A-Factor[a]	E/R	k(298 K)[a]	f(298 K)[b]	g	Notes
$O(^1D) + CH_3Br \rightarrow$ products	1.8×10^{-10}	0	1.8×10^{-10}	1.3	100	A15, A16
$O(^1D) + CH_2Br_2 \rightarrow$ products	2.7×10^{-10}	0	2.7×10^{-10}	1.3	100	A15, A17
$O(^1D) + CHBr_3 \rightarrow$ products	6.6×10^{-10}	0	6.6×10^{-10}	1.5	100	A15, A18
$O(^1D) + CH_3F \rightarrow$ products (HFC-41)	1.5×10^{-10}	0	1.5×10^{-10}	1.2	100	A15, A19
$O(^1D) + CH_2F_2 \rightarrow$ products (HFC-32)	5.1×10^{-11}	0	5.1×10^{-11}	1.3	100	A15, A20
$O(^1D) + CHF_3 \rightarrow$ products (HFC-23)	9.1×10^{-12}	0	9.1×10^{-12}	1.2	100	A15, A21
$O(^1D) + CHCl_2F \rightarrow$ products (HCFC-21)	1.9×10^{-10}	0	1.9×10^{-10}	1.3	100	A15, A22
$O(^1D) + CHClF_2 \rightarrow$ products (HCFC-22)	1.0×10^{-10}	0	1.0×10^{-10}	1.2	100	A15, A23
$O(^1D) + CCl_3F \rightarrow$ products (CFC-11)	2.3×10^{-10}	0	2.3×10^{-10}	1.2	100	A2, A15
$O(^1D) + CCl_2F_2 \rightarrow$ products (CFC-12)	1.4×10^{-10}	0	1.4×10^{-10}	1.3	100	A2, A15
$O(^1D) + CClF_3 \rightarrow$ products (CFC-13)	8.7×10^{-11}	0	8.7×10^{-11}	1.3	100	A15, A24
$O(^1D) + CClBrF_2 \rightarrow$ products (Halon-1211)	1.5×10^{-10}	0	1.5×10^{-10}	1.3	100	A15, A25
$O(^1D) + CBr_2F_2 \rightarrow$ products (Halon-1202)	2.2×10^{-10}	0	2.2×10^{-10}	1.3	100	A15, A26
$O(^1D) + CBrF_3 \rightarrow$ products (Halon-1301)	1.0×10^{-10}	0	1.0×10^{-10}	1.3	100	A15, A27
$O(^1D) + CF_4 \rightarrow CF_4 + O$ (CFC-14)	–	–	2.0×10^{-14}	1.5	–	A15, A28
$O(^1D) + CH_3CH_2F \rightarrow$ products (HFC-161)	2.6×10^{-10}	0	2.6×10^{-10}	1.3	100	A15, A29
$O(^1D) + CH_3CHF_2 \rightarrow$ products (HFC-152a)	2.0×10^{-10}	0	2.0×10^{-10}	1.3	100	A15, A30
$O(^1D) + CH_3CCl_2F \rightarrow$ products (HCFC-141b)	2.6×10^{-10}	0	2.6×10^{-10}	1.3	100	A15, A31
$O(^1D) + CH_3CClF_2 \rightarrow$ products (HCFC-142b)	2.2×10^{-10}	0	2.2×10^{-10}	1.3	100	A15, A32
$O(^1D) + CH_3CF_3 \rightarrow$ products (HFC-143a)	1.0×10^{-10}	0	1.0×10^{-10}	3.0	100	A15, A33
$O(^1D) + CH_2ClCClF_2 \rightarrow$ products (HCFC-132b)	1.6×10^{-10}	0	1.6×10^{-10}	2.0	100	A15, A34
$O(^1D) + CH_2ClCF_3 \rightarrow$ products (HCFC-133a)	1.2×10^{-10}	0	1.2×10^{-10}	1.3	100	A15, A35
$O(^1D) + CH_2FCF_3 \rightarrow$ products (HFC-134a)	4.9×10^{-11}	0	4.9×10^{-11}	1.3	100	A15, A36
$O(^1D) + CHCl_2CF_3 \rightarrow$ products (HCFC-123)	2.0×10^{-10}	0	2.0×10^{-10}	1.3	100	A15, A37
$O(^1D) + CHClFCF_3 \rightarrow$ products (HCFC-124)	8.6×10^{-11}	0	8.6×10^{-11}	1.3	100	A15, A38

Reaction	A-Factor[a]	E/R	k(298 K)[a]	f(298 K)[b]	g	Notes
$O(^1D) + CHF_2CF_3 \rightarrow$ products (HFC-125)	1.2×10^{-10}	0	1.2×10^{-10}	2.0	100	A15, A39
$O(^1D) + CCl_3CF_3 \rightarrow$ products (CFC-113a)	2×10^{-10}	0	2×10^{-10}	2.0	100	A15, A40
$O(^1D) + CCl_2FCClF_2 \rightarrow$ products (CFC-113)	2×10^{-10}	0	2×10^{-10}	2.0	100	A15, A41
$O(^1D) + CCl_2FCF_3 \rightarrow$ products (CFC-114a)	1×10^{-10}	0	1×10^{-10}	2.0	100	A15, A42
$O(^1D) + CClF_2CClF_2 \rightarrow$ products (CFC-114)	1.3×10^{-10}	0	1.3×10^{-10}	1.3	100	A15, A43
$O(^1D) + CClF_2CF_3 \rightarrow$ products (CFC-115)	5×10^{-11}	0	5×10^{-11}	1.3	100	A15, A44
$O(^1D) + CBrF_2CBrF_2 \rightarrow$ products (Halon-2402)	1.6×10^{-10}	0	1.6×10^{-10}	1.3	100	A15, A45
$O(^1D) + CF_3CF_3 \rightarrow O + CF_3CF_3$ (CFC-116)	–	–	1.5×10^{-13}	1.5	–	A15, A46
$O(^1D) + CHF_2CF_2CF_2CHF_2 \rightarrow$ products (HFC-338pcc)	1.8×10^{-11}	0	1.8×10^{-11}	1.5	100	A15, A47
$O(^1D) + c\text{-}C_4F_8 \rightarrow$ products	–	–	8×10^{-13}	1.3	–	A15, A48
$O(^1D) + CF_3CHFCHFCF_2CF_3 \rightarrow$ products (HFC-43-10mee)	2.1×10^{-10}	0	2.1×10^{-10}	4	100	A15, A49
$O(^1D) + C_5F_{12} \rightarrow$ products (CFC-41-12)	–	–	3.9×10^{-13}	2	–	A15, A50
$O(^1D) + C_6F_{14} \rightarrow$ products (CFC-51-14)	–	–	1×10^{-12}	2	–	A15, A51
$O(^1D) + 1,2\text{-}(CF_3)_2c\text{-}C_4F_6 \rightarrow$ products	–	–	2.8×10^{-13}	2	–	A15, A52
$O(^1D) + SF_6 \rightarrow$ products	–	–	1.8×10^{-14}	1.5	–	A53
Singlet O_2 Reactions						
$O_2(^1\Delta) + O \rightarrow$ products	–	–	$<2\times10^{-16}$	–	–	A54
$O_2(^1\Delta) + O_2 \rightarrow$ products	3.6×10^{-18}	220	1.7×10^{-18}	1.2	100	A55
$O_2(^1\Delta) + O_3 \rightarrow O + 2O_2$	5.2×10^{-11}	2840	3.8×10^{-15}	1.2	500	A56
$O_2(^1\Delta) + H_2O \rightarrow$ products	–	–	4.8×10^{-18}	1.5	–	A57
$O_2(^1\Delta) + N \rightarrow NO + O$	–	–	$<9\times10^{-17}$	–	–	A58
$O_2(^1\Delta) + N_2 \rightarrow$ products	–	–	$<10^{-20}$	–	–	A59
$O_2(^1\Delta) + CO_2 \rightarrow$ products	–	–	$<2\times10^{-20}$	–	–	A60
$O_2(^1\Sigma) + O \rightarrow$ products	–	–	8×10^{-14}	5.0	–	A61
$O_2(^1\Sigma) + O_2 \rightarrow$ products	–	–	3.9×10^{-17}	1.5	–	A62

Reaction	A-Factor[a]	E/R	k(298 K)[a]	f(298 K)[b]	g	Notes
$O_2(^1\Sigma) + O_3 \rightarrow$ products	2.2×10^{-11}	0	2.2×10^{-11}	1.2	200	A63
$O_2(^1\Sigma) + H_2O \rightarrow$ products	–	–	5.4×10^{-12}	1.3	–	A64
$O_2(^1\Sigma) + N \rightarrow$ products	–	–	$<10^{-13}$	–	–	A65
$O_2(^1\Sigma) + N_2 \rightarrow$ products	2.1×10^{-15}	0	2.1×10^{-15}	1.2	200	A66
$O_2(^1\Sigma) + CO_2 \rightarrow$ products	4.2×10^{-13}	0	4.2×10^{-13}	1.2	200	A67
HO_x Reactions						
$O + OH \rightarrow O_2 + H$	2.2×10^{-11}	–120	3.3×10^{-11}	1.2	100	B 1
$O + HO_2 \rightarrow OH + O_2$	3.0×10^{-11}	–200	5.9×10^{-11}	1.1	50	B 2
$O + H_2O_2 \rightarrow OH + HO_2$	1.4×10^{-12}	2000	1.7×10^{-15}	2.0	1000	B 3
$H + O_2 \xrightarrow{M} HO_2$	(See Table 2-1)					
$H + O_3 \rightarrow OH + O_2$	1.4×10^{-10}	470	2.9×10^{-11}	1.25	200	B 4
$H + HO_2 \rightarrow$ products	8.1×10^{-11}	0	8.1×10^{-11}	1.3	100	B 5
$OH + O_3 \rightarrow HO_2 + O_2$	1.7×10^{-12}	940	7.3×10^{-14}	1.2	80	B 6
$OH + H_2 \rightarrow H_2O + H$	5.5×10^{-12}	2000	6.7×10^{-15}	1.1	100	B 7
$OH + HD \rightarrow$ products	5.0×10^{-12}	2130	4.0×10^{-15}	1.2	200	B 8
$OH + OH \rightarrow H_2O + O$	4.2×10^{-12}	240	1.9×10^{-12}	1.4	240	B 9
$\xrightarrow{M} H_2O_2$	(See Table 2-1)					
$OH + HO_2 \rightarrow H_2O + O_2$	4.8×10^{-11}	–250	1.1×10^{-10}	1.3	100	B10
$OH + H_2O_2 \rightarrow H_2O + HO_2$	2.9×10^{-12}	160	1.7×10^{-12}	1.15	50	B11
$HO_2 + O_3 \rightarrow OH + 2O_2$	1.0×10^{-14}	490	1.9×10^{-15}	1.15	+160 –80	B12
$HO_2 + HO_2 \rightarrow H_2O_2 + O_2$	2.3×10^{-13}	–600	1.7×10^{-12}	1.3	200	B13
$\xrightarrow{M} H_2O_2 + O_2$	1.7×10^{-33}[M]	–1000	4.9×10^{-32}[M]	1.3	400	B13
NO_x Reactions						
$O + NO \xrightarrow{M} NO_2$	(See Table 2-1)					
$O + NO_2 \rightarrow NO + O_2$	5.6×10^{-12}	–180	1.0×10^{-11}	1.1	50	C1

Reaction	A-Factor[a]	E/R	k(298 K)[a]	f(298 K)[b]	g	Notes
$O + NO_2 \xrightarrow{M} NO_3$	(See Table 2-1)					
$O + NO_3 \rightarrow O_2 + NO_2$	1.0×10^{-11}	0	1.0×10^{-11}	1.5	150	C 2
$O + N_2O_5 \rightarrow$ products			$<3.0\times10^{-16}$			C 3
$O + HNO_3 \rightarrow OH + NO_3$			$<3.0\times10^{-17}$			C 4
$O + HO_2NO_2 \rightarrow$ products	7.8×10^{-11}	3400	8.6×10^{-16}	3.0	750	C 5
$H + NO_2 \rightarrow OH + NO$	4.0×10^{-10}	340	1.3×10^{-10}	1.3	300	C 6
$OH + NO \xrightarrow{M} HONO$	(See Table 2-1)					
$OH + NO_2 \xrightarrow{M} HNO_3$	(See Table 2-1)					
$OH + NO_3 \rightarrow$ products			2.2×10^{-11}	1.5		C 7
$OH + HONO \rightarrow H_2O + NO_2$	1.8×10^{-11}	390	4.5×10^{-12}	1.5	+200 –500	C 8
$OH + HNO_3 \rightarrow H_2O + NO_3$	(See Note)			1.2		C 9
$OH + HO_2NO_2 \rightarrow$ products	1.3×10^{-12}	–380	4.6×10^{-12}	1.3	+270 –500	C10
$OH + NH_3 \rightarrow H_2O + NH_2$	1.7×10^{-12}	710	1.6×10^{-13}	1.2	200	C11
$HO_2 + NO \rightarrow NO_2 + OH$	3.5×10^{-12}	–250	8.1×10^{-12}	1.15	50	C12
$HO_2 + NO_2 \xrightarrow{M} HO_2NO_2$	(See Table 2-1)					
$HO_2 + NO_2 \rightarrow HONO + O_2$	(See Note)					C13
$HO_2 + NO_3 \rightarrow$ products			3.5×10^{-12}	1.5		C14
$HO_2 + NH_2 \rightarrow$ products			3.4×10^{-11}	2.0		C15
$N + O_2 \rightarrow NO + O$	1.5×10^{-11}	3600	8.5×10^{-17}	1.25	400	C16
$N + O_3 \rightarrow NO + O_2$			$<2.0\times10^{-16}$			C17
$N + NO \rightarrow N_2 + O$	2.1×10^{-11}	–100	3.0×10^{-11}	1.3	100	C18
$N + NO_2 \rightarrow N_2O + O$	5.8×10^{-12}	–220	1.2×10^{-11}	1.5	100	C19
$NO + O_3 \rightarrow NO_2 + O_2$	3.0×10^{-12}	1500	1.9×10^{-14}	1.1	200	C20
$NO + NO_3 \rightarrow 2NO_2$	1.5×10^{-11}	–170	2.6×10^{-11}	1.3	100	C21
$NO_2 + O_3 \rightarrow NO_3 + O_2$	1.2×10^{-13}	2450	3.2×10^{-17}	1.15	150	C22

Reaction	A-Factor[a]	E/R	k(298 K)[a]	f(298 K)[b]	g	Notes
$NO_2 + NO_3 \rightarrow NO + NO_2 + O_2$ $NO_2 + NO_3 \xrightarrow{M} N_2O_5$	(See Note) (See Table 2-1)					C23
$NO_3 + NO_3 \rightarrow 2NO_2 + O_2$	8.5×10^{-13}	2450	2.3×10^{-16}	1.5	500	C24
$NH_2 + O_2 \rightarrow$ products			$<6.0\times10^{-21}$			C25
$NH_2 + O_3 \rightarrow$ products	4.3×10^{-12}	930	1.9×10^{-13}	3.0	500	C26
$NH_2 + NO \rightarrow$ products	4.0×10^{-12}	–450	1.8×10^{-11}	1.3	150	C27
$NH_2 + NO_2 \rightarrow$ products	2.1×10^{-12}	–650	1.9×10^{-11}	3.0	250	C28
$NH + NO \rightarrow$ products	4.9×10^{-11}	0	4.9×10^{-11}	1.5	300	C29
$NH + NO_2 \rightarrow$ products	3.5×10^{-13}	–1140	1.6×10^{-11}	2.0	500	C30
$O_3 + HNO_2 \rightarrow O_2 + HNO_3$			$<5.0\times10^{-19}$			C31
$N_2O_5 + H_2O \rightarrow 2HNO_3$			$<2.0\times10^{-21}$			C32
$N_2(A,v) + O_2 \rightarrow$ products			2.5×10^{-12}, v=0	1.5		C33
$N_2(A,v) + O_3 \rightarrow$ products			4.1×10^{-11}, v=0	2.0		C34
Reactions of Organic Compounds						
$O + CH_3 \rightarrow$ products	1.1×10^{-10}	0	1.1×10^{-10}	1.3	250	D 1
$O + HCN \rightarrow$ products	1.0×10^{-11}	4000	1.5×10^{-17}	10	1000	D 2
$O + C_2H_2 \rightarrow$ products	3.0×10^{-11}	1600	1.4×10^{-13}	1.3	250	D 3
$O + H_2CO \rightarrow$ products	3.4×10^{-11}	1600	1.6×10^{-13}	1.25	250	D 4
$O + CH_3CHO \rightarrow CH_3CO + OH$	1.8×10^{-11}	1100	4.5×10^{-13}	1.25	200	D 5
$O_3 + C_2H_2 \rightarrow$ products	1.0×10^{-14}	4100	1.0×10^{-20}	3	500	D 6
$O_3 + C_2H_4 \rightarrow$ products	1.2×10^{-14}	2630	1.7×10^{-18}	1.25	100	D 7
$O_3 + C_3H_6 \rightarrow$ products	6.5×10^{-15}	1900	1.1×10^{-17}	1.2	200	D 8
$OH + CO \rightarrow$ Products	$1.5\times10^{-13}\times(1+0.6P_{atm})$	0	$1.5\times10^{-13}\times(1+0.6P_{atm})$	1.3	300	D 9
$OH + CH_4 \rightarrow CH_3 + H_2O$	2.45×10^{-12}	1775	6.3×10^{-15}	1.1	100	D10
$OH + {}^{13}CH_4 \rightarrow {}^{13}CH_3 + H_2O$	(See Note)					D11

Reaction	A-Factor[a]	E/R	k(298 K)[a]	f(298 K)[b]	g	Notes
$OH + CH_3D \rightarrow$ products	3.5×10^{-12}	1950	5.0×10^{-15}	1.15	200	D12
$OH + H_2CO \rightarrow H_2O + HCO$	9.0×10^{-12}	0	9.0×10^{-12}	1.2	100	D13
$OH + CH_3OH \rightarrow$ products	7.3×10^{-12}	620	9.1×10^{-13}	1.15	250	D14
$OH + CH_3OOH \rightarrow$ products	3.8×10^{-12}	–200	7.4×10^{-12}	1.4	150	D15
$OH + HC(O)OH \rightarrow$ products	4.0×10^{-13}	0	4.0×10^{-13}	1.2	100	D16
$OH + HCN \rightarrow$ products	1.2×10^{-13}	400	3.1×10^{-14}	3	150	D17
$OH + C_2H_2 \xrightarrow{M}$ products	(See Table 2-1)					
$OH + C_2H_4 \xrightarrow{M}$ products	(See Table 2-1)					
$OH + C_2H_6 \rightarrow H_2O + C_2H_5$	8.7×10^{-12}	1070	2.4×10^{-13}	1.1	100	D18
$OH + C_3H_8 \rightarrow H_2O + C_3H_7$	1.0×10^{-11}	660	1.1×10^{-12}	1.2	100	D19
$OH + CH_3CHO \rightarrow CH_3CO + H_2O$	5.6×10^{-12}	–270	1.4×10^{-11}	1.2	200	D20
$OH + C_2H_5OH \rightarrow$ products	6.9×10^{-12}	230	3.2×10^{-12}	1.2	100	D21
$OH + CH_3C(O)OH \rightarrow$ products	4.0×10^{-13}	–200	8.0×10^{-13}	1.25	200	D22
$OH + CH_3C(O)CH_3 \rightarrow$ products	(See Note)					D23
$OH + CH_3CN \rightarrow$ products	7.8×10^{-13}	1050	2.3×10^{-14}	1.5	200	D24
$OH+ CH_3ONO_2 \rightarrow$ products	5.0×10^{-13}	810	3.3×10^{-14}	1.5	250	D25
$OH + CH_3C(O)O_2NO_2$ (PAN) $\rightarrow$ products			$<4 \times 10^{-14}$			D26
$OH+ C_2H_5ONO_2 \rightarrow$ products	6.8×10^{-13}	320	2.3×10^{-13}	1.5	200	D27
$OH + 1\text{–}C_3H_7ONO_2 \rightarrow$ products	7.1×10^{-13}	0	7.1×10^{-13}	1.5	200	D28
$OH + 2\text{–}C_3H_7ONO_2 \rightarrow$ products	1.2×10^{-12}	320	4.1×10^{-13}	1.5	200	D29
$HO_2 + CH_2O \rightarrow$ adduct	6.7×10^{-15}	–600	5.0×10^{-14}	5	600	D30
$HO_2 + CH_3O_2 \rightarrow CH_3OOH + O_2$	4.1×10^{-13}	–750	5.2×10^{-12}	1.3	150	D31
$HO_2 + C_2H_5O_2 \rightarrow C_2H_5OOH + O_2$	7.5×10^{-13}	–700	8.0×10^{-12}	1.5	250	D32
$HO_2 + CH_3C(O)O_2 \rightarrow$ products	4.3×10^{-13}	–1040	1.4×10^{-11}	2	500	D33
$HO_2 + CH_3C(O)CH_2O_2 \rightarrow$ products	8.6×10^{-13}	–700	9.0×10^{-12}	2	300	D34

Reaction	A-Factor[a]	E/R	k(298 K)[a]	f(298 K)[b]	g	Notes
$NO_3 + CO \rightarrow$ products			$<4.0\times10^{-19}$			D35
$NO_3 + CH_2O \rightarrow$ products			5.8×10^{-16}	1.3		D36
$NO_3 + CH_3CHO \rightarrow$ products	1.4×10^{-12}	1900	2.4×10^{-15}	1.3	300	D37
$CH_3 + O_2 \rightarrow$ products			$<3.0\times10^{-16}$			D38
$CH_3 + O_2 \xrightarrow{M} CH_3O_2$	(See Table 2-1)					
$CH_3 + O_3 \rightarrow$ products	5.4×10^{-12}	220	2.6×10^{-12}	2	150	D39
$HCO + O_2 \rightarrow CO + HO_2$	5.2×10^{-12}	0	5.2×10^{-12}	1.4	100	D40
$CH_2OH + O_2 \rightarrow CH_2O + HO_2$	9.1×10^{-12}	0	9.1×10^{-12}	1.3	200	D41
$CH_3O + O_2 \rightarrow CH_2O + HO_2$	3.9×10^{-14}	900	1.9×10^{-15}	1.5	300	D42
$CH_3O + NO \rightarrow CH_2O + HNO$ $CH_3O + NO \xrightarrow{M} CH_3ONO$	(See Note) (See Table 2-1)					D43
$CH_3O + NO_2 \rightarrow CH_2O + HONO$ $CH_3O + NO_2 \xrightarrow{M} CH_3ONO_2$	1.1×10^{-11} (See Table 2-1)	1200	2.0×10^{-13}	5	600	D44
$CH_3O_2 + O_3 \rightarrow$ products	2.9×10^{-16}	1000	1.0×10^{-17}	3	500	D45
$CH_3O_2 + CH_3O_2 \rightarrow$ products	9.5×10^{-14}	–390	3.5×10^{-13}	1.2	100	D46
$CH_3O_2 + NO \rightarrow CH_3O + NO_2$	2.8×10^{-12}	–300	7.7×10^{-12}	1.15	100	D47
$CH_3O_2 + NO_2 \xrightarrow{M} CH_3O_2NO_2$	(See Table 2-1)					
$CH_3O_2 + CH_3C(O)O_2 \rightarrow$ products	2.0×10^{-12}	–500	1.1×10^{-11}	1.5	250	D48
$CH_3O_2 + CH_3C(O)CH_2O_2 \rightarrow$ products	7.5×10^{-13}	–500	4.0×10^{-12}	2	300	D49
$C_2H_5 + O_2 \rightarrow C_2H_4 + HO_2$ $C_2H_5 + O_2 \xrightarrow{M} C_2H_5O_2$	 (See Table 2-1)		$<2.0\times10^{-14}$			D50
$C_2H_5O + O_2 \rightarrow CH_3CHO + HO_2$	6.3×10^{-14}	550	1.0×10^{-14}	1.5	200	D51
$C_2H_5O + NO \xrightarrow{M}$ products	(See Table 2-1)					
$C_2H_5O + NO_2 \xrightarrow{M}$ products	(See Table 2-1)					
$C_2H_5O_2 + C_2H_5O_2 \rightarrow$ products	6.8×10^{-14}	0	6.8×10^{-14}	2	300	D52

Reaction	A-Factor[a]	E/R	k(298 K)[a]	f(298 K)[b]	g	Notes
$C_2H_5O_2 + NO \rightarrow$ products	2.6×10^{-12}	–365	8.7×10^{-12}	1.2	150	D53
$CH_3C(O)O_2 + CH_3C(O)O_2 \rightarrow$ products	2.9×10^{-12}	–500	1.5×10^{-11}	1.5	150	D54
$CH_3C(O)O_2 + NO \rightarrow$ products	8.1×10^{-12}	–270	2.0×10^{-11}	1.5	100	D55
$CH_3C(O)O_2 + NO_2 \xrightarrow{M}$ products	(See Table 2-1)					
$CH_3C(O)CH_2O_2 + NO \rightarrow$ products	2.9×10^{-12}	–300	8.0×10^{-12}	1.5	300	D56
FO_x Reactions						
$O + FO \rightarrow F + O_2$	2.7×10^{-11}	0	2.7×10^{-11}	3.0	250	E 1
$O + FO_2 \rightarrow FO + O_2$	5.0×10^{-11}	0	5.0×10^{-11}	5.0	250	E 2
$OH + CH_3F \rightarrow CH_2F + H_2O$ (HFC–41)	2.5×10^{-12}	1430	2.1×10^{-14}	1.15	150	E 3
$OH + CH_2F_2 \rightarrow CHF_2 + H_2O$ (HFC-32)	1.7×10^{-12}	1500	1.1×10^{-14}	1.15	150	E 4
$OH + CHF_3 \rightarrow CF_3 + H_2O$ (HFC-23)	6.3×10^{-13}	2300	2.8×10^{-16}	1.2	200	E 5
$OH + CH_3CH_2F \rightarrow$ products (HFC-161)	2.5×10^{-12}	730	2.2×10^{-13}	1.15	150	E 6
$OH + CH_3CHF_2 \rightarrow$ products (HFC-152a)	9.4×10^{-13}	990	3.4×10^{-14}	1.1	100	E 7
$OH + CH_2FCH_2F \rightarrow CHFCH_2F + H_2O$ (HFC-152)	1.1×10^{-12}	730	9.7×10^{-14}	1.1	150	E 8
$OH + CH_3CF_3 \rightarrow CH_2CF_3 + H_2O$ (HFC-143a)	1.1×10^{-12}	2010	1.3×10^{-15}	1.1	100	E 9
$OH + CH_2FCHF_2 \rightarrow$ products (HFC-143)	3.9×10^{-12}	1620	1.7×10^{-14}	1.2	200	E10
$OH + CH_2FCF_3 \rightarrow CHFCF_3 + H_2O$ (HFC-134a)	1.05×10^{-12}	1630	4.4×10^{-15}	1.1	200	E11
$OH + CHF_2CHF_2 \rightarrow CF_2CHF_2 + H_2O$ (HFC-134)	1.6×10^{-12}	1660	6.1×10^{-15}	1.2	200	E12
$OH + CHF_2CF_3 \rightarrow CF_2CF_3 + H_2O$ (HFC-125)	6.0×10^{-13}	1700	2.0×10^{-15}	1.2	150	E13
$OH + CH_3CHFCH_3 \rightarrow$ products (HFC-281ea)	3.0×10^{-12}	490	5.8×10^{-13}	1.2	100	E14
$OH + CF_3CH_2CH_3 \rightarrow$ products (HFC-263fb)	–	–	4.2×10^{-14}	1.5	–	E15
$OH + CH_2FCF_2CHF_2 \rightarrow$ products (HFC-245ca)	2.1×10^{-12}	1620	9.2×10^{-15}	1.2	150	E16
$OH + CHF_2CHFCHF_2 \rightarrow$ products (HFC-245ea)	–	–	1.6×10^{-14}	2.0	–	E17
$OH + CF_3CHFCH_2F \rightarrow$ products (HFC-245eb)	–	–	1.5×10^{-14}	2.0	–	E18
$OH + CHF_2CH_2CF_3 \rightarrow$ products (HFC-245fa)	6.1×10^{-13}	1330	7.0×10^{-15}	1.2	150	E19

Reaction	A-Factor[a]	E/R	k(298 K)[a]	f(298 K)[b]	g	Notes
OH + $CF_3CF_2CH_2F \rightarrow CF_3CF_2CHF + H_2O$ (HFC-236cb)	*1.3×10^{-12}*	*1700*	*4.4×10^{-15}*	2.0	*200*	E20
OH + $CF_3CHFCHF_2 \rightarrow$ products (HFC-236ea)	9.4×10^{-13}	1550	5.2×10^{-15}	1.2	200	E21
OH + $CF_3CH_2CF_3 \rightarrow CF_3CHCF_3 + H_2O$ (HFC–236fa)	1.45×10^{-12}	2500	3.3×10^{-16}	1.15	150	E22
OH + $CF_3CHFCF_3 \rightarrow CF_3CFCF_3+H_2O$ (HFC-227ea)	4.3×10^{-13}	1650	1.7×10^{-15}	1.1	150	E23
OH + $CF_3CH_2CF_2CH_3 \rightarrow$ products (HFC-365mfc)	1.8×10^{-12}	1660	6.9×10^{-15}	1.3	150	E24
OH + $CF_3CH_2CH_2CF_3 \rightarrow$ products (HFC-356mff)	3.4×10^{-12}	1820	7.6×10^{-15}	1.2	300	E25
OH + $CF_3CF_2CH_2CH_2F \rightarrow$ products (HFC-356mcf)	1.7×10^{-12}	1100	4.2×10^{-14}	1.3	150	E26
OH + $CHF_2CF_2CF_2CF_2H \rightarrow$ products (HFC-338pcc)	7.7×10^{-13}	1540	4.4×10^{-15}	1.2	150	E27
OH + $CF_3CH_2CF_2CH_2CF_3 \rightarrow$ products (HFC-458mfcf)	1.1×10^{-12}	1800	2.6×10^{-15}	1.5	200	E28
OH + $CF_3CHFCHFCF_2CF_3 \rightarrow$ products (HFC-43-10mee)	5.2×10^{-13}	1500	3.4×10^{-15}	1.2	150	E29
OH + $CF_3CF_2CH_2CH_2CF_2CF_3 \rightarrow$ products (HFC–55-10-mcff)	*3.5×10^{-12}*	*1800*	8.3×10^{-15}	1.5	*300*	E30
OH + $CH_2{=}CHF \rightarrow$ products	1.5×10^{-12}	–390	5.5×10^{-12}	1.3	150	E31
OH + $CH_2{=}CF_2 \rightarrow$ products	*6.2×10^{-13}*	*–350*	2.0×10^{-12}	1.5	*150*	E32
OH + $CF_2{=}CF_2 \rightarrow$ products	3.4×10^{-12}	–320	1.0×10^{-11}	1.15	100	E33
OH + $CF_3OH \rightarrow CF_3O + H_2O$			$<2\times10^{-17}$			E34
OH + $CH_2(OH)CF_3 \rightarrow$ products	1.6×10^{-12}	830	9.8×10^{-14}	1.15	200	E35
OH + $CH_2(OH)CF_2CF_3 \rightarrow$ products	1.15×10^{-12}	730	1.0×10^{-13}	1.2	200	E36
OH + $CF_3CH(OH)CF_3 \rightarrow$ products	5.1×10^{-13}	900	2.5×10^{-14}	1.3	200	E37
OH + $CH_3OCHF_2 \rightarrow$ products (HFOC-152a)	6.0×10^{-12}	1530	3.5×10^{-14}	1.3	200	E38
OH + $CF_3OCH_3 \rightarrow CF_3OCH_2 + H_2O$ (HFOC-143a)	1.5×10^{-12}	1450	1.2×10^{-14}	1.1	150	E39
OH + $CF_2HOCF_2H \rightarrow CF_2OCF_2H + H_2O$ (HFOC-134)	1.1×10^{-12}	1830	2.4×10^{-15}	1.15	150	E40
OH + $CF_3OCHF_2 \rightarrow CF_3OCF_2 + H_2O$ (HFOC-125)	4.6×10^{-13}	2040	4.9×10^{-16}	1.2	200	E41
OH + $CHF_2OCH_2CF_3 \rightarrow$ products (HFOC-245fa)	3.1×10^{-12}	1660	1.2×10^{-14}	1.2	200	E42
OH + $CH_3OCF_2CHF_2 \rightarrow$ products	1.7×10^{-12}	1300	2.2×10^{-14}	1.3	200	E43
OH + $CH_3OCF_2CF_3 \rightarrow$ products	1.1×10^{-12}	1370	1.1×10^{-14}	1.2	150	E44

Reaction	A-Factor[a]	E/R	k(298 K)[a]	f(298 K)[b]	g	Notes
$OH + CH_3OCF_2CF_2CF_3 \rightarrow$ products	1.4×10^{-12}	1440	1.1×10^{-14}	1.15	150	E45
$OH + CH_3OCF(CF_3)_2 \rightarrow$ products	1.3×10^{-12}	1330	1.5×10^{-14}	1.3	200	E46
$OH + CHF_2OCH_2CF_2CHF_2 \rightarrow$ products	1.8×10^{-12}	1410	1.6×10^{-14}	1.3	200	E47
$OH + CHF_2OCH_2CF_2CF_3 \rightarrow$ products	1.6×10^{-12}	1510	1.0×10^{-14}	1.3	200	E48
$F + O_2 \xrightarrow{M} FO_2$	(See Table 2-1)					
$F + O_3 \rightarrow FO + O_2$	2.2×10^{-11}	230	1.0×10^{-11}	1.5	200	E49
$F + H_2 \rightarrow HF + H$	1.4×10^{-10}	500	2.6×10^{-11}	1.2	200	E50
$F + H_2O \rightarrow HF + OH$	1.4×10^{-11}	0	1.4×10^{-11}	1.3	200	E51
$F + NO \xrightarrow{M} FNO$	(See Table 2-1)					
$F + NO_2 \xrightarrow{M} FNO_2$	(See Table 2-1)					
$F + HNO_3 \rightarrow HF + NO_3$	6.0×10^{-12}	–400	2.3×10^{-11}	1.3	200	E52
$F + CH_4 \rightarrow HF + CH_3$	1.6×10^{-10}	260	6.7×10^{-11}	1.4	200	E53
$FO + O_3 \rightarrow$ products			$<1 \times 10^{-14}$			E54
$FO + NO \rightarrow NO_2 + F$	8.2×10^{-12}	–300	2.2×10^{-11}	1.5	200	E55
$FO + NO_2 \xrightarrow{M} FONO_2$	(See Table 2-1)					
$FO + FO \rightarrow 2F + O_2$	1.0×10^{-11}	0	1.0×10^{-11}	1.5	250	E56
$FO_2 + O_3 \rightarrow$ products			$<3.4\times10^{-16}$			E57
$FO_2 + NO \rightarrow FNO + O_2$	7.5×10^{-12}	690	7.5×10^{-13}	2.0	400	E58
$FO_2 + NO_2 \rightarrow$ products	3.8×10^{-11}	2040	4.0×10^{-14}	2.0	500	E59
$FO_2 + CO \rightarrow$ products			$<5.1\times10^{-16}$			E60
$FO_2 + CH_4 \rightarrow$ products			$<2\times10^{-16}$			E61
$CF_3 + O_2 \xrightarrow{M} CF_3O_2$	(See Table 2-1)					
$CF_3O + M \rightarrow F + CF_2O + M$	(See Table 2-1)					
$CF_3O + O_2 \rightarrow FO_2 + CF_2O$	$<3 \times 10^{-11}$	5000	$<1.5 \times 10^{-18}$	1.3	–	E62
$CF_3O + O_3 \rightarrow CF_3O_2 + O_2$	2×10^{-12}	1400	1.8×10^{-14}		600	E63

Reaction	A-Factor[a]	E/R	k(298 K)[a]	f(298 K)[b]	g	Notes
$CF_3O + H_2O \rightarrow OH + CF_3OH$	3×10^{-12}	>3600	$<2 \times 10^{-17}$	1.2	–	E64
$CF_3O + NO \rightarrow CF_2O + FNO$	3.7×10^{-11}	–110	5.4×10^{-11}		70	E65
$CF_3O + NO_2 \rightarrow$ products $\xrightarrow{M} CF_3ONO_2$	(See Note) (See Table 2-1)					E66
$CF_3O + CO \rightarrow$ products $\xrightarrow{M} CF_3OCO$	(See Table 2-1)		$<2 \times 10^{-15}$			E67
$CF_3O + CH_4 \rightarrow CH_3 + CF_3OH$	2.6×10^{-12}	1420	2.2×10^{-14}	1.1	200	E68
$CF_3O + C_2H_6 \rightarrow C_2H_5 + CF_3OH$	4.9×10^{-12}	400	1.3×10^{-12}	1.2	100	E69
$CF_3O_2 + O_3 \rightarrow CF_3O + 2O_2$			$<3 \times 10^{-15}$			E70
$CF_3O_2 + CO \rightarrow CF_3O + CO_2$			$<5 \times 10^{-16}$			E71
$CF_3O_2 + NO \rightarrow CF_3O + NO_2$	5.4×10^{-12}	–320	1.6×10^{-11}	1.1	150	E72
$CF_3O_2 + NO_2 \xrightarrow{M} CF_3O_2NO_2$	(See Table 2-1)					
ClO_x Reactions						
$O + ClO \rightarrow Cl + O_2$	3.0×10^{-11}	–70	3.8×10^{-11}	1.15	70	F 1
$O + OClO \rightarrow ClO + O_2$	2.4×10^{-12}	960	1.0×10^{-13}	2.0	300	F 2
$O + OClO \xrightarrow{M} ClO_3$	(See Table 2-1)					
$O + Cl_2O \rightarrow ClO + ClO$	2.7×10^{-11}	530	4.5×10^{-12}	1.3	150	F 3
$O + HCl \rightarrow OH + Cl$	1.0×10^{-11}	3300	1.5×10^{-16}	2.0	350	F 4
$O + HOCl \rightarrow OH + ClO$	1.7×10^{-13}	0	1.7×10^{-13}	3.0	300	F 5
$O + ClONO_2 \rightarrow$ products	2.9×10^{-12}	800	2.0×10^{-13}	1.5	200	F 6
$O_3 + OClO \rightarrow$ products	2.1×10^{-12}	4700	3.0×10^{-19}	2.5	1000	F 7
$O_3 + Cl_2O_2 \rightarrow$ products	–	–	$<1.0\times10^{-19}$	–	–	F 8
$OH + Cl_2 \rightarrow HOCl + Cl$	1.4×10^{-12}	900	6.7×10^{-14}	1.2	400	F 9
$OH + ClO \rightarrow Cl + HO_2$ $\rightarrow HCl + O_2$	7.4×10^{-12} 6.0×10^{-13}	–270 –230	1.8×10^{-11} 1.3×10^{-12}	1.4 3.0	100 150	F10
$OH + OClO \rightarrow HOCl + O_2$	4.5×10^{-13}	–800	6.8×10^{-12}	2.0	200	F11

Reaction	A-Factor[a]	E/R	k(298 K)[a]	f(298 K)[b]	g	Notes
$OH + HCl \rightarrow H_2O + Cl$	2.6×10^{-12}	350	8.0×10^{-13}	1.1	100	F12
$OH + HOCl \rightarrow H_2O + ClO$	3.0×10^{-12}	500	5.0×10^{-13}	3.0	500	F13
$OH + ClNO_2 \rightarrow HOCl + NO_2$	2.4×10^{-12}	1250	3.6×10^{-14}	2.0	300	F14
$OH + ClONO_2 \rightarrow$ products	1.2×10^{-12}	330	3.9×10^{-13}	1.5	200	F15
$OH + CH_3Cl \rightarrow CH_2Cl + H_2O$	2.4×10^{-12}	1250	3.6×10^{-14}	1.15	100	F16
$OH + CH_2Cl_2 \rightarrow CHCl_2 + H_2O$	1.9×10^{-12}	870	1.0×10^{-13}	1.15	100	F17
$OH + CHCl_3 \rightarrow CCl_3 + H_2O$	2.2×10^{-12}	920	1.0×10^{-13}	1.15	150	F18
$OH + CCl_4 \rightarrow$ products	*~1.0×10⁻¹²*	*>2300*	$<5.0\times10^{-16}$	–	–	F19
$OH + CH_2FCl \rightarrow CHClF + H_2O$ (HCFC-31)	2.4×10^{-12}	1210	4.1×10^{-14}	1.15	200	F20
$OH + CHFCl_2 \rightarrow CFCl_2 + H_2O$ (HCFC-21)	1.2×10^{-12}	1100	3.0×10^{-14}	1.2	150	F21
$OH + CHF_2Cl \rightarrow CF_2Cl + H_2O$ (HCFC-22)	1.05×10^{-12}	1600	4.8×10^{-15}	1.1	150	F22
$OH + CFCl_3 \rightarrow$ products (CFC-11)	*~1.0×10⁻¹²*	*>3700*	$<5.0\times10^{-18}$	–	–	F23
$OH + CF_2Cl_2 \rightarrow$ products (CFC-12)	*~1.0×10⁻¹²*	*>3600*	$<6.0\times10^{-18}$	–	–	F24
$OH + CH_2ClCH_3 \rightarrow$ products	5.4×10^{-12}	800	3.7×10^{-13}	1.2	100	F25
$OH + CH_3CCl_3 \rightarrow CH_2CCl_3 + H_2O$	1.6×10^{-12}	1520	1.0×10^{-14}	1.15	100	F26
$OH + CH_3CFCl_2 \rightarrow CH_2CFCl_2 + H_2O$ (HCFC-141b)	1.25×10^{-12}	1600	5.8×10^{-15}	1.15	150	F27
$OH + CH_3CF_2Cl \rightarrow CH_2CF_2Cl + H_2O$ (HCFC-142b)	1.3×10^{-12}	1770	3.4×10^{-15}	1.2	150	F28
$OH + CH_2ClCF_2Cl \rightarrow CHClCF_2Cl + H_2O$ (HCFC-132b)	3.6×10^{-12}	1600	1.7×10^{-14}	1.5	200	F29
$OH + CH_2ClCF_3 \rightarrow CHClCF_3 + H_2O$ (HCFC-133a)	5.6×10^{-13}	1100	1.4×10^{-14}	1.3	200	F30
$OH + CHCl_2CF_2Cl \rightarrow CCl_2CF_2Cl$ (HCFC-122) $+ H_2O$	7.7×10^{-13}	810	5.1×10^{-14}	1.2	150	F31
$OH + CHFClCFCl_2 \rightarrow CFClCFCl_2$ (HCFC-122a) $+ H_2O$	7.1×10^{-13}	1140	1.6×10^{-14}	1.3	150	F32
$OH + CHCl_2CF_3 \rightarrow CCl_2CF_3 + H_2O$ (HCFC-123)	6.3×10^{-13}	850	3.6×10^{-14}	1.2	100	F33
$OH + CHFClCF_2Cl \rightarrow CFClCF_2Cl + H_2O$ (HCFC-123a)	8.6×10^{-13}	1250	1.3×10^{-14}	1.3	200	F34
$OH + CHFClCF_3 \rightarrow CFClCF_3 + H_2O$ (HCFC-124)	7.1×10^{-13}	1300	9.0×10^{-15}	1.15	100	F35
$OH + CH_3CF_2CFCl_2 \rightarrow$ products (HCFC-243cc)	7.7×10^{-13}	1720	2.4×10^{-15}	1.3	200	F36

Reaction	A-Factor[a]	E/R	k(298 K)[a]	f(298 K)[b]	g	Notes
$OH + CHCl_2CF_2CF_3 \rightarrow$ products (HCFC-225ca)	6.3×10^{-13}	960	2.5×10^{-14}	1.2	200	F37
$OH + CHFClCF_2CF_2Cl \rightarrow$ products (HCFC-225cb)	5.5×10^{-13}	1230	8.9×10^{-15}	1.2	150	F38
$OH + CH_2{=}CHCl \rightarrow$ products	1.3×10^{-12}	–500	6.9×10^{-12}	1.2	100	F39
$OH + CH_2{=}CCl_2 \rightarrow$ products	1.9×10^{-12}	–530	1.1×10^{-11}	1.15	150	F40
$OH + CHCl{=}CCl_2 \rightarrow$ products	8.0×10^{-13}	–300	2.2×10^{-12}	1.2	100	F41
$OH + CCl_2{=}CCl_2 \rightarrow$ products	4.7×10^{-12}	990	1.7×10^{-13}	1.2	200	F42
$OH + CH_3OCl \rightarrow$ products	2.5×10^{-12}	370	7.1×10^{-13}	2.0	150	F43
$OH + CCl_3CHO \rightarrow H_2O + CCl_3CO$	9.1×10^{-12}	580	1.3×10^{-12}	1.3	200	F44
$HO_2 + Cl \rightarrow HCl + O_2$	1.8×10^{-11}	–170	3.2×10^{-11}	1.5	200	F45
$\rightarrow OH + ClO$	4.1×10^{-11}	450	9.1×10^{-12}	2.0	200	F45
$HO_2 + ClO \rightarrow HOCl + O_2$	2.7×10^{-12}	–220	5.6×10^{-12}	1.3	200	F46
$H_2O + ClONO_2 \rightarrow$ products	–	–	$<2.0\times10^{-21}$	–	–	F47
$NO + OClO \rightarrow NO_2 + ClO$	2.5×10^{-12}	600	3.4×10^{-13}	2.0	300	F48
$NO + Cl_2O_2 \rightarrow$ products	–	–	$<2.0\times10^{-14}$	–	–	F49
$NO_3 + OClO \xrightarrow{M} O_2ClONO_2$	(See Table 2-1)					
$NO_3 + HCl \rightarrow HNO_3 + Cl$	–	–	$<5.0\times10^{-17}$	–	–	F50
$HO_2NO_2 + HCl \rightarrow$ products	–	–	$<1.0\times10^{-21}$	–	–	F51
$Cl + O_2 \xrightarrow{M} ClOO$	(See Table 2-1)					
$Cl + O_3 \rightarrow ClO + O_2$	2.3×10^{-11}	200	1.2×10^{-11}	1.15	100	F52
$Cl + H_2 \rightarrow HCl + H$	3.7×10^{-11}	2300	1.6×10^{-14}	1.25	200	F53
$Cl + H_2O_2 \rightarrow HCl + HO_2$	1.1×10^{-11}	980	4.1×10^{-13}	1.3	300	F54
$Cl + NO \xrightarrow{M} NOCl$	(See Table 2-1)					
$Cl + NO_2 \xrightarrow{M} ClONO\ (ClNO_2)$	(See Table 2-1)					
$Cl + NO_3 \rightarrow ClO + NO_2$	2.4×10^{-11}	0	2.4×10^{-11}	1.5	400	F55
$Cl + N_2O \rightarrow ClO + N_2$	(See Note)					F56

Reaction	A-Factor[a]	E/R	k(298 K)[a]	f(298 K)[b]	g	Notes
$Cl + HNO_3 \rightarrow$ products	–	–	$<2.0\times10^{-16}$	–	–	F57
$Cl + HO_2NO_2 \rightarrow$ products			$<1\times10^{-13}$			F58
$Cl + CO \xrightarrow{M} ClCO$	(See Table 2-1)					
$Cl + CH_4 \rightarrow HCl + CH_3$	9.6×10^{-12}	1360	1.0×10^{-13}	1.05	75	F59
$Cl + CH_3D \rightarrow$ products	–	–	7.4×10^{-14}	2.0	–	F60
$Cl + H_2CO \rightarrow HCl + HCO$	8.1×10^{-11}	30	7.3×10^{-11}	1.15	100	F61
$Cl + HC(O)OH \rightarrow$ products			2.0×10^{-13}	1.5		F62
$Cl + CH_3O_2 \rightarrow$ products	–	–	1.6×10^{-10}	1.5	–	F63
$Cl + CH_3OH \rightarrow CH_2OH + HCl$	5.5×10^{-11}	0	5.5×10^{-11}	1.2	100	F64
$Cl + CH_3OOH \rightarrow$ products			5.7×10^{-11}	2.0		F65
$Cl + CH_3ONO_2 \rightarrow$ products	*1.3×10^{-11}*	*1200*	2.3×10^{-13}	1.5	*300*	F66
$Cl + C_2H_2 \xrightarrow{M} ClC_2H_2$	(See Table 2-1)					
$Cl + C_2H_4 \xrightarrow{M} ClC_2H_4$	(See Table 2-1)					
$Cl + C_2H_6 \rightarrow HCl + C_2H_5$	7.7×10^{-11}	90	5.7×10^{-11}	1.1	90	F67
$Cl + C_2H_5O_2 \rightarrow ClO + C_2H_5O$	–	–	7.4×10^{-11}	2.0	–	F68
$\rightarrow HCl + C_2H_4O_2$		–	7.7×10^{-11}	2.0	–	F68
$Cl + CH_3CH_2OH \rightarrow$ products	9.6×10^{-11}	0	9.6×10^{-11}	1.2	100	F69
$Cl + CH_3C(O)OH \rightarrow$ products			2.8×10^{-14}	2.0		F70
$Cl + CH_3CN \rightarrow$ products	1.6×10^{-11}	2140	1.2×10^{-14}	2.0	300	F71
$Cl + C_2H_5ONO_2 \rightarrow$ products	*1.5×10^{-11}*	*400*	3.9×10^{-12}	1.5	*200*	F72
$Cl + CH_3CO_3NO_2 \rightarrow$ products	–	–	$<1\times10^{-14}$		–	F73
$Cl + C_3H_8 \rightarrow HCl + C_3H_7$	1.2×10^{-10}	–40	1.4×10^{-10}	1.3	250	F74
$Cl + CH_3C(O)CH_3 \rightarrow CH_3C(O)CH_2 + HCl$	7.7×10^{-11}	1000	2.7×10^{-12}	1.3	500	F75
$Cl + C_2H_5CO_3NO_2 \rightarrow$ products			1.1×10^{-12}	2.0		F76
$Cl + 1\text{-}C_3H_7ONO_2 \rightarrow$ products	*4.5×10^{-11}*	*200*	2.3×10^{-11}	1.5	*200*	F77

Reaction	A-Factor[a]	E/R	k(298 K)[a]	f(298 K)[b]	g	Notes
$Cl + 2\text{-}C_3H_7ONO_2 \rightarrow$ products	*2.3×10^{-11}*	*400*	6.0×10^{-12}	2.0	*200*	F78
$Cl + OClO \rightarrow ClO + ClO$	3.4×10^{-11}	–160	5.8×10^{-11}	1.25	200	F79
$Cl + ClOO \rightarrow Cl_2 + O_2$	2.3×10^{-10}	0	2.3×10^{-10}	3.0	250	F80
$\rightarrow ClO + ClO$	1.2×10^{-11}	0	1.2×10^{-11}	3.0	250	F80
$Cl + Cl_2O \rightarrow Cl_2 + ClO$	6.2×10^{-11}	–130	9.6×10^{-11}	1.2	130	F81
$Cl + Cl_2O_2 \rightarrow$ products	–	–	1.0×10^{-10}	2.0	–	F82
$Cl + HOCl \rightarrow$ products	2.5×10^{-12}	130	1.6×10^{-12}	1.5	250	F83
$Cl + ClNO \rightarrow NO + Cl_2$	5.8×10^{-11}	–100	8.1×10^{-11}	1.5	200	F84
$Cl + ClONO_2 \rightarrow$ products	6.5×10^{-12}	–135	1.0×10^{-11}	1.2	50	F85
$Cl + CH_3Cl \rightarrow CH_2Cl + HCl$	3.2×10^{-11}	1250	4.8×10^{-13}	1.2	200	F86
$Cl + CH_2Cl_2 \rightarrow HCl + CHCl_2$	3.1×10^{-11}	1350	3.3×10^{-13}	1.5	500	F87
$Cl + CHCl_3 \rightarrow HCl + CCl_3$	8.2×10^{-12}	1325	9.6×10^{-14}	1.3	300	F88
$Cl + CH_3F \rightarrow HCl + CH_2F$ (HFC-41)	2.0×10^{-11}	1200	3.5×10^{-13}	1.3	500	F89
$Cl + CH_2F_2 \rightarrow HCl + CHF_2$ (HFC-32)	1.2×10^{-11}	1630	5.0×10^{-14}	1.5	500	F90
$Cl + CF_3H \rightarrow HCl + CF_3$ (HFC-23)	–	–	3.0×10^{-18}	5.0	–	F91
$Cl + CH_2FCl \rightarrow HCl + CHFCl$ (HCFC-31)	1.2×10^{-11}	1390	1.1×10^{-13}	2.0	500	F92
$Cl + CHFCl_2 \rightarrow HCl + CFCl_2$ (HCFC-21)	5.5×10^{-12}	1675	2.0×10^{-14}	1.3	200	F93
$Cl + CHF_2Cl \rightarrow HCl + CF_2Cl$ (HCFC-22)	5.9×10^{-12}	2430	1.7×10^{-15}	1.3	200	F94
$Cl + CH_3CCl_3 \rightarrow CH_2CCl_3 + HCl$	2.8×10^{-12}	1790	7.0×10^{-15}	2.0	400	F95
$Cl + CH_3CH_2F \rightarrow HCl + CH_3CHF$ (HFC-161)	1.8×10^{-11}	290	6.8×10^{-12}	3.0	500	F96
$\rightarrow HCl + CH_2CH_2F$	1.4×10^{-11}	880	7.3×10^{-13}	3.0	500	F96
$Cl + CH_3CHF_2 \rightarrow HCl + CH_3CF_2$ (HFC-152a)	6.4×10^{-12}	950	2.6×10^{-13}	1.3	500	F97
$\rightarrow HCl + CH_2CHF_2$	7.2×10^{-12}	2390	2.4×10^{-15}	3.0	500	F97
$Cl + CH_2FCH_2F \rightarrow HCl + CHFCH_2F$ (HFC-152)	2.6×10^{-11}	1060	7.5×10^{-13}	3.0	500	F98
$Cl + CH_3CFCl_2 \rightarrow HCl + CH_2CFCl_2$ (HCFC-141b)	1.8×10^{-12}	2000	2.2×10^{-15}	1.2	300	F99

Reaction	A-Factor[a]	E/R	k(298 K)[a]	f(298 K)[b]	g	Notes
$Cl + CH_3CF_2Cl \rightarrow HCl + CH_2CF_2Cl$ (HCFC-142b)	1.4×10^{-12}	2420	4.2×10^{-16}	1.2	500	F100
$Cl + CH_3CF_3 \rightarrow HCl + CH_2CF_3$ (HFC-143a)	1.2×10^{-11}	3880	2.6×10^{-17}	5.0	500	F101
$Cl + CH_2FCHF_2 \rightarrow HCl + CH_2FCF_2$ (HFC-143)	5.5×10^{-12}	1610	2.5×10^{-14}	3.0	500	F102
$\rightarrow HCl + CHFCHF_2$	7.7×10^{-12}	1720	2.4×10^{-14}	3.0	500	F102
$Cl + CH_2ClCF_3 \rightarrow HCl + CHClCF_3$ (HCFC-133a)	1.8×10^{-12}	1710	5.9×10^{-15}	3.0	500	F103
$Cl + CH_2FCF_3 \rightarrow HCl + CHFCF_3$ (HFC-134a)	–	–	1.5×10^{-15}	1.2	–	F104
$Cl + CHF_2CHF_2 \rightarrow HCl + CF_2CHF_2$ (HCF-134)	7.5×10^{-12}	2430	2.2×10^{-15}	1.5	500	F105
$Cl + CHCl_2CF_3 \rightarrow HCl + CCl_2CF_3$ (HCFC-123)	4.4×10^{-12}	1750	1.2×10^{-14}	1.3	500	F106
$Cl + CHFClCF_3 \rightarrow HCl + CFClCF_3$ (HCFC-124)	1.1×10^{-12}	1800	2.7×10^{-15}	1.3	500	F107
$Cl + CHF_2CF_3 \rightarrow HCl + CF_2CF_3$ (HFC-125)	–	–	2.4×10^{-16}	1.3	–	F108
$Cl + C_2Cl_4 \xrightarrow{M} C_2Cl_5$	(See Table 2-1)					
$ClO + O_3 \rightarrow ClOO + O_2$	–	–	$<1.4\times10^{-17}$	–	–	F109
$\rightarrow OClO + O_2$	*1.0×10^{-12}*	*>4000*	$<1.0\times10^{-18}$	–	–	F109
$ClO + H_2 \rightarrow$ products	*~1.0×10^{-12}*	*>4800*	$<1.0\times10^{-19}$	–	–	F110
$ClO + NO \rightarrow NO_2 + Cl$	6.4×10^{-12}	–290	1.7×10^{-11}	1.15	100	F111
$ClO + NO_2 \xrightarrow{M} ClONO_2$	(See Table 2-1)					
$ClO + NO_3 \rightarrow ClOO + NO_2$	4.7×10^{-13}	0	4.7×10^{-13}	1.5	400	F112
$ClO + N_2O \rightarrow$ products	~1.0×10^{-12}	>4300	$<6.0\times10^{-19}$	–	–	F113
$ClO + CO \rightarrow$ products	~1.0×10^{-12}	>3700	$<4.0\times10^{-18}$	–	–	F114
$ClO + CH_4 \rightarrow$ products	~1.0×10^{-12}	>3700	$<4.0\times10^{-18}$	–	–	F115
$ClO + H_2CO \rightarrow$ products	~1.0×10^{-12}	>2100	$<1.0\times10^{-15}$	–	–	F116
$ClO + CH_3O_2 \rightarrow$ products	3.3×10^{-12}	115	2.2×10^{-12}	1.5	115	F117
$ClO + ClO \rightarrow Cl_2 + O_2$	1.0×10^{-12}	1590	4.8×10^{-15}	1.5	300	F118
$\rightarrow ClOO + Cl$	3.0×10^{-11}	2450	8.0×10^{-15}	1.5	500	F118
$\rightarrow OClO + Cl$	3.5×10^{-13}	1370	3.5×10^{-15}	1.5	300	F118

Reaction	A-Factor[a]	E/R	k(298 K)[a]	f(298 K)[b]	g	Notes
$ClO + ClO \xrightarrow{M} Cl_2O_2$	(See Table 2-1)					
$ClO + OClO \xrightarrow{M} Cl_2O_3$	(See Table 2-1)					
$HCl + ClONO_2 \rightarrow$ products	–	–	$<1.0\times10^{-20}$	–	–	F119
$CH_2Cl + O_2 \xrightarrow{M} CH_2ClO_2$	(See Table 2-1)					
$CHCl_2 + O_2 \xrightarrow{M} CHCl_2O_2$	(See Table 2-1)					
$CCl_3 + O_2 \xrightarrow{M} CCl_3O_2$	(See Table 2-1)					
$CFCl_2 + O_2 \xrightarrow{M} CFCl_2O_2$	(See Table 2-1)					
$CF_2Cl + O_2 \xrightarrow{M} CF_2ClO_2$	(See Table 2-1)					
$CCl_3O_2 + NO_2 \xrightarrow{M} CCl_3O_2NO_2$	(See Table 2-1)					
$CFCl_2O_2 + NO_2 \xrightarrow{M} CFCl_2O_2NO_2$	(See Table 2-1)					
$CF_2ClO_2 + NO_2 \xrightarrow{M} CF_2ClO_2NO_2$	(See Table 2-1)					
$CH_2ClO + O_2 \rightarrow CHClO + HO_2$	–	–	6×10^{-14}	5	–	F120
$CH_2ClO_2 + HO_2 \rightarrow CH_2ClO_2H + O_2$	3.3×10^{-13}	–820	5.2×10^{-12}	1.5	200	F121
$CH_2ClO_2 + NO \rightarrow CH_2ClO + NO_2$	7×10^{-12}	–300	1.9×10^{-11}	1.5	200	F122
$CCl_3O_2 + NO \rightarrow CCl_2O + NO_2 + Cl$	7.3×10^{-12}	–270	1.8×10^{-11}	1.3	200	F123
$CCl_2FO_2 + NO \rightarrow CClFO + NO_2 + Cl$	4.5×10^{-12}	–350	1.5×10^{-11}	1.3	200	F124
$CClF_2O_2 + NO \rightarrow CF_2O + NO_2 + Cl$	3.8×10^{-12}	–400	1.5×10^{-11}	1.2	200	F125
BrO_x Reactions						
$O + BrO \rightarrow Br + O_2$	1.9×10^{-11}	–230	4.1×10^{-11}	1.5	150	G 1
$O + HBr \rightarrow OH + Br$	5.8×10^{-12}	1500	3.8×10^{-14}	1.3	200	G 2
$O + HOBr \rightarrow OH + BrO$	1.2×10^{-10}	430	2.8×10^{-11}	3.0	300	G 3
$OH + Br_2 \rightarrow HOBr + Br$	4.2×10^{-11}	0	4.2×10^{-11}	1.3	600	G 4
$OH + BrO \rightarrow$ products	–	–	7.5×10^{-11}	3.0	–	G 5
$OH + HBr \rightarrow H_2O + Br$	1.1×10^{-11}	0	1.1×10^{-11}	1.2	250	G 6
$OH + CH_3Br \rightarrow CH_2Br + H_2O$	2.35×10^{-12}	1300	3.0×10^{-14}	1.1	100	G 7

Reaction	A-Factor[a]	E/R	k(298 K)[a]	f(298 K)[b]	g	Notes
$OH + CH_2Br_2 \rightarrow CHBr_2 + H_2O$	2.0×10^{-12}	840	1.2×10^{-13}	1.15	150	G 8
$OH + CHBr_3 \rightarrow CBr_3 + H_2O$	1.35×10^{-12}	600	1.8×10^{-13}	1.5	100	G 9
$OH + CHF_2Br \rightarrow CF_2Br + H_2O$	1.0×10^{-12}	1380	1.0×10^{-14}	1.1	100	G10
$OH + CH_2ClBr \rightarrow CHClBr + H_2O$	2.4×10^{-12}	920	1.1×10^{-13}	1.1	100	G11
$OH + CF_2ClBr \rightarrow$ products (Halon-1211)	*$\sim1\times10^{-12}$*	*>2600*	$<1.5\times10^{-16}$	–	–	G12
$OH + CF_2Br_2 \rightarrow$ products (Halon-1202)	*$\sim1\times10^{-12}$*	*>2200*	$<5.0\times10^{-16}$	–	–	G13
$OH + CF_3Br \rightarrow$ products (Halon-1301)	*$\sim1\times10^{-12}$*	*>3600*	*$<6.0\times10^{-18}$*	–	–	G14
$OH + CH_2BrCH_3 \rightarrow$ products	2.9×10^{-12}	640	3.4×10^{-13}	1.2	150	G15
$OH + CH_2BrCF_3 \rightarrow CHBrCF_3 + H_2O$	1.4×10^{-12}	1340	1.6×10^{-14}	1.2	150	G16
$OH + CHFBrCF_3 \rightarrow CFBrCF_3 + H_2O$	7.3×10^{-13}	1120	1.7×10^{-14}	1.2	100	G17
$OH + CHClBrCF_3 \rightarrow CClBrCF_3 + H_2O$	1.1×10^{-12}	940	4.7×10^{-14}	1.2	150	G18
$OH + CHFClCF_2Br \rightarrow CFClCF_2Br + H_2O$	8.4×10^{-13}	1220	1.4×10^{-14}	1.3	200	G19
$OH + CF_2BrCF_2Br \rightarrow$ products (Halon-2402)	*$\sim1\times10^{-12}$*	*>3600*	*$<6\times10^{-18}$*	–	–	G20
$OH + CH_2BrCH_2CH_3 \rightarrow$ products	3.0×10^{-12}	330	1.0×10^{-12}	1.1	50	G21
$OH + CH_3CHBrCH_3 \rightarrow$ products	1.85×10^{-12}	270	7.5×10^{-13}	1.15	50	G22
$HO_2 + Br \rightarrow HBr + O_2$	1.5×10^{-11}	600	2.0×10^{-12}	2.0	600	G23
$HO_2 + BrO \rightarrow$ products	3.4×10^{-12}	–540	2.1×10^{-11}	1.5	200	G24
$NO_3 + HBr \rightarrow HNO_3 + Br$	–	–	$<1.0\times10^{-16}$	–	–	G25
$Cl + CH_2ClBr \rightarrow HCl + CHClBr$	1.5×10^{-11}	1070	4.1×10^{-13}	1.2	300	G26
$Cl + CH_3Br \rightarrow HCl + CH_2Br$	1.7×10^{-11}	1080	4.5×10^{-13}	1.1	100	G27
$Cl + CH_2Br_2 \rightarrow HCl + CHBr_2$	6.7×10^{-12}	825	4.2×10^{-13}	1.15	150	G28
$Cl + CHBr_3 \rightarrow CBr_3 + HCl$	4.85×10^{-12}	850	2.8×10^{-13}	1.5	250	G29
$Br + O_3 \rightarrow BrO + O_2$	1.7×10^{-11}	800	1.2×10^{-12}	1.2	200	G30
$Br + H_2O_2 \rightarrow HBr + HO_2$	1.0×10^{-11}	>3000	$<5.0\times10^{-16}$	–	–	G31
$Br + NO_2 \xrightarrow{M} BrNO_2$	(See Table 2-1)					

Reaction	A-Factor[a]	E/R	k(298 K)[a]	f(298 K)[b]	g	Notes
$Br + NO_3 \rightarrow BrO + NO_2$	–	–	1.6×10^{-11}	2.0	–	G32
$Br + H_2CO \rightarrow HBr + HCO$	1.7×10^{-11}	800	1.1×10^{-12}	1.3	200	G33
$Br + OClO \rightarrow BrO + ClO$	2.6×10^{-11}	1300	3.4×10^{-13}	2.0	300	G34
$Br + Cl_2O \rightarrow BrCl + ClO$	2.1×10^{-11}	470	4.3×10^{-12}	1.3	150	G35
$Br + Cl_2O_2 \rightarrow$ products	–	–	3.0×10^{-12}	2.0	–	G36
$BrO + O_3 \rightarrow$ products	$\sim1.0\times10^{-12}$	>3200	$<2.0\times10^{-17}$	–	–	G37
$BrO + NO \rightarrow NO_2 + Br$	8.8×10^{-12}	–260	2.1×10^{-11}	1.15	130	G38
$BrO + NO_2 \xrightarrow{M} BrONO_2$	(See Table 2-1)					
$BrO + NO_3 \rightarrow$ products	–	–	1.0×10^{-12}	3.0	–	G39
$BrO + ClO \rightarrow Br + OClO$	9.5×10^{-13}	–550	6.0×10^{-12}	1.25	150	G40
$\rightarrow Br + ClOO$	2.3×10^{-12}	–260	5.5×10^{-12}	1.25	150	G40
$\rightarrow BrCl + O_2$	4.1×10^{-13}	–290	1.1×10^{-12}	1.25	150	G40
$BrO + BrO \rightarrow$ products	1.5×10^{-12}	–230	3.2×10^{-12}	1.15	150	G41
$CH_2BrO_2 + NO \rightarrow CH_2O + NO_2 + Br$	4×10^{-12}	–300	1.1×10^{-11}	1.5	200	G42
IO_x Reactions						
$O + I_2 \rightarrow IO + I$	1.4×10^{-10}	0	1.4×10^{-10}	1.4	250	H 1
$O + IO \rightarrow O_2 + I$			1.2×10^{-10}	2.0		H 2
$OH + I_2 \rightarrow HOI + I$			1.8×10^{-10}	2.0		H 3
$OH + HI \rightarrow H_2O + I$			3.0×10^{-11}	2.0		H 4
$OH + CH_3I \rightarrow H_2O + CH_2I$	2.9×10^{-12}	1100	7.2×10^{-14}	1.5	300	H 5
$OH + CF_3I \rightarrow HOI + CF_3$	2.5×10^{-11}	2070	2.4×10^{-14}	1.3	200	H 6
$HO_2 + I \rightarrow HI + O_2$	1.5×10^{-11}	1090	3.8×10^{-13}	2.0	500	H 7
$HO_2 + IO \rightarrow HOI + O_2$			8.4×10^{-11}	1.5		H 8
$NO_3 + HI \rightarrow HNO_3 + I$	(See Note)					H 9
$Cl + CH_3I \rightarrow CH_2I + HCl$	2.9×10^{-11}	1000	1.0×10^{-12}	1.5	250	H10

Reaction	A-Factor[a]	E/R	k(298 K)[a]	f(298 K)[b]	g	Notes
$I + O_3 \rightarrow IO + O_2$	2.3×10^{-11}	870	1.2×10^{-12}	1.2	200	H11
$I + NO \xrightarrow{M} INO$	(See Table 2-1)					
$I + NO_2 \xrightarrow{M} INO_2$	(See Table 2-1)					
$I + BrO \rightarrow IO + Br$	–	–	1.2×10^{-11}	2.0		H12
$IO + NO \rightarrow I + NO_2$	9.1×10^{-12}	–240	2.0×10^{-11}	1.2	150	H13
$IO + NO_2 \xrightarrow{M} IONO_2$	(See Table 2-1)					
$IO + ClO \rightarrow$ products	5.1×10^{-12}	–280	1.3×10^{-11}	2.0	200	H14
$IO + BrO \rightarrow$ products	–	–	6.9×10^{-11}	1.5	–	H15
$IO + IO \rightarrow$ products	1.5×10^{-11}	–500	8.0×10^{-11}	1.5	500	H16
$INO + INO \rightarrow I_2 + 2NO$	8.4×10^{-11}	2620	1.3×10^{-14}	2.5	600	H17
$INO_2 + INO_2 \rightarrow I_2 + 2NO_2$	2.9×10^{-11}	2600	4.7×10^{-15}	3.0	1000	H18
SO_x Reactions						
$O + SH \rightarrow SO + H$	–	–	1.6×10^{-10}	5.0	–	I 1
$O + CS \rightarrow CO + S$	2.7×10^{-10}	760	2.1×10^{-11}	1.1	250	I 2
$O + H_2S \rightarrow OH + SH$	9.2×10^{-12}	1800	2.2×10^{-14}	1.7	550	I 3
$O + OCS \rightarrow CO + SO$	2.1×10^{-11}	2200	1.3×10^{-14}	1.2	150	I 4
$O + CS_2 \rightarrow CS + SO$	3.2×10^{-11}	650	3.6×10^{-12}	1.2	150	I 5
$O + SO_2 \xrightarrow{M} SO_3$	(See Table 2-1)					
$O + CH_3SCH_3 \rightarrow CH_3SO + CH_3$	1.3×10^{-11}	–410	5.0×10^{-11}	1.1	100	I 6
$O + CH_3SSCH_3 \rightarrow CH_3SO + CH_3S$	5.5×10^{-11}	–250	1.3×10^{-10}	1.3	100	I 7
$O_3 + H_2S \rightarrow$ products	–	–	$<2.0\times10^{-20}$	–	–	I 8
$O_3 + CH_3SCH_3 \rightarrow$ products	–	–	$<1.0\times10^{-18}$	–	–	I 9
$O_3 + SO_2 \rightarrow SO_3 + O_2$	3.0×10^{-12}	>7000	$<2.0\times10^{-22}$	–	–	I10
$OH + H_2S \rightarrow SH + H_2O$	6.0×10^{-12}	75	4.7×10^{-12}	1.2	75	I11
$OH + OCS \rightarrow$ products	1.1×10^{-13}	1200	1.9×10^{-15}	2.0	500	I12

Reaction	A-Factor[a]	E/R	k(298 K)[a]	f(298 K)[b]	g	Notes
$OH + CS_2 \rightarrow$ products	(See Note)	–	–	–	–	I13
$OH + CH_3SH \rightarrow CH_3S + H_2O$	9.9×10^{-12}	–360	3.3×10^{-11}	1.2	100	I14
$OH + CH_3SCH_3 \rightarrow H_2O + CH_2SCH_3$	1.2×10^{-11}	260	5.0×10^{-12}	1.15	100	I15
$OH + CH_3SSCH_3 \rightarrow$ products	6.0×10^{-11}	–400	2.3×10^{-10}	1.2	200	I16
$OH + S \rightarrow H + SO$	–	–	6.6×10^{-11}	3.0	–	I17
$OH + SO \rightarrow H + SO_2$	–	–	8.6×10^{-11}	2.0	–	I18
$OH + SO_2 \xrightarrow{M} HOSO_2$	(See Table 2-1)					
$HO_2 + H_2S \rightarrow$ products	–	–	$<3.0\times10^{-15}$	–	–	I19
$HO_2 + CH_3SH \rightarrow$ products	–	–	$<4.0\times10^{-15}$	–	–	I19
$HO_2 + CH_3SCH_3 \rightarrow$ products	–	–	$<5.0\times10^{-15}$	–	–	I19
$HO_2 + SO_2 \rightarrow$ products	–	–	$<1.0\times10^{-18}$	–	–	I20
$NO_2 + SO_2 \rightarrow$ products	–	–	$<2.0\times10^{-26}$	–	–	I21
$NO_3 + H_2S \rightarrow$ products	–	–	$<8.0\times10^{-16}$	–	–	I22
$NO_3 + OCS \rightarrow$ products	–	–	$<1.0\times10^{-16}$	–	–	I23
$NO_3 + CS_2 \rightarrow$ products	–	–	$<4.0\times10^{-16}$	–	–	I24
$NO_3 + CH_3SH \rightarrow$ products	4.4×10^{-13}	–210	8.9×10^{-13}	1.25	210	I25
$NO_3 + CH_3SCH_3 \rightarrow CH_3SCH_2 + HNO_3$	1.9×10^{-13}	–500	1.0×10^{-12}	1.2	200	I26
$NO_3 + CH_3SSCH_3 \rightarrow$ products	1.3×10^{-12}	270	5.3×10^{-13}	1.4	270	I27
$NO_3 + SO_2 \rightarrow$ products	–	–	$<7.0\times10^{-21}$	–	–	I28
$N_2O_5 + CH_3SCH_3 \rightarrow$ products	–	–	$<1.0\times10^{-17}$	–	–	I29
$CH_3O_2 + SO_2 \rightarrow$ products	–	–	$<5.0\times10^{-17}$	–	–	I30
$F + CH_3SCH_3 \rightarrow$ products	–	–	$2.4.\times10^{-10}$	2.0	–	I31
$Cl + H_2S \rightarrow HCl + SH$	3.7×10^{-11}	–210	7.4×10^{-11}	1.25	100	I32
$Cl + OCS \rightarrow$ products	–	–	$<1.0\times10^{-16}$	–	–	I33
$Cl + CS_2 \rightarrow$ products	–	–	$<4.0\times10^{-15}$	–	–	I34

Reaction	A-Factor[a]	E/R	k(298 K)[a]	f(298 K)[b]	g	Notes
$Cl + CH_3SH \rightarrow CH_3S + HCl$	1.2×10^{-10}	–150	2.0×10^{-10}	1.25	50	I35
$Cl + CH_3SCH_3 \rightarrow$ products	(See Note)	–	–	–	–	I36
$ClO + OCS \rightarrow$ products	–	–	$<2.0\times10^{-16}$	–	–	I37
$ClO + CH_3SCH_3 \rightarrow$ products	–	–	9.5×10^{-15}	2.0	–	I38
$ClO + SO \rightarrow Cl + SO_2$	2.8×10^{-11}	0	2.8×10^{-11}	1.3	50	I39
$ClO + SO_2 \rightarrow Cl + SO_3$	–	–	$<4.0\times10^{-18}$	–	–	I37
$Br + H_2S \rightarrow HBr + SH$	1.4×10^{-11}	2750	1.4×10^{-15}	2.0	300	I40
$Br + CH_3SH \rightarrow CH_3S + HBr$	9.2×10^{-12}	390	2.5×10^{-12}	2.0	100	I40
$Br + CH_3SCH_3 \rightarrow$ products	(See Note)					I41
$BrO + CH_3SCH_3 \rightarrow$ products	1.5×10^{-14}	–850	2.6×10^{-13}	1.3	200	I42
$BrO + SO \rightarrow Br + SO_2$			5.7×10^{-11}	1.4		I43
$IO + CH_3SH \rightarrow$ products			6.6×10^{-16}	2.0		I44
$IO + CH_3SCH_3 \rightarrow$ products			1.2×10^{-14}	1.5		I45
$S + O_2 \rightarrow SO + O$	2.3×10^{-12}	0	2.3×10^{-12}	1.2	200	I46
$S + O_3 \rightarrow SO + O_2$			1.2×10^{-11}	2.0		I47
$SO + O_2 \rightarrow SO_2 + O$	2.6×10^{-13}	2400	8.4×10^{-17}	2.0	500	I48
$SO + O_3 \rightarrow SO_2 + O_2$	3.6×10^{-12}	1100	9.0×10^{-14}	1.2	200	I49
$SO + NO_2 \rightarrow SO_2 + NO$	1.4×10^{-11}	0	1.4×10^{-11}	1.2	50	I50
$SO + OClO \rightarrow SO_2 + ClO$			1.9×10^{-12}	3.0		I51
$SO_3 + H_2O \rightarrow$ products	(See Note)		–	–		I52
$SO_3 + NH_3 \rightarrow$ products	(See Table 2-1)		–	–		
$SO_3 + NO_2 \rightarrow$ products			1.0×10^{-19}	10.0		I53
$SH + O_2 \rightarrow OH + SO$			$<4.0\times10^{-19}$	–		I54
$SH + O_3 \rightarrow HSO + O_2$	9.0×10^{-12}	280	3.5×10^{-12}	1.3	200	I55
$SH + H_2O_2 \rightarrow$ products			$<5.0\times10^{-15}$	–		I56

Reaction	A-Factor[a]	E/R	k(298 K)[a]	f(298 K)[b]	g	Notes
$SH + NO \xrightarrow{M} HSNO$	(See Table 2-1)					
$SH + NO_2 \rightarrow HSO + NO$	2.9×10^{-11}	–240	6.5×10^{-11}	1.2	50	I57
$SH + Cl_2 \rightarrow ClSH + Cl$	1.7×10^{-11}	690	1.7×10^{-12}	2.0	200	I58
$SH + BrCl \rightarrow$ products	2.3×10^{-11}	–350	7.4×10^{-11}	2.0	200	I58
$SH + Br_2 \rightarrow BrSH + Br$	6.0×10^{-11}	–160	1.0×10^{-10}	2.0	160	I58
$SH + F_2 \rightarrow FSH + F$	4.3×10^{-11}	1390	4.0×10^{-13}	2.0	200	I58
$HSO + O_2 \rightarrow$ products			$<2.0\times10^{-17}$	–		I59
$HSO + O_3 \rightarrow$ products			1.0×10^{-13}	1.3		I60
$HSO + NO \rightarrow$ products			$<1.0\times10^{-15}$	–		I61
$HSO + NO_2 \rightarrow HSO_2 + NO$			9.6×10^{-12}	2.0		I61
$HSO_2 + O_2 \rightarrow HO_2 + SO_2$			3.0×10^{-13}	3.0		I62
$HOSO_2 + O_2 \rightarrow HO_2 + SO_3$	1.3×10^{-12}	330	4.4×10^{-13}	1.2	200	I63
$CS + O_2 \rightarrow OCS + O$			2.9×10^{-19}	2.0		I64
$CS + O_3 \rightarrow OCS + O_2$			3.0×10^{-16}	3.0		I65
$CS + NO_2 \rightarrow OCS + NO$			7.6×10^{-17}	3.0		I65
$CH_3S + O_2 \rightarrow$ products			$<3.0\times10^{-18}$	–		I66
$CH_3S + O_3 \rightarrow$ products	2.0×10^{-12}	–290	5.3×10^{-12}	1.15	100	I67
$CH_3S + NO \rightarrow$ products $CH_3S + NO \xrightarrow{M}$ products	(See Table 2-1)		$<1.0\times10^{-13}$	–		I68
$CH_3S + NO_2 \rightarrow CH_3SO + NO$	2.1×10^{-11}	–320	6.1×10^{-11}	1.15	100	I69
$CH_2SH + O_2 \rightarrow$ products			6.5×10^{-12}	2.0		I70
$CH_2SH + O_3 \rightarrow$ products			3.5×10^{-11}	2.0		I71
$CH_2SH + NO \rightarrow$ products			1.9×10^{-11}	2.0		I72
$CH_2SH + NO_2 \rightarrow$ products			5.2×10^{-11}	2.0		I73
$CH_3SO + O_3 \rightarrow$ products			6.0×10^{-13}	1.5		I74

Reaction	A-Factor[a]	E/R	k(298 K)[a]	f(298 K)[b]	g	Notes
$CH_3SO + NO_2 \rightarrow CH_3SO_2 + NO$			1.2×10^{-11}	1.4		I75
$CH_3SOO + O_3 \rightarrow$ products			$<8.0\times10^{-13}$	–		I76
$CH_3SOO + NO \rightarrow$ products	1.1×10^{-11}	0	1.1×10^{-11}	2.0	100	I76
$CH_3SO_2 + NO_2 \rightarrow$ products	2.2×10^{-11}	0	2.2×10^{-11}	2.0	100	I77
$CH_3SCH_2 + O_2 \xrightarrow{M} CH_3SCH_2O_2$	(See Table 2-1)					
$CH_3SCH_2 + NO_3 \rightarrow$ products			3.0×10^{-10}	2.0		I78
$CH_3SCH_2O_2 + NO \rightarrow CH_3SCH_2O + NO_2$			1.9×10^{-11}	2.0		I79
$CH_3SS + O_3 \rightarrow$ products			4.6×10^{-13}	2.0		I80
$CH_3SS + NO_2 \rightarrow$ products			1.8×10^{-11}	2.0		I81
$CH_3SSO + NO_2 \rightarrow$ products			4.5×10^{-12}	2.0		I81
Metal Reactions						
$Na + O_2 \xrightarrow{M} NaO_2$	(See Table 2-1)					
$Na + O_3 \rightarrow NaO + O_2$	1.0×10^{-9}	95	7.3×10^{-10}	1.2	50	J 1
$\rightarrow NaO_2 + O$	–	–	$<4.0\times10^{-11}$	–	–	J 1
$Na + N_2O \rightarrow NaO + N_2$	2.8×10^{-10}	1600	1.3×10^{-12}	1.2	400	J 2
$Na + Cl_2 \rightarrow NaCl + Cl$	7.3×10^{-10}	0	7.3×10^{-10}	1.3	200	J 3
$NaO + O \rightarrow Na + O_2$	3.7×10^{-10}	0	3.7×10^{-10}	3.0	400	J 4
$NaO + O_2 \xrightarrow{M} NaO_3$	(See Table 2-1)					
$NaO + O_3 \rightarrow NaO_2 + O_2$	1.1×10^{-9}	570	1.6×10^{-10}	1.5	300	J 5
$\rightarrow Na + 2O_2$	6.0×10^{-11}	0	6.0×10^{-11}	3.0	800	J 5
$NaO + H_2 \rightarrow NaOH + H$	2.6×10^{-11}	0	2.6×10^{-11}	2.0	600	J 6
$NaO + H_2O \rightarrow NaOH + OH$	2.2×10^{-10}	0	2.2×10^{-10}	2.0	400	J 7
$NaO + NO \rightarrow Na + NO_2$	1.5×10^{-10}	0	1.5×10^{-10}	4.0	400	J 8
$NaO + CO_2 \xrightarrow{M} NaCO_3$	(See Table 2-1)					
$NaO + HCl \rightarrow$ products	2.8×10^{-10}	0	2.8×10^{-10}	3.0	400	J 9

Reaction	A-Factor[a]	E/R	k(298 K)[a]	f(298 K)[b]	g	Notes
$NaO_2 + O \rightarrow NaO + O_2$	2.2×10^{-11}	0	2.2×10^{-11}	5.0	600	J10
$NaO_2 + NO \rightarrow NaO + NO_2$	–	–	$<10^{-14}$	–	–	J11
$NaO_2 + HCl \rightarrow$ products	2.3×10^{-10}	0	2.3×10^{-10}	3.0	400	J12
$NaOH + HCl \rightarrow NaCl + H_2O$	2.8×10^{-10}	0	2.8×10^{-10}	3.0	400	J13
$NaOH + CO_2 \xrightarrow{M} NaHCO_3$	(See Table 2-1)					

Shaded areas indicate changes or additions since JPL 97-4/JPL 00-3. Italicized entries denote estimates.

[a] Units are cm^3 $molecule^{-1}$ s^{-1}.

[b] f(298 K) is the uncertainty factor at 298 K. To calculate the uncertainty at other temperatures, use the expression:

$$f(T) = f(298)\exp\left|g\left(\frac{1}{T} - \frac{1}{298}\right)\right|$$

Note that the exponent is absolute value.

1.3 Notes to Table 1

A1. $O + O_3$. The recommended rate expression is from Wine et al. [1316] and is a linear least squares fit of all data (unweighted) from Davis et al. [319], McCrumb and Kaufman [795], West et al. [1294], Arnold and Comes [29], and Wine et al. [1316].

A2. $O(^1D)$ Reactions. The rate constants are for the disappearance of $O(^1D)$, which includes physical quenching or deactivation. Where information is available, product yields are given. The rate constant recommendations are based on averages of the absolute rate constant measurements reported by Streit et al. [1123], Davidson et al. [312] and Davidson et al. [311] for N_2O, H_2O, CH_4, H_2, N_2, O_2, O_3, CCl_4, $CFCl_3$, CF_2Cl_2, NH_3, and CO_2; by Amimoto et al. [18], Amimoto et al. [17], and Force and Wiesenfeld [405,406] for N_2O, H_2O, CH_4, N_2, H_2, O_2, O_3, CO_2, CCl_4, $CFCl_3$, CF_2Cl_2, and CF_4; by Wine and Ravishankara [1317–1319] for N_2O, H_2O, N_2, H_2, O_3, CO_2, and CF_2O; by Brock and Watson (private communication, 1980) for N_2, O_2 and CO_2; by Lee and Slanger [701,702] for H_2O and O_2; by Gericke and Comes [427] for H_2O; and by Shi and Barker [1057] for N_2 and CO_2, and Talukdar and Ravishankara [1157] for H_2. The weight of the evidence from these studies indicates that the results of Heidner and Husain [494], Heidner et al. [493] and Fletcher and Husain [399,400] contain a systematic error. For the critical atmospheric reactants, such as N_2O, H_2O, and CH_4, the recommended absolute rate constants are in good agreement with the previous relative measurements when compared with N_2 as the reference reactant. A similar comparison with O_2 as the reference reactant gives somewhat poorer agreement.

A3. $O(^1D) + O_2$. The deactivation of $O(^1D)$ by O_2 leads to the production of $O_2(^1\Delta)$ with an efficiency of 80±20%: Noxon [901], Biedenkapp and Bair [119], Snelling [1096], and Lee and Slanger [701]. The $O_2(^1\Delta)$ is produced in the v=0, 1, and 2 vibrational levels in the amounts 60%, 40%, and <3%, Gauthier and Snelling [424] and Lee and Slanger [701].

A4. $O(^1D) + O_3$. The branching result for reaction of $O(^1D)$ with O_3 to give $O_2 + O_2$ or $O_2 + O + O$ is from Davenport et al. [306]. This is supported by measurements of Amimoto et al. [18] who reported that on average one ground state O is produced per $O(^1D)$ reaction with O_3. It seems unlikely that this could result from 100% quenching of the $O(^1D)$ by O_3.

A5. $O(^1D) + H_2$. Wine and Ravishankara [1318] have determined the yield of $O(^3P)$ is <4.9%. The major products are H + OH. Koppe et al. [649] report a 2.7 times larger rate coefficient at a kinetic energy of 0.12eV. This does not agree with the observations of Davidson et al. [312], who reported that k is independent of temperature (200–350 K) and Matsumi et al. [791] who report no change in k when hot $O(^1D)$ is moderated with Ar.

A6. $O(^1D) + H_2O$. Measurements of the $O_2 + H_2$ product yield were made by Zellner et al. [1361] (1 +0.5 or –1)% and by Glinski and Birks [445] (0.6 +0.7 or –0.6)%. The yield of $O(^3P)$ from $O(^1D) + H_2O$ is reported to be <(4.9±3.2)% by Wine and Ravishankara [1318] and (2±1)% by Takahashi et al. [1146].

To calculate the rates of OH production via $O(^1D)$ reactions in the atmosphere, the quantities of interest are the ratios of the rate coefficients for the reaction of $O(^1D)$ with H_2O to those with N_2 and with O_2. The ratios of the rate coefficients for $O(^1D)$ reactions measured using the same method (and often the same apparatus) are more accurate (and precise) than the individual rate constants that are quoted in Table 1. Ratio data are given in the original references for this reaction.

A7. $O(^1D) + N_2O$. The branching ratio for the reaction of $O(^1D)$ with N_2O to give $N_2 + O_2$ or NO + NO is an average of the values reported by Davidson et al. [309]; Volltrauer et al. [1236]; Marx et al. [790] and Lam et al. [675], with a spread in R=k(NO + NO)/k(Total) = 0.52 – 0.62. Cantrell et al. [198] reported a measurement of R=0.57 and an analysis of all measurements from 1957–1994 leads them to recommend a value of R=0.61±0.06, where the uncertainty indicates their 95% confidence interval. The recommended branching ratio agrees well with earlier measurements of the quantum yield from N_2O photolysis (Calvert and Pitts [189]). The $O(^1D)$ translational energy and temperature dependence effects are not clearly resolved. Wine and Ravishankara [1318] have determined that the yield of $O(^3P)$ from $O(^1D) + N_2O$ is <4.0%. The uncertainty for this reaction includes factors for both the overall rate coefficient and the branching ratio. A direct measurement by Greenblatt and Ravishankara [455] of the NO yield from the $O(^1D) + N_2O$ reaction in synthetic air agrees very well with the value predicted using the recommended $O(^1D)$ rate constants for N_2, O_2, and N_2O and the $O(^1D) + N_2O$ product branching ratio. These authors suggest that their results support the recommendations and reduce the uncertainty in the collected rate parameters by over a factor of two.

To calculate the rates of NO production via $O(^1D)$ reactions in the atmosphere, the quantities of interest are the ratios of the rate coefficients for the reaction of $O(^1D)$ with N_2O to those with N_2 and with O_2. The ratios of the rate coefficients for $O(^1D)$ reactions measured using the same method (and often the same apparatus)

are more accurate and precise than the individual rate constants that are quoted in Table 1. Ratio data are given in the original references for this reaction.

A8. O(1D) + NH3. Sanders et al. [1024] have detected the products NH(a1Δ) and OH formed in the reaction. They report that the yield of NH(a1Δ) is in the range 3–15% of the amount of OH detected.

A9. $O(^1D) + CH_4$. The reaction products are (a) $CH_3 + OH$, (b) CH_3O or $CH_2OH + H$ and (c) $CH_2O + H_2$. Lin and DeMore [739] analyzed the final products of N_2O/CH_4 photolysis mixtures and concluded that (a) accounted for about 90% and that CH_2O and H_2 (c) accounted for about 9%. Addison et al. [9] reported an OH yield of 80%. Casavecchia et al. [202] used a molecular beam experiment to observe H and CH_3O (or CH_2OH) products. They reported that the yield of H_2 was <25% of the yield of H from (b). Satyapal et al. [1029] observed the production of H atoms in a pulsed laser experiment and reported a yield of H of (25±8)%. Matsumi et al. [791] measured the yields of H and $O(^3P)$ in low pressure gas mixtures and reported the yield of H was (15±3)% and the yield of $O(^3P)$ was <5%. Wine and Ravishankara [1318] reported that the yield of $O(^3P)$ was <4.3%. Takahashi et al. [1146] reported that the $O(^3P)$ yield is <1%. We recommend the following branching ratios: (a) (75±15)%, (b) (20±7)%, (c) (5±5)%.

A10. O(1D) + HCl. The recommendation is the average of measurements by Davidson et al. [312] and Wine et al. [1325]. Product studies by the latter indicate: O(3P) + HCl (9±5)%; H + ClO (24±5)%; and OH + Cl (67±10)%. Takahashi et al. [1146] report the O(3P) yield is (15±4)%.

A11. $O(^1D) + HF$. Rate coefficient and product yield measured by Wine et al. (1984, private communication). The $O(^3P)$ yield is less than 4%.

A12. $O(^1D) + HBr$. Rate coefficient and products measured by Wine et al. [1325]. Product yields: $HBr + O(^3P)$ (20±7)%, H + BrO <4.5%, and OH + Br (80±12)%.

A13. $O(^1D) + Cl_2$. Rate coefficient and $O(^3P)$ product were measured by Wine et al. [1314], who reported $Cl_2 + O(^3P)$ (25±10)%. Takahashi et al. [1146] reported that the ClO yield is (74±15)%, in excellent agreement. An indirect study by Freudenstein and Biedenkapp [409] is in reasonable agreement on the yield of ClO.

A14. $O(^1D) + COCl_2$, COClF and COF_2. For the reactions of $O(^1D)$ with $COCl_2$ and COClF the recommended rate constants are derived from data of Fletcher and Husain [401]. For consistency, the recommended values for these rate constants were derived using a scaling factor (0.5) which corrects for the difference between rate constants from the Husain laboratory and the recommendations for other $O(^1D)$ rate constants in this table. The recommendation for COF_2 is from the data of Wine and Ravishankara [1319]. Their result is preferred over the value of Fletcher and Husain [401] because it appears to follow the pattern of decreased reactivity with increased fluorine substitution observed for other halocarbons. These reactions have been studied only at 298 K. Based on consideration of similar $O(^1D)$ reactions, it is assumed that E/R equals zero, and therefore the value shown for the A-factor has been set equal to k(298 K).

A15. $O(^1D)$ + halocarbons. The halocarbon rate constants are for the total disappearance of $O(^1D)$ and probably include physical quenching. Products of the reactive channels may include $CX_3O + X$, $CX_2O + X_2$ (or 2X), and $CX_3 + XO$, where X = H, F, Cl, or Br in various combinations. Bromine, chlorine and hydrogen are more easily displaced than fluorine from halocarbons. Some values have been reported for the fractions of the total rate of disappearance of $O(^1D)$ proceeding through physical quenching and reactive channels. For CCl_4: quenching = (14±6)% and reaction = (86±6)% (Force and Wiesenfeld [405]), ClO yield = (90±19)% (Takahashi et al. [1146]; for $CFCl_3$: quenching = (25±10)%, ClO formation = (60±15)% (Donovan, private communication, 1980), ClO yield = (88±18)% (Takahashi et al.); for CF_2Cl_2: quenching = (14±7)% and reaction = (86±14)% (Force and Wiesenfeld [405]), quenching = (20±10)%, ClO formation = (55±15)% (Donovan), quenching = (19±5)% and ClO formation = (87±18%) (Takahashi et al.).

A16. $O(^1D) + CH_3Br$. The recommendation is based on data from Thompson and Ravishankara [1165]. They report that the yield of $O(^3P)$ from physical quenching is 0±7%.

A17. $O(^1D) + CH_2Br_2$. The recommendation is based on data from Thompson and Ravishankara [1165]. They report that the yield of $O(^3P)$ from physical quenching is (5±7)%.

A18. $O(^1D) + CHBr_3$. The recommendation is based on data from Thompson and Ravishankara [1165]. The rate coefficient is somewhat large compared to analogous compounds. They report that the yield of $O(^3P)$ from physical quenching is (32±8)%.

A19. $O(^1D) + CH_3F$ (HFC-41). The recommendation is the average of measurements of Force and Wiesenfeld [405] and Schmoltner et al. [1039]. The $O(^3P)$ product yield was reported to be (25±3)% by Force and Wiesenfeld, (11±5)% by Schmoltner et al., and (19±5)% by Takahashi et al. [1146]. Burks and Lin [175] reported observing vibrationally excited HF as a product. Park and Wiesenfeld [929] observed OH.

A20. $O(^1D) + CH_2F_2$ (HFC-32). The recommendation is based upon the measurement of Schmoltner et al. [1039], who reported that the yield of $O(^3P)$ is (70±11)%. Green and Wayne [453] measured the loss of CH_2F_2 relative to the loss of N_2O. Their value when combined with our recommendation for $O(^1D) + N_2O$ yields a rate coefficient for reactive loss of CH_2F_2 that is about three times the result of Schmoltner et al. Burks and Lin [175] reported observing vibrationally excited HF as a product.

A21. $O(^1D) + CHF_3$ (HFC-23). The recommendation is the average of measurements of Force and Wiesenfeld [405] and Schmoltner et al. [1039]. The $O(^3P)$ product yield was reported to be (77±15)% by Force and Wiesenfeld and (102±3)% by Schmoltner et al. Although physical quenching is the dominant process, detectable yields of vibrationally excited HF have been reported by Burks and Lin [175] and Aker et al. [15], which indicate the formation of HF + CF_2O products.

A22. $O(^1D) + CHCl_2F$ (HCFC-21). The recommendation is based upon the measurement by Davidson et al. [311] of the total rate coefficient (physical quenching and reaction). Takahashi et al. [1146] report the yield of ClO is (74±15)%.

A23. $O(^1D) + CHClF_2$ (HCFC-22). The recommendation is based upon the measurements by Davidson et al. [311] and Warren et al. [1277] of the total rate coefficient. A measurement of the rate of reaction (halocarbon removal) relative to the rate of reaction with N_2O by Green and Wayne [453] agrees very well with this value when the $O(^1D) + N_2O$ recommendation is used to obtain an absolute value. A relative measurement by Atkinson et al. [41] gives a rate coefficient about a factor of two higher. Addison et al. [9] reported the following product yields: ClO (55±10)%, CF_2 (45±10)%, $O(^3P)$ (28 +10 or –15)%, and OH 5%, where the $O(^3P)$ comes from a branch yielding CF_2 and HCl. Warren et al. [1277] also report a yield of $O(^3P)$ of (28±6)%, which they interpret as the product of physical quenching.

A24. $O(^1D) + CClF_3$ (CFC-13). The recommendation is based on the measurement by Ravishankara et al.[985] who report (31±10)% physical quenching. Takahashi et al. [1146] report the yields of $O(^3P)$ (16±5)% and ClO (85±18)%.

A25. $O(^1D) + CClBrF_2$ (Halon 1211). The recommendation is based on data from Thompson and Ravishankara [1165]. They report that the yield of $O(^3P)$ from physical quenching is (36±4)%.

A26. $O(^1D) + CBr_2F_2$ (Halon 1202). The recommendation is based on data from Thompson and Ravishankara [1165]. They report that the yield of $O(^3P)$ from physical quenching is (54±6)%.

A27. $O(^1D) + CBrF_3$ (Halon 1301). The recommendation is based on data from Thompson and Ravishankara [1165]. They report that the yield of $O(^3P)$ from physical quenching is (59±8)%. Lorenzen-Schmidt et al. [753] measured the Halon removal rate relative to the N_2O removal rate and report that the rate coefficient for the Halon destruction path is $(4.0\pm0.4) \times 10^{-11}$, which is in excellent agreement with Thompson and Ravishankara.

A28. $O(^1D) + CF_4$ (CFC-14). The recommendation is based upon the measurement by Ravishankara et al. [985], who report (92±8)% physical quenching. Force and Wiesenfeld [405] measured a quenching rate coefficient about 10 times larger. Shi and Barker [1057] report an upper limit that is consistent with the recommendation. The small rate coefficient for this reaction makes it vulnerable to interference from reactant impurities. For this reason the recommendation should probably be considered an upper limit.

A29. $O(^1D) + CH_3CH_2F$ (HFC 161). The recommendation is based on data from Schmoltner et al. [1039]. They report that the yield of $O(^3P)$ from physical quenching is (18±5)%.

A30. $O(^1D) + CH_3CHF_2$ (HFC-152a). The recommendation is based on the measurements of Warren et al. [1277], who report (54±7)% physical quenching.

A31. $O(^1D) + CH_3CCl_2F$ (HCFC-141b). The recommendation is based upon the measurement of Warren et al. [1277], who report (31±5)% physical quenching.

A32. $O(^1D) + CH_3CClF_2$ (HCFC-142b). The recommendation is based upon the measurement of Warren et al. [1277], who report (26±5)% physical quenching. This agrees very well with Green and Wayne [453], who measured the loss of CH_3CF_2Cl relative to the loss of N_2O, when the recommendation for N_2O is used.

A33. $O(^1D) + CH_3CF_3$ (HFC-143a). The recommendation is based upon the relative rate measurement of Green and Wayne [453], who measured the loss of CH_3CF_3 relative to the loss of N_2O. The recommendation for N_2O is used to obtain the value given. It is assumed that there is no physical quenching, although the reported physical quenching by CH_2FCF_3 and CH_3CHF_2 suggests some quenching is possible.

A34. $O(^1D) + CH_2ClCClF_2$ (HCFC-132b). The recommendation is based upon the relative rate measurement of Green and Wayne [453], who measured the loss of CH_2ClCF_2Cl relative to the loss of N_2O. The recommendation for N_2O is used to obtain the value given. It is assumed that there is no physical quenching.

A35. $O(^1D) + CH_2ClCF_3$ (HCFC-133a). The recommendation is based upon the measurement of Warren et al. [1277], who report (20±5)% physical quenching. This agrees with Green and Wayne [453] who measured the loss of CH_2ClCF_3 relative to the loss of N_2O, when the recommendation for N_2O is used.

A36. $O(^1D) + CH_2FCF_3$ (HFC-134a). The recommendation is based on the measurement of Warren et al. [1277] who report (94+6/–1)% physical quenching. The predominance of physical quenching is surprising, considering the presence of C–H bonds, which are usually reactive toward $O(^1D)$.

A37. $O(^1D) + CHCl_2CF_3$ (HCFC-123). The recommendation is based upon measurements by Warren et al. [1277]. The relative rate measurement of Green and Wayne [453], who measured the loss of $CHCl_2CF_3$ relative to the loss of N_2O, agrees well with the recommendation when the recommendation for N_2O is used. Warren et al. report (21 ± 8)% physical quenching.

A38. $O(^1D) + CHClFCF_3$ (HCFC-124). The recommendation is based upon the measurement of Warren et al. [1277], who report (31 ± 10)% physical quenching.

A39. $O(^1D) + CHF_2CF_3$ (HFC-125). The recommendation is based upon the measurement of Warren et al. [1277], who report (85+15/–22)% physical quenching. Green and Wayne [453] measured the loss of CHF_2CF_3 relative to the loss of N_2O and report a loss corresponding to about 40% of the recommended rate coefficient. This reaction is much faster than one would predict by analogy to similar compounds, such as CH_2FCF_3.

A40. $O(^1D) + CCl_3CF_3$ (CFC-113a). The recommendation is an estimate based on analogy to similar compounds.

A41. $O(^1D) + CCl_2FCClF_2$ (CFC-113). The recommendation is an estimate based on analogy to similar compounds.

A42. $O(^1D) + CCl_2FCF_3$ (CFC-114a). The recommendation is an estimate based on analogy to similar compounds.

A43. $O(^1D) + CClF_2CClF_2$ (CFC-114). The recommendation is based on the measurement by Ravishankara et al. [985], who report (25 ± 9)% physical quenching.

A44. $O(^1D) + CClF_2CF_3$ (CFC-115). The recommendation is based on the measurement by Ravishankara et al.[985], who report (70 ± 7)% physical quenching.

A45. $O(^1D) + CBrF_2CBrF_2$ (Halon 2402). The recommendation is based on data from Thompson and Ravishankara [1165]. They report that the yield of $O(^3P)$ from physical quenching is (25±7)%. Lorenzen-Schmidt et al. [753] measured the Halon removal rate relative to the N_2O removal rate and report that the rate coefficient for the Halon destruction path is $(8.8 \pm 1.2) \times 10^{-11,}$ in fair agreement with the result of Thompson and Ravishankara.

A46. $O(^1D) + C_2F_6$ (CFC-116). The recommendation is based on a measurement by Ravishankara et al. [985], who report (85 ± 15)% physical quenching. The small rate coefficient for this reaction makes it vulnerable to interference from reactant impurities. For this reason the recommendation should probably be considered an upper limit.

A47. $O(^1D) + CHF_2CF_2CF_2CHF_2$ (HFC 338 pcc). The recommendation is based on data from Schmoltner et al. [1039]. They report that the yield of $O(^3P)$ from physical quenching is (97 ± 9)%.

A48. $O(^1D) + c\text{-}C_4F_8$. The recommendation for perfluorocyclobutane is based upon the measurement by Ravishankara et al. [985], who report (100 +0 /–15)% physical quenching. The small rate coefficient for this reaction makes it vulnerable to interference from reactant impurities. For this reason the recommendation should probably be considered an upper limit.

A49. $O(^1D) + CF_3CHFCHFCF_2CF_3$ (HFC 43-10 mee). The recommendation is based on data from Schmoltner et al. [1039]. The rate coefficients for this compound and CHF_2CF_3 do not follow the reactivity trend of other HFCs. Schmoltner et al. report that the yield of $O(^3P)$ from physical quenching is (91±4)%.

A50. $O(^1D) + C_5F_{12}$ (CFC 41-12). The recommendation is based on data from Ravishankara et al. [985]. They report that the yield of $O(^3P)$ from physical quenching is (79±12)%.

A51. $O(^1D) + C_6F_{14}$ (CFC 51-14). The recommendation is based on data from Ravishankara et al. [985]. They report that the yield of $O(^3P)$ from physical quenching is (75±9)%.

A52. $O(^1D) + 1,2\text{-}(CF_3)_2c\text{-}C_4F_6$. The recommendation is based on data from Ravishankara et al. [985]. They report that the yield of $O(^3P)$ from physical quenching is (84±16)%.

A53. $O(^1D) + SF_6$. The recommendation is based upon measurements by Ravishankara et al. [985] who report (32±10)% physical quenching. The small rate coefficient for this reaction makes it vulnerable to interference from reactant impurities. For this reason the recommendation should probably be considered an upper limit.

A54. $O_2(^1\Delta) + O$. The recommendation is based on the upper limit reported by Clark and Wayne [232].

A55. $O_2(^1\Delta) + O_2$. The recommendation is the average of eight room temperature measurements: Steer et al. [1108], Findlay and Snelling [392], Borrell et al. [140], Leiss et al. [706], Tachibana and Phelps [1140], Billington and Borrell [127], Raja et al. [977], and Wildt et al. [1306]. The temperature dependence is derived from the data of Findlay and Snelling and Billington and Borrell. Several other less direct measurements of the rate coefficient agree with the recommendation, including Clark and Wayne [231], Findlay et al. [391], and McLaren et al. [797]. Wildt et al. [1307] report observations of weak emissions in the near IR due to collision-induced radiation. Wildt et al. [1308] give rate coefficients for this process.

A56. $O_2(^1\Delta) + O_3$. The recommendation is the average of the room temperature measurements of Clark et al. [230], Findlay and Snelling [393], Becker et al. [95], and Collins et al. [266]. Several less direct measurements agree well with the recommendation (McNeal and Cook [798], Wayne and Pitts [1290], and Arnold and Comes [30]). The temperature dependence is from Findlay and Snelling and Becker et al., who agree very well, although both covered a relatively small temperature range. An earlier study by Clark et al. covered a much larger range, and found a much smaller temperature coefficient. The reason for this discrepancy is not clear. The yield of $O + 2O_2$ products appears to be close to unity, based on many studies of the quantum yield of O_3 destruction near the peak of the Hartley band. For example, measurements of the number of O_3 molecules destroyed per photon absorbed: Von Ellenrieder et al. [1237], Ravishankara et al. [991], Lissi and Heicklen [746], and references cited therein and measurements of O_3 loss and O atom temporal profiles in pulsed experiments Klais et al. [633] and Arnold and Comes [30]. Anderson et al. [26] report that the rate coefficient for atom exchange between $O_2(^1\Delta)$ and O_3 is $< 5\times10^{-16}$ at 300 K.

A57. $O_2(^1\Delta) + H_2O$. The recommendation is the average of the measurements reported by Becker et al. [94] and Findlay and Snelling [392]. An earlier study by Clark and Wayne [231] reported a value about three times larger.

A58. $O_2(^1\Delta) + N$. The recommendation is an upper limit based upon the measurement reported by Westenberg et al. [1301], who used ESR to detect $O_2(X^3\Sigma$ and $a^1\Delta)$, $O(^3P)$ and $N(^4S)$ with a discharge flow reactor. They used an excess of $O_2(^1\Delta)$ and measured the decay of N and the appearance of O at 195 and 300 K. They observed that the reaction of N with $O_2(^1\Delta)$ is somewhat slower than its reaction with $O_2(^3\Sigma)$. The recommended rate constant value for the latter provides the basis for the recommendation. Clark and Wayne [232,233] and Schmidt and Schiff [1036] reported observations of an $O_2(^1\Delta)$ reaction with N that is about 30 times faster than the recommended limit. Schmidt and Schiff attribute the observed loss of $O_2(^1\Delta)$ in excess N to a rapid energy exchange with some constituent in discharged nitrogen, other than N.

A59. $O_2(^1\Delta) + N_2$. The recommendation is based upon the measurements by Findlay et al. [391] and Becker et al. [94]. Other studies obtained higher values for an upper limit: Clark and Wayne [231] and Steer et al. [1108].

A60. $O_2(^1\Delta) + CO_2$. The recommendation is based on the measurements reported by Findlay and Snelling [392] and Leiss et al. [706]. Upper limit rate coefficients reported by Becker et al. [94], McLaren et al. [797], and Singh et al. [1074] are consistent with the recommendation.

A61. $O_2(^1\Delta) + O$. The recommendation is based on the measurement reported by Slanger and Black [1088].

A62. $O_2(^1\Delta) + O_2$. The recommendation is the average of values reported by Martin et al. [788], Lawton et al. [686], and Lawton and Phelps [687], who are in excellent agreement. Measurements by Thomas and Thrush [1164], Chatha et al. [214], and Knickelbein et al. [639] are in reasonable agreement with the recommendation. Knickelbein et al. report an approximate unit yield of $O_2(^1\Delta)$ product.

A63. $O_2(^1\Delta) + O_3$. The recommendation is based upon the room temperature measurements of Gilpin et al. [439], Slanger and Black [1088], Choo and Leu [229], and Shi and Barker [1057]. Measurements by Snelling [1096], Amimoto and Wiesenfeld [19], Ogren et al. [903], and Turnipseed et al. [1208] are in very good agreement with the recommendation. The temperature dependence is derived from the results of Choo and Leu. The yield of
$O + 2O_2$ products is reported to be (70±20)% by Slanger and Black and Amimoto and Wiesenfeld.

A64. $O_2(^1\Delta) + H_2O$. The recommendation is the average of room temperature measurements reported by Stuhl and Niki [1127], Filseth et al. [390], Wildt et al. [1306], and Shi and Barker [1057]. These data cover a range of about a factor of two. Measurements reported by O'Brien and Myers [902], Derwent and Thrush [342], and Thomas and Thrush [1164] are in good agreement with the recommendation. Wildt et al. [1306] report that the yield of $O_2(^1\Delta) \geq 90\%$.

A65. $O_2(^1\Delta) + N$. The recommendation is based on the limit reported by Slanger and Black [1088].

A66. $O_2(^1\Delta) + N_2$. The recommendation is the average of measurements reported by Izod and Wayne [566], Stuhl and Welge [1130], Filseth et al. [390], Martin et al. [788], Kohse-Höinghaus and Stuhl [646], Choo and Leu [229], Wildt et al. [1306], and Shi and Barker [1057]. Less direct measurements reported by Noxon [901], Myers and O'Brien [843], and Chatha et al. [214] are consistent with the recommendation. Kohse-Höinghaus and Stuhl observed no significant temperature dependence over the range 203–349 K.

A67. $O_2(^1\Delta) + CO_2$. The recommendation is the average of measurements reported by Filseth et al. [390], Davidson et al. [310], Avilés et al. [51], Muller and Houston [840], Choo and Leu [229], Wildt et al. [1306], and Shi and Barker [1057] at room temperature. The temperature dependence is from the work of Choo and Leu. Muller and Houston and Singh and Setser [1075] give evidence that $O_2(^1\Delta)$ is a product. Wildt et al. report that the yield of $O_2(^1\Delta) \geq 90\%$.

B1. O + OH. The rate constant for O + OH is a fit to three temperature dependence studies: Westenberg et al. [1300], Lewis and Watson [727], and Howard and Smith [532]. This recommendation is consistent with earlier work near room temperature as reviewed by Lewis and Watson [727] and with the measurements of Brune et al. [160]. The ratio $k(O + HO_2)/k(O + OH)$ measured by Keyser [621] agrees with the rate constants recommended here.

B2. $O + HO_2$. The recommended values are based on the results of studies over a range of temperatures by Keyser [620] and Nicovich and Wine [871] and the room temperature studies of Sridharan et al. [1099], Ravishankara et al. [991], and Brune et al. [160]. Earlier studies by Hack et al. [467] and Burrows et al. [176,179] are not considered, because the $OH + H_2O_2$ reaction was important in these studies and the value used for its rate constant in their analyses has been shown to be in error. Data from Ravishankara et al. [991] at 298 K show no dependence on pressure between 10 and 500 torr N_2. The ratio $k(O + HO_2)/k(O + OH)$ measured by Keyser [621] agrees with the rate constants recommended here. Sridharan et al. [1097] showed that the reaction products correspond to abstraction of an oxygen atom from HO_2 by the O reactant. Keyser et al. [625] reported <1% $O_2(^1\Delta)$ yield.

B3. $O + H_2O_2$. There are two direct studies of the $O + H_2O_2$ reaction: Davis et al. [320] and Wine et al. [1316]. The recommended value is a fit to the combined data. Wine et al. suggest that the earlier measurements may be too high because of secondary chemistry. The A-factor for both data sets is quite low compared to similar atom-molecule reactions. An indirect measurement of the E/R by Roscoe [1006] is consistent with the recommendation.

B4. $H + O_3$. The recommendation is an average of the results of Lee et al. [693] and Keyser [616], which are in excellent agreement over the 200–400 K range. An earlier study by Clyne and Monkhouse [251] is in very good agreement on the T dependence in the range 300–560 K but lies about 60% below the recommended values. Although we have no reason not to believe the Clyne and Monkhouse values, we prefer the two studies that are in excellent agreement, especially since they were carried out over the T range of interest. Results by Finlayson-Pitts and Kleindienst [397] agree well with the present recommendations. Reports of a channel forming $HO_2 + O$ (Finlayson-Pitts and Kleindienst [397]: ~25%, and Force and Wiesenfeld [406]: ~40%) have been contradicted by other studies (Howard and Finlayson-Pitts [531]: <3%; Washida et al. [1280]: <6%; Finlayson-Pitts et al. [398]: <2%; and Dodonov et al. [357]: <0.3%). Secondary chemistry is believed to be responsible for the observed O-atoms in this system. Washida et al. [1281] measured a low limit (<0.1%) for the production of singlet molecular oxygen in the reaction $H + O_3$.

B5. $H + HO_2$. There are five studies of this reaction: Hack et al. [471], Hack et al. [469], Thrush and Wilkinson [1171], Sridharan et al. [1099] and Keyser [623]. Related early work and combustion studies are referenced in the Sridharan et al. paper. All five studies used discharge flow systems. It is difficult to obtain a direct measurement of the rate constant for this reaction because both reactants are radicals and the products OH and O are very reactive toward the HO_2 reactant. The recommendation is based on the data of Sridharan et al. and Keyser because their measurements were the most direct and required the fewest corrections. The other measurements, $(5.0\pm1.3) \times 10^{-11}$ cm^3 molecule^{-1} s^{-1} by Thrush and Wilkinson [1171] and $(4.65\pm1) \times 10^{-11}$ by Hack et al. [469] are in reasonable agreement with the recommended value. Three of the studies reported the product channels: (a) 2OH, (b) $H_2O + O$, and (c) $H_2 + O_2$. Hack et al. [471] $k_a/k = 0.69$, $k_b/k = 0.02$, and $k_c/k = 0.29$; Sridharan et al. [1099] $k_a/k = 0.87\pm0.04$, $k_b/k = 0.02\pm0.02$, $k_c/k = 0.09\pm.045$; and Keyser [623] $k_a/k = 0.90\pm0.04$, $k_b/k = 0.02\pm0.02$, and $k_c/k = 0.08\pm0.04$. Hislop and Wayne [511], Keyser et al. [625], and Michelangeli et al. [825] reported on the yield of $O_2(b^1\Sigma)$ formed in channel (c) as $(2.8\pm1.3) \times 10^{-4}$, $<8 \times 10^{-3}$, and $<2.1 \times 10^{-2}$ respectively of the total reactions. Keyser found the rate coefficient and product yields to be independent of temperature for $245 < T < 300$ K.

B6. $OH + O_3$. Recommended values are based on the results of studies over a range of temperatures by Anderson and Kaufman [23], Ravishankara et al. [990], Smith et al. [1091] and Nizkorodov et al. [895] and the room

temperature measurements of Kurylo [660], Zahniser and Howard [1353], and Kulcke et al. [655]. The recommended E/R and k(298 K) values are based on averages of the individual E/R and k(298 K) values obtained in the above-mentioned studies. The values reported by Kulcke et al. [655] and Nizkorodov et al. [899] have been corrected for a minor contribution from k(HO_2 + O_3).

B7. OH + H_2. The OH + H_2 reaction has been the subject of numerous studies (see Ravishankara et al. [983] for a review of experimental and theoretical work). The recommendation is fixed to the average of nine studies at 298 K: Greiner [457], Stuhl and Niki [1129], Westenberg and de Haas [1298], Smith and Zellner [1093], Atkinson et al. [43], Overend et al. [923], Tully and Ravishankara [1198], Zellner and Steinert [1360], and Ravishankara et al. [983]. Results reported by Talukdar et al. [1153] are in excellent agreement.

B8. OH + HD. The recommendation is based on direct measurements made by Talukdar et al. [1153] using pulsed photolysis-laser induced fluorescence over the temperature range 248–418 K. The recommendation is in excellent agreement with the ratio k(OH + H_2)/k(OH + HD) = 1.65±0.05 at 298 K reported by Ehhalt et al. [375] when combined with the recommended k(OH + H_2).

B9. OH + OH. The recommendation for the OH + OH reaction is the average of six measurements near 298 K: Westenberg and de Haas [1297], McKenzie et al. [796], Clyne and Down [240], Trainor and von Rosenberg [1185], Farquharson and Smith [384], and Wagner and Zellner [1239]. The rate constants for these studies all fall between (1.4 and 2.3) × 10^{-12} cm^3 $molecule^{-1}$ s^{-1}. The temperature dependence is from Wagner and Zellner, who reported rate constants for the range T = 250–580 K.

B10. OH + HO_2. A study by Keyser [624] appears to resolve a discrepancy among low-pressure discharge flow experiments that all gave rate coefficients near 7 × 10^{-11} cm^3 $molecule^{-1}$ s^{-1} : Keyser [619], Thrush and Wilkinson [1170], Sridharan et al. [1098,1100], Temps and Wagner [1160], and Rozenshtein et al. [1010], and atmospheric pressure studies that gave rate coefficients near 11 × 10^{-11}: Lii et al. [735], Hochanadel et al. [517], DeMore [329], Cox et al. [278], Burrows et al. [178], and Kurylo et al. [666]. Laboratory measurements using a discharge flow experiment and a chemical model analysis of the results by Keyser [624] demonstrate that the previous discharge flow measurements were probably subject to interference from small amounts of O and H. In the presence of excess HO_2 these atoms generate OH and result in a rate coefficient measurement that falls below the true value.

The temperature dependence is from Keyser [624], who covered the range 254 to 382 K. A flow tube study by Schwab et al. [1043] reported k = (8.0 +3/–4) × 10^{-11}. These workers measured the concentrations of HO_2, OH, O, and H and used a computer model of the relevant reactions to test for interference. A flow tube study by Dransfeld and Wagner [365] employing an isotope labelled ^{18}OH reactant obtained k = (11±2) × 10^{-11} in good agreement with the recommendation. They attributed about half of the reactive events to isotope scrambling because control experiments with ^{16}OH gave k = 6 × 10^{-11}. It should be noted that their control experiments were subject to the errors described by Keyser [624] due to the presence of small amounts of H and O, whereas their ^{18}OH measurements were not. Kurylo et al. [666] found no evidence of significant scrambling in isotope studies of the OH and HO_2 reaction. An additional careful study of the reaction temperature dependence would be useful. Hippler and Troe [509] have analysed data for this reaction at temperatures up to 1250 K. In summary, this has historically been a difficult reaction to study. Earlier problems appear to have been resolved, as discussed above, and results now tend to converge on a central value, but the recommended value is still subject to a large uncertainty.

B11. OH + H_2O_2. The recommendation is a fit to the temperature dependence studies of Keyser [618], Sridharan et al. [1101], Wine et al. [1320], Kurylo et al. [670], and Vaghjiani et al. [1224]. The data from these studies have been revised to account for the H_2O_2 UV absorption cross section recommendations in this evaluation. The first two references contain a discussion of some possible reasons for the discrepancies with earlier work and an assessment of the impact of the new value on other kinetic studies. All of these measurements agree quite well and overlap one another. Measurements by Lamb et al. [676] agree at room temperature but indicate a quite different temperature dependence with k increasing slightly with decreasing temperature. Their data were not incorporated in the fit. Measurements at room temperature by Marinelli and Johnston [781] and Turnipseed et al. [1208] agree well with the recommendation. Hippler and Troe [509] have analysed data for this reaction at temperatures up to 1250 K.

B12. HO_2 + O_3. The recommended values are based on results of studies over a range of temperatures by DeMore [327] at 231 to 334 K, Zahniser and Howard [1353] at 245 to 365 K, Manzanares et al. [772] at 298 K, Sinha et al. [1084] at 243 to 413 K, Wang et al. [1275] at 233 to 400 K and Herndon et al. [501] at 200 to 298 K. The data of Simonaitis and Heicklen [1069] and DeMore and Tschuikow-Roux [338] were not considered. The temperature dependence studies show varying degrees of curvature in the Arrhenius plots, with the E/R decreasing at lower temperature. This is especially evident in the low temperature data of Herndon et al

where a number of measures were taken to control potential kinetic complications. The recommended E/R and
k(298 K) values are based on averages of the individual E/R and k(298 K) values. Furthermore, only data at temperatures less than 298 K were used for the E/R determination, accordingly the recommendation is not valid for T>298 K. Additional temperature dependence data are needed for this reaction over a larger range to more fully characterize the non-linear behavior of the rate constant. The mechanism of the reaction has been studied using ^{18}O labelled HO_2 by Sinha et al. [1084], who reported that the reaction occurs 75±10% via H atom transfer at 297 K and by Nelson and Zahniser [851], who reported branching ratios for H transfer vs O transfer over the range 226–355 K. They report that the H atom transfer decreases from 94±5% at 226±11 K to 88±5% at 355±8 K.

B13. $HO_2 + HO_2$. Two separate expressions are given for the rate constant for the $HO_2 + HO_2$ reaction. The effective rate constant is given by the sum of these two equations. This reaction has been shown to have a pressure-independent bimolecular component and a pressure-dependent termolecular component. Both components have negative temperature coefficients. The bimolecular expression is obtained from data of Cox and Burrows [277], Thrush and Tyndall [1167,1168], Kircher and Sander [627], Takacs and Howard [1144,1145], Sander [1016] and Kurylo et al. [672]. Data of Rozenshtein et al. [1010] are consistent with the low pressure recommendation, but they report no change in k with pressure up to 1 atm. Results of Thrush and Wilkinson [1169] and Dobis and Benson [355] are inconsistent with the recommendation. The termolecular expression is obtained from data of Sander et al. [1021], Simonaitis and Heicklen [1071], and Kurylo et al. [672] at room temperature and Kircher and Sander [627] for the temperature dependence. This equation applies to M = air. On this reaction system there is general agreement among investigators on the following aspects of the reaction at high pressure (P ~1 atm): (a) the HO_2 UV absorption cross section: Paukert and Johnston [934], Cox and Burrows [277], Hochanadel et al. [517], Sander et al. [1021], Kurylo et al. [673], and Crowley et al. [295]; (b) the rate constant at 300K: Paukert and Johnston [934], Hamilton and Lii [476], Cox and Burrows [277], Lii et al. [734], Tsuchiya and Nakamura [1190], Sander et al. [1021], Simonaitis and Heicklen [1071], Kurylo et al. [672], Andersson et al. [27], and Crowley et al. [295] (all values fall in the range (2.5 to 4.7) $\times 10^{-12}$ cm^3 $molecule^{-1}$ s^{-1}); (c) the rate constant temperature dependence: Cox and Burrows [277], Lii et al. [734], and Kircher and Sander [627]; (d) the rate constant water vapor dependence: Hamilton [475], Hochanadel et al. [516], Hamilton and Lii [476], Cox and Burrows [277], DeMore [327], Lii et al. [736], Sander et al. [1021], and Andersson et al. [27]; (e) the H/D isotope effect: Hamilton and Lii [476] and Sander et al. [1021]; and (f) the formation $H_2O_2 + O_2$ as the major products at 300 K: Su et al. [1133], Niki et al. [887], Sander et al. [1021], and Simonaitis and Heicklen [1071]. Sahetchian et al. [1014,1015] give evidence for the formation of a small amount of H_2 (~10%) at temperatures near 500 K, but Baldwin et al. [58] and Ingold [560] give evidence that the yield must be much less. Glinski and Birks [445] report an upper limit of 1% H_2 yield at a total pressure of about 50 torr and 298 K, but their experiment may have interference from wall reactions. A smaller limit to H_2 production (0.01%) was later determined in the same laboratory (Stephens et al. [1112]). For systems containing water vapor, the multiplicative factor given by Lii et al. [736] and Kircher and Sander [627] can be used: $1 + 1.4 \times 10^{-21}$ $[H_2O]$ exp(2200/T). Lightfoot et al. [732] reported atmospheric pressure measurements over the temperature range 298–777 K that are in agreement with the recommended value at room temperature but indicate an upward curvature in the Arrhenius plot at elevated temperature. A high temperature study by Hippler et al. [510] confirms the strong curvature.

C1. $O + NO_2$. The recommended values are based on the results of studies over a range of temperatures by Gierczak et al. [428], Ongstad and Birks [909], Slanger et al. [1089] and Geers-Muller and Stuhl [425] and the room temperature study of Paulson et al. [935]. In the most recent study of Gierczak et al. [428], special emphasis was placed on accurate measurement of the NO_2 concentration and on measurements at low temperatures. The results of earlier studies by Davis et al. [315] and Bemand et al. [110] were not used in deriving the recommended values either because of possible complications from decomposition of NO_2 at higher temperatures or lack of direct NO_2 detection.

C2. $O + NO_3$. Based on the study of Graham and Johnston [451] at 298 K and 329 K. While limited in temperature range, the data indicate no temperature dependence. Furthermore, by analogy with the reaction of O with NO_2, it is assumed that this rate constant is independent of temperature. Clearly, temperature-dependence studies are needed.

C3. $O + N_2O_5$. Based on Kaiser and Japar [600].

C4. $O + HNO_3$. The upper limit reported by Chapman and Wayne [212] is accepted.

C5. $O + HO_2NO_2$. The recommended value is based on the study of Chang et al. [211]. The large uncertainty in E/R and k at 298 K are due to the fact that the recommendation is based on a single study.

C6. $H + NO_2$. The recommended value of k_{298} is derived from the studies of Wagner et al. [1241], Bemand and Clyne [108], Clyne and Monkhouse [251], Michael et al. [820] and Ko and Fontijn [644]. The temperature dependence is from the studies of Wagner et al. and Ko and Fontijn. The data from Wategaonkar and Setser [1284] and Agrawalla et al. [14] were not considered.

C7. $OH + NO_3$. The recommendation is derived from an average of the results of Boodaghians et al. [137], Mellouki et al. [806], Becker et al. [91] and Mellouki et al. [809]. There are no temperature dependence data. The reaction products are probably $HO_2 + NO_2$.

C8. OH + HONO. The recommended rate expression is derived from the work of Jenkin and Cox [577], which supersedes the earlier room temperature study of Cox et al. [284]. Recent results from the Ravishankara group [173] suggest that the reaction may have a small negative temperature dependence.

C9. $OH + HNO_3$. The recent study of Brown et al. [159] furnishes the most comprehensive set of rate measurements for N_2 as the bath gas over a significant range of temperature (200–350 K) and pressure (20–500 torr). They analyzed their results in terms of the mechanism proposed by Smith et al. [1091], involving the formation of a bound, relatively long-lived $HO{\cdot}HNO_3$ complex, as well as the direct reaction channel. Studies of the effects of isotopic substitution on the reactions $OD+DNO_3$, $OH+DNO_3$, $OD+HNO_3$ and $^{18}OH+HNO_3$. by Brown et al. [158] support this mechanism and suggest that the structure of the intermediate consists of a H-bonded six-membered ring. Thus, the P dependence can be represented by combining a low pressure (bimolecular) limit, k_0, with a Lindemann-Hinshelwood expression for the p-dependence:

$$k([M],T)=k_o + \frac{k_3[M]}{1+\frac{k_3[M]}{k_2}} \qquad \left\{\begin{array}{l} k_o = 2.4x10^{-14}\exp(460/T) \\ k_2 = 2.7x10^{-17}\exp(2199/T) \\ k_3 = 6.5x10^{-34}\exp(1335/T) \end{array}\right\}$$

The coefficients k_3 and k_2 are the termolecular and high pressure limits for the "association" channel. The value of k at high pressures is the sum $k_0 + k_2$.

This expression for k([M],T) and the values of the Arrhenius parameters for k_0, k_2, and k_3 derived by Brown et al. [159] for N_2 as the bath gas constitute the recommended values for this rate coefficient. These recommended values are derived from a fit to the data of Brown et al. [159], Stachnik et al. [1103], Devolder et al. [343] and Margitan and Watson [776].

The reaction yield of NO_3 (per OH removed) is assumed to be unity at all temperatures for either reaction channel. These assumptions are supported by the isotopic studies of Brown et al. [158] and the theoretical calculations of Xia and Lin [1338].

C10. $OH + HO_2NO_2$. The recommendation for both k at 298 K and the Arrhenius expression is based upon the data of Trevor et al. [1186], Barnes et al. [64], C. A. Smith et al. [1091] and Barnes et al. [66]. Trevor et al. studied this reaction over the temperature range 246–324 K and reported a temperature invariant value of 4.0×10^{-12} cm^3 $molecule^{-1}$ s^{-1}, although a weighted least squares fit to their data yields an Arrhenius expression with an E/R value of (193±193) K. In contrast, Smith et al. studied the reaction over the temperature range 240–300 K and observed a negative temperature dependence with an E/R value of –(650±30) K. The early Barnes et al. study [64] was carried out only at room temperature and 1 torr total pressure while their later study was performed in the pressure range 1–300 torr N_2 and temperature range 268–295 K with no rate constant variation being observed. In addition, k_{298} derived in Barnes et al. [64] was revised upward in the later study from 4.1×10^{-12} to 5.0×10^{-12} due to a change in the rate constant for the reference reaction. The values of k at 298 K from the four studies are in excellent agreement. An unweighted least squares fit to the data from the above-mentioned studies yields the recommended Arrhenius expression. The less precise value for k at 298 K reported by Littlejohn and Johnston [747] is in fair agreement with the recommended value. The error limits on the recommended E/R are sufficient to encompass the results of both Trevor et al. and Smith et al. It should be noted that the values of k at 220 K deduced from the two studies differ by a factor of 2. Clearly, additional studies of k as a function of temperature and the identification of the reaction products are needed.

C11. $OH + NH_3$. The recommended value at 298 K is the average of the values reported by Stuhl [1125], Smith and Zellner [1094], Perry et al. [943], Silver and Kolb [1061], Stephens [1111] and Diau et al. [346]. The values reported by Pagsberg et al. [925] and Cox et al. [283] were not considered because these studies involved the analysis of a complex mechanism and the results are well outside the error limits implied by the above six direct studies. The results of Kurylo [660] and Hack et al. [465] were not considered because of their large discrepancies with the other direct studies (factors of 3.9 and 1.6 at room temperature, respectively). Because the Arrhenius plot displays considerable curvature, the temperature dependence is

based only on the data below 300 K, i.e., the studies of Smith and Zellner [1094] and Diau et al. [346], and the A-factor has been selected to fit the recommended room temperature value.

C12. HO_2 +NO. The recommendation for HO_2 + NO is based on the average of eight measurements of the rate constant at room temperature and below: Howard and Evenson [530], Leu [713], Howard [527], Glaschick-Schimpf et al. [440], Hack et al. [468], Thrush and Wilkinson [1170] and Jemi-Alade Thrush [574], and Seeley et al. [1047]. All of these are in quite good agreement. The results of Imamura and Washida [559] were not considered due to the relatively large uncertainty limits reported in this study. An earlier study, Burrows et al. [176] has been disregarded because of an error in the reference rate constant, k(OH + H_2O_2). The room temperature study of Rozenshtein et al. [1010] has also been disregarded due to an inadequate treatment of possible secondary reactions. The recommended Arrhenius parameters are obtained from a fit to all the data. The recommended value of k(298 K) is obtained from the Arrhenius line.

C13. HO_2 + NO_2 . Tyndall et al. [1212] obtained an upper limit to the rate coefficient of 5×10^{-16} cm^3 $molecule^{-1}$ s^{-1} based on static photolysis experiments with FTIR analysis at 296 K and 760 torr of N_2.

C14. HO_2 + NO_3. The recommendation for k_{298} is based on a weighted average of the data of Hall et al. [473], Mellouki et al. [806], Becker et al. [91] and Mellouki et al. [809]. There are insufficient data on which to base the temperature dependence of the rate coefficient. The measured branching ratios for the OH + NO_2 + O_2 channel range from 0.57 to 1.0. The most direct measurement is derived from the study of Mellouki et al. [809], which obtained a value of 1.0 +0.0/–0.3 at 298 K**.**

C15. HO_2 + NH_2. There is a fairly good agreement on the value of k at 298 K between the direct study of Kurasawa and Lesclaux [659] and the relative studies of Cheskis and Sarkisov [225] and Pagsberg et al. [925]. The recommended value is the average of the values reported in these three studies. The identity of the products is not known; however, Kurasawa and Lesclaux suggest that the most probable reaction channels give either NH_3 + O_2 or HNO + H_2O as products.

C16. N + O_2. The recommended expression is derived from a least squares fit to the data of Kistiakowsky and Volpi [629], Wilson [1310], Becker et al. [93], Westenberg et al. [1301], Clark and Wayne [233], Winkler et al. [1328] and Barnett et al. [74]. k(298 K) is derived from the Arrhenius expression and is in excellent agreement with the average of all of the room temperature determinations.

C17. N + O_3. The recommendation is based on the results of Barnett et al. [74]. The value of $(1.0 \pm 0.2) \times 10^{-16}$ cm^3 $molecule^{-1}$ s^{-1} reported by Barnett et al. should probably be considered an upper limit rather than a determination. The low values reported by Barnett et al., Stief et al. [1121] and Garvin and Broida [423] cast doubt on the much faster rates reported by Phillips and Schiff [948], and Chen and Taylor [221].

C18. N + NO. The recommended temperature dependence is based on the discharge flow-resonance fluorescence studies of Wennberg and Anderson [1293], and the discharge flow-resonance fluorescence and flash photolysis-resonance fluorescence studies of Lee et al. [695]. There is relatively poor agreement between these studies and the results of Clyne and McDermid [248], Kistiakowsky and Volpi [630], Herron [502], Phillips and Schiff [948], Lin et al. [741], Ishikawa et al. [563], Sugawara et al. [1134], Cheah and Clyne [215], Husain and Slater [549], Clyne and Ono [255], Brunning and Clyne [161] and Jeoung et al. [587].

C19. N + NO_2. The recommendation for k_{298} is from the discharge flow-resonance fluorescence study of Wennberg and Anderson [1293]. The latter study had significantly better sensitivity for $N(^4S)$ than the discharge flow-resonance fluorescence study of Clyne and Ono [255], which obtained a value about four times smaller. The results of Husain and Slater [549] and Clyne and McDermid [248] are not considered. The temperature dependence is obtained from the study of Wennberg and Anderson. In the latter study, atomic oxygen was shown to be the principal reaction product, in agreement with Clyne and McDermid. A recent study by Iwata et al. [564] suggested an upper limit of 3.3×10^{-13} cm^3 $molecule^{-1}$ s^{-1} for the corresponding reaction involving $N(^2D)$ and $N(^2P)$ atoms (sum of all reaction channels).

C20. NO + O_3. The recommended values are based on the results of studies over a range of temperatures by Birks et al. [129], Lippmann et al. [743], Ray and Watson [997], Michael et al. [814], Borders and Birks [139] and Moonen et al. [833] and the room temperature studies of Stedman and Niki [1105] and Bemand et al. [110]. The six temperature-dependent studies were given equal weighting in the recommendation by averaging over the E/R's from each individual data set. Following the Moonen et al. recommendation, the 200-K data point from their study has been excluded from the fit. All of the temperature dependence studies show some curvature in the Arrhenius plot at temperatures below 298 K. Increasing scatter between the data sets is evident at the lower temperatures. Clough and Thrush [236], Birks et al., Schurath et al. [1042], and Michael

et al. have reported individual Arrhenius parameters for the two primary reaction channels producing ground and excited molecular oxygen.

C21. $NO + NO_3$. The recommendation is based on the studies of Hammer et al. [477], Sander and Kircher [1020] and Tyndall et al. [1213], which are in excellent agreement.

C22. $NO_2 + O_3$. The recommended expression is derived from a least squares fit to the data of Davis et al. [318], Graham and Johnston [450], Huie and Herron [543], and Cox and Coker [279]. The data of Verhees and Adema [1228] and Stedman and Niki [1105] were not considered because of systematic discrepancies with the other studies.

C23. $NO_2 + NO_3$. The existence of the reaction channel forming $NO + NO_2 + O_2$ has not been firmly established. However, studies of N_2O_5 thermal decomposition that monitor NO_2 (Daniels and Johnston [304]; Johnston and Tao [591]; Cantrell et al. [196]) and NO (Hjorth et al. [512], and Cantrell et al. [199]) require reaction(s) that decompose NO_3 into $NO + O_2$. The rate constant from the first three studies is obtained from the product kK_{eq}, where K_{eq} is the equilibrium constant for $NO_2 + NO_3 \rightarrow N_2O_5$, while for the latter two studies the rate constant is obtained from the ratio $k/k(NO + NO_3)$, where $k(NO + NO_3)$ is the rate constant for the reaction $NO + NO_3 \rightarrow 2NO_2$. Using K_{eq} and $k(NO + NO_3)$ from this evaluation, the rate expression that best fits the data from all five studies is 4.5×10^{-14} exp (–1260/T) cm^3 $molecule^{-1}$ s^{-1} with an overall uncertainty factor of 2.

C24. $NO_3 + NO_3$. . The recommendation for k(298 K) is from the studies of Graham and Johnston [451] and Biggs et al. [123]. The temperature dependence is from Graham and Johnston.

C25. $NH_2 + O_2$. This reaction has several product channels which are energetically possible, including $NO + H_2O$ and HNO + OH. With the exception of the studies of Hack et al. [464] and Jayanty et al. [572] and several studies at high temperature, there is no evidence for a reaction. The following upper limits have been measured (cm^3 $molecule^{-1}$ s^{-1}): 3×10^{-18} (Lesclaux and Demissy [708]), 8×10^{-15} (Pagsberg et al. [925]), 1.5×10^{-17} (Cheskis and Sarkisov [225]), 3×10^{-18} (Lozovsky et al. [760]), 1×10^{-17} (Patrick and Golden [933]) and 7.7×10^{-18} (Michael et al. [816]) and 6×10^{-21} (Tyndall et al. [1215]). The recommendation is based on the study of Tyndall et al., which was sensitive to reaction paths leading to the products NO, NO_2 and N_2O. The reaction forming NH_2O_2 cannot be ruled out, but is apparently not important in the atmosphere.

C26. $NH_2 + O_3$. There is poor agreement among the recent studies of Cheskis et al. [224], k(298) = 1.5×10^{-13} cm^3 s^{-1}, Patrick and Golden [933], k(298 K) = 3.25×10^{-13} cm^3 s^{-1}, Hack et al. [463], 1.84×10^{-13} cm^3 s^{-1}, Bulatov et al. [166], 1.2×10^{-13} cm^3 s^{-1}, and Kurasawa and Lesclaux [658], 0.63×10^{-13} cm^3 s^{-1}. The very low value of Kurasawa and Lesclaux may be due to regeneration of NH_2 from secondary reactions (see Patrick and Golden), and it is disregarded here. The discharge flow value of Hack et al. is nearly a factor of two less than the recent Patrick and Golden flash photolysis value. The large discrepancy between Bulatov et al. and Patrick and Golden eludes explanation. The recommendation is the k(298 K) average of these four studies, and E/R is an average of Patrick and Golden (1151 K) with Hack et al. (710 K).

C27. $NH_2 + NO$. The recommended value for k at 298 K is the average of the values reported by Lesclaux et al. [710], Hancock et al. [478], Sarkisov et al. [1028], Stief et al. [1119], Andresen et al. [28] Whyte and Phillips [1302], Dreier and Wolfrum [367], Atakan et al. [33], Wolf et al. [1329], Diau et al. [344] and Imamura and Washida [559]. The results of Gordon et al. [447], Gehring et al. [426], Hack et al. [470] and Silver and Kolb [1062] were not considered because they lie at least 2 standard deviations from the average of the previous group. The results tend to separate into two groups. The flash photolysis results average 1.8×10^{-11} cm^3 $molecule^{-1}$ s^{-1} (except for the pulse radiolysis study of Gordon et al.), while those obtained using the discharge flow technique average 0.9×10^{-11} cm^3 $molecule^{-1}$ s^{-1}. The apparent discrepancy cannot be due simply to a pressure effect as the pressure ranges of the flash photolysis and discharge flow studies overlapped and none of the studies observed a pressure dependence for k. Whyte and Phillips have suggested that the difference may be due to decomposition of the adduct NH_2NO, which occurs on the timescale of the flow experiments, but not the flash experiments. There have been many studies of the temperature dependence but most have investigated the regime of interest to combustion and only two have gone below room temperature (Hack et al. from 209–505 K and Stief et al. from 216–480 K. Each study reported k to decrease with increasing temperature The recommended temperature dependence is taken from a fit of to the Stief et al. data at room temperature and below. The reaction proceeds along a complex potential energy surface, which results in product branching ratios that are strongly dependent on temperature. *Ab initio* calculations by Walch [1244] show the existence of four saddle points in the potential surface leading to $N_2 + H_2O$ without a reaction barrier. Elimination to form $OH + HN_2$ can occur at any point along the surface. While results from early studies on the branching ratio for OH formation different significantly, the most

recent studies (Hall et al., Dolson [359], Silver and Kolb [1065], Atakan et al., Stephens et al. [1110], Park and Lin [930]) agree on a value around 0.1 at 300 K, with N_2+H_2O making up the balance.

C28. NH_2 + NO_2. There have been four studies of this reaction (Hack et al. [470]; Kurasawa and Lesclaux [657]; Whyte and Phillips [1302]; and Xiang et al. [1339]). There is very poor agreement among these studies both for k at 298 K (factor of 2.3) and for the temperature dependence of k ($T^{-3.0}$ and $T^{-1.3}$). The recommended values of k at 298 K and the temperature dependence of k are averages of the results reported in these four studies. Hack et al. have shown that the predominant reaction channel (>95%) produces N_2O + H_2O. Just as for the NH_2 + NO reaction, the data for this reaction seem to indicate a factor of two discrepancy between flow and flash techniques, although the data base is much smaller.

C29. NH + NO. The recommendation is derived from the room temperature results of Hansen et al. [481], Cox et al. [274] and Harrison et al. [483]. The temperature dependence is from Harrison et al.

C30. NH + NO_2. The recommendation is derived from the temperature-dependence study of Harrison et al. [483].

C31. O_3 + HNO_2. Based on Kaiser and Japar [599] and Streit et al. [1124].

C32. N_2O_5 + H_2O. The recommended value at 298 K is based on the studies of Tuazon et al. [1193], Atkinson et al. [49] and Hjorth et al. [513]. Sverdrup et al. [1136] obtained an upper limit that is a factor of four smaller than that obtained in the other studies, but the higher upper limit is recommended because of the difficulty of distinguishing between homogeneous and heterogeneous processes in the experiment. See Table 59 for heterogeneous rate data for this reaction.

C33. N_2(A,v) + O_2. Rate constants for the overall reaction for the v=0, 1 and 2 vibrational levels of N_2(A) have been made by Dreyer et al. [368], Zipf [1374], Piper et al. [951], Iannuzzi and Kaufman [557], Thomas and Kaufman [1163] and De Sousa et al. [324]. The results of these studies are in relatively good agreement. The recommended values are (2.5±0.4), (4.0±0.6) and (4.5±0.6) ($\times 10^{-12}$ cm^3 $molecule^{-1}$ s^{-1}), from the work of De Sousa et al. The only temperature dependence data are from De Sousa et al., who obtained $k(T,v)=k(v,298K)(T/300)^{0.55}$ for v=0,1,2. The observation of high N_2O production initially reported by Zipf [1374] has not been reproduced by other groups, and the branching ratio for this channel is probably less than 0.02 (Iannuzzi et al. [556], Black et al. [132], De Sousa et al. [324], Fraser and Piper [407]). The branching ratios for the other channels are poorly established, although there is strong evidence for the formation of both $O(^3P)$ and $O_2(B^3\Sigma_u^-)$.

C34. N_2(A,v) + O_3. The only study is that of Bohmer and Hack [136], who obtained 298 K rate constants of 4.1±1.0, 4.1±1.2, 8.0±2.3, and 10±3.0 ($\times 10^{-11}$ cm^3 $molecule^{-1}$ s^{-1}) for the v=0–3 vibrational levels of N_2(A), respectively. This study determined that the NO channel accounts for about 20% of the reaction products.

D1. O + CH_3. The recommended k(298 K) is the weighted average of three measurements by Washida and Bayes [1282], Washida [1279], and Plumb and Ryan [956]. The E/R value is based on the results of Washida and Bayes [1282], who found k to be independent of temperature between 259 and 341 K.

D2. O + HCN. Because it is a very slow reaction, there are no studies of this reaction below 450 K. Davies and Thrush [313] studied this reaction between 469 and 574 K while Perry and Melius [945] studied it between 540 and 900 K. Results of Perry and Melius are in agreement with those of Davies and Thrush. Our recommendation is based on these two studies. The higher-temperature (T>1000 K) combustion-related studies Roth et al. [1007], Szekely et al. [1137], and Louge and Hanson [754]] have not been considered. This reaction has two reaction pathways: O + HCN $\rightarrow$ H + NCO, ΔH = –2 kcal/mol (k_a); and O + HCN $\rightarrow$ CO + NH (k_b), ΔH = –36 kcal/mol. The branching ratio k_a/k_b for these two channels has been measured to be ~2 at T = 860 K. The branching ratio at lower temperatures, which is likely to vary significantly with temperature, is unknown.

D3. O + C_2H_2. The value at 298 K is an average of ten measurements (Arrington et al. [31], Sullivan and Warneck [1135], Brown and Thrush [156], Hoyermann et al. [533,534], Westenberg and deHaas [1295], James and Glass [569], Stuhl and Niki [1128], Westenberg and deHaas [1299], and Aleksandrov et al. [16]). There is reasonably good agreement among these studies. Arrington et al. [31] did not observe a temperature dependence, an observation that was later shown to be erroneous by Westenberg and deHaas [1295]. Westenberg and deHaas [1295], Hoyermann et al. [534] and Aleksandrov et al. [16] are the only authors, who have measured the temperature dependence below 500 K. Westenberg and deHaas observed a curved Arrhenius plot at temperatures higher than 450 K. In the range 194–450 K, Arrhenius behavior provides an adequate description and the E/R obtained by a fit of the data from these three groups in this temperature range is recommended. The A-factor was calculated to reproduce k(298 K). This reaction can have two sets of products, i.e., C_2HO + H or CH_2 + CO. Under molecular beam conditions C_2HO has been shown to be the major product. The study by Aleksandrov et al. using a discharge flow-resonance fluorescence method (under

undefined pressure conditions) indicates that the C_2HO + H channel contributes no more than 7% to the net reaction at 298 K, while a similar study by Vinckier et al. [1234] suggests that both CH_2 and C_2HO are formed.

D4. O + H_2CO. The recommended values for A, E/R and k(298 K) are the averages of those determined by Klemm [635] (250 to 498 K) using flash photolysis-resonance fluorescence, by Klemm et al. [636] (298 to 748 K) using discharge flow-resonance fluorescence, and Chang and Barker [208] (296 to 436 K) using discharge flow-mass spectrometry techniques. All three studies are in good agreement. The k(298 K) value is also consistent with the results of Niki et al. [884], Herron and Penzhorn [504], and Mack and Thrush [762]. Although the mechanism for O + H_2CO has been considered to be the abstraction reaction yielding OH + HCO, Chang and Barker suggest that an additional channel yielding H + HCO_2 may be occurring to the extent of 30% of the total reaction. This conclusion is based on an observation of CO_2 as a product of the reaction under conditions where reactions such as O + HCO $\rightarrow$ H + CO_2 and O + HCO $\rightarrow$ OH + CO apparently do not occur. This interesting suggestion needs independent confirmation.

D5. O + CH_3CHO. The recommended k(298 K) is the average of three measurements by Cadle and Powers [185], Mack and Thrush [763], and Singleton et al. [1078], which are in good agreement. Cadle and Powers and Singleton et al. studied this reaction as a function of temperature between 298 and 475 K and obtained very similar Arrhenius parameters. The recommended E/R value was obtained by considering both sets of data. This reaction is known to proceed via H-atom abstraction (Mack and Thrush [763], Avery and Cvetanovic [50], and Singleton et al. [1078]).

D6. O_3 + C_2H_2. The database for this reaction is not well established. Room temperature measurements (Cadle and Schadt [186]; DeMore [325]; DeMore [326]; Stedman and Niki [1106]; Pate et al. [932]; and Atkinson and Aschmann [34]) disagree by as much as an order of magnitude. It is probable that secondary reactions involving destruction of ozone by radical products resulted in erroneously high values for the rate constants in several of the previous measurements. The present recommendation for k(298 K) is based on the room temperature value of Atkinson and Aschmann [34], which is the lowest value obtained and therefore perhaps the most accurate. The temperature dependence is estimated, based on an assumed A-factor of 10^{-14} cm^3 s^{-1} similar to that for the O_3 + C_2H_4 reaction and corresponding to the expected five-membered ring structure for the transition state (DeMore [325,326]). Further studies, particularly of the temperature dependence, are needed. Major products in the gas phase reaction are CO, CO_2, and HCOOH, and chemically-activated formic anhydride has been proposed as an intermediate of the reaction (DeMore [326], and DeMore and Lin [336]). The anhydride intermediates in several alkyne ozonations have been isolated in low temperature solvent experiments (DeMore and Lin [336]).

D7. O_3 + C_2H_4. The rate constant of this reaction is well established over a large temperature range, 178 to 360 K. Our recommendation is based on the data of DeMore [325], Stedman et al. [1107], Herron and Huie [503], Japar et al. [570,571], Toby et al. [1176], Su et al. [1132], Adeniji et al. [10], Kan et al. [606], Atkinson et al. [38], and Bahta et al. [55].

D8. O_3 + C_3H_6. The rate constant of this reaction is well established over the temperature range 185 to 360 K. The present recommendation is based largely on the data of Herron and Huie [503], in the temperature range 235–362 K. (Note that a typographical error in Table 2 of that paper improperly lists the lowest temperature as 250 K, rather than the correct value, 235 K.) The recommended Arrhenius expression agrees within 25% with the low temperature (185–195 K) data of DeMore [325], and is consistent with, but slightly lower (about 40%) than the data of Adeniji et al. [10] in the temperature range 260–294 K. Room temperature measurements of Cox and Penkett [290], Stedman et al. [1107], Japar et al. [570,571], and Atkinson et al. [38] are in good agreement (10% or better) with the recommendation.

D9. OH + CO. The recommendation allows for an increase in k with pressure. The zero pressure value was derived by averaging direct low pressure determinations (those listed in Baulch et al. [89]) and the values reported by Dreier and Wolfrum [366], Husain et al. [547], Ravishankara and Thompson [986], Paraskevopoulos and Irwin [927], Hofzumahaus and Stuhl [518]. The results of Jonah et al. [593] are too high and were not included. An increase in k with pressure has been observed by a large number of investigators (Overend and Paraskevopoulos [922], Perry et al. [944], Chan et al. [207], Biermann et al. [121], Cox et al. [284], Butler et al. [184], Paraskevopoulos and Irwin [926,927], DeMore [330], Hofzumahaus and Stuhl [518], Hynes et al. [554]). In addition, Niki et al. [892] have measured k relative to OH + C_2H_4 in one atmosphere of air by following CO_2 production using FTIR. The recommended 298 K value was obtained by using a weighted nonlinear least squares analysis of all pressure-dependent data in N_2 (Paraskevopoulos and Irwin [927], DeMore [330], Hofzumahaus and Stuhl [518], and Hynes et al. [554]) as well as those in air (Niki et al. [894], Hynes et al. [554]), to the form k = (A+BP)/(C+DP), where P is pressure in atmospheres. The data were best fit with D = 0 and therefore a linear form is recommended.

Previous controversy regarding the effect of small amounts of O_2 (Biermann et al. [121]) has been resolved and is attributed to secondary reactions (DeMore [330], Hofzumahaus and Stuhl [518]). The results of Butler et al. [184] have to be re-evaluated in the light of refinements in the rate coefficient for the OH + H_2O_2 reaction. The corrected rate coefficient is in approximate agreement with the recommended value. Currently, there are no indications to suggest that the presence of O_2 has any effect on the rate coefficient other than as a third body. The E/R value in the pressure range
50–760 torr has been shown to be essentially zero between 220 and 298 K by Hynes et al. [554]. Further substantiation of the temperature independence of k at 1 atm. may be worthwhile. Beno et al. [111] observe an enhancement of k with water vapor, which is in conflict with the flash photolysis studies; e.g., Ravishankara and Thompson [986], Paraskevopoulos and Irwin [927], and Hynes et al. [554]. The uncertainty factor is for 1 atm. of air.

The bimolecular channel yields H + CO_2 while the addition leads to HOCO. In the presence of O_2, the HOCO intermediate is converted to HO_2 + CO_2 (DeMore [330], Miyoshi et al. [827]). Miyoshi et al. report a rate constant for the reaction of HOCO with O_2 of ~1.5×10^{-12} cm^3 $molecule^{-1}$ s^{-1} at 298 K). Therefore, for atmospheric purposes, the products can be taken to be HO_2 and CO_2.

D10. OH + CH_4. This reaction has been extensively studied. The most recent data are from Vaghjiani and Ravishankara [1223], Saunders et al. [1030], Finlayson-Pitts et al. [396], Dunlop and Tully [370] , Mellouki et al. [812], and Gierczak et al. [434], who measured the absolute rate coefficients for this reaction using discharge flow and pulsed photolysis techniques. Sharkey and Smith [1056] have reported a high value (7.7×10^{-15} cm^3 $molecule^{-1}$ s^{-1}) for k(298 K), and this value has not been considered here. The current recommendation for k(298 K) was derived from the results of Vaghjiani and Ravishankara, Dunlop and Tully, Saunders et al., Mellouki et al., Finlayson-Pitts et al., and Gierczak et al. The temperature dependence of this rate coefficient has been measured by Vaghjiani and Ravishankara (223–420 K), Dunlop and Tully (above 298 K), Finlayson-Pitts et al. (278–378 K), and Mellouki et al. (233–343 K). Gierczak et al have extended the measurements of k to 195 K, and it appears that the rate coefficient does not strictly follow an Arrhenius expression. The recommended E/R was obtained from these results using data below 300 K. A more accurate representation of the rate constant as a function of temperature is obtained by using the three-parameter expression: $k = 2.80\times10^{-14}\, T^{0.667} \exp(-1575/T)$. This three-parameter fit may be preferred for lower stratosphere and upper troposphere calculations.

D11. OH + $^{13}CH_4$. This reaction has been studied relative to the OH + CH_4 reaction, since the ratio of the rate coefficients is the quantity needed for quantifying methane sources. Rust and Stevens [1011], Davidson et al. [308], and Cantrell et al. [200] have measured k_{12}/k_{13} at 298 K to be 1.003, 1.010, and 1.0055, respectively. Cantrell et al.'s data supersede the results of Davidson et al. The recommended value of 1.005 ± 0.002 is based on the results of Rust and Stevens and Cantrell et al. Cantrell et al. find k_{12}/k_{13} to be independent of temperature between 273 and 353 K.

D12. OH + CH_3D. The rate coefficient for this reaction has been measured between 249 and 422 K using a pulsed laser photolysis-laser induced fluorescence system by Gierczak et al. [433]. The recommended values of k (298 K) and E/R are from this study. The recommendation agrees within about 10% at 298 K with the rate constant measured by DeMore [334] in a relative rate study over the temperature range 298 – 360 K. The difference, while small in an absolute sense, is nevertheless significant for the isotopic fractionation of atmospheric CH_3D and CH_4 by OH. An earlier result of Gordon and Mulac at 416 K [448] is in good agreement with the extrapolated data of both of these determinations. However, that measurement has not been explicitly included in this recommendation because the experiments were carried out at higher temperatures and therefore are less applicable to the atmosphere. The rate coefficients for the reactions of OH with other deuterated methanes have also been measured. (Dunlop and Tully [370], Gierczak et al. [1153], Gordon and Mulac [448]).

D13. OH + H_2CO. The value for k(298 K) is the average of those determined by Niki et al. [893], Atkinson and Pitts [46], Stief et al. [1120], Yetter et al. [1345], and Temps and Wagner [1161]. The value reported by Morris and Niki [836] agrees within the stated uncertainty. There are two relative values that are not in agreement with the recommendations. The value of Niki et al. [886] relative to OH + C_2H_4 is higher, while the value of Smith [1095] relative to OH + OH is lower. The latter data are also at variance with the negligible temperature dependence observed in the two flash photolysis studies. The later report of Niki et al. [893] is assumed to supersede the earlier rate constant. The rate coefficient reported by Zabarnick et al. [1348] at and above 298 K are consistently higher than the average value recommended here, but overlap within the combined uncertainty. The combined data set suggests E/R = 0, although a slight negative temperature dependence cannot be ruled out The abstraction reaction shown in the table is the major channel (Temps and Wagner [1161], Niki et al. [892]); other channels may contribute to a small extent (Horowitz et al. [525]).

D14. OH + CH_3OH. The recommended value for k(298 K) is the average of seven direct studies (Overend and Paraskevopoulos [921], Ravishankara and Davis [979], Hagele et al. [472], Meier et al. [800], Greenhill and O'Grady [456], Wallington and Kurylo [1264], and Hess and Tully [506]). When these measurements were not at exactly 298 K, their values have been recalculated for 298 K by using the E/R recommended here. Indirect measurements by Campbell et al. [190], Barnes et al. [65], Tuazon et al. [1194] and Klopffer et al. [638] are in good agreement with the recommended value. The temperature dependence of k has been measured by Hagele et al., Meier et al., Greenhill and O'Grady, Wallington and Kurylo, and Hess and Tully. The recommended value of E/R was calculated using the results obtained in the temperature range of 240 to 400 K by Greenhill and O'Grady [456], Wallington and Kurylo [1264], Hess and Tully, Meier et al., and Haegle et al. Hess and Tully report a curved Arrhenius plot over the temperature range 298 – 1000 K, while Meier et al. do not observe such a curvature. This reaction has two pathways: abstraction of the H-atom from the methyl group to give CH_2OH + H_2O or from the OH group to give CH_3O + H_2O. The results of Hagele et al., Meier et al., and Hess and Tully suggest that H abstraction from the methyl group to give CH_2OH + H_2O is the dominant channel below room temperature. At 298 K, for example, the branching ratio for the formation of CH_2OH is about 0.85 and increases as the temperature decreases. In the Earth's atmosphere, the eventual products of OH + CH_3OH reaction are the same: CH_2O and HO_2.

D15. OH + CH_3OOH. The recommended value for k(298 K) is the average of the rate coefficients measured by Niki et al. [891] and Vaghjiani and Ravishankara [1222], which differ by nearly a factor of two. Niki et al. measured the rate coefficient relative to that for OH with C_2H_4 (= 8.0×10^{-12} cm^3 $molecule^{-1}$ s^{-1}) by monitoring CH_3OOH disappearance using an FTIR system. Vaghjiani and Ravishankara monitored the disappearance of OH, OD, and ^{18}OH in excess CH_3OOH in a pulsed photolysis-LIF system. They measured k between 203 and 423 K and report a negative activation energy with E/R = –190 K; the recommended E/R is based on their results. The reaction of OH with CH_3OOH occurs via abstraction of H from the oxygen end to produce the CH_3OO radical and from the CH_3 group to produce the CH_2OOH radical, as originally proposed by Niki et al. and confirmed by Vaghjiani and Ravishankara. CH_2OOH is unstable and falls apart to CH_2O and OH within a few microseconds. The possible reaction of CH_2OOH with O_2 is unimportant under atmospheric conditions (Vaghjiani and Ravishankara). The recommended branching ratios are,

$$OH + CH_3OOH \rightarrow CH_3O_2 + H_2O \qquad \text{(a) } 70\%$$

$$OH + CH_3OOH \rightarrow CH_2OOH + H_2O \qquad \text{(b) } 30\%,$$

(from Vaghjiani and Ravishankara) and are nearly independent of temperature.

D16. OH + HC(O)OH. The recommended value of k(298 K) is the average of those measured by Zetzsch and Stuhl [1363], Wine et al. [1311], Jolly et al. [592], Dagaut et al. [303], and Singleton et al. [1083]. The temperature dependence of k has been studied by Wine et al. and by Singleton et al., who observed k to be essentially independent of T.

Wine et al. found the rate coefficient for the OH + HC(O)OH reaction to be the same as that for OH + DC(O)OH reaction. Jolly et al. found the formic acid dimer to be unreactive toward OH, i.e., abstraction of the H atom attached to C was not the major pathway for the reaction. A comprehensive study of Singleton et al. showed that reactivity of HC(O)OH is essentially the same as that of DC(O)OH, but DC(O)OD reacts much slower than HC(O)OH and DC(O)OH. These observations show that the reaction proceeds via abstraction of the acidic H atom. Wine et al. and Jolly et al. also found that H atoms are produced in the reaction, which is consistent with the formation of HC(O)O, which would rapidly fall apart to CO_2 and H. End product studies are also consistent with the formation of CO_2 and H_2O in this reaction (Singleton et al. [1083]). The products of this reaction would be mostly HC(O)O and H_2O. The fate of HC(O)O in the atmosphere will be to give HO_2 either directly via reaction with O_2 or via thermal decomposition to H atom, which adds to O_2.

Wine et al. have suggested that, in the atmosphere, the formic acid could be hydrogen bonded to a water molecule and its reactivity with OH could be lowered because the hydrogen bonded water would obstruct the abstraction of the H atom. This suggestion needs to be checked.

D17. OH + HCN. This reaction is pressure dependent. The recommended value is the high pressure limit measured by Fritz et al. [414] using a laser photolysis-resonance fluorescence apparatus. Phillips [947] studied this reaction using a discharge flow apparatus at low pressures and found the rate coefficient to have reached the high pressure limit at ~10 torr at 298 K. Fritz et al.'s results contradict this finding. They agree with Phillip's measured value, within a factor of two, at 7 torr, but they find k to increase further with pressure. The products of the reaction are unknown.

D18. OH + C_2H_6. There are nineteen studies of this reaction at 298 K (Greiner [458], Howard and Evenson [529], Overend et al. [923], Lee and Tang [697], Leu [713], Tully et al. [1199], Jeong et al. [584], Tully et al.

[1197], Nielsen et al. [879], Zabarnick et al. [1348], Wallington et al. [1266], Smith et al. [1091], Baulch et al. [88], Bourmada et al. [144], Abbatt et al. [2], Schiffman et al. [1033], Talukdar et al. [1155], Sharkey and Smith [1056] and Anderson and Stephens [24]). The recommended value is obtained by averaging the results of the recent investigations by Tully et al., Wallington et al., Abbatt et al., Schiffman et al., Talukdar et al. and Anderson and Stephens. The results of Sharkey and Smith are approximately 20% higher than those recommended here. When the measurements were not carried out at exactly 298 K, we have recalculated k using an E/R of 1070 K. The temperature dependence of the rate coefficient below 298 K has been measured only by Jeong et al., Wallington et al., Talukdar et al. and Anderson and Stephens. The last three studies are in good agreement. The recommended E/R is obtained from an analysis of the data of these three studies. The ratio of the rate coefficients for OH reactions with C_2H_6 and C_3H_8 has been measured by Finlayson-Pitts [396]. Our recommendations are in reasonable agreement with this ratio. Crowley et al. [294] have measured k at 247, 294, and 303 K, and the results are in agreement with the recommendations.

D19. OH + C_3H_8. There are many measurements of the rate coefficients at 298 K. In this evaluation we have considered only the direct measurements (Greiner [458], Tully et al. [1199], Droege and Tully [369], Schmidt et al. [1037], Baulch et al. [88], Bradley et al. [147], Abbatt et al. [2], Schiffman et al. [1033], Talukdar et al. [1155], Anderson and Stephens [24] and Mellouki et al. [812]). The 298 K value is the average of these ten studies. Greiner, Tully et al. [1196], Droege and Tully, Talukdar et al. and Mellouki et al. have measured the temperature dependence of this reaction. The recommended E/R was obtained from a linear least squares analysis of the data of Droege and Tully below 400 K and the data of Talukdar et al., Anderson and Stephens, and Mellouki et al. The A-factor was adjusted to reproduce k(298 K). This reaction has two possible channels, i.e., abstraction of the primary and the secondary H-atom. Therefore, non-Arrhenius behavior is exhibited over a wide temperature range, as shown by Tully et al. and Droege and Tully. The branching ratios were estimated from the latter study:

$$k_{primary} = 6.3 \times 10^{-12} \exp(-1050/T) \text{ cm}^3 \text{ molecule}^{-1} \text{ s}^{-1}$$

$$k_{secondary} = 6.3 \times 10^{-12} \exp(-580/T) \text{ cm}^3 \text{ molecule}^{-1} \text{ s}^{-1}$$

These numbers are in reasonable agreement with the older data of Greiner. The ratio of the rate coefficients for OH reactions with C_2H_6 and C_3H_8 has been measured by Finlayson-Pitts et al. [396]. Our recommendations are in reasonable agreement with this ratio.

D20. OH + CH_3CHO. There are six measurements of this rate coefficient at 298 K (Morris et al. [838], Niki et al. [886], Atkinson and Pitts [46], Kerr and Sheppard [613], Semmes et al. [1054], and Michael et al. [815]). The recommended value of k(298 K) is the average of these measurements. Atkinson and Pitts, Semmes et al., and Michael et al. measured the temperature dependence of this rate coefficient and found it to exhibit a negative temperature dependence. The recommended E/R is the average value of these studies. The A-factor has been adjusted to yield the recommended value of k(298 K).

D21. OH + C_2H_5OH. The recommended value for k(298 K) is the average of those reported by Campbell et al. [190], Overend and Paraskevopoulos [921], Ravishankara and Davis [979], Cox and Goldstone [288], Kerr and Stocker [614], Wallington and Kurylo [1264], and Hess and Tully [505]. The value reported by Meier et al. is nearly a factor of two lower than that recommended here. The recommended value of E/R was obtained by using the data of Wallington and Kurylo, Hess and Tully, and Meier et al. The temperature dependent rate coefficient values of Meier et al. were assumed to have the same systematic error that , hence, would not be reflected in the derivation of the E/R value. The A-factor has been adjusted to yield the recommended value of k(298 K). This reaction has three possible product channels: (a) $CH_3CH_2O + H_2O$, (b) $CH_3CHOH + H_2O$, and (c) $CH_2CH_2OH+H_2O$. At atmospheric temperatures, channel (b) is the major pathway (Meier et al. [801], Hess and Tully [505]), accounting for more than 75% of the reaction. The branching ration for channel (b) is expected to increase with decreasing temperature, based on the work of Hess and Tully [505]. The CH_3CHOH radical that is produced in channel (b) and CH_3CH_2O radical formed in channel (a) will both rapidly react with O_2 leading to CH_3CHO and HO_2. However, the CH_2CH_2OH radical produced in channel (c) will lead to a different set of products in the atmosphere. The exact values for these reaction pathways under atmospheric temperatures have not been quantified. Extrapolations of the higher temperature data to atmospheric temperatures may not be valid.

D22. OH + $CH_3C(O)OH$. The recommended k(298K) is the average of the values obtained by Dagaut et al. [303] and Singleton et al. [1082]. The earlier results of Zetzsch and Stuhl [1363] are lower than these values, but within the uncertainty of the recommended value. The temperature dependence has been studied by Dagaut et al., who observe a very slight increase in k with temperature between 298 and 440 K and by Singleton et al., who observe a significant decrease with increase in temperature between 298 and 446 K. Further, Singleton et al. observe that the Arrhenius plot is curved. While Dagaut et al. observed that the acetic acid dimer reacts twice as fast as the monomer, Singleton et al. found the dimer to be essentially unreactive toward OH! The

latter observations are consistent with the mechanism for the OH + HC(O)OH reaction, which is discussed in the note for that reaction. It is also consistent with the decrease in reactivity upon D substitution on the carboxylic site and no change upon substitution on the methyl group (Singleton et al. [1082]). Thus, there is some uncertainty as to the T dependence and the reaction mechanism. Here we recommend a slightly negative T dependence, based on an average of both temperature dependence studies but with an uncertainty that encompasses both the studies. The A factor and E/R suggest that this reaction may not be a simple metathesis reaction. Based on the analogy with OH + HC(O)OH reaction and the evidence of Singleton et al., the products are expected to be mostly $CH_3C(O)O + H_2O$. In the atmosphere, $CH_3C(O)O$ is expected to give $CH_3 + CO_2$.

D23. OH + $CH_3C(O)CH_3$. The rate coefficient for this reaction has been measured at temperatures close to 298 K by Cox et al. [286], Zetzsch [1362], Chiorboli et al. [227], Kerr and Stocker [614], Wallington and Kurylo [1265], LeCalve et al. [690], Wollenhaupt et al. [1330], and Gierczak et al. [429]. Cox reported only an upper limit of $<5 \times 10^{-13}$ cm^3 $molecule^{-1}s^{-1}$, which is consistent with this recommendation. The primary aim of Chiorboli et al. was to examine the atmospheric degradation of styrene, which produces acetone. They employed a relative rate measurement and reported a value of k(298 K) that is almost three times faster than the recommended value. Because of possible complications in their system, we have not included their results in arriving at the recommended value. Wallington and Kurylo, LeCalve et al., Wollenhaupt et al. and Gierczak et al. have reported k as a function of temperature; all these studies directly measured the rate constant using the pulsed photolysis method where the temporal profile of OH was measured using resonance fluorescence or laser induced fluorescence. The extensive data of Wollenhaupt et al. and Gierczak et al. seem to show that this rate coefficient does not follow an Arrhenius expression. The results of LeCalve et al. and Wallington et al. are in general agreement with the results of Wollenhaupt et al. and Gierczak et al. The non-Arrhenius behavior was not evident in the results of Wallington et al. and LeCalve et al. because they measured the rate constant at a few temperatures and did not explore temperature below 240 K, where the curvature becomes increasingly evident. The following recommendation reproduces all reported data, except that of Chiorboli et al. within the recommended uncertainty of 25% at all temperatures:

$$k(T) = 1.33 \times 10^{-13} + 3.82 \times 10^{-11}\exp(-2000/T)$$

This reaction can proceed via the abstraction of an H atom or via the formation of a complex that decomposes to give many different products, which include $CH_3 + CH_3C(O)OH$, $CH_3OH + CH_3C(O)$, $CH_4 + CH_3CO_2$, $H_2O + CH_3C(O)CH_2$. The branching ratios for the formation of different sets of products will, most likely, vary with temperature. Wollenhaupt and Crowley (2000) have deduced that CH_3 radicals are produced with a yield of ~50% at 298 K and ~30% at 233 K. A similar branching ratio has also been reported by Vasvari et al. [1227]. The results of Gierczak et al. on OH + $CD_3C(O)CD_3$ reaction, whose rate coefficient nearly obeys an Arrhenius expression between 240 and 400 K and is nearly an order of magnitude smaller than the non-deuterated analog at 250 K, suggests that H abstraction may be the dominant channel. Because of this conflicting evidence, we have not recommended the products of this reaction.

D24. OH + CH_3CN. This rate coefficient has been measured as a function of temperature by Harris et al. [482] between 298 and 424 K, Kurylo and Knable [667] between 250 and 363 K, Rhasa [1002] between 295 and 520 K, and Hynes and Wine [552] between 256 and 388 K. In addition, the 298 K value has been measured by Poulet et al. [961]. The 298 K results of Harris et al. are in disagreement with all other measurements and therefore have not been included. The recommended 298 K value is a weighted average of all other studies. The temperature dependence was computed using the results of Kurylo and Knable, the lower temperature values (i.e., 295–391 K) of Rhasa, and the data of Hynes and Wine. Three points are worth noting: (a) Rhasa observed a curved Arrhenius plot even in the temperature range of 295 to 520 K, and therefore extrapolation of the recommended expression could lead to large errors; (b) Hynes and Wine observed a pressure dependent increase of k(298 K) that levels off at about 1 atmosphere, and this observation is contradictory to the results of other investigations; (c) Hynes and Wine have carried out extensive pressure, temperature, O_2 concentration, and isotope variations in this reaction. Hynes and Wine postulate that the reaction proceeds via addition as well as abstraction pathways. They observe OH regeneration in the presence of O_2. The recommended k(298 K) and E/R are applicable for only lower tropospheric conditions. Because of the unresolved questions of pressure dependence and reaction mechanism, the recommended value may not be applicable under upper tropospheric and stratospheric conditions.

D25. OH + CH_3ONO_2. The rate coefficient for this reaction at 298 K has been measured by Kerr and Stocker [614], Nielsen et al. [881], Gaffney et al. [417], Talukdar et al. [417], Kakesu et al. [604] and Shallcross et al. [1055]. The results of Kerr and Stocker and of Nielsen et al. are a factor of ten higher than those reported by the other groups There are no obvious reasons for the reported differences but the lower values are preferred for a number of reasons. Firstly, Talukdar et al. have carried out a large number of checks which ruled out possible effects in their system due to the regeneration of OH via secondary reactions, to bath gas pressure,

and to formation of an adduct that could undergo further reaction in the presence of oxygen. Secondly, the lower values are more consistent with reactivity predictions of Atkinson and Aschmann [36], who assumed that the series of nitrate reactions proceed by H-atom abstraction pathways. Kinetic measurements of Talukdar et al. performed with isotopically substituted hydroxyl radical (OH, ^{18}OH, and OD) and methyl nitrate (CH_3ONO_2 and CD_3ONO_2) are all consistent with this reaction proceeding via an H-atom abstraction pathway.. Accordingly, the recommended value of k(298 K) is based on an average of the values given by Gaffney et al, Talukdar et al., Kakesu et al. and Shallcross et al. Further verification of the reaction mechanism by identification of the products of the reaction is needed. The temperature dependence of the rate coefficient has been measured by Nielsen et al, Talukdar et al and Shallcross et al. While Nielsen et al. report a negative activation energy, Talukdar et al. and Shallcross et al. report positive values. For the reasons given above, the temperature dependence recommended here is based on an average of Talukdar et al. and Shallcross et al.

D26. OH + $CH_3C(O)O_2NO_2$ (PAN). This reaction has been studied by four groups, Winer et al. [1326], Wallington et al. [1248], Tsalkani et al. [1187], and Talukdar et al. [1152]. Winer et al. obtained only an upper limit for the rate coefficient. Tsalkani et al. noted that their system was very ill-behaved and obtained a value of k(298 K) that is a factor of ~2 lower than that obtained by Wallington et al. The pulsed photolysis study of Wallington et al. yielded consistent results, but PAN was not directly measured and photodissociation of H_2O in the vacuum UV, where PAN absorbs strongly, was used as the OH source. The recent study of Talukdar et al. [1152] yielded much lower rate coefficients. These investigators measured the PAN concentration directly in their system, minimized secondary reactions due to the photodissociation of PAN, and carried out extensive tests for decomposition of PAN, impurities, and secondary reactions. The recommended upper limit is a factor two higher than the highest value measured by Talukdar et al. at 298 K and at 272 K. The quoted upper limit is expected to be valid at all atmospheric temperatures. The products of the reaction are not known. Further measurements of the rate coefficients and information on the reaction pathways are needed.

D27. OH + $C_2H_5ONO_2$. The rate constant for this reaction at 298 K has been measured by Kerr and Stocker [614], Nielsen et al. [881], Talukdar et al. [1154], Kakesu et al. [604], and Shallcross et al. [1055]. As in the case of the reaction of OH with CH_3ONO_2, the results of Kerr and Stocker and of Nielsen et al. are larger (by a factor of 3) than those of the more recent studies . The reasons for the differences are not clear. Because of the exhaustive tests carried out (see the note for the OH + CH_3ONO_2 reaction), the values of Talukdar et al., Kakesu et al., and Shallcross et al. are recommended, with a large uncertainty. Nielsen et al., Talukdar et al., and Shallcross et al. have measured the rate constant as a function of temperature. As with the OH + CH_3ONO_2 reaction, Nielsen et al. report a negative activation energy while Talukdar et al. and Shallcross et al. have observed a small positive activation energy. Talukdar et al. note that the rate coefficient for this reaction does not strictly follow Arrhenius behavior, consistent with the abstraction of both the primary and the secondary H atoms. Above 298 K, E/R values measured by Shallcross et al and Talukdar et al. are in excellent agreement. Only Talukdar et al have kinetics data below 298 K and the recommended E/R value was obtained by fitting the rate coefficients measured by Talukdar et al. at ≤ 298 K. The large uncertainty encompasses the results of Kerr and Stocker and Nielsen et al.

D28. OH + 1-$C_3H_7ONO_2$. The reaction has been studied by Kerr and Stocker [614] and Atkinson and Aschmann [36] at room temperature and by Nielsen et al. [881] between 298 and 368 K. The results of the three studies are in good agreement at room temperature. Nielsen et al. find that the reaction is temperature independent within the measurement uncertainty over the range studied. However as discussed above, the Nielson et al. results for the analogous reactions of OH with CH_3ONO_2 and $C_2H_5ONO_2$, yield negative activation energies that disagree with the positive activation energies obtained by others. Judging from the E/R's for the analogous reactions, one might expect the E/R for this reaction to be on the order of 300 kcal/mole. Accordingly, we place a large uncertainty on the recommended temperature dependence. A thorough investigation of the temperature dependence of this reaction is needed.

D29. OH + 2-$C_3H_7ONO_2$. The reaction has been studied by Atkinson and Aschman [36], Atkinson et al [37] and Becker and Wirtz [98] at room temperature and by Talukdar et al. [1117] over the range 233 and 395 K. The results of Atkinson and Aschmann supersede those of Atkinson et al. There is fair agreement between the results of the three studies at room temperature, with roughly a factor of two spread in the values. The recommendation is based on an average of the room temperature values and the E/R measured by Talukdar et al.

D30. HO_2 + CH_2O. There is sufficient evidence to suggest that HO_2 adds to CH_2O (Su et al. [1131,1133], Veyret et al. [1231], Zabel et al. [1349], Barnes et al. [70], and Veyret et al. [1230]). The recommended k(298 K) is the average of values obtained by Su et al. [1131], Veyret et al. [1231], and Veyret et al. [1230]. The temperature dependence observed by Veyret et al. [1230] is recommended. The value reported by Barnes et al. at 273 K is consistent with this recommendation. The adduct HO_2•CH_2O seems to isomerize to $HOCH_2OO$ reasonably

rapidly and reversibly. There is a great deal of discrepancy between measured values of the equilibrium constants for this reaction.

D31. $HO_2 + CH_3O_2$. This recommendation is from Tyndall et al. [1210]. The kinetics of this reaction has been studied by using UV absorption following pulsed photolytic production of the radicals. These authors first analyzed the available data for the products of the reaction and concluded that the major products are CH_3OOH and O_2. They used this product yield information with their evaluated UV absorption cross sections for HO_2 and CH_3O_2 to reanalyze the UV absorption profiles measured in kinetics experiments by Dagaut et al. [301] and by Lightfoot et al. [733], the two groups that carried out the most extensive studies. They found that rate coefficients reported by these two groups need to be increased by ~20%. The recommended value is based on the average of the corrected data from these two groups. The temperature dependence was evaluated by Tyndall et al. by assuming that the absorption cross sections of CH_3O_2 and HO_2 are independent of temperature at the wavelengths used for the kinetics studies.

D32. $HO_2 + C_2H_5O_2$. The recommended value is the weighted average of those measured by Cattell et al. [205], Dagaut et al. [302], Fenter et al. [389], and Maricq and Szente [778]. In all experiments the rate coefficient was obtained by modeling the reaction system. Also, the calculated rate coefficients depended on the UV absorption cross sections of both $C_2H_5O_2$ and HO_2. The absorption cross section of $C_2H_5O_2$ is not well-defined. The value reported by Dagaut et al. would be ~30% higher if the cross sections used by Maricq and Szente were used. The recommended E/R is that measured by Dagaut et al., Fenter et al., and Maricq and Szente. Wallington and Japar [1263] have shown that $C_2H_5O_2H$ and O_2 are the only products of this reaction.

D33. $HO_2 + CH_3C(O)O_2$. This recommendation is from Tyndall et al. [1210]. This reaction has two sets of products:

$$CH_3C(O)O_2 + HO_2 \xrightarrow{k_a} CH_3C(O)O_2H + O_2 \text{ (a)}$$

$$CH_3C(O)O_2 + HO_2 \xrightarrow{k_b} CH_3C(O)OH + O_3 \text{ (b)}$$

The majority of the reaction proceeds via channel (a), but there is clear evidence for channel (b). Tyndall et al. reevaluated the available data on end products of this reaction, particularly those of Crawford et al. [293], Moortgat et al. [834], and Horie and Moortgat [522], and concluded that channel (a) contributes ~80% while channel (b) contributes ~20% at 298 K. They also concluded that $k_a/k_b = 37 \times \exp(-660/T)$ with a large uncertainty in this value. They derived the overall rate coefficient for this reaction, which has been measured only by following the radical concentrations via UV absorption. They based their recommendation mostly on the results of Moortgat et al [834] and Tomas et al. [1180].

D34. $HO_2 + CH_3C(O)CH_2O_2$. This recommendation is from Tyndall et al. [1210]. This reaction has been studied by only Bridier et al. [152] and Tyndall et al. based their recommendation on this one study.

D35. $NO_3 + CO$. The upper limit is based on the results of Hjorth et al. [514], who monitored isotopically labeled CO loss in the presence of NO_3 by FTIR. Burrows et al. [180] obtained an upper limit of 4×10^{-16} cm^3 molecule^{-1} s^{-1}, which is consistent with the Hjorth et al. study. Products are expected to be $NO_2 + CO_2$, if the reaction occurs.

D36. $NO_3 + CH_2O$. There are three measurements of this rate coefficient at 298 K: Atkinson et al. [48], Cantrell et al. [201], and Hjorth et al. [515]. The value reported by Atkinson et al. [48], $k = (3.23 \pm 0.26) \times 10^{-16}$ cm^3 molecule^{-1} s^{-1}, is corrected to 5.8×10^{-16} cm^3 molecule^{-1} s^{-1} to account for the different value of the equilibrium constant for the $NO_3 + NO_2 \rightarrow N_2O_5$ reaction that was measured subsequent to this study by the same group using the same apparatus. This correction is in accordance with their suggestion (Tuazon et al. [1195]). The values reported by Cantrell et al. and Hjorth et al., $k = 6.3 \times 10^{-16}$ cm^3 molecule^{-1} s^{-1} and $(5.4\pm1.1) \times 10^{-16}$ cm^3 molecule^{-1} s^{-1}, respectively, are in good agreement with the corrected value of Atkinson et al. The recommended value is the average of these three studies. Cantrell et al. have good evidence to suggest that HNO_3 and CHO are the products of this reaction. The temperature dependence of this rate coefficient is unknown, but comparison with the analogous $NO_3 + CH_3CHO$ reaction suggests a large E/R.

D37. $NO_3 + CH_3CHO$. There are four measurements of this rate constant: Morris and Niki [837], Atkinson et al. [48], Cantrell et al. [195], and Dlugokencky and Howard [349]. The value reported by Atkinson et al. [48], $k = (1.34\pm0.28) \times 10^{-15}$ cm^3 molecule^{-1} s^{-1}, is corrected to 2.4×10^{-15} cm^3 molecule^{-1} s^{-1} as discussed for the $NO_3 + H_2CO$ reaction above and as suggested by Tuazon et al. [1195]. The recommended value is the average of the values obtained by Atkinson et al., Cantrell et al., and Dlugokencky and Howard. The results of Morris and Niki agree with the recommended value when their original data is re-analyzed using a more recent value for the equilibrium constant for the reaction $NO_2 + NO_3 \leftrightarrow N_2O_5$ as shown by Dlugokencky and

Howard. Dlugokencky and Howard have studied the temperature dependence of this reaction. Their measured value of E/R is recommended. The A-factor has been calculated to yield the k(298K) recommended here. Morris and Niki, and Cantrell et al. observed the formation of HNO_3 and PAN in their studies, which strongly suggests that HNO_3 and CH_3CO are the products of this reaction.

D38. $CH_3 + O_2$. This bimolecular reaction is not expected to be important, based on the results of Baldwin and Golden [57], who found $k < 5 \times 10^{-17}$ cm^3 molecule^{-1} s^{-1} for temperatures up to 1200 K. Klais et al. [632] failed to detect OH (via $CH_3 + O_2 \rightarrow CH_2O + OH$) at 368 K and placed an upper limit of 3×10^{-16} cm^3 molecule^{-1} s^{-1} for this rate coefficient. Bhaskaran et al. [116] measured $k = 1\times10^{-11} \exp(-12{,}900/T)$ cm^3 molecule^{-1} s^{-1} for $1800 < T < 2200$ K. The latter two studies thus support the results of Baldwin and Golden. Studies by Selzer and Bayes [1053] and Plumb and Ryan [956] confirm the low value for this rate coefficient. Previous studies of Washida and Bayes [1282] are superseded by those of Selzer and Bayes. Plumb and Ryan have placed an upper limit of 3×10^{-16} cm^3 molecule^{-1} s^{-1} based on their inability to find HCHO in their experiments. A study by Zellner and Ewig [1359] suggests that this reaction is important at combustion temperature but is unimportant for the atmosphere.

D39. $CH_3 + O_3$. The recommended A-factor and E/R are those obtained from the results of Ogryzlo et al. [904]. The results of Simonaitis and Heicklen [1070], based on an analysis of a complex system, are not used. Washida et al. [1281] used $O + C_2H_4$ as the source of CH_3. Studies on the $O + C_2H_4$ reaction (Schmoltner et al. [1038], Kleinermanns and Luntz [634], Hunziker et al. [544], and Inoue and Akimoto [561]) have shown this reaction to be a poor source of CH_3. Therefore, the results of Washida et al. are also not used.

D40. $HCO + O_2$. The value of k(298 K) is the average of the determinations by Washida et al. [1283], Shibuya et al. [1059], Veyret and Lesclaux [1229], Langford and Moore [680], Nesbitt et al. [859], Temps et al. [1161] and Ninomiya et al. [896]. There are three measurements of k where HCO was monitored via the intracavity dye laser absorption technique (Reilly et al. [998], Nadtochenko et al. [844], and Gill et al. [435]). Even though these studies agree with the recent measurements of Nesbitt et al., the only recent measurement to obtain a low value, they have not been included in deriving the recommended value of k(298 K). However, the uncertainty has been increased to overlap with those measurements. The main reason for not including them in the average is the possible depletion of O_2 in those static systems (as suggested by Veyret and Lesclaux). Also, these experiments were designed more for the study of photochemistry than kinetics. The temperature dependence of this rate coefficient has been measured by Veyret and Lesclaux, Timonen et al. [1175] and Nesbitt et al. While Timonen et al. obtain a slightly positive activation energy, Veyret and Lesclaux, and Nesbitt et al. measure slightly negative activation energy. It is very likely that the Arrhenius expression is curved. We recommend an E/R value of zero, with an uncertainty of 100 K. Veyret and Lesclaux preferred a T^n form ($k = 5.5 \times 10^{-11}\ T^{-(0.4\pm0.3)}$ cm^3 molecule^{-1} s^{-1}). Hsu et al.[535] suggest that this reaction proceeds via addition at low temperature and abstraction at higher temperatures.

D41. $CH_2OH + O_2$. The rate coefficient was first measured directly by Radford [973] by detecting the HO_2 product in a laser magnetic resonance spectrometer. The wall loss of CH_2OH could have introduced a large error in this measurement. Radford also showed that the previous measurement of Avramenko and Kolesnikova [52] was in error. Wang et al. [1273] measured a value of 1.4×10^{-12} cm^3 molecule^{-1} s^{-1} by detecting the HO_2 product. Recently, Dobe et al. [352], Grotheer et al. [460], Payne et al. [937], Grotheer et al. [461] and Nesbitt et al. [862] have measured k(298 K) to be close to 1.0×10^{-11} cm^3 molecule^{-1} s^{-1} under conditions where wall losses are small. This reaction appears to exhibit a very complex temperature dependence. Based on the recent data of Grotheer et al. [461] and Nesbitt et al. [862], k appears to increase from 200 K to approximately 250 K in an Arrhenius fashion, levels off at approximately 300 K, decreases from 300 to 500 K, and finally increases as temperature is increased. This complex temperature dependence is believed to be due to the formation of a $CH_2(OH)\bullet O_2$ adduct which can isomerize to $CH_2O\bullet HO_2$ or decompose to reactants. The $CH_2O\bullet HO_2$ isomer can also decompose to CH_2O and HO_2 or reform the original adduct. At temperatures less than 250 K, the data of Nesbitt et al. suggests an E/R value of ~1700 K. For atmospheric purposes, the value E/R = 0 is appropriate.

D42. $CH_3O + O_2$. The recommended value for k(298 K) is the average of those reported by Lorenz et al. [752] and Wantuck et al. [1276]. The recommended E/R was obtained using the results of Gutman et al. [462] (413 to 608 K), Lorenz et al. [752] (298 to 450 K), and Wantuck et al. [1276] (298 to 498 K). These investigators have measured k directly under pseudo–first order conditions by following CH_3O via laser induced fluorescence. Wantuck et al. measured k up to 973 K and found the Arrhenius plot to be curved; only their lower temperature data are used in the fit to obtain E/R. The A factor has been adjusted to reproduce the recommended k(298 K). The previous high temperature measurements (Barker et al. [61] and Batt and Robinson [85]) are in reasonable agreement with the derived expression. This value is consistent with the

298 K results of Cox et al. [285], obtained from an end product analysis study, and with the upper limit measured by Sanders et al. [1025]. The A-factor appears low for a hydrogen atom transfer reaction. The reaction may be more complicated than a simple abstraction. At 298 K, the products of this reaction are HO_2 and CH_2O, as shown by Niki et al. [889].

D43. CH_3O + NO. The reaction of CH_3O with NO proceeds mainly via addition to form CH_3ONO (Batt et al. [84], Wiebe and Heicklen [1305], Frost and Smith [415], and Ohmori et al. [905]). However, a fraction of the energized CH_3ONO adducts decompose to CH_2O + HNO, and appear to be a bimolecular channel. This reaction has been investigated recently by direct detection of CH_3O via laser-induced fluorescence (Zellner [1357]; Frost and Smith [415]; Ohmori et al. [905]). The previous end-product studies (Batt et al. [84], Wiebe and Heicklen [1305]) are generally consistent with this conclusion. Since the fraction of the CH_3ONO adduct that falls apart to CH_2O + HNO decreases with increases in pressure and decreases in temperature, it is not possible to derive a "bimolecular" rate coefficient. A value of $k < 8\times10^{-12}$ cm^3 $molecule^{-1}$ s^{-1} can be deduced from the work of Frost and Smith [415] and Ohmori et al.[905] for lower atmospheric conditions.

D44. $CH_3O + NO_2$. The reaction of CH_3O with NO_2 proceeds mainly via the formation of CH_3ONO_2. However, a fraction of the energized adducts fall apart to yield $CH_2O + HNO_2$. The bimolecular rate coefficient reported here is for the fraction of the reaction that yields CH_2O and HNO_2. It is not meant to represent a bimolecular metathesis reaction. The recommended value was derived from the study of McCaulley et al.[794] and is discussed in the section on association reactions.

D45. $CH_3O_2 + O_3$. This recommendation is from Tyndall et al. [1210]. Their recommendation is based mostly on the recent study by Tyndall et al. [1220]. The temperature dependence is based on the assumption that the only possible reaction which can occur is the O atom transfer from the CH_3O_2 radical and that the activation energy of ~2 kcal mol^{-1} for this O-atom transfer is similar to that in the $HO_2 + O_3$ reaction.

D46. $CH_3O_2 + CH_3O_2$. This recommendation is from Tyndall et al. [1210]. There are two confirmed sets of products for this reaction.

$$CH_3O_2 + CH_3O_2 \xrightarrow{k_a} CH_3O + CH_3O + O_2 \text{ (a)}$$

$$CH_3O_2 + CH_3O_2 \xrightarrow{k_b} CH_3OH + HCHO + O_2 \text{ (b)}$$

The relative product yield, k_a/k_b, was evaluated by Tyndall et al. to be $(26.2 \pm 6.6) \times \exp((-1130 \pm 240)/T)$. They concluded that there was no evidence for the formation of the CH_3OOCH_3. The kinetics of this reaction has been studied by using UV absorption following pulsed photolytic production of the radicals. Tyndall et al. used the values of k/σ measured by a large number of groups along with the σ values from their evaluation to calculate k. (σ is the absorption cross section of the radical at the wavelength at which it was monitored.) They only used the kinetics data obtained at wavelengths larger than 240 nm, since the absorption by HO_2 radicals that are unavoidably produced in these measurements can significantly contribute to the measure UV profiles at shorter wavelengths. They noted that the values of k/σ measured by various groups were much more accurate than the values of σ measured by the same groups. The value of k obtained by this method was then corrected using the above branching ratio for the production of CH_3O that leads to the unavoidable occurrence of the $CH_3O_2 + HO_2$ side reaction; this side reaction consumes another CH_3O_2 radical.

D47. CH_3O_2 + NO. This recommendation is from Tyndall et al. [1210]. They evaluated the available information to deduce that the main set of products under atmospheric conditions is $CH_3O + NO_2$. They noted, however, that a very small yield, <0.5%, of CH_3ONO_2 is also possible. The rate coefficient for the reaction at 298 K and its temperature dependence is based on numerous direct studies of this reaction that have been reported.

D48. $CH_3O_2 + CH_3C(O)O_2$. This recommendation is from Tyndall et al. [1210]. This reaction has two sets of products:

$$CH_3C(O)O_2 + CH_3O_2 \xrightarrow{k_a} CH_3 + CO_2 + CH_3O + O_2 \text{ (a)}$$

$$CH_3C(O)O_2 + CH_3O_2 \xrightarrow{k_b} CH_3C(O)OH + HCHO + O_2 \text{ (b)}$$

Tyndall et al. reanalyzed the previously available data on the branching ratios for this reaction and concluded that the branching ratio for channel (a) was $k_a/k = 0.9\pm0.1$ and $k_b/k = 0.1\pm0.1$ at 298 K. They also concluded that branching ratios could not be derived for other temperatures from the existing data and therefore did not make a recommendation for the temperature dependence. The recommendation from Tyndall et al. is based on the work of Roehl et al. [1005] and Villenave et al. [1232]. Their recommended temperature dependence for the overall rate coefficient is based on analogy with other RO_2 reactions.

D49. $CH_3O_2 + CH_3C(O)CH_2O_2$. This recommendation is from Tyndall et al. [1210]. This reaction has three possible sets of products:

$$CH_3C(O)CH_2O_2 + CH_3O_2 \xrightarrow{k_a} CH_3C(O) + HCHO + CH_3O + O_2 \text{ (a)}$$

$$CH_3C(O)CH_2O_2 + CH_3O_2 \xrightarrow{k_b} CH_3C(O)CH_2OH + HCHO + O_2 \text{ (b)}$$

$$CH_3C(O)CH_2O_2 + CH_3O_2 \xrightarrow{k_c} CH_3C(O)CHO + CH_3OH + O_2 \text{ (c)}$$

The branching ratios for these channels, $k_a/k = 0.3\pm0.1$, $k_b/k = 0.2\pm0.1$, and $k_c/k = 0.5\pm0.1$, are based on the work of Bridier et al. [152] and Jenkin et al. [578]. The overall rate coefficient for this reaction has been studied only at 298 K by Bridier et al. and the recommendation is based on this value. The recommended values of E/R and g are based on analogy with other RO_2 reactions.

D50. $C_2H_5 + O_2$. This is a complex reaction that involves the formation of an $C_2H_5O_2$ adduct, which can either be stabilized by collisions or fall apart to HO_2 and C_2H_4 (Wagner et al. [1238], Bozzelli and Dean [146], and Kaiser et al. [601]). The fraction of the energized adducts that fall apart to give HO_2 and C_2H_4 will decrease with increasing pressure and decreasing temperature, i.e., as the $C_2H_5O_2$ formation increases. The C_2H_4-formation channel cannot be separated from the addition reaction. We recommend a conservative upper limit as a guide to the extent of this reaction. This upper limit is applicable only for lower atmospheric pressure and temperature conditions.

D51. $C_2H_5O + O_2$. The recommendation is based on the pulsed laser photolysis studies of Gutman et al. [462] and Hartmann et al. [484]. In both these studies, removal of C_2H_5O in an excess of O_2 was directly monitored via laser induced fluorescence. Gutman et al. measured k at only two temperatures, while Hartmann et al. measured k at 5 temperatures between 295 and 411 K. The E/R is from Hartmann et al. The 298 K value deduced from an indirect study by Zabarnick and Heicklen [1347] is in reasonable agreement with the recommended value.

D52. $C_2H_5O_2 + C_2H_5O_2$. k(298 K) has been studied by Adachi et al. [7], Anastasi et al. [22], Munk et al. [841], Cattell et al. [205], Anastasi et al. [21], Wallington et al. [1254], Bauer et al. [87], and Fenter et al. [389]. All the above determinations used only UV absorption to monitor $C_2H_5O_2$ and hence measured k/σ, where σ is the absorption cross section of $C_2H_5O_2$ at the monitoring wavelength. These investigators also measured the σ that was used in evaluating the rate coefficient. There are large discrepancies in the measured values of σ. For this evaluation, we have used the cross sections recommended here and recalculated the values of k from each investigation. The recommended k is based on the results of Cattell et al., Wallington et al., Bauer et al., and Fenter et al. In all these experiments the observed rate coefficient is higher than the true rate coefficient because of secondary reactions involving HO_2. HO_2 is formed by the reaction of CH_3CH_2O with O_2 and it reacts with $C_2H_5O_2$ to enhance the observed rate coefficient (see Wallington et al. [1256] or Lightfoot et al. [731] for further discussion). Based on product branching ratios discussed below, which determine the magnitude of the necessary correction, the recommended rate coefficient is 0.6 times the average observed rate coefficient. The recommended value of E/R was obtained from the results of Anastasi et al., Wallington et al., Anastasi et al., Cattell et al., Bauer et al. and Fenter et al. The observed products (Niki et al. [890]), suggest that at 298 K the channel to yield 2 $C_2H_5O + O_2$ accounts for about 60% of the reaction; the channel to yield $CH_3CHO + C_2H_5OH + O_2$ accounts for about 40% of the reaction; and the channel to yield $C_2H_5O_2C_2H_5 + O_2$ accounts for less than 5% of the reaction. These branching ratios were used above to obtain the true rate coefficient from the observed rate coefficient.

D53. $C_2H_5O_2 + NO$. The recommended k(298 K) is obtained from the results of Plumb et al. [958], Sehested et al. [1051], Daele et al. [300], Eberhard and Howard [371], and Maricq and Szente [779]. The value reported by Adachi and Basco [6], which is a factor of three lower than the recommended value, was not used. The rate coefficient for the $CH_3O_2 + NO$ reaction measured by Basco and co-workers (Adachi et al. [7]), using the same apparatus, is also much lower than the value recommended here. The recommended temperature dependence is derived from Eberhardt and Howard and Maricq and Szente, which are in good agreement.

D54. $CH_3C(O)O_2 + CH_3C(O)O_2$. This reaction has been studied by Addison et al. [8], Basco and Parmar [83], Moortgat et al. [834] Maricq and Szente [779], and Roehl et al. [1005], using UV absorption techniques. The recommended value is obtained from the data of Moortgat et al., Maricq and Szente, and Roehl et al. As pointed out by Moortgat et al., the six times lower value of k obtained by Addison et al. is likely due to the use of incorrect UV absorption cross sections for the peroxyradical. The k obtained by Basco and Parmar is ~2 times lower than the recommended value. This discrepancy is possibly due to neglecting the UV absorption of CH_3O_2 and other stable products in their data analysis (Moortgat et al., Maricq and Szente). The recommended temperature dependence was calculated from the data of Moortgat et al. and Maricq and

Szente. Addison et al. reported the formation of O_3, which was attributed to the reaction channel which produces $CH_3C(O)OCH_3C(O) + O_3$. Moortgat et al. place an upper limit of 2% for this channel. The main products of this reaction appear to be $CH_3C(O)O + O_2$. The $CH_3C(O)O$ radicals rapidly decompose to give CH_3 and CO_2.

D55. $CH_3C(O)O_2 + NO$. This recommendation is from Tyndall et al. [1210]. These authors have argued that the only set of products of importance in the atmosphere is the production of $CH_3 + CO_2 + NO_2$. This is because the alkoxy radical produced upon O abstraction from the peroxy radical by NO will be unstable towards decomposition to give CH_3 and CO_2. The rate coefficient for the reaction was deduced primarily from direct studies, but was found to be consistent with the relative rate studies. In the relative rate studies, this rate coefficient was measured relative to the rate coefficient for the reaction of $CH_3C(O)O_2$ with NO_2. The temperature dependence of this rate coefficient were derived from a set of direct measurement and kept consistent with the observed temperature dependence of the rate coefficient for the $CH_3C(O)O_2 + NO_2$ reaction.

D56. $CH_3C(O)CH_2O_2 + NO$. This recommendation is from Tyndall et al. [1210]. They deduced, based on the results of Sehested et al. [1048], Jenkin et al. [578] and Orlando et al. [918], that the products of this reaction are $CH_3C(O)CH_2O + NO_2$. The $CH_3C(O)CH_2O$ radical decomposes rapidly to give $CH_3C(O) + CH_2O$. The only kinetics study of this reaction by Sehested et al. forms the basis for the rate coefficient at 298 K. This value is uncertain because of the corrections that had to be made in the study of Sehested et al. to account for the production of NO_2, the monitored species, via the reaction of peroxy radicals (such as $CH_3C(O)O_2$ and CH_3O_2) with NO. The temperature dependence of the reaction is derived based on analogy with other peroxy radical reactions.

E1. O + FO. The recommended value is based on results of the room temperature study of Bedzhanyan et al. [106] The temperature dependence of the rate constant is expected to be small, as it is for the analogous ClO reaction.

E2. $O + FO_2$. No experimental data. The rate constant for such a radical-atom process is expected to approach the gas collision frequency, and is not expected to exhibit a strong temperature dependence.

E3. $OH + CH_3F$ (HFC-41). The recommended values for k(298 K) and E/R are averages of these parameters derived from fits to the data of Schmoltner et al. [1039], Nip et al [898], Hsu and DeMore [538], and DeMore [335] (with the relative rate constants from the last two studies recalculated based on the current recommendations for the rate constants for the $OH + CH_3CHF_2$ and $OH + CH_3Cl$ reference reactions respectively.) The A factor was then calculated. The renormalization procedure for relative rate measurements referenced to the $OH + CH_3CHF_2$ reaction is discussed in the note for that reaction. The results of Howard and Evenson [528], Jeong and Kaufman [586], and Wallington and Hurley [1260] appear to be systematically lower than those of the other studies over the temperature region of interest and were not used to derive the recommended parameters.

E4. $OH + CH_2F_2$ (HFC-32). The recommended value of k(298 K) is an average from the studies of Nip et al. [898], Jeong and Kaufman [586], Talukdar et al. [1150], Hsu and DeMore [538] (recalculated based on the current recommendation for the rate constant for the $OH + CH_3CHF_2$ reference reaction, as described in the note for that reaction), and Szilagyi et al. [1138]. The recommended value for E/R is derived from an Arrhenius fit to the data from these same five studies below 400 K. The results of Howard and Evenson [528], Clyne and Holt [244], and Bera and Hanrahan [113] were not used in deriving the recommended parameters.

E5. $OH + CHF_3$ (HFC-23). The recommended values for k(298 K) and E/R are averages of the values Schmoltner et al. [1039], and Hsu and DeMore [538] (recalculated based on the current recommendation for the rate constant for the $OH + CHF_2CF_3$ reference reaction). The results of Jeong and Kaufman [586], and Medhurst et al. [799], being predominantly above room temperature, were not used in deriving the recommended parameters. The results from Clyne and Holt [244] and Bera and Hanrahan [113] were also not used due to their inconsistency with the other studies. The room temperature values of Howard and Evenson [528] and Nip et al [898] are encompassed within the 2σ confidence limits.

E6. $OH + CH_3CH_2F$ (HFC-161). The recommended value for k(298 K) is an average of the values from Nip et al. [898], Schmoltner et al. [1039], and Kozlov et al. [651]. The value of E/R is based on a fit to the data from these three studies from room temperature and below. The relative rate study by Hsu and DeMore [538] reports a temperature dependence that is markedly different from those of Schmoltner et al. [1039] and Kozlov et al. [651], which are in excellent agreement. This difference is due to significantly lower rate constant values being obtained in the Hsu and DeMore study in the region near room temperature. Given the most recent results for the reaction of $OH + CH_3CHF_2$ (HFC-152a), it seems likely that the HFC-161 reaction also has two channels with different activation energies and that the temperature dependence below room

temperature should be less than that recommended for HFC-152a, consistent with the present recommendation. Curvature in the Arrhenius plot is evident from the study by Kozlov et al. [651], which was conducted over an extended temperature range above and below room temperature. Singleton et al. [1080] determined that 85 ± 3% of the abstraction by OH is from the fluorine substituted methyl group at room temperature. Hence this curvature is quite possibly due to the increasing importance of hydrogen abstraction from the unsubstituted methyl group with increasing temperature. Due to such occurrence, the recommended parameters should not be used for calculating rate constants above room temperature.

E7. OH + CH_3CHF_2 (HFC-152a). The recommended value for k(298 K) is an average of the values from Howard and Evenson [529], Handwerk and Zellner [480], Nip et al. [898], Gierczak et al. [431] (two different absolute determinations), Hsu and DeMore [538] (two relative rate determinations which have been recalculated based on the current recommendations for the rate constants of the OH + CH_4 and OH + CH_3CCl_3 reference reactions), and Kozlov et al [651]. There are systematic differences in the temperature dependencies determined in the absolute studies (particularly below room temperature) and relative studies (conducted at room temperature and above). Curvature in the Arrhenius plot (as suggested by the data of Gierczak et al. [431]) has been more clearly demonstrated by the study of Kozlov et al. [651] and seems to explain the earlier cited differences between the relative and absolute rate data. This curvature is likely due to the presence of two hydrogen-abstraction reaction channels. Hence, care must be taken in deriving a recommended rate expression suitable for atmospheric modeling (in the temperature region below room temperature).

In spite of the noticeable Arrhenius curvature over the temperature range from 480 K to 210 K, the data below 300 K can be well represented by a two-parameter Arrhenius expression. Thus, the recommended value for E/R is derived from a fit to the data (T ≤ 300 K) of Gierczak et al. and Kozlov et al. The results from Clyne and Holt [244], Brown et al. [154], Nielsen [875], and Liu et al. [749] (superceded by the study of Kozlov et al.) were not used in deriving the recommended parameters.

Clearly, in light of the observed Arrhenius curvature, the above procedure for deriving our recommendation for E/R below 300 K does not yield a parameter suitable for use in recalculating rate constants from relative rate studies in which the OH + CH_3CHF_2 reaction was the reference and which were conducted at temperatures above 300 K. Use of the below-room-temperature value for E/R for such purposes results in rate constant values that are systematically different from those determined relative to other reactions or determined by absolute techniques. For such renormalization purposes, one should use an Arrhenius expression derived from data over the appropriate temperature range. A fit to the absolute rate data of Gierczak et al. [431] and Kozlov et al. [651] between room temperature and 400 K yields the Arrhenius expression

$$k_{abs} = 2.36 \times 10^{-12} \exp\{-1255/T\}$$

This is in good agreement with the expression derived from the relative rate data of Hsu and DeMore [538]

$$k_{rel} = 2.1 \times 10^{-12} \exp\{-1265/T\}$$

The small difference in the pre-exponential factors results from a slight systematic difference in the actual rate constants determined in these three studies that is probably within the combined uncertainties of the determinations. Thus, the following expression derived from the above room temperature E/R value and the recommended k(298 K) has been used for renormalization purposes in this evaluation.

$$k_{T\geq 300K} = 2.33 \times 10^{-12} \exp\{-1260/T\}$$

However, this expression should not be used below 298 K, as erroneous values for OH + CH_3CHF_2 reaction rate constants would be obtained.

E8. OH + CH_2FCH_2F (HFC-152). The recommended value for k(298 K) is an average of the values from Martin and Paraskevopoulos [787], Kozlov et al. [651], and DeMore et al. [341] (three relative rate studies using HFC-152a, cyclopropane, and ethane as reference reactants). The value for E/R is from a fit to the data of Kozlov et al. [651] at room temperature and below. The A factor was then calculated to yield the recommended value for k(298 K). The data above room temperature from Kozlov et al [651] are in excellent agreement with the three relative rate data sets of DeMore et al. [341]. Together, they show a pronounced curvature in the Arrhenius plot, which may indicate the existence of different conformers for HFC-152, each with differing temperature populations and reactivities.

E9. OH + CH_3CF_3 (HFC-143a). The recommended value for k(298 K) is an average of the values from Martin and Paraskevopoulos [787], Orkin et al. [910], Talukdar et al. [1150] (two different determinations), and Hsu and DeMore [538] (two relative rate determinations which have been recalculated based on the current recom-mendations for the rate constants of the OH + CH_4 and OH + CHF_2CF_3 reference reactions). The value for E/R is an average of the E/R values from the last three of these studies which are in excellent agreement

(Martin and Paraskevopoulos having made measurements only at room temperature). The data of Clyne and Holt [244] were not used due to their inconsistency with the other studies.

E10. OH + CH_2FCHF_2 (HFC-143). The recommended temperature dependence is based on results of the relative rate study of Barry et al. [79] normalized to the value of the rate constant for the reference reaction (OH + CH_3CCl_3) recommended in this evaluation. The value for k(298 K) is an average of the room temperature values of Martin and Paraskevopoulos [787] and Barry et al. The significantly higher values reported by Clyne and Holt [244] were not used in the derivation of the recommended parameters.

E11. OH + CH_2FCF_3 (HFC-134a). The recommended value for k(298 K) is an average of the values from Martin and Paraskevopoulos [787], Bednarek et al. [101], Orkin and Khamaganov [912], Leu and Lee [711], Gierczak et al. [431] (two different determinations), Liu et al. [749], and DeMore [333] (three determinations which have been recalculated based on the current recommendations for the rate constants for the reference reactions OH + CH_4, OH + CH_3CCl_3, and OH + CHF_2CF_3). The value for E/R is an average of the E/R values from the last five of these investigations (the studies by Martin and Paraskevopoulos and by Bednarek et al. being conducted only at room temperature). The 270 K result of Zhang et al. [1365] is in excellent agreement with the recommendation. The data of Jeong et al. [584], Brown et al. [154], and Clyne and Holt [244] were not used in deriving the recommended parameters.

E12. OH + CHF_2CHF_2 (HFC-134). The preferred rate expression is based on results of the three relative rate measurements by DeMore [333] (which have been recalculated based on the current rate constant recommendations for the OH + CH_3CCl_3, OH + CH_2FCF_3, and OH + CHF_2CF_3 reference reactions). The room temperature value of Clyne and Holt [244] agrees within the 2σ confidence limits.

E13. OH + CHF_2CF_3 (HFC-125). The recommended rate expression is derived from a combined fit to the temperature dependence data of Talukdar et al. [1150] and DeMore [333] and the room temperature data of Martin and Paraskevopoulos [787]. The data of Brown et al. [154] and Clyne and Holt [244] were not used in deriving the recommended parameters.

E14. OH + CH_3CHFCH_3 (HFC-281ea). The recommended parameters were derived from a fit to the data of DeMore and Wilson [340] who conducted five independent relative rate determinations. Using infrared detection, these investigators based their determinations on the reference reactions of OH with C_2H_6, C_3H_8, and C_2H_5Cl. Using gas chromatographic detection, they based their determinations on the reference reactions of OH with C_2H_6 and C_3H_8. All of the data were recalculated based on the current recommendations for the reference rate constants.

E15. OH + $CH_3CH_2CF_3$ (HFC-263fb). Based on room temperature measurement of Nelson et al. [853].

E16. OH + $CH_2FCF_2CHF_2$ (HFC-245ca). The absolute rate constant results of Zhang et al. [1368] differ from the relative rate data (Hsu and DeMore [538]) by approximately 30 to 40% over the temperature region of measurement overlap. Both studies, however, derive nearly identical T-dependencies. The recommended rate expression, hence, averages both the k(298 K) and E/R values from these studies (with the results of Hsu and DeMore [538] recalculated using the current recommendation for the rate constant of the OH + CH_4 reference reaction).

E17. OH + $CHF_2CHFCHF_2$ (HFC-245ea). Based on room temperature measurement of Nelson et al. [853].

E18. OH + $CH_2FCHFCF_3$ (HFC-245eb). Based on room temperature measurement of Nelson et al. [853].

E19. OH + $CHF_2CH_2CF_3$ (HFC-245fa). The recommended room temperature value is the mean of the values reported by Orkin et al. [910] and Nelson et al. [853], which are in good agreement. The temperature dependence is from Orkin et al. The A-factor has been calculated to fit the recommended room temperature value.

E20. OH + $CH_2FCF_2CF_3$ (HFC-236cb). The recommended rate expression is estimated as being the same as that for the reaction of OH with CH_2FCF_3 (HFC-134a), since these reactions are expected to have very similar Arrhenius parameters. This estimate is preferred over the results reported by Garland et al. [420], the only published experimental study. The A-factor reported in that study is much lower than expected and the value reported for E/R (1107 K) in lower than that reported for any similar halocarbon reaction.

E21. OH + CHF_2CHFCF_3 (HFC-236ea). The recommended value for k(298 K) averages the values reported by Hsu and DeMore [538] by a relative rate method (recalculated based on the current recommendation for the rate constant of the OH + CH_4 reference reaction) and by Nelson et al. [853] by an absolute technique. The temperature dependence is from Hsu and DeMore [538], with the A-factor adjusted to fit the recommended room temperature value. The higher and somewhat more scattered values of Garland et al. [420] and Zhang et al. [1368] were not used in deriving the recommended expression.

E22. OH + $CF_3CH_2CF_3$ (HFC-236fa). The recommended rate expression is derived from a combined fit to the data from the relative rate study of Hsu and DeMore [538] (recalculated based on the current recommendation for the rate constant for the reference reaction OH + CHF_2CF_3) and the absolute rate study of Gierczak et al. [432]. The higher results of Nelson et al. [853] and of Garland and Nelson [421], which superseded the earlier results of Garland et al. [421], were not used. A relative rate determination at room temperature by Barry et al. [77] yields a rate constant in excellent agreement with the recommended value. However, the extremely small rate constant ratio measured (relative to OH + $CH_3CF_2CH_2CF_3$) resulted in fairly large uncertainties. Hence this determination was not directly used in the evaluation.

E23. OH + CF_3CHFCF_3 (HFC-227ea). The recommended rate expression is derived from a combined fit to the data (below 400 K) from the absolute studies of Nelson et al. [849], Zellner et al. [1358], and Zhang et al. [1368] and the relative rate studies of Hsu and DeMore [538] (two determinations which have been recalculated based on the current recommendations for the rate constants for the reference reactions OH + CH_4 and
OH + CHF_2CF_3).

E24. OH + $CH_3CF_2CH_2CF_3$ (HFC-365mfc). The recommended value of k(298 K) is an average of the values obtained from the individual rate expressions by Mellouki et al. [813] and Barry et al. [77] (renormalized to the current recommendation for the rate constant for the reference reaction OH + CH_3CCl_3). The value for E/R is an average of the values for this parameter from the same two studies.

E25. OH + $CF_3CH_2CH_2CF_3$ (HFC-356mff). The recommended value of k(298 K) is an average of the values from Nelson et al.[853] and Zhang et al. [1368]. The temperature dependence is from a fit to the data of Zhang et al. excluding the lowest temperature points (at 260 K), which are somewhat higher than an extrapolation from their other data would indicate. The A-factor has been calculated to fit the recommended room temperature value.

E26. OH + $CH_2FCH_2CF_2CF_3$ (HFC-356mcf). The recommended parameters are based on a fit to the data of Nelson et al. [853].

E27. OH + $CHF_2CF_2CF_2CHF_2$ (HFC-338pcc). The recommended values for both k(298 K) and E/R are averages of these values taken from the individual fits to the data of Schmoltner et al. [1039] and Zhang et al. [1370].

E28. OH + $CF_3CH_2CF_2CH_2CF_3$ (HFC-458mfcf). The recommended values for both k(298 K) and E/R are from a fit to the data of Nelson et al. [853].

E29. OH + $CF_3CHFCHFCF_2CF_3$. (HFC-43-10mee). The recommended rate expression is derived from a combined fit to the data from Schmoltner et al. [1039] and Zhang et al. [1370].

E30. OH + $CF_3CF_2CH_2CH_2CF_2CF_3$ (HFC-55-10mcff). The recommended value for k(298 K) is based on Nelson et al. [853]. As expected, the rate constant is similar to that for $CF_3CH_2CH_2CF_3$. Hence the recommendation for E/R is estimated as being approximately the same as for this reaction, with the A-factor calculated to yield k(298 K).

E31. OH + CH_2=CHF. The recommended parameters were derived from a fit to the data of Perry et al. [941].

E32. OH + CH_2=CF_2. The recommended value for k(298 K) is from Howard [526]. The value of E/R was estimated as being similar to that for the reactions of OH with CH_2=CHF and with CF_2=CF_2, and the value for A was then calculated.

E33. OH + CF_2=CF_2. The recommended value for k(298 K) is an average of the values determined in the studies of Acerboni et al. [5] (two relative rate determinations referenced to the rate constants for the reactions of OH with propene and cyclohexane) and the absolute rate studies of Orkin et al. [911], and Orkin et al. [916]. The value for E/R is from a fit to the data of Orkin et al [916], with the value for A calculated to yield the recommended value for k(298 K).

E34. OH + CF_3OH. There are no measurements of the rate coefficient of this reaction. The recommendation is based on the recommended limit for the reverse reaction rate coefficient and an estimated equilibrium constant. The thermochemistry of CF_3O and CF_3OH are taken from *ab initio* calculations (Montgomery et al. [832] and Schneider and Wallington [1040]) and laboratory measurements (Huey et al. [542]) to estimate ΔG°_{298}(OH + $CF_3OH \rightarrow CF_3O + H_2O$) to be about (2±4) kcal mol^{-1}. In considering the large uncertainty in the free energy change, the estimated rate coefficient limit is based on the assumption that the reaction is approximately thermoneutral.

E35. OH + $CH_2(OH)CF_3$. The recommended value for k(298 K) is an average of the values reported by Wallington et al. [1255], Inoue et al. [562], and Tokuhashi et al. [1177] (two independent studies). The recommended

value for E/R is derived from the data of and Tokuhashi et al. [1177]. The A factor was calculated to agree with the recommended value for k(298 K).

E36. OH + $CH_2(OH)CF_2CF_3$. The recommended parameters were derived from a combined fit to the data of Tokuhashi et al. [1177] (two independent absolute measurement studies) and the relative rate study of Chen et al. [220] (recalculated based on the current recommendation for the rate constant for the OH + CH_2Cl_2 reference reaction).

E37. OH + $CF_3CH(OH)CF_3$. The recommended parameters were derived from a fit to the data (below 400 K) of Tokuhashi et al. [1177] (two independent absolute measurement studies).

E38. OH + CH_3OCHF_2 (HFOC-152a). The recommended rate expression is derived from a fit to the data of Orkin et al. [914] below 400 K.

E39. OH + CH_3OCF_3 (HFOC-143a). The preferred rate expression is derived from a combined fit to the data of Orkin et al. [914] and Hsu and DeMore [539] (two relative rate determinations which have been recalculated based on the current recommendations for the rate constants of the OH + CH_3CHF_2 and OH + CH_2F_2 reference reactions). The renormalization procedure for relative rate measurements referenced to the OH + CH_3CHF_2 reaction is discussed in the note for that reaction. The room temperature result of Zhang et al. [1371] was not used in the derivation since it is significantly higher than the values of the other studies and may be influenced by the presence of reactive impurities.

E40. OH + CHF_2OCHF_2 (HFOC-134). The recommended values of k(298 K) and E/R were derived from a combined fit to the data of Hsu and DeMore [539] (a relative rate study whose results have been recalculated using the current recommendation for the rate constant of the OH + CH_3CCl_3 reference reaction), Orkin et al. [917], and Wilson et al. [1309]. The more scattered measurements of Garland et al. [420] were not used in derivation of the preferred value.

E41. OH + CHF_2OCF_3 (HFOC-125). The recommended rate expression is based on results of the relative rate study of Hsu and DeMore [539] (recalculated using the rate constant for the CHF_3 reference reaction given in this evaluation). Additional measurements by Hsu and DeMore [539] relative to CHF_2CF_3 and CH_4 are encompassed well within the 2σlimits, but were not used for assigning the recommended rate expression due to the large differences in reactivity between these two species and the target molecule. The room temperature result of Zhang et al. [1371] lies significantly higher than the recommended value, possibly due to the presence of reactive impurities in the sample.

E42. OH + $CHF_2OCH_2CF_3$ (HFOC-245fa). The recommended rate expression is derived from a fit to the data of Orkin et al. [914] below 400 K.

E43. OH + $CH_3OCF_2CHF_2$. The recommended parameters were derived from a fit to the data (below 400 K) of Tokuhashi et al. [1179] (two independent absolute measurement studies). A room temperature measurement by Heathfield et al. [490] is nearly an order of magnitude higher than recommended and may be affected by reactive impurities.

E44. OH + $CH_3OCF_2CF_3$. The recommended parameters were derived from a fit to the data (below 400 K) of Tokuhashi et al. [1178] (two independent absolute measurement studies). The expression, as expected, is similar to those for the OH + CH_3OCF_3 and OH + $CH_3OCF_2CF_2CF_3$ reactions.

E45. OH + $CH_3OCF_2CF_2CF_3$. The recommended value for k(298 K) is an average of the values reported by Tokuhashi et al. [1178] (two independent absolute measurement studies) and Nonomiya et al. [896] (two relative rate determinations which have been recalculated based on the current recommendations for the rate constants of the OH + CH_4 and OH + CH_3Cl reference reactions). The value for E/R was determined from a fit to the data (below 400 K) of Tokuhashi et al. and the A factor calculated to agree with the value for k(298 K). The expression, as expected, is similar to those for the OH + CH_3OCF_3 and OH + $CH_3OCF_2CF_3$ reactions.

E46. OH + $CH_3OCF(CF_3)_2$. The recommended parameters were derived from a fit to the data (below 400 K) of Tokuhashi et al. [1178] (two independent absolute measurement studies).The rate constants from this study are surprisingly somewhat larger than those for the similar OH + CH_3OCF_3 and OH + $CH_3OCF_2CF_3$ reactions.

E47. OH + $CHF_2OCH_2CF_2CHF_2$. The recommended parameters were derived from a fit to the data (below 400 K) of Tokuhashi et al. [1179] (two independent absolute measurement studies).

E48. OH + $CHF_2OCH_2CF_2CF_3$. The recommended parameters were derived from a fit to the data (below 400 K) of Tokuhashi et al. [1179] (two independent absolute measurement studies).

E49. $F + O_3$. The recommended value is based on results of the room temperature study of Bedzhanyan et al. [103] and the temperature-dependent study of Wagner et al. [1242]. The value appears to be quite reasonable in view of the well-known reactivity of atomic chlorine with O_3.

E50. $F + H_2$. The value of k at 298 K seems to be well established with the results reported by Zhitneva and Pshezhetskii [1373], Heidner et al. [491,492], Wurzberg and Houston [1337], Dodonov et al. [356], Clyne et al. [249], Bozzelli [145], Igoshin et al. [558], Clyne and Hodgson [242] and Stevens et al. [1115] being in excellent agreement (range of k being $2.3–3.0 \times 10^{-11}$ cm^3 $molecule^{-1}$ s^{-1}). The preferred value at 298 K is taken to be the mean of the values reported in these references. Values of E/R range from 433–595 K (Heidner et al.; Wurzberg and Houston; Igoshin et al.; and Stevens et al.). The preferred value of E/R is derived from a fit to the data in these studies. The A-factor was chosen to fit the recommended room temperature value.

E51. $F + H_2O$. The recommended temperature-independent value is based on results reported in the study by Stevens et al. [1115] over the temperature range 240–373 K using a discharge flow system with chemical conversion of fluorine atoms to deuterium atoms and detection of the latter by resonanace fluorescence. This value is in excellent agreement with the room temperature results of Frost et al. [416] and Walther and Wagner [1268]. The latter authors in a limited temperature-dependent study reported an E/R value of 400 K. Although these data have not been included in the derivation of the preferred value, with the exception of the one low temperature data point, they are encompassed within the indicated uncertainty limits.

E52. $F + HNO_3$. The recommendation is based on results of the temperature-dependent study of Wine et al. [1324] and the room temperature results of Mellouki et al. [805], Rahman et al. [975] and Becker et al. [90]. The values at room temperature are in good agreement. The study of Wine et al. [1324] was over the temperature range 260–373 K. Below 320 K the data were fitted with the Arrhenius expression recommended here, whereas at higher temperatures a temperature-independent value was found, suggesting the occurrence of different mechanisms in the two temperature regimes.

E53. $F + CH_4$. The recommended room temperature value is the mean of the results of Wagner et al. [1240], Clyne et al. [249], Kompa and Wanner [648], Foon and Reid [404], Fasano and Nogar [386], and Persky et al. [946]. The temperature dependence is that reported by Persky et al. in a competitive study using the reaction $F + D_2$ as the reference reaction. These results are preferred over the temperature dependences reported in the earlier studies of Wagner et al. and Foon and Reid.

E54. $FO + O_3$. Recommended upper limit is based on the results of Li et al. [729] in a study using a discharge flow-mass spectrometric technique. FO was produced in the reaction of F atoms with excess O_3. No appreciable decay of FO, and only a small increase in FO_2, was detected, allowing an upper limit to the rate constant of
10^{-14} cm^3 $molecule^{-1}s^{-1}$ to be derived. A two orders of magnitude higher upper limit was derived by Sehested et al. [1052]. A lower value of the upper limit was derived by Colussi and Grela [268] from a re-analysis of data on the quantum yields for ozone destruction in F_2/O_3 mixtures reported by Starrico et al. [1104]. The results of the recent, more direct, study of Li et al. [729] are preferred over the earlier results of Starrico et al. There are two possible pathways which are exothermic, resulting in the production of $F + 2O_2$ or $FO_2 + O_2$.

E55. FO + NO. The recommended value is based on results of the temperature-dependent study of Bedzhanyan et al. [105] and the value reported by Ray and Watson [996] for k at 298 K using the discharge flow-mass spectrometric technique.

E56. FO + FO. The recommended value is based on the results of Bedzhanyan et al. [104] and Clyne and Watson [260]. Wagner et al. [1242], in a less direct study, report a higher value. The results of Bedzhanyan et al. indicate the predominant reaction channel is that to produce $2F + O_2$.

E57. $FO_2 + O_3$. Recommended value is based on results of Sehested et al. [1052]. A higher upper limit has been reported by Li et al. [729].

E58. $FO_2 + NO$. Recommended values are based on results of Li et al. [729], the only temperature-dependent study. The room temperature value is nearly a factor of 2 less than the previous recommendation, which was based on the results of Sehested et al. [1052].

E59. $FO_2 + NO_2$. Recommended values are based on results of Li et al. [729], the only temperature-dependent study. The room temperature value is a factor of 2.5 less than the previous recommendation, which was based on the results of Sehested et al. [1052]. This discrepancy might be attributable to a small NO impurity in the NO_2 sample used in the Sehested et al. study.

E60. $FO_2 + CO$. Recommended value is based on results of Sehested et al. [1052], the only published study of this reaction.

E61. $FO_2 + CH_4$. Recommended value is based on results of Li et al. [729]. This upper limit is a factor of 20 less than the previously recommended upper limit, which was based on the results of Sehested et al. [1052].

E62. $CF_3O + O_2$. The recommendation is based upon the results of Turnipseed et al. [1202] who reported $k(373\ K) \leq 4 \times 10^{-17}$. Assuming an E/R of 5000 K, which is equal to the reaction endothermicity, yields the recommended A and k(298 K) limits. By comparison to other reactions involving abstraction by O_2 the A-factor is likely to be much smaller.

E63. $CF_3O + O_3$. The recommendation is based on the average of room temperature measurements reported by Turnipseed et al. [1202], Wallington and Ball [1251] , and Bourbon et al. [141]. Turnipseed et al. and Bourbon et al. made direct measurements using LIF detection of CF_3O with pulsed photolysis and flow tube reactors, respectively. Wallington and Ball used a competetive reaction scheme with IR absorption detection and $CF_3O + CH_4$ as the reference reaction. The recommended A factor is estimated by comparison to other CF_3O reactions, and the E/R is calculated to give the recommended k(298 K). Upper limits reported by Maricq and Szente [777], Nielsen and Sehested [880], and Wallington et al. [1261] are consistent with the k(298 K) recommendation. Measurements reported by Fockenberg et al. [402] and Meller and Moortgat [802] gave rate coefficients about an order of magnitude less than the recommended value. Although the reason for this discrepancy is not known, both studies appear to have the possibility of significant secondary chemistry. The reaction products have not been observed.

E64. $CF_3O + H_2O$. The recommendation is based upon the measurement $k(381) \leq 2 \times 10^{-16}$ reported by Turnipseed et al. [1200]. The A factor is estimated and the E/R is calculated to fit k(381). The limits $k = (0.2–40) \times 10^{-17}$ at 296 ± 2 K given by Wallington et al. [1262] are consistent with the recommendation.

E65. $CF_3O + NO$. The recommendation is based upon the room temperature rate coefficients reported by Sehested and Nielsen [1050], Turnipseed et al. [1202], and Jensen et al. [581] which are in very good agreement. An earlier low value given by Bevilacqua et al. [115] is superseded by Jensen et al. The temperature-dependence is derived from measurements by Turnipseed (233–360 K) and Jensen et al. (231–393 K). Room temperature results from Bourbon et al. [142] and Bhatnagar and Carr [117] and a temperature dependence study by Dibble et al. [347] are in good agreement with the recommendation. The reaction products have been reported by Chen et al. [218] Bevilacqua et al. [115], Bhatnagar and Carr and Dibble et al.

E66. $CF_3O + NO_2$. There are no published measurements of the rate coefficient for this reaction. The reaction products have been reported by Chen et al. [217] who used photolysis of CF_3NO to prepare CF_3O_2 and subsequently CF_3O in 700 torr of air at 297±2 K. They considered two product channels: (a) CF_3ONO_2 obtained via three-body recombination and (b) $CF_2O + FNO_2$ obtained via fluorine transfer. Products from both channels were observed and found to be thermally stable in their reactor. They report $k_a/(k_a + k_b) \geq 90\%$ and $k_b/(k_a + k_b) \leq 10\%$, thus the formation of CF_3ONO_2 is the dominant channel at 700 torr and 297 K.

E67. $CF_3O + CO$. The kinetics of this reaction were studied by Turnipseed et al. [1200], who used pulsed laser photolysis with pulsed laser-induced fluorescence detection and a flow tube reactor with chemical ionization detection to obtain data at temperatures from 233 to 332 K and at pressures from 0.8 to about 300 torr in He and at about 300 torr in SF_6. The reaction was found to be predominantly a three-body recombination, presumably producing CF_3OCO as described in Table 2. The bimolecular reaction has at least two product channels: (a) $CF_2O + CFO$ and (b) $CF_3 + CO_2$. The recommended bimolecular rate coefficient limit is derived from the low pressure results of Turnipseed et al., where the reaction was in the fall-off region. Their low pressure data indicate that $k_b < 4 \times 10^{-16}$ cm^3 molecule^{-1} s^{-1} at 298 K. The fate of the CF_3OCO adduct is uncertain, and it may lead to the regeneration of CF_3 or CF_3O radicals in the atmosphere. Wallington and Ball [1252] report a yield of 96±8% CO_2 at one atmosphere and 296±2 K.

E68. $CF_3O + CH_4$. The absolute rate coefficients reported by Saathoff and Zellner [1013], Barone et al. [75], Jensen et al. [581], Bourbon et al. [143], and Bednarek et al. [102] at room temperature are in excellent agreement. Kelly et al. [611] used a relative method with FTIR detection to determine the ratio $k(CF_3O + CH_4)/k(CF_3O + C_2H_6) = R = 0.01±0.001$ at 298±2 K. This does not agree with the ratio of our recommended values, which is 0.017. A relative rate measurement reported by Chen et al. [219] using FTIR methods also gives a low result for the rate coefficient. A relative rate measurement reported by Wallington and Ball [1252], R = 0.0152±0.0023 at 296 K, is in good agreement with the recommended rate coefficients. The temperature dependence is from the data of Barone et al. (247–360 K), Jensen et al. (231–385 K), and Bednarek et al. (235–401 K), who agree very well. Measurements at higher temperatures by Bourbon et al. (296–573 K) gave a higher E/R (1606 K). The k(298 K) is the average of the three absolute studies. The CF_3OH product was observed by Jensen et al. and Bevilacqua et al. [115].

E69. $CF_3O + C_2H_6$. The room temperature recommendation is based on results reported by Saathoff and Zellner [1013], Barone et al. [75], and Bourbon et al. [143]. These workers are in excellent agreement. Chen et al. [219] measured the rate coefficient relative to that for the $CF_3O + NO$ reaction in 700 torr of air at 297 K. Their ratio is in good agreement with the values recommended in this evaluation. Kelly et al. [611] used a relative method with FTIR detection to determine the ratio $k(CF_3O + CH_4)/k(CF_3O + C_2H_6) = 0.01\pm0.001$ at 298±2 K. This does not agree with the ratio of our recommended values, which is 0.017. A relative rate measurement reported by Wallington and Ball [1252], R = 0.0152±0.0023 at 296 K is in good agreement with the recommended rate coefficients. The temperature dependence is from the work of Barone et al., who studied the reaction over the temperature range from 233 to 360 K. Measurements by Bourbon et al. (295–573 K) gave a higher E/R (642 K). The products are inferred by analogy to other reactions of CF_3O with organic compounds.

E70. $CF_3O_2 + O_3$. The recommended upper limit is given by the measurements reported by Ravishankara et al. [987] who used chemical ionization detection of CF_3O_2 with a flow tube reactor. No measurable reaction was observed in their study. The less direct studies of Nielsen and Sehested [880], Maricq and Szente [777] and Turnipseed et al. [1202] all report somewhat larger upper limits to the rate coefficient. An observable reaction was reported in an indirect measurement by Meller and Moortgat [802]. Their result for the $CF_3O + O_3$ reaction is not consistent with the value recommended above. Their study may have interference from unknown reactions. The products are assumed to be $CF_3O + 2O_2$.

E71. $CF_3O_2 + CO$. The recommended upper limit is reported by Turnipseed et al. [1200] who used chemical ionization mass spectrometric detection of CF_3OO with a flow tube reactor at 296 K. This result is at odds with an earlier study by Czarnowski and Schumacher [298], who deduced a "fast reaction" when they observed the thermal decomposition of CF_3OOOCF_3 to accelerate in the presence of CO at 315–343K. It is possible that the reaction of CF_3O with CO could account for their observations.

E72. $CF_3O_2 + NO$. The recommendation is an average of the room temperature rate coefficients reported by Plumb and Ryan [957], Dognon et al. [358], Peeters et al. [939], Bevilacqua et al. [115], Sehested and Nielsen [1050], Turnipseed et al. [1202], Bourbon et al. [142], and Bhatnagar and Carr [117], all of whom are in excellent agreement. The temperature dependence is derived from the results of Dognon et al. Several studies have confirmed the identity of the products.

F1. O + ClO. There have been five studies of this rate constant over an extended temperature range using a variety of techniques: Leu [716]; Margitan [775]; Schwab et al. [1044]; Ongstad and Birks [909]; and Nicovich et al. [873]. The recommended value is based on a least squares fit to the data reported in these studies and in the earlier studies of Zahniser and Kaufman [1354] and Ongstad and Birks [908]. Values reported in the early studies of Bemand et al. [109] and Clyne and Nip [254] are significantly higher and were not used in deriving the recommended value. Leu and Yung [725] were unable to detect $O_2(^1\Delta)$ or $O_2(^1\Sigma)$ and set upper limits to the branching ratios for their production of 4.4×10^{-4} and 2.5×10^{-2} respectively.

F2. O + OClO. The recommended value is based on results of the DF-RF study of Gleason et al. [443]. Over the temperature range from 400 K down to 240 K their data are well fitted by this Arrhenius expression, but at lower temperatures down to 200 K their data show an abrupt change to a negative temperature dependence. At 200 K the value measured is a factor of 3 higher than that calculated from the Arrhenius expression. Similar results were obtained in a recent study (Toohey, Avallone, and Anderson, private communication). Over the temperature range 413 – 273 K their data showed a temperature dependence very similar to that reported by Gleason et al. over the same temperature range. Moreover, as the temperature was lowered further their rate constant values also levelled off and then increased at the lowest temperature. Their rate constant values were nearly 50% lower than the values of Gleason et al. from 400 K down to 273 K and 30% lower at 253 K. Colussi [267], using a laser-flash photolysis–resonance fluorescence technique over an extended pressure range, reported a value of the bimolecular rate coefficient at room temperature 50% higher than the recommended value. Colussi et al. [269] extended these measurements down to 248 K; in contrast to the positive temperature dependence over this temperature range reported by Gleason et al., these authors report a negative temperature dependence. The bimolecular rate constants reported by Colussi et al. are not directly measured but are derived quantities which are consistent with fall-off curves fitted to the experimental data over the pressure range 20–600 torr. It appears that the experiments of Bemand et al. [109], were complicated by secondary chemistry. The results of Colussi and Colussi et al. over an extended pressure range demonstrate the importance of the termolecular reaction $O + OClO + M \rightarrow ClO_3 + M$ (see entry for this reaction in Table 2). It should be noted that the termolecular rate constants derived by Gleason et al. on the basis of their low temperature data are not consistent with the termolecular rate constant expression recommended in this evaluation (factor of 3 difference). The recommended expression is based on the results of Colussi [267] and Colussi et al. [269].

F3. O + Cl_2O. Recommended value is based on the results of Stevens and Anderson [1114] and Miziolek and Molina [828], which are in good agreement. The significantly lower values of Wecker et al. [1291] are not included, nor are earlier results by Basco and Dogra [82] and Freeman and Phillips [408] due to data analysis difficulties in both studies.

F4. O + HCl. Fair agreement exists between the results of Brown and Smith [157], Wong and Belles [1331], Ravishankara et al. [984], Hack et al. [466] and Singleton and Cvetanovic [1077] at 300 K (some of the values for k(300 K) were obtained by extrapolation of the experimentally determined Arrhenius expressions), but these are a factor of ~7 lower than that of Balakhnin et al. [56]. Unfortunately, the values reported for E/R are in complete disagreement, ranging from 2260–3755 K. The preferred value was based on the results reported by Brown and Smith, Wong and Belles, Ravishankara et al., Hack et al. and Singleton and Cvetanovic, but not on those reported by Balakhnin et al.

F5. O + HOCl. Recommended value is based on results of Schindler et al. [1035]. In this study the rate constant was found to be practically independent of temperature in the range 213–298 K. Product analysis indicated that Cl atom abstraction is the predominant primary reaction channel.

F6. O + $ClONO_2$. The results reported by Molina et al. [830] and Kurylo [661] are in good agreement, and these data have been used to derive the preferred Arrhenius expression. The value reported by Ravishankara et al. [980] at 245 K is a factor of 2 greater than those from the other studies, and this may possibly be attributed to (a) secondary kinetic complications, (b) the presence of NO_2 as a reactive impurity in the $ClONO_2$, or (c) formation of reactive photolytic products. None of the studies reported identification of the reaction products. The room temperature result of Adler-Golden and Wiesenfeld [11] is in good agreement with the recommended value.

F7. O_3 + OClO. The recommended value is based on results over the temperature range 262–296 K reported by Wongdontri-Stuper et al. [1332]. Within the indicated uncertainty limits it also encompasses the somewhat lower room temperature result of Birks et al. [128].

F8. O_3 + Cl_2O_2. The recommended upper limit is that determined by DeMore and Tschuikow-Roux [339]. It refers to a temperature of 195 K, and while the reaction possibly could be faster at higher temperatures, the value of the rate at the higher temperatures would be of no significance because of the thermal decomposition of the dimer.

F9. OH + Cl_2. The recommended room temperature value is the average of the results reported by Boodaghians et al. [138], Loewenstein and Anderson [750], Ravishankara et al. [981], and Leu and Lin [721]. The temperature dependence is from Boodaghians et al. Loewenstein and Anderson determined that the exclusive products are Cl + HOCl.

F10. OH + ClO. The reaction has two known product channels under atmospheric conditions: OH + ClO → Cl + HO_2 and OH + ClO → HCl + O_2. Most studies measure the rate coefficients for the overall reaction (OH + ClO → products) that is presumably the sum of the two channels. The recommendation for the Cl + HO_2 channel is obtained from the difference between a critical assessment of the measurements of the overall reaction and the recommendation for the HCl + O_2 channel as discussed below. The assessment of the overall reaction (OH + ClO → products) is based on a fit to the 219–373 K data of Hills and Howard [508], the 208–298 K data of Lipson et al. [745], the 234–356 K data of Kegley-Owen et al. [610] and the 298 K data of Poulet et al. [965]. Data reported in the studies of Burrows et al. [181], Ravishankara et al. [981], and Leu and Lin [721] were not used in deriving the recommended value because ClO was not measured directly in these studies and the concentration of ClO was determined by an indirect method. Recent measurements of the overall rate constant by Wang and Keyser (218–298 K) [1269], Bedjanian et al. (230–360 K) [100] and Tyndall et al. (298 K) [1211] are consistent with the recommendation.

The minor reaction channel forming HCl poses significant experimental difficulties due to the complications associated with the measurement of the HCl reaction product. Early studies inferred the HCl branching ratio without measuring HCl. These included the 298 K measurements of Leu and Lin [721] (>0.65); Burrows et al. [181] (0.85±0.2) and Hills and Howard [508] (0.86±0.14). Poulet et al. [965] measured the HCl product yield to be 0.98±0.12 using mass spectroscopy but their HCl sensitivity was marginal. These studies were not considered in the evaluation. Later studies using mass spectroscopy [744] and diode laser spectroscopy [1270] improved the precision of the HCl product channel measurements. Lipson et al. measured rate constants for the HCl channel over the temperature range 207–298 K while Wang and Keyser [1270] measured the HCl yield between 218–298 K. obtaining (9.0±4.8) %, independent of temperature. The recommendation for the HCl channel is based on an average of the results of Lipson et al. and the rate expression obtained from the product of the HCl yield of Wang and Keyser and the evaluated overall rate constant as discussed above. Recent measurements by Tyndall et al. [1211] and Bedjanian et al. [100] are noted but are not considered in this evaluation.

F11. OH + OClO. The recommended value is that reported by Poulet et al. [969], the only reported study of this rate constant, using a discharge flow system in which OH decay was measured by LIF or EPR over the temperature range 293–473 K. Product HOCl was detected by modulated molecular beam mass spectrometry. The branching ratio for the channel to produce HOCl + O_2 was determined to be close to unity, but experimental uncertainty would allow it to be as low as 0.80.

F12. OH + HCl. The recommended value is based on a least squares fit to the data over the temperature range 240–300 K reported in the studies by Molina et al. [831], Keyser [622], Ravishankara et al. [993] and Battin-Leclerc et al. [86]. In these studies particular attention was paid to the determination of the absolute concentration of HCl by UV and IR spectrophotometry. Earlier studies by Takacs and Glass [1143], Zahniser et al. [1355], Smith and Zellner [1093], Ravishankara et al. [984], Hack et al. [466], Husain et al. [547], Cannon et al. [191], Husain et al. [548], and Smith and Williams [1092] had reported somewhat lower room temperature values. The data of Sharkey and Smith [1056] over the temperature range 138–216 K and Battin-Leclerc et al. [86] below 240 K depart from normal Arrhenius behavior. It is unknown whether this is due to an effect such as tunneling at low temperature or a systematic experimental error. Additional work at low temperature is needed.

F13. OH + HOCl. In the only reported study of this system Ennis and Birks [379] reported the value of this rate constant at room temperature to lie in the range $(1.7 – 9.5) \times 10^{-13}$ cm^3 $molecule^{-1}$ s^{-1}. A temperature-dependent expression has been estimated by choosing a pre-exponential factor by analogy with the OH + H_2O_2 reaction and selecting the midpoint of the experimental range for the room temperature rate constant. The large uncertainty factor is needed to encompass the entire range.

F14. OH + $ClNO_2$. The recommended value is based on results of the direct study of Ganske et al. [418,419] using the discharge flow-resonance fluorescence technique. Mass spectrometric studies showed HOCl to be the major chlorine-containing product, with no evidence for a channel to produce $HONO_2$ + Cl.

F15. OH + $ClONO_2$. The results reported by Zahniser et al. [1352] and Ravishankara et al. [980] are in good agreement at ~245 K (within 25%), considering the difficulties associated with handling $ClONO_2$. The preferred value is that of Zahniser et al. Neither study reported any data on the reaction products.

F16. OH + CH_3Cl. The recommended rate expression is derived from a combined fit (for T ≤ 400 K) of the data from the relative rate study by Hsu and DeMore [537] (recalculated based on the current recommendation for the rate constant for the OH + CH_3CHF_2 reference reaction, as described in the note for that reaction) and the absolute rate studies of Orkin et al. [914] and Herndon et al. [500]. Data from the earlier studies of Howard and Evenson [528], Perry et al. [942], Davis et al. [317], Paraskevopoulos et al. [928], Taylor et al. [1158], and Jeong and Kaufman [586] are reasonably well encompassed within the 2σ limits. The room temperature value from Taylor et al. [1158] is inconsistent with the higher temperature results in the same study and with the other investigations and lies outside of the 2σ band, as do the higher room temperature values of Cox et al. [281] and Brown et al. [155].

F17. OH + CH_2Cl_2. The recommended values for k(298 K) and E/R are averages of the values from the absolute rate studies of Villenave et al. [1233] and Herndon et al. [500] and the relative rate study of Hsu and DeMore [537] (two determinations which have been recalculated based on the current recommendations for the rate constants of the OH + CH_3CHF_2 and OH + CH_3CH_2F reference reactions). The renormalization procedure for relative rate measurements referenced to the OH + CH_3CHF_2 reaction is discussed in the note for that reaction. The rate constant determined relative to the rate constant of the OH + CH_3CH_2F was renormalized using a rate constant of the reference reaction calculated from the data of Schmoltner et al. [1039] and Kozlov et al. [650] above room temperature. The results of Cox et al. [281] and Davis et al. [317] support this recommendation. The results from Taylor et al. [1159], Jeong and Kaufman [586], Perry et al. [942] and Howard and Evenson [528] lie considerably higher and were not used in deriving the recommended parameters.

F18. OH + $CHCl_3$. The recommended value for k(298 K) is an average of the values from the relative rate study of Hsu and DeMore [537] (which has been recalculated based on the current recommendation for the rate constant of the OH + CH_3CHF_2 reference reaction, as described in the note for that reaction) and the absolute rate studies of Taylor et al. [1159] (which superseded Taylor et al. [1158]), Jeong and Kaufman [586], Davis et al. [317], and Howard and Evenson [528]. The recommended value of E/R is an average of values for this parameter derived in the first four of the above studies.

F19. OH + CCl_4. The recommended upper limit at 298 K is based on the upper limit reported in the competitive study by Cox et al. [281]. The value given there has been increased by a factor of four to allow for uncertainties in the number of NO molecules oxidized. The recommendation is compatible with the less sensitive upper limits reported by Howard and Evenson [528] and Clyne and Holt [243]. None of these

investigators reported any evidence for reaction between these species. The A-factor was estimated and a lower limit for E/R was derived.

F20. OH + CH_2FCl (HCFC-31). The recommended value for k(298 K) is an average of the values from the relative rate study of DeMore [335] (which has been recalculated based on the current recommendation for the rate constant of the OH + CH_2Cl_2 reference reaction) and the absolute rate studies of Howard and Evenson [528], Paraskevopoulos et al. [928], Watson et al. [1286], Handwerk and Zellner [480] and Jeong and Kaufman [586]. The recommended value for E/R is an average of the values for this parameter determined by DeMore and by Watson et al., Handwerk and Zellner, and Jeong and Kaufman below 400 K.

F21. OH + $CHFCl_2$ (HCFC-21). The recommended rate expression is derived from a combined fit to the data of Howard and Evenson [528], Perry et al. [942], Watson et al. [1286], Chang and Kaufman [209], Paraskevopoulos et al. [928], Jeong and Kaufman [586], and Fang et al. [382]. The rate constants reported by Clyne and Holt [244] are significantly higher than those from the other seven studies and were not used in deriving the recommended parameters.

F22. OH + CHF_2Cl (HCFC-22). Results for this compound show very good agreement among both absolute and relative rate constant measurements. The recommended rate expression is derived from a combined fit to the relative rate data of Hsu and DeMore [538] (which has been recalculated based on the current recommendation for the rate constant of the OH + CH_4 reference reaction), and the absolute rate studies of Orkin and Khamaganov [912], Fang et al. [382], Atkinson et al. [43], Watson et al. [1286], Chang and Kaufman [209], Paraskevopoulos et al. [928] and Jeong and Kaufman [586]. The more scattered results of Handwerk and Zellner [480] are in general agreement. The results from the studies of Howard and Evenson [528] and Clyne and Holt [244] are significantly different from those of the other studies and were not used in the derivation.

F23. OH + $CFCl_3$ (CFC-11). The A-factor was estimated, and a lower limit for E/R was derived by using the upper limit for the rate constant reported by Chang and Kaufman [210] at about 480 K. This expression is compatible with the upper limits reported by Atkinson et al. [43], Howard and Evenson [528], Cox et al. [281] and Clyne and Holt [243]. None of the investigators reported any evidence for reaction.

F24. OH + CF_2Cl_2 (CFC-12). The A-factor was estimated, and a lower limit for E/R was derived by using the upper limit for the rate constant reported by Chang and Kaufman [210] at about 480 K. This expression is compatible with the upper limits reported by Atkinson et al. [43], Howard and Evenson [528], Cox et al. [281] and Clyne and Holt [243]. None of the investigators reported any evidence for reaction.

F25. OH + CH_2ClCH_3. The recommended value for k(298 K) is an average of the values reported by Howard and Evenson [529], Paraskevopoulos et al. [928], Kasner et al. [608], and Herndon et al. [500]. The recommended value for E/R is an average of the values for this parameter determined by Kasner et al. and Herndon et al. with the value for A calculated to yield the recommended value for k(298 K). Data from the study by Markert and Nielsen [782] were not used to derive the recommended parameters, as they are somewhat more scattered.

F26. OH + CH_3CCl_3. The recommended value for k(298 K) is an average of the values from the absolute rate studies of Talukdar et al. [1156] and Finlayson-Pitts et al. [395], and a relative rate study of DeMore [332] (recalculated based on the current recommendation for the rate constant of the OH + CH_4 reference reaction). The temperature dependence is a fit to the data between 243 K and 379 K of Talukdar et al. [1156]. These studies indicate both a lower k(298 K) and E/R than was reported in earlier studies: Nelson et al. [856], Jeong and Kaufman [585], and Kurylo et al. [664]. More recent measurements by Jiang et al. [588] and Lancar et al. [678] yield rate constants that are slightly higher at 298 K than this recommendation.

F27. OH + CH_3CFCl_2 (HCFC-141b). Both absolute and relative rate measurements are in excellent agreement for this compound, and the data are linear over a wide temperature range. The recommended rate expression is derived from a combined fit to the data of Huder and DeMore [541] (two relative rate determinations which have been recalculated based on the current recommendations for the rate constants for the reference reactions OH + CH_4 and OH + CH_3CCl_3), Lancar et al. [678], Zhang et al. [1365] (together with the data at 330 K and above from Liu et al. [749], Talukdar et al. [1150] above 253 K (two studies), and Mors et al.[839]. The temperature-dependence data of Brown et al. [154] were not considered because the relatively large rate constants and Arrhenius curvature are suggestive of sample impurities.

F28. OH + CH_3CF_2Cl (HCFC-142b). The recommended value for k(298 K) is an average of the values from Howard and Evenson [529], Cox et al. [281], Paraskevopoulos et al. [928], Mors et al. [839], Watson et al. [1286], Handwerk and Zellner [480], Liu et al. [749], Gierczak et al. [431], and Fang et al. [383]. The recommended value of E/R is an average of values for this parameter derived in the last five of these studies. The data from Brown et al. [154] and Clyne and Holt [244] were not used to derive the recommended parameters. The 270 K data of Zhang et al. [1365] are in reasonable agreement with the recommendation.

F29. OH + CH_2ClCF_2Cl (HCFC-132b). The recommended rate expression was derived from the data of Watson et al. [1288], which were corrected by these authors for the presence of alkene impurities. The data of Jeong et al. [584], indicating faster rate constants, may have been affected by such impurities; hence they were not included in deriving the recommendation.

F30. OH + CH_2ClCF_3 (HCFC-133a). The recommended value of k_{298} is the average of the values of Howard and Evenson [529] and Handwerk and Zellner [480] adjusted to 298 K. The recommended temperature dependence was derived from the data of Handwerk and Zellner [480]. The data of Clyne and Holt [244] were not used in deriving the recommended parameters but (below 400 K) are encompassed within the 2σ limits.

F31. OH + $CHCl_2CF_2Cl$ (HCFC-122). The recommended rate expression is derived from a combined fit to the data of Orkin and Khamaganov [912] (below 400 K) and DeMore [335] (two determinations which have been recalculated based on the current recommendations for the rate constants of the OH + CH_2Cl_2 and OH + $CHCl_2CF_3$ reference reactions).

F32. OH + $CHFClCFCl_2$ (HCFC-122a). The recommended rate expression was derived from the relative rate data of Hsu and DeMore [538] (recalculated based on the current recommendation for the rate constant for the OH + CH_3CHF_2 reference reaction, as discussed in the note for that reaction).

F33. OH + $CHCl_2CF_3$ (HCFC-123). The recommended value of k_{298} is the average of the values from the absolute studies of Gierczak et al. [431] (two determinations) Liu et al. [749], and Yamada et al. [1342], and from the relative rate study by Hsu and DeMore [538] (recalculated based on the current recommendation for the rate constant for the OH + CH_3CHF_2 reference reaction, as discussed in the note for that reaction). The recommen-dation for the temperature dependence is derived from a fit to the data of these same five investigations. The temperature dependence data of Nielsen [875], Watson et al. [1288], Clyne and Holt [244], and Brown et al. [154] and the room temperature data of Howard and Evenson [529] were not used in the derivations.

F34. OH + $CHFClCF_2Cl$ (HCFC-123a). The recommended rate expression is based on the data of Orkin and Khamaganov [912].

F35. OH + $CHFClCF_3$ (HCFC-124). The recommended value for k(298 K) is an average of the values from the studies of Watson et al. [1288], Gierczak et al. [431] (2 studies), Yamada et al. [1342], and Hsu and DeMore [538] (two relative rate determinations which have been recalculated based on the current recommendations for the rate constants of the OH + CH_4 and OH + CHF_2CHF_2 reference reactions). The room temperature rate constant of Howard and Evenson [529] is considerably higher than these other values and was not included in the average. The recommended temperature dependence is an average of the dependencies derived from these same studies (but using only data below 400 K from Gierczak et al. [431] and Yamada et al. [1342].

F36. OH + $CH_3CF_2CFCl_2$ (HCFC-243cc). The recommended rate expression is derived from the temperature-dependence data of Nelson et al. [852]. Although there is only a single study of this reaction, the uncertainties have been assigned to reflect our belief that the rate constant for this reaction should be less than that for OH + CH_3CF_2Cl.

F37. OH + $CHCl_2CF_3CF_2$ (HCFC-225ca). The recommended value for k(298 K) is an average of the values from Nelson et al. [852] and Zhang et al. [1366]. The recommendation for E/R is taken from Nelson et al. [852]. The temperature-dependence data of Brown et al. [153] were not considered because the relatively large rate constants at and below room temperature and the Arrhenius curvature are suggestive of sample impurities. The temperature dependence results of Zhang et al. [1366] are in reasonable agreement with those of Nelson et al. [852] over the temperature range of measurement overlap. However, the complete Zhang et al. [1366] data set yields a value for E/R much larger than currently recommended for the OH + $CHCl_2CF_3$ (HFC-123) reaction, for which the activation energy should be similar.

F38. OH + CF_2ClCF_2CHFCl (HCFC-225cb). The recommended rate expression is derived from a combined fit to the temperature-dependence data of Nelson et al. [852] and Zhang et al. [1366], which are in excellent agreement.

F39. OH + CH_2=CHCl. The recommended value for k(298 K) is an average of the values reported by Howard [526], Perry et al. [941], Liu et al. [748] and [1343]. The recommended value for E/R is an average of the values for this parameter derived from fits to the data of Perry et al., Liu et al. and Yamada et al. at temperatures below about 400 K. In the 400–500 K region the rate constant levels off before increasing at higher temperatures, suggesting the stronger importance of an abstraction mechanism at the higher temperatures.

F40. OH + CH_2=CCl_2. The recommended value for k(298 K) is an average of the values reported by Edney et al. [373], Tuazon et al. [1191], Abbatt and Anderson [1], Zhang et al. [1367], Canosa-Mas et al. [193] and [1341]. The recommended value for E/R comes from a combined fit to the data of Abbatt and Anderson, Zhang et al. and Yamada et al. The data of Kirchner et al. [628] were not used in deriving the recommended parameters since they were obtained at very low pressure and the much stronger temperature dependence obtained may be indicative of a pressure dependence above room temperature.

F41. OH + CHCl=CCl_2. The recommended value for k(298 K) is the mean of the values reported by Howard [526], Chang and Kaufman [209], Kirchner et al. [628], Klopffer et al. [638], Edney et al. [373] and Tichenor et al. [1172]. The recommended value of E/R is an average of values for this parameter derived by Chang and Kaufman [209], Kirchner et al. [628] and Tichenor et al. [1172]. The value for k(298 K) derived from a relative rate study by Winer et al. [1327] is a factor of ~2 greater than the other values and is not considered in deriving the preferred value. An absolute study by Jiang et al. [589] yielding a significantly higher value for k(298 K) as well as a considerably stronger temperature dependence (E/R = –970 K) is assumed to be superseded by Tichenor et al. [1172].

F42. OH + CCl_2=CCl_2. The recommended value for k(298 K) is the mean of the values reported by Howard [526], Chang and Kaufman [209], and Kirchner et al. [628]. The room temperature value reported by Winer et al. [1327] is more than a factor of 10 greater and was not used in deriving the recommendation. The recommended value for E/R is an average of values for this parameter derived by Chang and Kaufman [209] and Kirchner et al. [628]. A study by Tichenor et al. [1173] yields a value for k(298 K) slightly lower than these other studies, but a temperature dependence less than half of that recommended. While these latest results were not used in deriving the recommendations, they are encompassed within the 95% confidence limits.

F43. OH + CH_3OCl. The recommended rate expression is derived from a fit to the data of Crowley et al. [294], the only reported study of this reaction.

F44. OH + CCl_3CHO. The recommended value for k(298 K) is an average of the values reported by Barry et al. [78] (using three independent techniques), Dobe et al. [350], Nelson et al. [856], Ballestra-Garcia et al. [59], and Scollard et al. [1045]. The temperature dependence is derived from a fit to the data of Dobe et al. [350]. The A factor was then calculated to agree with the recommended value for k(298 K).

F45. HO_2 + Cl. The recommendations for the two reaction channels are based upon the results by Lee and Howard [703] using a discharge flow system with laser magnetic resonance detection of HO_2, OH, and ClO. The total rate constant is temperature independent with a value of $(4.2\pm0.7) \times 10^{-11}$ cm^3 $molecule^{-1}$ s^{-1} over the temperature range 250–420 K. This value for the total rate constant is in agreement with the results of indirect studies relative to Cl + H_2O_2 (Leu and DeMore [717], Poulet et al. [967], Burrows et al. [176]] or to Cl + H_2 (Cox [275]). The contribution of the reaction channel producing OH + ClO (21% at room temperature) is much higher than the upper limit reported by Burrows et al. (1% of total reaction). Cattell and Cox [206], using a molecular modulation-UV absorption technique over the pressure range 50–760 torr, report results in good agreement with those of Lee and Howard both for the overall rate constant and for the relative contribution of the two reaction channels. A study by Dobis and Benson [355] reports a total rate constant in good agreement with this recommendation but a much lower contribution (5±3%) of the channel producing OH + ClO. The rate constant for the channel producing ClO + OH can be combined with that for the reaction ClO + OH > Cl + HO_2 to give an equilibrium constant from which a value of the heat of formation of HO_2 at 298 K of 3.0 kcal/mol can be derived.

F46. HO_2 + ClO. Three new studies by Nickolaisen et al [865], Knight et al. [640], and Laszlo et al. [682] have been added to the previous five studies of this rate constant (Reimann and Kaufman, [999]; Stimpfle et al. [1122]; Leck et al. [691]; Burrows and Cox [177]; Cattell and Cox [206]). The studies span a wide variety of pressure conditions and detection techniques. The studies of Cattell and Cox and Nickolaisen et al. were performed over extended pressure ranges and indicate that the reaction is pressure independent. However, the room temperature rate constant obtained by averaging the five low pressure (< 10 torr) studies is slightly lower (5.1±1.5 vs. 6.5±1.2 in units of 10^{-12} cm^3 $molecule^{-1}$ s^{-1}) than that obtained by averaging the higher pressure measurements (> 50 torr). Although within the combined uncertainty, this offset may suggest possible systematic experimental complications (e.g. unknown secondary reactions) in the low or high pressure experiments. The recommended value for k(298 K) is the mean of the eight studies. Temperature-dependence data has been obtained by Stimpfle et al., Nickolaisen et al., Knight et al., and Laszlo et al. The earliest study (Stimpfle et al.) observed nonlinear Arrhenius behavior. The data were best described by a four parameter equation of the form $k=A\exp(-B/T)+CT^n$, possibly suggesting that two different mechanisms may be occurring. The more recent studies find the T-dependence to display linear Arrhenius behavior over the entire temperature range. Moreover, they derive much smaller E/R values (17 to 312) than that obtained

by Stimpfle (E/R ≈ 700 for T<300 K). The recommended value for E/R is based on an average of the four studies over their entire temperature ranges. The two most probable pairs of reaction products are, (1) HOCl + O_2 and (2) HCl + O_3. Leu [715], Leck et al., Knight et al., and Laszlo et al. used mass spectrometric detection of ozone to place upper limits on channel 2 of 1.5%, 2%, 1%, and 2%, respectively at 298 K. In addition, Leck et al. and Laszlo set upper limits of 3.0% (248 K); and 5.0% (243 K), respectively, on k_2/k. Burrows and Cox report an upper limit of 0.3% for k_2/k at 300 K. Finkbeiner et al. [394], using matrix-isolation/FTIR spectroscopy, studied product formation between 210 and 300 K at 700 torr. HOCl was observed as the dominant product (> 95% at all temperatures). The branching ratio values for k_2/k were determined to be <1% at 300 K and 270 K, 2±1% at 240 K, and 5±2% at 210 K. No evidence for any other product channel was found. Theoretical calculations by Nickolaisen et al. suggest that the reaction to channel (1) proceeds mainly through the ClO-HO_2 complex on the triplet potential surface. However, these calculations also suggest that collisionally stabilized HOOOCl formed on the singlet surface will possess an appreciable lifetime. Further studies on possible formation of HOOOCl are warranted.

F47. H_2O + $ClONO_2$. This recommendation is based on the upper limits to the homogeneous bimolecular rate constant reported by Atkinson et al. [49], and by Hatakeyama and Leu [487,488]. Atkinson et al. observed by FTIR analysis the decay of $ClONO_2$ in the presence of H_2O in large-volume (2500 and 5800 liters) Teflon or Teflon-coated chambers. Their observed decay rate gives an upper limit to the homogeneous gas phase rate constant, and they conclude that the decay observed is due to heterogeneous processes. Hatakeyama and Leu, using a static photolysis system with FTIR analysis, derive a similar upper limit. Rowland et al. [1008] concluded that the decay they observed resulted from rapid heterogeneous processes. The homogeneous reaction is too slow to have any significant effect on atmospheric chemistry.

F48. NO + OClO. The Arrhenius expression was estimated based on 298 K data reported by Bemand, Clyne and Watson [109].

F49. NO + Cl_2O_2. The recommended upper limit is that determined by Friedl (private communication) in a study using a DF-MS technique.

F50. NO_3 + HCl. The recommended upper limit is that reported by Mellouki et al. [807] in a study using DF-EPR techniques. This upper limit shows that this reaction is of negligible importance in stratospheric chemistry. Somewhat lower upper limits have been reported by Cantrell et al. [197] and Canosa-Mas et al. [194]; the latter study also reports Arrhenius parameters at higher temperatures (333–473 K).

F51. HO_2NO_2 + HCl. This upper limit is based on results of static photolysis-FTIR experiments reported by Leu et al. [720].

F52. Cl + O_3. The results reported for k(298 K) by Watson et al. [1287], Zahniser et al. [1356], Kurylo and Braun [665], Clyne and Nip [253], Nicovich et al. [868] and Seeley et al. [1046] are in good agreement, and have been used to determine the preferred value at this temperature. The values reported by Leu and DeMore [717] (due to the wide error limits) and Clyne and Watson [259] (the value is inexplicably high) are not considered. The six Arrhenius expressions are in fair agreement within the temperature range 205–300 K. In this temperature range, the rate constants at any particular temperature agree to within 30–40%. Although the values of the activation energy obtained by Watson et al. and Kurylo and Braun are in excellent agreement, the value of k in the study of Kurylo and Braun is consistently (~17%) lower than that of Watson et al. This may suggest a systematic underestimate of the rate constant, as the values from the other three agree so well at 298 K. The two most recent studies (Nicovich et al. and Seeley et al.) obtained significantly smaller temperature dependences than those observed in the earlier studies. There is no reason to prefer any one set of data to any other; therefore, the preferred Arrhenius expression shown above was obtained by computing the mean of the six results between 205 and 298 K. DeMore [331] directly determined the ratio k(Cl + O_3)/k(Cl + CH_4) at 197–217 K to be within 15% of that calculated from the absolute rate constant values recommended here.

Vanderzanden and Birks [1226] have interpreted their observation of oxygen atoms in this system as evidence for some production (0.1–0.5%) of O_2 ($^1\Sigma_g^+$) in this reaction. The possible production of singlet molecular oxygen in this reaction has also been discussed by DeMore [328], in connection with the Cl_2 photosensitized decomposition of ozone. However Choo and Leu [228] were unable to detect $O_2(^1\Sigma)$ or $O_2(^1\Delta)$ in the Cl + O_3 system and set upper limits to the branching ratios for their production of 5×10^{-4} and 2.5×10^{-2}, respectively. They suggested two possible mechanisms for the observed production of oxygen atoms, involving reactions of vibrationally excited ClO radicals with O_3 or with Cl atoms, respectively. Burkholder et al. [172], in a study of infrared line intensities of the ClO radical, present evidence in support of the second mechanism. In their experiments with excess Cl atoms, the vibrationally excited ClO radicals produced in the Cl + O_3 reaction can react with Cl atoms to give Cl_2 and oxygen atoms, which can then remove additional ClO radicals. These authors point out the possibility for systematic error from assuming a

1:1 stoichiometry for $[Cl]:[O_3]_o$ when using the $Cl + O_3$ reaction as a quantitative source of ClO radicals for kinetic and spectroscopic studies.

F53. $Cl + H_2$. This Arrhenius expression is based on the data below 300 K reported by Watson et al. [1285], Lee et al. [694], Miller and Gordon [826], and Kita and Stedman [631]. The results of these studies are in excellent agreement below 300 K; the data at higher temperatures are in somewhat poorer agreement. The results of Watson et al., Miller and Gordon, and Kita and Stedman agree well (after extrapolation) with the results of Benson et al. [112] and Steiner and Rideal [1109] at higher temperatures. For a discussion of the large body of rate data at high temperatures, see the review by Baulch et al. [89][86]. The room temperature value of Kumaran et al. [656], in a study primarily at high temperatures, is in excellent agreement with this recommendation. Miller and Gordon and Kita and Stedman also measured the rate of the reverse reaction, and found the ratio to be in good agreement with equilibrium constant data.

F54. $Cl + H_2O_2$. The absolute rate coefficients determined at ~298 K by Watson et al. [1287], Leu and DeMore [717], Michael et al. [824], Poulet et al. [967] and Keyser [617] range in value from $(3.6–6.2) \times 10^{-13}$. The studies of Michael et al., Keyser, and Poulet et al. are presently considered to be the most reliable. The preferred value for the Arrhenius expression is taken to be that reported by Keyser. The A-factor reported by Michael et al. is considerably lower than that expected from theoretical considerations and may possibly be attributed to decomposition of H_2O_2 at temperatures above 300 K. The data of Michael et al. at and below 300 K are in good agreement with the Arrhenius expression reported by Keyser. More data are required before the Arrhenius parameters can be considered to be well-established. Heneghan and Benson [498], using mass spectrometry, confirmed that this reaction proceeds only by the abstraction mechanism giving HCl and HO_2 as products.

F55. $Cl + NO_3$. The recommended value at room temperature is based on the discharge flow-EPR study of Mellouki et al. [805] and the discharge flow-mass spectrometric study of Becker et al. [92]. The results of these direct absolute rate studies are preferred over results of the earlier relative rate studies of Cox et al. [276], Burrows et al. [180], and Cox et al. [287], in all of which NO_3 was monitored in the photolysis of Cl_2-$ClONO_2$-N_2 mixtures. Complications in the chemistry of the earlier systems probably contributed to the spread in reported values. This radical-radical reaction is expected to have negligible temperature dependence, which is consistent with the results from the study of Cox et al. [287] in which the complications must have been temperature independent.

F56. $Cl + N_2O$. This rate coefficient has been determined in a study of the halogen-catalyzed decomposition of nitrous oxide at about 1000 K by Kaufman et al. [609]. The largest value reported was 10^{-17} cm^3 $molecule^{-1}$ s^{-1}, with an activation energy of 34 kcal/mol. Extrapolation of these results to low temperature shows that this reaction cannot be of any significance in atmospheric chemistry.

F57. $Cl + HNO_3$. The recommended upper limit at room temperature is that reported in the study of Wine et al. [1324], in which long-path laser absorption spectroscopy was used to look for the appearance of NO_3 following the pulsed laser photolysis of Cl_2-HNO_3 mixtures with no evidence for NO_3 production was observed. In the same study a less sensitive upper limit was derived from monitoring Cl atom decay by resonance fluorescence. A less sensitive upper limit was also found in the discharge flow-EPR study of Zagogianni et al. [1350]. Higher values obtained in earlier studies (Leu and DeMore [717], Kurylo et al. [671], and Clark et al. [234]) as well as the higher temperature results of Poulet et al. [967] are not used.

F58. $Cl + HO_2NO_2$. The only study of this reaction is by Simonaitis and Leu [1072] using the low pressure discharge flow technique coupled with resonance fluorescence detection of Cl and mass spectrometric detection of HO_2NO_2 ion fragments. Consistent results were obtained monitoring either Cl or HO_2NO_2 decays and retrieved rate constants were less than 1×10^{-13} cm^3 $molecule^{-1}$ s^{-1} for all conditions. Impurities in the HO_2NO_2 sample (especially H_2O_2) complicated the measurements. A limited temperature study over the 298–399 K range suggests that E/R is in the range of 500 – 1500. Given the experimental difficulties, only an upper limit is recommended for the reaction rate.

F59. $Cl + CH_4$. The values of k at 298 K reported from thirteen absolute rate constant studies (Manning and Kurylo [770], Whytock et al. [1303], Michael and Lee [817], Lin et al. [740], Zahniser et al. [1351], Keyser [615], Ravishankara and Wine [988], Heneghan et al. [499], Dobis and Benson [353], Sawerysyn et al. [1031], Beichert et al. [107], Seeley et al. [1046], and Pilgrim et al. [950]) fall in the range $(0.92 – 1.13) \times 10^{-13}$, with a mean value of 0.99×10^{-13}. An earlier absolute study by Watson et al. [1287] gives rate constant values slightly higher than those of the aforementioned studies, which may be due to uncertainties in correcting the data for OH loss via reaction with trace levels of ethane and propane in the methane samples used.

The values derived for k at 298 K from the competitive chlorination studies of Pritchard et al. [970], Pritchard et al. [971], Knox [641], Knox and Nelson [643], Lee and Rowland [692], and Lin et al. [740]

range from
$(0.8–1.6) \times 10^{-13}$ when the original data are referenced to the presently recommended rate constant values for the reactions of Cl with H_2 and C_2H_6. Of these relative rate studies, that of Lin et al. [740], yields a room temperature rate constant (1.07×10^{-13}) that is most consistent with the absolute measured values. Thus, the recommended value for k at 298 K (1.0×10^{-13}) is derived from an unweighted average of the rate constants from the thirteen preferred absolute studies and the relative rate study of Lin et al. [740].

There have been nine absolute studies of the temperature dependence of k in which the measurements extend below 300 K (Watson et al. [1287], Manning and Kurylo [770], Whytock et al. [1303], Lin et al. [740], Zahniser et al. [1351], Keyser [615], Ravishankara and Wine [988], Heneghan et al. [499], and Seeley et al. [1046]). In general, the agreement among most of these studies is quite good. However, systematic differences in activation energies are apparent when calculated using data obtained below 300 K versus data from above 300 K. Three resonance fluorescence studies have been performed over the temperature region between 200 and 500 K (Whytock et al. [1303], Zahniser et al. [1351] and Keyser [615]), and in each case a strong non-linear Arrhenius behavior was observed. Ravishankara and Wine [988] also noted nonlinear Arrhenius behavior over a more limited temperature range. This behavior tends to partially explain the variance in the values of E/R reported between those investigators who mainly studied this reaction below 300 K (Watson et al. [1287], Manning and Kurylo [770], and Seeley et al. [1046])] and those who only studied it above 300 K (Clyne and Walker [258], Poulet et al. [966], and Lin et al. [740]). The agreement between all studies below 300 K is reasonably good, with values of E/R ranging from (1063–1320) K, and k(230 K) in the range
$(2.6–3.2) \times 10^{-14}$. There have not been any absolute studies at stratospheric temperatures other than those which utilized the resonance fluorescence technique. Ravishankara and Wine [988] have suggested that the results obtained using the discharge flow and competitive chlorination techniques may be in error at the lower temperatures (<240 K) due to a non-equilibration of the $^2P_{1/2}$ and $^2P_{3/2}$ states of atomic chlorine. Ravishankara and Wine observed that at temperatures below 240 K the apparent bimolecular rate constant was dependent upon the chemical composition of the reaction mixture; i.e., if the mixture did not contain an efficient spin equilibrator, e.g., Ar or CCl_4, the bimolecular rate constant decreased at high CH_4 concentrations. The chemical composition in each of the flash photolysis studies contained an efficient spin equilibrator, whereas this was not the case in the discharge flow studies. However, the reactor walls in the discharge flow studies could have been expected to have acted as an efficient spin equilibrator. Consequently, until the hypothesis of Ravishankara and Wine is proven it is assumed that the discharge flow and competitive chlorination results are reliable. A composite unweighted Arrhenius fit to all of the temperature dependent absolute studies with data in the temperature region ≤300 K (with the exception of the data of Watson et al. [1287], which appear to be systematically high due to reactive impurities) yields E/R = 1253 K and k(298 K) = 1.0×10^{-13}.

The competitive chlorination results differ from those obtained in the absolute studies in that linear Arrhenius behavior is observed. The values of E/R are consistently larger than those obtained from the absolute studies, with an average value of approximately 1500 K. Until the hypothesis of Ravishankara and Wine [988] is re-examined, the preferred Arrhenius expression attempts to best fit the results obtained between 200 and 300 K from all sources. Thus, using the relative rate results of Lin et al. [740] (referenced to the current recommendation for the Cl + C_2H_6 reaction) as representative of the relative rate studies below 300 K, together with the composite fit to the absolute studies given above, we obtain a recommended E/R value of 1360 K. Taken with the recommended value for k(298 K) = 1.0×10^{-13}, we compute an Arrhenius A factor of 9.6×10^{-12}. However, the A-factor thus derived seems somewhat low (on a per hydrogen atom basis) when compared with the A-factors for some similar reactions.

F60. Cl + CH_3D. Recommended value is based on results of Wallington and Hurley [1259].

F61. Cl + H_2CO. The results from five of the six published studies (Michael et al. [821], Anderson and Kurylo [25], Niki et al. [885], Fasano and Nogar [385] and Poulet et al. [962]) are in good agreement at ~298 K, but are ~50% greater than the value reported by Foon et al. [403]. The preferred value at 298 K was obtained by combining the absolute values reported by Michael et al., Anderson and Kurylo, and Fasano and Nogar, with the values obtained by combining the ratio of k(Cl + H_2CO)/k(Cl + C_2H_6) reported by Niki et al. (1.3±0.1) and by Poulet et al. (1.16±0.12) with the preferred value of 5.7×10^{-11} for k(Cl + C_2H_6) at 298 K. The preferred value of E/R was obtained from a least squares fit to all the data reported in Michael et al. and in Anderson and Kurylo. The A-factor was adjusted to yield the preferred value at 298 K.

F62. Cl + HC(O)OH. The room temperature kinetics of this reaction have been studied by Wallington et al. [1245] and Li et al. [728]. Wallington et al. used a relative rate technique at atmospheric pressure while Li et al. employed flash photolysis and operated at 10 torr. The results of the two studies are in excellent agreement and have been averaged together to derive the recommended value. Reaction products have been investigated

by Tyndall et al. [1221] at room temperature and 700 torr pressure. They measured the CO_2 yield to be 96 ± 5% and suggested that the HOCO complex reacted with either O_2 or Cl_2 in their experiment to give the observed product.

F63. Cl + CH_3O_2. Recommended value is based on results of Maricq et al. [780], Jungkamp et al. [598], and Daele and Poulet [299]. All three studies agree that this overall reaction is very fast. However, there is a discrepancy in the reported values of the branching ratios for the two pathways producing ClO + CH_3O (a) and HCl + CH_2O_2 (b). The branching ratio for the reaction channels producing HCl + CH_2O_2 (b) has been reported to be 50% by both Maricq et al. [780] and Jungkamp et al., but has been reported to be 90% by Daele and Poulet. Because of this large discrepancy no branching ratios are recommended.

F64. Cl + CH_3OH. This recommendation at 298 K) is based on results of the absolute rate studies of Michael et al. [822], Payne et al. [937], Dobe et al. [351], Pagsberg et al. [924] and Tyndall et al. [1214], and results obtained in the competitive chlorination studies of Wallington et al. [1267], Lightfoot et al. [733], Nelson et al. [855] and Tyndall et al. The temperature independence of the rate constant was reported by Michael et al. in a direct study. This is consistent with the indirect results of Lightfoot et al. who deduced the rate coefficient for this reaction relative to that for methane as a function of temperature. This reaction can have two sets of products: CH_2OH + HCl, channel (a) and CH_3O + HCl, channel (b). Product analysis and isotopic substitution have established that the reaction proceeds via channel (a) rather than via channel (b). See Radford [973], Radford et al. [974], Meier et al. [800], and Payne et al. [937]. This reaction has been used in the laboratory as a source of CH_2OH and as a source of HO_2 by the reaction of CH_2OH with O_2.

F65. Cl + CH_3OOH. The only study of this reaction was by Wallington et al [1245], who measured the rate relative to Cl + C_2H_6 at 295 K and atmospheric pressure.

F66. Cl + CH_3ONO_2. This reaction has been studied at 298 K by Nielsen et al [881] using a relative rate technique. The reference compound was ethane. The recommended value is adjusted from that given by Nielsen et al. using the currently recommended value for k (Cl + C_2H_6). The temperature dependence is estimated by assuming an A-factor equal to approximately 20 times that of OH + CH_3ONO_2. This is consistent with observed OH/Cl A-factor ratios for primary H-abstraction from alkanes.

F67. Cl + C_2H_6. The absolute rate coefficients reported in all four studies (Davis et al. [314], Manning and Kurylo [770], Lewis et al. [726], and Ray et al. [995]) are in good agreement at 298 K. The value reported by Davis et al. was probably overestimated by ~10% (the authors assumed that I_f was proportional to $[Cl]^{0.9}$, whereas a linear relationship between I_f and [Cl] probably held under their experimental conditions). The preferred value at 298 K was taken to be a simple mean of the four values (the value reported by Davis et al. was reduced by 10%), i.e., 5.7×10^{-11}. The two values reported for E/R are in good agreement; E/R = 61 K (Manning and Kurylo) and E/R = 130 K (Lewis et al.). A simple least squares fit to all the data would unfairly weight the data of Lewis et al. due to the larger temperature range covered. Therefore, the preferred value of
$7.7 \times 10^{-11} \exp(-90/T)$ is an expression which best fits the data of Lewis et al. and Manning and Kurylo between 220 and 350 K. The recent temperature-dependent results of Dobis and Benson [354] and room temperature results of Kaiser et al. [602], Hooshiyar and Niki [521] and Beichert et al. [107] are in good agreement with the recommendation.

F68. Cl + $C_2H_5O_2$. Recommended value is based on results of Maricq et al. [780].

F69. Cl + CH_3CH_2OH. The rate coefficient for this reaction has been studied at 298 K by four groups using a relative rate technique: Nelson et al. [855] (relative to Cl + cyclohexane), Wallington et al. [1267] (relative to Cl + C_2H_6), Edelbuttel-Einhaus et al. [372] (relative to Cl + C_2H_6), and Taatjes et al. [1139]. Nelson et al measured this rate constant relative to the Cl + cyclohexane while the others used the Cl + C_2H_6 reaction. Taatjes et al. also measured this rate coefficient by measuring the temporal profile of the HCl product. The agreement between these five measurements is quite good, yielding an average value that is recommended. The temperature dependence of this rate coefficient is based on the results of Taatjes et al., who studied this reaction above 298 K and found it to be essentially independent of temperature. We recommend the same independence of temperature at atmospheric temperatures.

This reaction can have three sets of products: CH_2CH_2OH + HCl, channel (a); CH_3CHOH, channel (b); and CH_3CH_2O channel (c). Taatjes et al. have deduced that channel (c) is negligible and that channel (a) is about 8% at 298 K. Therefore, the majority of reaction is expected to occur via channel (b). It is very unlikely that these branching ratios will change significantly at lower atmospheric temperatures.

F70. Cl + $CH_3C(O)OH$. Koch and Moortgat [645] have studied this reaction at room temperature using the relative rate technique. Deuterium substitution of the methyl hydrogens decreased the observed rate by a factor of 3.75. In addition, CO and CO_2 reaction products were observed in a stoichiometric ratio of 1:1. These

observations were interpreted in terms of methyl hydrogen abstraction from acetic acid to form the $CH_2C(O)OH$ radical followed by reaction with O_2 to form a peroxy radical. Thermal decomposition of the peroxy radical produces HCHO, CO_2, and atomic H. In the laboratory system, the HCHO reacts with atomic chlorine to yield CO.

F71. Cl + CH_3CN. The recommendation is based on results of the study of Tyndall et al. [1216]. The results of this study, using both relative and absolute methods and measured over a wide range of experimental conditions are preferred over the results of earlier studies of Kurylo and Knable [667], Poulet et al. [961], and Olbregts et al. [906]. Product studies reported by Tyndall et al. show that reaction proceeds predominantly by hydrogen atom abstraction.

F72. Cl + $C_2H_5ONO_2$. Wallington et al. [1258] and Nielsen et al [881] have measured the rate of this reaction at room temperature relative to atomic chlorine reactions with ethyl chloride and ethane, respectively. The two studies are in excellent agreement and the recommended value is based on an average of the two. The values given in Wallington et al and Nielsen et al. were adjusted based on the currently accepted values of the reference rate constants. The temperature dependence is estimated by assuming an A-factor equal to approximately 20 times that of OH + CH_3ONO_2. This is consistent with observed OH/Cl A-factor ratios for primary H-abstraction from alkanes.

F73. Cl + $CH_3CO_3NO_2$ (PAN). The recommended value is based on results of the relative rate study of Wallington et al. [1245]. In this study no reaction of PAN was observed in the presence of Cl atoms. These results are preferred over the results of the direct study of Tsalkani et al. [1187] using a discharge flow system with EPR detection of Cl atom decay (in which study the authors reported a rate constant of $(3.7\pm1.7) \times 10^{-13}$ cm^3 molecule^{-1} s^{-1}). In both studies the major impurity in the PAN samples would be the alkane solvent. The presence of 0.1% tridecane in the PAN sample used by Tsalkani et al. could account for the observed Cl atom decay; however, solvent impurities in the PAN sample would be of no consequence in the relative rate study of Wallington et al.

F74. Cl + C_3H_8. The recommended room temperature value is the mean of results of the competitive chlorination studies of Pritchard et al. [971], Knox and Nelson [643], Atkinson and Aschmann [35], Wallington et al. [1267], and Hooshiyar and Niki [521], and the absolute rate studies of Lewis et al. [726] and Beichert et al. [107]. The temperature dependence is from Lewis et al. The A-factor from that study has been adjusted slightly to fit the recommended room temperature value.

F75. Cl + $CH_3C(O)CH_3$. The rate coefficient for this reaction has only been reported at 298 K. Wallington et al. [1267] and Olsson et al. [907] report values of 2.37×10^{-12} and 1.69×10^{-12} cm^3 molecule^{-1} s^{-1} at 298 K measured via relative rate methods. The only direct measurement of this rate constant is by Notario et al. [900] who report a value of $(3.06 \pm 0.38) \times 10^{-12}$ cm^3 molecule^{-1} s^{-1} at 298 K. Because of the reasons noted by Wallington et al. [1267], the value reported by Olsson et al. is suspect and is not considered here. The average of the results from Wallington et al. and Notario et al. is recommended for k(298 K). In the absence of temper-ature dependent measurements, based on analogy with other Cl atom reactions with halogenated hydrocarbons whose rate coefficients at 298 K are close to that for Cl + $CH_3C(O)CH_3$, we recommend an E/R value of 1000 K with a g value of 500 K. Such a temperature dependence is consistent with this reaction proceeding via H atom abstraction. This E/R and k(298 K) lead to an A factor of 7.7×10^{-11} cm^3 molecule^{-1} s^{-1} . This A factor is the same as that for the reaction of Cl atom with ethane, which also contains six primary C–H bonds. End product studies clearly show that the products of this reaction are $CH_3C(O)CH_2$ and HCl.

F76. Cl + $C_2H_5CO_3NO_2$. Wallington et al. [1245] have measured this rate constant relative to Cl + CH_3Cl. The recommended value is adjusted from that given by Wallington et al. using the currently recommended value for the reference reaction rate constant.

F77. Cl + 1-$C_3H_7ONO_2$. Wallington et al. [1258] and Nielsen et al [881] have measured the rate of this reaction at room temperature relative to atomic chlorine reactions with ethyl chloride and ethane, respectively. The two studies are in excellent agreement and the recommended value is based on an average of the two. The values given in Wallington et al and Nielsen et al. were adjusted based on the currently accepted values of the reference rates. The temperature dependence is estimated by assuming an A-factor equal to approximately 20 times that of OH + CH_3ONO_2. This is consistent with observed OH/Cl A-factor ratios for primary H-abstraction from alkanes.

F78. Cl + 2-$C_3H_7ONO_2$. This reaction has been measured by Wallington et al [1258] at 295 K relative to Cl + C_2H_5Cl. The reported ratio of 0.46 ± 0.03 has been converted to an absolute rate using the currently recommended value for the ethyl chloride reaction rate. The temperature dependence is estimated by assuming an A-factor equal to approximately 20 times that of OH + CH_3ONO_2. This is consistent with observed OH/Cl A-factor ratios for primary H-abstraction from alkanes.

F79. Cl + OClO. The data of Toohey [1181] are in good agreement with the results of Bemand et al. [109] at room temperature, and the recommended value at room temperature is the mean of the values reported in these two studies. The slight negative temperature dependence reported by Toohey [1181] is accepted but with error limits that encompass the temperature independence reported in the earlier study.

F80. Cl + ClOO. The recommended value is based on the results of studies by Mauldin et al. [792] and Baer et al. [54], in which ClOO was formed by the pulsed photolysis of Cl_2/O_2 mixtures and its overall loss rate was monitored by UV absorption. In both studies k was found to be independent of temperature. These results are preferred over the results of the earlier, indirect studies of Johnston et al. [590], Cox et al. [282], and Ashford et al. [32]. The earlier studies did show that the predominant reaction pathway is that yielding $Cl_2 + O_2$ as products. From the branching ratio data of Cox et al., Ashford et al., and Nicholas and Norrish [863], it can be estimated that this reaction channel constitutes 95% of the overall reaction with ClO + ClO the products of the minor (5%) reaction channel.

F81. Cl + Cl_2O. The preferred value was determined from results of the temperature-dependent study of Stevens and Anderson [1114] and the results of two independent absolute rate coefficient studies reported by Ray et al. [995], which used the discharge flow-resonance fluorescence and discharge flow-mass spectrometric techniques. This value has been confirmed by Burrows and Cox [177], who determined the ratio $k(Cl + Cl_2O)/k(Cl + H_2) = 6900$ in modulated photolysis experiments. The earlier value reported by Basco and Dogra [80] has been rejected.

F82. Cl + Cl_2O_2. The recommended value is that determined by Friedl (private communication) in a study using a DF-MS technique. It is in agreement with the value reported by Cox and Hayman [289] in a study using a static photolysis technique with photodiode array UV spectroscopy.

F83. Cl + HOCl. This recommendation is based on results over the temperature range 243–365 K reported by Cook et al. [270] and the room temperature result of Vogt and Schindler [1235]. There is a significant discrepancy in the reported values of the product branching ratios. Ennis and Birks [378] reported that the major reaction channel is that to give the products Cl_2 + OH with a yield of 91±6%, whereas Vogt and Schindler report this yield to be 24±11%, with the major reaction channel giving HCl + ClO as products.

F84. Cl + ClNO. The discharge flow-resonance fluorescence study of Abbatt et al. [4] provides the first reliable data on the temperature dependence. The laser photolysis-LMR study of Chasovnikov et al. [213] provides rate data for each Cl atom spin state, and they attribute the low value reported by Nelson and Johnston [854] in a laser flash photolysis-resonance fluorescence study to reaction of the Cl $^2P_{1/2}$ state. Adsorption and decomposition of ClNO on the walls of their static system may account for the very low value of Grimley and Houston [459]. The results of Clyne and Cruse [239] in a discharge flow-resonance fluorescence study are significantly lower than all recent results. The recommended value at room temperature is the mean of the values reported by Abbatt et al. [4], Chasovnikov et al. [213], Nesbitt et al. [861], and Kita and Stedman [631]. The recommended temperature dependence is from the study of Abbatt et al. [4].

F85. Cl + $ClONO_2$. Recommended value is based on the results of Yokelson et al. [1346] and those of Margitan [773]. These results are in excellent agreement; the slightly higher values of Kurylo et al. [668] are encompassed within the stated uncertainties. Yokelson et al. report that at 298 K, more than 95% of this reaction proceeds by the reaction channel giving $Cl_2 + NO_3$ as products.

F86. Cl + CH_3Cl. The recommended room temperature value is the mean of results of the absolute rate studies of Manning and Kurylo [770] and Beichert et al. [107] and the relative rate study of Wallington et al. [1245]. The temperature dependence is from Manning and Kurylo. The A-factor from that study has been adjusted slightly to fit the recommended room temperature value. The results reported by Clyne and Walker [258] and Manning and Kurylo [770] are in good agreement at 298 K. However, the value of the activation energy measured by Manning and Kurylo is significantly lower than that measured by Clyne and Walker. Both groups of workers measured the rate constant for the Cl + CH_4 and, similarly, the activation energy measured by Manning and Kurylo was significantly lower than that measured by Clyne and Walker. It is suggested that the discharge flow-mass spectrometric technique used by Clyne and Walker was in this case subject to a systematic error, and that the flash photolysis results of Manning and Kurylo provide the basis for the recommended rate constant.

F87. Cl + CH_2Cl_2. The recommended value is based on results of the relative rate study of Tschuikow-Roux et al. [1188] normalized to the value of the rate constant for the reference reaction (Cl + CH_4) recommended in this evaluation. The room temperature value is in good agreement with results of the relative rate study of Niki et al. [888] and the absolute rate study of Beichert et al. [107]. The higher results of Clyne and Walker [258] were not used.

F88. Cl + $CHCl_3$. There have been three recent studies of this reaction. In the studies of Beichert et al. [107] by an absolute technique and Brahan et al. [148] by a relative technique, room temperature values about 50% greater than the previous recommendation, which was based on the relative study of Knox [642], were reported. Talhaoui et al. [1148] in a temperature-dependent absolute rate study by the discharge flow-mass spectrometric technique reported a room temperature value in excellent agreement with the previous recommendation. The recommended room temperature value is the mean of the values reported in the studies of Knox , Beichert et al., Brahan et al., and Talhaoui et al. The temperature dependence is from Talhaoui et al. and Knox. The A-factor has been fitted to the recommended room temperature value.

F89. Cl + CH_3F (HFC-41). The recommended value is based on results of the temperature-dependent relative rate study of Tschuikow-Roux et al. [1188] and the relative rate studies of Tuazon et al. [1192] and Wallington et al. [1253] at room temperature. The results of the absolute rate study of Manning and Kurylo [770] are in good agreement at room temperature but show a weaker temperature dependence, which is encompassed within the error limits.

F90. Cl + CH_2F_2 (HFC-32). The recommended room temperature value is the mean of results of the relative rate studies of Tschuikow-Roux et al. [1189] and of Nielsen et al. [876], both normalized to the value of the rate constant for the reference reaction (Cl + CH_4) recommended in this evaluation. The temperature dependence is from Tschuikow-Roux et al. The A-factor from that study has been adjusted to fit the recommended room temperature value.

F91. Cl + CF_3H (HFC-23). Recommended value is based on results of Coomber and Whittle [271].

F92. Cl + CH_2FCl (HCFC-31). The recommended value is based on the room temperature results of Tuazon et al. [1192] and the temperature dependence reported by Tschuikow-Roux et al. [1188], normalized to the value of the rate constant for the reference reaction (Cl + CH_4) recommended in this evaluation.

F93. Cl + $CHFCl_2$ (HCFC-21). The recommended room temperature value is the mean of results of the relative rate study of Tuazon et al. [1192] and the absolute rate study of Talhaoui et al. [1148]. The temperature dependence is from Talhaoui et al. The A-factor from that study has been adjusted to fit the recommended room temperature value. These results are preferred over the earlier results of Glavas and Heicklen [441].

F94. Cl + CHF_2Cl (HCFC-22). The recommended room temperature value is the mean of results of the relative rate studies of Tuazon et al. [1192] and the absolute rate studies of Sawerysyn et al. [1032] and Talhaoui et al. [1148]. The temperature dependence is from Talhaoui et al. The A-factor from that study has been adjusted to fit the recommended room temperature value.

F95. Cl + CH_3CCl_3. Recommended value is based on results of the absolute rate study of Talhaoui et al. [1149]. It is consistent with the previous recommendation, which was a much higher upper limit reported by Wine et al. [1321] in a study in which it was concluded that a reactive impurity accounted for a significant fraction of the Cl atom removal. The value reported by Platz et al. [955] is in agreement with the recommendation.

F96. Cl + CH_3CH_2F (HFC-161). The recommended values for the two reaction channels are based on results of the relative rate study of Tschuikow-Roux et al. [1189], normalized to the value of the rate constant for the reference reaction (Cl + CH_4) recommended in this evaluation.

F97. Cl + CH_3CHF_2 (HFC-152a). The recommended values for the two reaction channels are based on results of the relative rate study of Yano and Tschuikow-Roux [1344], normalized to the value of the rate constant for the reference reaction (Cl + C_2H_6) recommended in this evaluation. The overall rate constant value is in good agreement with results of the room temperature relative rate studies of Wallington and Hurley [1259], and Tuazon et al. [1192].

F98. Cl + CH_2FCH_2F (HFC-152). The recommended value is based on results of the relative rate study of Yano and Tschuikow-Roux [1344], normalized to the value of the rate constant for the reference reaction (Cl + C_2H_6) recommended in this evaluation.

F99. Cl + CH_3CFCl_2 (HCFC-141b). The recommended value is based on results of absolute rate studies of Talhaoui et al. [1149] by the discharge flow - mass spectrometric technique and Warren and Ravishankara [1278] by the pulsed photolysis-resonance fluorescence technique and the relative rate studies of Wallington and Hurley [1259] and Tuazon et al. [1192].

F100. Cl + CH_3CF_2Cl (HCFC-142b). The recommended room temperature value is based on results of the relative rate studies of Wallington and Hurley [1259], and Tuazon et al. [1192], and the absolute rate study of Talhaoui et al. [1149]. The temperature dependence is from Talhaoui et al. The A-factor from that study has been adjusted to fit the recommended room temperature value.

F101. Cl + CH_3CF_3 (HFC-143a). The recommended value is based on results of the relative rate study of Tschuikow-Roux et al. [1189], normalized to the value of the rate constant for the reference reaction (Cl + CH_4) recommended in this evaluation.

F102. Cl + CH_2FCHF_2 (HFC-143). The recommended values for the two reaction channels are based on results of the relative rate study of Tschuikow-Roux et al. [1189] normalized to the value of the rate constant for the reference reaction (Cl + CH_4) recommended in this evaluation.

F103. Cl + CH_2ClCF_3 (HCFC-133a). The recommended value is based on results of the direct study of Jourdain et al. [595] using the discharge flow-mass spectrometric technique to monitor the decay of the HCFC in the presence of a large excess of Cl atoms. The A-factor is lower than expected.

F104. Cl + CH_2FCF_3 (HFC-134a). The recommended value is based on results of the relative rate studies of Wallington and Hurley [1259], and Tuazon et al. [1192], and the absolute rate study of Sawerysyn et al. [1032].

F105. Cl + CHF_2CHF_2 (HFC-134). The recommended value is based on results of the relative rate study of Nielsen et al. [877] and that of Yano and Tschuikow-Roux [1344], normalized to the value of the rate constant for the reference reaction (Cl + C_2H_6) recommended in this evaluation.

F106. Cl + $CHCl_2CF_3$ (HCFC-123). The recommended value is based on results of the temperature-dependent study of Warren and Ravishankara [1278] using the pulsed photolysis-resonance fluorescence technique, and the relative rate studies of Wallington and Hurley [1259] and Tuazon et al. [1192] at room temperature.

F107. Cl + $CHFClCF_3$ (HCFC-124). The recommended value is based on results of the temperature-dependent study of Warren and Ravishankara [1278] using the pulsed photolysis-resonance fluorescence technique and the relative rate study of Tuazon et al. [1192] at room temperature. The A-factor is lower than expected.

F108. Cl + CHF_2CF_3 (HFC-125). Recommended value is based on results of the relative rate studies of Tuazon et al. [1192] and Sehested et al. [1049].

F109. ClO + O_3. There are two possible channels for this reaction: ClO + O_3 → ClOO + O_2 (k_1); and ClO + O_3 → OClO + O_2 (k_2). The recommended upper limit for k_1 at 298 K is based on results of the recent study by Stevens and Anderson [1113]. These authors also report that $k_1 = (4\pm2) \times 10^{-16}$ cm^3 $molecule^{-1}$ s^{-1} at 413 K. These data can be combined to derive the Arrhenius parameters $A = 2 \times 10^{-12}$ cm^3 $molecule^{-1}$ s^{-1} and $E/R > 3600$ K. The upper limit for k_2 is based on results reported by DeMore et al. [337] and Wongdontri-Stuper et al. [1332]; the Arrhenius parameters for k_2 were estimated.

F110. ClO + H_2. The Arrhenius expression was estimated based on the ~600 K data of Walker (reported in Clyne and Watson [259]).

F111. ClO + NO. The absolute rate coefficients determined in the four discharge flow-mass spectrometric studies (Clyne and Watson [259], Leu and DeMore [719], Ray and Watson [996] and Clyne and MacRobert [245]) and the discharge flow laser magnetic resonance study of Lee et al. [704] are in excellent agreement at 298 K, and are averaged to yield the preferred value. The value reported by Zahniser and Kaufman [1354] from a competitive study is not used in the derivation of the preferred value as it is about 33% higher. The magnitudes of the temperature dependences reported by Leu and DeMore [719] and Lee et al. are in excellent agreement. Although the E/R value reported by Zahniser and Kaufman [1354] is in fair agreement with the other values, it is not considered as it is dependent upon the E/R value assumed for the Cl + O_3 reaction. The Arrhenius expression was derived from a least squares fit to the data reported by Clyne and Watson, Leu and DeMore, Ray and Watson, Clyne and MacRobert, and Lee et al.

F112. ClO + NO_3. The recommended value is based on results reported by Cox et al. [276], Cox et al. [287] Biggs et al. [124], and Kukui et al. [652]. Biggs et al. report the rate constant to be independent of temperature, consistent with the results of Cox et al. [287]. This recent study of Kukui et al. supersedes the earlier study of Becker et al. [92] from the same laboratory, which had indicated the major products to be OClO + NO_2. There is now agreement among all studies that the major reaction channel forms ClOO + NO_2 (see Biggs et al. [124] Cox et al. [287], and Kukui et al. From a study of the OClO/NO_3 system Friedl et al. [413] conclude that at 220 K the formation of ClOO + NO_2 is favored.

F113. ClO + N_2O. The Arrhenius expression was estimated based on the ~600 K data of Walker (reported in Clyne and Watson [259]).

F114. ClO + CO. The Arrhenius expression was estimated based on the ~600 K data of Walker (reported in Clyne and Watson [259]).

F115. ClO + CH_4. The Arrhenius expression was estimated based on the ~600 K data of Walker (reported in Clyne and Watson [259]).

F116. $ClO + H_2CO$. Poulet et al. [968] have reported an upper limit of 10^{-15} cm^3 $molecule^{-1}$ s^{-1} for k at 298 K using the discharge flow-EPR technique.

F117. $ClO + CH_3O_2$. The recommended expressions for the overall rate constant is based on the results of Helleis et al. [495]. It is consistent with the room temperature measurements of Simon et al. [1067] and Kenner et al. [612]. The results of Kukui et al. [654] for the overall reaction are in agreement with the recommendation at room temperature, but these values show a slight negative temperature dependence in contrast with the slight positive temperature dependence recommended here. There is general agreement that the only important reaction channels are the two channels resulting in the production of $ClOO + CH_3O$ (a) and $CH_3OCl + O_2$ (b). However, there is severe disagreement on their relative importance; at room temperature reaction channel (a) is reported to be the major channel by Helleis et al. [495], Simon et al. [1067], Kukui et al. and Helleis et al. [496] but it is reported to be the minor channel by Biggs et al. [122] and Daele and Poulet [299]. Because of this large discrepancy, no branching ratios are recommended. The branching ratio studies that go down to low temperatures (Helleis et al. [495], Kukui et al. , and Helleis et al. [496]) report that reaction channels (a) and (b) are both significant down to lower polar stratospheric temperatures.

F118. $ClO + ClO$. There are three bimolecular channels for this reaction: $ClO + ClO \rightarrow Cl_2 + O_2$ (k_1); $ClO + ClO \rightarrow ClOO + Cl$ (k_2); and $ClO + ClO \rightarrow OClO + Cl$ (k_3). The recommended values for the individual reaction channels are from the study of Nickolaisen et al. [864]. This study, using a flash photolysis/long path ultraviolet absorption technique, is the most comprehensive study of this system, covering a wide range of temperature and pressure. These results are preferred over the results of earlier studies of the total bimolecular rate coefficient at low pressures by Clyne and Coxon [237], Clyne and White [263], and Clyne et al. [250], and those of other studies reported by Hayman et al. [489], Cox and Derwent [280], Simon et al. [1068], Horowitz et al. [523], and Horowitz et al. [524]. The room temperature branching ratio are k_1:k_2:k_3 = 0.29:0.50:0.21. The reaction exhibits both bimolecular and termolecular reaction channels (see entry in Table 2). The termolecular reaction dominates at pressures higher than about 10 torr. The equilibrium constant for formation of the Cl_2O_2 dimer is given in Table 3.

F119. $HCl + ClONO_2$. Results of four studies of the kinetics of this system have been published, in which the following upper limits to the homogeneous bimolecular rate constant were reported: 10^{-19} cm^3 $molecule^{-1}$ s^{-1} by a static wall-less long-path UV absorption technique and a steady-state flow FTIR technique (Molina et al. [829]); 5×10^{-18} using a flow reactor with FTIR analysis (Friedl et al. [411]); and 8.4×10^{-21} using a static photolysis system with FTIR analysis (Hatakeyama and Leu [487] and Leu et al. [720]), and 1.5×10^{-19} by FTIR analysis of the decay of $ClONO_2$ in the presence of HCl in large-volume (2500 and 5800 liters) Teflon or Teflon-coated chambers (Atkinson et al. [40]). Earlier, Birks et al. [128] had reported a higher upper limit. All studies found this reaction to be catalyzed by surfaces. The differences in the reported upper limits can be accounted for in terms of the very different reactor characteristics and detection sensitivities of the various studies. The homogeneous reaction is too slow to have any significant effect on atmospheric chemistry.

F120. $CH_2ClO + O_2$. The CH_2ClO radical is reported to be resistant to unimolecular dissociation into $Cl + CH_2O$ products, according to chain reaction/product analysis studies by Sanhueza and Heicklen [1026] and Niki et al. [888] and kinetics studies by Catoire et al. [204]. The recommendation is based on the work of Kaiser and Wallington [603] who studied the competition between reaction with O_2 and HCl elimination in a complex photochemical reaction system using FTIR detection of stable products. The recommendation is a factor of 5 higher than estimated using the empirical relationship given by Atkinson and Carter [42]. The fate of CH_2ClO in the atmosphere is this reaction with O_2.

F121. $CH_2ClO_2 + HO_2$. The recommendation is based on the measurement reported by Catoire et al. [204], who used pulsed photolysis with UV absorption detection at 1 atm pressure and 251–588 K.

F122. $CH_2ClO_2 + NO$. The recommendation is based on the value reported by Sehested et al. [1051], who used pulsed radiolysis and UV absorption detection of NO_2 to measure the rate coefficient. The temperature dependence is estimated by analogy to similar $RO_2 + NO$ reactions.

F123. $CCl_3O_2 + NO$. The recommendation is based upon the measurements of Ryan and Plumb [1012] and Dognon et al. [358], who agree well at room temperature. The temperature dependence is derived from the data of Dognon et al., who covered the temperature range 228–413 K. The CCl_3O primary product of the reaction of CCl_3O_2 with NO decomposes rapidly to eliminate Cl, according to Lesclaux et al. [709].

F124. $CCl_2FO_2 + NO$. The recommendation is based on the measurements made by Dognon et al. [358] using pulsed photolysis with mass spectrometry detection at 1–10 torr and 228–413 K. These results supersede the earlier study of Lesclaux and Caralp [707]. The CCl_2FO radical primary product of the $CCl_2FO_2 + NO$ reaction is reported by Lesclaux et al.[709] and Wu and Carr [1336] to rapidly decompose to eliminate Cl and to give the products indicated.

F125. $CClF_2O_2$ + NO. The recommendation is based on the measurements made by Dognon et al. [358], who used pulsed photolysis with mass spectrometry detection at 1–10 torr and 228–413 K, and Sehested et al. [1051], who used pulsed radiolysis with UV absorption detection of the NO_2 product at one atm and 298 K. Wu and Carr [1336] observed the $CClF_2O$ radical primary product to rapidly dissociate to CF_2O and Cl.

G1. O + BrO. The preferred value is based on the value reported by Thorn et al. [1166] using a dual laser flash photolysis/long path absorption/resonance fluorescence technique. Clyne et al. [252] reported a value approximately 40% lower.

G2. O + HBr. Results of the flash photolysis-resonance fluorescence study of Nava et al. [846] for 221–455 K and the laser flash photolysis-resonance fluorescence study of Nicovich and Wine [872] for 250–402 K provide the only data at stratospheric temperatures. Results reported include those of Singleton and Cvetanovic [1076] for 298–554 K by a phase-shift technique, and discharge flow results of Brown and Smith [157] for 267–430 K and Takacs and Glass [1142] at 298 K. The preferred value is based on the results of Nava et al., as well as those of Nicovich and Wine and those of Singleton and Cvetanovic over the same temperature range, since these results are less subject to complications due to secondary chemistry than are the results using discharge flow techniques. The uncertainty at 298 K has been set to encompass these latter results.

G3. O + HOBr. Recommended room temperature value is the mean of results of Monks et al. [1166] and Kukui et al. [653]. The temperature dependence is from Nesbitt et al. [860]. The A-factor from that study has been adjusted to fit the recommended room temperature value. Kukui et al. determined that the Br atom abstraction channel is the only pathway at room temperature.

G4. OH + Br_2. The recommended room temperature value is the average of the values reported by Boodaghians et al. [138], Loewenstein and Anderson [750], and Poulet et al. [963]. The temperature independence is from Boodaghians et al. Loewenstein and Anderson determined that the exclusive products are Br + HOBr.

G5. OH + BrO. Recommended room temperature value is that reported by Bogan et al. [135]. This study, using discharge flow reactor techniques and beam sampling mass spectrometry, is the only experimental measurement of this rate constant. Because of the difficulty of analyzing the data, we assign a large uncertainty factor. The authors suggest that the reaction proceeds by recombination to form vibrationally excited HOOBr that dissociates to Br + HO_2.

G6. OH + HBr. The preferred value at room temperature is the average of the values reported by Ravishankara et al. [989] using FP-RF, by Jourdain et al. [597] using DF-DPR, by Cannon et al. [191] using FP-LIF, and by Ravishankara et al. [992] using LFP-RF and LFP-LIF techniques. In this latest study the HBr concentration was directly measured in-situ in the slow flow system by UV absorption. The rate constant determined in this re-investigation is identical to the value recommended here. The data of Ravishankara et al. [989] show no dependence on temperature over the range 249–416 K. Values reported by Takacs and Glass [1141] and by Husain et al. [547] are a factor of 2 lower and were not included in the derivation of the preferred value. Data by Sims et al. [1073] are in good agreement with the reommendation at 298 K but show a negative temperature dependence at lower temperatures.

G7. OH + CH_3Br. The recommended rate expression is derived from a combined fit to the data from the relative rate study of Hsu and DeMore [537] (recalculated based on the current recommendation for the rate constant for the OH + CH_3CHF_2 reference reaction, as discussed in the note for that reaction) and the absolute determinations by Chichinin et al. [226], Mellouki et al. [811] and Zhang et al. [1369]. The results of these extensive studies are in excellent agreement and are preferred over the higher values reported in the earlier studies of Davis et al. [317] and Howard and Evenson [528].

G8. OH + CH_2Br_2. The recommended value for k(298 K) is an average of the values from the absolute studies of Mellouki et al. [811] and Zhang et al. [1364] and from the relative rate measurements of DeMore [335] (recalculated based on the current recommendation for the rate constant for the OH + CH_2Cl_2 reference reaction) and Orlando et al. [920] (recalculated based on the current recommendation for the rate constant for the OH + $CH_3(CO)CH_3$ reference reaction). The recommended value of E/R is from the study of Mellouki et al. [811].

G9. OH + $CHBr_3$. The recommended rate expression is derived from a fit to the data from the relative rate study of DeMore [335] (recalculated based on the current recommendation for the rate constant for the OH + CH_2Cl_2 reference reaction). The results of Orkin et al. [914] are higher by a factor of 2 but have the same temperature dependence. They are encompassed within the 2σconfidence limits.

G10. OH + CHF_2Br. The recommended values for k(298 K) and E/R are derived from a fit to the data of Talukdar et al. [1151] (two studies), Orkin and Khamaganov [913], and Hsu and DeMore [538] (a relative rate measurement recalculated using the current recommendation for the rate constant for the OH + CH_4 reference reaction). These data are preferred over the consistently higher results reported by Brown et al. [153].

G11. OH + CH_2ClBr. The recommended value for k(298 K) is an average of the values from two relative rate studies by DeMore [335] (recalculated based on the current recommendation for the rate constant for the OH + CH_2Cl_2 reference reaction) and Bilde et al. [126] (recalculated using the current recommendation for the rate constant for the OH + CH_2Br_2 reference reaction) and two absolute determinations by Orkin et al. [915], all of which are in good agreement. The recommended E/R is obtained from a fit to the data of DeMore and Orkin et al.. The A factor was then calculated.

G12. OH + CF_2ClBr. The A-factor was estimated, and a lower limit for E/R was derived using the upper limit for the rate constant at 298 K reported by Burkholder et al. [174] in a study using pulsed photolysis-LIF and DF-LMR techniques. A less sensitive upper limit was reported by Clyne and Holt [243].

G13. OH + CF_2Br_2. The A-factor was estimated, and a lower limit for E/R was derived by using the upper limit for the rate constant at 298 K reported by Burkholder et al. [174] in a study using pulsed photolysis-LIF and DF-LMR techniques.

G14. OH + CF_3Br. The A-factor was estimated and a lower limit for E/R was derived by using the upper limit for the rate constant at 460 K reported by Orkin and Khamaganov [913]. These parameters were then used to calculate an upper limit for k(298 K). The upper limit for k(298 K) determined by Burkholder et al. [174] in a study using pulsed photolysis-LIF and DF-LMR techniques at room temperature is understandably higher. A less sensitive upper limit was also reported by Le Bras and Combourieu [688].

G15. OH + CH_2BrCH_3. The recommended values for k(298 K) and E/R are derived from a fit to the data ($T \leq 300$ K) of Herndon et al. [500]. These data suggest a curvature of the Arrhenius plot similar to that found for the OH reaction with CH_3CH_2F. The data of Qiu et al. [972] (which include earlier data reported by the same research group in Xing et al. [1340]) were not used because they were obtained mainly at above room temperature and exhibit a very steep temperature dependence resulting in a value for E/R that is larger than the E/R value obtained from data at $T > 298$ K for the OH reaction with CH_3CH_2F. The k(300 K) value reported by Donaghy et al. [363] seems too low for this reaction when compared with the recommendation for presumably slower (and better studied) OH reaction with CH_3CH_2F.

G16. OH + CH_2BrCF_3. The recommended values for k(298 K) and E/R are from a combined fit to the data of Nelson et al. [849] and Orkin and Khamaganov [913].

G17. OH + $CHFBrCF_3$. The recommended rate expression is derived from a combined fit to the data (below 400 K) of Orkin and Khamaganov [913] and Brown et al. [153].

G18. OH + $CHClBrCF_3$. The recommended rate expression is derived from a fit to the data of Orkin and Khamaganov [913] (for $T \leq 400$ K). The room temperature value measured by Brown et al. [154] lies somewhat higher than this recommendation but is encompassed within the 2σ confidence limits.

G19. OH + $CHFClCF_2Br$. The recommended rate expression is derived from a fit to the data from the relative rate study of DeMore [335] (recalculated based on the current recommendation for the rate constant for the OH + CH_3CCl_3 reference reaction).

G20. OH + CF_2BrCF_2Br. The A-factor was estimated and a lower limit for E/R was derived by using the upper limit for the rate constant at 460 K reported by Orkin and Khamaganov [913]. These parameters were then used to calculate an upper limit for k(298 K). The upper limit for k(298 K) determined by Burkholder et al. [174] in a study using pulsed photolysis-LIF and DF-LMR techniques at room temperature is understandably higher.

G21. OH + $CH_2BrCH_2CH_3$. The recommended values for k(298 K) and E/R are derived from a fit to the data ($T \leq 300$ K) from Donaghy et al. [363], Teton et al. [1162], Nelson et al. [850], Herndon et al. [500], Gilles et al. [436], and Kozlov et al. [650]. Significant curvature in the Arrhenius plot has been observed over the 480 to 210 K temperature range, due to the three different hydrogen-abstraction reaction channels that occur. These channels have been quantified in the study of Gilles et al. In spite of the noticeable Arrhenius curvature, the data below 300 K can be well represented by a two-parameter Arrhenius fit.

G22. OH + $CH_3CHBrCH_3$. The recommended values for k(298 K) and E/R are averages of the parameters derived from a fit to the data ($T \leq 300$ K) of Herndon et al. [500] and Kozlov et al. [650] which are in excellent agreement. The A factor was then calculated. The room temperature relative rate determination by Donaghy et al. [363] and the absolute temperature dependent data of Teton et al. [1162] lie systematically higher than those from these two more recent studies. Significant curvature in the Arrhenius plot has been observed over the 480 K to 210 K temperature range by Kozlov et al., presumably due to the two different hydrogen-abstraction reaction channels that occur. In spite of the noticeable Arrhenius curvature, the data below 300 K can be well represented by a two-parameter Arrhenius fit.

G23. HO_2 + Br. This recommendation is based on results obtained over the 260–390 K temperature range in the study by Toohey et al. [1183], using a discharge flow system with LMR detection of HO_2 decay in excess Br. The room temperature value reported in this study is a factor of 3 higher than that reported by Poulet et al. [964] using LIF and MS techniques and is an order of magnitude larger than the value of Posey et al. [959]. The uncertainty in E/R is set to encompass the value E/R = O, as it is for other radical-radical reactions. The value determined by Laverdet et al. [685] using DF-EPR techniques is in good agreement with this recommendation. The reactions of Br atoms with H_2O_2, HCHO, and HO_2 are all slower than the corresponding reactions of Cl atoms by one to two orders of magnitude.

G24. HO_2 + BrO. The recommendation is based on results of the temperature-dependent studies of Larichev et al. [681], Elrod et al. ([377], and Li et al. [730]. The studies of Larichev et al. and Elrod et al. were done under pseudo–first-order conditions with excess HO_2; the study of Li et al. was done under pseudo–first-order conditions with either HO_2 or BrO in excess. The recommended room temperature value is the mean of the values reported in these studies, with the values of Li et al. under both conditions included. These studies all report a similar negative temperature dependence. The room temperature value of Bridier et al. [151], which was not obtained under pseudo–first-order decay conditions, was not included in derivation of the recommendation. Larichev et al. have determined an upper limit of 1.5% for production of HBr and O_3. From a study of the reverse reaction above room temperature, Mellouki et al. [810] determined by extrapolation that the yield of HBr + O_3 is an insignificant fraction (<0.01%) of the total reaction down to 200 K.

G25. NO_3 + HBr. The recommended upper limit is the upper limit reported by Mellouki et al. [807] in a study using DF-EPR techniques. This upper limit shows that this reaction is of negligible importance in stratospheric chemistry. Canosa-Mas et al. [194] reported a value that is consistent, within experimental error, with the upper limit of Mellouki et al.

G26. Cl + CH_2ClBr. Recommended value is based on results of Tschuikow-Roux et al. [1188] (normalized to the value of the rate constant for the reference reaction (Cl + CH_4) recommended in this evaluation) and Bilde et al. [126] (normalized to most recent values for the rate coefficients for the reference reactions, i.e., the rate coefficients for the Cl + CH4 reaction given in JPL 00-3 [1019] and for Cl + CH_2Br_2 given in the current recommendation, respectively.) The products of this reaction are expected to be CHClBr and HCl.

G27. Cl + CH_3Br. Recommended value is based on results of the absolute rate studies of Gierczak et al. [430], Orlando et al. [920], Kambanis et al. [605] and Piety et al. [949]. Results of these studies are in excellent agreement. Results of the relative rate study Tschuikow-Roux et al. [1188] were not used in derivation of the recommended value. The product of this reaction is expected to be mostly CH_2Br and HCl. The possible production of CH_3Cl + Br is very small in the atmosphere [446].

G28. Cl + CH_2Br_2. Recommended value is based on results of the absolute rate studies of Gierczak et al. [430], Orlando et al. [920], and Kambanis et al. [605]. Results of these studies are in excellent agreement. Results of the relative rate study of Tschuikow-Roux et al. [1188] were not used in derivation of the recommended value. The products of this reaction are expected to be $CHBr_2$ and HCl.

G29. Cl + $CHBr_3$. The recommendation is based on the only reported study of this reaction by Kambanis et al. [605], who employed a very low pressure reactor and monitored reactants and products using mass spectrometry. The products of this reaction are CBr_3 and HCl.

G30. Br + O_3. The results reported for k(298 K) by Clyne and Watson [261], Leu and DeMore [718], Michael et al. [818], Michael and Payne [823], and Toohey et al. [1184] are in excellent agreement. The preferred value at 298 K is derived by taking a simple mean of these five values. The temperature dependences reported for k by Leu and DeMore and by Toohey et al. are in good agreement, but they can only be considered to be in fair agreement with those reported by Michael et al. and Michael and Payne. The preferred value was synthesized to best fit all the data reported from these five studies. The results of Nicovich et al. [868] are in excellent agreement with this recommendation.

G31. Br + H_2O_2. The recommended upper limit to the value of the rate constant at room temperature is based on results reported in the study by Toohey et al. [1183] using a discharge flow-resonance fluorescence/laser magnetic resonance technique. Their upper limit determined over the temperature range 298–378 K is consistent with less sensitive upper limits determined by Leu [714] and Posey et al. [959] using the discharge flow-mass spectrometric technique. The much higher value reported by Heneghan and Benson [498] may result from the presence of excited Br atoms in the very low pressure reactor. The pre-exponential factor was chosen to be consistent with that for the Cl + H_2O_2 rate constant, and the E/R value was fitted to the upper limit at 298 K. Mellouki et al. [810] have measured the rate of the reverse reaction.

G32. Br + NO_3. The recommended value is that reported by Mellouki et al. [807] in a study using DF-DPR techniques.

G33. Br + H_2CO. There have been two studies of this rate constant as a function of temperature: Nava et al. [848], using the flash photolysis–resonance fluorescence technique, and Poulet et al. [962], using the discharge flow-mass spectrometric technique. These results are in reasonably good agreement. The Arrhenius expression was derived from a least squares fit to the data reported in these two studies. The higher room temperature value of Le Bras et al. [689], using the discharge flow–EPR technique, has been shown to be in error due to secondary chemistry (Poulet et al.).

G34. Br + OClO. The recommended value at room temperature is the mean of the values reported by Clyne and Watson [262] and Toohey [1181]. In the study of Clyne and Watson, correction for the effect of the rapid reverse reaction was required. The temperature dependence reported by Toohey [1181] is accepted but with increased error limits.

G35. Br + Cl_2O. The recommended value is based on results reported by Stevens and Anderson [1114] and by Sander and Friedl [1018], which are in good agreement.

G36. Br + Cl_2O_2. The recommended value is that determined by Friedl (private communication) in a study using a DF-MS technique.

G37. BrO + O_3. There have been two recent studies of this reaction. Rattigan et al. [978] report an overall rate constant of ~10^{-17} cm^3 $molecule^{-1}s^{-1}$ over the temperature range 318–343 K. Rowley et al. [1009] report a room temperature upper limit of 2×10^{-17} cm^3 $molecule^{-1}s^{-1}$. Both papers report a value of ~2×10^{-18} cm^3 $molecule^{-1}$ s^{-1} for the channel to produce OBrO + O_2. The recommended upper limit of 2×10^{-17} cm^3 $molecule^{-1}s^{-1}$ is a factor of 2.5 less than the previously recommended upper limit of 5×10^{-17}, which was based on Mauldin et al. [793]. The pre-exponential factor was estimated, and E/R was calculated.

G38. BrO + NO. The results of the three low pressure mass spectrometric studies (Clyne and Watson [261]; Ray and Watson [996]; Leu [712]) and the high pressure UV absorption study (Watson et al. [1289]), which all used pseudo–first-order conditions, are in excellent agreement at 298 K and are thought to be much more reliable than the earlier low pressure UV absorption study (Clyne and Cruse [238]). The results of the two temperature-dependence studies are in good agreement and both show a small negative temperature dependence. The preferred Arrhenius expression was derived from a least squares fit to all the data reported in the four recent studies. By combining the data reported by Watson et al. with those from the three mass spectrometric studies, it can be shown that this reaction does not exhibit any observable pressure dependence between 1 and 700 torr total pressure. The temperature dependences of k for the analogous ClO and HO_2 reactions are also negative and are similar in magnitude.

G39. BrO + NO_3. The recommended value is the geometric mean of the lower and upper limits reported by Mellouki et al. [807] in a study using DF-DPR techniques. These reported limits are encompassed within the indicated uncertainty limits.

G40. BrO + ClO. Friedl and Sander [412], using DF/MS techniques, measured the overall rate constant over the temperature range 220–400 K and also over this temperature range determined directly branching ratios for the reaction channels producing BrCl and OClO. The same authors in a separate study using flash photolysis–ultraviolet absorption techniques (Sander and Friedl [1018]) determined the overall rate constant over the temperature range 220–400 K and pressure range 50–750 torr and also determined at 220 K and 298 K the branching ratio for OClO production. The results by these two independent techniques are in excellent agreement, with the overall rate constant showing a negative temperature dependence. Toohey and Anderson [1182], using DF/RF/LMR techniques, reported room temperature values of the overall rate constant and the branching ratio for OClO production. They also found evidence for the direct production of BrCl in a vibrationally excited Π state. Poulet et al. [960], using DF/MS techniques, reported room temperature values of the overall rate constant and branching ratios for OClO and BrCl production. Overall room temperature rate constant values reported also include those from the DF/MS study of Clyne and Watson [262] and the very low value derived in the flash photolysis study of Basco and Dogra [81] using a different interpretation of the reaction mechanism. The recommended Arrhenius expressions for the individual reaction channels are taken from the study of Friedl and Sander [412] and Turnipseed et al. [1205] . These studies contain the most comprehensive sets of rate constant and branching ratio data. The overall rate constants reported in these two studies are in good agreement (20%) at room temperature and in excellent agreement at stratospheric temperatures. Both studies report that OClO production by channel (1) accounts for 60% of the overall reaction at 200 K. Both studies report a BrCl yield by channel (3) of about 8%, relatively independent of temperature. The recommended expressions are consistent with the body of data from all studies except those of Hills et al. [507] and Basco and Dogra [81].

G41. BrO + BrO. Measurements of the overall rate constant can be divided into categories—those in which BrO was monitored by UV absorption and those in which BrO was monitored by mass spectrometer. Gilles et al. [438] have re-analyzed the results of the UV absorption studies and scaled the reported values of the rate

constant to the UV absorption cross sections reported in their paper. When scaled in this manner, the room temperature rate constant values reported in the UV absorption studies (Sander and Watson [1023], Mauldin et al. [793], Bridier et al. [151], Rowley et al. [1009], Laszlo et al. [683], and Gilles et al.) come into very good agreement among themselves and also with results of the mass spectrometric studies of Clyne and Watson [261] and Lancar et al. [677]. This provides the basis for the reommended room temperature value. The temperature dependence is based on results of Sander and Watson, Turnipseed et al. [1204] and Gilles et al.

There are two possible bimolecular channels for this reaction: $BrO + BrO \rightarrow 2Br + O_2$ (k_1) and $BrO + BrO \rightarrow Br_2 + O_2$ (k_2). The partitioning of the total rate constant into its two components, k_1 and k_2, has been measured at room temperature by Sander and Watson [1023], Turnipseed et al. [1204] and Lancar et al. [677], by Jaffe and Mainquist [568] from 258 to 333 K, by Cox et al. [292] from 278 to 348 K and by Mauldin et al. [793] from 220 to 298 K. All are in agreement that $k_1/k = 0.85 \pm 0.03$ at 298 K. From the values of $k_1/k = 0.85$ at 298 K (all studies) and 0.68 at 220 K (Mauldin et al. and Cox et al. extrapolated), one can derive the temperature-dependent expression $k_1/k = 1.60 \exp(-190/T)$. From the recommended Arrhenius expression for the overall rate constant $k = k_1 + k_2$ and the expression for the branching ratio k_1/k, one can derive the following Arrhenius expressions for the individual reaction channels: $k_1 = 2.4 \times 10^{-12} \exp(40/T)$ cm^3 molecule^{-1}s^{-1} and $k_2 = 2.8 \times 10^{-14} \exp(860/T)$ cm^3 molecule^{-1}s^{-1}.

G42. $CH_2BrO_2 + NO$. The recommendation is based on the 298 K measurement of Sehested et al. [1051], who used pulsed radiolysis with UV absorption detection of the NO_2 product formation rate. The temperature dependence is estimated based on analogy to similar $RO_2 + NO$ reactions. The CH_2BrO product has been shown to undergo rapid unimolecular decomposition to yield $CH_2O + Br$ by Chen et al. [216] and Orlando et al. [919] The domination of this channel over the reaction of CH_2BrO with O_2 is consistent with the fate of other alkoxy radicals (Chen et al. and Orlando et al.), but contradicts the earlier result of Nielson et al. [878].

H1. $O + I_2$. Based on the room temperature data of Ray and Watson [996] and Laszlo et al. [684]. The molecular beam study of Parrish and Herschbach [931] suggests a zero activation energy, consistent with the near gas kinetic value of k at 298 K.

H2. O + IO. Based on results of Laszlo et al. [684], the only reported study of this rate constant. This value was derived from modeling a system in which the concentrations of I_2 and IO were monitored simultaneously. This rate constant is a factor of 4 greater than the values for the corresponding reactions of O with ClO and BrO.

H3. $OH + I_2$. Based on the data of Loewenstein and Anderson [751] and Jenkin et al. [575].

H4. OH + HI. Based on the data of Lancar et al. [679] and MacLeod et al. [765].

H5. $OH + CH_3I$. The recommended rate expression is derived from a fit to the data of Brown et al. [155], the only reported study of this reaction.

H6. $OH + CF_3I$. The recommended rate expression is derived from a fit to the data of Gilles et al. [437]. The results from the studies by Garraway and Donovan [422] and Berry et al. [114] were not used in deriving the recommendation as the results were possibly influenced by reactant photolysis. The room temperature value from the discharge flow/resonance fluorescence study of Brown et al. [155]agrees within the 2σ limits.

H7. $HO_2 + I$. Based on the data of Jenkin et al. [580], the only reported study of this reaction.

H8. $HO_2 + IO$. The recommended value is the average of the values reported by Jenkin et al. [579] and Maguin et al. [768].

H9. $NO_3 + HI$. No recommendation is given, based on the potential for severe complications resulting from secondary chemistry in the only reported study of the reaction (Lancar et al. [679]).

H10. $Cl + CH_3I$. This reaction, thought to be a simple H abstraction reaction, has been shown by Ayhens et al. [53] to be quite complex. At low temperatures, Cl atom reversibly adds to CH_3I to form CH_3ICl. Thus, there are at least two channels for this reaction,

$$Cl + CH_3I \rightarrow CH_2I + HCl \qquad (a)$$

$$Cl + CH_3I \leftrightarrow CH_3ICl \qquad (b)$$

The rate coefficient for channel (a) has been measured by Ayhens et al. above 364 K, Kambanis et al. [605] between 273 and 363 K, Bilde and Wallington [125] at 298 K, and Cotter et al. [273] at 298 K. The recommendation is based on these studies.

Under atmospheric conditions reaction (b) to form the adduct is about two orders of magnitude faster than reaction (a). However, the fate of the CH_3ICl adduct in the atmosphere is unclear. Its lifetime, based on the

studies of Ayhens et al., can be as long as a few seconds at 200 K and a few hundred Torr pressure. Therefore, it is possible that it could react with O_2 or be photolyzed. At 298 K, in one atmosphere of O_2, it appears that the overall fate of the CH_3ClI is to decompose back to the reactants, based on the work of Bilde and Wallington [125]. Therefore, if O_2 were to react with CH_3ICl, this rate coefficient has to be less than about
10^{-17} cm^3 molecule^{-1} s^{-1} , using the rate coefficient for its decomposition measured by Ayhens et al. If the rate coefficient for $CH_3ICl + O_2$ were to remain approximately the same, i.e., 10^{-17} cm^3 molecule^{-1} s^{-1}, at lower temperatures, the possible loss of CH_3ICl via reaction with O_2 cannot be ignored. Further, the possible atmospheric photolysis of CH_3ICl may be important if it has a J-value greater than 0.1 s^{-1}.

There is a third possible product channel for this reaction to yield $CH_3Cl + I$ (Goliff and Rowland [446]). Based on the results of Bilde and Wallington and Goliff and Rowland, we recommend that the rate coefficient for the $Cl + CH_3I \rightarrow CH_3Cl + I$ reaction to be less than $0.2k_a$ at 298 K. Since such a reaction is likely to have a significant barrier in the gas phase, even though it is exothermic by ~14 kcal mol^{-1} at 298 K, the branching ratio for the production of CH_3Cl and I in the atmosphere will be likely less than that at 298 K.

H11. $I + O_3$. Based on the room temperature data of Jenkin and Cox [576] and Sander [1017], and the temperature dependent data of Buben et al. [164] and Turnipseed et al. [1207].

H12. I + BrO. Based on results of Laszlo et al. [683], the only reported study of this rate constant. This value was derived from modeling the simultaneous decay of BrO and IO in a $Br_2/I_2/N_2O$ system.

H13. IO + NO. Based on the data of Ray and Watson [996], Daykin and Wine [322], Buben et al. [165], and Turnipseed et al. [1207].

H14. IO + ClO. Based on results of Turnipseed et al. [1206], the only reported study of this reaction. These authors also reported the product yield for channel(s) yielding an I atom to be 0.8 ± 0.2.

H15. IO + BrO. Based primarily on results of Laszlo et al. [683]. Gilles et al. [438] reported the following Arrhenius expression for non-iodine atom producing channels: $2.5 \times 10^{-11} \exp(260/T)$ cm^3 molecule^{-1}s^{-1}. They also reported a branching ratio of <0.35 for channels producing I atoms. From their data they could constrain the value of the overall rate constant to be: $6 \times 10^{-11} < k < 10 \times 10^{-11}$ cm^3 molecule^{-1}s^{-1}, the range of which is consistent with the results of Laszlo et al.

H16. IO + IO. Changed from the previous recommendation, which was based on the results of Sander [1017]. In that study, over the temperature range 250–373 K, a negative temperature dependence was reported for the overall rate constant and for the absorption cross section at 427.2 nm. In the recent study of Harwood et al. [485], the overall rate constant and the absorption cross section were found to be independent of temperature from 253 to 320 K. The recommended room temperature value is the average of the values reported by Sander, Harwood et al., and Laszlo et al. [684]. The recommended temperaure dependence is the average of the values reported by Sander and by Harwood et al., with an uncertainty sufficient to encompass the two reported values. The A-factor has been fitted to the recommended room temperature rate constant and the recom-mended temperature dependence. The overall rate constant for the decay of IO in the absence of ozone has been found to be independent of pressure by Sander, Laszlo et al., and Harwood et al. A comparison of the overall rate observed in excess ozone to that in the absence of ozone was interpreted by Sander and by Harwood et al. to imply that formation of the dimer I_2O_2 is the dominant reaction channel in the IO self-reaction.

H17. INO + INO. Based on the data of Van den Bergh and Troe [1225].

H18. $INO_2 + INO_2$. Based on the data of Van den Bergh and Troe [1225].

I1. O + SH. This recommendation accepts the results of Cupitt and Glass [296]. The large uncertainty reflects the absence of any confirming investigation.

I2. O + CS. The room temperature recommendation is an average of the rate constants determined by Slagle et al. [1087], Bida et al. [118], Lilenfeld and Richardson [737], and Hancock and Smith [479]. The temperature dependence is that of Lilenfeld and Richardson, with the A-factor adjusted to yield the recommended value of k(298 K).

I3. $O + H_2S$. This recommendation is derived from an unweighted least squares fit of the data of Singleton et al. [1079] and Whytock et al. [1304]. The results of Slagle et al. [1085] show very good agreement for E/R in the temperature region of overlap (300 – 500 K) but lie systematically higher at every temperature. The uncertainty factor at 298 K has been chosen to encompass the room temperature rate constant values of Slagle et al. [1085] and Hollinden et al. [519]. Other than the 263 K data point of Whytock et al. and the 281 K point of Slagle et al., the main body of rate constant data below 298 K comes from the study of Hollinden et al., which indicates a dramatic change in E/R in this temperature region. Thus, ΔE/R was set to account for

these observations. Such a nonlinearity in the Arrhenius plot might indicate a change in the reaction mechanism from abstraction (as written) to addition. An addition channel (resulting in H atom displacement) has been proposed by Slagle et al. [1085], Singleton et al. [1079], and Singleton et al. [1081]. In the latter two studies, an upper limit of 20% was placed on the displacement channel. Direct observations of product HSO was made in the reactive scattering experiments of Clemo et al. [235] and Davidson et al. [307]. A threshold energy of 3.3 kcal/mole was observed (similar to the activation energy measured in earlier studies), suggesting the importance of this direct displacement channel. Addition products from this reaction have been seen in a matrix by Smardzewski and Lin [1090]. Further kinetic studies in the 200–300-K temperature range, as well as quantitative direct mechanistic information, could clarify these issues. However, this reaction is thought to be of limited importance in stratospheric chemistry.

I4. O + OCS. The value of k(298 K) is the average of the determinations by Westenberg and de Haas [1296], Klemm and Stief [637], Wei and Timmons [1292], Manning et al. [771], and Breckenridge and Miller [150]. The recommended value of E/R is the average value taken from the first three listed studies. Hsu et al. [536] report that this reaction proceeds exclusively by a stripping mechanism. The vibrational and rotational state distributions in the SO and CO products have been reported by Chen et al. [222] and Nickolaisen et al. [866] respectively.

I5. O + CS_2. The value of k(298 K) is an average of the rate constants determined by Wei and Timmons [1292], Westenberg and de Haas [1296], Slagle et al. [1086], Callear and Smith [188], Callear and Hedges [187], Homann et al. [520], and Graham and Gutman [449]. The E/R value is an average of the determinations by Wei and Timmons and Graham and Gutman. The g value has been set to encompass the limited temperature data of Westenberg and de Haas. The principal reaction products are thought to be CS + SO. However, Hsu et al. [536] report that 1.4% of the reaction at 298 K proceeds through a channel yielding CO + S_2 and calculate a rate constant for the overall process in agreement with that recommended. Graham and Gutman [449] have found that 9.6% of the reaction proceeds to yield OCS + S at room temperature. Using time-resolved diode laser spectroscopy, Cooper and Hershberger [272] determined the branching ratios for the CO and OCS producing channels to be (3.0±1.0)% and (8.5±1.0)% respectively.

I6. O + CH_3SCH_3. This recommendation is based on a fit of the data from Nip et al. [897], Lee et al. [700], and Lee et al. [699]. Product studies by Cvetanovic et al. [297] indicate that the reaction proceeds almost entirely by addition followed by rapid fragmentation to the products as written. Pavanaja et al. [936] examined the pressure and reactant ratio dependencies of OH($A^2\Sigma^+$) and SO_2(^3B, ^1B) emissions in this reaction system. Their observations are consistent with initial product formation as written, followed by secondary generation of both OH and SO_2.

I7. O + CH_3SSCH_3. This recommendation averages the 298 K rate constants of Nip et al. [897] and Lee et al. [696], which differ by nearly a factor of 2. The temperature dependence is that of Nip et al.; Lee et al. having reported no temperature dependence over the limited range of 270–329 K. The A-factor has been adjusted to yield the recommended (averaged) value of k(298 K). Product studies by Cvetanovic et al. [297] indicate that the reaction proceeds mainly by addition followed by rapid fragmentation to the products as written. Pavanaja et al. [936] examined the pressure and reactant ratio dependencies of OH($A^2\Sigma^+$) and SO_2(^3B, ^1B) emissions in this reaction system. Their observations are consistent with initial product formation as written, followed by secondary generation of both OH and SO_2.

I8. O_3 + H_2S. This upper limit was determined by Becker et al. [96] from measurements of the rates of SO_2 production and O_3 consumption. The heterogeneous reaction between H_2S and O_3 is far more efficient in most laboratory systems.

I9. O_3 + CH_3SCH_3. This rate constant upper limit is based on the measurements of Martinez and Herron [789], which represent the only reported study of this reaction.

I10. SO_2 + O_3. This recommendation is based on the limited data of Davis et al. [318] at 300 K and 360 K in a stopped flow investigation using mass spectrometric and UV spectroscopic detection.

I11. OH + H_2S. The values of k(298 K) and E/R are derived from a composite unweighted least squares fit to the individual data points of Perry et al. [943], Cox and Sheppard [291], Wine et al. [1313], Leu and Smith [723], Michael et al. [819], Lin [738], Lin et al. [742], Barnes et al. [63], and Lafage et al. [674]. The studies of Leu and Smith [723], Lin et al. [742], Lin [738], and Lafage et al. [674] show a slight parabolic temperature dependence of k with a minimum occurring near room temperature. However, with the error limits stated in this evaluation, all data are fit reasonably well by an Arrhenius expression. Lafage et al. and Michael et al. discuss the results in terms of a two-channel reaction scheme involving direct H atom abstraction and complex (adduct) formation. Lafage et al. analyzed their results above room temperature to yield an apparent E/R = 400 K for the abstraction channel, in good agreement with the E/R value determined above room

temperature by Westenberg and de Haas [1297]. The results of these latter workers lie systematically higher (by about 70%), presumably due to secondary reactions. The room temperature value measured by Stuhl [1126] lies just outside the 2σ error limit set for k(298 K).

I12. OH + OCS. The value of k(298 K) is an average of the determinations by Wahner and Ravishankara [1243] and Cheng and Lee [223]. The room temperature rate constants from these studies are a factor of 3 higher than the earlier determination by Leu and Smith [722]. As discussed in the later studies, this difference may be due to an overcorrection of the Leu and Smith data to account for OH reaction with H_2S impurities and also to possible regeneration of OH. Nevertheless, the uncertainty factor at 298 K has been set to encompass the earlier study within 2σ. The work by Wahner and Ravishankara [1243] supersedes the study of Ravishankara et al. [982], which minimized complications due to secondary and/or excited state reactions that presumably were interfering with the experiments of Atkinson et al. [45] and of Kurylo [663]. The upper limit for
k(298 K) reported by Cox and Sheppard [291] is too insensitive to permit comparison with the more recent studies. The room temperature measurements of Wahner and Ravishankara demonstrate the lack of an effect of total pressure (or O_2 partial pressure) on the rate constant and are supported by the more limited pressure and O_2 studies of Cheng and Lee. The recommendation for E/R is based on the study of Cheng and Lee who determined a value considerably lower than reported by Leu and Smith, although this difference may be due in part to the earlier mentioned overcorrection of the data by the latter authors.

Product observations by Leu and Smith indicate that SH is a primary product of this reaction and tentatively confirm the suggestion of Kurylo and Laufer [669] that the predominant reaction pathway is to produce SH + CO_2 through a complex (adduct) mechanism similar to that observed for the OH + CS_2 reaction. However, the absence of an O_2/pressure effect for OH + OCS is in marked contrast with the strong dependence seen in studies of OH + CS_2 (see note for the latter reaction).

Experiments by Greenblatt and Howard [454] have shown that oxygen atom exchange in the reaction of ^{18}OH with OCS is relatively unimportant, leading to an upper limit of 10^{-15} being set on the rate constant of the exchange reaction.

I13. OH + CS_2. There is a consensus of experimental evidence that this reaction proceeds very slowly as a direct bimolecular process. Wine et al. [1322] set an upper limit on k(298 K) of 1.5×10^{-15} cm^3 molecule^{-1} s^{-1}. A consistent upper limit is also reported by Iyer and Rowland [565] for the rate of direct product of OCS, suggesting that OCS and SH are primary products of the bimolecular process. This mechanistic interpretation is further supported by the studies of Leu and Smith [724] and of Biermann et al. [120], which set somewhat higher upper limits on k(298 K). The more rapid reaction rates measured by Atkinson et al. [45], Kurylo [663], and Cox and Sheppard [291] may be attributable to severe complications arising from excited state and secondary chemistry in their photolytic systems. The Cox and Sheppard study in particular may have been affected by the reaction of electronically excited CS_2 (produced via the 350 nm photolysis) with O_2 (in the 1-atm synthetic air mixture) as well as by the accelerating effect of O_2 on the OH + CS_2 reaction itself, which has been observed by other workers as summarized below. The possible importance of electronically excited CS_2 reactions in the tropospheric oxidation of CS_2 to OCS has been discussed by Wine et al. [1312].

An accelerating effect of O_2 on the OH + CS_2 reaction rate has been observed by Jones et al. [594], Barnes et al. [69], and Hynes et al. [553], along with a near unity product yield for SO_2 and OCS. In the latter two studies the effective bimolecular rate constant was found to be a function of total pressure (O_2 + N_2), and exhibited an appreciably negative temperature dependence. These observations are consistent with the formation of a long-lived adduct as postulated by Kurylo [663] and Kurylo and Laufer [669] followed by its reaction with O_2:

$$OH + CS_2 + M \underset{k_b}{\overset{k_a}{\rightleftharpoons}} HOCS_2 + M$$

$$HOCS_2 + O_2 \xrightarrow{k_c} \text{Products}$$

Hynes et al. [553], Murrells et al. [842], Becker et al. [97], and Bulatov et al. [167] directly observed the approach to equilibrium in this reversible adduct formation. In the Hynes et al. study, the equilibrium constant was measured as a function of temperature, and the heat of formation of $HOCS_2$ was calculated (–27.4 kcal/mole). A rearrangement of this adduct followed by dissociation into OCS and SH corresponds to the bimolecular (low k) channel referred to earlier. Hynes et al. [553] measured the rate constant for this process in the absence of O_2 (at approximately one atmosphere of N_2) to be $< 8 \times 10^{-16}$ cm^3 molecule^{-1} s^{-1}. Hynes et al. [553], Murrells et al. [842], and Diau and Lee [345] agree quite well on the value of k_c, with an average value of 2.9×10^{-14} being reported independent of temperature and pressure. Diau and Lee also

report the rate constants for the reactions of the adduct (CS_2OH) with NO and NO_2 to be 7.3×10^{-13} and 4.2×10^{-11} respectively.

The effective second order rate constant for CS_2 or OH removal in the above reaction scheme can be expressed as

$$1/k_{eff} = (k_b/k_a k_c)(1/P_{O2}) + (1/k_a)(1/P_M)$$

where P_{O_2} is the partial pressure of O_2 and P_M equals $P_{O_2} + P_{N_2}$. The validity of this expression requires that k_a and k_b are invariant with the P_{O_2}/P_{N_2} ratio. A 1/k vs $1/P_{O_2}$ plot of the data of Jones et al. [594] taken at atmospheric pressure exhibits marked curvature, suggesting a more complex mechanistic involvement of O_2, whereas the data of Barnes et al. [69] and Hynes et al. [553] are more satisfactorily represented by this analytical expression. Nevertheless, while the qualitative features of the data from all three laboratories agree, there are some quantitative inconsistencies. First, under similar conditions of O_2 and N_2 pressures, the Barnes et al. rate constants lie approximately 60% higher than those of Jones et al. and up to a factor of 2 higher than those derived by Hynes et al. Secondly, two fits each of both the Barnes et al. and Hynes et al. data can be made: one at fixed P_M and varying P_{O_2}, and the other at fixed P_{O_2} and varying P_M (i.e., varying added N_2). Within each data set, rate constants calculated from both fits agree reasonably well for mole fractions of O_2 near 0.2 (equivalent to air) but disagree by more than a factor of 2 for measurements in a pure O_2 system. Finally, the temperature dependence (from 264–293 K) of the k_{eff} values from Barnes et al. varies systematic-cally from an E/R of –1300 K for experiments in pure O_2 (at 700 torr total pressure) to –2900 K for experi-ments in a 50 torr O_2 plus 650 torr N_2 mixture. An Arrhenius fit of the Hynes et al. data (from 251–348 K) recorded in synthetic air at 690 torr yields an E/R = –3300 K, although the data show marked curvature over the temperature range of study. These observations suggest that k_a and k_b may not be independent of the identity of M. For this reason, we limit our recommendation to air mixtures (i.e., $P_{O_2}/P_{N_2} = 0.25$) at atmospheric pressure. Since most CS_2 is oxidized within the atmospheric boundary layer, such restriction does not limit the applicability of this recommendation in atmospheric modeling.

The present recommendation accepts the measurements of Hynes et al. [553], which appear to be the most sensitive of the three investigations. Thus, k(298 K) is derived from the Arrhenius fit of the data near room temperature.

$$k(298\ K) = 1.2 \times 10^{-12}\ cm^3\ molecule^{-1}\ s^{-1}$$

The uncertainty factor, f(298 K) = 1.5, encompasses the results of Barnes et al. [69] within 2σ. To compute values of k below 298 K, we have accepted the analysis of Hynes et al.

$$k(T) = \{1.25 \times 10^{-16} \exp(4550/T)\}/\{T + 1.81 \times 10^{-3} \exp(3400/T)\}$$

This recommendation is only valid for one atmosphere pressure of air. It is interesting to note that measurements by Hynes et al. [553] at approximately 250 K and 700 torr total pressure result in k_{eff} values that are independent of the amount of O_2 for partial pressures between 145–680 torr. This suggests that the adduct is quite stable with respect to dissociation into the reactants (OH + CS_2) at this low temperature and the that effective rate constant for reactant removal approaches the elementary rate constant for adduct formation.

From a mechanistic viewpoint, the primary products of reaction c determine the products of CS_2 oxidation in air. Lovejoy et al. [757] have shown that the yields of both HO_2 and SO_2 are equal and near unity. Together with the earlier mentioned unity yield of OCS, these observations suggest that the oxidation equation

$$OH + CS_2 + 2O_2 \rightarrow OCS + HO_2 + SO_2$$

describes this atmospheric system. Further insight is provided by the mechanistic study of Stickel et al. [1116], who observe OCS and CO product yields of (0.83±0.08) and (0.16±0.03) respectively. The results from this study are interpreted to imply that OCS and CO are formed either as primary products of the $CS_2OH + O_2$ reaction or as products of a secondary reaction between a primary product and O_2. These same authors report an SO_2 yield of (1.15±0.10), with the results suggesting that only about 75% of the SO_2 formed as a prompt product, with the remainder generated via a slow reaction of SO (generated as a prompt product of the
$CS_2OH + O_2$ reaction) with O_2. Insight into the specific reaction pathways can be gleaned from the study of Lovejoy et al. [756] in which k_c for the reaction of $DOCS_2 + O_2$ was found to be the same as that for $HOCS_2$, indicating that simple H atom abstraction is not the likely process. Rather, HO_2 production most likely involves complex formation followed by HO_2 elimination. Lovejoy et al. [758] found that the ^{18}O atom in the ^{18}OH reactant is transferred predominantly (90 ± 20)% to the SO_2 product. These findings are consistent with an S–O-bonded CS_2–OH adduct and preservation of the S–O bond in the steps leading to SO_2 formation.

Additional work involving direct intermediate observations would be helpful in elucidating this reaction mechanism.

I14. OH + CH_3SH. This recommendation is based on a composite fit to the data of Atkinson et al. [44], Wine et al. [1313], Wine et al. [1323], and Hynes and Wine [551], which are in excellent agreement. The results from the relative rate study of Barnes et al. [63] are in agreement with this recommendation and indicate that the higher value of Cox and Sheppard [291] is due to complications resulting from the presence of O_2 and NO in their reaction system. MacLeod et al. [766,767] and Lee and Tang [698] obtained rate constants at 298 K approximately 50% lower than recommended here. These authors also obtained lower values for the ethanethiol reaction in comparison with results from studies upon which the methanethiol recommendation is made. Wine et al. [1323] present evidence that this reaction proceeds via adduct formation to produce a species that is thermally stable over the temperature range and time scales of the kinetic measurements. Tyndall and Ravishankara [1218] have determined the yield of CH_3S (via laser–induced fluorescence) to be unity, indicating that any adduct must be short lived (less than 100 μs). Longer lifetimes would have led to anomalies in the OH decay kinetics used for the rate constant determinations. Hynes and Wine [551] failed to observe any effect of O_2 on the rate constant.

I15. OH + CH_3SCH_3. This recommendation is based on the results of Hynes et al. [555], Wine et al. [1313], Hsu et al. [540], Abbatt et al. [3], and Barone et al.[76]. The earlier higher rate constant values of Atkinson et al. [45] and Kurylo [662] are presumably due to reactive impurities, while those of MacLeod et al. [767] were most likely overestimated because of heterogeneous reactions. Absolute determinations lower than those recommended were obtained by Martin et al. [785], Wallington et al. [1247], and Nielsen et al. [883]. While the reasons for these differences are not readily apparent, these results are encompassed within the 2σ error limits of the 298 K recommendation. Hynes et al. have demonstrated the importance of a second reaction channel involving addition of OH to dimethyl sulfide (approximately 30% in 1 atmosphere of air at 298 K). More recently, Hynes et al. and Barone et al. have examined the reaction mechanism in more detail using fully deuterated DMS. Both groups report similar rate constants for the bimolecular (non–adduct–forming) rate constant and adduct bond strengths (13.0 and 10.1 kcal/mole—Hynes et al.; 10.2 and 10.7 kcal/mole—Barone et al.) from second and third law calculations, respectively. Values of the rate constant for the reaction of the adduct with O_2 were also nearly identical (8×10^{-13} cm^3 $molecule^{-1}$ s^{-1} from Hynes et al., and 10^{-12} cm^3 $molec^{-1}$ s^{-1} from Barone et al for both DMS and d^6–DMS) independent of pressure and temperature.

The recommendation given here is for the abstraction reaction only. Confirmation of the products as written is obtained from the study of Stickel et al. [1118] who determined an HDO product yield of (0.84±0.15) for the OD + CH_3SCH_3. Further mechanistic insight comes from the studies of Barnes et al. [72,73] and Turnipseed et al. [1203] who find that the abstraction product, CH_3SCH_2, leads predominantly to CH_3S under atmospheric conditions. Barnes et al. measure a 0.7% yield of OCS under low NO_x conditions, which they attribute to further oxidation of CH_3S. Both Barnes et al. and Turnipseed et al. find a significant (20–30%) yield of dimethyl sulfoxide, apparently produced via the reaction of the DMS–OH adduct with O_2. Zhao et al. [1372] determined an upper yield of 0.07 for CH_3 elimination in the OD + CH_3SCH_3 reaction system.

Due to the rapid decomposition of a DMS–OH adduct, only the direct abstraction channel is measured in the absence of O_2. The reaction of the adduct with O_2, as quantified most recently by Hynes et al. and Barone et al., is responsible for the majority of the products formed in the atmospheric oxidation of DMS. An increase in the observed rate constant (k_{obs}) with increasing O_2 concentration has clearly been observed by Hynes et al. [555], Wallington et al. [1247], Barnes et al. [62], Nielsen et al. [883], Barone et al. [76], and Hynes et al. [550]. This O_2 effect has been suggested as an explanation for the higher rate constants obtained in many of the earlier relative rate studies. Hynes et al. give the following expression for the observed rate constant in one atmosphere of air:

$$k_{obs} = \frac{T\exp(-234/T) + 8.46x10^{-10}\exp(7230/T) + 2.68x10^{-10}\exp(7810/T)}{1.04x10^{11}T + 88.1\exp(7460/T)}$$

This expression was derived empirically from the analysis of a complex data set, which also yielded a value of the rate constant for reaction of the adduct with O_2 that was a factor of 4 larger than the values derived by Hynes et al. [550] and Barone et al. [76] and appeared to be both pressure and temperature dependent. The effect of these revisions in the adduct + O_2 rate constant on the k_{obs} expression is not easily ascertained.

I16. OH + CH_3SSCH_3. This recommendation is based on the temperature–dependent studies of Wine et al. [1313] and Abbatt et al. [3] and the room temperature relative rate study of Cox and Sheppard [291]. Domine and Ravishankara [361] have observed both CH_3S (via laser–induced fluorescence) and CH_3SOH (via photo-ionization mass spectrometry) as products of this reaction. At 298 K, the yield of CH_3S alone was quantified

at approximately 30%. An FTIR product study of the photooxidation of dimethyl disulfide by Barnes et al. [71] presents evidence that oxidation of the CH_3SOH product is the principal source of the methane sulfonic acid observed.

I17. OH + S. This recommendation is based on the study by Jourdain et al. [596]. Their measured value for k(298 K) compares favorably with the recommended value of k(O + OH) when one considers the slightly greater exothermicity of the present reaction.

I18. OH + SO. The value recommended for k(298 K) is an average of the determinations by Fair and Thrush [380] and Jourdain et al. [596]. Both sets of data have been corrected using the present recommendation for the O + OH reaction.

I19. $HO_2 + H_2S$, $HO_2 + CH_3SH$, $HO_2 + CH_3SCH_3$. These upper limits are taken from the discharge flow laser magnetic resonance study of Mellouki and Ravishankara [808]. The H_2S value disagrees with the rate constant reported by Bulatov et al. [171] by approximately three orders of magnitude. The reason for this difference is not readily apparent. However, the recommended upper limit is consistent with the values for CH_3SH and CH_3SCH_3, which respectively agree with upper limits from the work of Barnes et al. [63] and Niki (reported as a private communication in the Mellouki and Ravishankara paper).

I20. $HO_2 + SO_2$. This upper limit is based on the atmospheric pressure study of Graham et al. [452]. A low pressure laser magnetic resonance study by Burrows et al. [176] places a somewhat higher upper limit on k(298 K) of
4×10^{-17} (determined relative to $OH + H_2O_2$). Their limit is based on the assumption that the products are OH and SO_3. The weight of evidence from both studies suggests an error in the earlier determination by Payne et al. [938].

I21. $NO_2 + SO_2$. This recommendation is based on the study of Penzhorn and Canosa [940] using second derivative UV spectroscopy. While these authors actually report a measured value for k(298 K), their observations of strong heterogeneous and water vapor catalyzed effects prompt us to accept their measurement as an upper limit. This value is approximately two orders of magnitude lower than that for a dark reaction observed by Jaffe and Klein [567], much of which may have been due to heterogeneous processes. Penzhorn and Canosa suggest that the products of this reaction are $NO + SO_3$.

I22. $NO_3 + H_2S$. This recommendation accepts the upper limit set by Dlugokencky and Howard [348] based on experiments in which NO_3 loss was followed in the presence of large concentrations of H_2S. Less sensitive upper limits for the rate constant have been reported by Wallington et al. [1249] and Cantrell et al. [197].

I23. NO_3 + OCS. This upper limit is based on the relative rate data of MacLeod et al. [764].

I24. $NO_3 + CS_2$. This upper limit is based on the study of Burrows et al. [180]. A somewhat higher upper limit was derived in the relative rate data of MacLeod et al. [764].

I25. $NO_3 + CH_3SH$. The recommended values are derived from a composite fit to the data of Wallington et al. [1249], Rahman et al. [975], and Dlugokencky and Howard [348]. The room temperature rate constant derived in the relative rate experiments of MacLeod et al. [764] is in good agreement with the recommended value. The suite of investigations shows the rate constant to be pressure independent over the range 1–700 torr. Dlugokencky and Howard place an upper limit of 5% on the production of NO_2 via this reaction at low pressure. Based on the product distribution observed in their investigation, Jensen et al. [583] propose a reaction mechanism initiated by abstraction of the hydrogen atom from the SH group, possibly after formation of an initial adduct as suggested by Wallington et al. and Dlugokencky and Howard.

I26. $NO_3 + CH_3SCH_3$. The recommended values are derived from a composite fit to the data of Wallington et al. [1249], Tyndall et al. [1209], and Dlugokencky and Howard [348]. The relative rate study of Atkinson et al. [47] yields a rate constant at room temperature in good agreement with that recommended. The experimental data from all investigations demonstrate the pressure independence of the rate constant over the range 1–740 torr. Room temperature investigations by Daykin and Wine [323] and Wallington et al. [1250] are also in agreement with the recommended value. Jensen et al. [582] propose a mechanism that involves hydrogen abstraction as the first step to explain their observed product distribution. In a later study, Jensen et al. [583] measured a kinetic isotope effect for the rate constant for CH_3SCH_3 vs. that for CD_3SCD_3 of $k_H/k_D = (3.8 \pm 0.6)$, providing further confirmation of such abstraction. Butkovskaya and Le Bras [182] utilized chemical titration of the primary radical produced from $NO_3 + CH_3SCH_3$ in a discharge flow mass spectrometer system to show that the reaction produces predominantly $CH_3SCH_2 + HNO_3$. An upper limit of 2% was placed on the reaction channel yielding $CH_3 + CH_3SONO_2$.

I27. $NO_3 + CH_3SSCH_3$. The recommended values were derived from a composite fit to the data of Wallington et al. [1249] and Dlugokencky and Howard [348]. The investigation by Atkinson et al. [39] indicates that the

relative rate technique cannot be considered as yielding reliable rate data for this reaction due to chemical complexities. Thus, the much lower room temperature results from the study of MacLeod et al. [764] can be considered to be erroneous. Based on their observations of intermediate and end products, Jensen et al. [583] proposed a reaction mechanism in which the initial addition of NO_3 to one of the sulfur atoms results in formation of $CH_3S + CH_3SO + NO_2$.

I28. $NO_3 + SO_2$. This recommended upper limit for k(298 K) is based on the study by Daubendiek and Calvert [305]. Considerably higher upper limits have been derived by Burrows et al. [180], Wallington et al. [1249], Canosa–Mas et al. [192], and Dlugokencky and Howard [348].

I29. $N_2O_5 + CH_3SCH_3$. This recommendation is based on the value estimated by Tyndall and Ravishankara [1219] from the study by Atkinson et al. [47].

I30. $CH_3O_2 + SO_2$. This recommendation accepts the results from the study of Sander and Watson [1022], which is believed to be the most appropriate for stratospheric modeling purposes. These authors conducted experiments using much lower CH_3O_2 concentrations than employed in the earlier investigations of Sanhueza et al. [1027] and Kan et al. [607], both of which resulted in k(298 K) values approximately 100 times greater. A later report by Kan et al. [606] postulates that these differences are due to the reactive removal of the $CH_3O_2SO_2$ adduct at high CH_3O_2 concentrations prior to its reversible decomposition into CH_3O_2 and SO_2. They suggest that such behavior of $CH_3O_2SO_2$ or its equilibrated adduct with O_2 ($CH_3O_2SO_2O_2$) would be expected in the studies yielding high k values, while decomposition of $CH_3O_2SO_2$ into reactants would dominate in the Sander and Watson experiments. It does not appear likely that such secondary reactions involving CH_3O_2, NO, or other radical species would be rapid enough, if they occur under normal stratospheric conditions to compete with the adduct decomposition. This interpretation, unfortunately, does not explain the high rate constant derived by Cocks et al. [265] under conditions of low [CH_3O_2].

I31. $F + CH_3SCH_3$. This recommendation is based on the discharge flow mass spectrometric study by Butkovskaya et al. [183]. The uncertainty placed on this recommendation has been increased over that estimated by the authors to reflect the lack of any confirming investigations. Titration of the primary organic radical products indicated that the reaction proceeds via two channels to produce $HF + CH_3SCH_2$ and $CH_3 + CH_3SF$ with a branching ratio of approximately 0.8/0.2 respectively.

I32. $Cl + H_2S$. This recommendation is based on the study by Nicovich et al. [870], who conducted an elaborate study with attention to sources of possible systematic error. The rate constant at 298 K is in good agreement with that determined by Nesbitt and Leone [857], who refined the data of Braithwaite and Leone [149], but is significantly greater than the values reported by Clyne and Ono [256], Clyne et al. [247], and Nava et al. [847]. The small, but clearly observed, negative activation energy determined by Nicovich et al. contrasts with the lack of a temperature dependence observed by Nava et al.. In fact, at the lowest temperature of overlap, the results from these two studies differ by 50%. Nevertheless, the Nicovich et al. study yields consistent results for both H_2S and CH_3SH as well as for D_2S and CD_3SD. While the reason for these differences remains to be determined, the full range of reported values is encompassed within the 2σ error limits recommended. Lu et al. [761] also measured a temperature–independent rate constant but report a value at 298 K, about 40% greater than that of Nicovich et al. However, the presence of 4000 torr of CF_3Cl bath gas in the Lu et al. may suggest a slight pressure dependence of the reaction, although Nicovich et al. observed no pressure dependence for pressures ranging up to 600 torr with N_2.

I33. Cl + OCS. This upper limit is based on the minimum detectable decrease in atomic chlorine measured by Eibling and Kaufman [376]. Based on the observation of product SCl, these authors set a lower limit on k(298 K) of 10^{-18} for this reaction channel. Considerably higher upper limits on k(298 K) were determined in the studies of Clyne et al. [247] and Nava et al. [847].

I34. $Cl + CS_2$. This upper limit for the overall reaction is based on determinations by Nicovich et al. [869] and Wallington et al. [1246]. The first authors confirm that the reaction proceeds via reversible adduct formation as suggested by Martin et al. [783]. The much larger rate constant values determined by Martin et al. may possibly be attributed to reactive impurities in the CS_2 sample. Nicovich et al. set an upper limit on the rate constant for the adduct (CS_2Cl) reacting with O_2 of 2.5×10^{-16} at room temperature.

I35. $Cl + CH_3SH$. This recommendation is based on the results of Nicovich et al. [870], who used laser photolysis with resonance fluorescence detection to study the reactions of Cl with H_2S, D_2S, CH_3SH, and CD_3SD. The room temperature determination by Nesbitt and Leone [857] is in good agreement with the value recommended. The k(298 K) value from the study by Mellouki et al. [804] is nearly a factor of 2 lower. However, the low sensitivity of EPR detection of Cl atoms did not permit these latter authors to conduct a precise determination of k under pseudo–first–order conditions, and a more complex analysis of experiments conducted under second–order conditions was required. Nesbitt and Leone [858] report that less than 2% of the reaction occurs via abstraction of an H atom from the CH_3 group.

I36. Cl + CH_3SCH_3. Stickel et al. [1117] have used laser photolysis resonance fluorescence to measure that rate constant between 240–421 K, over the pressure range of 3–700 torr. The rate constant is near collisional but increases with increasing pressure from a low pressure limit of 1.8×10^{-10} to a value of 3.3×10^{-10} at 700 torr. The yield of HCl at 297 K, measured by diode laser spectroscopy, decreased from near unity at low pressure to a value of approximately 0.5 at 203 torr, suggesting that stabilization of a $(CH_3)_2SCl$ adduct becomes competitive with hydrogen atom abstraction with increasing pressure. These investigators also observed a negative temperature dependence for the reaction. Butkovskaya et al. [183] conducted a discharge flow mass spectrometric study at 298 K, in which they determined that the reaction proceeds to form HCl + CH_3SCH_2 almost exclusively at 1 torr total pressure. The sum of all other possible channels was estimated at less than 3%. Zhao et al. [1372] used laser photolysis coupled with CH_3 detection by time–resolved tunable diode laser absorption spectroscopy to determine an upper limit for CH_3 elimination at 298 K and pressures between 10–30 torr. Room temperature measurements by Nielsen et al. [882] at 740 torr and Kinnison et al. [626] at 760 torr agree quite well with the results of Stickel et al. Kinnison et al. also observed the rate constant to increase from 3.6×10^{-10} to 4.2×10^{-10} cm^3 $molec^{-1}$ s^{-1} when the bath gas was changed from pure N_2 to synthetic air, suggesting that the $(CH_3)_2SCl$ adduct reacts with O_2.

I37. ClO + OCS; ClO + SO_2. These recommendations are based on the discharge flow mass spectrometric data of Eibling and Kaufman [376]. The upper limit on k(298 K) for ClO + OCS was set from the minimum detectable decrease in ClO. No products were observed. The upper limit on k(298 K) for ClO + SO_2 is based on the authors' estimate of their SO_3 detection limit. The upper limit for this same reaction based on the minimum detectable decrease in ClO was not used due to the potential problem of ClO reformation from the Cl + O_3 source reaction.

I38. ClO + CH_3SCH_3. This recommendation is based on the study by Barnes et al. [67] using discharge flow mass spectrometry. The authors prefer the present value of the rate constant to one a factor of 4 higher, which they determined in an earlier version of their apparatus. The uncertainty factor reflects the absence of any confirming investigations.

I39. ClO + SO. The value of k(298 K) is an average of the determinations by Clyne and MacRobert [246] and Brunning and Stief [162]. The temperature independence is taken from the latter study with the A–factor recalculated to fit the k(298 K) recommendation.

I40. Br + H_2S, Br + CH_3SH. These recommendations are based on the study by Nicovich et al. [867] who measured both the forward and reverse reactions by time–resolved resonance fluorescence detection of Br atoms. The uncertainties placed on these recommendations have been increased over those estimated by the authors to reflect the absence of any confirming investigations.

I41. Br + CH_3SCH_3. Wine et al. [1315] used laser photolysis resonance fluorescence to study reversible adduct formation in the Br + CH_3SCH_3 reaction system over the temperature range 260 – 310 K from which they derive a $(CH_3)_2S$–Br bond strength of 14.5 ± 1.2 kcal $mole^{-1}$. Above 375 K, adduct decomposition is so rapid that the addition channel is effectively negligible. Extrapolation of these data to conditions typical of the springtime Arctic boundary layer (760 torr, 230 – 270 K) leads these authors to suggest that under such conditions, the addition of Br to CH_3SCH_3 proceeds with a rate constant of approximately 1.3×10^{-10} cm^3 $molecule^{-1}$ s^{-1}. Researchers from the same laboratory (Jefferson et al. [573]) studied the abstraction reaction over the temperature range 386 – 604 K. These authors observed the reactants to be in equilibrium with the products HBr + CH_3SCH_2 and determined Arrhenius expressions for the forward and reverse reactions respectively of 9.0×10^{-11} exp(–2386/T) cm^3 $molecule^{-1}$ s^{-1} and 8.6×10^{-13} exp(836/T) cm^3 $molecule^{-1}$ s^{-1}. Analysis of the equilibrium data also permitted determination of the heat of formation of CH_3SCH_2 (see Appendix 1).

I42. BrO + CH_3SCH_3. This recommendation is based on the discharge flow mass spectrometric study by Bedjanian et al. [99], performed at 1 torr over the temperature range 233–320 K. The rate constant at 298 K is nearly identical to that derived by Barnes et al. [67], using a similar experimental system. Bedjanian et al. also determined a near unity yield for the production of dimethylsulfoxide and suggest that the reaction proceeds via production of an adduct that decomposes into the sulfoxide and bromine atoms.

I43. BrO + SO. This recommendation is based on the measurements of Brunning and Stief [163] performed under both excess BrO and excess SO conditions. The rate constant is supported by the lower limit assigned by Clyne and MacRobert [246] from measurements of SO_2 production.

I44. IO + CH_3SH. The value of k(298 K) comes from the study by Maguin et al. [769] using discharge flow mass spectrometry. The investigators establish a branching ratio near unity for the production of HOI. The uncertainty factor reflects the absence of any confirming investigations.

I45. IO + CH_3SCH_3. This recommendation comes from the studies by Daykin and Wine [321] using laser photolysis absorption spectroscopy and by Maguin et al. [769] and Barnes et al. [67] using discharge flow mass spectroscopy. These groups obtained rate constants of $\leq 3.5 \times 10^{-14}$, 1.5×10^{-14}, and 8.8×10^{-15} respectively. The last two studies supersede earlier, less direct measurements by the same groups, which resulted in rate constants of 1.5×10^{-11} (Martin et al. [784]) and 3.0×10^{-11} (Barnes et al. [68]).

I46. S + O_2. This recommendation is based primarily on the study of Davis et al. [316]. Modest agreement at 298 K is found in the studies of Fair and Thrush [380], Fair et al. [381], Donovan and Little [364], and Clyne and Townsend [257]. The study by Clyne and Whitefield [264], which indicates a slightly negative E/R between 300 and 400 K, is encompassed by the assigned uncertainty limits.

I47. S + O_3. This recommendation accepts the only available experimental data of Clyne and Townsend [257]. In this study the authors measure a value of the rate constant for S + O_2 in reasonable agreement with that recommended above.

I48. SO + O_2. This recommendation is based on the low temperature measurements of Black et al. [133,134]. The room temperature value accepts the results of the more recent paper as recommended by the authors. The uncertainties cited reflect the need for further confirmation and the fact that these results lie significantly higher than an extrapolation of the higher temperature data of Homann et al. [520]. A room temperature upper limit on k set by Breckenridge and Miller [150] is consistent with the Black et al. data.

I49. SO + O_3. The value of k(298 K) is an average of the determinations by Halstead and Thrush [474], Robertshaw and Smith [1004], and Black et al. [133,134] using widely different techniques. The value of E/R is an average of the values reported by Halstead and Thrush and Black et al. [134], with the A-factor recalculated to fit the recommendation for k(298 K).

I50. SO + NO_2. The value of k(298 K) is an average of the determinations by Clyne and MacRobert [245], Black et al. [133], and Brunning and Stief [162], which agree quite well with the rate constant calculated from the relative rate measurements of Clyne et al. [241]. The Arrhenius parameters are taken from Brunning and Stief.

I51. SO + OClO. This recommendation is based on the room temperature study by Clyne and MacRobert [246]. The uncertainty reflects the absence of any confirming investigation.

I52. SO_3 + H_2O. Several research groups have attempted to quantify the rate of sulfuric acid formation via this reaction in the gas phase. Reiner and Arnold [1000] placed an upper limit of 2.4×10^{-15} cm^3 $molec^{-1}$ s^{-1} on the rate constant, slightly lower than that determined by Wang et al. [1274]. The inability to cite the results as other than an upper limit is due to the difficulty in excluding all heterogeneous effects from the experiments. The higher rate constant reported earlier by Castleman et al. [203] may have resulted from an underestimation of the effects of such heterogeneous reactions. Subsequently, Reiner and Arnold [1001] sought to improve their rate constant determination by more detailed quantification of heterogeneous contributions. They derived a value of 1.2×10^{-15} cm^3 $molec^{-1}$ s^{-1}, independent of pressure (from 31–260 mbar of synthetic air). Evidence was also obtained that H_2SO_4 was, indeed, the product of the reaction.

Kolb et al. [647] attempted to measure the gas phase reaction using a turbulent flow reactor designed to minimize wall effects. Their results, when analyzed as representing a bimolecular reaction, support a rate constant between $(1 – 7) \times 10^{-15}$ cm^3 $molec^{-1}$ s^{-1}. However, a more considered analysis of the data indicated that the gas phase reaction was second order in water vapor. The reaction rate was also observed to increase as the temperature was lowered from 333 K to 243 K. These observations, together with calculations by Morokuma and Mugurama [835], led the latter authors to suggest that SO_3 consumption likely involved its reaction with the water dimer or the reaction of $SO_3 \cdot H_2O$ + H_2O, leading to the formation of sulfuric acid.

A laminar flow reactor study by Lovejoy et al. [755] over the temperature range 256–360 K also revealed SO_3 loss to be second order in water concentration and independent of pressure (from 20 to 80 torr of N_2 at 300 K). These latter authors measured a strong negative temperature dependence for the rate constant and a significant kinetic isotope effect ($k_{H2O} \approx 2k_{D2O}$), leading them to describe the reaction as proceeding via the rapid association between SO_3 and H_2O followed by a slower reaction between the adduct and water to form sulfuric acid. Lovejoy at al.'s measurement of a –13 kcal mol^{-1} "activation" energy was viewed as energetically inconsistent with the SO_3 + water dimer reaction mechanism since it would require a large negative activation energy for the SO_3 + $(H_2O)_2$ step. The first order expression for SO_3 loss derived by these authors is 2.26×10^{-43} T exp(6544/T) $[H_2O]^2$ and is recommended here.

I53. SO_3 + NO_2. This recommendation is based on the study of Penzhorn and Canosa [940] using second derivative UV spectroscopy. These authors observe the production of a white aerosol, which they interpret to be the adduct NSO_5. This claim is supported by ESCA spectra.

I54. SH + O_2. This upper limit for k(298 K) is based on the study by Stachnik and Molina [1102] utilizing experiments sensitive to the production of OH. Somewhat higher upper limits of 1.0×10^{-17} and 1.5×10^{-17} were assigned by Friedl et al. [410] and Wang et al. [1272] respectively from the detection sensitivities for OH detection and SH decay respectively. An even higher upper limit by Black [130], based on the lack of SH decay, may have been complicated by SH regeneration. Much less sensitive upper limits have been calculated by Tiee et al. [1174], Nielsen [874], and Cupitt and Glass [296]. Stachnik and Molina [1102] also report a somewhat higher upper limit ($< 1.0 \times 10^{-18}$) for the rate constant for the sum of the two SH + O_2 reaction channels (producing OH + SO and H + SO_2).

I55. SH + O_3. The value for k(298 K) is an average of the determinations by Friedl et al. [410] (laser–induced fluorescence detection of SH), Schonle et al. [1041] (mass spectrometric detection of reactant SH and product HSO) as revised by Schindler and Benter [1034], and Wang and Howard [1271] (laser magnetic resonance detection of SH). The temperature dependence is from Wang and Howard with the A–factor calculated to agree with the recommended value for k(298 K). $\Delta E/R$ reflects the fact that the temperature dependence comes from measurements above room temperature and, thus, extrapolation to lower temperatures may be subject to additional uncertainties. Wang and Howard report observing a minor reaction channel that produces H + SO + O_2.

I56. SH + H_2O_2. This recommended upper limit for k(298 K) is based on the study of Friedl et al. [410]. Their value is calculated from the lack of SH decay (measured by laser–induced fluorescence) and the lack of OH production (measured by resonance fluorescence). The three possible product channels yield: H_2S + HO_2, HSOH + OH, and HSO + H_2O.

I57. SH + NO_2. This recommendation is based on the measurements of Wang et al. [1272]. These authors suggest that the lower values of k(298 K) reported by Black [130], Friedl et al. [410], and Bulatov et al. [168] are due to SH regeneration from the H_2S source compound. In the study by Stachnik and Molina [1102], attempts were made at minimizing such regeneration, and the reported value of k(298 K) was significantly higher than that from the earlier studies, but still 30% lower than that measured by Wang et al., who used two independent SH source reactions. A slightly higher rate constant measured by Schonle et al. [1041], as revised by Schindler and Benter [1034], has not been recommended due to the somewhat more limited database for their determination. The reaction as written represents the most exothermic channel. In fact, HSO has been detected as a product by Leu and Smith [723], Bulatov et al. [168], Schonle et al. [1041], and Wang et al. [1272]. The absence of a primary deuterium isotope effect, as observed by Wang et al. [1272], coupled with the large magnitude of the rate constant suggests that the (four–center intermediate) channels producing SO + HNO and OH + SNO are of minor importance. No evidence for a three–body combination reaction was found by either Black [130] or Friedl et al. [410]. Based on a pressure independence of the rate constant between 30–300 torr, Black set an upper limit of 7.0×10^{-31} for the termolecular rate constant. Similarly, Stachnik and Molina [1102] saw no change in decay rate between 100 and 730 torr with O_2 (although these O_2 experiments were designed primarily to limit SH regeneration). The recommendation given here is supported by the recent discharge flow laser–induced fluorescence study of the SD + NO_2 reaction by Fenter and Anderson [388]. These investigators report a rate constant at 298 K of 6.8×10^{-11} cm^3 $molec^{-1}$ s^{-1}, which compares favorably with the value of 7.1×10^{-11} cm^3 $molecule^{-1}$ s^{-1} determined in the Wang et al. of the same reaction. Fenter and Anderson also obtained an E/R value of –210 K, very similar to the –237 K value derived by Wang et al. for the SH reaction.

I58. SH + Cl_2; SH + BrCl; SH + Br_2; SH + F_2. The recommendations for these reactions are derived from the data of Fenter and Anderson [387] for the SD radical. The uncertainties have been increased over those estimated by the investigators to reflect the absence of any confirming investigations and the influence of the secondary isotope effect. For the BrCl reaction, the channel producing ClSD + Br was found to be described by the rate expression $k = 2.3 \times 10^{-11} \exp(100/T)$.

I59. HSO + O_2. This recommendation is based on the study by Lovejoy et al. [759], who employed laser magnetic resonance monitoring of HSO in a discharge flow system. The upper limit thus derived for k(298 K) is nearly two orders of magnitude lower than measured by Bulatov et al. [170].

I60. HSO + O_3. This recommendation is based on the determinations by Friedl et al. [410] and Wang and Howard [1271]. In the first study, performed at higher O_3 concentrations, greater quantities of HSO were produced in the flow tube and SH approached a steady state due to its generation via HSO + O_3. The rate constant for this reaction was thus determined relative to SH + O_3 from measurements of the steady state SH concentration as a function of the initial SH concentration. In the second study, the rate constant and its branching ratio were measured at two temperatures. At room temperature, the overall rate constant is in excellent agreement with that of Friedl et al. More recently, Lee et al. [705] determined a room temperature rate constant of 4.7×10^{-14} for the sum of all reaction channels not producing HS. This value is approximately 30% greater than that

measured by Wang and Howard for the same channels. Lee et al. derive an Arrhenius activation energy of 1120 K for these channels from data between 273–423 K, in agreement with the more limited temperature data of Wang and Howard.

The lack of an isotope effect when SD was employed in the Friedl et al. study suggests that the products of the HSO + O_3 reaction are SH + $2O_2$ (analogous to those for HO_2 + O_3). However, Wang and Howard found that only 70% of the reaction leads to HS formation. In addition, their observations of HO_2 production in the presence of O_2 suggests the existence of a reaction channel producing HSO_2 + O_2 followed by $HSO_2 + O_2 \rightarrow HO_2 + SO_2$. At the present time, no recommendation is given for the product channels. Further mechanistic work is suggested, since it is important to understand whether this reaction in the atmosphere leads to HS regeneration or to oxidation of the sulfur.

I61. HSO + NO; HSO + NO_2. The recommendations for these reactions are based on the study by Lovejoy et al. [759] in which laser magnetic resonance was used to monitor HSO in a discharge flow system. Their upper limit for the NO reaction is a factor of 25 lower than the rate constant measured by Bulatov et al. [169] using intracavity laser absorption at pressures between 10 and 100 torr. Since it is unlikely that this reaction rate undergoes a factor of 25 increase between 1 torr (the pressure of the Lovejoy et al. work) and 10 torr, the higher rate constant may be due to secondary chemistry associated with the HSO production methods employed.

The recommendation for the NO_2 reaction is a factor of 2 higher than the rate constant reported by Bulatov et al. [168]. Lovejoy et al. have attributed this difference to HSO regeneration under the experimental conditions used by Bulatov et al. [168]. The product assignment for this reaction is discussed in the note for the
HSO_2 + O_2 reaction.

I62. HSO_2 + O_2. This recommendation is based on the rate of HO_2 formation measured by Lovejoy et al. [759] upon addition of O_2 to the HSO + NO_2 reaction system. While HSO_2 was not observed directly, a consideration of the mechanistic possibilities for HSO + NO_2, coupled with measurements of the HO_2 production rate at various O_2 pressures, led these authors to suggest that HSO_2 is both a major product of the HSO + NO_2 reaction and a precursor for HO_2 via reaction with O_2.

I63. $HOSO_2$ + O_2. This recommendation is based on the studies of Gleason et al. [444] and Gleason and Howard [442] in which the $HOSO_2$ reactant was monitored using a chemical ionization mass spectrometric technique. Gleason and Howard conducted their measurements over the 297–423 K temperature range in the only temperature dependence investigation. Thus, $\Delta E/R$ has been increased from their quoted limits to account for the potential uncertainties in extrapolating their data to sub–ambient temperatures. The value of k(298 K) derives further support from the studies of Margitan [774] and Martin et al. [786], both of whom used modeling fits of OH radical decays in the OH + SO_2 + M reaction system in the presence of O_2 and NO. In this latter analysis, the $HOSO_2$ reacts with O_2, yielding HO_2, which subsequently regenerates OH through its reaction with NO. The infrared spectrum of $HOSO_2$ has been recorded in low temperature matrix isolation experiments by Hashimoto et al. [486] and Nagase et al. [845]. Mass spectrometric detection of $HOSO_2$ in the gas phase has also been reported by Egsgaard et al. [374].

I64. CS + O_2. The recommendation given for k(298 K) is based on the work of Black et al. [132] using laser–induced fluorescence to monitor CS. This value agrees with the somewhat less precise determination by Richardson [1003] using OCS formation rates. The latter author presents evidence that this reaction channel dominates over the one producing SO + CO by more than a factor of 10. Measurements by Richardson at 293 K and 495 K yield an E/R of 1860 K. However, use of this activation energy with the recommended value of k(298 K) results in an unusually low Arrhenius A-factor of 1.5×10^{-16}. In view of this, no recommendation is given for the temperature dependence.

I65. CS + O_3; CS + NO_2. The k(298 K) recommendations for both reactions accept the results of Black et al. [132], who used laser–induced fluorescence to monitor the CS reactant in a room temperature experiment. The uncertainty factors reflect the absence of any confirming measurements.

I66. CH_3S + O_2. This upper limit is based on the study by Tyndall and Ravishankara [1217]. Somewhat higher upper limits were derived in the earlier studies of Balla et al. [60] and Black and Jusinski [131].

I67. CH_3S + O_3. This recommendation is based on the temperature–dependent study of Turnipseed et al. [1201] and the room temperature determinations of Tyndall and Ravishankara [1218] and Domine et al. [362]. Domine et al. measured the yield of CH_3SO to be 15% at low pressure and used this value to revise the corrections applied in the Tyndall and Ravishankara investigation to account for CH_3S regeneration by CH_3SO + O_3. A failure to observe significant reaction in the study by Black and Jusinski [131] is interpreted

as due to rapid regeneration of CH_3S in their system. The value of g has been set larger than that derived by Turnipseed et al. to reflect the existence of only one temperature dependence investigation.

I68. $CH_3S + NO$. The upper limit for the bimolecular reaction between CH_3S and NO is based on estimates by Balla et al. [60], who conducted a temperature dependence study of the termolecular reaction.

I69. $CH_3S + NO_2$. This recommendation is based on the temperature dependent data of Turnipseed et al. [1201] and the room temperature results of Tyndall and Ravishankara [1217]. The room temperature value of Domine et al. [360] is encompassed by the recommended uncertainty factor. The value of $\Delta E/R$ has been set larger than that derived by Turnipseed et al. to reflect the existence of only one temperature dependence investigation. An earlier study by Balla et al. [60] yielded a room temperature rate constant nearly a factor of two higher than the present recommendation, which may be attributed to secondary reactions at higher radical concentrations. Tyndall and Ravishankara determined the NO yield to be (80 ± 20)%. Together with the unity yield of CH_3SO obtained by Domine et al., this implies that the primary reaction channel is as written.

I70. $CH_2SH + O_2$. This recommendis the ation average of the rate constant obtained by Rahman et al. [976] in a fast flow mass spectrometer system and that from Anastasi et al. [20] using a pulse radiolysis kinetic absorption apparatus. The value of Anastasi et al. is nearly twice that of Rahman et al. It is difficult at present to indicate a preference for the results of one study over the other, and the value of f(298 K) has been chosen to reflect this uncertainty. Since this is a fast bimolecular reaction, one would expect the products to be $HO_2 + CH_2S$, by analogy with the reaction between CH_2OH and O_2.

I71. $CH_2SH + O_3$. The value of k(298 K) comes from the study by Rahman et al. [976] using fast flow mass spectrometry. The uncertainty factor reflects the absence of any confirming investigations.

I72. $CH_2SH + NO$. The value of k(298 K) comes from the study by Anastasi et al. [20] using a pulse radiolysis kinetic absorption apparatus. The uncertainty factor reflects the absence of any confirming investigations.

I73. $CH_2SH + NO_2$. This recommendation averages the rate constant obtained by Rahman et al. [976] in a fast flow mass spectrometer system with that from Anastasi et al. [20], using a pulse radiolysis kinetic absorption apparatus. The value of Rahman et al. is nearly twice that of Anastasi et al. It is difficult at present to indicate a preference for the results of one study over the other, and the value of f(298 K) has been chosen to reflect this uncertainty.

I74. $CH_3SO + O_3$. This recommendation is based on the study by Domine et al. [362]. It is supported by the study of Tyndall and Ravishankara [1218], in which the rate constant was derived from a complex analysis of the $CH_3S + O_3$ reaction system. Domine et al. place the direct yield of CH_2SO at approximately 10% and that of CH_3S at 13% at low pressure.

I75. $CH_3SO + NO_2$. This recommendation is based on the direct measurements of Domine et al. [360]. The results are supported by somewhat less direct measurements of Tyndall and Ravishankara [1217] and Mellouki et al. [803].

I76. $CH_3SOO + O_3$, $CH_3SOO + NO$, $CH_3SOO + NO_2$. These recommendations are based on the experiments of Turnipseed et al. [1201] in which CH_3S was monitored by LIF in equilibrium with CH_3SOO. The upper limit for the O_3 reaction was determined from experiments at 227 K. The results for the NO and NO_2 reactions were independent of temperature over the ranges 227–256 K and 227–246 K, respectively. The uncertainties placed on these recommendations have been increased over those estimated by the authors to reflect the absence of any confirming investigations.

I77. $CH_3SO_2 + NO_2$. This recommendation is based on the study by Ray et al. [994] using a discharge flow reactor equipped with laser–induced fluorescence and mass spectrometric detection. The CH_3SO_2 was produced by the sequential oxidation of CH_3S and CH_3SO by NO_2 and is to be differentiated from the weakly bound adduct, CH_3SOO, formed by the reaction of CH_3S with O_2 at low temperature (Turnipseed et al [1201]). The uncertainty limit on the rate constant has been increased over that given by the authors to reflect the absence of any confirming investigation. However, some additional support for this recommendation does come from the study of the $CH_3S + NO_2$ reaction by Tyndall and Ravishankara [1217]. These authors observed fluorescence from a product species tentatively identified as CH_3SO_2, produced by the reaction of CH_3SO with NO_2. Computer simulation of the rise and fall of the fluorescence signal yielded an approximate rate constant value for the reaction $CH_3SO_2 + NO_2$ of 7.0×10^{-12} cm^3 $molec^{-1}$ s^{-1}. However, an unambiguous differentiation between the production and disappearance rate constants was not possible.

I78. $CH_3SCH_2 + NO_3$. This recommendation is based on the experiments of Butkovskaya and Le Bras [182]. The uncertainty factor reflects the absence of any confirming investigation.

I79. $CH_3SCH_2O_2$ + NO. This recommendation is based on the experiments of Wallington et al. [1257]. The uncertainty factor reflects the absence of any confirming investigation.

I80. $CH_3SS + O_3$. This recommendation is based on the discharge flow photoionization mass spectroscopy study by Domine et al. [362]. The uncertainty factor reflects the absence of any confirming investigations. The rate constant ratio for the reactions of CH_3SS with O_3 and NO_2 is consistent with the rate constant ration for the corresponding CH_3S reactions.

I81. $CH_3SS + NO_2$; $CH_3SSO + NO_2$. These recommendations are based on the discharge flow photoionization mass spectroscopy study by Domine et al. [360]. The rate constant ratio for these two reactions agrees with that observed for other RS/RSO radicals with NO_2. The assigned uncertainties reflect this agreement but acknowledge the absence of any confirming investigation. In the Domine et al. study, CH_3SSO was produced by reacting away all CH_3SS with high NO_2 concentrations. Thus, as expected, O atom transfer may be the primary channel in the CH_3SS reaction.

J1. $Na + O_3$. The recommendation is based on the measurements of Ager et al. [13], Worsnop et al. [1333] as corrected in Worsnop et al. [1334], and Plane et al. [953]. The data of Worsnop et al. supersede earlier work from that laboratory (Silver and Kolb [1063]). Measurements made by Husain et al. [546] at 500 K are somewhat lower, probably because they did not recognize that secondary chemistry, $NaO + O_3 \rightarrow Na + 2O_2$, interferes with the rate coefficient measurement. The temperature dependence is from results of Worsnop et al. [1334] (214–294 K) and Plane et al. [953] (208–377K). Ager et al. [13] estimate that the NaO_2 + O product channel is $\leq 5\%$. Evidence that the NaO product is in the $^2\Sigma^+$ excited electronic state was reported by Shi et al. [1058] and Wright et al. [1335].

J2. $Na + N_2O$. The recommendation incorporates the data of Husain and Marshall [545], Ager et al. [13], Plane and Rajasekhar [954], and Worsnop et al. [1334]. Silver and Kolb [1063] measured a rate coefficient at 295 K that is lower and is superseded by Worsnop et al. [1334]. Helmer and Plane [497] report a measurement at
300 K in excellent agreement with the recommendation. Earlier, less direct studies are discussed by Ager et al. [13]. The NaO product does not react significantly with N_2O at room temperature [k (for $Na + N_2 + O_2$ products) $\leq 10^{-16}$ and k (for $NaO_2 + N_2$ products) $\leq 2 \times 10^{-15}$ Ager et al.]. Wright et al. [1335] used UV photoelectron spectroscopy to determine the product NaO is formed predominantly in the excited $^2\Sigma^+$ state.

J3. $Na + Cl_2$. Two measurements of the rate coefficient for this reaction are in excellent agreement: Silver [1060] and Talcott et al. [1147]. The recommended value is the average of these room temperature results.

J4. NaO + O. The recommendation is based on a measurement at 573 K by Plane and Husain [952]. They reported that $\leq 1\%$ of the Na product is in the 3^2P excited state.

J5. $NaO + O_3$. This reaction was studied by Silver and Kolb [1063], Ager et al. [13], and Plane et al. [953], who agree on the rate coefficient and branching ratio. This agreement may be fortuitous because Silver and Kolb used an indirect method and an analysis based on their rate coefficient for the $Na + O_3$ reaction, which is about 1/2 of the recommended value. Ager et al. employed a somewhat more direct measurement, but the study is complicated by a chain reaction mechanism in the Na/O_3 system. Plane et al. reported rate coefficient measurements for the $NaO_2 + O_2$ product channel over the temperature range 207–377 K using pulsed photolysis LIF methods. The recommendation for that channel is based on all three studies, and the recommendation for the $Na + 2O_2$ channel is based upon the results of Silver and Kolb and Ager et al. The latter reaction channel may also have a significant temperature dependence.

J6. $NaO + H_2$. The recommendation is based on a measurement by Ager and Howard [12]. They also reported a significant $Na + H_2O$ product channel and that a small fraction of the Na from this channel is in the 3^2P excited state.

J7. $NaO + H_2O$. The recommendation is based on a measurement by Ager and Howard [12].

J8. NaO + NO. The recommendation is based on an indirect measurement reported by Ager et al. [13].

J9. NaO + HCl. There is only one indirect measurement of the rate coefficient for this reaction, that from the study by Silver et al. [1066]. They indicate that the products are NaCl and OH, although some NaOH and Cl production is not ruled out.

J10. NaO_2 + O. The recommendation is based on a flow tube study at 300 K by Helmer and Plane [497].

J11. NaO_2 + NO. This reaction is endothermic. The upper limit recommended is from an experimental study by Ager et al. [13].

J12. NaO_2 + HCl. The recommendation is based on a measurement reported by Silver and Kolb [1064]. They indicated that the products are NaCl + HO_2, but NaOOH + Cl may be possible products.

J13. NaOH + HCl. The recommendation is based on the study by Silver et al. [1066], which is the only published study of this reaction.

1.4 References

1. Abbatt, J. P. D. and J. G. Anderson, 1991, J. Phys. Chem. B, **95**, 2382–2390.
2. Abbatt, J. P. D., K. L. Demerjian and J. G. Anderson, 1990, J. Phys. Chem., **94**, 4566–4575.
3. Abbatt, J. P. D., F. F. Fentner and J. G. Anderson, 1992, J. Phys. Chem., **96**, 1780–1785.
4. Abbatt, J. P. D., D. W. Toohey, F. F. Fenter, P. S. Stevens, W. H. Brune and J. G. Anderson, 1989, J. Phys. Chem., **93**, 1022–1029.
5. Acerboni, G., N. R. Jensen, B. Rindone and J. JHjorth, 1999, Chem. Phys. Lett., **309**, 364–368.
6. Adachi, H. and N. Basco, 1979, Chem. Phys. Lett., **63**, 490.
7. Adachi, H., N. Basco and D. G. L. James, 1979, Int. J. Chem. Kinet., **11**, 1211–1229.
8. Addison, M. C., J. P. Burrows, R. A. Cox and R. Patrick, 1980, Chem. Phys. Lett., **73**, 283.
9. Addison, M. C., R. J. Donovan and J. Garraway, 1979, J. Chem. Soc. Faraday Disc., **67**, 286–296.
10. Adeniji, S. A., J. A. Kerr and M. R. Williams, 1981, Int. J. Chem. Kinet., **13**, 209.
11. Adler–Golden, S. M. and J. R. Wiesenfeld, 1981, Chem. Phys. Lett., **82**, 281.
12. Ager, J. W., III and C. J. Howard, 1987, J. Chem. Phys., **87**, 921–925.
13. Ager, J. W., III, C. L. Talcott and C. J. Howard, 1986, J. Chem. Phys., **85**, 5584–5592.
14. Agrawalla, B. S., A. S. Manocha and D. W. Setser, 1981, J. Phys. Chem., **85**, 2873–2877.
15. Aker, P. M., B. I. Niefer, J. J. Sloan and H. Heydtmann, 1987, J. Chem. Phys., **87**, 203–209.
16. Aleksandrov, E. N., V. S. Arutyunov and S. N. Kozlov, 1981, Kinetics and Catalysis, **22**, 391–394.
17. Amimoto, S. T., A. P. Force, R. G. Gulotty, Jr. and J. R. Wiesenfeld, 1979, J. Chem. Phys., **71**, 3640–3647.
18. Amimoto, S. T., A. P. Force and J. R. Wiesenfeld, 1978, Chem. Phys. Lett., **60**, 40–43.
19. Amimoto, S. T. and J. R. Wiesenfeld, 1980, J. Chem. Phys., **72**, 3899–3903.
20. Anastasi, C., M. Broomfield, O. J. Nielsen and P. Pagsberg, 1992, J. Phys. Chem., **96**, 696–701.
21. Anastasi, C., M. J. Brown, D. B. Smith and D. J. Waddington. Joint French and Italian sections of the Combustion Institute, 1987, Amalfi, Italy.
22. Anastasi, C., D. J. Waddington and A. Woolley, 1983, J. Chem. Soc. Faraday Trans., **79**, 505–516.
23. Anderson, J. G. and F. Kaufman, 1973, Chem. Phys. Lett., **19**, 483–486.
24. Anderson, L. G. and R. D. Stephens.
25. Anderson, P. C. and M. J. Kurylo, 1979, J. Phys. Chem., **83**, 2055.
26. Anderson, S. M., J. Morton, K. Mauersberger, Y. L. Yung and W. B. DeMore, 1992, Chem. Phys. Lett., **189**, 581–585.
27. Andersson, B. Y., R. A. Cox and M. E. Jenkin, 1988, Int. J. Chem. Kinetics, **20**, 283–295.
28. Andresen, P., A. Jacobs, C. Kleinermanns and J. Wolfrum. In *19th Symp. (Intl.) Combustion*, 1982; pp 11.
29. Arnold, I. and F. J. Comes, 1979, Chem. Phys., **42**, 231.
30. Arnold, I. and F. J. Comes, 1980, Chem. Phys., **47**, 125–130.
31. Arrington, C. A., W. Brennen, G. P. Glass, J. V. Michael and H. Niki, 1965, J. Chem. Phys., **43**, 525.
32. Ashford, R. D., N. Basco and J. E. Hunt, 1978, Int. J. Chem. Kinet., **10**, 1233–1244.
33. Atakan, B. A. Jacobs, M. Wahl, R. Weller and J. Wolfrum, 1989, Chem. Phys. Lett., **155**, 609–613.
34. Atkinson, R. and S. M. Aschmann, 1984, Int. J. Chem. Kinet., **16**, 259.
35. Atkinson, R. and S. M. Aschmann, 1985, Int. J. Chem. Kinet., **17**, 33–41.
36. Atkinson, R. and S. M. Aschmann, 1989, Int. J. Chem. Kinet., **21**, 1123–1129.
37. Atkinson, R., S. M. Aschmann, W. P. L. Carter and A. M. Winer, 1982, International Journal of Chemical Kinetics, **14**, 919–926.
38. Atkinson, R., S. M. Aschmann, D. R. Fitz, A. M. Winer and J. N. Pitts, Jr., 1982, Int. J. Chem. Kinet., **14**, 13.
39. Atkinson, R., S. M. Aschmann and J. N. Pitts, Jr., 1988, J. Geophys. Res., **93**, 7125–7126.
40. Atkinson, R., S. M. Aschmann, E. C. Tuazon, M. A. Goodman and A. M. Winer, 1987, J. Atmos. Chem., **5**, 83–90.
41. Atkinson, R., G. M. Breuer and J. N. Pitts, Jr., 1976, J. Geophys. Res., **81**, 5765–5770.
42. Atkinson, R. and W. P. L. Carter, 1991, J. Atmos. Chem., **13**, 195–210.
43. Atkinson, R., D. A. Hansen and J. N. Pitts, Jr., 1975, J. Chem. Phys., **63**, 1703–1706.
44. Atkinson, R., R. A. Perry and J. N. Pitts, Jr., 1977, J. Chem. Phys., **66**, 1578.
45. Atkinson, R., R. A. Perry and J. N. Pitts, Jr., 1978, Chem. Phys. Lett., **54**, 14.
46. Atkinson, R. and J. N. Pitts, Jr., 1978, J. Chem. Phys., **68**, 3581.
47. Atkinson, R., J. N. Pitts, Jr. and S. M. Aschmann, 1984, J. Phys. Chem., **88**, 1584.
48. Atkinson, R., C. N. Plum, W. P. L. Carter, A. M. Winer and J. N. Pitts, Jr., 1984, J. Phys. Chem., **88**, 1210–1215.
49. Atkinson, R., R. C. Tuazon, H. Macleod, S. M. Aschmann and A. M. Winer, 1986, Geophys. Res. Lett., **13**, 117–120.

50. Avery, H. E. and R. J. Cvetanovic, 1965, J. Chem. Phys., **43**, 3727–3733.
51. Aviles, R. G., D. F. Muller and P. L. Houston, 1980, Appl. Phys. Lett., **37**, 358–360.
52. Avramenko, L. I. and R. V. Kolesnikova, 1961, Bull. Acad. Sci. USSR, Div. Chem. Sci., 545.
53. Ayhens, Y. V., J. M. Nicovich, M. L. McKee and P. H. Wine, 1997, J. Phys. Chem. A, **101**, 9382–9390.
54. Baer, S., H. Hippler, R. Rahn, M. Siefke, N. Seitzinger and J. Troe, 1991, J. Chem. Phys., **95**, 6463–6470.
55. Bahta, A., R. Simonaitis and J. Heicklen, 1984, Int. J. Chem. Kinet. , **16**, 1227.
56. Balakhnin, V. P., V. I. Egorov and E. I. Intezarova, 1971, Kinetics and Catalysis **12**, 299.
57. Baldwin, A. C. and D. M. Golden, 1978, Chem. Phys. Lett., **55**, 350.
58. Baldwin, R. R., C. E. Dean, M. R. Honeyman and R. W. Walker, 1984, J. Chem. Soc. Faraday Trans. 1, **80**, 3187–3194.
59. Balestra–Garcia, C., G. Le Bras and H. MacLeod, 1992, J. Phys. Chem., **96**, 3312–3316.
60. Balla, R. J., H. H. Nelson and J. R. McDonald, 1986, Chem. Phys., **109**, 101.
61. Barker, J. R., S. W. Benson and D. M. Golden, 1977, Int. J. Chem. Kinet., **9**, 31.
62. Barnes, I., V. Bastian and K. H. Becker, 1988, Int. J. Chem. Kinet., **20**, 415–431.
63. Barnes, I., V. Bastian, K. H. Becker, E. H. Fink and W. Nelsen, 1986, J. Atmos. Chem., **4**, 445–466.
64. Barnes, I., V. Bastian, K. H. Becker, E. H. Fink and F. Zabel, 1981, Chem. Phys. Lett. , **83**, 459–464.
65. Barnes, I., V. Bastian, K. H. Becker, E. H. Fink and F. Zabel, 1982, Atmos. Environ., **16**, 545.
66. Barnes, I., V. Bastian, K. H. Becker, E. H. Fink and F. Zabel, 1986, Chem. Phys. Lett., **123**, 28–32.
67. Barnes, I., V. Bastian, K. H. Becker and R. D. Overath, 1991, Int. J. Chem. Kinet., **23**, 579–591.
68. Barnes, I., K. H. Becker, P. Carlier and G. Mouvier, 1987, Int. J. Chem. Kinet., **19**, 489–501.
69. Barnes, I., K. H. Becker, E. H. Fink, A. Reimer, F. Zabel and H. Niki, 1983, Int. J. Chem. Kinet., **15**, 631–645.
70. Barnes, I., K. H. Becker, E. H. Fink, A. Reimer, F. Zabel and H. Niki, 1985, Chem. Phys. Lett. , **115**, 1.
71. Barnes, I., K. H. Becker and N. Mihalopoulas, 1994, J. Atmos. Chem., **18**, 267–289.
72. Barnes, I., K. H. Becker and I. Patroescu, 1994, Geophys. Res. Lett., **21**, 2389–2392.
73. Barnes, I., K. H. Becker and I. Patroescu, 1996, Atmos. Environ., **30**, 1805–1814.
74. Barnett, A. J., G. Marston and R. P. Wayne, 1987, J. Chem. Soc. Faraday Trans. 2, **83**, 1453–1463.
75. Barone, S. B., A. A. Turnipseed and A. R. Ravishankara, 1994, J. Phys. Chem., **98**, 4602–4608.
76. Barone, S. B., A. A. Turnipseed and A. R. Ravishankara, 1996, J. Phys. Chem., **100**, 14694–14702.
77. Barry, J., G. Locke, D. Scollard, H. Sidebottom, J. Treacy, C. Clerbaux, R. Colin and J. Franklin, 1997, Int. J. Chem. Kinet., **29**, 607–617.
78. Barry, J., D. J. Scollard, J. J. Treacy, H. W. Sidebottom, G. Le Bras, G. Poulet, S. Teton, A. Chichinin, C. E. Canosa–Mas, D. J. Kinnison, R. P. Wayne and O. J. Nielsen, 1994, Chem. Phys. Lett., **221**, 353–358.
79. Barry, J., H. Sidebottom, J. Treacy and J. Franklin, 1995, Int. J. Chem. Kinet., **27**, 27–36.
80. Basco, N. and S. K. Dogra, 1971, Proc. Roy. Soc. A., **323**, 401.
81. Basco, N. and S. K. Dogra, 1971, Proc. Roy. Soc. A., **323**, 417–429.
82. Basco, N. and S. K. Dogra, 1971, Proc. Roy. Soc. A., **323**, 29.
83. Basco, N. and S. S. Parmar, 1985, Int. J. Chem. Kinet., **17**, 891.
84. Batt, L., R. T. Milne and R. D. McCulloch, 1977, Int. J. Chem. Kinet., **9**, 567–587.
85. Batt, L. and G. N. Robinson, 1979, Int. J. Chem. Kinet., **11**, 1045.
86. Battin–Leclerc, F., I. K. Kim, R. K. Talukdar, R. W. Portmann, A. R. Ravishankara, R. Steckler and D. Brown, 1999, J. Phys. Chem. A, **103**, 3237–3244.
87. Bauer, D., J. N. Crowley and G. K. Moortgat, 1992, J. Photochem and Photobiol., **A65**, 329–344.
88. Baulch, D. L., I. M. Campbell and S. M. Saunders, 1985, J. Chem. Soc. Faraday Trans. 1, **81**, 259–263.
89. Baulch, D. L., R. A. Cox, R. F. Hampson, Jr., J. A. Kerr, J. Troe and R. T. Watson, 1980, J. Phys. Chem. Ref. Data, **9**, 295–471.
90. Becker, E., T. Benter, R. Kampf, R. N. Schindler and U. Wille, 1991, Ber. Bunsenges. Phys. Chem., **95**, 1168–1173.
91. Becker, E., M. M. Rahman and R. N. Schindler, 1992, Ber. Bunsenges. Phys. Chem., **96**, 776–783.
92. Becker, E., U. Wille, M. M. Rahman and R. H. Schindler, 1991, Ber. Bunsenges. Phys. Chem., **95**, 1173–1179.
93. Becker, K. H., W. Groth and D. Kley, 1969, Z. Naturforsch, **A24**, 1280.
94. Becker, K. H., W. Groth and U. Schurath, 1971, Chem. Phys. Lett., **8**, 259–262.
95. Becker, K. H., W. Groth and U. Schurath, 1972, Chem. Phys. Lett. , **14**, 489–492.
96. Becker, K. H., M. A. Inocencio and U. Schurath, 1975, Int. J. Chem. Kinet., **Symp. No. 1**, 205–220.
97. Becker, K. H., W. Nelsen, Y. Su and K. Wirtz, 1990, Chem. Phys. Lett., **168**, 559–563.
98. Becker, K. H. and K. Wirtz, 1989, Journal of Atmospheric Chemistry, **9**, 419–433.
99. Bedjanian, Y., G. Poulet and G. Le Bras, 1996, Int. J. Chem. Kinet, **28**, 383–389.
100. Bedjanian, Y., V. Riffault and G. Le Bras, 2001, Int. J. Chem. Kin., **33**, 587–599.

101. Bednarek, G., M. Breil, A. Hoffman, J. P. Kohlman, V. Mors and R. Zellner, 1996, Ber. Bunsenges. Phys. Chem., **100**, 528–539.
102. Bednarek, G., J. P. Kohlmann, H. Saathoff and R. Zellner, 1995, Z, Phys. Chem., **188**, 1–15.
103. Bedzhanyan, Y. R., E. M. Markin and Y. M. Gershenzon, 1993, Kinetics and Catalysis, **33**, 594–601.
104. Bedzhanyan, Y. R., E. M. Markin and Y. M. Gershenzon, 1993, Kinetics and Catalysis, **33**, 601–606.
105. Bedzhanyan, Y. R., E. M. Markin and Y. M. Gershenzon, 1993, Kinetics and Catalysis, **34**, 1–3.
106. Bedzhanyan, Y. R., E. M. Markin, G. G. Politenkova and Y. M. Gershenzon, 1993, Kinetics and Catalysis, **33**, 797–801.
107. Beichert, P., L. Wingen, J. Lee, R. Vogt, M. J. Ezell, M. Ragains, R. Neavyn and B. J. Finlayson–Pitts, 1995, J. Phys. Chem., **99**, 13156–13162.
108. Bemand, P. P. and M. A. A. Clyne, 1977, J. Chem. Soc. Faraday Trans. 2, **73**, 394.
109. Bemand, P. P., M. A. A. Clyne and R. T. Watson, 1973, J. Chem. Soc. Faraday Trans. 1, **69**, 1356–1374.
110. Bemand, P. P., M. A. A. Clyne and R. T. Watson, 1974, J. Chem. Soc. Faraday Trans. 2, **70**, 564–576.
111. Beno, M. F., C. D. Jonah and W. A. Mulac, 1985, Int. J. Chem. Kinet., **17**, 1091–1101.
112. Benson, S. W., F. R. Cruickshank and R. Shaw, 1969, Int. J. Chem. Kinet., **1**, 29.
113. Bera, R. K. and R. J. Hanrahan, 1988, Radiation Physics and Chemistry, **32**, 579–584.
114. Berry, R., J. Yuan, A. Misra and P. Marshall, 1998, J. Phys. Chem. A, **102**, 5182–5188.
115. Bevilacqua, T. J., D. R. Hanson and C. J. Howard, 1993, J. Phys. Chem., **97**, 3750–3757.
116. Bhaskaran, K. A., P. Frank and T. Just. In *12th International Shock Tube Symposium* Jerusalem., 1979.
117. Bhatnagar, A. and R. W. Carr, 1994, Chem. Phys. Lett., **231**, 454–459.
118. Bida, G. T., W. H. Breckenridge and W. S. Kolln, 1976, J. Chem. Phys., **64**, 3296.
119. Biedenkapp, D. and E. J. Bair, 1970, J. Chem. Phys., **52**, 6119–6125.
120. Biermann, H. W., G. W. Harris and J. N. Pitts, Jr., 1982, J. Phys. Chem., **86**, 2958–2964.
121. Biermann, H. W., C. Zetzsch and F. Stuhl, 1978, Ber. Bunsenges Phys. Chem., **82**, 633.
122. Biggs, P., C. E. Canosa–Mas, J.–M. Fracheboud, D. E. Shallcross and R. P. Wayne, 1995, Geophys. Res. Lett., **22**, 1221–1224.
123. Biggs, P., C. E. Canosa–Mas, P. S. Monks, R. P. Wayne, T. Benter and R. N. Schindler, 1993, Int. J. Chem. Kinet., **25**, 805–817.
124. Biggs, P., M. H. Harwood, A. D. Parr and R. P. Wayne, 1991, J. Phys. Chem., **97**, 7746–7751.
125. Bilde, M. and T. J. Wallington, 1998, J. Phys. Chem., **102**, 1550–1555.
126. Bilde, M., T. J. Wallington, G. Ferronato, J. J. Orlando, G. S. Tyndall, E. Estupinan and S. Haberkorn, 1998, J. Phys.Chem. A, **102**, 1976–1986.
127. Billington, A. P. and P. Borrell, 1986, J. Chem. Soc. Faraday Trans. 2, **82**, 963–970.
128. Birks, J. W., B. Shoemaker, T. J. Leck, R. A. Borders and L. J. Hart, 1977, J. Chem. Phys., **66**, 4591–4599.
129. Birks, J. W., B. Shoemaker, T. J. Leck and D. M. Hinton, 1976, J. Chem. Phys., **65**, 5181–5185.
130. Black, G., 1984, J. Chem. Phys., **80**, 1103–1107.
131. Black, G. and L. E. Jusinski, 1986, J. Chem. Soc. Faraday Trans. 2, **86**, 2143.
132. Black, G., L. E. Jusinski and T. G. Slanger, 1983, Chem. Phys. Lett., **102**, 64–68.
133. Black, G., R. L. Sharpless and T. G. Slanger, 1982, Chem. Phys. Lett., **90**, 55–58.
134. Black, G., R. L. Sharpless and T. G. Slanger, 1982, Chem. Phys. Lett., **93**, 598–602.
135. Bogan, D. J., R. P. Thorn, F. L. Nesbitt and L. J. Stief, 1996, J. Phys. Chem., **100**, 14383–14389.
136. Bohmer, E. and W. Hack, 1991, Ber. Bunsenges. Phys. Chem., **95**, 1688–1690.
137. Boodaghians, R. B., C. E. Canosa–Mas, P. J. Carpenter and R. P. Wayne, 1988, J. Chem. Soc. Faraday Trans. 2, **84**, 931–948.
138. Boodaghians, R. B., I. W. Hall and R. P. Wayne, 1987, J. Chem. Soc. Faraday Trans. 2, **83**, 529–538.
139. Borders, R. A. and J. W. Birks, 1982, J. Phys. Chem., **86**, 3295–3302.
140. Borrell, P., P. M. Borrell and M. D. Pedley, 1977, Chem. Phys. Lett., **51**, 300–302.
141. Bourbon, C., M. Brioukov and P. Devolder, 1996, C.A. Acad. Sci. Paris, **322**, 181–188.
142. Bourbon, C., M. Brioukov, B. Hanoune, J. P. Sawerysyn and P. Devolder, 1996, Chem. Phys. Lett., **254**, 203–212.
143. Bourbon, C., C. Fittschen, J. P. Sawerysyn and P. Devolder, 1995, J. Phys. Chem., **99**, 15102–15107.
144. Bourmada, N., C. Lafage and P. Devolder, 1987, Chem. Phys. Lett., **136**, 209–214.
145. Bozzelli, J. W. *Ph.D. Thesis*; Dept. of Chemistry, Princeton University, (Diss. Abstr. Int. B 34(2) 608), 1973.
146. Bozzelli, J. W. and A. M. Dean, 1990, J. Phys. Chem., **94**, 3313–3317.
147. Bradley, J. N., W. Hack, K. Hoyermann and H. G. Wagner, 1973, J. Chem. Soc. Faraday Trans. 1, **69**, 1889.
148. Brahan, K. M., A. D. Hewitt, G. D. Boone and S. A. Hewitt, 1996, Int. J. Chem. Kinet., **28**, 397–404.
149. Braithwaite, M. and S. R. Leone, 1978, J. Chem. Phys., **69**, 839–845.

150. Breckenridge, W. H. and T. A. Miller, 1972, J. Chem. Phys., **56**, 465.
151. Bridier, I., B. Veyret and R. Lesclaux, 1993, Chem. Phys. Lett., **201**, 563–568.
152. Bridier, I., B. Veyret, R. Lesclaux and M. E. Jenkin, 1993, J. Chem. Soc. Faraday Trans., **89**, 2993–2997.
153. Brown, A. C., C. E. Canosa–Mas, A. D. Parr, K. Rothwell and R. P. Wayne, 1990, Nature, **347**, 541–543.
154. Brown, A. C., C. E. Canosa–Mas, A. D. Parr and R. P. Wayne, 1990, Atmos. Environ., **24A**, 2499–2511.
155. Brown, A. C., C. E. Canosa–Mas and R. P. Wayne, 1990, Atmos. Environ., **24A**, 361–367.
156. Brown, A. C. and B. A. Thrush, 1967, Trans. Faraday Soc., **63**, 630.
157. Brown, R. D. and I. W. M. Smith, 1975, Int. J. Chem. Kinet. , **7**, 301.
158. Brown, S. S., J. B. Burkholder, R. K. Talukdar and A. R. Ravishankara, 2001, Journal of Physical Chemistry A, **105**, 1605–1614.
159. Brown, S. S., R. K. Talukdar and A. R. Ravishankara, 1999, J. Phys. Chem. A, **103**, 3031–3037.
160. Brune, W. H., J. J. Schwab and J. G. Anderson, 1983, J. Phys. Chem., **87**, 4503–4514.
161. Brunning, J. and M. A. A. Clyne, 1984, J. Chem. Soc. Faraday Trans 2, **80**, 1001–1014.
162. Brunning, J. and L. J. Stief, 1986, J. Chem. Phys., **84**, 4371–4377.
163. Brunning, J. and L. J. Stief, 1986, J. Chem. Phys., **85**, 2591.
164. Buben, S. N., I. K. Larin, N. A. Messineva and E. M. Trofimova, 1990, Khim. Fiz., **9**, 116–126.
165. Buben, S. N., I. K. Larin, N. A. Messineva and E. M. Trofimova, 1991.
166. Bulatov, V. P., A. A. Buloyan, S. G. Cheskis, M. Z. Kozliner, O. M. Sarkisov and A. I. Trostin, 1980, Chem. Phys. Lett., **74**, 288.
167. Bulatov, V. P., S. G. Cheskis, A. A. Iogensen, P. V. Kulakov, O. M. Sarkisov and E. Hassinen, 1988, Chem. Phys. Lett., **153**, 258–262.
168. Bulatov, V. P., M. Z. Kozliner and O. M. Sarkisov, 1984, Khim. Fiz., **3**, 1300–1305.
169. Bulatov, V. P., M. Z. Kozliner and O. M. Sarkisov, 1985, Khimi Fiz. , **4**, 1353.
170. Bulatov, V. P., O. M. Sarkisov, M. Z. Kozliner and V. G. Ergorov, 1986, Khim. Fiz., **5**, 1031.
171. Bulatov, V. P., S. I. Vereschchuk, F. N. Dzegilenko, O. M. Sarkisov and V. N. Khabarov, 1990, Khim. Fiz., **9**, 1214.
172. Burkholder, J. B., P. D. Hammer, C. J. Howard and A. Goldman, 1989, J. Geophys. Res., **94**, 2225–2234.
173. Burkholder, J. B., A. Mellouki, R. Talukdar and A. R. Ravishankara, 1994, Int. J. Chem. Kinet., **24**, 711–725.
174. Burkholder, J. B., R. R. Wilson, T. Gierczak, R. Talukdar, S. A. McKeen, J. J. Orlando, G. L. Vaghjiani and A. R. Ravishankara, 1991, J. Geophys. Res., **96**, 5025–5043.
175. Burks, T. L. and M. C. Lin, 1981, Int. J. Chem. Kinet., **13**, 13977–13999.
176. Burrows, J. P., D. I. Cliff, G. W. Harris, B. A. Thrush and J. P. T. Wilkinson, 1979, Proc. Roy. Soc. (London), **A368**, 463–481.
177. Burrows, J. P. and R. A. Cox, 1981, J. Chem. Soc. Faraday Trans. 1, **77**, 2465.
178. Burrows, J. P., R. A. Cox and R. G. Derwent, 1981, J. Photochem., **16**, 147–168.
179. Burrows, J. P., G. W. Harris and B. A. Thrush, 1977, Nature, **267**, 233–234.
180. Burrows, J. P., G. S. Tyndall and G. K. Moortgat, 1985, J. Phys. Chem., **89**, 4848–4856.
181. Burrows, J. P., T. J. Wallington and R. P. Wayne, 1984, J. Chem. Soc. Faraday Trans. 2, **80**, 957–971.
182. Butkovskaya, N. I. and G. Le Bras, 1994, J. Phys. Chem., **98**, 2582–2591.
183. Butkovskaya, N. I., G. Poulet and G. Le Bras, 1995, J. Phys. Chem., **99**, 4536–4543.
184. Butler, R., I. J. Solomon and A. Snelson, 1978, Chem. Phys. Lett., **54**, 19.
185. Cadle, R. D. and J. W. Powers, 1967, J. Phys. Chem., **71**, 1702–1706.
186. Cadle, R. D. and C. Schadt, 1953, J. Phys. Chem., **21**, 163.
187. Callear, A. B. and R. E. M. Hedges, 1970, Trans. Faraday Soc., **66**, 605.
188. Callear, A. B. and I. W. M. Smith, 1967, Nature, **213**, 382.
189. Calvert, J. G. and J. N. Pitts. In *Photochemistry*; John Wiley & Sons, Inc., New York, 1966; pp 783.
190. Campbell, I. M., D. F. McLaughlin and B. J. Handy, 1976, Chem. Phys. Lett., **38**, 362–64.
191. Cannon, B. D., J. S. Robertshaw, I. W. M. Smith and M. D. Williams, 1984, Chem. Phys. Lett., **105**, 380–385.
192. Canosa–Mas, C., S. J. Smith, S. Toby and R. P. Wayne, 1988, J. Chem. Soc. Faraday Trans. 2, **84**, 247–262.
193. Canosa–Mas, C. E., R. J. Dillon, H. Sidebotom, K. C. Thompson and R. P. Wayne, 2001, Phys. Chem. Chem. Phys., **3**, 542–550.
194. Canosa–Mas, C. E., S. J. Smith, S. Toby and R. P. Wayne, 1989, J. Chem. Soc. Faraday Trans. 2, **85**, 709–725.
195. Cantrell, C. A., J. A. Davidson, K. L. Busarow and J. G. Calvert, 1986, J. Geophys. Res., **91**, 5347–5353.
196. Cantrell, C. A., J. A. Davidson, A. H. McDaniel, R. E. Shetter and J. G. Calvert, 1988, J. Chem. Phys., **88**, 4997–5006.

197. Cantrell, C. A., J. A. Davidson, R. E. Shetter, B. A. Anderson and J. G. Calvert, 1987, J. Phys. Chem., **91**, 6017–6021.
198. Cantrell, C. A., R. E. Shetter and J. G. Calvert, 1994, J. Geophys. Res., **99**, 3739–3743.
199. Cantrell, C. A., R. E. Shetter, A. H. McDaniel and J. G. Calvert, 1990, J. Geophys. Res., **95**, 20531–20537.
200. Cantrell, C. A., R. E. Shetter, A. J. McDaniel, J. G. Calvert, J. A. Davidson, D. C. Lowe, S. C. Tyler, R. J. Cicerone and J. P. Greenberg, 1990, J. Geophys. Res., **95**, 22455–22462.
201. Cantrell, C. A., W. R. Stockwell, L. G. Anderson, K. L. Busarow, D. Perner, A. Schmeltekopf, J. G. Calvert and H. S. Johnston, 1985, J. Phys. Chem., **89**, 139–146.
202. Casavecchia, P., R. J. Buss, S. J. Sibener and Y. T. Lee, 1980, J. Chem. Phys., **73**, 6351–6352.
203. Castleman, A. W., R. E. Davis, H. R. Munkelwitz, I. N. Tang and W. P. Wood, 1975, Int. J. Chem. Kinet., **Symp. 1**, 629.
204. Catoire, V., R. Lesclaux, P. D. Lightfoot and M.–T. Rayez, 1994, J. Phys. Chem., **98**, 2889–2898.
205. Cattell, F. C., J. Cavanagh, R. A. Cox and M. E. Jenkin, 1986, J. Chem. Soc. Faraday Trans. 2, **82**, 1999–2018.
206. Cattell, F. C. and R. A. Cox, 1986, J. Chem. Soc. Faraday Trans. 2, **82**, 1413–1426.
207. Chan, W. H., W. M. Uselman, J. G. Calvert and J. H. Shaw, 1977, Chem. Phys. Lett., **45**, 240.
208. Chang, J. S. and J. R. Barker, 1979, J. Phys. Chem., **83**, 3059.
209. Chang, J. S. and F. Kaufman, 1977, J. Chem. Phys., **66**, 4989.
210. Chang, J. S. and F. Kaufman, 1977, Geophys. Res. Lett., **4**, 192–194.
211. Chang, J. S., P. L. Trevor and J. R. Barker, 1981, Int. J. Chem. Kinet., **13**, 1151–1161.
212. Chapman, C. J. and R. P. Wayne, 1974, Int. J. Chem. Kinet., **6**, 617–630.
213. Chasovnikov, S. A., A. I. Chichinin and L. N. Krasnoperov, 1987, Chem. Phys., **116**, 91–99.
214. Chatha, J. P. S., P. K. Arora, N. Raja, P. B. Kulkarni and K. G. Vohra, 1979, Int. J. Chem. Kinetics, **11**, 175–185.
215. Cheah, C. T. and M. A. A. Clyne, 1980, J. Chem. Soc. Faraday Trans., **76**, 1543.
216. Chen, J., V. Catoire and H. Niki, 1995, Chem. Phys. Lett, **245**, 519–528.
217. Chen, J., V. Young, T. Zhu and H. Niki, 1993, J. Phys. Chem., **97**, 11696–11698.
218. Chen, J., T. Zhu and H. Niki, 1992, J. Phys. Chem., **96**, 6115–6117.
219. Chen, J., T. Zhu, H. Niki and G. J. Mains, 1992, Geophys. Res. Lett., **19**, 2215–2218.
220. Chen, L., F. Fukuda, N. Takenaka, H. Bandow and Y. Maeda, 2000, Int. J. Chem. Kinet., **25**, 73–78.
221. Chen, M. C. and H. A. Taylor, 1961, J. Chem. Phys., **34**, 1344–1347.
222. Chen, X., F. Wu and B. R. Weiner, 1995, Chem. Phys. Lett., **247**, 313–320.
223. Cheng, B.–M. and Y.–P. Lee, 1986, Int. J. Chem. Kinet., **18**, 1303–1314.
224. Cheskis, S. G., A. A. Iogansen, O. M. Sarkisov and A. A. Titov, 1985, Chem. Phys. Lett., **120**, 45–49.
225. Cheskis, S. G. and O. M. Sarkisov, 1979, Chem. Phys. Lett., **62**, 72.
226. Chichinin, A., S. Teton, G. Le Bras and G. Poulet, 1994, J. Atmos. Chem, **18**, 239–245.
227. Chiorboli, C., C. A. Bignozzi, A. Maldotti, P. F. Giardini, A. Rossi and V. Carassiti, 1983, Int. J. Chem. Kinet., **15**, 579–586.
228. Choo, K. Y. and M. T. Leu, 1985, J. Phys. Chem., **89**, 4832–4837.
229. Choo, K. Y. and M.–T. Leu, 1985, Int. J. Chem. Kinetics, **17**, 1155–1167.
230. Clark, I. D., I. T. N. Jones and R. P. Wayne, 1970, Proc. Roy. Soc. Lond. A., **317**, 407–416.
231. Clark, I. D. and R. P. Wayne, 1969, Proc. Roy. Soc. Lond. A., **314**, 111–127.
232. Clark, I. D. and R. P. Wayne, 1969, Chem. Phys. Lett., **3**, 405–407.
233. Clark, I. D. and R. P. Wayne, 1970, Proc. Roy. Soc. London. A., **316**, 539–550.
234. Clark, R. H., D. Husain and J. Y. Jezequel, 1982, J. Photochem., **18**, 39–46.
235. Clemo, A. R., F. E. Davidson, G. L. Duncan and R. Grice, 1981, Chem. Phys. Lett., **84**, 509–511.
236. Clough, P. N. and B. A. Thrush, 1967, Trans. Faraday Soc., **63**, 915–925.
237. Clyne, M. A. A. and J. A. Coxon, 1968, Proc. Roy. Soc. A, **303**, 207–231.
238. Clyne, M. A. A. and H. W. Cruse, 1970, Trans. Faraday Soc., **66**, 2227.
239. Clyne, M. A. A. and H. W. Cruse, 1972, J. Chem. Soc. Faraday Trans. 2, **68**, 1281.
240. Clyne, M. A. A. and S. Down, 1974, J. Chem. Soc. Faraday Trans. 2, **70**, 253–266.
241. Clyne, M. A. A., C. J. Halstead and B. A. Thrush, 1966, Proc. Soc. London Ser. A., **295**, 355.
242. Clyne, M. A. A. and A. Hodgson, 1985, J. Chem. Soc. Faraday Trans. 2, **81**, 443–455.
243. Clyne, M. A. A. and P. M. Holt, 1979, J. Chem. Soc. Faraday Trans. 2, **75**, 569–581.
244. Clyne, M. A. A. and P. M. Holt, 1979, J. Chem. Soc. Faraday Trans. 2, **75**, 582–591.
245. Clyne, M. A. A. and A. J. MacRobert, 1980, Int. J. Chem. Kinet., **12**, 79–96.
246. Clyne, M. A. A. and A. J. MacRobert, 1981, Int. J. Chem. Kinet., **13**, 187–197.
247. Clyne, M. A. A., A. J. MacRobert, T. P. Murrells and L. J. Stief, 1984, J. Chem. Soc. Faraday Trans. 2, **80**, 877–886.

248. Clyne, M. A. A. and I. S. McDermid, 1975, J. Chem. Soc. Faraday Trans. 1, **71**, 2189.
249. Clyne, M. A. A., D. J. McKenney and R. F. Walker, 1973, Can. J. Chem., **51**, 3596.
250. Clyne, M. A. A., D. J. McKenney and R. T. Watson, 1975, Chem. Soc. Faraday Trans. 1, **71**, 322–335.
251. Clyne, M. A. A. and P. Monkhouse, 1977, J. Chem. Soc. Faraday Trans. 2, **73**, 298–309.
252. Clyne, M. A. A., P. B. Monkhouse and L. W. Townsend, 1976, Int. J. Chem. Kinet., **8**, 425.
253. Clyne, M. A. A. and W. S. Nip, 1976, J. Chem. Soc. Faraday Trans. 2, **72**, 838–847.
254. Clyne, M. A. A. and W. S. Nip, 1976, J. Chem. Soc. Faraday Trans. 1, **72**, 2211–2217.
255. Clyne, M. A. A. and Y. Ono, 1982, Chem. Phys., **69**, 381–388.
256. Clyne, M. A. A. and Y. Ono, 1983, Chem. Phys. Lett., **94**, 597–602.
257. Clyne, M. A. A. and L. W. Townsend, 1975, Int. J. Chem. Kinet., **Symp. 1**, 73–84.
258. Clyne, M. A. A. and R. F. Walker, 1973, J. Chem. Soc. Faraday Trans. 1, **69**, 1547–1567.
259. Clyne, M. A. A. and R. T. Watson, 1974, J. Chem. Soc. Faraday Trans. 1, **70**, 2250–2259.
260. Clyne, M. A. A. and R. T. Watson, 1974, J. Chem. Soc. Faraday Trans. 1, **70**, 1109.
261. Clyne, M. A. A. and R. T. Watson, 1975, J. Chem. Soc. Faraday Trans. 1, **71**, 336.
262. Clyne, M. A. A. and R. T. Watson, 1977, J. Chem. Soc. Faraday Trans. 1, **73**, 1169–1187.
263. Clyne, M. A. A. and I. F. White, 1971, Trans. Faraday Soc., **67**, 2068–2076.
264. Clyne, M. A. A. and P. D. Whitefield, 1979, J. Chem. Soc. Faraday Trans. 2, **75**, 1327.
265. Cocks, A. T., R. P. Fernanado and I. S. Fletcher, 1986, Atmos. Environ., **20**, 2359–2366.
266. Collins, R. J., D. Husain and R. J. Donovan, 1973, J. Chem. Soc. Faraday Trans. 2, **69**, 145–157.
267. Colussi, A. J., 1990, J. Phys. Chem., **94**, 8922–8926.
268. Colussi, A. J. and M. A. Grela, 1994, Chem. Phys. Lett., **229**, 134–138.
269. Colussi, A. J., S. P. Sander and R. R. Friedl, 1992, J. Phys.Chem., **96**, 4442–4445.
270. Cook, J. L., C. A. Ennis, T. J. Leck and J. W. Birks, 1981, J. Chem. Phys., **74**, 545.
271. Coomber, J. W. and E. Whittle, 1966, Trans. Faraday Soc., **62**, 2183–2190.
272. Cooper, W. F. and J. F. Hershberger, 1992, J. Phys. Chem., **96**, 5405–5410.
273. Cotter, E. S. N., N. J. Booth, C. E. Canosa–Mas, D. J. Gray, D. E. Shallcross and R. P. Wayne, 2001, Chem. Phys. Phys. Chem, **3**, 402–408.
274. Cox, J. W., H. H. Nelson and J. R. McDonald, 1985, Chem. Phys., **96**, 175.
275. Cox, R. A., 1980, Int. J. Chem. Kinet., **12**, 649.
276. Cox, R. A., R. A. Barton, E. Ljungstrum and D. W. Stocker, 1984, Chem. Phys. Lett., **108**, 228–232.
277. Cox, R. A. and J. P. Burrows, 1979, J. Phys. Chem., **83**, 2560–2568.
278. Cox, R. A., J. P. Burrows and T. J. Wallington, 1981, Chem. Phys. Lett., **84**, 217–221.
279. Cox, R. A. and G. B. Coker, 1983, J. Atmos. Chem., **1**, 53.
280. Cox, R. A. and R. G. Derwent, 1979, J. Chem. Soc. Far. Trans. 1, **75**, 1635–1647.
281. Cox, R. A., R. G. Derwent, A. E. J. Egg1eton and J. E. Lovelock, 1976, Atmos. Environ., **10**, 305.
282. Cox, R. A., R. G. Derwent, A. E. J. Eggleton and H. J. Read, 1979, J. Chem. Soc. Faraday Trans. I, **75**, 1648–1666.
283. Cox, R. A., R. G. Derwent and P. M. Holt, 1975, Chemosphere, **4**, 201.
284. Cox, R. A., R. G. Derwent and P. M. Holt, 1976, J. Chem. Soc. Faraday Trans. 1, **72**, 2031.
285. Cox, R. A., R. G. Derwent, S. V. Kearsey, L. Batt and K. G. Patrick, 1980, J. Photochem., **13**, 149.
286. Cox, R. A., R. G. Derwent and M. R. Williams, 1980, Environ. Sci. and Technol., **14**, 57–61.
287. Cox, R. A., M. Fowles, D. Moulton and R. P. Wayne, 1987, J. Phys. Chem., **91**, 3361–3365.
288. Cox, R. A. and A. Goldstone. In *Proceedings of the 2nd European Symposium on the "Physico–Chemical Behaviour of the Atmospheric Pollutants"*; D. Reidel Publishing Co.: Varese, Italy, 1982; pp 112–119.
289. Cox, R. A. and G. D. Hayman, 1988, Nature, **332**, 796–800.
290. Cox, R. A. and S. A. Penkett, 1972, J. Chem. Soc., Faraday Trans. 1, **68**, 1735.
291. Cox, R. A. and D. Sheppard, 1980, Nature, **284**, 330–331.
292. Cox, R. A., D. W. Sheppard and M. P. Stevens, 1982, J. Photochem., **19**, 189–207.
293. Crawford, M. A., T. J. Wallington, J. J. Szente, M. M. Maricq and J. S. Francisco, 1999, J. Phys. Chem. A, **103**, 365–378.
294. Crowley, J. N., P. Campuzano–Jost and G. K. Moortgat, 1996, J. Phys. Chem., **100**, 3601–3606.
295. Crowley, J. N., F. G. Simon, J. P. Burrows, G. K. Moortgat, M. E. Jenkin and R. A. Cox, 1991, J. Photochem. and Photobiol. A: Chem., **60**, 1–10.
296. Cupitt, L. T. and G. P. Glass, 1975, Int. J. Chem. Kinet., **Symp. 1**, 39–50.
297. Cvetanovic, R. J., D. L. Singleton and R. S. Irwin, 1981, J. Am. Chem. Soc., **103**, 3530.
298. Czarnowski, J. and H. J. Schumacher, 1981, Int. J. Chem. Kinet., **13**, 639–649.
299. Daele, V. and G. Poulet, 1996, J. Chim. Phys., **93**, 1081–1099.
300. Daele, V., A. Ray, I. Vassali, G. Poulet and G. Le Bras, 1995, Int. J. Chem. Kinet., **27**, 1121–1133.
301. Dagaut, P., T. J. Wallington and M. J. Kurylo, 1988, J. Phys. Chem., **92**, 3833–3836.

302. Dagaut, P., T. J. Wallington and M. J. Kurylo, 1988, J. Phys. Chem., **92**, 3836–3839.
303. Dagaut, P., T. J. Wallington, R. Liu and M. J. Kurylo, 1988, Int. J. Chem. Kinet., **20**, 331–338.
304. Daniels, F. and E. H. Johnston, 1921, J. Am. Chem. Soc., **43**, 53.
305. Daubendiek, R. L. and J. G. Calvert, 1975, Environ. Lett., **8**, 103.
306. Davenport, J. E., B. Ridley, H. I. Schiff and K. H. Welge, 1972, J. Chem. Soc. Faraday Discussion, **53**, 230–231.
307. Davidson, F. E., A. R. Clemo, G. L. Duncan, R. J. Browett, J. H. Hobson and R. Grice, 1982, Molec. Phys., **46**, 33–40.
308. Davidson, J. A., C. A. Cantrell, S. C. Tyler, R. E. Shetter, R. J. Cicerone and J. G. Calvert, 1987, J. Geophys. Res., **92**, 2195–2199.
309. Davidson, J. A., C. J. Howard, H. I. Schiff and F. C. Fehsenfeld, 1979, J. Chem. Phys., **70**, 1697–1704.
310. Davidson, J. A., K. E. Kear and E. W. Abrahamson, 1972/1973, J. Photochem., **1**, 307–316.
311. Davidson, J. A., H. I. Schiff, T. J. Brown and C. J. Howard, 1978, J. Chem. Phys., **69**, 4277–4279.
312. Davidson, J. A., H. I. Schiff, G. E. Streit, J. R. McAfee, A. L. Schmeltekopf and C. J. Howard, 1977, J. Chem. Phys., **67**, 5021–5025.
313. Davies, P. B. and B. A. Thrush, 1968, Trans. Far. Soc., **64**, 1836.
314. Davis, D. D., W. Braun and A. M. Bass, 1970, Int. J. Chem. Kinet., **2**, 101.
315. Davis, D. D., J. T. Herron and R. E. Huie, 1973, J. Chem. Phys., **58**, 530–535.
316. Davis, D. D., R. B. Klemm and M. Pilling, 1972, Int. J. Chem. Kinet., **4**, 367–382.
317. Davis, D. D., G. Machado, B. Conaway, Y. Oh and R. T. Watson, 1976, J. Chem. Phys., **65**, 1268.
318. Davis, D. D., J. Prusazcyk, M. Dwyer and P. Kim, 1974, J. Phys. Chem., **78**, 1775–1779.
319. Davis, D. D., W. Wong and J. Lephardt, 1973, Chem. Phys. Lett., **22**, 273–278.
320. Davis, D. D., W. Wong and R. Schiff, 1974, J. Phys. Chem., **78**, 463–464.
321. Daykin, E. P. and P. H. Wine, 1990, J. Geophys. Res., **95**, 18547–18553.
322. Daykin, E. P. and P. H. Wine, 1990, J. Phys. Chem. , **94**, 4528–4535.
323. Daykin, E. P. and P. H. Wine, 1990, Int. J. Chem. Kinet., **22**, 1083–1094.
324. De Sousa, A. R., M. Touzeau and M. Petitdidier, 1985, Chem. Phys. Lett., **121**, 423–428.
325. DeMore, W. B., 1969, Int. J. Chem. Kinet., **1**, 209–220.
326. DeMore, W. B., 1971, Int. J. Chem. Kinet., **3**, 161–173.
327. DeMore, W. B., 1979, J. Phys. Chem., **83**, 1113–1118.
328. DeMore, W. B. 182nd National Meeting of the American Chemical Society, 1981, New York.
329. DeMore, W. B., 1982, J. Phys. Chem, **86**, 121–126.
330. DeMore, W. B., 1984, Int. J. Chem. Kinet., **16**, 1187–1200.
331. DeMore, W. B., 1991, J. Geophys. Res., **96**, 4995–5000.
332. DeMore, W. B., 1992, Geophys. Res. Lett., **19**, 1367–1370.
333. DeMore, W. B., 1993, Geophys. Res. Lett., **20**, 1359–1362.
334. DeMore, W. B., 1993, J. Phys. Chem., **97**, 8564–8566.
335. DeMore, W. B., 1996, J. Phys. Chem., **100**, 5813–5820.
336. DeMore, W. B. and C. L. Lin, 1973, J. Org. Chem., **38**, 985–989.
337. DeMore, W. B., C. L. Lin and S. Jaffe. 12th Informal Conference on Photochemistry, 1976.
338. DeMore, W. B. and E. Tschuikow–Roux, 1974, J. Phys. Chem., **78**, 1447–1451.
339. DeMore, W. B. and E. Tschuikow–Roux, 1990, J. Phys. Chem., **94**, 5856–5860.
340. DeMore, W. B. and E. W. Wilson Jr., 1999, J. Phys. Chem. A, **103**, 573–576.
341. DeMore, W. B., E. W. Wilson Jr., A. Jacoby, S. Kutka and A. S. Gilbert. 223rd American Chemical Society Meeting, 2002, Orlando.
342. Derwent, R. G. and B. A. Thrush, 1971, Trans. Faraday Soc., **67**, 2036–2043.
343. Devolder, P., M. Carlier, J. F. Pauwels and L. R. Sochet, 1984, Chem. Phys. Lett., **111**, 94–99.
344. Diau, E. W., T. Yu, M. A. G. Wagner and M. C. Lin, 1994, J. Phys. Chem., **98**, 4034–4042.
345. Diau, E. W.–G. and Y.–P. Lee, 1991, J. Phys. Chem., **95**, 7726–7732.
346. Diau, E. W.–G., T.–L. Tso and Y.–P. Lee, 1990, J. Phys. Chem., **94**, 5261–5265.
347. Dibble, T. S., M. M. Maricq, J. J. Szente and J. S. Francisco, 1995, J. Phys. Chem., **99**, 17394–17402.
348. Dlugokencky, E. J. and C. J. Howard, 1988, J. Phys. Chem., **92**, 1188–1193.
349. Dlugokencky, E. J. and C. J. Howard, 1989, J. Phys. Chem., **93**, 1091–1096.
350. Dobe, S., L. A. Khachatryan and T. Berces, 1989, Ber. Bunsenges. Phys. Chem., **93**, 847–852.
351. Dobe, S., M. Otting, F. Temps, H. G. Wagner and H. Ziemer, 1993, Ber. Bunsenges. Phys. Chem., **97**, 877–884.
352. Dobe, S., F. Temps, T. Bohland and H. G. Wagner, 1985, Z. Naturforsch., **40a**, 1289–1298.
353. Dobis, O. and S. W. Benson, 1987, Int. J. Chem. Kinet., **19**, 691–708.
354. Dobis, O. and S. W. Benson, 1991, J. Am. Chem. Soc., **113**, 6377–6386.

355. Dobis, O. and S. W. Benson, 1993, J. Am. Chem. Soc., **115**, 8798–8809.
356. Dodonov, A. F., G. K. Lavrovskaya, I. I. Morozov and V. L. Tal'rose, 1971, Dokl. Adak. Nauk USSR, 1971, Vol. 198, 622: Dokl. Phys. Chem. (Engl. Trans.), **198**, 440–442.
357. Dodonov, A. F., V. V. Zelenov, A. S. Kukui and E. A. P. V. L. Tal'Rose, 1985, Khim. Fiz., **4**, 1335–1343.
358. Dognon, A. M., F. Caralp and R. Lesclaux, 1985, J. Chim. Phys. Phys.–Chim. Biol., **82**, 349–352.
359. Dolson, D. A., 1986, J. Phys. Chem., **90**, 6714–6718.
360. Domine, F., T. P. Murrells and C. J. Howard, 1990, J. Phys. Chem., **94**, 5839–5847.
361. Domine, F. and A. R. Ravishankara, 1992, Int. J. Chem. Kinet., **24**, 943–951.
362. Domine, F., A. R. Ravishankara and C. J. Howard, 1992, J. Phys. Chem., **96**, 2171–2178.
363. Donaghy, T., I. Shanahan, M. Hande and S. Fitzpatrick, 1993, Int. J. Chem. Kinet., **25**, 273–284.
364. Donovan, R. J. and D. J. Little, 1972, Chem. Phys. Lett., **13**, 488.
365. Dransfeld, P. and H. G. Wagner, 1987, Z. Naturforsch., **42a**, 471–476.
366. Dreier, T. and J. Wolfrum. In *18th International Symposium on Combustion*; The Combustion Institute, 1980; pp 801–809.
367. Dreier, T. and J. Wolfrum. 20th International Symposium on Combustion, 1984.
368. Dreyer, J. W., D. Perner and C. R. Roy, 1974, J. Chem. Phys., **61**, 3164.
369. Droege, A. T. and F. P. Tully, 1986, J. Phys. Chem., **90**, 1949–1954.
370. Dunlop, J. R. and F. P. Tully, 1993, J. Phys. Chem., **97**, 11148–11150.
371. Eberhard, J. and C. J. Howard, 1996, Int. J. Chem. Kinet., **28**, 731–740.
372. Edelbuttel–Einhaus, J., K.–H. Hoyermann, G. Rohde and J. Seeba, 1992, Proc. Symp. (Int.) Combustion, **24**, 661+.
373. Edney, E. O., T. E. Kleindienst and E. W. Corse, 1986, Int. J. Chem. Kinet., **18**, 1355–1371.
374. Egsgaard, H., L. Carlson, H. Florencio, T. Drewello and H. Schwarz, 1988, Chem. Phys. Lett., **148**, 537–540.
375. Ehhalt, D. H., J. A. Davidson, C. A. Cantrell, I. Friedman and S. Tyler, 1989, J. Geophys. Res., **94**, 9831–9836.
376. Eibling, R. E. and M. Kaufman, 1983, Atmos. Environ., **17**, 429–431.
377. Elrod, M. J., R. F. Meads, J. B. Lipson, J. V. Seeley and M. J. Molina, 1996, J. Phys. Chem., **100**, 5808–5812.
378. Ennis, C. A. and J. W. Birks, 1985, J. Phys. Chem., **89**, 186–191.
379. Ennis, C. A. and J. W. Birks, 1988, J. Phys. Chem., **93**, 1119–1126.
380. Fair, R. W. and B. A. Thrush, 1969, Trans. Faraday Soc., **65**, 1557.
381. Fair, R. W., A. van Roodaelaar and O. P. Strausz, 1971, Can. J. Chem., **49**, 1659.
382. Fang, T. D., P. H. Taylor and B. Dellinger, 1996, J. Phys. Chem., **100**, 4048–4054.
383. Fang, T. D., P. H. Taylor, B. Dellinger, C. J. Ehlers and R. J. Berry, 1997, J. Phys. Chem. A, **101**, 5758–5764.
384. Farquharson, G. K. and R. H. Smith, 1980, Aust. J. Chem., **33**, 1425–1435.
385. Fasano, D. M. and N. S. Nogar, 1981, Int. J. Chem. Kinet., **13**, 325.
386. Fasano, D. M. and N. S. Nogar, 1982, Chem. Phys. Lett., **92**, 411–414.
387. Fenter, F. F. and J. G. Anderson, 1991, J. Phys. Chem., **95**, 3172–3180.
388. Fenter, F. F. and J. G. Anderson, 1994, Int. J. Chem. Kinet., **26**, 801–812.
389. Fenter, F. F., V. Catoire, R. Lesclaux and P. D. Lightfoot, 1993, J. Phys. Chem., **97**, 3530–3538.
390. Filseth, S. V., A. Zia and K. H. Welge, 1970, J. Chem. Phys., **52**, 5502–5510.
391. Findlay, F. D., C. J. Fortin and D. R. Snelling, 1969, Chem. Phys. Lett., **3**, 204–206.
392. Findlay, F. D. and D. R. Snelling, 1971, J. Chem. Phys., **55**, 545–551.
393. Findlay, F. D. and D. R. Snelling, 1971, J. Chem. Phys., **54**, 2750–2755.
394. Finkbeiner, M., J. N. Crowley, O. Horie, R. Muller, G. K. Moortgat and P. J. Crutzen, 1995, J. Phys. Chem., **99**, 16264–16275.
395. Finlayson–Pitts, B. J., M. J. Ezell, T. M. Jayaweera, H. N. Berko and C. C. Lai, 1992, Geophys. Res. Lett., **19**, 1371–1374.
396. Finlayson–Pitts, B. J., S. K. Hernandez and H. N. Berko, 1993, J. Phys. Chem., **97**, 1172–1177.
397. Finlayson–Pitts, B. J. and T. E. Kleindienst, 1979, J. Chem. Phys., **70**, 4804–4806.
398. Finlayson–Pitts, B. J., T. E. Kleindienst, J. J. Ezell and D. W. Toohey, 1981, J. Chem. Phys., **74**, 4533–4543.
399. Fletcher, I. S. and D. Husain, 1976, Can. J. Chem., **54**, 1765–1770.
400. Fletcher, I. S. and D. Husain, 1976, J. Phys. Chem., **80**, 1837–1840.
401. Fletcher, I. S. and D. Husain, 1978, J. Photochem., **8**, 355–361.
402. Fockenberg, C., H. Saathoff and R. Zellner, 1994, Chem. Phys. Lett., **218**, 21–28.
403. Foon, R., G. Le Bras and J. Combourieu, 1979, C.R. Acad. Sci. Paris, **Series C 288**, 241.

404. Foon, R. and G. P. Reid, 1971, Trans. Faraday Soc., **67**, 3513.
405. Force, A. P. and J. R. Wiesenfeld, 1981, J. Phys. Chem., **85**, 782–785.
406. Force, A. P. and J. R. Wiesenfeld, 1981, J. Chem. Phys., **74**, 1718–1723.
407. Fraser, M. E. and L. G. Piper, 1989, J. Phys. Chem., **93**, 1107–1111.
408. Freeman, C. G. and L. F. Phillips, 1968, J. Phys. Chem., **72**, 3025.
409. Freudenstein, K. and D. Biedenkapp, 1976, Ber. Bunsenges. Phys. Chem., **80**, 42–48.
410. Friedl, R. R., W. H. Brune and J. G. Anderson, 1985, J. Phys. Chem., **89**, 5505–5510.
411. Friedl, R. R., J. H. Goble and S. P. Sander, 1986, Geophys. Res. Lett., **13**, 1351–1354.
412. Friedl, R. R. and S. P. Sander, 1989, J. Phys. Chem., **93**, 4756–4764.
413. Friedl, R. R., S. P. Sander and Y. L. Yung, 1992, J. Phys. Chem., **96**, 7490–7493.
414. Fritz, B., K. Lorenz, W. Steinert and R. Zellner, 1984, Oxidation Communications, **6**, 363–370.
415. Frost, M. J. and I. W. M. Smith, 1990, J. Chem. Soc. Farad. Trans., **86**, 1757–1762.
416. Frost, R. J., D. S. Green, M. K. Osborn and I. W. M. Smith, 1986, Int. J. Chem. Kinet., **18**, 885–898.
417. Gaffney, J. S., R. Fajer, G. I. Senum and J. H. Lee, 1986, Int. J. Chem. Kinet., **18**, 399–407.
418. Ganske, J. A., H. N. Berko, M. J. Ezell and B. J. Finlayson–Pitts, 1992, J. Phys. Chem., **96**, 2568–2572.
419. Ganske, J. A., M. J. Ezell, H. N. Berko and B. J. Finlayson–Pitts, 1991, Chem. Phys. Lett., **179**, 204–210.
420. Garland, N. L., L. J. Medhurst and H. H. Nelson, 1993, J. Geophys. Res. D., **98**, 23107–23111.
421. Garland, N. L. and H. H. Nelson, 1996, Chem. Phys. Lett., **248**, 296–300.
422. Garraway, J. and R. J. Donovan, 1979, J. Chem. Soc. Chem. Commun., 1108.
423. Garvin, D. and H. P. Broida. 9th Symposium on Combustion, 1963.
424. Gauthier, M. J. E. and D. R. Snelling, 1974, Can. J. Chem., **52**, 4007–4015.
425. Geers–Muller, R. and F. Stuhl, 1987, Chem. Phys. Lett., **135**, 263–268.
426. Gehring, M., K. Hoyermann, H. Sahaeke and J. Wolfrum. 14th Int. Symposium on Combustion, 1973.
427. Gericke, K.–H. and F. J. Comes, 1981, Chem. Phys. Lett., **81**, 218–222.
428. Gierczak, T., J. B. Burkholder and A. R. Ravishankara, 1999, J. Phys. Chem. A, **103**, 877–883.
429. Gierczak, T., M. K. Gilles and A. R. Ravishankara, 2002, J. Phys. Chem., submitted.
430. Gierczak, T., L. Goldfarb, D. Sueper and A. R. Ravishankara, 1994, Int. J. Chem. Kinet., **26**, 719–728.
431. Gierczak, T., R. Talukdar, G. L. Vaghjiani, E. R. Lovejoy and A. R. Ravishankara, 1991, J. Geophys. Res., **96**, 5001–5011.
432. Gierczak, T., R. K. Talukdar, J. B. Burkholder, R. W. Portmann, J. S. Daniel, S. Solomon and A. R. Ravishankara, 1996, J. Geophys. Res., **101**, 12905–12911.
433. Gierczak, T., R. K. Talukdar and A. R. Ravishankara, 1997, J. Phys. Chem., in press.
434. Gierczak, T., S. Talukdar, S. Herndon, G. L. Vaghjiani and A. R. Ravishankara, 1997, J. Phys. Chem. A, **101**, 3125–3134.
435. Gill, R. J., W. D. Johnson and G. H. Atkinson, 1981, Chem. Phys., **58**, 29.
436. Gilles, M. K., J. B. Burkholder, Gierczak, P. Marshall and A. R. Ravishankara, 2002, J. Phys.Chem. A, **104**, 8945–8950.
437. Gilles, M. K., R. K. Talukdar and A. R. Ravishankara, 2000, J. Phys. Chem. A, **104**, 8945–8950.
438. Gilles, M. K., A. A. Turnipseed, J. B. Burkholder, A. R. Ravishankara and S. Solomon, 1996, manuscript.
439. Gilpin, R., H. I. Schiff and K. H. Welge, 1971, J. Chem. Phys., **55**, 1087–1093.
440. Glaschick–Schimpf, I., A. Leiss, P. B. Monkhouse, U. Schurath, K. H. Becker and E. H. Fink, 1979, Chem. Phys. Lett., **67**, 318–323.
441. Glavas, S. and J. Heicklen, 1985, J. Photochem., **31**, 21–28.
442. Gleason, J. F. and C. J. Howard, 1988, J. Phys. Chem. , **92**, 3414–3417.
443. Gleason, J. F., F. L. Nesbitt and L. J. Stief, 1994, J. Phys. Chem., **98**, 126–131.
444. Gleason, J. F., A. Sinha and C. J. Howard, 1987, J. Phys. Chem., **91**, 719–724.
445. Glinski, R. J. and J. W. Birks, 1985, J. Phys. Chem., **89**, 3449–3453.
446. Goliff, W. S. and F. S. Rowland, 1997, Geophys. Res. Lett., **23**, 3029–3032.
447. Gordon, S., W. Mulac and P. Nangia, 1971, J. Phys. Chem., **75** 2087.
448. Gordon, S. and W. A. Mulac, 1975, Int. J. Chem. Kinet., **Symp. 1**, 289–299.
449. Graham, R. A. and D. J. Gutman, 1977, J. Phys. Chem., **81**, 207.
450. Graham, R. A. and H. S. Johnston, 1974, J. Chem. Phys., **60**, 4628.
451. Graham, R. A. and H. S. Johnston, 1978, J. Phys. Chem., **82**, 254–268.
452. Graham, R. A., A. M. Winer, R. Atkinson and J. N. Pitts, Jr., 1979, J. Phys. Chem., **83**, 1563.
453. Green, R. G. and R. P. Wayne, 1976/77, J. Photochem., **6**, 371–374.
454. Greenblatt, G. D. and C. J. Howard, 1989, J. Phys. Chem., **93**, 1035–1042.
455. Greenblatt, G. D. and A. R. Ravishankara, 1990, J. Geophys. Res., **95**, 3539–3547.
456. Greenhill, P. G. and B. V. O'Grady, 1986, Aust. J. Chem., **39**, 1775–1787.
457. Greiner, N. R., 1969, J. Chem. Phys., **51**, 5049–5051.

458. Greiner, N. R., 1970, J. Chem. Phys., **53**, 1284–1285.
459. Grimley, A. J. and P. L. Houston, 1980, J. Chem. Phys., **72**, 1471–1475.
460. Grotheer, H. H., G. Riekert, U. Meier and T. Just, 1985, Ber. Bunsenges. Phys. Chem., **89**, 187–191.
461. Grotheer, H. H., G. Riekert, D. Walter and T. Just, 1988, J. Phys. Chem., **92**, 4028.
462. Gutman, D., N. Sanders and J. E. Butler, 1982, J. Phys. Chem., **86**, 66.
463. Hack, W., O. Horie and H. G. Wagner, 1981, Ber. Bunsenges. Phys. Chem., **85**, 72.
464. Hack, W., O. Horie and H. G. Wagner, 1982, J. Phys. Chem. , **86**, 765.
465. Hack, W., K. Hoyermann and H. G. Wagner, 1974, Ber. Bunsenges. Phys. Chem., **78**, 386.
466. Hack, W., G. Mex and H. G. Wagner, 1977, Ber. Bunsenges. Phys. Chem., **81**, 677–684.
467. Hack, W., A. W. Preuss, F. Temps and H. G. Wagner, 1979, Ber. Bunsenges. Phys. Chem., **83**, 1275–1279.
468. Hack, W., A. W. Preuss, F. Temps, H. G. Wagner and K. Hoyermann, 1980, Int. J. Chem. Kinet., **12**, 851–860.
469. Hack, W., A. W. Preuss, H. G. Wagner and K. Hoyermann, 1979, Ber. Bunsenges. Phys. Chem., **83**, 212–217.
470. Hack, W., H. Schacke, M. Schroter and H. G. Wagner. 17th International Symposium on Combustion, 1979.
471. Hack, W., H. G. Wagner and K. Hoyermann, 1978, Ber. Bunsenges. Phys. Chem., **82**, 713–719.
472. Hagele, J., K. Lorenz, D. Rhasa and R. Zellner, 1983, Ber. Bunsenges. Phys. Chem., **87**, 1023–1026.
473. Hall, I. W., R. P. Wayne, R. A. Cox, M. E. Jenkin and G. D. Hayman, 1988, J. Phys. Chem., **92**, 5049–5054.
474. Halstead, C. J. and B. A. Thrush, 1966, Proc. Roy. Soc. London, **Ser. A 295**, 380
475. Hamilton, E. J., Jr., 1975, J. Chem. Phys., **63**, 3682–3683.
476. Hamilton, E. J., Jr. and R.–R. Lii, 1977, Int. J. Chem. Kinet., **9**, 875–885.
477. Hammer, P. D., E. J. Dlugokencky and C. J. Howard, 1986, J. Phys. Chem., **90**, 2491–2496.
478. Hancock, G., W. Lange, M. Lenzi and K. H. Welge, 1975, Chem. Phys. Lett., **33**, 168.
479. Hancock, G. and I. W. M. Smith, 1971, Trans. Faraday Soc., **67**, 2586.
480. Handwerk, V. and R. Zellner, 1978, Ber. Bunsenges. Phys. Chem., **82**, 1161–1166.
481. Hansen, I., K. Hoinghaus, C. Zetzsch and F. Stuhl, 1976, Chem. Phys. Lett., **42**, 370–372.
482. Harris, G. W., T. E. Kleindienst and J. N. Pitts, Jr., 1981, Chem. Phys. Lett., **80**, 479–483.
483. Harrison, J. A., A. R. Whyte and L. F. Phillips, 1986, Chem. Phys. Lett., **129**, 346–352.
484. Hartmann, D., J. Karthauser, J. P. Sawerysyn and R. Zellner, 1990, Ber. Bunsenges. Phys. Chem., **94**, 639–645.
485. Harwood, M. H., J. B. Burkholder, M. Hunter, R. W. Fox and A. R. Ravishankara, 1997, J. Phys. Chem. A, **101**, 853–863.
486. Hashimoto, S., G. Inoue and H. Akimoto, 1984, Chem. Phys. Lett., **107**, 198–202.
487. Hatakeyama, S. and M. T. Leu, 1986, Geophys. Res. Lett., **13**, 1343–1346.
488. Hatakeyama, S. and M. T. Leu, 1989, J. Phys. Chem., **93**, 5784–5789.
489. Hayman, G. D., J. M. Davies and R. A. Cox, 1986, Geophys. Res. Lett., **13**, 1347–1350.
490. Heathfield, A. E., C. Anastasi, P. Pagsberg and A. McCulloch, 1998, Atmos. Environ., **32**, 711–717.
491. Heidner, R. F., J. F. Bott, C. E. Gardner and J. E. Melzer, 1979, J. Chem. Phys., **70**, 4509.
492. Heidner, R. F., J. F. Bott, C. E. Gardner and J. E. Melzer, 1980, J. Chem. Phys., **72**, 4815.
493. Heidner, R. F., III , D. Husain and J. R. Weisenfeld, 1973, J. Chem. Soc. Faraday Trans. 2, **69**, 927–938.
494. Heidner, R. F., III and D. Husain, 1973, Int. J. Chem. Kinet., **5**, 819–831.
495. Helleis, F., J. N. Crowley and G. K. Moortgat, 1993, J. Phys. Chem., **97**, 11464–11473.
496. Helleis, F., J. N. Crowley and G. K. Moortgat, 1994, Geophys. Res. Lett., **21**, 1795–1798.
497. Helmer, M. and J. M. C. Plane, 1993, J. Geophys. Res., **98**, 23207–23222.
498. Heneghan, S. P. and S. W. Benson, 1983, Int. J. Chem. Kinet., **15**, 1311–1319.
499. Heneghan, S. P., P. A. Knoot and S. W. Benson, 1981, Int. J. Chem. Kinet., **13**, 677–691.
500. Herndon, S. C., Gierczak, R. K. Talukdar and A. R. Ravishankara, 2001, Phys. Chem. Chem. Phys., **3**, 4529–4535.
501. Herndon, S. C., P. W. Villalta, D. D. Nelson, J. T. Jayne and M. S. Zahniser, 2001, J. Phys. Chem. A, **105**, 1583–1591.
502. Herron, J. T., 1961, J. Chem. Phys., **35**, 1138.
503. Herron, J. T. and R. E. Huie, 1974, J. Phys. Chem., **78**, 2085
504. Herron, J. T. and R. D. Penzhorn, 1969, J. Phys. Chem., **73**, 191.
505. Hess, W. P. and F. P. Tully, 1988, Chem. Phys. Lett., **152**, 183–189.
506. Hess, W. P. and F. P. Tully, 1989, J. Phys. Chem., **93**, 1944–1947.
507. Hills, A. J., R. J. Cicerone, J. G. Calvert and J. W. Birks, 1988, J. Phys. Chem., **92**, 1853–1858.

508. Hills, A. J. and C. J. Howard, 1984, J. Chem. Phys., **81**, 4458–4465.
509. Hippler, H. and J. Troe, 1992, Chem. Phys. Lett., **192**, 333–337.
510. Hippler, H., J. Troe and J. Willner, 1990, J. Chem. Phys., **93**, 1755–1760.
511. Hislop, J. R. and R. P. Wayne, 1977, J. Chem. Soc. Faraday Trans. 2, **73**, 506–516.
512. Hjorth, J., F. Cappellani, C. J. Nielsen and G. Restelli, 1989, J. Phys. Chem., **93**, 5458–5461.
513. Hjorth, J., G. Ottobrini, F. Cappellani and G. Restelli, 1987, J. Phys. Chem., **91**, 1565–1568.
514. Hjorth, J., G. Ottobrini and G. Restelli, 1986, Int. J. Chem. Kinet., **18**, 819–828.
515. Hjorth, J., G. Ottobrini and G. Restelli, 1988, J. Phys. Chem., **92**, 2669.
516. Hochanadel, C. J., J. A. Ghormley and P. J. Ogren, 1972, J. Chem. Phys., **56**, 4426–4432.
517. Hochanadel, C. J., T. J. Sworski and P. J. Ogren, 1980, J. Phys. Chem., **84**, 3274–3277.
518. Hofzumahaus, A. and F. Stuhl, 1984, Ber. Bunsenges Phys. Chem., **88**, 557–561.
519. Hollinden, G. A., M. J. Kurylo and R. B. Timmons, 1970, J. Phys. Chem., **74**, 988–991.
520. Homann, K. H., G. Krome and H. G. Wagner, 1968, Ber. Bunsenges. Phys. Chem., **72**, 998.
521. Hooshiyar, P. A. and H. Niki, 1995, Int. J. Chem. Kinet., **27**, 1197–1206.
522. Horie, O. and G. K. Moortgat, 1992, J. Chem. Soc. Faraday Trans., **88**, 3305–3312.
523. Horowitz, A., D. Bauer, J. N. Crowley and G. K. Moortgat, 1993, Geophys. Res. Lett., **20**, 1423–1426.
524. Horowitz, A., J. N. Crowley and G. K. Moortgat, 1994, J. Phys. Chem., **98**, 11924–11930.
525. Horowitz, A., F. Su and J. G. Calvert, 1978, Int. J. Chem. Kinet., **10**, 1099.
526. Howard, C. J., 1976, J. Chem. Phys., **65**, 4771.
527. Howard, C. J., 1979, J. Chem. Phys., **71**, 2352–2359.
528. Howard, C. J. and K. M. Evenson, 1976, J. Chem. Phys., **64**, 197.
529. Howard, C. J. and K. M. Evenson, 1976, J. Chem. Phys., **64**, 4303.
530. Howard, C. J. and K. M. Evenson, 1977, Geophys. Res. Lett., **4**, 437–440.
531. Howard, C. J. and B. J. Finlayson–Pitts, 1980, J. Chem. Phys., **72**, 3842–3843.
532. Howard, M. J. and I. W. M. Smith, 1981, J. Chem. Soc. Faraday Trans. 2, **77**, 997–1008.
533. Hoyermann, K., H. G. Wagner and J. Wolfrum, 1967, Z. Phys. Chem., **55**, 72.
534. Hoyermann, K., H. G. Wagner and J. Wolfrum, 1969, Z. Phys. Chem., **63**, 193.
535. Hsu, C.–C., A. M. Mebel and M. C. Lin, 1996, J. Chem. Phys., **105**, 2346.
536. Hsu, D. S. Y., W. M. Shaub, T. L. Burks and M. C. Lin, 1979, Chem Phys., **44**, 143–150.
537. Hsu, K. J. and W. B. DeMore, 1994, Geophys. Res. Lett., **21**, 805–808.
538. Hsu, K. J. and W. B. DeMore, 1995, J. Phys. Chem., **99**, 1235–1244.
539. Hsu, K. J. and W. B. DeMore, 1995, J. Phys. Chem., **99**, 11141–11930.
540. Hsu, Y.–C., D.–S. Chen and Y.–P. Lee, 1987, Int. J. Chem. Kinet., **19** 1073–1082.
541. Huder, K. J. and W. B. DeMore, 1993, Geophys. Res. Lett., **20**, 1575–1577.
542. Huey, L. G., E. J. Dunlea and C. J. Howard, 1996, J. Phys. Chem, **100**, 6504–6508.
543. Huie, R. E. and J. T. Herron, 1974, Chem. Phys. Lett., **27**, 411.
544. Hunziker, H. E., H. Kneppe and H. R. Wendt, 1981, J. Photochem., **17**, 377.
545. Husain, D. and P. Marshall, 1985, Combust. and Flame, **60**, 81–87.
546. Husain, D., P. Marshall and J. M. C. Plane, 1985, J. Chem. Soc. Chem. Comm., 1216–1218.
547. Husain, D., J. M. C. Plane and N. K. H. Slater, 1981, J. Chem. Soc. Faraday Trans. 2, **77**, 1949–1962.
548. Husain, D., J. M. C. Plane and C. C. Xiang, 1984, J. Chem. Soc. Faraday Trans. 2, **80**, 713–728.
549. Husain, D. and N. K. H. Slater, 1980, J. Chem. Soc. Faraday Trans. 2, **76**, 606–619.
550. Hynes, A. J., R. B. Stocker, A. J. Pounds, T. Mckay, J. D. Bradshaw, J. M. Nicovich and P. H. Wine, 1995, J. Phys. Chem., **99**, 16967–16975.
551. Hynes, A. J. and P. H. Wine, 1987, J. Phys. Chem., **91**, 3672.
552. Hynes, A. J. and P. H. Wine, 1991, J. Phys. Chem., **95**, 1232–1240.
553. Hynes, A. J., P. H. Wine and J. M. Nicovich, 1988, J. Phys. Chem., **92**, 3846–3852.
554. Hynes, A. J., P. H. Wine and A. R. Ravishankara, 1986, J. Geophys. Res., **91**, 815–820.
555. Hynes, A. J., P. H. Wine and D. H. Semmes, 1986, J. Phys. Chem., **90**, 4148–4156.
556. Iannuzzi, M. P., J. B. Jeffries and F. Kaufman, 1982, Chem. Phys. Lett., **87**, 570–574.
557. Iannuzzi, M. P. and F. Kaufman, 1981, J. Phys. Chem., **85**, 2163
558. Igoshin, V. I., L. V. Kulakov and A. I. Nikitin, 1974, Sov. J. Quant. Electron., **3**, 306.
559. Imamura, T. and N. Washida, 1995, Laser Chem., **16**, 43–51.
560. Ingold, K. U., 1988, J. Phys. Chem., **92**, 4568–4569.
561. Inoue, G. and H. Akimoto, 1981, J. Chem. Phys., **84**, 425–433.
562. Inoue, G., K. Izumi and V. A. Lozovsky, 1993, presented at the Third International Conference on Chemical Kinetics, Gaithersburg, MD.
563. Ishikawa, Y., K. Sugawara and S. Sato *Abstracts of Papers*; ACS/CSJ Chemical Congress, 1979; Vol. 1.
564. Iwata, R., R. A. Ferrieri and A. P. Wolf, 1986, J. Phys. Chem., **90**, 6722–6726.

565. Iyer, R. S. and F. S. Rowland, 1980, Geophys. Res. Lett., **7**, 797–800.
566. Izod, T. P. J. and R. P. Wayne, 1968 Proc. Roy. Soc. A, **308**, 81–94.
567. Jaffe, S. and F. S. Klein, 1966, Trans. Faraday Soc., **62**, 2150–2157.
568. Jaffe, S. and W. K. Mainquist, 1980, J. Phys. Chem, **84**, 3277.
569. James, G. S. and G. P. Glass, 1970, J . Chem . Phys . **50**, 2268
570. Japar, S. M., C. H. Wu and H. Niki, 1974, J. Phys. Chem., **78**, 2318.
571. Japar, S. M., C. H. Wu and H. Niki, 1976, J. Phys. Chem., **80**, 2057.
572. Jayanty, R. K. M., R. Simonaitis and J. Heicklen, 1976, J. Phys. Chem., **80**, 443.
573. Jefferson, A., J. M. Nicovich and P. H. Wine, 1994, J. Phys. Chem., **98**, 7128–7135.
574. Jemi–Alade, A. A. and B. A. Thrush, 1990, J. Chem. Soc. Faraday Trans. 2, **86**, 3355–3363.
575. Jenkin, M. E., K. C. Clemitshaw and R. A. Cox, 1984, J. Chem. Soc. Faraday Trans. 2, **80**, 1633–1641.
576. Jenkin, M. E. and R. A. Cox, 1985, J. Phys. Chem., **89**, 192–199.
577. Jenkin, M. E. and R. A. Cox, 1987, Chem. Phys. Lett., **137**, 548–552.
578. Jenkin, M. E., R. A. Cox, M. Emrich and G. K. Moortgat, 1993, J. Chem. Soc. Faraday Trans., **89**, 2983–2991.
579. Jenkin, M. E., R. A. Cox and G. D. Hayman, 1991, Chem. Phys. Lett., **177**, 272–278.
580. Jenkin, M. E., R. A. Cox, A. Mellouki, G. Le Bras and G. Poulet, 1990, J. Phys. Chem., **94**, 2927–2934.
581. Jensen, N. R., D. R. Hanson and C. J. Howard, 1994, J. Phys. Chem., **98**, 8574–8579.
582. Jensen, N. R., J. Hjorth, C. Lohse, H. Skov and G. Restelli, 1991, Atmos. Environ., **24A**, 1897–1904.
583. Jensen, N. R., J. Hjorth, C. Lohse, H. Skov and G. Restelli, 1992, J. Atmos. Chem., **14**, 95–108.
584. Jeong, K. M., K. J. Hsu, J. B. Jeffries and F. Kaufman, 1984, J. Phys. Chem., **88**, 1222–1226.
585. Jeong, K. M. and F. Kaufman, 1979, Geophys. Res. Lett., **6**, 757–759.
586. Jeong, K. M. and F. Kaufman, 1982, J. Phys. Chem., **86**, 1808–1815.
587. Jeoung, S. C., K. Y. Choo and S. W. Benson, 1991, J. Phys. Chem., **95**, 7282–7290.
588. Jiang, Z., P. H. Taylor and B. Dellinger, 1992, J. Phys. Chem., **96**, 8961–8964.
589. Jiang, Z., P. H. Taylor and B. Dellinger, 1993, J. Phys. Chem., **97**, 5050–5053.
590. Johnston, H. S., E. D. Morris, Jr. and J. Van den Bogaerde, 1969, J. Am. Chem. Soc., **91**, 7712–7727.
591. Johnston, H. S. and Y.–S. Tao, 1951, J. Am. Chem Soc., **73**, 2948.
592. Jolly, G. S., D. J. McKenney, D. L. Singleton, G. Paraskevopoulos and A. R. Bossard, 1986, J. Phys. Chem., **90**, 6557–6562.
593. Jonah, C. D., W. A. Mulac and P. Zeglinski, 1984, J. Phys. Chem., **88**, 4100–4104.
594. Jones, B. M. R., J. P. Burrows, R. A. Cox and S. A. Penkett, 1982, Chem. Phys. Lett., **88**, 372–376.
595. Jourdain, J. L., G. Le Bras and J. Combourieu, 1978, J. Chim. Phys., **75**, 318–323.
596. Jourdain, J. L., G. Le Bras and J. Combourieu, 1979, Int. J. Chem. Kinet., **11**, 569–577.
597. Jourdain, J. L., G. Le Bras and J. Combourieu, 1981, Chem. Phys. Lett., **78**, 483.
598. Jungkamp, T. P., A. Kukui and R. N. Schindler, 1995, Ber. Bunsenges. Phys. Chem., **99**, 1057–1066.
599. Kaiser, E. W. and S. M. Japar, 1977, Chem. Phys . Lett., **52**, 121.
600. Kaiser, E. W. and S. M. Japar, 1978, Chem. Phys. Lett., **54**, 265.
601. Kaiser, E. W., I. M. Lorkovic and T. J. Wallington, 1990, J. Phys. Chem., **94**, 3352–3354.
602. Kaiser, E. W., L. Rimai, E. Schwab and E. C. Lim, 1992, J. Phys. Chem., **96**, 303–306.
603. Kaiser, E. W. and T. J. Wallington, 1994, J. Phys. Chem., **98**, 5679–5685.
604. Kakesu, M., H. Bandow, N. Takenaka, Y. Maeda and N. Washida, 1997, International Journal of Chemical Kinetics, **29**, 933–941.
605. Kambanis, K. G., Y. G. Lazarou and P. J. Papagiannakopoulos, 1997, J. Phys. Chem., **101**, 8496.
606. Kan, C. S., J. G. Calvert and J. H. Shaw, 1981, J. Phys. Chem., **85**, 1126–1132.
607. Kan, C. S., R. D. McQuigg, M. R. Whitbeck and J. G. Calvert, 1979, Int. J. Chem. Kinet., **11**, 921.
608. Kasner, J. H., P. H. Taylor and B. Dellinger, 1990, J. Phys.Chem., **94**, 3250–3253.
609. Kaufman, F., N. J. Gerri and D. A. Pascale, 1956, J. Chem. Phys., **24**, 32–34.
610. Kegley–Owen, C. S., M. K. Gilles, J. B. Burkholder and A. R. Ravishankara, 1999, J. Phys. Chem. A, **103**, 5040–5048.
611. Kelly, C., J. Treacy, H. W. Sidebottom and O. J. Nielsen, 1993, Chem. Phys. Lett., **207**, 498–503.
612. Kenner, R. D., K. R. Ryan and I. C. Plumb, 1993, Geophys. Res. Lett., **20**, 1571–1574.
613. Kerr, J. A. and D. W. Sheppard, 1981, Environ. Sci. and Technol., **15**, 960.
614. Kerr, J. A. and D. W. Stocker, 1986, J. Atmos. Chem., **4**, 253–262.
615. Keyser, L. F., 1978, J. Chem. Phys., **69**, 214–218.
616. Keyser, L. F., 1979, J. Phys. Chem., **83**, 645–648.
617. Keyser, L. F., 1980, J. Phys. Chem., **84**, 11–14.
618. Keyser, L. F., 1980, J. Phys. Chem., **84** 1659–1663.
619. Keyser, L. F., 1981, J. Phys. Chem., **85**, 3667–3673.

620. Keyser, L. F., 1982, J. Phys. Chem., **86**, 3439–3446.
621. Keyser, L. F., 1983, J. Phys. Chem., **87**, 837–841.
622. Keyser, L. F., 1984, J. Phys. Chem., **88**, 4750–4758.
623. Keyser, L. F., 1986, J. Phys. Chem., **90**, 2994–3003.
624. Keyser, L. F., 1988, J. Phys. Chem., **92**, 1193–1200.
625. Keyser, L. F., K. Y. Choo and M. T. Leu, 1985, Int. J. Chem. Kinet., **17**, 1169–1185.
626. Kinnison, D. J., W. Mengon and J. A. Kerr, 1996, J. Chem. Soc. Faraday Trans., **92**, 369–372.
627. Kircher, C. C. and S. P. Sander, 1984, J. Phys. Chem., **88**, 2082–91.
628. Kirchner, K., D. Helf, P. Ott and S. Vogt, 1990, Ber. Bunsenges. Phys. Chem., **94**, 77–83.
629. Kistiakowsky, G. B. and G. G. Volpi, 1957, J. Chem. Phys., **27**, 1141–1149.
630. Kistiakowsky, G. B. and G. G. Volpi, 1958, J. Chem. Phys., **28**, 665.
631. Kita, D. and D. H. Stedman, 1982, J. Chem. Soc. Faraday Trans. 2, **78**, 1249–1259.
632. Klais, O., P. C. Anderson, A. H. Laufer and M. J. Kurylo, 1979, Chem. Phys. Lett., **66**, 598.
633. Klais, O., A. H. Laufer and M. J. Kurylo, 1980, J. Chem. Phys., **73**, 2696–2699.
634. Kleinermanns, K. and A. C. Luntz, 1981, J. Phys. Chem., **85**, 1966.
635. Klemm, R. B., 1979, J. Chem. Phys. , **71**, 1987.
636. Klemm, R. B., E. G. Skolnik and J. V. Michael, 1980, J. Chem. Phys., **72**, 1256.
637. Klemm, R. B. and L. J. Stief, 1974, J. Chem. Phys., **61**, 4900.
638. Klopffer, W., R. Frank, E. G. Kohl and F. Haag, 1986, Chemiker–Zeitung, **110**, 57–61.
639. Knickelbein, M. B., K. L. Marsh, O. E. Ulrich and G. E. Busch, 1987, J. Chem. Phys., **87**, 2392–2393.
640. Knight, G. P., T. Beiderhase, F. Helleis, G. K. Moortgat and J. N. Crowley, 2000, Journal of Physical Chemistry A, **104**, 1674–1685.
641. Knox, J. H., 1955, Chemistry and Industry, 1631–1632.
642. Knox, J. H., 1962, Trans. Faraday Soc., **58**, 275.
643. Knox, J. H. and R. L. Nelson, 1959, Trans. Far. Soc., **55**, 937–946.
644. Ko, T. and A. Fontijn, 1991, J. Phys. Chem. , **95**, 3984–3987.
645. Koch, S. and G. K. Moortgat, 1990, Chem. Phys. Lett., **173**, 531–536.
646. Kohse–HÖinghaus, K. and F. Stuhl, 1980, J. Chem. Phys., **72**, 3720–3726.
647. Kolb, C. E., J. T. Jayne, D. R. Worsnop, M. J. Molina, R. F. Meads and A. A. Viggiano, 1994, J. Am. Chem. Soc., **116**, 10314–10315.
648. Kompa, K. L. and J. Wanner, 1972, Chem. Phys. Lett., **12**, 560.
649. Koppe, S., T. Laurent, P. D. Naik, H.–R. Volpp, J. Wolfrum, T. Arusi–Parpar, I. Bar and S. Rosenwaks, 1993, Chem. Phys. Lett., **214**, 546–552.
650. Kozlov, S., V. L. Orkin, R. E. Huie and M. J. Kurylo, 2002, J. Phys.Chem. A, **submitted**.
651. Kozlov, S., V. L. Orkin and M. J. Kurylo, 2002, J. Phys.Chem. A, **submitted**.
652. Kukui, A., T. P. W. Jungkamp and R. N. Schindler, 1994, Ber. Bunsenges. Phys. Chem., **98**, 1619–1621.
653. Kukui, A., U. Kirchner, T. Benter and R. N. Schindler, 1996, Ber. Bunsenges. Phys. Chem., **100**, 455–461.
654. Kukui, A. S., T. P. W. Jungkamp and R. N. Schindler, 1994, Ber. Bunsenges. Phys. Chem., **98**, 1298–1302.
655. Kulcke, A., B. Blackman, W. B. Chapman, I. K. Kim and D. J. Nesbitt, 1998, J. Phys. Chem. A, **102**, 1965–1972.
656. Kumaran, S. S., K. P. Lim and J. V. Michael, 1994, J. Chem. Phys., **101**, 9487–9498.
657. Kurasawa, H. and R. Lesclaux, 1979, Chem. Phys. Lett., **66**, 602.
658. Kurasawa, H. and R. Lesclaux, 1980, Chem. Phys. Lett., **72**, 437.
659. Kurasawa, H. and R. Lesclaux. 14th Informal Photochemistry Conference, 1980, Newport Beach, CA.
660. Kurylo, M. J., 1973, Chem. Phys. Lett., **23**, 467–471.
661. Kurylo, M. J., 1977, Chem. Phys. Lett., **49**, 467.
662. Kurylo, M. J., 1978, Chem. Phys. Lett., **58**, 233.
663. Kurylo, M. J., 1978, Chem. Phys. Lett., **58**, 238–242.
664. Kurylo, M. J., P. C. Anderson and O. Klais, 1979, Geophys. Res. Lett., **6**, 760–762.
665. Kurylo, M. J. and W. Braun, 1976, Chem. Phys. Lett., **37**, 232–235.
666. Kurylo, M. J., O. Klais and A. H. Laufer, 1981, J. Phys. Chem., **85**, 3674–3678.
667. Kurylo, M. J. and G. L. Knable, 1984, J. Phys. Chem., **88**, 3305–3308.
668. Kurylo, M. J., G. L. Knable and J. L. Murphy, 1983, Chem. Phys. Lett., **95**, 9–12.
669. Kurylo, M. J. and A. H. Laufer, 1979, J. Chem. Phys., **70**, 2032–2033.
670. Kurylo, M. J., J. L. Murphy, G. S. Haller and K. D. Cornett, 1982, Int. J. Chem. Kinet, **14**, 1149–1161.
671. Kurylo, M. J., J. L. Murphy and G. L. Knable, 1983, Chem. Phys. Lett., **94**, 281–284.
672. Kurylo, M. J., P. A. Ouellette and A. H. Laufer, 1986, J. Phys. Chem., **90**, 437–440.
673. Kurylo, M. J., T. J. Wallington and P. A. Ouellette, 1987, J. Photochem., **39**, 201–215.

674. Lafage, C., J.–F. Pauwels, M. Carlier and P. Devolder, 1987, J. Chem. Soc. Faraday Trans. 2, **83**, 731–739.
675. Lam, L., D. R. Hastie, B. A. Ridley and H. I. Schiff, 1981, J. Photochem., **15**, 119–130.
676. Lamb, J. J., L. T. Molina, C. A. Smith and M. J. Molina, 1983, J. Phys. Chem., **87**, 4467–4470.
677. Lancar, I., G. Laverdet, G. Le Bras and G. Poulet, 1991, Int. J. Chem. Kinet., **23**, 37–45.
678. Lancar, I., G. Le Bras and G. Poulet, 1993, J. Chim. Physique, **90**, 1897–1908.
679. Lancar, I., A. Mellouki and G. Poulet, 1991, Chem. Phys. Lett., **177**, 554–558.
680. Langford, A. O. and C. B. Moore, 1984, J. Chem. Phys., **80**, 4211–4221.
681. Larichev, M., F. Maguin, G. Le Bras and G. Poulet, 1995, J. Phys. Chem., **99**, 15911–15918.
682. Laszlo, B., R. R. Friedl and S. P. Sander, J. Phys. Chem. A, **to be submitted**.
683. Laszlo, B., R. E. Huie, M. J. Kurylo and A. W. Miziolek, 1997, J. Geophys. Res., **102**, 1523–1532.
684. Laszlo, B., M. J. Kurylo and R. E. Huie, 1995, J. Phys. Chem., **99**, 11701–11707.
685. Laverdet, G., G. Le Bras, A. Mellouki and G. Poulet, 1990, Chem. Phys. Lett., **172**, 430–434.
686. Lawton, S. A., S. E. Novick, H. P. Broida and A. V. Phelps, 1977, J. Chem. Phys., **66**, 1381–1382.
687. Lawton, S. A. and A. V. Phelps, 1978, J. Chem. Phys., **69**, 1055–1068.
688. Le Bras, G. and J. Combourieu, 1978, Int. J. Chem. Kinet., **10**, 1205–1213.
689. Le Bras, G., R. Foon and J. Combourieu, 1980, Chem. Phys. Lett., **73**, 357.
690. Le Calve, S., D. Hitier, G. Le Bras and A. Mellouki, 1998, J. Phys. Chem. A, **102**, 4579–4584.
691. Leck, T. J., J. E. Cook and J. W. Birks, 1980, J. Chem. Phys., **72**, 2364–2373.
692. Lee, F. S. C. and F. S. Rowland, 1977, J. Phys. Chem., **81**, 86–87.
693. Lee, J. H., J. V. Michael, W. A. Payne, Jr. and L. J. Stief, 1978, J. Chem. Phys., **69**, 350–353.
694. Lee, J. H., J. V. Michael, W. A. Payne, Jr. and L. J. Stief, 1977, J. Chem. Soc. Faraday Trans. 1, **73**, 1530–1536.
695. Lee, J. H., J. V. Michael, W. A. Payne, Jr. and L. J. Stief, 1978, J. Chem. Phys., **69**, 3069–3076.
696. Lee, J. H. and I. N. Tang, 1980, J. Chem. Phys., **72**, 5718–5720.
697. Lee, J. H. and I. N. Tang, 1982, J. Chem. Phys., **77**, 4459–63.
698. Lee, J. H. and I. N. Tang, 1983, J. Chem. Phys., **78**, 6646.
699. Lee, J. H., I. N. Tang and R. B. Klemm, 1980, J. Chem. Phys., **72**, 1793–1796.
700. Lee, J. H., R. B. Timmons and L. J. Stief, 1976, J. Chem. Phys., **64**, 300–305.
701. Lee, L. C. and T. G. Slanger, 1978, J. Chem. Phys., **69**, 4053–4060.
702. Lee, L. C. and T. G. Slanger, 1979, Geophys. Res. Lett., **6**, 165–166.
703. Lee, Y.–P. and C. J. Howard, 1982, J. Chem. Phys., **77** 756–763.
704. Lee, Y.–P., R. M. Stimpfle, R. A. Perry, J. A. Mucha, K. M. Evenson, D. A. Jennings and C. J. Howard, 1982, Int. J. Chem. Kinet., **14**, 711–732.
705. Lee, Y.–Y., Y.–P. Lee and N. S. Wang, 1994, J. Chem. Phys., **100**, 387–392.
706. Leiss, A., U. Schurath, K. H. Becker and E. H. Fink, 1978, J. Photochem., **8**, 211–214.
707. Lesclaux, R. and F. Caralp, 1984, Int. J. Chem. Kinet., **16**, 1117–1128.
708. Lesclaux, R. and M. Demissy, 1977, Nouv. J. Chim., **1**, 443.
709. Lesclaux, R., A. M. Dognon and F. Caralp, 1987, J. Photochem. and Photobiol., **A41**, 1–11.
710. Lesclaux, R., P. V. Khe, P. Dezauzier and J. C. Soulignac, 1975, Chem. Phys. Lett., **35**, 493.
711. Leu, G.–H. and Y.–P. Lee, 1994, J. Chin. Chem. Soc., **41**, 645–649.
712. Leu, M. T., 1979, Chem. Phys. Lett., **61**, 275–279.
713. Leu, M. T., 1979, J. Chem. Phys., **70**, 1662–1666.
714. Leu, M. T., 1980, Chem. Phys. Lett., **69**, 37–39.
715. Leu, M. T., 1980, Geophys. Res. Lett., **7**, 173–175.
716. Leu, M. T., 1984, J. Phys. Chem., **88**, 1394–1398.
717. Leu, M. T. and W. B. DeMore, 1976, Chem. Phys. Lett. , **41**, 121–124.
718. Leu, M. T. and W. B. DeMore, 1977, Chem. Phys. Lett., **48**, 317.
719. Leu, M. T. and W. B. DeMore, 1978, J. Phys. Chem., **82**, 2049.
720. Leu, M. T., S. Hatkeyama and K. J. Hsu, 1989, J. Phys. Chem., **93**, 5778–5784.
721. Leu, M. T. and C. L. Lin, 1979, Geophys. Res. Lett., **6**, 425–428.
722. Leu, M. T. and R. H. Smith, 1981, J. Phys. Chem., **85**, 2570–2575.
723. Leu, M. T. and R. H. Smith, 1982, J. Phys. Chem., **86**, 73–81.
724. Leu, M. T. and R. H. Smith, 1982, J. Phys. Chem., **86**, 958–961.
725. Leu, M. T. and Y. L. Yung, 1987, Geophys. Res. Lett., **14**, 949–952.
726. Lewis, R. S., S. P. Sander, S. Wagner and R. T. Watson, 1980, J. Phys. Chem., **84**, 2009–2015.
727. Lewis, R. S. and R. T. Watson, 1980, J. Phys. Chem., **84**, 3495–3503.
728. Li, Q., M. C. Osborne and I. W. M. Smith, 2000, Int. J. Chem. Kin., **32**, 85–91.
729. Li, Z., R. R. Friedl and S. P. Sander, 1995, J. Phys. Chem., **99**, 13445–13451.
730. Li, Z., R. R. Friedl and S. P. Sander, 1997, J. Chem. Soc. Farad. Trans., submitted.

731. Lightfoot, P. D., R. A. Cox, J. N. Crowley, M. Destriau, G. D. Hayman, M. E. Jenkin, G. K. Moortgat and F. Zabel, 1992, Atmos. Environ., **26A**, 1805–1961.
732. Lightfoot, P. D., B. Veyret and R. Lesclaux, 1988, Chem. Phys. Lett., **150**, 120–126.
733. Lightfoot, P. D., B. Veyret and R. Lesclaux, 1990, J. Phys. Chem., **94**, 708–714.
734. Lii, R.–R., R. A. Gorse, Jr., M. C. Sauer, Jr. and S. Gordon, 1979, J. Phys. Chem., **83**, 1803–1804.
735. Lii, R.–R., R. A. Gorse, Jr., M. C. Sauer, Jr. and S. Gordon, 1980, J. Phys. Chem., **84**, 819–821.
736. Lii, R.–R., M. C. Sauer, Jr. and S. Gordon, 1981, J. Phys. Chem., **85**, 2833–2834.
737. Lilenfeld, H. V. and R. J. Richardson, 1977, J. Chem. Phys., **67**, 3991.
738. Lin, C. L., 1982, Int. J. Chem. Kinet., **14**, 593–598.
739. Lin, C. L. and W. B. DeMore, 1973, J. Phys. Chem., **77** 863–869.
740. Lin, C. L., M. T. Leu and W. B. DeMore, 1978, J. Phys. Chem., **82**, 1772–1777.
741. Lin, C.–L., D. A. Parkes and F. Kaufman, 1970, J. Chem. Phys., **53**, 3896–3900.
742. Lin, Y.–L., N.–S. Wang and Y.–P. Lee, 1985, Int. J. Chem. Kinet., **17**, 1201–1214.
743. Lippmann, H. H., B. Jesser and U. Schurath, 1980, Int. J. Chem. Kinet., **12**, 547–554.
744. Lipson, J. B., T. W. Beiderhase, L. T. Molina, M. J. Molina and M. Olzmann, 1999, J. Phys. Chem. A, **103**, 6540–6551.
745. Lipson, J. B., M. J. Elrod, T. W. Beiderhase, L. T. Molina and M. J. Molina, 1997, J. Chem. Soc. Faraday Trans., **93**, 2665–2673.
746. Lissi, E. and J. Heicklen, 1972, J. Photochem., **1**, 39–68.
747. Littlejohn, D. and H. S. Johnston, 1980, EOS, **61**, 966.
748. Liu, A., W. A. Mulac and C. D. Jonah, 1989, J. Phys. Chem., **93**, 4092–4094.
749. Liu, R., R. E. Huie and M. J. Kurylo, 1990, J. Phys. Chem., **94**, 3247–3249.
750. Loewenstein, L. M. and J. G. Anderson, 1984, J. Phys. Chem., **88**, 6277–6286.
751. Loewenstein, L. M. and J. G. Anderson, 1985, J. Phys. Chem., **89**, 5371–5379.
752. Lorenz, K., D. Rhasa, R. Zellner and B. Fritz, 1985, Ber. Bunsenges. Phys. Chem., **89**, 341–342.
753. Lorenzen–Schmidt, H., R. Weller and O. Schrems, 1994, Ber. Bunsenges. Phys. Chem., **98**, 1622–1629.
754. Louge, M. Y. and R. K. Hanson, 1984, Twentieth Symposium (International) on Combustion, 665–672.
755. Lovejoy, E. R., D. R. Hanson and L. G. Huey, 1996, J. Phys. Chem., **100**, 19911–19916.
756. Lovejoy, E. R., K. S. Kroeger and A. R. Ravishankara, 1990, Chem. Phys. Lett., **167**, 183–187.
757. Lovejoy, E. R., T. P. Murrells, A. R. Ravishankara and C. J. Howard, 1990, J. Phys. Chem., **94**, 2386–2393.
758. Lovejoy, E. R., A. R. Ravishankara and C. J. Howard, 1994, Int. J. Chem. Kinet., **26**, 551–560.
759. Lovejoy, E. R., N. S. Wang and C. J. Howard, 1987, J. Phys. Chem., **91**, 5749–5755.
760. Lozovsky, V. A., M. A. Ioffe and O. M. Sarkisov, 1984, Chem. Phys. Lett., **110**, 651–654.
761. Lu, E. C. C., R. S. Iyer and F. S. Rowland, 1986, J. Phys. Chem., **90**, 1988–1990.
762. Mack, G. P. R. and B. Thrush, 1973, J. Chem. Soc. Faraday Trans. 1, **69**, 208.
763. Mack, G. P. R. and B. Thrush, 1974, J. Chem. Soc. Faraday Trans. 1, **70**, 173–186.
764. MacLeod, H., S. M. Aschmann, R. Atkinson, E. C. Tuazon, J. A. Sweetman, A. M. Winer and J. N. Pitts, Jr., 1986, J. Geophys. Res., **91**, 5338.
765. MacLeod, H., C. Balestra, J. L. Jourdain, G. Laverdet and G. Le Bras, 1990, Int. J. Chem. Kinet., **22**, 1167–1176.
766. MacLeod, H., J. L. Jourdain, G. Poulet and G. Le Bras, 1984, Atmos. Environ., **18**, 2621.
767. MacLeod, H., G. Poulet and G. Le Bras, 1983, J. Chim. Phys., **80**, 287.
768. Maguin, F., G. Laverdet, G. Le Bras and G. Poulet, 1992, J. Phys. Chem., **96**, 1775–1780.
769. Maguin, F., A. Mellouki, G. Laverdet, G. Poulet and G. Le Bras, 1991, Int. J. Chem. Kinet., **23**, 237–245.
770. Manning, R. and M. J. Kurylo, 1977, J. Phys. Chem., **81**, 291–296.
771. Manning, R. G., W. Braun and M. J. Kurylo, 1976, J. Chem. Phys., **65**, 2609.
772. Manzanares, E. R., M. Suto, L. C. Lee and D. Coffey, 1986, J. Chem. Phys., **85**, 5027–5034.
773. Margitan, J. J., 1983, J. Phys. Chem., **87**, 674–679.
774. Margitan, J. J., 1984, J. Phys. Chem., **88**, 3314–3318.
775. Margitan, J. J., 1984, J. Phys. Chem., **88**, 3638–3643.
776. Margitan, J. J. and R. T. Watson, 1982, J. Phys. Chem., **86**, 3819–3824.
777. Maricq, M. M. and J. J. Szente, 1993, Chem. Phys. Lett., **213**, 449–456.
778. Maricq, M. M. and J. J. Szente, 1994, J. Phys. Chem., **98**, 2078–2082.
779. Maricq, M. M. and J. J. Szente, 1996, J. Phys. Chem., **100**, 12374.
780. Maricq, M. M., J. J. Szente, E. W. Kaiser and J. Shi, 1994, J. Phys. Chem., **98**, 2083–2089.
781. Marinelli, W. J. and H. S. Johnston, 1982, J. Chem. Phys., **77**, 1225–1234.
782. Markert, F. and O. J. Nielsen, 1992, Chem. Phys. Lett., **194**, 123–127.
783. Martin, D., I. Barnes and K. H. Becker, 1987, Chem. Phys. Lett., **140**, 195.

784. Martin, D., J. L. Jourdain, G. Laverdet and G. Le Bras, 1987, Int. J. Chem. Kinet., **19**, 503–512.
785. Martin, D., J. L. Jourdain and G. Le Bras, 1985, Int. J. Chem. Kinet., **17**, 1247.
786. Martin, D., J. L. Jourdain and G. Le Bras, 1986, J. Phys. Chem., **90**, 4143–4147.
787. Martin, J.–P. and G. Paraskevopoulos, 1983, Can. J. Chem., **61**, 861–865.
788. Martin, L. R., R. B. Cohen and J. F. Schatz, 1976, Chem. Phys. Lett., **41**, 394–396.
789. Martinez, R. I. and J. T. Herron, 1978, Int. J. Chem. Kinet., **10**, 433.
790. Marx, W., F. Bahe and U. Schurath, 1979, Ber. Bunsenges. Phys. Chem., **83**, 225–230.
791. Matsumi, Y., K. Tonokura, Y. Inagaki and M. Kawasaki, 1993, J. Phys. Chem., **97**, 6816–6821.
792. Mauldin, R. L., III, J. B. Burkholder and A. R. Ravishankara, 1992, J. Phys. Chem., **96**, 2582–2588.
793. Mauldin, R. L., III, A. Wahner and A. R. Ravishankara, 1993, J. Phys. Chem., **97**, 7585–7596.
794. McCaulley, J. A., S. M. Anderson, J. B. Jeffries and F. Kaufman, 1985, Chem Phys. Lett., **115**, 180.
795. McCrumb, J. L. and F. Kaufman, 1972, J. Chem. Phys., **57**, 1270–1276.
796. McKenzie, A., M. F. R. Mulcahy and J. R. Steven, 1973, J. Chem. Phys. , **59**, 3244–3254.
797. McLaren, I. A., N. W. Morris and R. P. Wayne, 1981, J. Photochem., **16**, 311–319.
798. McNeal, R. J. and G. R. Cook, 1967, J. Chem. Phys., **47**, 5385–5389.
799. Medhurst, L. J., J. Fleming and H. H. Nelson, 1977, Chem. Phys. Lett., **266**, 607–611.
800. Meier, U., H. H. Grotheer and T. Just, 1984, Chem. Phys. Lett., **106**, 97–101.
801. Meier, U., H. H. Grotheer, G. Riekert and T. Just, 1985, Chem. Phys. Lett., **115**, 221–225.
802. Meller, R. and G. K. Moortgat, 1995, J. Photochem. Photobio. A: Chem., **86**, 15–25.
803. Mellouki, A., J. L. Jourdain and G. Le Bras, 1988, Chem. Phys. Lett., **148**, 231–236.
804. Mellouki, A., G. Laverdet, L. Jourdain and G. Poulet, 1989, Int. J. Chem. Kinet., **21**, 1161–1172.
805. Mellouki, A., G. Le Bras and G. Poulet, 1987, J. Phys. Chem., **91**, 5760–5764.
806. Mellouki, A., G. Le Bras and G. Poulet, 1988, J. Phys. Chem., **92**, 2229–2234.
807. Mellouki, A., G. Poulet, G. Le Bras, R. Singer, J. P. Burrows and G. K. Moortgat, 1989, J. Phys. Chem., **93**, 8017–8021.
808. Mellouki, A. and A. R. Ravishankara, 1994, Int. J. Chem. Kinet., **26**, 355–365.
809. Mellouki, A., R. K. Talukdar, A. M. R. P. Bopegedera and C. J. Howard, 1993, Int. J. Chem. Kinet., **25**, 25–39.
810. Mellouki, A., R. K. Talukdar and C. J. Howard, 1994, J. Geophys. Res., **99**, 22949–22954.
811. Mellouki, A., R. K. Talukdar, A.–M. Schmoltner, T. Gierczak, M. J. Mills, S. Soloman and A. R. Ravishankara, 1992, Geophys. Res. Lett., **19**, 2059–2062.
812. Mellouki, A., S. Teton, G. Laverdet, A. Quilgars and G. Le Bras, 1994, J. Chem. Physique, **91**, 473–487.
813. Mellouki, A., S. Teton and G. Le Bras, 1995, Geophys. Res. Lett., **22**, 389–392.
814. Michael, J. V., J. E. Allen, Jr. and W. D. Brobst, 1981, J. Phys. Chem., **85**, 4109–4117.
815. Michael, J. V., D. G. Keil and R. B. Klemm, 1985, J. Chem. Phys., **83** 1630–1636.
816. Michael, J. V., R. B. Klemm, W. D. Brobst, S. R. Bosco and D. F. Nava, 1985, J. Phys. Chem., **89**, 3335–3337.
817. Michael, J. V. and J. H. Lee, 1977, Chem. Phys. Lett., **51**, 303–306.
818. Michael, J. V., J. H. Lee, W. A. Payne and L. J. Stief, 1978, J. Chem. Phys., **68**, 4093.
819. Michael, J. V., D. F. Nava, W. Brobst, R. P. Borkowski and L. J. Stief, 1982, J. Phys. Chem., **86**, 81–84.
820. Michael, J. V., D. F. Nava, W. A. Payne, J. H. Lee and L. J. Stief, 1979, J. Phys. Chem., **83**, 2818.
821. Michael, J. V., D. F. Nava, W. A. Payne and L. J. Stief, 1979, J. Chem. Phys., **70**, 1147.
822. Michael, J. V., D. F. Nava, W. A. Payne and L. J. Stief, 1979, J. Chem. Phys., **70**, 3652.
823. Michael, J. V. and W. A. Payne, 1979, Int. J. Chem. Kinet., **11**, 799.
824. Michael, J. V., D. A. Whytock, J. H. Lee, W. A. Payne and L. J. Stief, 1977, J. Chem. Phys., **67**, 3533.
825. Michelangeli, D. V., K.–Y. Choo and M. T. Leu, 1988, Int. J. Chem. Kinet., **20**, 915–938.
826. Miller, J. C. and R. J. Gordon, 1981, J. Chem. Phys., **75**, 5305.
827. Miyoshi, A., H. Matsui and N. Washida, 1994, J. Chem. Phys., **100**, 3532–3539.
828. Miziolek, A. W. and M. J. Molina, 1978, J. Phys. Chem., **82**, 1769.
829. Molina, L. T., M. J. Molina, R. A. Stachnik and R. D. Tom, 1985, J. Phys. Chem., **89**, 3779–3781.
830. Molina, L. T., J. E. Spencer and M. J. Molina, 1977, Chem. Phys. Lett., **45**, 158–162.
831. Molina, M. J., L. T. Molina and C. A. Smith, 1984, Int. J. Chem. Kinet., **16**, 1151–1160.
832. Montgomery, J. A., H. H. Michels and J. S. Francisco, 1994, Chem. Phys. Lett., **220**, 391–396.
833. Moonen, P. C., J. N. Cape, R. L. Storeton–West and R. McColm, 1998, J. Atmos. Chem., **29**, 299–314.
834. Moortgat, G. K., B. Veyret and R. Lesclaux, 1989, J. Phys. Chem., **93**, 2362–2368.
835. Morokuma, K. and C. Mugurama, 1994, J. Am. Chem. Soc., **116**, 10316–10317.
836. Morris, E. D., Jr. and H. Niki, 1971, J. Chem. Phys., **55**, 1991–1992.
837. Morris, E. D. and H. Niki, 1974, J. Phys. Chem., **78**, 1337–1338.
838. Morris, E. D., D. H. Stedman and H. Niki, 1971, J. Am. Chem. Soc., **93**, 3570.

839. Mors, V., A. Hoffman, W. Malms and R. Zellner, 1996, Ber. Bunsenges, Phys. Chem., **100**, 540–552.
840. Muller, D. F. and P. L. Houston, 1981, J. Phys. Chem., **85**, 3563–3565.
841. Munk, J., P. Pagsberg, E. Ratajczak and A. Sillesen, 1986, J. Phys. Chem. , **90**, 2752–2757.
842. Murrells, T. P., E. R. Lovejoy and A. R. Ravishankara, 1990, J. Phys. Chem., **94**, 2381–2386.
843. Myers, G. H. and R. J. O'Brien, Jr., 1970, Ann. N.Y. Acad. Sci., **171**, 224–225.
844. Nadtochenko, V. A., O. M. Sarkisov and V. I. Vedeneev, 1979, Doklady Akademii Nauk SSSR, **244**, 152.
845. Nagase, S., S. Hashimoto and H. Akimoto, 1988, J. Phys. Chem., **92**, 641–644.
846. Nava, D. F., S. R. Bosco and L. J. Stief, 1983, J. Chem. Phys., **78**, 2443–2448.
847. Nava, D. F., W. D. Brobst and L. J. Stief, 1985, J. Phys. Chem., **89**, 4703–4707.
848. Nava, D. F., J. V. Michael and L. J. Stief, 1981, J. Phys. Chem., **85**, 1896.
849. Nelson, D. D., Jr. , M. S. Zahniser and C. E. Kolb, 1993, Geophys. Res. Lett., **20**, 197–200.
850. Nelson, D. D., Jr., J. C. Wormhoudt, M. S. Zahniser, C. E. Kolb, M. K. W. Ko and D. K. Weisenstein, 1997, J. Phys. Chem. A, **101**, 4987–4990.
851. Nelson, D. D., Jr. and M. S. Zahniser, 1994, J. Phys. Chem., **98**, 2101–2104.
852. Nelson, D. D., Jr., M. S. Zahniser and C. E. Kolb, 1992, J. Phys. Chem., **96**, 249–253.
853. Nelson, D. D., M. S. Zahniser, C. E. Kolb and H. Magid, 1995, J. Phys. Chem., **99**, 16301–16306.
854. Nelson, H. H. and H. S. Johnston, 1981, J. Phys. Chem., **85**, 3891.
855. Nelson, L., O. Rattigan, R. Neavyn, H. Sidebottom, J. Treacy and O. J. Nielsen, 1990, Int. J. Chem. Kinet., **22**, 1111–1126.
856. Nelson, L., I. Shanahan, H. W. Sidebottom, J. Treacy and O. J. Nielsen, 1990, Int. J. Chem. Kinet., **22**, 577–590.
857. Nesbitt, D. J. and S. R. Leone, 1980, J. Chem. Phys., **72**, 1722–1732.
858. Nesbitt, D. J. and S. R. Leone, 1981, J. Chem. Phys., **75**, 4949.
859. Nesbitt, F. L., J. F. Gleason and L. J. Stief, 1999, J. Phys. Chem. A, **103**, 3038–3043.
860. Nesbitt, F. L., P. S. Monks, W. A. Payne, L. J. Stief and R. Toumi, 1995, Geophys. Res. Lett., **22**, 827–830.
861. Nesbitt, F. L., D. F. Nava, W. A. Payne and L. J. Stief, 1987, J. Phys. Chem., **91**, 5337–5340.
862. Nesbitt, F. L., W. A. Payne and L. J. Stief, 1988, J. Phys. Chem., **92**, 4030–4032.
863. Nicholas, J. E. and R. G. W. Norrish, 1968, Proc. Roy. Soc. A, **307**, 391.
864. Nickolaisen, S. L., R. R. Friedl and S. P. Sander, 1994, J. Phys. Chem., **98**, 155–169.
865. Nickolaisen, S. L., C. M. Roehl, L. K. Blakeley, R. R. Friedl, J. S. Francisco, R. F. Liu and S. P. Sander, 2000, Journal of Physical Chemistry A, **104**, 308–319.
866. Nickolaisen, S. L., D. W. Veney and H. E. Cartland, 1994, J. Chem. Phys., **100**, 4925–4931.
867. Nicovich, J. M., K. D. Kreutter, C. A. van Dijk and P. H. Wine, 1992, J. Phys. Chem., **96**, 2518–2528.
868. Nicovich, J. M., K. D. Kreutter and P. H. Wine, 1990, Int. J Chem. Kinet., **22**, 399–414.
869. Nicovich, J. M., C. J. Shackelford and P. H. Wine, 1990, J. Phys. Chem., **94**, 2896–2903.
870. Nicovich, J. M., S. Wang and P. H. Wine, 1995, Int. J. Chem. Kinet., **27**, 359–368.
871. Nicovich, J. M. and P. H. Wine, 1987, J. Phys. Chem., **91**, 5118–5123.
872. Nicovich, J. M. and P. H. Wine, 1990, Int. J. Chem. Kinet., **22**, 379–397.
873. Nicovich, J. M., P. H. Wine and A. R. Ravishankara, 1988, J. Chem. Phys., **89**, 5670–5679.
874. Nielsen, O. J. "Chemical Kinetics in the Gas Phase Pulse Radiolysis of Hydrogen Sulfide Systems," Riso–M–2216, Riso National Laboratory 1979.
875. Nielsen, O. J., 1991, Chem. Phys. Lett., **187**, 286–290.
876. Nielsen, O. J., T. Ellermann, E. Bartkiewicz, T. J. Wallington and M. D. Hurley, 1992, Chem. Phys. Lett., **192**, 82–88.
877. Nielsen, O. J., T. Ellermann, J. Sehested and T. J. Wallington, 1992, J. Phys. Chem., **96**, 10875–10879.
878. Nielsen, O. J., J. Munk, G. Locke and T. J. Wallington, 1991, J. Phys. Chem., **95**, 8714–8719.
879. Nielsen, O. J., J. Munk, P. Pagsberg and A. Sillesen, 1986, Chem. Phys. Lett., **128**, 168–171.
880. Nielsen, O. J. and J. Sehested, 1993, Chem. Phys. Lett., **213**, 433–441.
881. Nielsen, O. J., H. W. Sidebottom, M. Donlon and J. Treacy, 1991, Chem. Phys. Lett., **178**, 163–170.
882. Nielsen, O. J., H. W. Sidebottom, L. Nelson, O. Rattigan, J. J. Treacy and D. J. O'Farrell, 1990, Int. J. Chem. Kinet., **22**, 603–612.
883. Nielsen, O. J., H. W. Sidebottom, L. Nelson, J. J. Treacy and D. J. O'Farrell, 1989, Int. J. Chem. Kinet., **21**, 1101–1112.
884. Niki, H., E. E. Daby and B. Weinstock. In *Twelfth Symposium (International) on Combustion*; The Combustion Institute, 1969; pp 277.
885. Niki, H., P. D. Maker, L. P. Breitenbach and C. M. Savage, 1978, Chem. Phys. Lett., **57**, 596.
886. Niki, H., P. D. Maker, C. M. Savage and L. P. Breitenbach, 1978, J. Phys. Chem., **82**, 132.
887. Niki, H., P. D. Maker, C. M. Savage and L. P. Breitenbach, 1980, Chem. Phys. Lett., **73**, 43–46.

888. Niki, H., P. D. Maker, C. M. Savage and L. P. Breitenbach, 1980, Int. J. Chem. Kinet., **12**, 1001–1012.
889. Niki, H., P. D. Maker, C. M. Savage and L. P. Breitenbach, 1981, J. Phys. Chem., **85**, 877.
890. Niki, H., P. D. Maker, C. M. Savage and L. P. Breitenbach, 1982, J. Phys. Chem., **86**, 3825.
891. Niki, H., P. D. Maker, C. M. Savage and L. P. Breitenbach, 1983, J. Phys. Chem., **87**, 2190–2193.
892. Niki, H., P. D. Maker, C. M. Savage and L. P. Breitenbach, 1984, J. Phys. Chem., **88**, 2116–2119.
893. Niki, H., P. D. Maker, C. M. Savage and L. P. Breitenbach, 1984, J. Phys. Chem., **88**, 5342–5344.
894. Niki, H., P. D. Maker, C. M. Savage and L. P. Breitenbach, 1985, J. Phys. Chem., **89**, 588.
895. Nikzorodov, S. A., W. W. Harper, B. W. Blackmon and D. J. Nesbitt, 2000, J. Phys. Chem. A, **104**, 3964–3973.
896. Ninomiya, Y., M. Kawasaki, A. Guschin, L. T. Molina, M. J. Molina and T. J. Wallington, 2000, Environ. Sci. Technol., **34**, 2973–2978.
897. Nip, W. S., D. L. Singleton and R. J. Cvetanovic, 1981, J. Am. Chem. Soc., **103**, 3526.
898. Nip, W. S., D. L. Singleton, R. Overend and G. Paraskevopoulos, 1979, J. Phys. Chem., **83**, 2440–2443.
899. Nizkorodov, S. A. and P. O. Wennberg, 2002, J. Phys. Chem. A, **in press**.
900. Notario, A., A. Mellouki and G. Le Bras, 2000, Int. J. Chem. Kinet., **32**, 62–66.
901. Noxon, J. F., 1970, J. Chem. Phys. , **52**, 1852–1873.
902. O'Brien, R. J., Jr. and G. H. Myers, 1970, J. Chem. Phys., **53**, 3832–3835.
903. Ogren, P. J., T. J. Sworski, C. J. Hochanadel and J. M. Cassel, 1982, J. Phys. Chem., **86**, 238–242.
904. Ogryzlo, E. A., R. Paltenghi and K. D. Bayes, 1981, Int. J. Chem. Kinet., **13**, 667–675.
905. Ohmori, K., K. Yamasaki and H. Matsui, 1993, Bull. Chem. Soc. Jpn., **66**, 51–56.
906. Olbregts, J., G. Brasseur and E. J. Arijs, 1984, J. Photochem., **24**, 315–322.
907. Olsson, B., M. Hallquist, E. Ljungstrom and J. Davidsson, 1997, Int. J. Chem. Kinet., **29**, 195.
908. Ongstad, A. P. and J. W. Birks, 1984, J. Chem. Phys., **81**, 3922–3930.
909. Ongstad, A. P. and J. W. Birks, 1986, J. Chem. Phys., **85**, 3359–3368.
910. Orkin, V. L., R. E. Huie and M. J. Kurylo, 1996, J. Phys. Chem., **100**, 8907–8912.
911. Orkin, V. L., R. E. Huie and M. J. Kurylo, 1997, J. Phys. Chem. A, **101**, 9118–9124.
912. Orkin, V. L. and V. G. Khamaganov, 1993, J. Atmos. Chem., **16**, 157–167.
913. Orkin, V. L. and V. G. Khamaganov, 1993, J. Atmos. Chem., **16**, 169–178.
914. Orkin, V. L., V. G. Khamaganov, A. G. Guschin, R. E. Huie and M. J. Kurylo. International Symposium on Gas Kinetics, 1994, Dublin.
915. Orkin, V. L., V. G. Khamaganov, A. G. Guschin, R. E. Huie and M. J. Kurylo, 1997, J. Phys. Chem. A, **101**, 174–178.
916. Orkin, V. L., F. Louis, R. E. Huie and M. J. Kurylo, 2002, J. Phys. Chem. A, **106**, 10195–10199.
917. Orkin, V. L., E. Villenave, R. E. Huie and M. J. Kurylo, 1999, Journal of Physical Chemistry A, **103**, 9770–9779.
918. Orlando, J. J., G. S. Tyndall, L. Vereecken and J. Peeters, 2000, J. Phys. Chem. A, **104**, 11578–11588.
919. Orlando, J. J., G. S. Tyndall and T. J. Wallington, 1996, J. Phys. Chem., **100**, 7026–7033.
920. Orlando, J. J., G. S. Tyndall, T. J. Wallington and M. Dill, 1996, Int. J. Chem. Kinet., **28**, 433–442.
921. Overend, R. and G. Paraskevopoulos, 1978, J. Phys. Chem., **82**, 1329–1333.
922. Overend, R. P. and G. Paraskevopoulos, 1977, Chem. Phys. Lett., **49**, 109.
923. Overend, R. P., G. Paraskevopoulos and R. J. Cvetanovic, 1975, Canad. J. Chem., **53**, 3374–3382.
924. Pagsberg, P., J. Munk, A. Sillesen and C. Anastasi, 1988, Chem. Phys. Lett., **146**, 375–381.
925. Pagsberg, P. B., J. Erikson and H. C. Christensen, 1979, J. Phys. Chem., **83**, 582.
926. Paraskevopoulos, G. and R. S. Irwin. XV Informal Conference on Photochemistry, 1982, Stanford, CA.
927. Paraskevopoulos, G. and R. S. Irwin, 1984, J. Chem. Phys., **80**, 259–266.
928. Paraskevopoulos, G., D. L. Singleton and R. S. Irwin, 1981, J. Phys. Chem., **85**, 561.
929. Park, C. R. and J. R. Wiesenfeld, 1991, Chem. Phys. Lett., **186**, 170–176.
930. Park, J. and M. C. Lin, 1996, J. Phys. Chem., **100**, 3317–3319.
931. Parrish, D. D. and D. R. Herschbach, 1973, J. Am. Chem. Soc., **95**, 6133.
932. Pate, C. T., R. Atkinson and J. N. Pitts, Jr., 1976, J. Environ. Sci. Health, **A11**, 1.
933. Patrick, R. and D. M. Golden, 1984, J. Phys. Chem., **88**, 491–495.
934. Paukert, T. T. and H. S. Johnston, 1972, J. Chem. Phys., **56**, 2824–2838.
935. Paulson, S. E., J. J. Orlando, G. S. Tyndall and J. G. Calvert, 1995, Int. J. Chem. Kinet., **27**, 997–1008.
936. Pavanaja, U. B., H. P. Upadhyaya, A. V. Sapre, K. V. S. R. Rao and J. P. Mittal, 1994, J. Chem. Soc. Faraday. Trans., **90**, 825–829.
937. Payne, W. A., J. Brunning, M. B. Mitchell and L. J. Stief, 1988, Int. J. Chem. Kinet., **20**, 63–74.
938. Payne, W. A., L. J. Stief and D. D. Davis, 1973, J. Am. Chem. Soc., **95**, 7614.
939. Peeters, J., J. Vertommen and I. Langhans, 1992, Ber. Bunsenges. Phys. Chem., **96**, 431–436.
940. Penzhorn, R. D. and C. E. Canosa, 1983, Ber. Bunsenges. Phys. Chem., **87**, 648–654.

941. Perry, R. A., R. Atkinson and J. N. Pitts, 1977, J. Chem. Phys., **67**, 458–462.
942. Perry, R. A., R. Atkinson and J. N. Pitts, Jr., 1976, J. Chem. Phys., **64**, 1618.
943. Perry, R. A., R. Atkinson and J. N. Pitts, Jr., 1976, J. Chem. Phys., **64**, 3237.
944. Perry, R. A., R. Atkinson and J. N. Pitts, Jr., 1977, J. Chem. Phys., **67**, 5577.
945. Perry, R. A. and C. F. Melius. In *Twentieth Symposium (International) on Combustion*; The Combustion Institute, 1984; pp 639–646.
946. Persky, A., 1996, J. Phys. Chem., **100**, 689–693.
947. Phillips, L. F., 1978, Chem. Phys. Lett., **57**, 538–539.
948. Phillips, L. F. and H. I. Schiff, 1962, J. Chem. Phys., **36**, 1509–1517.
949. Piety, C. A., R. Soller, J. M. Nicovich, M. L. McKee and P. H. Wine, 1998, Chem. Phys., **231**, 155–169.
950. Pilgrim, J. S., A. McIlroy and C. A. Taatjes, 1997, J. Phys. Chem. A, **101**, 1873–1880.
951. Piper, L. G., G. E. Caledonia and J. P. Konnealy, 1981, J. Chem. Phys., **74**, 2888.
952. Plane, J. M. C. and D. Husain, 1986, J. Chem. Soc. Faraday 2, **82**, 2047–2052.
953. Plane, J. M. C., C.–F. Nien, M. R. Allen and M. Helmer, 1993, J. Phys. Chem., **97**, 4459–4467.
954. Plane, J. M. C. and B. Rajasekhar, 1989, J. Phys. Chem., **93**, 3135–3140.
955. Platz, J., O. J. Nielson, J. Sehested and T. J. Wallington, 1995, J. Phys. Chem., **99**, 6570–6579.
956. Plumb, I. C. and K. R. Ryan, 1982, Int. J. Chem. Kinet., **14**, 861–874.
957. Plumb, I. C. and K. R. Ryan, 1982 Chem. Phys. Lett., **92**, 236–238.
958. Plumb, I. C., K. R. Ryan, J. R. Steven and M. F. R. Mulcahy, 1982, Int. J. Chem. Kinet., **14**, 183.
959. Posey, J., J. Sherwell and M. Kaufman, 1981, Chem. Phys. Lett., **77**, 476–479.
960. Poulet, G., I. T. Lancar, G. Laverdet and G. Le Bras, 1990, J. Phys. Chem., **94**, 278–284.
961. Poulet, G., G. Laverdet, J. L. Jourdain and G. Le Bras, 1984, J. Phys. Chem., **88**, 6259–6263.
962. Poulet, G., G. Laverdet and G. Le Bras, 1981, J. Phys. Chem., **85**, 1892.
963. Poulet, G., G. Laverdet and G. Le Bras, 1983, Chem. Phys. Lett., **94**, 129–132.
964. Poulet, G., G. Laverdet and G. Le Bras, 1984, J. Chem. Phys., **80**, 1922–1928.
965. Poulet, G., G. Laverdet and G. Le Bras, 1986, J. Phys. Chem., **90**, 159–165.
966. Poulet, G., G. Le Bras and J. Combourieu, 1974, J. Chim. Physique, **71**, 101–106.
967. Poulet, G., G. Le Bras and J. Combourieu, 1978, J. Chem. Phys., **69**, 767.
968. Poulet, G., G. Le Bras and J. Combourieu, 1980, Geophys. Res. Lett., **7**, 413–414.
969. Poulet, G., H. Zagogianni and G. Le Bras, 1986, Int. J. Chem. Kinet., **18**, 847–859.
970. Pritchard, H. O., J. B. Pyke and A. F. Trotman–Dickenson, 1954, J. Amer. Chem. Soc., **76**, 1201–1202.
971. Pritchard, H. O., J. B. Pyke and A. F. Trotman–Dickenson, 1955, J. Amer. Chem. Soc., **77**, 2629–2633.
972. Qiu, L. X., S.–H. Shi, S. B. Xing and X. G. Chen, 1992, J. Phys.Chem., **96**, 685–689.
973. Radford, H. E., 1980, Chem. Phys. Lett., **71**, 195.
974. Radford, H. E., K. M. Evenson and D. A. Jennings, 1981, Chem. Phys. Lett., **78**, 589.
975. Rahman, M. M., E. Becker, T. Benter and R. N. Schindler, 1988, Ber. Bunsenges. Phys. Chem., **92**, 91–100.
976. Rahman, M. M., E. Becker, U. Wille and R. N. Schindler, 1992, Ber. Bunsenges. Phys. Chem., **96**, 783–787.
977. Raja, N., P. K. Arora and J. P. S. Chatha, 1986, Int. J. Chem. Kinetics, **18**, 505–512.
978. Rattigan, O. V., R. A. Cox and R. L. Jones, 1995, J. Chem. Soc. Faraday Soc. Trans., **91**, 4189–4197.
979. Ravishankara, A. R. and D. D. Davis, 1978, J. Phys. Chem., **82**, 2852–2853.
980. Ravishankara, A. R., D. D. Davis, G. Smith, G. Tesi and J. Spencer, 1977, Geophys. Res. Lett., **4**, 7.
981. Ravishankara, A. R., F. L. Eisele and P. H. Wine, 1983, J. Chem. Phys., **78**, 1140–1144.
982. Ravishankara, A. R., N. M. Kreutter, R. C. Shah and P. H. Wine, 1980, Geophys. Res. Lett., **7**, 861–864.
983. Ravishankara, A. R., J. M. Nicovich, R. L. Thompson and F. P. Tully, 1981, J. Phys. Chem., **85**, 2498–2503.
984. Ravishankara, A. R., G. Smith, R. T. Watson and D. D. Davis, 1977, J. Phys. Chem., **81**, 2220–2225.
985. Ravishankara, A. R., S. Solomon, A. A. Turnipseed and R. F. Warren, 1993, Science, **259**, 194–199.
986. Ravishankara, A. R. and R. L. Thompson, 1983, Chem. Phys. Lett., **99**, 377.
987. Ravishankara, A. R., A. A. Turnipseed, N. R. Jensen, S. Barone, M. Mills, C. J. Howard and S. Solomon, 1994, Science, **263**, 71–75.
988. Ravishankara, A. R. and P. H. Wine, 1980, J. Chem. Phys., **72**, 25–30.
989. Ravishankara, A. R., P. H. Wine and A. O. Langford, 1979, Chem. Phys. Lett., **63**, 479.
990. Ravishankara, A. R., P. H. Wine and A. O. Langford, 1979, J. Chem. Phys., **70**, 984–989.
991. Ravishankara, A. R., P. H. Wine and J. M. Nicovich, 1983, J. Chem. Phys., **78**, 6629–6639.
992. Ravishankara, A. R., P. H. Wine and J. R. Wells, 1985, J. Chem. Phys., **83**, 447–448.
993. Ravishankara, A. R., P. H. Wine, J. R. Wells and R. L. Thompson, 1985, Int. J. Chem. Kinet., **17**, 1281–1297.

994. Ray, A., I. Vassalli, G. Laverdet and G. Le Bras, 1996, J. Phys. Chem., **100**, 8895–8900.
995. Ray, G. W., L. F. Keyser and R. T. Watson, 1980, J. Phys. Chem., **84**, 1674–1681.
996. Ray, G. W. and R. T. Watson, 1981, J. Phys. Chem., **85**, 2955–2960.
997. Ray, G. W. and R. T. Watson, 1981, J. Phys. Chem., **85** 1673–1676.
998. Reilly, J. D., J. H. Clark, C. B. Moore and G. C. Pimentel, 1978, J. Chem. Phys., **69**, 4381.
999. Reimann, B. and F. Kaufman, 1978, J. Chem. Phys., **69**, 2925
1000. Reiner, T. and F. Arnold, 1993, Geophys. Res. Lett., **20**, 2659–2662.
1001. Reiner, T. and F. Arnold, 1994, J. Chem. Phys., **101**, 7399–7407.
1002. Rhasa, D. In *Diplomarbeit* Univ. of Gottingen FRG, 1983.
1003. Richardson, R. J., 1975, J. Phys. Chem., **79**, 1153–1158.
1004. Robertshaw, J. S. and I. W. M. Smith, 1980, Int . J . Chem. Kinet . **12**, 729
1005. Roehl, C. M., D. Bauer and G. K. Moortgat, 1996, J. Phys. Chem., **100**, 4038–4047.
1006. Roscoe, J. M., 1982, Int. J. Chem. Kinet., **14**, 471–478.
1007. Roth, P., R. Lohr and H. D. Hermanns, 1980, Ber. Bunsenges. Phys. Chem., **84**, 835–840.
1008. Rowland, F. S., H. Sato, H. Khwaja and S. M. Elliott, 1986, J. Phys. Chem., **90**, 1985 –1988.
1009. Rowley, D. M., M. H. Harwood, R. A. Freshwater and R. L. Jones, 1996, J. Phys. Chem., **100**, 3020–3029.
1010. Rozenshtein, V. B., Y. M. Gershenzon, S. O. Il'in and O. P. Kishkovitch, 1984, Chem. Phys. Lett., **112**, 473–478.
1011. Rust, F. and C. M. Stevens, 1980, Int. J. Chem. Kinet., **12**, 371–377.
1012. Ryan, K. R. and I. C. Plumb, 1984, Int. J. Chem. Kinet., **16**, 591–602.
1013. Saathoff, H. and R. Zellner, 1993, Chem. Phys. Lett., **206**, 349–354.
1014. Sahetchian, K. A., A. Heiss and R. Rigny, 1982, Can. J. Chem., **60**, 2896–2902.
1015. Sahetchian, K. A., A. Heiss and R. Rigny, 1987, J. Phys. Chem., **91**, 2382–2386.
1016. Sander, S. P., 1984, J. Phys. Chem., **88**, 6018–6021.
1017. Sander, S. P., 1986, J. Phys. Chem., **90**, 2194–2199.
1018. Sander, S. P. and R. R. Friedl, 1989, J. Phys. Chem., **93**, 4764–4771.
1019. Sander, S. P., R. R. Friedl, W. B. DeMore, D. M. Golden, M. J. Kurylo, R. F. Hampson, R. E. Huie, G. K. Moortgat, A. R. Ravishankara, C. E. Kolb and M. J. Molina "Chemical Kinetics and Photochemical Data for Use in Stratospheric Modeling, Evaluation Number 13," JPL Publication 00–3, Jet Propulsion Laboratory, California Institute of Technology, Pasadena, CA, 2000.
1020. Sander, S. P. and C. C. Kircher, 1986, Chem. Phys. Lett., **126**, 149–152.
1021. Sander, S. P., M. Peterson, R. T. Watson and R. Patrick, 1982, J. Phys. Chem., **86**, 1236–1240.
1022. Sander, S. P. and R. T. Watson, 1981, Chem. Phys. Lett., **77**, 473–475.
1023. Sander, S. P. and R. T. Watson, 1981, J. Phys. Chem., **85**, 4000.
1024. Sanders, N. D., J. E. Butler and J. R. McDonald, 1980, J. Chem. Phys., **73**, 5381–5383.
1025. Sanders, N. D., J. E. Butler, L. R. Pasternack and J. R. McDonald, 1980, Chem. Phys., **48**, 203.
1026. Sanhueza, E. and J. Heicklen, 1975, J. Phys. Chem., **79**, 7–11.
1027. Sanhueza, E., R. Simonaitis and J. Heicklen, 1979, Int. J. Chem. Kinet., **11**, 907.
1028. Sarkisov, O. M., S. G. Cheskis and E. A. Sviridenkov, 1978, Bull. Acad. Sci. USSR Chem., **Ser. 27**, 2336.
1029. Satyapal, S., J. Park, R. Bersohn and B. Katz, 1989, J. Chem. Phys., **91**, 6873–6879.
1030. Saunders, S. M., K. J. Hughes, M. J. Pilling, D. L. Baulch and P. I. Smurthwaite. "Reactions of hydroxyl radicals with selected hydrocarbons of importance in atmospheric chemistry"; Optical Methods in Atmospheric Chemistry, 1992, Berlin.
1031. Sawerysyn, J.–P., C. Lafage, B. Meriaux and A. Tighezza, 1987, J. Chim. Phys., **84**, 1187–1193.
1032. Sawerysyn, J. P., A. Talhaoui, B. Meriaux and P. Devolder, 1992, Chem. Phys. Lett., **198**, 197–199.
1033. Schiffman, A., D. D. Nelson, M. S. Robinson and D. J. Nesbitt, 1991, J. Phys. Chem., **95**, 2629–2636.
1034. Schindler, R. N. and T. Benter, 1988, Ber. Bunsenges. Phys. Chem., **92**, 558.
1035. Schindler, R. N., J. Dethlefs and M. Schmidt, 1996, Ber. Bunsenges. Phys. Chem., **100**, 1242–1249.
1036. Schmidt, C. and H. I. Schiff, 1973, Chem. Phys. Lett., **23**, 339–342.
1037. Schmidt, V., G. Y. Zhu, K. H. Becker and E. H. Fink, 1985, Ber. Bunsenges. Phys. Chem., **89**, 321.
1038. Schmoltner, A.–M., P. M. Chu, R. J. Brudzynski and Y. T. Lee, 1989, J. Chem. Phys., **91**, 6926–6936.
1039. Schmoltner, A. M., R. K. Talukdar, R. F. Warren, A. Mellouki, L. Goldfarb, T. Gierczak, S. A. McKeen and A. R. Ravishankara, 1993, J. Phys. Chem., **97**, 8976–8982.
1040. Schneider, W. F. and T. J. Wallington, 1994, J. Phys. Chem., **98**, 7448–7451.
1041. Schonle, G., M. M. Rahman and R. N. Schindler, 1987, Ber. Bunsenges. Phys. Chem., **91**, 66–75.
1042. Schurath, U., H. H. Lippmann and B. Jesser, 1981, Ber. Bunsenges. Phys. Chem., **85**, 807–813.
1043. Schwab, J. J., W. H. Brune and J. G. Anderson, 1989, J. Phys. Chem., **93**, 1030–1035.
1044. Schwab, J. J., D. W. Toohey, W. H. Brune and J. G. Anderson, 1984, J. Geophys. Res., **89**, 9581–9587.

1045. Scollard, D. J., J. J. Treacy, H. W. Sidebottom, C. Balestra–Garacia, G. Laverdet, G. Le Bras, H. MacLeod and S. Teton, 1993, J. Phys. Chem., **97**, 4683–4688.
1046. Seeley, J. V., J. T. Jayne and M. J. Molina, 1996, J. Phys. Chem., **100**, 4019–4025.
1047. Seeley, J. V., R. F. Meads, M. J. Elrod and M. J. Molina, 1996, J. Phys. Chem., **100**, 4026–4031.
1048. Sehested, J., L. K. Christensen, O. J. Nielsen, M. Bilde, T. J. Wallington, J. J. Schneider, J. J. Orlando and G. S. Tyndall, 1998, Int. J. Chem. Kinet., **30**, 475–489.
1049. Sehested, J., T. Ellermann, O. J. Nielsen, T. J. Wallington and M. D. Hurley, 1993, Int. J. Chem. Kinet., **25**, 701–717.
1050. Sehested, J. and O. J. Nielsen, 1993, Chem. Phys. Lett., **206**, 369–375.
1051. Sehested, J., O. J. Nielsen and T. J. Wallington, 1993, Chem. Phys. Lett., **213**, 457–464.
1052. Sehested, J., K. Sehested, O. J. Nielsen and T. J. Wallington, 1994, J. Phys. Chem., **98**, 6731–6739.
1053. Selzer, E. A. and K. D. Bayes, 1983, J. Phys. Chem., **87**, 392–394.
1054. Semmes, D. H., A. R. Ravishankara, C. A. Gump–Perkins and P. H. Wine, 1985, Int. J. Chem. Kinet., **17**, 303–313.
1055. Shallcross, D. E., P. Biggs, C. E. CanosaMas, K. C. Clemitshaw, M. G. Harrison, M. R. L. Alanon, J. A. Pyle, A. Vipond and R. P. Wayne, 1997, Journal of the Chemical Society–Faraday Transactions, **93**, 2807–2811.
1056. Sharkey, P. and I. W. M. Smith, 1993, J. Chem. Soc. Faraday Trans., **89**, 631–638.
1057. Shi, J. and J. R. Barker, 1990, Int. J. Chem. Kinetics, **20**, 1283–1301.
1058. Shi, X., D. R. Herschbach, D. R. Worsnop and C. E. Kolb, 1993, J. Phys. Chem., **97**, 2113–2122.
1059. Shibuya, K., T. Ebatu, K. Obi and I. Tanaka, 1977, J. Phys. Chem., **81**, 2292.
1060. Silver, J. A., 1986, J. Chem. Phys., **84**, 4718–4720.
1061. Silver, J. A. and C. E. Kolb, 1980, Chem. Phys. Lett., **75**, 191.
1062. Silver, J. A. and C. E. Kolb, 1982, J. Phys. Chem., **86**, 3240–3246.
1063. Silver, J. A. and C. E. Kolb, 1986, J. Phys. Chem., **90**, 3263–3266.
1064. Silver, J. A. and C. E. Kolb, 1986, J. Phys. Chem., **90**, 3267–3269.
1065. Silver, J. A. and C. E. Kolb, 1987, J. Phys. Chem., **91**, 3713–3714.
1066. Silver, J. A., A. D. Stanton, M. S. Zahniser and C. E. Kolb, 1984, J. Phys. Chem., **88**, 3123–3129.
1067. Simon, F. G., J. P. Burrows, W. Schneider, G. K. Moortgat and P. J. Crutzen, 1989, J. Phys. Chem., **93**, 7807–7813.
1068. Simon, F. G., W. Schneider, G. K. Moortgat and J. P. Burrows, 1990, J. Photochem. Photobiol., **A55**, 1–23.
1069. Simonaitis, R. and J. Heicklen, 1973, J. Phys. Chem, **77**, 1932–1935.
1070. Simonaitis, R. and J. Heicklen, 1975, J. Phys. Chem., **79**, 298.
1071. Simonaitis, R. and J. Heicklen, 1982, J. Phys. Chem., **86**, 3416–3418.
1072. Simonaitis, R. and M. T. Leu, 1985, Int. J. Chem. Kinet., **17**, 293–301.
1073. Sims, I. R., I. W. M. Smith, D. C. Clary, P. Bocherel and B. R. Rowe, 1994, J. Chem. Phys., **101**, 1748–1751.
1074. Singh, J. P., J. Bachar, D. W. Setser and S. Rosenwaks, 1985, J. Phys. Chem. , **89**, 5347–5353.
1075. Singh, J. P. and D. W. Setser, 1985, J. Phys. Chem., **89**, 5353–5358.
1076. Singleton, D. L. and R. J. Cvetanovic, 1978, Can. J. Chem., **56**, 2934.
1077. Singleton, D. L. and R. J. Cvetanovic, 1981, Int. J. Chem. Kinet., **13**, 945.
1078. Singleton, D. L., R. S. Irwin and R. J. Cvetanovic, 1977, Can. J. Chem., **55**, 3321–3327.
1079. Singleton, D. L., R. S. Irwin, W. S. Nip and R. J. Cvetanovic, 1979, J. Phys. Chem., **83**, 2195–2200.
1080. Singleton, D. L., G. Paraskevopoulos and R. S. Irwin, 1980, J. Phys. Chem., **84** 2339–2343.
1081. Singleton, D. L., G. Paraskevopoulos and R. S. Irwin, 1982, J. Phys. Chem., **86**, 2605–2609.
1082. Singleton, D. L., G. Paraskevopoulos and R. S. Irwin, 1989, J. Am. Chem. Soc., **111**, 5248–5251.
1083. Singleton, D. L., G. Paraskevopoulos, R. S. Irwin, G. S. Jolly and D. J. McKenney, 1988, J. Am. Chem. Soc., **110**, 7786–7790.
1084. Sinha, A., E. R. Lovejoy and C. J. Howard, 1987, J. Chem. Phys., **87**, 2122–2128.
1085. Slagle, I. R., F. Baiocchi and D. Gutman, 1978, J. Phys. Chem., **82** 1333.
1086. Slagle, I. R., J. R. Gilbert and D. Gutman, 1974, J. Chem. Phys., **61**, 704.
1087. Slagle, I. R., R. E. Graham, J. R. Gilbert and D. Gutman, 1975, Chem. Phys. Lett., **32**, 184.
1088. Slanger, T. G. and G. Black, 1979, J. Chem. Phys., **70**, 3434–3438.
1089. Slanger, T. G., B. J. Wood and G. Black, 1973, Int. J. Chem. Kinet., **5**, 615–620.
1090. Smardzewski, R. R. and M. C. Lin, 1977, J. Chem. Phys., **66**, 3197–3204.
1091. Smith, C. A., L. T. Molina, J. J. Lamb and M. J. Molina, 1984, Int. J. Chem. Kinet., **16**, 41–55.
1092. Smith, I. W. M. and M. D. Williams, 1986, J. Chem. Soc. Faraday Trans. 2, **82**, 1043–1055.
1093. Smith, I. W. M. and R. Zellner, 1974, J. Chem. Soc.. Faraday Trans. 2, **70**, 1045–1056.

1094. Smith, I. W. M. and R. Zellner, 1975, Int. J. Chem. Kinet., **Symp. 1**, 341.
1095. Smith, R. H., 1978, Int. J. Chem. Kinet., **10**, 519.
1096. Snelling, D. R., 1974, Can. J. Chem., **52**, 257–270.
1097. Sridharan, U. C., F. S. Klein and F. Kaufman, 1985, J. Chem. Phys., **82**, 592–593.
1098. Sridharan, U. C., L. X. Qiu and F. Kaufman, 1981, J. Phys. Chem., **85**, 3361–3363.
1099. Sridharan, U. C., L. X. Qiu and F. Kaufman, 1982, J. Phys. Chem., **86**, 4569–4574.
1100. Sridharan, U. C., L. X. Qiu and F. Kaufman, 1984, J. Phys. Chem., **88**, 1281–1282.
1101. Sridharan, U. C., B. Reimann and F. Kaufman, 1980, J. Chem. Phys., **73** 1286–1293.
1102. Stachnik, R. A. and M. J. Molina, 1987, J. Phys. Chem., **91**, 4603
1103. Stachnik, R. A., M. J. Molina and L. T. Molina, 1986, J. Phys. Chem., **90**, 2777–2780.
1104. Staricco, E. H., S. E. Sicre and H. J. Schumacher, 1962, Z. Phys . Chem. N.F., **31**, 385.
1105. Stedman, D. H. and H. Niki, 1973, J. Phys. Chem., **77**, 2604–2609.
1106. Stedman, D. H. and H. Niki, 1973, Environ. Lett., **4**, 303.
1107. Stedman, D. H., C. H. Wu and H. Niki, 1973, J. Phys. Chem., **77**, 2511.
1108. Steer, R. P., R. A. Ackerman and J. N. Pitts, Jr., 1969, J. Chem. Phys., **51**, 843–844.
1109. Steiner, H. and E. K. Rideal, 1939, Proc. Roy. Soc. (London) Sec. A., **173**, 503.
1110. Stephens, J. W., C. L. Morter, S. K. Farhat, G. P. Glass and R. F. Curl, 1993, J. Phys. Chem., **97**, 8944–8951.
1111. Stephens, R. D., 1984, J. Phys. Chem. , **88**, 3308–3313.
1112. Stephens, S. L., J. W. Birks and R. J. Glinski, 1989, J. Phys. Chem., **93**, 8384–8385.
1113. Stevens, P. S. and J. G. Anderson, 1990, Geophys. Res. Lett., **17**, 1287–1290.
1114. Stevens, P. S. and J. G. Anderson, 1992, J. Phys. Chem., **96**, 1708–1718.
1115. Stevens, P. S., W. H. Brune and J. G. Anderson, 1989, J. Phys. Chem., **93**, 4068–4079.
1116. Stickel, R. E., M. Chin, E. P. Daykin, A. J. Hynes, P. H. Wine and T. J. Wallington, 1993, J. Phys. Chem., **97**, 13653–13661.
1117. Stickel, R. E., J. M. Nicovich, S. Wang, Z. Zhao and P. H. Wine, 1992, J. Phys. Chem., **96**, 9875–9883.
1118. Stickel, R. E., Z. Zhao and P. H. Wine, 1993, Chem. Phys. Lett., **212**, 312–318.
1119. Stief, L. J., W. D. Brobst, D. F. Nava, R. P. Borkowski and J. V. Michael, 1982, J. Chem. Soc. Faraday Trans. 2, **78**, 1391–1401.
1120. Stief, L. J., D. F. Nava, W. A. Payne and J. V. Michael, 1980, J. Chem. Phys., **73**, 2254–2258.
1121. Stief, L. J., W. A. Payne, J. H. Lee and J. V. Michael, 1979, J. Chem. Phys., **70**, 5241–5243.
1122. Stimpfle, R., R. Perry and C. J. Howard, 1979, J. Chem. Phys., **71**, 5183–5190.
1123. Streit, G. E., C. J. Howard, A. L. Schmeltekopf, J. A. Davidson and H. I. Schiff, 1976, J. Chem. Phys., **65**, 4761–4764.
1124. Streit, G. E., J. S. Wells, F. C. Fehsenfeld and C. J. Howard, 1979, J. Chem. Phys., **70**, 3439–3443.
1125. Stuhl, F., 1973, J. Chem. Phys., **59**, 635.
1126. Stuhl, F., 1974, Ber. Bunsenges. Phys. Chem., **78**, 230.
1127. Stuhl, F. and H. Niki, 1970, Chem. Phys. Lett., **7**, 473–474.
1128. Stuhl, F. and H. Niki, 1971, J. Chem. Phys., **55**, 3954–3957.
1129. Stuhl, F. and H. Niki, 1972, J. Chem. Phys., **57**, 3671–3677.
1130. Stuhl, F. and K. H. Welge, 1969, Can. J. Chem., **47**, 1870–1871.
1131. Su, F., J. G. Calvert and J. H. Shaw, 1979, J. Phys. Chem., **83**, 3185–3191.
1132. Su, F., J. G. Calvert and J. H. Shaw, 1980, J. Phys. Chem., **84**, 239.
1133. Su, F., J. G. Calvert, J. H. Shaw, H. Niki, P. D. Maker, C. M. Savage and L. D. Breitenbach, 1979, Chem. Phys. Lett., **65**, 221–225.
1134. Sugawara, K., Y. Ishikawa and S. Sato, 1980, Bull. Chem. Soc. Japan, **53**, 3159.
1135. Sullivan, J. O. and P. Warneck, 1965, J. Phys. Chem., **69**, 1749.
1136. Sverdrup, G. M., C. W. Spicer and G. F. Ward, 1987, Int. J. Chem. Kinet., **19**, 191–205.
1137. Szekely, A., R. K. Hanson and C. Bowman. In *Twentieth Symposium (International) on Combustion*; The Combustion Institute, 1984; pp 647–654.
1138. Szilagyi, I., S. Dobe and T. Berces, 2000, Reaction Kinetics and Catalysis Letters, **70**, 319–324.
1139. Taatjes, C. A., L. K. Christensen, M. D. Hurley and T. J. Wallington, 1999, J. Phys.Chem. A, **103**, 9805.
1140. Tachibana, K. and A. V. Phelps, 1981, J. Chem. Phys., **75**, 3315–3320.
1141. Takacs, G. A. and G. P. Glass, 1973, J. Phys. Chem., **77**, 1060.
1142. Takacs, G. A. and G. P. Glass, 1973, J. Phys. Chem., **77**, 1182.
1143. Takacs, G. A. and G. P. Glass, 1973, J. Phys. Chem., **77**, 1948–1951.
1144. Takacs, G. A. and C. J. Howard, 1984, J. Phys. Chem. , **88**, 2110.
1145. Takacs, G. A. and C. J. Howard, 1986, J. Phys. Chem., **90**, 687–690.
1146. Takahashi, K., R. Wada, Y. Matsumi and M. Kawasaki, 1996, J. Phys. Chem., **100**, 10145–10149.

1147. Talcott, C. L., J. W. Ager, III and C. J. Howard, 1986, J. Chem. Phys., **84**, 6161–6169.
1148. Talhaoui, A., B. Louis, B. Meriaux, P. Devolder and J. P. Sawerysyn, 1996, J. Phys. Chem., **100**, 2107–2113.
1149. Talhaoui, A., F. Louis, P. Devolder, B. Meriaux, J. P. Sawerysyn, M. T. Rayez and J. C. Rayez, 1996, J. Phys. Chem., **100**, 13531–13538.
1150. Talukdar, R., A. Mellouki, T. Gierczak, J. B. Burkholder, S. A. McKeen and A. R. Ravishankara, 1991, J. Phys. Chem., **95**, 5815–5821.
1151. Talukdar, R., A. Mellouki, T. Gierczak, J. B. Burkholder, S. A. McKeen and A. R. Ravishankara, 1991, Science, **252**, 693–695.
1152. Talukdar, R. K., J. B. Burkholder, A.–M. Schmoltner, J. M. Roberts, R. Wilson and A. R. Ravishankara, 1995, J. Geophys. Res., **100**, 14163–14173.
1153. Talukdar, R. K., T. Gierczak, L. Goldfarb, Y. Rudich, B. S. Madhava Rao and A. R. Ravishankara, 1996, J. Phys. Chem., **100**, 3037–3043.
1154. Talukdar, R. K., S. C. Herndon, J. B. Burkholder, J. M. Roberts and A. R. Ravishankara, 1997, Journal of the Chemical Society–Faraday Transactions, **93**, 2787–2796.
1155. Talukdar, R. K., A. Mellouki, T. Gierczak, S. Barone, S.–Y. Chiang and A. R. Ravishankara, 1994, Int. J. Chem. Kinet., **26**, 973–990.
1156. Talukdar, R. K., A. Mellouki, A.–M. Schmoltner, T. Watson, S. Montzka and A. R. Ravishankara, 1992, Science, **257**, 227–230.
1157. Talukdar, R. K. and A. R. Ravishankara, 1996, Chem. Phys. Lett., **253**, 177–183.
1158. Taylor, P. H., J. A. D'Angelo, M. C. Martin, J. H. Kasner and B. Dellinger, 1989, Int. J. Chem. Kinet., **21**, 829–846.
1159. Taylor, P. H., Z. Jiang and B. Dellinger, 1993, Int. J. Chem. Kinet., **25**, 9–23.
1160. Temps, F. and H. G. Wagner, 1982, Ber. Bunsenges. Phys. Chem., **86**, 119–125.
1161. Temps, F. and H. G. Wagner, 1984, Ber. Bunsenges Phys. Chem., **88**, 415.
1162. Teton, S., A. El–Boudali and A. Mellouki, 1996, J. Chim. Phys., **93**, 274–282.
1163. Thomas, J. W. and F. Kaufman, 1985, J. Chem. Phys., **83**, 2900–2903.
1164. Thomas, R. G. O. and B. A. Thrush, 1975, J. Chem. Soc. Faraday Trans. 2, **71**, 664–667.
1165. Thompson, J. E. and A. R. Ravishankara, 1993, Int. J. Chem. Kinet., **25**, 479–487.
1166. Thorn, R. P., J. M. Conkhite, J. M. Nicovich and P. H. Wine, 1995, J. Chem. Phys., **102**, 4131–4142.
1167. Thrush, B. A. and G. S. Tyndall, 1982, J. Chem. Soc. Faraday 2, **78**, 1469–1475.
1168. Thrush, B. A. and G. S. Tyndall, 1982, Chem. Phys. Lett., **92**, 232–235.
1169. Thrush, B. A. and J. P. T. Wilkinson, 1979, Chem. Phys. Lett., **66**, 441–443.
1170. Thrush, B. A. and J. P. T. Wilkinson, 1981, Chem. Phys. Lett., **81**, 1–3.
1171. Thrush, B. A. and J. P. T. Wilkinson, 1981, Chem. Phys. Lett., **84**, 17–19.
1172. Tichenor, L. B., A. El–Sinawi, T. Yamada, P. H. Taylor, J. P. Peng, X. Hu and P. Marshall, 2001, Chemosphere, **42**, 571–577.
1173. Tichenor, L. B., J. L. Graham, T. Yamada, P. H. Taylor, J. P. Peng, X. H. Hu and P. Marshall, 2000, Journal of Physical Chemistry A, **104**, 1700–1707.
1174. Tiee, J. J., F. B. Wampler, R. C. Oldenborg and W. W. Rice, 1981, Chem. Phys. Lett., **82**, 80–84.
1175. Timonen, R. S., E. Ratajczak and D. Gutman, 1988, J. Phys. Chem., **92**, 651–655.
1176. Toby, F. S., S. Toby and H. E. O'Neal, 1976, Int. J. Chem. Kinet., **8**, 25.
1177. Tokuhashi, K., H. Nagai, A. Takahashi, M. Kaise, S. Kondo, A. Sekiya, M. Takahashi, Y. Gotoh and A. Suga, 1999, J. Phys. Chem. A, **103**, 2664–2672.
1178. Tokuhashi, K., A. Takahashi, M. Kaise, S. Kondo, A. Sekiya, S. Yamashita and H. Ito, 1999, Int. J. Chem. Kinet., **31**, 846–853.
1179. Tokuhashi, K., A. Takahashi, M. Kaise, S. Kondo, A. Sekiya, S. Yamashita and H. Ito, 2000, J. Phys. Chem. A, **104**, 1165–1170.
1180. Tomas, A. E., E. Villenave and R. Lesclaux, 2001, J. Phys. Chem. A, **105**, 3505–3514.
1181. Toohey, D. W. Kinetic and Mechanistic Studies of Reactions of Bromine and Chlorine Species Important in the Earth's Stratosphere. Ph. D. Thesis, Harvard University, 1988.
1182. Toohey, D. W. and J. G. Anderson, 1988, J. Phys. Chem., **92**, 1705–1708.
1183. Toohey, D. W., W. H. Brune and J. G. Anderson, 1987, J. Phys. Chem. , **91**, 1215–1222.
1184. Toohey, D. W., W. H. Brune and J. G. Anderson, 1988, Int. J. Chem. Kinet., **20**, 131–144.
1185. Trainor, D. W. and C. W. von Rosenberg, Jr., 1974, J. Chem. Phys., **61**, 1010–1015.
1186. Trevor, P. L., G. Black and J. R. Barker, 1982, J. Phys. Chem., **86**, 1661.
1187. Tsalkani, N., A. Mellouki, G. Poulet, G. Toupance and G. Le Bras, 1988, J. Atmos. Chem., **7**, 409–419.
1188. Tschuikow–Roux, E., F. Faraji, S. Paddison, J. Niedzielski and K. Miyokawa, 1988, J. Phys. Chem., **92**, 1488–1495.

1189. Tschuikow–Roux, E., T. Yano and J. Niedzielski, 1985, J. Chem. Phys., **82** 65–74.
1190. Tsuchiya, S. and T. Nakamura, 1979, Bull. Chem. Soc. Japan, **52**, 1527–1528.
1191. Tuazon, E. C., R. Atkinson, S. M. Aschmann, M. A. Goodman and A. M. Winer, 1988, Int. J. Chem. Kinet., **20**, 241–265.
1192. Tuazon, E. C., R. Atkinson and S. B. Corchnoy, 1992, Int. J. Chem. Kinet., **24**, 639–648.
1193. Tuazon, E. C., R. Atkinson, C. N. Plum, A. M. Winer and J. N. Pitts, 1983, Geophys. Res. Lett., **10**, 953–956.
1194. Tuazon, E. C., W. P. L. Carter, R. Atkinson and J. N. Pitts, Jr., 1983, Int. J. Chem. Kinet., **15**, 619–629.
1195. Tuazon, E. C., E. Sanhueza, R. Atkinson, W. P. L. Carter, A. M. Winer and J. N. Pitts, Jr., 1984, J. Phys. Chem., **88**, 3095–3098.
1196. Tully, F. P., 1983, Chem. Phys. Lett., **96**, 148–153.
1197. Tully, F. P., A. T. Droege, M. L. Koszykowski and C. F. Melius, 1986, J. Phys. Chem., **90**, 691–698.
1198. Tully, F. P. and A. R. Ravishankara, 1980, J. Phys. Chem., **84**, 3126–3130.
1199. Tully, F. P., A. R. Ravishankara and K. Carr, 1983, Inter. J. Chem. Kinet., **15**, 1111–1118.
1200. Turnipseed, A. A., S. B. Barone, N. R. Jensen, D. R. Hanson, C. J. Howard and A. R. Ravishankara, 1995, J. Phys. Chem., **99**, 6000–6009.
1201. Turnipseed, A. A., S. B. Barone and A. R. Ravishankara, 1993, J. Phys. Chem., **97**, 5926–5934.
1202. Turnipseed, A. A., S. B. Barone and A. R. Ravishankara, 1994, J. Phys. Chem., **98**, 4594–4601.
1203. Turnipseed, A. A., S. B. Barone and A. R. Ravishankara, 1996, J. Phys. Chem., **100**, 14703–14713.
1204. Turnipseed, A. A., J. W. Birks and J. G. Calvert, 1990, J. Phys. Chem., **94**, 7477–7482.
1205. Turnipseed, A. A., J. W. Birks and J. G. Calvert, 1991, J. Phys. Chem., **95**, 4356–4364.
1206. Turnipseed, A. A., M. K. Gilles, J. B. Burkholder and A. R. Ravishankara, manuscript.
1207. Turnipseed, A. A., M. K. Gilles, J. B. Burkholder and A. R. Ravishankara, 1995, Chem. Phys. Lett., **242**, 427–434.
1208. Turnipseed, A. A., G. L. Vaghjiani, T. Gierczak, J. E. Thompson and A. R. Ravishankara, 1991, J. Chem. Phys., **95**, 3244–3251.
1209. Tyndall, G. S., J. P. Burrows, W. Schneider and G. K. Moortgat, 1986, Chem. Phys. Lett., **130**, 463–466.
1210. Tyndall, G. S., R. A. Cox, C. Granier, R. Lesclaux, G. K. Moortgat, M. J. Pilling, A. R. Ravishankara and T. J. Wallington, 2001, J. Geophys. Res., **106**, 12157–12182.
1211. Tyndall, G. S., C. S. Kegley–Owen, G. S. Orlando and A. Fried, 2002, J. Phys.Chem. A, **106**, 1567–1575.
1212. Tyndall, G. S., J. J. Orlando and J. G. Calvert, 1995, Environ. Sci. Technol., **29**, 202–206.
1213. Tyndall, G. S., J. J. Orlando, C. A. Cantrell, R. E. Shetter and J. G. Calvert, 1991, J. Phys. Chem., **95**, 4381–4386.
1214. Tyndall, G. S., J. J. Orlando, C. S. Kegley–Owen, T. J. Wallington and M. D. Hurley, 1999, Int. J. Chem. Kinet., **31**, 776–784.
1215. Tyndall, G. S., J. J. Orlando, K. E. Nickerson, C. A. Cantrell and J. G. Calvert, 1991, J. Geophys. Res., **96**, 20761–20768.
1216. Tyndall, G. S., J. J. Orlando, T. J. Wallington, J. Sehested and O. J. Nielsen, 1996, J. Phys. Chem., **100**, 660–668.
1217. Tyndall, G. S. and A. R. Ravishankara, 1989, J. Phys. Chem., **93**, 2426–2435.
1218. Tyndall, G. S. and A. R. Ravishankara, 1989, J. Phys. Chem., **93**, 4707–4710.
1219. Tyndall, G. S. and A. R. Ravishankara, 1991, Int. J. Chem. Kinet., **23**, 483–527.
1220. Tyndall, G. S., T. J. Wallington and J. C. Ball, 1998, J. Phys. Chem. A, **102**, 2547–2554.
1221. Tyndall, G. S., T. J. Wallington and A. R. Potts, 1991, Chemical Physics Letters, **186**, 149–153.
1222. Vaghjiani, G. L. and A. R. Ravishankara, 1989, J. Phys. Chem., **93**, 1948.
1223. Vaghjiani, G. L. and A. R. Ravishankara, 1991, Nature, **350**, 406–409.
1224. Vaghjiani, G. L., A. R. Ravishankara and N. Cohen, 1989, J. Phys. Chem., **93**, 7833–7837.
1225. Van den Bergh, H. and J. Troe, 1976, J. Chem. Phys., **64**, 736–742.
1226. Vanderzanden, J. W. and J. W. Birks, 1982, Chem. Phys. Lett., **88**, 109–114.
1227. Vasvari, G., I. Szilagyi, A. Bencsura, S. Dobe, T. Berces, E. Heron, S. Canneaux and F. Bohr, 2001, Phys. Chem. Chem. Phys., **3**, 551–555.
1228. Verhees, P. W. C. and E. H. Adema, 1985, J. Atmos. Chem., **2**, 387.
1229. Veyret, B. and R. Lesclaux, 1981, J. Phys. Chem., **85**, 1918.
1230. Veyret, B., R. Lesclaux, M.–T. Rayez, J.–C. Rayez, R. A. Cox and G. K. Moortgat, 1989, J. Phys. Chem. , **93**, 2368–2374.
1231. Veyret, B., J. C. Rayez and R. Lesclaux, 1982, J. Phys. Chem., **86**, 3424–3430.
1232. Villenave, E. and R. Lesclaux, 1996, J. Phys. Chem., **100**, 14372–14382.
1233. Villenave, E., V. L. Orkin, R. E. Huie and M. J. Kurylo, 1997, J. Phys. Chem. A, **101**, 8513–8517.
1234. Vinckier, C., M. Schaekers and J. Peeters, 1985, J. Phys. Chem., **89**, 508–512.

1235. Vogt, R. and R. N. Schindler, 1993, Ber. Bunsenges. Phys. Chem., **97**, 819–829.
1236. Volltrauer, H. N., W. Felder, R. J. Pirkle and A. Fontijn, 1979, J. Photochem., **11**, 173–181.
1237. Von Ellenrieder, G., E. Castellano and H. J. Schumacher, 1971, Chem. Phys. Lett., **9**, 152–156.
1238. Wagner, A. F., I. R. Slagle, D. Sarzynski and D. Gutman, 1990, J. Phys. Chem., **94**, 1853–1864.
1239. Wagner, G. and R. Zellner, 1981, Ber. Bunsenges. Phys. Chem., **85**, 1122–1128.
1240. Wagner, H. G., J. Warnatz and C. Zetzsch, 1971, Anales Assoc. Quim. Argentina, **59**, 169–177.
1241. Wagner, H. G., U. Welzbacher and R. Zellner, 1976, Ber Bunsenges. Phys. Chem., **80**, 1023–1027.
1242. Wagner, H. G., C. Zetzsch and J. Warnatz, 1972, Ber. Bunsenges. Phys. Chem., **76**, 526.
1243. Wahner, A. and A. R. Ravishankara, 1987, J. Geophys. Res. , **92**, 2189–2194.
1244. Walch, S. P., 1993, J. Chem. Phys., **99**, 5295–5300.
1245. Wallington, T. J., J. M. Andino, J. C. Ball and S. M. Japar, 1990, J. Atmos. Chem., **10**, 301–313.
1246. Wallington, T. J., J. M. Andino, A. R. Potts and P. H. Wine, 1991, Chem. Phys. Lett., **176**, 103–108.
1247. Wallington, T. J., R. Atkinson, E. C. Tuazon and S. M. Aschmann, 1986, Int. J. Chem. Kinet., **18**, 837–846.
1248. Wallington, T. J., R. Atkinson and A. M. Winer, 1984, Geophys. Res. Lett., **11**, 861–864.
1249. Wallington, T. J., R. Atkinson, A. M. Winer and J. N. Pitts, Jr., 1986, J. Phys. Chem., **90**, 5393–5396.
1250. Wallington, T. J., R. Atkinson, A. M. Winer and J. N. Pitts Jr., 1986, J. Phys. Chem., **90**, 4640–4644.
1251. Wallington, T. J. and J. C. Ball, 1995, Chem. Phys. Lett., **234**, 187–194.
1252. Wallington, T. J. and J. C. Ball, 1995, J. Phys. Chem., **99**, 3201–3205.
1253. Wallington, T. J., J. C. Ball, O. J. Nielsen and E. Bartkiewicz, 1992, J. Phys. Chem. , **96**, 1241–1246.
1254. Wallington, T. J., P. Dagaut and M. J. Kurylo, 1988, J. Photochem. Photobiol. A: Chemistry, **42**, 173–185.
1255. Wallington, T. J., P. Dagaut and M. J. Kurylo, 1988, J. Phys. Chem., **92**, 5024–5028.
1256. Wallington, T. J., P. Dagaut and M. J. Kurylo, 1992, Chem. Rev., **92**, 667–710.
1257. Wallington, T. J., T. Ellermann and O. J. Nielsen, 1993, J. Phys. Chem., **97**, 8442–8449.
1258. Wallington, T. J., M. M. Hinman, J. M. Andino, W. O. Siegl and S. M. Japar, 1990, International Journal of Chemical Kinetics, **22**, 665–671.
1259. Wallington, T. J. and M. D. Hurley, 1992, Chem. Phys. Lett., **189**, 437–442.
1260. Wallington, T. J. and M. D. Hurley, 1993, Environ. Sci. Technol., **27**, 1448–1452.
1261. Wallington, T. J., M. D. Hurley and W. F. Schneider, 1993, Chem. Phys. Lett., **213**, 442–448.
1262. Wallington, T. J., M. D. Hurley, W. F. Schneider, J. Sehested and O. J. Nielsen, 1993, J. Phys. Chem., **97**, 7606–7611.
1263. Wallington, T. J. and S. M. Japar, 1990, Chem. Phys. Lett., **166**, 495–499.
1264. Wallington, T. J. and M. J. Kurylo, 1987, Int. J. Chem. Kinet., **19**, 1015–1023.
1265. Wallington, T. J. and M. J. Kurylo, 1987, J. Phys. Chem., **91**, 5050–5054.
1266. Wallington, T. J., D. M. Neuman and M. J. Kurylo, 1987, Int. J. Chem. Kinet., **19**, 725–739.
1267. Wallington, T. J., L. M. Skewes, W. O. Siegl, C. H. Wu and S. M. Japar, 1988, Int. J. Chem. Kinet., **20**, 867–875.
1268. Walther, C.–D. and H. G. Wagner, 1983, Ber. Bunsenges. Phys. Chem., **87**, 403–409.
1269. Wang, J. J. and L. F. Keyser, 2001, J. Phys.Chem. A, **105**, 10544–10552.
1270. Wang, J. J. and L. F. Keyser, 2001, J. Phys.Chem. A, **105**, 6479–6489.
1271. Wang, N. S. and C. J. Howard, 1990, J. Phys. Chem., **94**, 8787–8794.
1272. Wang, N. S., E. R. Lovejoy and C. J. Howard, 1987, J. Phys. Chem., **91**, 5743–5749.
1273. Wang, W. C., M. Suto and L. C. Lee, 1984, J. Chem. Phys., **81**, 3122–3126.
1274. Wang, X., Y. G. Jin, M. Suto and L. C. Lee, 1988, J. Chem. Phys., **89**, 4853–4860.
1275. Wang, X., M. Suto and L. C. Lee, 1988, J. Chem. Phys., **88** 896–899.
1276. Wantuck, P. J., R. C. Oldenberg, S. L. Baughcum and K. R. Winn, 1987, J. Phys. Chem., **91**, 4653.
1277. Warren, R., T. Gierczak and A. R. Ravishankara, 1991, Chem. Phys. Lett., **183**, 403–409.
1278. Warren, R. F. and A. R. Ravishankara, 1993, Int. J. Chem. Kinet., **25**, 833–844.
1279. Washida, N., 1980, J. Chem. Phys., **73**, 1665.
1280. Washida, N., H. Akimoto and M. Okuda, 1980, J. Chem. Phys., **72**, 5781–5783.
1281. Washida, N., H. Akimoto and M. Okuda, 1980, Bull. Chem. Soc. Japan, **53**, 3496–3503.
1282. Washida, N. and K. D. Bayes, 1976, Int. J. Chem. Kinet., **8**, 777
1283. Washida, N., R. J. Martinez and K. D. Bayes, 1974, Z. Naturforsch., **29A**, 251.
1284. Wategaonkar, S. J. and D. W. Setser, 1989, J. Chem. Phys., **90**, 251–264.
1285. Watson, R. T., E. S. Machado, R. L. Schiff, S. Fischer and D. D. Davis. In *Proceedings of the 4th CIAP Conference*; Dept. of Transportation Washington D.C: Cambridge, MA, 1975; Vol. DOT–TSC–OST–75–38.
1286. Watson, R. T., G. Machado, B. C. Conaway, S. Wagner and D. D. Davis, 1977, J. Phys. Chem. , **81**, 256.
1287. Watson, R. T., G. Machado, S. Fischer and D. D. Davis, 1976, J. Chem. Phys., **65**, 2126–2138.

1288. Watson, R. T., A. R. Ravishankara, G. Machado, S. Wagner and D. D. Davis, 1979, Int. J. Chem. Kinet., **11**, 187–197.
1289. Watson, R. T., S. P. Sander and Y. L. Yung, 1979, J. Phys. Chem., **83**, 2936.
1290. Wayne, R. P. and J. N. Pitts, Jr., 1969, J. Chem. Phys., **50**, 3644–3645.
1291. Wecker, D., R. Johanssen and R. N. Schindler, 1982, Ber. Bunsenges. Phys. Chem., **86**, 532–538.
1292. Wei, C. N. and R. B. Timmons, 1975, J. Chem. Phys., **62**, 3240.
1293. Wennberg, P. O., J. G. Anderson and D. K. Weisenstein, 1994, J. Geophys. Res., **99**, 18839–18846.
1294. West, G. A., R. E. Weston, Jr. and G. W. Flynn, 1978, Chem. Phys. Lett., **56**, 429.
1295. Westenberg, A. A. and N. de Haas, 1969, J. Phys. Chem., **73**, 1181.
1296. Westenberg, A. A. and N. de Haas, 1969, J. Chem. Phys., **50**, 707–709.
1297. Westenberg, A. A. and N. de Haas, 1973, J. Chem. Phys., **58**, 4066–4071.
1298. Westenberg, A. A. and N. de Haas, 1973, J. Chem. Phys., **58**, 4061–4065.
1299. Westenberg, A. A. and N. de Haas, 1977, J. Chem. Phys., **66**, 4900.
1300. Westenberg, A. A., N. de Haas and J. M. Roscoe, 1970, J. Phys. Chem., **74**, 3431.
1301. Westenberg, A. A., J. M. Roscoe and N. de Haas, 1970, Chem. Phys. Lett., **7**, 597–599.
1302. Whyte, A. R. and L. F. Phillips, 1983, Chem. Phys. Lett., **102**, 451–454.
1303. Whytock, D. A., J. H. Lee, J. V. Michael, W. A. Payne and L. J. Stief, 1977, J. Chem. Phys., **66**, 2690–2695.
1304. Whytock, D. A., R. B. Timmons, J. H. Lee, J. V. Michael, W. A. Payne and L. J. Stief, 1976, J. Chem. Phys., **65**, 2052–2055.
1305. Wiebe, H. A. and J. Heicklen, 1973, J. Am. Chem. Soc., **95**, 1–7.
1306. Wildt, J., G. Bednarek, E. H. Fink and R. P. Wayne, 1988, Chem. Phys., **122**, 463–470.
1307. Wildt, J., E. H. Fink, P. Biggs and R. P. Wayne, 1989, Chem. Phys., **139**, 401–407.
1308. Wildt, J., E. H. Fink, P. Biggs, R. P. Wayne and A. F. Vilesov, 1992, Chem. Phys., **159**, 127–140.
1309. Wilson, E. W., A. A. Sawyer and H. A. Sawyer, 2001, J. Phys. Chem. A, **105**, 1445–1448.
1310. Wilson, W. E., 1967, J. Chem. Phys., **46**, 2017–2018.
1311. Wine, P. H., R. J. Astalos and R. L. Mauldin, III, 1985, J. Phys. Chem., **89**, 2620–2624.
1312. Wine, P. H., W. L. Chameides and A. R. Ravishankara, 1981, Geophys. Res. Lett., **8** 543–546.
1313. Wine, P. H., N. M. Kreutter, C. A. Gump and A. R. Ravishankara, 1981, J. Phys. Chem., **85**, 2660–2665.
1314. Wine, P. H., J. M. Nicovich and A. R. Ravishankara, 1985, J. Phys. Chem., **89**, 3914–3918.
1315. Wine, P. H., J. M. Nicovich, R. E. Stickel, Z. Zhao, C. J. Shackelford, K. D. Kreutter, E. P. Daykin and S. Wang *The Tropospheric Chemistry of Ozone in the Polar Regions*; Springer–Verlag: Berlin, 1993; Vol. 17.
1316. Wine, P. H., J. M. Nicovich, R. J. Thompson and A. R. Ravishankara, 1983, J. Phys. Chem., **87**, 3948–3954.
1317. Wine, P. H. and A. R. Ravishankara, 1981, Chem. Phys. Lett., **77**, 103–109.
1318. Wine, P. H. and A. R. Ravishankara, 1982, Chem. Phys., **69**, 365–373.
1319. Wine, P. H. and A. R. Ravishankara, 1983, Chem. Phys. Lett., **96**, 129–132.
1320. Wine, P. H., D. H. Semmes and A. R. Ravishankara, 1981, J. Chem. Phys., **75**, 4390–4395.
1321. Wine, P. H., D. H. Semmes and A. R. Ravishankara, 1982, Chem. Phys. Lett., **90**, 128–132.
1322. Wine, P. H., R. C. Shah and A. R. Ravishankara, 1980, J. Phys. Chem., **84**, 2499–2503.
1323. Wine, P. H., R. J. Thompson and D. H. Semmes, 1984, Int. J. Chem. Kinet., **16**, 1623.
1324. Wine, P. H., J. R. Wells and J. M. Nicovich, 1988, J. Phys. Chem., **92**, 2223–2228.
1325. Wine, P. H., J. R. Wells and A. R. Ravishankara, 1986, J. Chem. Phys., **84**, 1349–1354.
1326. Winer, A. M., A. C. Lloyd, K. R. Darnall, R. Atkinson and J. N. Pitts, Jr., 1977, Chem. Phys. Lett., **51**, 221–226.
1327. Winer, A. M., A. C. Lloyd, K. R. Darnall and J. N. Pitts, Jr., 1976, J. Phys. Chem., **80**, 1635.
1328. Winkler, I. C., R. A. Stachnik, J. I. Steinfeld and S. M. Miller, 1986, J. Chem. Phys., **85**, 890.
1329. Wolf, M., D. L. Yang and J. L. Durant, 1994, J. Photochem. Photobiol. A: Chem., **80**, 85–93.
1330. Wollenhaupt, M., S. A. Carl, A. Horowitz and J. N. Crowley, 2000, Journal of Physical Chemistry A, **104**, 2695–2705.
1331. Wong, E. L. and F. R. Belles; NASA TN D–6495 NASA Washington, D. C., 1971.
1332. Wongdontri–Stuper, W., R. K. M. Jayanty, R. Simonaitis and J. Heicklen, 1979, J. Photochem., **10**, 163.
1333. Worsnop, D. R., M. S. Zahniser and C. E. Kolb, 1991, J. Phys. Chem., **95**, 3960–3964.
1334. Worsnop, D. R., M. S. Zahniser and C. E. Kolb, 1992, J. Phys. Chem., **96**, 9088.
1335. Wright, T. G., A. M. Ellis and J. M. Dyke, 1993, J. Chem. Phys., **98**, 2891–2907.
1336. Wu, F. and R. W. Carr, 1992, J. Phys. Chem., **96**, 1743–1748.
1337. Wurzburg, E. and P. L. Houston, 1980, J. Chem. Phys., **72**, 4811.
1338. Xia, W. S. and M. C. Lin, 2001, Journal of Chemical Physics, **114**, 4522–4532.
1339. Xiang, T., M. L. Torres and W. A. Guillory, 1985, J. Chem. Phys., **83**, 1623–1629.

1340. Xing, S. B., S.–H. Shi and L. X. Qiu, 1992, Int. J. Chem. Kinet., **24**, 1–10.
1341. Yamada, T., A. El–Sinawi, M. Siraj, P. H. Taylor, J. Peng, X. Hu and P. Marshall, 2001, J. Phys.Chem. A, **105**, 7588–7597.
1342. Yamada, T., T. D. Fang, P. H. Taylor and R. J. Berry, 2000, J. Phys. Chem. A, **104**, 5013–5022.
1343. Yamada, T., M. Siraj, P. H. Taylor, J. Peng, X. Hu and P. Marshall, 2001, J. Phys.Chem. A, **105**, 9436–9444.
1344. Yano, T. and E. Tschuikow–Roux, 1986, J. Photochem., **32**, 25–37.
1345. Yetter, R. A., H. Rabitz, F. L. Dryer, R. G. Maki and R. B. Klemm, 1989, J. Chem. Phys., **91**, 4088–4097.
1346. Yokelson, R. J., J. B. Burkholder, L. Goldfarb, R. W. Fox, M. K. Gilles and A. R. Ravishankara, 1995, J. Phys. Chem., **99**, 13976–13983.
1347. Zabarnick, S. and J. Heicklen, 1985, Int. J. Chem. Kinet., **17**, 455–476.
1348. Zabarnick, S., J. W, Fleming and M. C. Lin, 1988, Int. J. Chem. Kinet., **20**, 117–129.
1349. Zabel, F., K. A. Sahetchian and C. Chachaty, 1987, Chem. Phys. Lett., **134**, 433.
1350. Zagogianni, H., A. Mellouki and G. Poulet, 1987, C. R. Acad. Sci. Paris, **Series II 304**, 573–578.
1351. Zahniser, M. S., B. M. Berquist and F. Kaufman, 1978, Int. J. Chem. Kinet., **10**, 15–29.
1352. Zahniser, M. S., J. Chang and F. Kaufman, 1977, J. Chem. Phys., **67**, 997–1003.
1353. Zahniser, M. S. and C. J. Howard, 1980, J. Chem. Phys., **73**, 1620–1626.
1354. Zahniser, M. S. and F. Kaufman, 1977, J. Chem. Phys., **66**, 3673–3681.
1355. Zahniser, M. S., F. Kaufman and J. G. Anderson, 1974, Chem. Phys. Lett., **27**, 507–510.
1356. Zahniser, M. S., F. Kaufman and J. G. Anderson, 1976, Chem. Phys. Lett., **37**, 226–231.
1357. Zellner, R., 1987, J. Chem. Phys., **84**, 403.
1358. Zellner, R., G. Bednarek, A. Hoffmann, J. P. Kohlmann, V. Mors and H. Saathoff, 1994, Ber. Bunsenges. Phys. Chem., **98**, 141–146.
1359. Zellner, R. and F. Ewig, 1988, J. Phys Chem., **92**, 2971.
1360. Zellner, R. and W. Steinert, 1981, Chem. Phys. Lett., **81**, 568–572.
1361. Zellner, R., G. Wagner and B. Himme, 1980, J. Phys. Chem., **84**, 3196–3198.
1362. Zetzsch, C. "Rate constants for the reactions of OH with acetone and methylethylketone in the gas phase"; 7th International Symposium on Gas Kinetics, 1982, Goettingen, Germany.
1363. Zetzsch, C. and F. Stuhl. In *Proceedings of the 2nd European Symposium on the Physico–Chemical Behaviour of Atmospheric Pollutants*; D. Reidel Publishing Co.: Dordrecht, Holland, 1982; pp 129–137.
1364. Zhang, D. Q., J. X. Zhong and L. X. Qiu, 1997, J. Atmos. Chem., **27**, 209–215.
1365. Zhang, Z., R. E. Huie and M. J. Kurylo, 1992, J. Phys. Chem., **96**, 1533–1535.
1366. Zhang, Z., R. Liu, R. E. Huie and M. J. Kurylo, 1991, Geophys. Res. Lett., **18**, 5–7.
1367. Zhang, Z., R. F. Liu, R. E. Huie and M. J. Kurylo, 1991, J. Phys. Chem., **95**, 194–196.
1368. Zhang, Z., S. Padmaja, R. D. Saini, R. E. Huie and M. J. Kurylo, 1994, J. Phys. Chem., **98**, 4312–4315.
1369. Zhang, Z., R. D. Saini, M. J. Kurylo and R. E. Huie, 1992, Geophys. Res. Lett., **19**, 2413–2416.
1370. Zhang, Z., R. D. Saini, M. J. Kurylo and R. E. Huie, 1992, Chem. Phys. Lett., **200**, 230–234.
1371. Zhang, Z., R. D. Saini, M. J. Kurylo and R. E. Huie, 1992, J. Phys. Chem., **96**, 9301–9304.
1372. Zhao, Z., R. E. Stickel and P. H. Wine, 1996, Chem. Phys. Lett., **251**, 59–66.
1373. Zhitneva, G. P. and S. Y. Pshezhetskii, 1978, Kinetika i Kataliz, **19**, 296.
1374. Zipf, E. C., 1980, Nature (London), **287**, 523–525.

SECTION 2. TERMOLECULAR REACTIONS

Table of Contents

section 2. Termolecular Reactions 2-1
2.1 Introduction 2-1
2.2 Low–Pressure-Limiting Rate Constant, $k_o^x(T)$ 2-1
2.3 Temperature Dependence of Low–Pressure Limiting Rate Constants: T^n 2-2
2.4 High-Pressure-Limit Rate Constants, $k_\infty(T)$ 2-2
2.5 Temperature Dependence of High-Pressure-Limiting Rate Constants: T^m 2-3
2.6 Uncertainty Estimates 2-3
2.7 Notes to Table 2 2-8
2.8 References 2-16

Tables

Table 2–1. Rate Constants for Termolecular Reactions 2-4

2.1 Introduction

Rate constants for association reactions (Table 2–1) of the type A + B ↔ [AB]* $\xrightarrow{M}$ AB can be pressure dependent. The low-pressure-limiting rate constants are given in the form:

$$k_o(T) = k_o^{300}\left(\frac{T}{300}\right)^{-n} \text{ cm}^6 \text{ molecule}^{-2} \text{ s}^{-1},$$

(where k_o^{300} has been adjusted for air as the third body), together with a recommended value of n. The limiting high-pressure rate constant is given in a similar form:

$$k_\infty(T) = k_\infty^{300}\left(\frac{T}{300}\right)^{-m} \text{ cm}^3 \text{ molecule}^{-1} \text{ s}^{-1}.$$

To obtain the effective second-order rate constant for a given condition of temperature and pressure (altitude), the following formula is used:

$$k_f([M],T) = \left(\frac{k_o(T)[M]}{1+\frac{k_o(T)[M]}{k_\infty(T)}}\right) 0.6^{\left\{1+\left[\log_{10}\left(\frac{k_o(T)[M]}{k_\infty(T)}\right)\right]^2\right\}^{-1}}$$

The fixed value 0.6 that appears in this formula fits the data for all listed reactions adequately, although in principle this quantity may be different for each reaction, and also temperature dependent.

Thus, a compilation of rate constants of this type requires the stipulation of the four parameters, $k_o(300)$, n, $k_\infty(300)$, and m. These can be found in Table 2–1. The discussion that follows outlines the general methods we have used in establishing this table, and the notes to the table discuss specific data sources. Recent advances in theory have allowed direct calculation of rate constants for some reactions using RRKM/Master Equation methods.

2.2 Low-Pressure-Limiting Rate Constant, $k_o^x(T)$

Troe [259] has described a simple method for obtaining low-pressure-limiting rate constants. In essence this method depends on the definition:

$$k_o^x(T) \equiv \beta_x k_{o,sc}^x$$

Here sc signifies "strong" collisions, x denotes the bath gas, and β_x is an efficiency parameter ($0 < \beta_x < 1$), which provides a measure of energy transfer.

The coefficient β_x is related to the average energy transferred in a collision with gas x, $\langle \Delta E \rangle_x$, via:

$$\frac{\beta_x}{\left(1-\sqrt{\beta_x}\right)} = \frac{\langle \Delta E \rangle_x}{F_E kT}$$

Notice that $\langle \Delta E \rangle$ is quite sensitive to β. F_E is the correction factor of the energy dependence of the density of states (a quantity of the order of 1.1 for most species of stratospheric interest).

For some of the reactions of possible stratospheric interest reviewed here, there exist data in the low-pressure limit (or very close thereto), and we have chosen to evaluate and unify this data by calculating $k_o^x(T)$ for the appropriate bath gas x and computing the value of β_x corresponding to the experimental value (Troe [259]). A compilation (Patrick and Golden [211]) gives details for many of the reactions considered here.

From the β_x values (most of which are for N_2, i.e., β_{N_2}), we compute $\langle \Delta E \rangle_X$ according to the above equation. Values of $\langle \Delta E \rangle_{N_2}$ of approximately 0.3–1 kcal mole^{-1} are generally expected. If multiple data exist, we average the values of $\langle \Delta E \rangle_{N_2}$ and recommend a rate constant corresponding to the β_{N_2} computed in the equation above.

Where no data exist we have sometimes estimated the low-pressure rate constant by taking $\beta_{N_2} = 0.3$ at T = 300 K, a value based on those cases where data exist.

2.3 Temperature Dependence of Low–Pressure Limiting Rate Constants: T^n

The value of n recommended here comes from measurements or, in some cases, a calculation of $\langle \Delta E \rangle_{N_2}$ from the data at 300 K, and a computation of β_{N_2} (200 K) assuming that $\langle \Delta E \rangle_{N_2}$ is independent of temperature in this range. This β_{N_2} (200 K) value is combined with the computed value of k_o^{sc} (200 K) to give the expected value of the actual rate constant at 200 K. This latter, in combination with the value at 300 K, yields the value of n.

This procedure can be directly compared with measured values of k_o (200 K) when those exist. Unfortunately, very few values at 200 K are available. There are often temperature-dependent studies, but some ambiguity exists when one attempts to extrapolate these down to 200 K. If data are to be extrapolated beyond the measured temperature range, a choice must be made as to the functional form of the temperature dependence.

There are two general ways of expressing the temperature dependence of rate constants. Either the Arrhenius expression

$$k_o(T) = A \exp(-E/RT)$$

or the form

$$k_o(T) = A' T^{-n}$$

is employed. Since neither of these extrapolation techniques is soundly based, and since they often yield values that differ substantially, we have used the method explained earlier as the basis of our recommendations.

2.4 High-Pressure-Limit Rate Constants, $k_\infty(T)$

High-pressure rate constants can often be obtained experimentally, but those for the relatively small species of atmospheric importance usually reach the high-pressure limit at inaccessibly high pressures. This leaves two sources of these numbers, the first being guesses based upon some model, and the second being extrapolation of fall-off data up to higher pressures.

Stratospheric conditions generally render reactions of interest much closer to the low-pressure limit and thus are fairly insensitive to the high-pressure value. This means that while the extrapolation is long, and the value of $k_\infty(T)$ not very accurate, a "reasonable guess" of $k_\infty(T)$ will then suffice. In some cases we have declined to guess since the low-pressure limit is effective over the entire range of stratospheric conditions.

2.5 Temperature Dependence of High-Pressure-Limiting Rate Constants: T^m

There are very few data upon which to base a recommendation for values of m. Values in Table 2–1 are often estimated, based on models for the transition state of bond-association reactions and whatever data are available.

2.6 Uncertainty Estimates

For three-body reactions (Table 2–1) uncertainties are assigned using a procedure that is analogous to that employed for bimolecular reactions. Values of f(298 K) are given for these rate constants at room temperature and assumed to be valid at all pressures. The additional uncertainty arising from the temperature extrapolation has in previous evaluations been expressed as an uncertainty in the temperature coefficients n and m. In this evaluation, those reactions that have been re-evaluated or added have uncertainties expressed with a g-factor as in Table 1–1. In future evaluations we will continue to update this format.

Table 2–1. Rate Constants for Termolecular Reactions

Reaction	Low-Pressure Limit[a] $k_o(T) = k_o^{300}(T/300)^{-n}$		High-Pressure Limit[b] $k_\infty(T) = k_\infty^{300}(T/300)^{-m}$		f	g	Notes
	k_o^{300}	n	k_∞^{300}	m			
O_x Reactions							
$O + O_2 \xrightarrow{M} O_3$	(6.0) (–34)	2.4	–	–	1.1	50	A1
$O(^1D)$ Reactions							
$O(^1D) + N_2 \xrightarrow{M} N_2O$	(3.5±3.0) (–37)	$0.6\pm^{2.0}_{0.6}$	–	–			A2
HO_x Reactions							
$H + O_2 \xrightarrow{M} HO_2$	(5.7±0.5) (–32)	1.6±0.5	(7.5±4.0) (–11)	0±1.0			B1
$OH + OH \xrightarrow{M} H_2O_2$	(6.9) (–31)	1.0	(2.6) (–11)	0	1.5	100	B2
NO_x Reactions							
$O + NO \xrightarrow{M} NO_2$	(9.0±2.0) (–31)	1.5±0.3	(3.0±1.0) (–11)	0±1.0			C1
$O + NO_2 \xrightarrow{M} NO_3$	(2.5) (–31)	1.8	(2.2) (–11)	0.7	1.3	100	C2
$OH + NO \xrightarrow{M} HONO$	(7.0±1.0) (–31)	2.6±0.3	(3.6±1.0) (–11)	0.1±0.5			C3
$OH + NO_2 \xrightarrow{M} HONO_2$ (See Note)	(2.0) (–30)	3.0	(2.5) (–11)	0	1.3	100	C4
$HO_2 + NO_2 \xrightarrow{M} HO_2NO_2$	(1.8±0.3) (–31)	3.2±0.4	(4.7±1.0) (–12)	1.4±1.4			C5
$NO_2 + NO_3 \xrightarrow{M} N_2O_5$	(2.0) (–30)	4.4	(1.4) (–12)	0.7	1.2	100	C6
$NO_3 \xrightarrow{M} NO + O_2$	See Note						C7
Hydrocarbon Reactions							
$CH_3 + O_2 \xrightarrow{M} CH_3O_2$	(4.5±1.5) (–31)	3.0±1.0	(1.8±0.2) (–12)	1.7±1.7			D1
$C_2H_5 + O_2 \xrightarrow{M} C_2H_5O_2$	(1.5±1.0) (–28)	3.0±1.0	(8.0±1.0) (–12)	0±1.0			D2
$OH + C_2H_2 \xrightarrow{M} HOCHCH$	(5.5±2.0) (–30)	0.0±0.2	(8.3±1.0) (–13)	$-2\pm^{2}_{1}$			D3
$OH + C_2H_4 \xrightarrow{M} HOCH_2CH_2$	(1.0±0.6) (–28)	0.8±2.0	(8.8±0.9) (–12)	$0\pm^{0}_{2}$			D4
$CH_3O + NO \xrightarrow{M} CH_3ONO$	(1.4±0.5) (–29)	3.8±1.0	(3.6±1.6) (–11)	0.6±1.0			D5
$CH_3O + NO_2 \xrightarrow{M} CH_3ONO_2$	(5.3) (–29)	4.4	(1.9) (–11)	1.8	1.1	0	D6
$C_2H_5O + NO \xrightarrow{M} C_2H_5ONO$	(2.8±1.0) (–27)	4.0±2.0	(5.0±1.0) (–11)	1.0±1.0			D7

Reaction	Low-Pressure Limit[a] $k_o(T) = k_o^{300}(T/300)^{-n}$		High-Pressure Limit[b] $k_\infty(T) = k_\infty^{300}(T/300)^{-m}$		f	g	Notes
	k_o^{300}	n	k_∞^{300}	m			
$C_2H_5O + NO_2 \xrightarrow{M} C_2H_5ONO_2$	(2.0±1.0) (–27)	4.0±2.0	(2.8±0.4) (–11)	1.0±1.0			D8
$CH_3O_2 + NO_2 \xrightarrow{M} CH_3O_2NO_2$	(1.5±0.8) (–30)	4.0±2.0	(6.5±3.2) (–12)	2.0±2.0			D9
$C_2H_5O_2 + NO_2 \xrightarrow{M} C_2H_5O_2NO_2$	(1.2)(–29)	4.0	(9.0)(–12)	0.0	1.3	50	D10
$CH_3C(O)O_2 + NO_2 \xrightarrow{M} CH_3C(O)O_2NO_2$	(9.7±3.8) (–29)	5.6±2.8	(9.3±0.4)(–12)	1.5±0.3			D11
$CH_3CH_2C(O)O_2 + NO_2. \xrightarrow{M} CH_3CH_2C(O)O_2NO_2$	(9.0) (–28)	8.9	(7.7) (–12)	0.2	2.0	100	D12
$CH_3C(O)CH_2 + O_2 \xrightarrow{M} CH_3C(O)CH_2O_2$	See Note						D13
FO_x Reactions							
$F + O_2 \xrightarrow{M} FO_2$	(4.4±0.4) (–33)	1.2±0.5	–	–			E1
$F + NO \xrightarrow{M} FNO$	(1.8±0.3) (–31)	1.0±10	(2.8±1.4) (–10)	0.0±1.0			E2
$F + NO_2 \xrightarrow{M} FNO_2$	(6.3±3.0) (–32)	2.0±2.0	(2.6±1.3) (–10)	0.0±1.0			E3
$FO + NO_2 \xrightarrow{M} FONO_2$	(2.6±2.0) (–31)	1.3±1.3	(2.0±1.0) (–11)	1.5±1.5			E4
$CF_3 + O_2 \xrightarrow{M} CF_3O_2$	(3.0±0.3) (–29)	4.0±2.0	(4.0±1.0) (–12)	1.0±1.0			E5
$CF_3O + NO_2 \xrightarrow{M} CF_3ONO_2$	3.1(–28)	2.0	1.5(–11)	2.8	1.1	50	E6
$CF_3O_2 + NO_2 \xrightarrow{M} CF_3O_2NO_2$	(2.2±0.5) (–29)	5.0±1.0	(6.0±1.0) (–12)	2.5±1.0			E7
$CF_3O + CO \xrightarrow{M} CF_3OCO$	(2.5±0.2) (–31)	–	(6.8±0.4) (–14)	–1.2			E8
$CF_3O \xrightarrow{M} CF_2O + F$	See Note						E9
ClO_x Reactions							
$Cl + O_2 \xrightarrow{M} ClOO$	(2.7±1.0) (–33)	1.5±0.5	–	–			F1
$Cl + NO \xrightarrow{M} ClNO$	(9.0±2.0) (–32)	1.6±0.5	–	–			F2
$Cl + NO_2 \xrightarrow{M} ClONO$	(1.3±0.2) (–30)	2.0±1.0	(1.0±0.5) (–10)	1.0±1.0			F3
$\xrightarrow{M} ClNO_2$	(1.8±0.3) (–31)	2.0±1.0	(1.0±0.5) (–10)	1.0±1.0			
$Cl + CO \xrightarrow{M} ClCO$	(1.3±0.5) (–33)	3.8±0.5	–	–			F4
$Cl + C_2H_2 \xrightarrow{M} ClC_2H_2$	((5.9±1.0) (–30)	2.1±1.0	(2.1±0.4) (–10)	1.0±0.5			F5
$Cl + C_2H_4 \xrightarrow{M} ClC_2H_4$	(1.6) (–29)	3.3	(3.1) (–10)	1.0	1.5	50	F6
$Cl + C_2Cl_4 \xrightarrow{M} C_2Cl_5$	(1.4) (–28)	8.5	(4.0) (–11)	1.2	1.2	50	F7

Reaction	Low-Pressure Limit[a] $k_o(T) = k_o^{300}(T/300)^{-n}$		High-Pressure Limit[b] $k_\infty(T) = k_\infty^{300}(T/300)^{-m}$		f	g	Notes
	k_o^{300}	n	k_∞^{300}	m			
$ClO + NO_2 \xrightarrow{M} ClONO_2$	(1.8±0.3) (–31)	3.4±0.2	(1.5±0.4) (–11)	1.9±0.5			F8
$OClO + NO_3 \xrightarrow{M} O_2ClONO_2$	See Note						F9
$ClO + ClO \xrightarrow{M} Cl_2O_2$	(1.6) (–32)	4.5	(2.0) (–12)	2.4	1.1	25	F10
$ClO + OClO \xrightarrow{M} Cl_2O_3$	(6.2±1.0) (–32)	4.7±0.6	(2.4±1.2) (–11)	0±1.0			F11
$OClO + O \xrightarrow{M} ClO_3$	(1.9±0.5) (–31)	1.1±1.0	(3.1±0.8) (–11)	0±1.0			F12
$CH_2Cl + O_2 \xrightarrow{M} CH_2ClO_2$	(1.9±0.1) (–30)	3.2±0.2	(2.9±0.2) (–12)	1.2±0.6			F13
$CHCl_2 + O_2 \xrightarrow{M} CHCl_2O_2$	(1.3±0.1) (–30)	4.0±0.2	(2.8±0.2) (–12)	1.4±0.6			F14
$CCl_3 + O_2 \xrightarrow{M} CCl_3O_2$	(6.9±0.2) (–31)	6.4±0.3	(2.4±0.2) (–12)	2.1±0.6			F15
$CFCl_2 + O_2 \xrightarrow{M} CFCl_2O_2$	(5.0±0.8) (–30)	4.0±2.0	(6.0±1.0) (–12)	1.0±1.0			F16
$CF_2Cl + O_2 \xrightarrow{M} CF_2ClO_2$	(3.0±1.5) (–30)	4.0±2.0	(3±2) (–12)	1.0±1.0			F17
$CCl_3O_2 + NO_2 \xrightarrow{M} CCl_3O_2NO_2$	(5.0±1.0) (–29)	5.0±1.0	(6.0±1.0) (–12)	2.5±1.0			F18
$CFCl_2O_2 + NO_2 \xrightarrow{M} CFCl_2O_2NO_2$	(3.5±0.5) (–29)	5.0±1.0	(6.0±1.0) (–12)	2.5±1.0			F19
$CF_2ClO_2 + NO_2 \xrightarrow{M} CF_2ClO_2NO_2$	(3.3±0.7) (–29)	6.7±1.3	(4.1±1.9) (–12)	2.8±0.7			F20
BrO_x Reactions							
$Br + NO_2 \xrightarrow{M} BrNO_2$	(4.2±0.8) (–31)	2.4±0.5	(2.7±0.5) (–11)	0±1.0			G1
$BrO + NO_2 \xrightarrow{M} BrONO_2$	(5.2±0.4) (–31)	3.2±0.8	(6.9±0.4) (–12)	2.9±0.1			G2
IO_x Reactions							
$I + NO \xrightarrow{M} INO$	(1.8±0.5) (–32)	1.0±0.5	(1.7±1.0) (–11)	0±1.0			H1
$I + NO_2 \xrightarrow{M} INO_2$	(3.0±1.5) (–31)	1.0±1.0	(6.6±5.0) (–11)	0±1.0			H2
$IO + NO_2 \xrightarrow{M} IONO_2$	(5.9±2.0) (–31)	3.5±1.0	(9.0±1.0) (–12)	1.5±1.0			H3
SO_x Reactions							
$HS + NO \xrightarrow{M} HSNO$	(2.4±0.4) (–31)	3.0±1.0	(2.7±0.5) (–11)	$0\pm^{0}_{2}$			I1
$CH_3S + NO \xrightarrow{M} CH_3SNO$	(3.2±0.4) (–29)	4.0±1.0	(3.9±0.6) (–11)	2.7±1.0			I2
$O + SO_2 \xrightarrow{M} SO_3$	$(1.3\pm^{1.3}_{0.7})(-33)$	–3.6±0.7					I3
$OH + SO_2 \xrightarrow{M} HOSO_2$	(3.0±1.0) (–31)	3.3±1.5	(1.5±0.5) (–12)	$0\pm^{0}_{2}$			I4

Reaction	Low-Pressure Limit[a] $k_o(T) = k_o^{300}(T/300)^{-n}$		High-Pressure Limit[b] $k_\infty(T) = k_\infty^{300}(T/300)^{-m}$		f	g	Notes
	k_o^{300}	n	k_∞^{300}	m			
$CH_3SCH_2 + O_2 \xrightarrow{M} CH_3SCH_2O_2$	See Note						I5
$SO_3 + NH_3 \xrightarrow{M} H_3NSO_3$	(3.9±0.8) (–30)	3.0±3.0	(4.7±1.3) (–11)	0±1.0			I6
Metal Reactions							
$Na + O_2 \xrightarrow{M} NaO_2$	(3.2±0.3) (–30)	1.4±0.3	(6.0±2.0) (–10)	0±1.0			J1
$NaO + O_2 \xrightarrow{M} NaO_3$	(3.5±0.7) (–30)	2.0±2.0	(5.7±3.0) (–10)	0±1.0			J2
$NaO + CO_2 \xrightarrow{M} NaCO_3$	(8.7±2.6) (–28)	2.0±2.0	(6.5±3.0) (–10)	0±1.0			J3
$NaOH + CO_2 \xrightarrow{M} NaHCO_3$	(1.3±0.3) (–28)	2.0±2.0	(6.8±4.0) (–10)	0±1.0			J4

Shaded areas indicate changes or additions since JPL 97–4 and/or JPL 00–03.
The values quoted are suitable for air as the third body, M.
a Units are cm^6/molecule^2-s.
b Units are cm^3/molecule-s.
f(298 K) is the uncertainty factor at 298 K. To calculate the uncertainty at other temperatures, use the expression:

$$f(T) = f(298)\exp\left|g\left(\frac{1}{T} - \frac{1}{298}\right)\right|$$

Note that the exponent is absolute value

2.7 Notes to Table 2

A1. O + O2. Low pressure limit and T dependence are an average of Klais et al. [145], Huie et al. [127] and Lin and Leu [167]. These studies in N_2 and Ar are in the temperature range (200<T/K<268). The result is in agreement with the study of Hippler et al. [119] and the extrapolated recommendation fits their lower pressure N_2 data down to 100 K. High pressure studies by Croce de Cobos and Troe [72] are in agreement with this recommendation. Rawlins et al. [224] estimate values in Ar between 80 and 150 K from nascent vibrational distributions that are a factor of two higher than the recommendation extrapolated to 80 K. The temperature dependence of the rate constant determined from the experimental data is in excellent agreement with the value of n=2.36 determined from the calculations of Patrick and Golden [211].

Kaye [139] has calculated isotope effects for this reaction, using methods similar to those discussed in the Introduction of this document (see Troe [259] and Patrick and Golden [211].) Isotope effects have been reported by Anderson et al. [8] and Gross and Billing [111]. Measurements of isotopic fractionation by Mauersberger and colleagues [288] and Thiemens and co–workers [236] reveal distinctly non–statistical effects. Various attempts at theoretical explanations exist [115], but the detailed knowledge of the potential energy surface required is unavailable.

A2. $O(^1D) + N_2$. Low pressure limit from Kajimoto and Cvetanovic [138]. The T dependence is obtained by assuming a constant β. The rate constant is extremely low in this special system due to electronic curve crossing. Maric and Burrows [174] extract $(8.8\pm3.3)\times10^{-37}$ $cm^6\ s^{-1}$ from a study of the photolysis of synthetic air, in agreement with the recommended value within mutual error limits.

B1. $H + O_2$. Kurylo [151], Wong and Davis [290] and Hsu et al. [126] are averaged to obtain the low pressure limiting value at 300 K. The first two studies include T dependence, as does a study by Hsu et al. [125]. The recommended value is chosen with constant $\langle\Delta E\rangle_{N2}$ ~0.05 kcal mol^{-1}. This very low number reflects rotational effects. The high pressure limit is from Cobos et al. [59]. The temperature dependence is estimated. Cobos et al. [59] estimate
m = –0.6, which is within our uncertainty. High temperature measurements in Ar by Pirraglia et al. [216] are in good agreement. Measurements in the range 298<T/K<750 by Carleton et al. [51] agree within error limits. High temperature theoretical and experimental studies examining wide ranges of pressure and temperature [260], [24] are in good agreement with the recommendation.

B2. OH + OH. Recommended values are from fits of measurements by Zellner et al. [297] in N_2, by Forster et al. [99] and Fulle et al. [105] in 1–150 bar He scaled to N_2. A study by Fagerstrom et al. [94] in 85–1000 mbar SF_6 gives slightly different values. A pressure independent bimolecular channel to H_2O + O with a rate $4.2\times10^{-12} * \exp(-240/T)$ is observed (see Table 1–1). Zellner et al. used somewhat different values for this rate constant to make substantial corrections to their measured values. Changing to the accepted value will make large changes in the Zellner et al. values and it is unclear how to evaluate this. Trainor and von Rosenberg [258] report a value at 300 K that is lower than recommended by a factor of 2.7.

C1. O + NO. Low pressure limit and n from direct measurements of Schieferstein et al. [237] and their re–analysis of the data of Whytock et al. [284]. Error limits encompass other studies. High pressure limit and m from Baulch et al. [26] and Baulch et al. [25], slightly modified. Hippler et al. [120] report higher values for the high pressure limiting rate constant. Atkinson et al. [14] use $F_c = \exp(-T/1850)$. This yields rate constants 10–20% higher than obtained from Table 2–1. Shock tube measurements by Yarwood et al. [293] in argon from 300–1300 K are consistent with the values in Table 2–1.

C2. $O + NO_2$. Values of rate constants and temperature dependences from a combination of the study by Burkholder and Ravishankara [44] and that of Hahn et al. [112]. At 300K these studies almost overlap at the highest pressure of Burkholder and Ravishankara and the lowest pressure studied by Hahn et al.. The former values are larger by a factor of 2.2 under these conditions. This recommendation is in reasonable agreement with the evaluation of Baulch et al. [26], which fits the Hahn et al. values very well.

C3. OH + NO. The low pressure limit rate constant has been reported by Anderson and Kaufman [6], Stuhl and Niki [254], Morley and Smith [185], Westenberg and de Haas [283], Anderson et al. [7], Howard and Evenson [124], Harris and Wayne [114], Atkinson et al. [16], Overend et al. [201], Anastasi and Smith [5], Burrows et al. [46] and Atkinson and Smith [11]. The general agreement is good, and the recommended values of both the rate constant and the temperature dependence are weighted averages. Studies by Sharkey et al. [242] and Donahue et al. [88] in the transition regime between low and high pressure limits are in agreement and serve to reduce the uncertainty. These latter studies yield a value for the high pressure limiting rate constant in

agreement with the results of Forster et al. [99], whose study reached pressures of 100 bar in He. The temperature dependence of the high pressure limiting rate constant is from the data of Anastasi and Smith [5] and Sharkey et al. (Both cis- and trans-HONO are expected to be formed.) Fulle et al. [106] report a high pressure limit in agreement with Forster et al. [99]. Pagsberg et al. [202] report low pressure values in SF_6 that are compatible (i.e. the ratio of collision efficiencies is about a factor of two.) with the recommendation. A study by Zabarnick [294] is noted.

C4. $OH + NO_2$. This reaction has been the subject of detailed study. Golden and Smith [108] concluded that there were two pathways, one to $HONO_2$ (nitric acid) and the other to HOONO (pernitrous acid). They offered parameters in the format of this recommendation that were given in the note in JPL 00-3.[232] Donahue et al. [87] support the finding of two pathways in an analysis of isotopic effects. The low pressure limit and the high pressure limiting rate constants and their temperature dependences in JPL 00-3 are from a fit to the data of Anastasi and Smith [4] Wine et al. [286], Donahue et al. [88], Dransfield et al. [90], Brown et al. [39] and D'Ottone et al.[89]. (Brown et al. report that O_2 is about 30% less efficient than N_2 as a collider and suggest that air might therefore have a total efficiency of 0.94 relative to N_2) Data from Anderson et al. [7] Howard and Evenson [89], Burrows et al. [46], and Erler et al. [93] are in essential agreement. Data of Forster et al [99] and Fulle et al. [106] appear to be about 30% too high [118]. Experiments up to about 100 bar at 300 K and the finding of a double exponential decay of OH at 430 K and 100 bar implicate a second pathway [118]. Burkholder et al. [42] and Dransfield et al. [90] have searched for the isomer HOONO and have been unable to identify it. Nizkorodov and Wennberg [193] report 5% HOONO at 253K and 20 Torr of an N_2/He buffer gas . The presence of the HOONO isomer at 300 and 430 K can be accounted for with model transition states and RRKM calculations. However, this description of the reaction between HO and NO_2, requires that the data obtained at lower than 300 K represent the sum of the two pathways. Thus the fate of HOONO might have to be included in models. If this fate involves rapid loss due to reaction or photolysis, the effect of the second pathway is the diminution of the $HONO_2$ forming rate constant. However, evaluation of data, taking into account both pathways, indicates that the contribution of the HOONO forming reaction is quite small under atmospheric conditions. Thus, the recommendation is to use only the $HONO_2$ forming reaction. The following parameters relating to HOONO are provided for the purposes of model evaluation only and are not part of the Panel's recommendation for reaction C4.

Extrapolation of the model transition states used to fit the higher temperature results allows the formulation below.

Fits to individual product species in Table 2–1 format:

$$HONO_2: k_o(300) = 2.0 \times 10^{-30};\ n = 3.0;\ k_\infty(300) = 2.5 \times 10^{-11};\ m = 0$$

$$HOONO: k_o(300) = 1.0 \times 10^{-31};\ n = 4.0;\ k_\infty(300) = 1.0 \times 10^{-10};\ m = 0$$

For the HOONO case, the reverse reaction must be taken into account through the equilibrium constant. In the format of Table 3-1:

$$A = 4.66 \times 10^{-27};\ B = 10028;\ K(298\ K) = 1.92 \times 10^{-12} \text{ and } f(298\ K) = 10$$

C5. $HO_2 + NO_2$. Kurylo and Ouellette [152] have remeasured the 300-K rate constants. Kurylo and Ouellette [153] have also remeasured the temperature dependence. The recommended values are taken from this latter reference wherein their data were combined with that of Sander and Peterson [233]. The recommended k_o (300 K) is consistent with Howard [123]. Other studies by Simonaitis and Heicklen [245] and Cox and Patrick [70] are in reasonable agreement with the recommendation, as is the value of Christensen et al. [56].

C6. $NO_2 + NO_3$. Data with N_2 as the bath gas from Kircher et al. [143], Smith et al. [248], Burrows et al. [45], Wallington et al. [272] and Orlando et al. [199] ranging from 236 to 358 K were used to obtain k_o, k_∞, n and m. Values from Croce de Cobos et al. [71] are excluded due to arguments given by Orlando et al. [199], who point out that a reanalysis of these data using better values for the rate constant for $NO_3 + NO \rightarrow 2NO_2$ yields a negative value for $NO_2 + NO_3 + M$. The study of Fowles et al. [100] is noted, but not used. Johnston et al. [130] have reviewed this reaction. Hahn et al. [112] have studied this reaction between 300 and 400 K at pressures from 30 to 900 bar. Their suggested parameterization yields values indistinguishable from those in this recommendation under most atmospheric conditions. (There are deviations of 30 to 50% at pressures less than a mbar and greater than
5 bar.)

A study of the reverse reaction has been carried out by Cantrell et al. [47]. These data are in excellent agreement with those obtained by Connell and Johnston [62] and Viggiano et al. [267]. The equilibrium

constant recommended in Table 3-1 is the one given in Cantrell et al. [47], who computed it from the ratio of the rate constant of Orlando et al. [199] and their rate constants for the reverse reaction.

C7. $O_2 + NO_3$. Johnston et al. [130] and Davidson et al. [78] have suggested significant thermal decomposition of NO_3. This has been disputed by Russell et al. [227]. Davis et al. [80] claim that the barrier to thermal dissociation is
47.3 kcal mol^{-1}. This would seem to rule out such a process in the atmosphere.

D1. $CH_3 + O_2$. Low pressure limit from Selzer and Bayes [240]. (These workers determined the rate constants as a function of pressure in N_2, Ar, O_2, and He. Only the N_2 points were used directly in the evaluation, but the others are consistent.) Plumb and Ryan [218] report a value in He which is consistent within error limits with the work of Selzer and Bayes. Pilling and Smith [215] have measured this process in Ar (32–490 Torr). Their low pressure limiting rate constant is consistent with this evaluation, but their high pressure value is a little low. Cobos et al. [58] have made measurements in Ar and N_2 from 0.25 to 150 atmospheres. They report parameters somewhat different than recommended here, but their data are reproduced well by the recommended values. The work of Laguna and Baughcum [154] seems to be in the fall–off region. Results of Pratt and Wood [220] in Ar are consistent with this recommendation, although the measurements are indirect. Their T dependence is within our estimate. As can be seen from Patrick and Golden [211], the above value leads to a very small β, ~0.02, and thus temperature dependence is hard to calculate. The suggested value accommodates the values of Keiffer et al. [140], who measured the process in Ar between 20 and 600 Torr and in the range $334 \leq T/K \leq 582$. Ryan and Plumb [230] suggest that the same type of calculation as employed by Patrick and Golden yields a reasonable value of β. We have not been able to reproduce their results. The high-pressure rate constant fits the data of Cobos et al. [58]. The temperature dependence is an estimate. (Data of van den Bergh and Callear [266], Hochanadel et al. [121], Basco et al. [23], Washida and Bayes [282], Laufer and Bass [156], and Washida [281] are also considered.) The fit to Keiffer et al. [140] is very good, suggesting that the temperature dependence for the high pressure limit is also reasonable. Kaiser [134] has determined values in reasonable agreement (±30%) with the recommended values.

D2. $C_2H_5 + O_2$. A relative rate study by Kaiser et al. [136] yields $k_\infty = (9.2 \pm 0.9) \times 10^{-12}$ cm^3 $molecule^{-1}s^{-1}$ and $k_o = (6.5 \pm 2.0) \times 10^{-29}$ cm^6 $molecule^{-2}s^{-1}$ in He at 298 K and pressures between 3 and 1500 Torr. Their k_∞ agrees with the value calculated by Wagner et al. [269] ($k_\infty = 7 \times 10^{-12}$ cm^3 $molecule^{-1}s^{-1}$) using variational RRKM theory. The extrapolation to the low-pressure limit is difficult due to the complex potential energy surface, but agrees with a Patrick and Golden–type calculation [211] using $\Delta H^o_o = 32.4$ kcal mol^{-1}. The recommended values use the calculated temperature dependence and a 2.5 times higher rate constant for air as the bath gas.

D3. $OH + C_2H_2$. The rate constant for this complex process has been re-examined by Smith et al. [249] in the temperature range from 228 to 1400 K, and in the pressure range 1 to 760 Torr. Their analysis, which is cast in similar terms to those used here, is the source of the rate constants and temperature dependences at both limits. The negative value of m reflects the fact that their analysis includes a 1.2 kcal/mol barrier for the addition of OH to C_2H_2. The data analyzed include those of Pastrana and Carr [210], Perry et al. [213], Michael et al. [181], and Perry and Williamson [214]. Other data of Wilson and Westenberg [285], Breen and Glass [35], Smith and Zellner [252], and Davis et al. [79] were not included. Studies by Liu et al. [168] and Lai et al. [155] are in general agreement with the recommendation. Calculations of k_o via the methods of Patrick and Golden [211] yield values compatible with those of Smith et al. [249].

D4. $OH + C_2H_4$. Experimental data of Tully [262], Davis et al. [79], Howard [122], Greiner [109], Morris et al. [186], and Overend and Paraskevopoulos [200] in helium, Atkinson et al. [17] in argon, and Lloyd et al. [169] and Cox [64] and Klein et al. [146] in nitrogen/oxygen mixtures, have been considered in the evaluation. This well–studied reaction is considerably more complex than most others in this table. The parameters recommended here fit exactly the same curve proposed by Klein et al. [146] at 298 K. Discrepancies remain and the effect of multiple product channels is not well understood. Kuo and Lee [150] report very strong temperature dependence for the low-pressure limit (n=4). Calculations of the type in Patrick and Golden [211] yield the recommended value. The high-pressure limit temperature dependence has been determined by several workers. Almost all obtain negative activation energies, the Zellner and Lorenz [298] value being equivalent to m = +0.8 over the range ($296<T/K<524$) at about 1 atmosphere. Although this could theoretically arise as a result of reversibility, the equilibrium constant is too high for this possibility. If there is a product channel that proceeds with a low barrier via a tight transition state, a complex rate constant may yield the observed behavior.

The actual addition process (OH + C_2H_4) may even have a small positive barrier. The recommended limits encompass the reported values. A new high temperature measurement has been reported by Diau and Lee [84].

D5. CH_3O + NO. The recommended values are taken from the results of Frost and Smith [103] in argon. Temperature dependences are from their higher temperature results. The low pressure rate constant is consistent with the measurement of McCaulley et al. [179] and Daele et al. [73] in helium and half the value from Troe–type calculations. A bimolecular (chemical activation) path also exists, forming HNO + CH_2O (Frost and Smith [103]). Studies by Ohmori et al. [195] and Dobé et al. [86] are in general agreement with Frost and Smith with respect to both the addition and bimolecular pathways. (See the note in Table 1-1 for the bimolecular pathway.)

D6. CH_3O + NO_2. The recommended values are from the work of Wollenhaupt and Crowley [289]. Agreement is good with earlier work at 298 K from the study of Frost and Smith [102] in argon (corrected by Frost and Smith [104] and that of Biggs et al [28] in He. Low pressure results agree within a factor of two with the measurements of McCaulley et al. [178] in helium. A minor bimolecular (chemical activation) pathway is also observed. (See Table 1-1.)

D7 C_2H_5O + NO. High-pressure data at 298 K in Ar from Frost and Smith [103] and low-pressure measurements in He by Daele et el. [74] are scaled to N_2 and fit with an expression summing the bimolecular and termolecular channels. The low pressure value agrees with theory. The bimolecular channel with an estimated rate of about 10^{-12} needs to be verified by direct studies. The temperature dependence is estimated.

D8. C_2H_5O + NO_2. High-pressure rate constant at 298 K from Frost and Smith [102]. Other values estimated from similar reactions.

D9. CH_3O_2 + NO_2. Parameters from a reasonable fit to the temperature- and pressure-dependent data in Sander and Watson [235] and Ravishankara et al. [221]. These references report $F_c = 0.4$, and their parameters are a somewhat better fit at all temperatures than those recommended here. We do not adopt them since they are not much better in the stratospheric range, and they would require both a change in our $F_c = 0.6$ format and the adoption of a quite large negative activation energy for k_∞. A study of the reverse reaction by Zabel et al. [295] also uses $F_c = 0.4$. The values recommended herein, taken with the value of the equilibrium constant in Table 3-1, fit the data in Zabel et al. [295] very well. Destriau and Troe [83] have fit the above data with k_∞ independent of temperature and $F_c = 0.36$. Bridier et al. [37] are in good agreement with this recommendation at one atmosphere and 298 K.

D10. $C_2H_5O_2$ + NO_2. The only experimental study is that of Elfers et al. [91] who measured the rate constant relative to the $C_2H_5O_2$ + NO reaction between 10 and 1000 mbar. Elfers et al. used a value of $k = 8.9 \times 10^{-12}$ cm^3 molecule^{-1} s^{-1} for the reference reaction. By comparison the recommended rate constant for the reference reaction from Table 1-1 of this evaluation is 1.1×10^{-11} cm^3 molecule^{-1} s^{-1} at 254 K. There are three data points. An evaluation of the Elfers et al. work by Destriau and Troe [83] cast the data in the format used in the IUPAC evaluation [14]. The parameters in Table 2–1 are adjusted to agree with the data corrected for the change in the reference reaction, using the simpler formula employed in this recommendation.

D11. $CH_3C(O)O_2$ + NO_2. The recommended parameters are from the data of Bridier et al. [36], who report in the format represented here, but using $F_c = 0.3$. Their values are: $k_o^{300} = (2.7 \pm 1.5) \times 10^{-28}$, $k_\infty^{300} = (12.1 \pm 2.0) \times 10^{-12}$, with n = 7.1 ± 1.7 and m= 0.9 ± 0.15. Studies of the decomposition of $CH_3C(O)O_2NO_2$ [PAN] by Roberts and Bertman [226], Grosjean et al. [110], and Orlando et al. [198] are in accord with Bridier et al. [36]. In the former study it was shown that PAN decomposition yields only peroxyacetyl radical and NO_2; no methyl nitrate.

D12. $CH_3CH_2C(O)O_2$ + NO_2. This reaction, forming peroxypropionyl nitrate (PPN), has been studied in the reverse direction by Schurath and Wipprecht [238], Mineshos and Glavas [182], Grosjean et al. [110] and Kirchner et al. [144]. The measured values are very similar to those for $CH_3C(O)O_2$ + NO_2 forming peroxyacetyl nitrate (PAN). Group additivity considerations indicate that the equilibrium constant for both PAN and PPN will be the same (both sides of the equilibrium for PPN differ from those for PAN by the group C-(C)(CO)$(H)_2$.) Therefore, the recommended value for the association reaction is taken from the decomposition studies multiplied by the same equilibrium constant as for PAN. Conservative error limits are estimated.

D13. CH_3COCH_2 + O_2. Cox et al. [69] reported a value of $k = (1.5 +/- 0.3) \times 10^{-12}$ cm^3 molecule^{-1}s^{-1} at 298 K and 1 atm of SF_6 in which a pulse radiolysis study was modeled. This should be close to the high-pressure limit, but Cox et al point out that it is a bit low. (Using group additivity to calculate the entropy change yields about $10^{14.3}$ s^{-1} for the decomposition A-factor. This compares with almost 10^{15} s^{-1} for $C_2H_5O_2$ decomposition.)

E1. $F + O_2$. A study by Pagsberg et al. [206] reports k_o in argon = 4.38×10^{-33} $(T/300)^{-1.2}$. This is in good agreement with earlier values of Smith and Wrigley [251], Smith and Wrigley [250], Shamonina and Kotov [241], Arutyunov et al. [9] and slightly lower than the values of Chen et al. [54] and Chegodaev et al. [53]. Wallington and Nielsen [278], Wallington et al. [277] and Ellerman et al. [92] confirm the value of Pagsberg et al. [206]. Lyman and Holland [172] report a slightly lower value in Ar at 298K. We assume that $\beta_{Ar} = \beta_{N_2}$ at all temperatures. Pagsberg et al. [206], also determined the equilibrium constant and thus ΔH_f (FO_2). See $F + O_2$, Table 2–1. A calculation such as described in Patrick and Golden [211], using the new value yields: $k_o = 1.06 \times 10^{-33}$ $(T/300)^{-1.5}$ using $\beta_{N2} = 0.3$ (i.e., $\langle\Delta E\rangle = 2$ kJ mol^{-1}). This is not good agreement.

E2. F + NO. A study by Pagsberg et al [203], taking into account data from Zetzsch [299], Skolnik et al. [246], Kim et al. [142], Pagsberg et al. [205] and Wallington et al. [275], reports rate constants for this reaction in several bath gases. Converting their values to the form used in this compilation yields the recommended parameters.

E3. $F + NO_2$. A study by Pagsberg et al. [204], taking into account the experimental data of Fasano and Nogar [95] and Zetzsch [299], was used to determine both the high and low pressure limits at 300 K. Converting their values to the form used in this compilation yields the recommended parameters. Treatment of the data for this system requires knowledge of the relative stabilities of FNO_2 and FONO. Patrick and Golden [211] assumed that the difference between these would be the same as between the $ClNO_2$ isomers. Theoretical work by Dixon and Christie [85], Lee and Rice [159] and Amos et al. [3] indicates that FNO_2 is 35–40 kcal mol^{-1} more stable than FONO, and therefore the measured rate refers to FNO_2 formation. The value of n = 2 is from Patrick and Golden, but consistent with Pagsberg et al. The value of m is a rough estimate from similar reactions, but is also consistent with Pagsberg et al.

E4. $FO + NO_2$. Low pressure limit from strong collision calculation and $\beta = 0.33$. T dependence from resultant $\langle\Delta E\rangle = 0.523$ kcal mol^{-1}, high-pressure limit and T dependence estimated. A theoretical study by Rayez and Destriau [225] indicates that the product is the single isomer $FONO_2$. Bedzhanyan et al. [27] report a value extracted from a complex mixture of bath gases.

E5. $CF_3 + O_2$. Caralp et al. [49] have measured the rate constant in N_2 between 1 and 10 Torr. This supplants the value from Caralp and Lesclaux [48]. Kaiser et al. [137] have extended the pressure range to 580 Torr. They both recommend different parameters, but the data are well represented by the currently recommended values. Data of Ryan and Plumb [229] are in agreement.

E6. $CF_3O + NO_2$. Fockenberg et al. [98] report values in nitrogen with 250<T/K<302 and 7<p/mbar<107. They report large error limits. Their values, including two sigma errors, using the previous format are: $k_0 = (3.1 \pm 3.0)\times10^{-28}$; n = (2.0 ± 2.0) $k_\infty = (1.5 \pm 0.5)\times10^{-28}$; m = (2.8 ± 2.0). The reaction products agree with those reported by Chen et al. [55], who used photolysis of CF_3NO to prepare CF_3O_2 and subsequently CF_3O in 700 Torr of air at 297 + 2 K. They considered two product channels: (a) CF_3ONO_2 obtained via three–body recombination and (b) $CF_2O + FNO_2$ obtained via fluorine transfer. Both products were observed and found to be thermally stable in their reactor. They report $k_a/(k_a+k_b) > 90\%$ and $k_b/(k_a+k_b) < 10\%$, thus the formation of CF_3ONO_2 is the dominant channel at 700 Torr and 297 K.

E7. $CF_3O_2 + NO_2$. Based on experiments in O_2 of Caralp et al. [50], who suggest a somewhat different fitting procedure, but the values recommended here fit the data just as well. Destriau and Troe [83] use yet a different fitting procedure that does not represent the data quite as well as that recommended here. Reverse rate data are given by Köppenkastrop and Zabel [148].

E8. $CF_3O + CO$. Values taken from Turnipseed et al. [263]. The numbers were obtained for Ar as the bath gas and are assumed to hold for N_2 as well. The temperature dependence of the high-pressure rate constant was determined over the range 233<T/K<332 in SF_6. No temperature dependence of the low-pressure-limiting rate constant was reported. Wallington and Ball [273] report values in good agreement with Turnipseed et al.

E9. $CF_3O + M$. The activation energy for thermal decomposition of CF_3O to $CF_2O + F$ has been reported to be 31 kcal mol^{-1} by Kennedy and Levy [141]. Thermochemical data yield $\Delta H^o(298) = 23$ kcal mol^{-1}. This implies an intrinsic barrier of about 8 kcal mol^{-1} to elimination of F from CF_3O. Electronic structure calculations by Li and Francisco [166] support this observation. Adopting the A-factor for unimolecular dissociation, $A = 3 \times 10^{14}$ s^{-1} and E = 31 kcal mol^{-1} from Kennedy and Levy, k_∞ (298 K) is about 6×10^{-9}s^{-1}. This corresponds to a lifetime of about 6 years; therefore, thermal decomposition of CF_3O is unimportant throughout the atmosphere.

F1. $Cl + O_2$. Nicovich et al. [189] measure $k_o = (9 \pm 3)$ 10^{-33} cm^6 molecule^{-2}s^{-1} at T = 187 ± 6 K in O_2. Using the methods described in Patrick and Golden [211], but adjusting the thermochemistry of ClO_2 such that

$S^o_{298\,K}$ = 64.3 cal mol^{-1} K^{-1} and $\Delta H_{f,298}$ = 23.3 ± 0.6 kcal mol^{-1} (Cl + O_2, Table 3), we calculate $k_o = 5.4 \times 10^{-33}$ cm^6 molecule^{-2} s^{-1} at T = 185 K. The collisional efficiency of the bath gas is taken from the formula $[\beta/(1-\beta^{1/2})] = \langle\Delta E\rangle/F_E kT$ and $\langle\Delta E\rangle \sim 0.5$ kcal mol^{-1} (i.e., $\beta_{185} = 0.42$ and $\beta_{300} = 0.30$). Since O_2 may be particularly efficient for this process, we use this calculation with broader error limits. The value from the calculation at 300 K (i.e., 2.7×10^{-33} cm^6 molecules^{-2} s^{-1}) compares with an older value of Nicholas and Norrish [187] of 1.7×10^{-33} in an $N_2 + O_2$ mixture. The temperature dependence is from the calculation. Baer et al. [18] report a value at 298 K in good agreement with the value recommended here, but the temperature dependence is strikingly different, as noted by the authors.

F2. Cl + NO. Low-pressure limit is from Lee et al. [158], Clark et al. [57], Ashmore and Spencer [10], and Ravishankara et al. [222]. Temperature dependence is from Lee et al. [158] and Clark et al. [57].

F3. Cl + NO_2. Low-pressure limit and T dependence from Leu [164]. (Assuming similar T dependence in N_2 and He.) Leu [164] confirms the observation of Niki et al. [192] that both ClONO and $ClNO_2$ are formed, with the former dominating. This has been explained by Chang et al. [52], with detailed calculations in Patrick and Golden [211]. The temperature dependence is as predicted in Patrick and Golden [211]. Leu's results are in excellent agreement with those reported in Ravishankara et al. [223]. The latter work extends to 200 Torr, and the high-pressure limit was chosen to fit these measurements. The temperature dependence of the high-pressure limit is estimated. A turbulent flow study by Seeley et al. [239] that extends results to 250 Torr of Ar is in agreement with earlier work.

F4. Cl + CO. From Nicovich et al. [190], who measured the process in N_2 for 185 ≤ T/K ≤ 260.

F5. Cl + C_2H_2. The recommended values are taken from the work of Kaiser [133] and Kaiser and Wallington [132], which extends the pressure range to 0.3–6000 Torr. The data are in reasonable agreement with earlier measurements of Brunning and Stief [40] and Wallington et al. [271], although the derived temperature dependence is much less than obtained by Brunning and Stief [40]. These values are compatible with earlier studies of Poulet et al. [219], Atkinson and Aschmann [12], Lee and Rowland [157] and Wallington et al. [279]. Using FTIR, Zhu et al. [300] reported branching of 16% and 84% to the trans and cis adduct isomers, respectively, at 700 Torr N_2 and 295 K.

F6. Cl + C_2H_4. Values at 300K are from a relative rate study by Wallington et al. [271]. A relative rate study by Kaiser and Wallington [132] extends the pressure range to 0.3–6000 Torr and is compatible with earlier studies. Temperature dependence of k_o is taken from Kaiser and Wallington [135]. The temperature dependence of k_∞ is estimated. Values are in reasonable agreement with studies by Maricq et al. [175], Lee and Rowland [157], Iyer et al. [129], Atkinson and Aschmann [12], Atkinson and Aschmann [13] and Wallington et al. [280]. A study in He by Stutz et al. [255] is noted, as is a comment on it by Kaiser and Wallington [135]. Knyasev et al. [147] have done an extensive experimental and theoretical analysis. Their values agree with this recommendation.

F7 Cl + C_2Cl_4. Recommendation is from the flash-photolysis study of Nicovich et al. [191] done at 231–390 K in 3–700 Torr N_2. A study by Thuner et al. is in agreement [257].

F8. ClO + NO_2. The low-pressure-limit recommendation and uncertainties are based on temperature-dependent values from Zahniser et al. [296], Lee et al. [161], Birks et al. [31], Leu et al. [165], Wallington and Cox [274], Cox et al. [65] and Molina et al. [183]. All of these data were collected in N_2 bath gas, except for several points from Lee et al. [161] collected in O_2.

The high-pressure-limit recommendation is based on the RRKM calculations of Smith and Golden . There are several pressure-dependent data sets in the literature, such as Percival et al. [212], Handwerk and Zellner [113], Dasch et al. [77] and Cox and Lewis [68]; however, they are too disparate to extract unambiguous values. These data are all reproduced within two-sigma error limits by the current recommendation.

F9. OClO + NO_3. Friedl et al. [101], studied this system at 1 ≤ P/Torr ≤ 5 for helium and 220 ≤ T/K ≤ 298. They deduced values for the rate constant consistent with their data of $k_o \approx 10^{-31}$ and $k_\infty \approx 10^{-11}$. They also suggest a value for the equilibrium constant: K/cm^3 molecule^{-1} = 1×10^{-28} exp (9300/T). However, Boyd et al. [34] have raised the question of possible heterogeneous effects in this system, and further work is needed.

F10. ClO + ClO. The recommendation is based on a simultaneous fit to data from Bloss et al. (183–245 K) [33], (which supersedes earlier work of Sander et al. (194–247 K) [231]), Nickolaisen et al. (260–390 K) [188] and Trolier et al. (200–263 K) [261]. The latter data have been corrected for the effect of Cl_2 as third body, as suggested by Nickolaisen et al. With this adjustment all the data are in reasonable agreement. Error limits are from the statistical fit. The k_o value for N_2 is not in accord with a Patrick and Golden–type calculation [211].

This may be due to uncertainty in the ClOOCl thermochemistry, which is based on the equilibrium constants reported by Nickolaisen et al. and Cox and Hayman [67] (See Table 3.). Other previous rate constant measurements, such as those of Hayman et al. [116], Cox and Derwent [66], Basco and Hunt [22], Walker [270], and Johnston et al. [131], range from $1–5 \times 10^{-32}$ cm^6 s^{-1}, with N_2 or O_2 as third bodies. The major dimerization product is chlorine peroxide (Birk et al. [30], DeMore and Tschuikow-Roux [82], Slanina and Uhlik [247], Stanton et al. [253] and Lee et al. [160]).

F11. ClO + OClO. Data are from Burkholder et al. [43], who measured the rate constant in N_2 at $200 \leq T/K \leq 260$ and densities from $(1.1–10.9) \times 10^{18}$ molecules cm^{-3}. They also measured the equilibrium constant. Parr et al. [208] also report a value for the rate constant in reasonable agreement with the recommendation.

F12. O + OClO. The recommendation is based on data of Colussi et al. [61] and Colussi [60], who measured the pressure dependence between 248 and 312 K. Their results are consistent with calculations. A zero-pressure rate constant of
$(1.6 \pm 0.4) \times 10^{-13}$ cm^3 s^{-1} is reported for the chemical activation channel producing ClO + O_2, and their value of $\Delta H_f^o(ClO_3)$ = 52 kcal mol^{-1} is derived at 298 K. A low-pressure study by Gleason et al. [107] suggests a direct abstraction as well. See Table 1-1.

F13. $CH_2Cl + O_2$. Measured by Fenter et al. [96] over the range $298 \leq T/K \leq 448$ and $1 \leq P/Torr \leq 760$ in nitrogen. Two different techniques were employed: laser photolysis/photoionization mass spectrometry in the range 1–10 Torr and laser photolysis/UV absorption for the range 20–760 Torr. A study by Bilde et al. [29] in N_2 relative to the reaction $CH_2Cl + Cl_2 \rightarrow CH_2Cl_2 + Cl$ is in excellent agreement.

F14. $CHCl_2 + O_2$. Measured by Fenter et al. [96] over the range $298 \leq T/K \leq 383$ and $1 \leq P/Torr \leq 760$ in nitrogen. Two different techniques were employed: laser photolysis/photoionization mass spectrometry in the range 1–10 Torr and laser photolysis/UV absorption for the range 20–760 Torr. A study by Nottingham et al. [194], in He, is in agreement.

F15. $CCl_3 + O_2$. The recommendation incorporates studies by Fenter et al. [97], Danis et al. [76] and Luther et al. [171]. Experimental data of Ryan and Plumb [230] have been considered in the evaluation. A study by Nottingham et al. [194], in He, is in agreement. A Patrick and Golden–type calculation using the thermochemistry of Russell et al. [228] yields $k_0^{300} = 1.5 \times 10^{-30}$, with $\beta = 0.3$. A value of $k_\infty^{300} = 5 \times 10^{-12}$ has been reported by Cooper et al. [63]. The value of the high-pressure-limiting rate constant recommended here is slightly below that of Luther et al., but within their error limits. If we use their value the fit to lower-pressure data in the atmospherically important regions is less good.

F16. $CFCl_2 + O_2$. Values for both low- and high-pressure limits at 300 K are from Caralp and Lesclaux [48]. Temperature dependences are rough estimates based on calculations and similar reactions.

F17. $CF_2Cl + O_2$. Values estimated from other reactions in this series.

F18. $CCl_3O_2 + NO_2$. Based on experiments in O_2 of Caralp et al. [50], who suggest a somewhat different fitting procedure, but the values recommended here fit the data as well. Destriau and Troe [83] use yet a different fitting procedure that does not represent the data quite as well as that recommended herein. Reverse rate data are given by Köppenkastrop and Zabel [148].

F19. $CFCl_2O_2 + NO_2$. Based on experiments in O_2 of Caralp et al. [50], who suggest a somewhat different fitting procedure, but the values recommended here fit the data as well. Destriau and Troe [83] use yet a different fitting procedure that does not represent the data quite as well as that recommended herein. Reverse rate data are given by Köppenkastrop and Zabel [148].

F20. $CF_2ClO_2 + NO_2$. A study by Wu and Carr [291] supersedes the earlier work of Moore and Carr [184] and is recommended here. Reverse rate data are given by Köppenkastrop and Zabel [148] and Xiong and Carr [292].

G1. Br+NO_2. The recommended values are from a study by Kreutter et al. [149]. Their k_o value agrees with the measurement of Mellouki et al. [180] at 300 K. A Patrick-and-Golden-type calculation using the known structure of the more stable $BrNO_2$ isomer and the measured equilibrium by Kreutter et al. [149] underpredicts k_o by an order of magnitude. Participation by other electronic states and isomers such as BrONO as suggested in JPL 97-4, in keeping with the chlorine analog, has been shown in studies by Broske and Zabel [38] and Orlando and Burkholder [196].

G2. BrO + NO_2. Values from a study by Thorn et al. [256] that is in excellent agreement with Sander et al. [234] are recommended. Error limits are from a reanalysis of the data. Danis et al. [75] give slightly lower values for the

low-pressure-limiting rate constant and a smaller temperature dependence as well. This latter study may be hampered by heterogeneous effects. A theoretical study by Rayez and Destriau [225] suggests that the bond-dissociation energy in $BrONO_2$ is higher than that in $ClONO_2$, thus rationalizing the relative values of the low-pressure-limiting rate constants for these two processes. This is confirmed by a more detailed study by Parthiban and Lee. [209] as well as by Orlando and Tyndall [197], who measured $BrONO_2$ decomposition and thus an equilibrium constant.

H1. I + NO. Evaluation taken from IUPAC [128]. The data is from van den Bergh et al. [264] and Basco and Hunt [21]. Although IUPAC recommends $F_c = 0.75$, any differences will be insignificant, since this reaction is in the low pressure limit under atmospheric conditions.

H2. I + NO_2. Evaluation taken from IUPAC [128]. The data is from van den Bergh et al. [264], Mellouki et al. [180], Buben et al. [41] and van den Bergh and Troe [265]. IUPAC uses $F_c = 0.63$, which is the same as the universal value adopted here of $F_c = 0.6$. (No evidence of possible isomers [INO_2 or IONO] is reported.)

H3. IO + NO_2. Data taken from Daykin and Wine [81]. They suggest $k_o = 7.7 \times 10^{-31}$ $(T/300)^{-5.0}$, $k_\infty = 1.5 \times 10^{-11}$ and $F_c = 0.4$. The values recommended here fit the data as well.

I1. HS + NO. Data and analysis are from the work of Black et al. [32]. The temperature dependence of k has been estimated.

I2. CH_3S + NO. The recommended values are from the study by Balla et al. [19] at 296K in nitrogen. Temperature dependences are derived from the higher temperature results of the same study.

I3 O + SO_2. The recommendation is taken from Atkinson et al. [15] and was transformed to the format used herein.

I4. OH + SO_2. Values of the rate constant as a function of pressure at 298 K are from Leu [163], Paraskevopoulos et al. [207], and Wine et al. [287]. The value of the low-pressure limit is from Leu [163], corrected for fall–off. The high-pressure limit is from a fit to all the data. The value of n comes from the above data combined with calculations such as those of Patrick and Golden [211], except that the heat of formation of $HOSO_2$ is raised by 4 kcal mol^{-1}, as suggested by the work of Margitan [173]. The value of m is estimated. This is not a radical–radical reaction and is unlikely to have a positive value of m. The limit of m = –2 corresponds to a real activation energy of ~1 kcal mol^{-1}. Earlier data listed in Baulch et al. [26] and Baulch et al. [25] are noted. Work of Martin et al. [177], Barnes et al. [20], and Lee et al. [162] confirm the current evaluation.

I5. CH_3SCH_2 + O_2 . Wallington et al. [276] have employed a pulse radiolysis technique, allowing the derivation of $k = 5.7 \pm 0.4 \times 10^{-12}$ in 992 mbar of SF_6 at room temperature.

I6 SO_3 + NH_3. Recommendation is from Lovejoy and Hanson [170], who studied this reaction from 10–400 Torr N_2 at 295 K. They observe that the adduct isomerizes rapidly to sulfamic acid and clusters efficiently with itself and sulfuric acid. Observed sulfamic acid dimerization rate constant exceeds 5×10^{-11}. Measurements of Shen et al. [243] made at 1–2 Torr He are much higher than those of Lovejoy and Hanson. Temperature dependences are rough estimates.

J1. Na + O_2. A study by Plane and Rajasekhar [217] finds $k_o = (2.9 \pm 0.7) \times 10^{-30}$ at 300 K with n = 1.30 ± .04. They also estimate k_∞ to be about $6 \times 10^{-10,}$ with a small positive temperature dependence. Another study by Helmer and Plane [117] yields $k_o = (3.1 \pm 0.2) \times 10^{-30}$ at 300 K with n = 1.52±0.27. The recommended values are taken from these studies. They are consistent with values measured by Marshall et al. [176] at 600 K and those measured by Vinckier et al. [268] at higher temperature. The k_o value is about 60% higher than that of Silver et al. [244].

J2. NaO + O_2. Ager and Howard [1] have measured the low- pressure limit at room temperature in several bath gases. Their value in N_2 is used in the recommendation. They performed a Troe calculation, as per Patrick and Golden [211], to obtain collision efficiency and temperature dependence. They obtained a high-pressure-limit rate constant by use of a simple model. The temperature dependence is estimated.

J3. NaO + CO_2. Ager and Howard [1] have measured the rate constant for this process in the "fall–off" regime. Their lowest pressures are very close to the low-pressure limit. The temperature dependence is an estimate. Ager and Howard calculate the high-pressure rate constant from a simple model.

J4. NaOH + CO_2. Ager and Howard [2] have measured the low-pressure-limiting rate constant. The temperature dependence is an estimate. Ager and Howard have calculated the high-pressure limit using a simple model.

2.8 References

1. Ager, J. W., III and C. J. Howard, 1986, Geophys. Res. Lett., **13**, 1395–1398.
2. Ager, J. W., III and C. J. Howard, 1987, J. Geophys. Res., **92**, 6675–6678.
3. Amos, R. D., C. W. Murray and N. C. Handy, 1993, Chem. Phys. Lett., **202**, 489–494.
4. Anastasi, C. and I. W. M. Smith, 1976, J. Chem. Soc. Faraday Trans. 2, **72**, 1459–1468.
5. Anastasi, C. and I. W. M. Smith, 1978, J. Chem. Soc. Faraday Trans. 2, **74**, 1056.
6. Anderson, J. G. and F. Kaufman, 1972, Chem. Phys. Lett., **16**, 375–379.
7. Anderson, J. G., J. J. Margitan and F. Kaufman, 1974, J. Chem. Phys., **60**, 3310.
8. Anderson, S. M., D. Hulsebusch and Mauersberger, 1997, J. Chem. Phys., **107**, 5385–5392.
9. Arutyunov, V. S., L. S. Popov and A. M. Chaikin, 1976, Kinet. Katal., **17**, 286.
10. Ashmore, P. G. and M. S. Spencer, 1959, Trans. Faraday Soc., **55**, 1868.
11. Atkinson, D. B. and M. A. Smith, 1994, J. Phys. Chem., **98**, 5797–5800.
12. Atkinson, R. and S. M. Aschmann, 1985, Int. J. Chem. Kinet., **17**, 33–41.
13. Atkinson, R. and S. M. Aschmann, 1987, Int. J. Chem. Kinet., **19**, 1097–1105.
14. Atkinson, R., D. L. Baulch, R. A. Cox, J. Hampson, R. F., J. A. Kerr, M. J. Rossi and J. Troe, 1997, J. Phys. Chem. Ref. Data, **26**, 1329–1499.
15. Atkinson, R., D. L. Baulch, R. A. Cox, R. F. Hampson, J. A. Kerr and J. Troe, 1992, J. Phys. Chem. Ref. Data, **21**, 1125–1568.
16. Atkinson, R., D. A. Hansen and J. N. Pitts, Jr., 1975, J. Chem. Phys., **62**, 3284–3288.
17. Atkinson, R., R. A. Perry and J. N. Pitts, Jr., 1977, J. Chem. Phys., **66**, 1197.
18. Baer, S., H. Hippler, R. Rahn, M. Siefke, N. Seitzinger and J. Troe, 1991, J. Chem. Phys., **95**, 6463–6470.
19. Balla, R. J., H. H. Nelson and J. R. McDonald, 1986, Chem. Phys., **109**, 101.
20. Barnes, I., V. Bastian, K. H. Becker, E. H. Fink and W. Nelsen, 1986, J. Atmos. Chem., **4**, 445–466.
21. Basco, N. and J. E. Hunt, 1978, Int. J. Chem Kinet., **10**, 733–743.
22. Basco, N. and J. E. Hunt, 1979, Int. J. Chem. Kinet., **11**, 649–664.
23. Basco, N., D. G. L. James and F. C. James, 1972, Int. J. Chem. Kinet. , **4**, 129.
24. Bates, R. W., D. M. Golden, R. K. Hanson and C. T. Bowman, 2001, Phys. Chem. Chem. Phys., **3**, 2337–2342.
25. Baulch, D. L., R. A. Cox, P. J. Crutzen, R. F. Hampson, Jr., J. A. Kerr, J. Troe and R. T. Watson, 1982, J. Phys. Chem. Ref. Data, **11**, 327–496.
26. Baulch, D. L., R. A. Cox, R. F. Hampson, Jr., J. A. Kerr, J. Troe and R. T. Watson, 1980, J. Phys. Chem. Ref. Data, **9**, 295–471.
27. Bedzhanyan, Y. R., E. M. Markin and Y. M. Gershenzon, 1993, Kinetics and Catalysis, **34**, 190–193.
28. Biggs, P., C. E. Canosa–Mas, J. M. Fracheboud, D. E. Shallcross, R. P. Wayne and F. Caralp, 1993, J. Chem. Soc. Faraday Trans., **89**, 4163–4169.
29. Bilde, M., J. Sehested, O. J. Nielsen, T. J. Wallington, R. J. Meagher, M. E. McIntosh, C. A. Piety, J. M. Nicovich and P. H. Wine, 1997, J. Phys.Chem. A, **101**, 8035–8041.
30. Birk, M., R. R. Friedl, E. A. Cohen, H. M. Pickett and S. P. Sander, 1989, J. Chem. Phys., **91**, 6588–6597.
31. Birks, J. W., B. Shoemaker, T. J. Leck, R. A. Borders and L. J. Hart, 1977, J. Chem. Phys., **66**, 4591–4599.
32. Black, G., R. Patrick, L. E. Jusinski and T. G. Slanger, 1984, J. Chem. Phys., **80**, 4065.
33. Bloss, W. J., S. L. Nickolaisen, R. J. Salawitch, R. R. Friedl and S. P. Sander, 2001, J. Phys. Chem. A, **105**, 11226–11239.
34. Boyd, A. A., G. Marston and R. P. Wayne, 1996, J. Phys. Chem., **100**, 130–137.
35. Breen, J. E. and G. P. Glass, 1971, Int. J. Chem. Kinet., **3**, 145.
36. Bridier, I., F. Caralp, H. Loirat, R. Lesclaux, B. Veyret, K. H. Becker, A. Reimer and F. Zabel, 1991, J. Phys. Chem., **95**, 3594–3600.
37. Bridier, I., R. Lesclaux and B. Veyret, 1992, Chem. Phys. Lett., **191**, 259–263.
38. Broske, R. and F. Zabel, 1998, J. Phys.Chem. A, **102**, 8626–8631.
39. Brown, S. S., R. K. Talukdar and A. R. Ravishankara, 1999, Chem. Phys. Lett., **299**, 277–284.
40. Brunning, J. and L. J. Stief, 1985, J. Chem. Phys., **83**, 1005–1009.
41. Buben, S. N., I. K. Larin, N. A. Messineva and E. M. Trofimova, 1990, Kinetika i Kataliz, **31**, 973.
42. Burkholder, J. B., P. D. Hammer and C. J. Howard, 1987, J. Phys. Chem., **91**, 2136–2144.
43. Burkholder, J. B., R. L. Mauldin, R. J. Yokelson, S. Solomon and A. R. Ravishankara, 1993, J. Phys. Chem., **97**, 7597–7605.
44. Burkholder, J. B. and A. R. Ravishankara, 2000, J. Phys. Chem. A, **104**, 6752–6757.
45. Burrows, J. P., G. S. Tyndall and G. K. Moortgat, 1985, J. Phys. Chem., **89**, 4848–4856.

46. Burrows, J. P., T. J. Wallington and R. P. Wayne, 1983, J. Chem. Soc. Faraday Trans. 2, **79**, 111–122.
47. Cantrell, C. A., R. E. Shetter, J. G. Calvert, G. S. Tyndall and J. J. Orlando, 1993, J. Phys. Chem., **97**, 9141–9148.
48. Caralp, F. and R. Lesclaux, 1983, Chem. Phys. Lett., **102**, 54–58.
49. Caralp, F., R. Lesclaux and A. M. Dognon, 1986, Chem. Phys. Lett., **129**, 433–438.
50. Caralp, F., R. Lesclaux, M. T. Rayez, J.–C. Rayez and W. Forst, 1988, J. Chem. Soc. Faraday Trans. 2, **84**, 569–585.
51. Carleton, K. J., W. J. Kessler and W. J. Marinelli, 1993, J. Phys. Chem., **97**, 6412–6417.
52. Chang, J. S., A. C. Baldwin and D. M. Golden, 1979, Chem. Phys., **71**, 2021.
53. Chegodaev, P. P. and V. I. Tubikov, 1973, Dokl. Akad. Nauk. SSSR, **210**, 647.
54. Chen, H. L., D. W. Trainor, R. E. Center and W. T. Fyfe, 1977, J. Chem. Phys., **66**, 5513.
55. Chen, J., V. Young, T. Zhu and H. Niki, 1993, J. Phys. Chem., **97**, 11696–11698.
56. Christensen, L. E., B. Laszlo, C. E. Miller, J. J. Sloan, M. Okumura and S. P. Sander, 2002, to be submitted.
57. Clark, T. C., M. A. A. Clyne and D. H. Stedman, 1966, Trans. Faraday Soc., **62**, 3354.
58. Cobos, C. J., H. Hippler, K. Luther, A. R. Ravishankara and J. Troe, 1985, J. Phys. Chem., **89**, 4332–4338.
59. Cobos, C. J., H. Hippler and J. Troe, 1985, J. Phys. Chem., **89**, 342–349.
60. Colussi, A. J., 1990, J. Phys. Chem., **94**, 8922–8926.
61. Colussi, A. J., S. P. Sander and R. R. Friedl, 1992, J. Phys.Chem., **96**, 4442–4445.
62. Connell, P. S. and H. S. Johnston, 1979, Geophys. Res. Lett., **6**, 553–556.
63. Cooper, R., J. B. Cumming, S. Gordon and W. A. Mulac, 1980, Radiat. Phys. Chem., **16**, 169.
64. Cox, R. A., 1975, Int. J. Chem. Kinet. Symp., **1**, 379.
65. Cox, R. A., J. P. Burrows and G. B. Coker, 1984, Int. J. Chem. Kinet., **16**, 445–67.
66. Cox, R. A. and R. G. Derwent, 1979, J. Chem. Soc. Far. Trans. 1, **75**, 1635–1647.
67. Cox, R. A. and G. D. Hayman, 1988, Nature, **332**, 796–800.
68. Cox, R. A. and R. Lewis, 1979, J. Chem. Soc. Faraday Trans. 1, **75**, 2649–2661.
69. Cox, R. A., J. Munk, O. J. Nielsen, P. Pagsberg and E. Ratajczak, 1990, Chem. Phys. Lett., **173**, 206–210.
70. Cox, R. A. and R. Patrick, 1979, Int. J. Chem. Kinet., **11**, 635.
71. Croce de Cobos, A. E., H. Hippler and J. Troe, 1984, J. Phys. Chem., **88**, 5083–5086.
72. Croce de Cobos, A. E. and J. Troe, 1984, Int. J. Chem. Kinet., **16**, 1519–1530.
73. Daele, V., G. Laverdet, G. Le Bras and G. Poulet, 1995, J. Phys. Chem., **99**, 1470–1477.
74. Daele, V., A. Ray, I. Vassali, G. Poulet and G. Le Bras, 1995, Int. J. Chem. Kinet., **27**, 1121–1133.
75. Danis, F., F. Caralp, J. Masanet and R. Lesclaux, 1990, Chem. Phys. Lett., **167**, 450.
76. Danis, F., F. Caralp, M. Rayez and R. Lesclaux, 1991, J. Phys. Chem., **95**, 7300–7307.
77. Dasch, W., K.–H. Sternberg and R. N. Schindler, 1981, Ber. Bunsenges. Phys. Chem., **85**, 611–615.
78. Davidson, J. A., C. A. Cantrell, R. E. Shetter, A. H. McDaniel and J. G. Calvert, 1990, J. Geophys. Res., **95**, 13963–13969.
79. Davis, D. D., S. Fischer, R. Schiff, R. T. Watson and W. Bollinger, 1975, J. Chem. Phys., **63**, 1707.
80. Davis, H. F., B. Kim, H. S. Johnston and Y. T. Lee, 1993, J. Phys. Chem., **97**, 2172–2180.
81. Daykin, E. P. and P. H. Wine, 1990, J. Phys. Chem. , **94**, 4528–4535.
82. DeMore, W. B. and E. Tschuikow–Roux, 1990, J. Phys. Chem., **94**, 5856–5860.
83. Destriau, M. and J. Troe, 1990, Int. J. Chem. Kinet., **22**, 915–934.
84. Diau, E. W.–G. and Y.–P. Lee, 1992, J. Chem. Phys., **96**, 377–386.
85. Dixon, D. A. and K. O. Christie, 1992, J. Phys. Chem., **95**, 1018–1021.
86. Dobe, S., G. Lendvay, I. Szilagyi and T. Berces, 1994, Int. J. Chem. Kinet., **26**, 887–901.
87. Donahue, N., personal communication.
88. Donahue, N. M., M. K. Dubey, R. Mohrschladt, K. Demerjian and J. G. Anderson, 1997, J. Geophys. Res., **102**, 6159–6168.
89. D'Ottone, L., P. Campuzano–Jost, D. Bauer and A. J. Hynes, 2001, J. Phys. Chem. A, **105**, 10538–10543.
90. Dransfield, T. J., K. K. Perkins, N. M. Donahue, J. G. Anderson, M. M. Sprengnether and K. Demerjian, 1999, Geophys. Res. Lett., **26**, 687–690.
91. Elfers, G., F. Zabel and K. H. Becker, 1990, chem. Phys. Lett., **168**, 14–19.
92. Ellerman, T., J. Sehested, O. J. Nielson, P. Pagsberg and T. J. Wallington, 1994, Chem. Phys. Lett., **218**, 287–294.
93. Erler, K., D. Field, R. Zellner and I. W. M. Smith, 1977, Ber. Bunsenges. Phys. Chem., **81**, 22.
94. Fagerstrom, K., A. Lund, G. Mahmound, J. T. Jodkowski and E. Ratajczak, 1994, Chem. Phys. Lett., **224**, 43–50.
95. Fasano, D. M. and N. S. Nogar, 1983, J. Chem. Phys., **78**, 6688–6694.

96. Fenter, F. F., P. D. Lightfoot, F. Caralp, R. Lesclaux, J. T. Niranen and D. Gutman, 1993, J. Phys. Chem., **97**, 4695–4703.
97. Fenter, F. F., P. D. Lightfoot, J. T. Niranen and D. Gutman, 1993, J. Phys. Chem., **97**, 5313–5320.
98. Fockenberg, C., H. Somnitz, G. Bednarek and R. Zellner, 1997, Ber. Bunsenges. Phys. Chem., **101**, 1411–1420.
99. Forster, R., M. Frost, D. Fulle, H. F. Hamann, H. Hippler, Schlepegreli and J. Troe, 1995, J. Chem. Phys., **103**, 2949–2958.
100. Fowles, M., D. N. Mitchell, J. W. L. Morgan and R. P. Wayne, 1982, J. Chem. Soc. Faraday Trans. 2, **78**, 1239–1248.
101. Friedl, R. R., S. P. Sander and Y. L. Yung, 1992, J. Phys. Chem., **96**, 7490–7493.
102. Frost, M. J. and I. W. M. Smith, 1990, J. Chem. Soc. Farad. Trans., **86**, 1751–1756.
103. Frost, M. J. and I. W. M. Smith, 1990, J. Chem. Soc. Farad. Trans., **86**, 1757–1762.
104. Frost, M. J. and I. W. M. Smith, 1993, J. Chem. Soc. Faraday Trans, **89**, 4251.
105. Fulle, D., H. F. Hamann, H. Hippler and J. Troe, 1996, J. Chem. Phys., **105**, 1001–1006.
106. Fulle, D. H., H. F. Hamann, H. Hippler and J. Troe, 1998, J. Chem. Phys., **108**, 5391–5397.
107. Gleason, J. F., F. L. Nesbitt and L. J. Stief, 1994, J. Phys. Chem., **98**, 126–131.
108. Golden, D. M. and J. P. Smith, 2000, J. Phys. Chem. A, **104**, 3991–3997.
109. Greiner, N. R., 1970, J. Chem. Phys., **53**, 1284–1285.
110. Grosjean, D., E. Grosjean and E. L. Williams, 1994, J. Air and Waste Manage. Assoc., **44**, 391–396.
111. Gross, A. and G. D. Billing, 1997, Chem. Phys., **217**, 1–18.
112. Hahn, J., K. Luther and J. Troe, 2000, Phys. Chem. Chem. Phys., **2**, 5098–5104.
113. Handwerk, V. and R. Zellner, 1984, Ber. Bunsenges. Phys. Chem., **88**, 405.
114. Harris, G. W. and R. P. Wayne, 1975, J. Chem. Soc. Faraday Trans. 1, **71**, 610.
115. Hathorn, B. C. and R. A. Marcus, 2000, J. Chem. Phys., **113**, 9497–9509.
116. Hayman, G. D., J. M. Davies and R. A. Cox, 1986, Geophys. Res. Lett., **13**, 1347–1350.
117. Helmer, M. and J. M. C. Plane, 1993, J. Geophys. Res., **98**, 23207–23222.
118. Hippler, H., S. Nasterlack and F. Striebel, 2002, Phys. Chem. Chem. Phys., **4**, 2959–2964.
119. Hippler, H., R. Rahn and J. Troe, 1990, J. Chem. Phys., **93**, 6560.
120. Hippler, H., M. Siefke, H. Stark and J. Troe, 1999, Phys. Chem. Chem. Phys., **1**, 57–61.
121. Hochanadel, C. J., J. A. Ghormley, J. W. Boyle and P. J. Ogren, 1977, J. Phys. Chem., **81**, 3.
122. Howard, C. J., 1976, J. Chem. Phys., **65**, 4771.
123. Howard, C. J., 1977, J. Chem. Phys., **67**, 5258.
124. Howard, C. J. and K. M. Evenson, 1974, J. Chem. Phys., **61**, 1943.
125. Hsu, K. J., S. M. Anderson, J. L. Durant and F. Kaufman, 1989, J. Phys. Chem., **93**, 1018.
126. Hsu, K. J., J. L. Durant and F. Kaufman, 1987, J. Phys. Chem., **91**, 1895–1899.
127. Huie, R. E., J. T. Herron and D. D. Davis, 1972, J. Phys. Chem., **76**, 2653–2658.
128. IUPAC, 1992, J. Phys. Chem. Ref. Data, **21**, 1125–1568.
129. Iyer, R. S., P. J. Rogers and F. S. Rowland, 1983, J. Phys. Chem., **87**, 3799.
130. Johnston, H. S., C. A. Cantrell and J. G. Calvert, 1986, J. Geophys. Res., **91**, 5159–5172.
131. Johnston, H. S., E. D. Morris, Jr. and J. Van den Bogaerde, 1969, J. Am. Chem. Soc., **91**, 7712–7727.
132. Kaiser, E. W. and T. J. Wallington, 1996, J. Phys. Chem., **100**, 4111–4119.
133. Kaiser, E. W., 1992, Int. J. Chem. Kinet., **24**, 179–189.
134. Kaiser, E. W., 1993, J. Phys. Chem., **97**, 11681–11688.
135. Kaiser, E. W. and T. J. Wallington, 1998, J. Phys. Chem. A, **102**, 6054–6055.
136. Kaiser, E. W., T. J. Wallington and J. M. Andino, 1990, Chem. Phys. Lett., **168**, 309.
137. Kaiser, E. W., T. J. Wallington and M. D. Hurley, 1995, Int. J. Chem. Kinet., **27**, 205–218.
138. Kajimoto, O. and R. J. Cvetanovic, 1976, J. Chem. Phys., **64**, 1005.
139. Kaye, J. A., 1986, J. Geophys. Res., **91**, 7865–7874.
140. Keiffer, M., M. J. Pilling and M. J. C. Smith, 1987, J. Phys. Chem., **91**, 6028–6034.
141. Kennedy, R. C. and J. B. Levy, 1972, J. Phys. Chem., **76**, 3480–3488.
142. Kim, P., D. I. MacLean and W. G. Valence, 1980, J. Phys. Chem., **84**, 1806.
143. Kircher, C. C., J. J. Margitan and S. P. Sander, 1984, J. Phys. Chem., **88**, 4370–4375.
144. Kirchner, F., A. Mayer–Figge, F. Zabel and K. H. Becker, 1999, Int. J. Chem. Kin., **31**, 127–144.
145. Klais, O., P. C. Anderson and M. J. Kurylo, 1980, Int. J. Chem. Kinet., **12**, 469–490.
146. Klein, T., I. Barnes, K. H. Becker, E. H. Fink and F. Zabel, 1984, J. Phys. Chem., **88**, 5020–5025.
147. Knyazev, V. D., I. J. Kalinovski and I. R. Slagle, 1999, J. Phys. Chem. A, **103**, 3216–3221.
148. Köppenkastrop, D. and F. Zabel, 1991, Int. J. Chem. Kinet., **23**, 1–15.

149. Kreutter, K. D., J. M. Nicovich and P. H. Wine, 1991, J. Phys. Chem., **95**, 4020.
150. Kuo, C. H. and Y. P. Lee, 1991, J. Phys. Chem., **95**, 1253.
151. Kurylo, M. J., 1972, J. Phys. Chem., **76**, 3518.
152. Kurylo, M. J. and P. A. Ouellette, 1986, J. Phys. Chem., **90**, 441–444.
153. Kurylo, M. J. and P. A. Ouellette, 1987, J. Phys. Chem., **91**, 3365–3368.
154. Laguna, G. A. and S. L. Baughcum, 1982, Chem. Phys. Lett., **88**, 568–71.
155. Lai, L.–H., Y.–C. Hsu and Y.–P. Lee, 1992, J. Chem. Phys., **97**, 3092–3099.
156. Laufer, A. H. and A. M. Bass, 1975, Int. J. Chem. Kinet., **7**, 639.
157. Lee, F. S. C. and F. S. Rowland, 1977, J. Phys. Chem., **81**, 86–87.
158. Lee, J. H., J. V. Michael, W. A. Payne, Jr. and L. J. Stief, 1978, J. Chem. Phys., **68**, 5410–5413.
159. Lee, T. J. and J. E. Rice, 1992, J. Chem. Phys., **97**, 4223–4232.
160. Lee, T. J., C. M. Rohlfing and J. E. Rice, 1992, J. Chem. Phys., **97**, 6593–6605.
161. Lee, Y.–P., R. M. Stimpfle, R. A. Perry, J. A. Mucha, K. M. Evenson, D. A. Jennings and C. J. Howard, 1982, Int. J. Chem. Kinet., **14**, 711–732.
162. Lee, Y.–Y., W. C. Kao and Y.–P. Lee, 1990, J. Phys. Chem., **94**, 4535.
163. Leu, M. T., 1982, J. Phys. Chem., **86**, 4558.
164. Leu, M. T., 1984, Int. J. Chem. Kinet., **16**, 1311–1320.
165. Leu, M. T., C. L. Lin and W. B. DeMore, 1977, J. Phys. Chem., **81**, 190–195.
166. Li, Z. and J. S. Francisco, 1989, J. Am. Chem. Soc., **111**, 5660–5667.
167. Lin, C. L. and M. T. Leu, 1982, Int. J. Chem. Kinet., **14**, 417.
168. Liu, A., W. A. Mulac and C. D. Jonah, 1988, J. Phys. Chem., **92**, 5942–5945.
169. Lloyd, A. C., K. R. Darnall, A. M. Winer and J. N. Pitts, Jr., 1976, J. Phys. Chem., **80**, 789.
170. Lovejoy, E. R. and D. R. Hanson, 1996, J. Phys. Chem., **100**, 4459–4465.
171. Luther, K., K. Oum and J. Troe, 2001, J. Phys.Chem. A, **105**, 5535–5541.
172. Lyman, J. and R. Holland, 1988, J. Phys. Chem., **92**, 7232–7241.
173. Margitan, J. J., 1984, J. Phys. Chem., **88**, 3314–3318.
174. Maric, D. and J. P. Burrows, 1992, J.Photochem. Photobiol. A: Chem., **66**, 291–312.
175. Maricq, M. M., J. J. Szente and E. W. Kaiser, 1993, J. Phys. Chem., **97**, 7970–7977.
176. Marshall, P., A. S. Narayan and A. Fontijn, 1990, J. Phys. Chem., **94**, 2998.
177. Martin, D., J. L. Jourdain and G. Le Bras, 1986, J. Phys. Chem., **90**, 4143–4147.
178. McCaulley, J. A., S. M. Anderson, J. B. Jeffries and F. Kaufman, 1985, Chem Phys. Lett., **115**, 180.
179. McCaulley, J. A., A. M. Moyle, M. F. Golde, S. M. Anderson and F. Kaufman, 1990, J. Chem Soc. Farad. Trans., **86**, 4001–4009.
180. Mellouki, A., G. Laverdet, J. L. Jourdain and G. Poulet, 1989, Int. J. Chem. Kinet., **21**, 1161.
181. Michael, J. V., D. F. Nava, R. P. Borkowski, W. A. Payne and L. J. Stief, 1980, J. Chem. Phys., **73**, 6108.
182. Mineshos, G. and S. Glavas, 1991, React. Kinet. Catal. Lett., **45**, 305–312.
183. Molina, M. J., L. T. Molina and T. Ishiwata, 1980, J. Phys. Chem., **84**, 3100–3104.
184. Moore, S. B. and R. W. Carr, 1990, J. Phys. Chem., **94**, 1393.
185. Morley, C. and I. W. M. Smith, 1972, J. Chem. Soc. Faraday Trans., **68**, 1016.
186. Morris, E. D., D. H. Stedman and H. Niki, 1971, J. Am. Chem. Soc., **93**, 3570.
187. Nicholas, J. E. and R. G. W. Norrish, 1968, Proc. Roy. Soc. A, **307**, 391.
188. Nickolaisen, S. L., R. R. Friedl and S. P. Sander, 1994, J. Phys. Chem., **98**, 155–169.
189. Nicovich, J. M., K. D. Kreutter, C. J. Shackelford and P. H. Wine, 1991, Chem. Phys. Lett., **179**, 367–373.
190. Nicovich, J. M., K. D. Kreutter and P. H. Wine, 1990, J. Chem. Phys., **92**, 3539–3544.
191. Nicovoch, J. M., S. Wang, M. L. McKee and P. H. Wine, 1996, J. Phys. Chem., **100**, 680–688.
192. Niki, H., P. D. Maker, C. M. Savage and L. P. Breitenbach, 1978, Chem. Phys. Lett., **59**, 78.
193. Nizkorodov, S. A. and P. O. Wennberg, 2002, J. Phys. Chem. A, **in press**.
194. Nottingham, W. C., R. N. Rudolph, K. P. Andrews, J. H. Moore and J. A. Tossell, 1994, Int. J. Chem. Kinet., **26**, 749–756.
195. Ohmori, K., K. Yamasaki and H. Matsui, 1993, Bull. Chem. Soc. Jpn., **66**, 51–56.
196. Orlando, J. J. and J. B. Burkholder, 2000, J. Phys.Chem. A, **104**, 2048–2053.
197. Orlando, J. J. and G. S. Tyndall, 1996, J. Phys. Chem., **100**, 19398–19405.
198. Orlando, J. J., G. S. Tyndall and J. G. Calvert, 1992, Atmos. Environ., **26A**, 3111–3118.
199. Orlando, J. J., G. S. Tyndall, C. A. Cantrell and J. G. Calvert, 1991, J. Chem. Soc. Far. Trans., **87**, 2345–2349.
200. Overend, R. P. and G. Paraskevopoulos, 1977, J. Chem. Phys., **67**, 674.
201. Overend, R. P., G. Paraskevopoulos and C. Black, 1976, J. Chem. Phys., **64**, 4149.

202. Pagsberg, P., E. Bjergbakke, E. Ratajczak and A. Sillesen, 1997, Chem. Phys. Lett., **272**, 383–390.
203. Pagsberg, P., A. Sillesen, J. T. Jodowski and E. Ratajczak, 1996, Chem. Phys. Lett., **249**, 358–364.
204. Pagsberg, p., A. Sillesen, J. T. Jodowski and E. Ratajczak, 1996, Chem. Phys. Lett., **252**, 165–171.
205. Pagsberg, P., B. Sztuba, E. Ratajczak and A. Sillesen, 1991, Acta Chem. Scand., **45**, 329.
206. Pagsberg, P. B., E. Ratajczak, A. Sillesen and J. T. Jodkowski, 1987, Chem. Phys. Lett., **141**, 88–94.
207. Paraskevopoulos, G., D. L. Singleton and R. S. Irwin, 1983, Chem. Phys. Lett., **100**, 83–87.
208. Parr, A. D., R. P. Wayne, G. D. Hayman, M. E. Jenkin and R. A. Cox, 1990, Geophys. Res. Lett., **17**, 2357–2360.
209. Parthiban, P. and T. Lee, 1998, J. Chem. Phys., **109**, 525–530.
210. Pastrana, A. V. and R. W. Carr, Jr., 1974, Int. J. Chem. Kinet., **6**, 587.
211. Patrick, R. and D. M. Golden, 1983, Int. J. Chem. Kinet., **15**, 1189–1227.
212. Percival, C. J., G. D. Smith, L. T. Molina and M. J. Molina, 1997, J. Phys. Chem. A, **101**, 8830–8833.
213. Perry, R. A., R. Atkinson and J. N. Pitts, Jr., 1977, J. Chem. Phys., **67**, 5577.
214. Perry, R. A. and D. Williamson, 1982, Chem. Phys. Lett., **93**, 331–334.
215. Pilling, M. J. and M. J. C. Smith, 1985, J. Phys. Chem., **89**, 4713–4720.
216. Pirraglia, A. N., J. V. Michael, J. W. Sutherland and R. B. Klemm, 1989, J. Phys. Chem., **93**, 282–291.
217. Plane, J. M. C. and B. Rajasekhar, 1989, J. Phys. Chem., **93**, 3135–3140.
218. Plumb, I. C. and K. R. Ryan, 1982, Int. J. Chem. Kinet., **14**, 861–874.
219. Poulet, G., J. Barassin, G. Le Bras and J. Combourieu, 1973, Bull. Soc. Chim. Fr., **1**, 1.
220. Pratt, G. L. and S. W. Wood, 1984, J. Chem. Soc. Faraday Trans. 1, **80**, 3419–3427.
221. Ravishankara, A. R., F. L. Eisele and P. H. Wine, 1980, J. Chem. Phys., **73**, 3743.
222. Ravishankara, A. R., G. Smith and D. D. Davis. 13th Informal Photochemistry Conference, 1978, Clearwater Beach, Florida.
223. Ravishankara, A. R., G. J. Smith and D. D. Davis, 1988, Int. J. Chem. Kinet., **20**, 811–814.
224. Rawlins, W. T., G. E. Caledonia and R. A. Armstrong, 1987, J. Chem. Phys . **87**, 5209–5213
225. Rayez, M. T. and M. Destriau, 1993, Chem. Phys. Lett., **206**, 278–284.
226. Roberts, J. M. and S. B. Bertman, 1992, Int. J. Chem. Kinet., **24**, 297–307.
227. Russell, A. G., G. R. Cass and J. H. Seinfeld, 1986, Environ. Sci. Technol., **20**, 1167–1172.
228. Russell, J. J., J. A. Setula, D. Gutman, F. Danis, F.Caralp, P. D. Lightfoot, R. Lesclaux, C. F. Melius and S. M. Senkan, 1990, J. Phys. Chem., **94**, 3277–3283.
229. Ryan, K. R. and I. C. Plumb, 1982, J. Phys. Chem., **86**, 4678–4683.
230. Ryan, K. R. and I. C. Plumb, 1984, Int. J. Chem. Kinet., **16**, 591–602.
231. Sander, S. P., R. P. Friedl and Y. L. Yung, 1989, Science, **245**, 1095–1098.
232. Sander, S. P., R. R. Friedl, W. B. DeMore, D. M. Golden, M. J. Kurylo, R. F. Hampson, R. E. Huie, G. K. Moortgat, A. R. Ravishankara, C. E. Kolb and M. J. Molina "Chemical Kinetics and Photochemical Data for Use in Stratospheric Modeling, Evaluation Number 13," JPL Publication 00–3, Jet Propulsion Laboratory, California Institute of Technology, Pasadena, CA, 2000.
233. Sander, S. P. and M. Peterson, 1984, J. Phys. Chem., **88**, 1566–1571.
234. Sander, S. P., G. W. Ray and R. T. Watson, 1981, J. Phys. Chem., **85**, 199.
235. Sander, S. P. and R. T. Watson, 1980, J. Phys. Chem. , **84**, 1664.
236. Savarino, J. and M. Thiemens, 1999, J. Phys. Chem. A, **103**, 9221–9229.
237. Schieferstein, M., K. Kohse–Höinghaus and F. Stuhl, 1983, Ber. Bunsenges. Phys. Chem., **87**, 361–366.
238. Schurath, U. and V. Wipprecht. 1st European Symposium on Physico–Chemical Behavior of Atmospheric Pollutants, 1979, Ispra.
239. Seeley, J. V., J. T. Jayne and M. J. Molina, 1996, J. Phys. Chem., **100**, 4019–4025.
240. Selzer, E. A. and K. D. Bayes, 1983, J. Phys. Chem., **87**, 392–394.
241. Shamonina, N. F. and A. G. Kotov, 1979, Kinet. i Kataliz., **20**, 233.
242. Sharkey, P., I. R. Sims, I. W. M. Smith, P. Bocherl and B. R. Rowe, 1994, J. Chem. Soc. Far. Trans., **90**, 3609–3616.
243. Shen, G., M. Suto and L. C. Lee, 1990, J. Geophys. Res., **95**, 13981–13984.
244. Silver, J. A., M. S. Zahniser, A. C. Stanton and C. E. Kolb. In *20th International Symposium on Combustion* Pittsburgh, PA, 1984; pp 605–612.
245. Simonaitis, R. and J. Heicklen, 1978, Int. J. Chem. Kinet., **10**, 67–87.
246. Skolnik, E. D., M. G. Veysey, M. G. Ahmed and W. E. Jones, 1975, Can. J. Chem., **53**, 3188.
247. Slanina, Z. and F. Uhlik, 1991, Chem. Phys. Lett., **182**, 51–56.
248. Smith, C. A., A. R. Ravishankara and P. H. Wine, 1985, J. Phys. Chem., **89**, 1423–1427.
249. Smith, G. P., P. W. Fairchild and D. R. Crosley, 1984, J. Chem. Phys., **81**, 2667.

250. Smith, I. W. M. and D. J. Wrig1ey, 1981, Chem. Phys., **63**, 321.
251. Smith, I. W. M. and D. J. Wrigley, 1980, Chem. Phys. Lett., **70**, 481.
252. Smith, I. W. M. and R. Zellner, 1973, J. Chem. Soc. Faraday Trans. 2, **69**, 1617.
253. Stanton, J. F., C. M. L. Rittby, R. J. Bartlett and D. W. Toohey, 1991, J. Phys. Chem., **95**, 2107–2110.
254. Stuhl, F. and H. Niki, 1972, J. Chem. Phys., **57**, 3677–3679.
255. Stutz, J., M. J. Ezell and B. J. Finlayson–Pitts, 1997, J. Phys. Chem. A, **101**, 9187–9190.
256. Thorn, R. P., E. P. Daykin and P. H. Wine, 1993, Int J. Chem. Kinet., **25**, 521–537.
257. Thuner, L. P., I. Barnes, K. H. Becker, T. J. Wallington, L. K. Christensen, J. J. Orlando and B. Ramacher, 1999, J. Phys.Chem. A, **103**, 8657–8663.
258. Trainor, D. W. and C. W. von Rosenberg, Jr., 1974, J. Chem. Phys., **61**, 1010–1015.
259. Troe, J., 1977, J. Chem. Phys., **66**, 4745
260. Troe, J., 2001, Proc. Combust. inst., **28**, 1463–1469.
261. Trolier, M., R. L. Mauldin, III and A. R. Ravishankara, 1990, J. Phys. Chem., **94**, 4896–4907.
262. Tully, F. P., 1983, Chem. Phys. Lett., **96**, 148–153.
263. Turnipseed, A. A., S. B. Barone, N. R. Jensen, D. R. Hanson, C. J. Howard and A. R. Ravishankara, 1995, J. Phys. Chem., **99**, 6000–6009.
264. Van den Bergh, H., N. Benoit–Guyot and J. Troe, 1977, Int. J. Chem Kinet., **9**, 223–234.
265. Van den Bergh, H. and J. Troe, 1976, J. Chem. Phys., **64**, 736–742.
266. Van den Bergh, H. E. and A. B. Callear, 1971, Trans. Faraday Soc., **67**, 2017.
267. Viggiano, A. A., J. A. Davidson, F. C. Fehsenfeld and E. E. Ferguson, 1981, J. Chem. Phys., **74**, 6113–6125.
268. Vinckier, C., A. Dumoulin and S. DeJaegere, 1991, J. Chem. Soc. Faraday Trans., **87**, 1075–1081.
269. Wagner, A. F., I. R. Slagle, D. Sarzynski and D. Gutman, 1990, J. Phys. Chem., **94**, 1853–1864.
270. Walker, R. W. In *Ph.D. Thesis*; Queen Mary College University of London, 1972.
271. Wallington, T. J., J. M. Andino, I. M. Lorkovic, E. W. Kaiser and G. Marston, 1990, J. Phys. Chem., **94**, 3644–3648.
272. Wallington, T. J., R. Atkinson, A. M. Winer and J. N. Pitts, Jr., 1987, Int. J. Chem. Kinet., **19**, 243–249.
273. Wallington, T. J. and J. C. Ball, 1995, J. Phys. Chem., **99**, 3201–3205.
274. Wallington, T. J. and R. A. Cox, 1986, J. Chem. Soc. Faraday Trans. 2, **82**, 275–289.
275. Wallington, T. J., T. Ellerman, O. J. Nielsen and J. Sehested, 1994, J. Phys. Chem., **98**, 2346.
276. Wallington, T. J., T. Ellermann and O. J. Nielsen, 1993, J. Phys. Chem., **97**, 8442–8449.
277. Wallington, T. J., M. M. Mariq, T. Ellerman and O. J. Nielsen, 1992, J. Phys. Chem., **96**, 982–986.
278. Wallington, T. J. and O. J. Nielsen, 1991, Int. J. Chem. Kinet., **23**, 785–798.
279. Wallington, T. J., L. M. Skewes and W. O. Siegl, 1988, J. Photochem. Photobiol. A, **45**, 167.
280. Wallington, T. J., L. M. Skewes, W. O. Siegl, C. H. Wu and S. M. Japar, 1988, Int. J. Chem. Kinet., **20**, 867–875.
281. Washida, N., 1980, J. Chem. Phys., **73**, 1665.
282. Washida, N. and K. D. Bayes, 1976, Int. J. Chem. Kinet., **8**, 777
283. Westenberg, A. A. and N. de Haas, 1972, J. Chem. Phys., **57**, 5375–5378.
284. Whytock, D. A., J. V. Michael and W. A. Payne, 1976, Chem. Phys. Lett., **42**, 466–471.
285. Wilson, W. E. and A. A. Westenberg. In *11th Symposium on Combustion*; The Combustion Institute, Pittsburgh, 1967; pp 1143.
286. Wine, P. H., N. M. Kreutter and A. R. Ravishankara, 1979, J. Phys. Chem., **83**, 3191.
287. Wine, P. H., R. J. Thompson, A. R. Ravishankara, D. H. Semmes, C. A. Gump, A. Torabi and J. M. Nicovich, 1984, J. Phys. Chem., **88**, 2095.
288. Wolf, S., M. bitter, D. Krankowsky and K. Mauersberger, 2000, J. Chem. Phys., **113**, 2684–2686.
289. Wollenhaupt, M. and J. N. Crowley, 2000, J. Phys. Chem. A, **104**, 6429–6438.
290. Wong, W. D. and D. Davis, 1974, Int. J. Chem. Kinet., **6**, 401.
291. Wu, F. and R. W. Carr, 1991, Int. J. Chem. Kinet., **23**, 701–715.
292. Xiong, J. Q. and R. W. Carr, 1994, J. Phys. Chem., **98**, 9811–9822.
293. Yarwood, G., J. W. Sutherland, M. A. Wickramaaratchi and R. B. Klemm, 1991, J. Phys. Chem., **95**, 8771–8775.
294. Zabarnick, S., 1993, Chem Phys., **171**, 265–273.
295. Zabel, F., A. Reimer, K. H. Becker and E. H. Fink, 1989, J. Phys. Chem., **93**, 5500–5507.
296. Zahniser, M. S., J. Chang and F. Kaufman, 1977, J. Chem. Phys., **67**, 997–1003.
297. Zellner, R., F. Ewig, R. Paschke and G. Wagner, 1988, J. Phys. Chem., **92**, 4184–4190.
298. Zellner, R. and K. Lorenz, 1984, J. Phys. Chem., **88**, 984–989.
299. Zetzsch, C. European Symposium on Combustion, 1973.

300. Zhu, T., G. Yarwood, J. Chen and H. Niki, 1994, J. Phys. Chem., **98**, 5065–5067.

SECTION 3. EQUILIBRIUM CONSTANTS

Table of Contents

SECTION 3. EQUILIBRIUM CONSTANTS 3-1
3.1 Format 3-1
3.2 Definitions 3-1
3.3 Notes to Table 3 3-3
3.4 References 3-5

Tables

Table 3-1. Equilibrium Constants 3-2

3.1 Format

Some of the three-body reactions in Table 2-1 form products that are thermally unstable at atmospheric temperatures. In such cases the thermal decomposition reaction may compete with other loss processes, such as photodissociation or radical attack. Table 3-1 lists the equilibrium constants, K(T), for several reactions which may fall into this category. The table has three column entries, the first two being the parameters A and B which can be used to express K(T):

$$K(T)/cm^3\,molecule^{-1} = A\,\exp(B/T)\ (200 < T < 300\ K)$$

The third column entry in Table 3-1 is the calculated value of K at 298 K.

The data sources for K(T) are described in the individual notes to Table 3-1.

3.2 Definitions

When values of the heats of formation and entropies of all species are known at the temperature T, we note that:

$$\log_{10}\left[K(T)\,/\,cm^3 molecule^{-1}\right] = \frac{\Delta S_T^o}{2.303R} - \frac{\Delta H_T^o}{2.303RT} + \log_{10}(T) - 21.87$$

Where the superscript "o" refers to a standard state of one atmosphere. In some cases K values were calculated from this equation, using thermochemical data. In other cases the K values were calculated directly from kinetic data for the forward and reverse reactions. When available, JANAF values were used for the equilibrium constants. The following equations were then used to calculate the parameters A and B:

$$B/^oK = 2.303\left[\frac{(300 \bullet 200)}{(300-200)}\right]\log_{10}\left(\frac{K_{200}}{K_{300}}\right) = 1382\,\log_{10}\left(\frac{K_{200}}{K_{300}}\right)$$

$$\log_{10}(A) = \log_{10}\left(K(T)\right) - \frac{B}{2.303\ T}$$

The relationships between the parameters A and B and the quantities ΔS^o(298 K) and ΔH^o(298 K) are as follows:

$$A = \frac{eR'T}{N_{av}}\exp\left(\frac{\Delta S^o}{R}\right) = 3.7x10^{-22}\,T\exp\left(\frac{\Delta S^o}{R}\right)$$

where $R' = 82.1\ cm^3\ atm\ mole^{-1}K^{-1}$, and $N_{av} = 6.02 \times 10^{23}$ molecule $mole^{-1}$ and

$$B/^oK = -\frac{\Delta H^o}{R}$$

Table 3-1. Equilibrium Constants

Reaction	A/cm^3 molecule^{-1}	B/°K	K_{eq}(298 K)	f(298 K)[a]	g	Note
$HO_2 + NO_2 \rightarrow HO_2NO_2$	2.1×10^{-27}	10900	1.6×10^{-11}	5	1000	1
$NO + NO_2 \rightarrow N_2O_3$	3.3×10^{-27}	4667	2.1×10^{-20}	2	100	2
$NO_2 + NO_2 \rightarrow N_2O_4$	5.9×10^{-29}	6643	2.8×10^{-19}	1.2	250	3
$NO_2 + NO_3 \rightarrow N_2O_5$	3.0×10^{-27}	10990	3.1×10^{-11}	1.2	500	4
$CH_3O_2 + NO_2 \rightarrow CH_3O_2NO_2$	1.3×10^{-28}	11200	2.7×10^{-12}	2	1000	5
$CH_3C(O)O_2 + NO_2 \rightarrow CH_3C(O)O_2NO_2$	9.0×10^{-29}	14000	2.3×10^{-8}	2	200	6
$CH_3CH_2C(O)O_2 + NO_2 \rightarrow CH_3CH_2C(O)O_2NO_2$	9.0×10^{-29}	14000	2.3×10^{-8}	10	800	7
$CH_3C(O)CH_2 + O_2 \rightarrow CH_3C(O)CH_2O_2$	7×10^{-27}	13000	6×10^{-8}	10	800	8
$F + O_2 \rightarrow FOO$	3.2×10^{-25}	6100	2.5×10^{-16}	1 0	1200	9
$Cl + O_2 \rightarrow ClOO$	5.7×10^{-25}	2500	2.5×10^{-21}	2	750	10
$Cl + CO \rightarrow ClCO$	1.6×10^{-25}	4000	1.1×10^{-19}	5	500	11
$ClO + O_2 \rightarrow ClO\cdot O_2$	2.9×10^{-26}	<3700	$<7.2\times10^{-21}$			12
$ClO + ClO \rightarrow Cl_2O_2$	1.27×10^{-27}	8744	7.0×10^{-15}	1.3	500	13
$ClO + OClO \rightarrow Cl_2O_3$	1.1×10^{-24}	5455	9.8×10^{-17}	3	300	14
$OClO + NO_3 \rightarrow O_2ClONO_2$	1×10^{-28}	9300	3.6×10^{-15}	5	1000	15
$OH + CS_2 \rightarrow CS_2OH$	4.5×10^{-25}	5140	1.4×10^{-17}	1.4	500	16
$CH_3S + O_2 \rightarrow CH_3SO_2$	1.8×10^{-27}	5545	2.2×10^{-19}	1.4	300	17

K/cm3 molecule–1 = A exp (B/T) [200 < T/K < 300]

a f(298 K) is the uncertainty factor at 298 K, and g is a measure of the uncertainty in the quantity B . To calculate the uncertainty at temperatures other than 298 K, use the expression:

$$f(T) = f(298\ K)\exp\left[g\left(\frac{1}{T} - \frac{1}{298}\right)\right]$$

Shaded areas indicate changes or additions since JPL 97-4 and/or JPL 00-3

3.3 Notes to Table 3

1. $HO_2 + NO_2$. The value was obtained by combining the data from Table 1-1 for the rate constant of the reaction as written and that of Graham et al. [27] and Zabel [56] for the reverse reaction. Values for the entropy and heat of formation of pernitric acid may be extracted. These values are: S(298 K) = 71.7 cal mole^{-1} K^{-1} and ΔH_f(298 K) = –12.9 kcal mole^{-1}. If the entropy is calculated from the frequencies and moments of inertia given by Chen and Hamilton [19], the value becomes 71.0 and the heat is –13.1. The values in the Appendix to this report reflect these results.

2. $NO + NO_2$. The data are from JANAF [33] and Chao et al. [17]. This process is included because a measurement of the rate constant by Smith and Yarwood [50] and Markwalder et al. [36] shows that it is too slow to be an important process in most atmospheric and laboratory systems.

3. $NO_2 + NO_2$. The data are from JANAF [33] and Vosper [54], Chao et al. [18] and Amoruso et al. [1]. Rate data for this process are reported by Brunning et al. [11], Borrell et al. [8] Gozel et al. [25] and Markwalder et al. [35]. A direct study by Harwood and Jones [28] at low temperatures is in agreement with the recommendation. Re-evaluation of the data suggests lower error limits than recommended in JPL 97-4. A typographical error in JPL 97-4 has been corrected.

4. $NO_2 + NO_3$. The recommendation is from Cantrell et al. [15]. They report rate constants for the decomposition reaction, which they combine with the rate constants of Orlando et al. [42] to obtain the equilibrium constant. Agreement is quite good with the data of Burrows et al. [13] and Cantrell et al. [14], and the room temperature data of Tuazon et al. [51], Perner et al. [44] and Hjorth et al. [30]. An evaluation by Pritchard [47] is also in excellent agreement with the recommendation. Pritchard [47] examined the data of Cantrell et al. [14], Burrows et al. [13], Graham and Johnston [26], Wangberg et al [55], Schott and Davidson [48], and the room temperature data of Tuazon et al. [51], Perner et al. [44] and Hjorth et al. [30]. He also included the values given by Smith et al. [49], and Kircher et al. [34], who combined data on the forward reaction, tabulated in Table 2-1, with decomposition data of by Connell and Johnston [20] and Viggiano et al. [53]. The latter was used as the basis for the value in JPL 00-3, but some uncertainties in the entropies of NO_3 and N_2O_5 justify the reversion to the JPL 97-4 basis. Wangberg et al. [55] measured the equilibrium constant between 280 and 294 K and report results in agreement with this recommendation.

5. $CH_3O_2 + NO_2$. Thermochemical values at 300 K for $CH_3O_2NO_2$ and CH_3O_2 are from Baldwin [6]. In the absence of data, $\Delta H°$ and $\Delta S°$ were assumed to be independent of temperature. Bahta et al. [5] have measured k(dissociation) at 263 K. Using the values of k(recombination) suggested in this evaluation, they compute K(263 K) = (2.68 ± 0.26) × 10^{-10} cm^3. Our values predict 3.94 × 10^{-10} cm^3, in good agreement.

   Zabel et al. [57] have measured k(dissociation) as a function of pressure and temperature. ($CH_3O_2 + NO_2$, Table 2-1). Their values are in good agreement with Bahta et al. [5] and, taken together with k(recombination), would lead to A = 5.2 × 10^{-28} and B = 10,766. This is sufficiently close to the value in Table 3-1 to forego any change in parameters, but the uncertainty has been reduced. Bridier et al. [10] measure an equilibrium constant in good agreement with this recommendation.

6. $CH_3C(O)O_2 + NO_2$: From measurements of the rate constants in both directions by Bridier et al. [9].

7. $CH_3CH_2C(O)O_2 + NO_2$. Assumed to be the same as for PAN (Note 6). Both sides of the of the reaction differ from PAN by the group C–(C)(CO)$(H)_2$. Error limits are estimated and expanded from those for PAN.

8. $CH_3COCH_2 + O_2$. Estimated values of the entropy and enthalpy changes for the reaction are: ΔS = –33 e.u. and ΔH = –26 kcal/mole. The entropy is from group additivity and the enthalpy from group additivity for the hydroperoxide followed by assuming that the O–H bond dissociation energy is 88 kcal/mole. Error limits are estimated from the uncertainties in this procedure.

9. $F + O_2$. Calculated from JANAF thermochemical values except for $\Delta H_{f,298}(FO_2)$ = 6.24 ± 0.5 kcal mol^{-1}. The latter was taken from Pagsberg et al. [43]. This direct measurement, which falls between the earlier disputed values, would seem to settle that controversy, but the calculated value of k_o is not in good agreement with the experiment (see $F + O_2$ of Table 2-1).

10. $Cl + O_2$. Baer et al. [4] determined K in the temperature range 180 to 300 K. Their value at 185.4 K (5.23 × 10^{-19} cm^3 molecule^{-1}) compares well with the Nicovich et al. [40] measurement K = 4.77 × 10^{-19} cm^3 molecule^{-1}, and within error with the Mauldin et al. [37] value of 2.55 × 10^{-19} cm^3 molecule^{-1}. A different expression for K by Avallone et al. [3] gives $S°_{298}$(ClOO) = 61.8 cal K^{-1} moleculr^{-1} and $\Delta H°_{f,298}$ (ClOO) = 23.3 kcal mol^{-1}. Using known thermochemistry

for Cl and O_2 and computed entropy values for ClOO, $\Delta H_{f,298}$ (ClOO) = 23.3 ±0.6 kcal mole^{-1} is obtained from the Nicovich et al. [40] data. The value of $S°_{298}$ (ClOO) = 64.3 cal mole^{-1} K^{-1} used is computed from a structure with a 105° bond angle and Cl–O and O–O bond lengths of 0.173 and 0.130 nm respectively. Frequencies of 1441, 407, and 373 cm^{-1} are from Arkell and Schwager [2]. Symmetry number is 1 and degeneracy is 2.

11. Cl + CO. From Nicovich et al. [41] who measured both k and K between 185 and 260 K in N_2. They report $\Delta H_{f,298}$ (ClCO) = –5.2 ± 0.7 kcal mole^{-1}.

12. ClO + O_2. DeMore [22] reports K < 4 × 10^{-18} cm^3 molecule^{-1} at 197 K. His temperature dependence of the equilibrium constant is estimated using $S°_{298}$ (ClO·O_2) = 73 cal mol^{-1}K^{-1} and $\Delta H°_{298}$ <7.7 kcal mol^{-1}. A higher value of K has been proposed by Prasad [45], but it requires S°(ClO·O_2) to be about 83 cal mol^{-1} K^{-1}, which seems unreasonably high. Carter and Andrews [16] found no experimental evidence for ClO·O_2 in matrix experiments. Prasad and Lee [46] discuss these issues and question the validity of the upper limit reported by DeMore.

13. ClO + ClO. The value is from a third-law calculation based on the data from Cox and Hayman [21] (except for the two lowest temperature points) and Nickolaisen et al. [39]. The entropy of ClOOCl, the value of which is 72.2 cal mol^{-1} K^{-1} at 300 K, is calculated from structural and spectroscopic data given by Birk et al. [7]. The heat of formation at 300 K is $\Delta H°_{f,300}$ = 30.8 kcal mol^{-1}. A study of branching ratios of ClO + ClO channels in $Cl_2/O_2/O_3$ mixtures by Horowitz et al.[31] also finds the equilibrium constant in O_2 at 285 K to be in agreement with the recommendation.

14. ClO + OClO. The value in Table 3-1 is that of Burkholder et al. [12] who report a second law value combining their own data and those of Hayman and Cox [29] except for the lowest temperature point from the latter study. They deduce $\Delta H_f(Cl_2O_3) \approx 37$ kcal mol^{-1} and S° (Cl_2O_3) ≈ 95 cal mol^{-1} K^{-1}. The value from Hayman and Cox [29] is in agreement with entropy calculations based on molecular properties (3rd law). All calculations assume the chlorine chlorate structure ($ClOCl(O)_2$). The deviation that Burkholder et al. [12] observe from third law behavior may indicate that the reaction is more complex than written. Other structures might be stable at the lowest temperatures (i.e., ClOOClO, OClOClO, $OClCl(O)_2$).

15. OClO + NO_3. Deduced by Friedl et al. [24].

16. OH + CS_2. Average of the concordant recent measurements of Murrells et al. [38] and Diau and Lee [23] between 249 and 298 K. The measurements of Hynes et al. [32] indicate a less stable adduct, but agree within combined experimental error.

17. CH_3S + O_2. Turnipseed et al. [52] report the equilibrium constant for 216 ≤ T/K ≤ 258. From a third law analysis using $\Delta S°_{237}$ = –36.8 ± 2.6 eu, they obtain $\Delta H°_{237}$ = –11.5 ± 0.9 kcal/mole.

3.4 References

1. Amoruso, A., L. Crescentini, G. Fiocco and M. Volpe, 1993, J. Geophys. Res., **98**, 16857-16863.
2. Arkell, A. and I. Schwager, 1967, J. Amer. Chem. Soc., **89**, 5999-6006.
3. Avallone, L. M., D. W. Toohey and J. G. Anderson.
4. Baer, S., H. Hippler, R. Rahn, M. Siefke, N. Seitzinger and J. Troe, 1991, J. Chem. Phys., **95**, 6463-6470.
5. Bahta, A., R. Simonaitis and J. Heicklen, 1982, J. Phys. Chem. , **86**, 1849.
6. Baldwin, A. C. Thermochemistry of Peroxides. In *Chemistry of Functional Groups*; Patai, S., Ed.; John Wiley and Sons Inc.: New York, 1982.
7. Birk, M., R. R. Friedl, E. A. Cohen, H. M. Pickett and S. P. Sander, 1989, J. Chem. Phys., **91**, 6588-6597.
8. Borrell, P., C. J. Cobos and K. Luther, 1988, J. Phys. Chem., **92**, 4377-4384.
9. Bridier, I., F. Caralp, H. Loirat, R. Lesclaux, B. Veyret, K. H. Becker, A. Reimer and F. Zabel, 1991, J. Phys. Chem., **95**, 3594-3600.
10. Bridier, I., R. Lesclaux and B. Veyret, 1992, Chem. Phys. Lett., **191**, 259-263.
11. Brunning, J., M. J. Frost and I. W. M. Smith, 1988, Int. J. Chem. Kinetics, **20**, 957.
12. Burkholder, J. B., R. L. Mauldin, R. J. Yokelson, S. Solomon and A. R. Ravishankara, 1993, J. Phys. Chem., **97**, 7597-7605.
13. Burrows, J. P., G. S. Tyndall and G. K. Moortgat, 1985, Chem. Phys. Lett., **119**, 193-198.
14. Cantrell, C. A., J. A. Davidson, A. H. McDaniel, R. E. Shetter and J. G. Calvert, 1988, J. Chem. Phys., **88**, 4997-5006.
15. Cantrell, C. A., R. E. Shetter, J. G. Calvert, G. S. Tyndall and J. J. Orlando, 1993, J. Phys. Chem., **97**, 9141-9148.
16. Carter, R. O. and L. Andrews, 1981, J. Phys. Chem., **85**, 2351.
17. Chao, J., R. C. Wilhoit and B. J. Zwolinski, 1974, Thermochim. Acta, **10**, 359-360.
18. Chao, J., R. C. Wilhoit and B. J. Zwolinski, 1974, Thermochim. Acta, **10**, 361-371.
19. Chen, Z. and T. P. Hamilton, 1996, J. Phys. Chem., **100**, 15731-15734.
20. Connell, P. S. and H. S. Johnston, 1979, Geophys. Res. Lett., **6**, 553-556.
21. Cox, R. A. and G. D. Hayman, 1988, Nature, **332**, 796-800.
22. DeMore, W. B., 1990, Geophys. Res. Lett., **17**, 2353-2355.
23. Diau, E. W.-G. and Y.-P. Lee, 1991, J. Phys. Chem., **95**, 379.
24. Friedl, R. R., S. P. Sander and Y. L. Yung, 1992, J. Phys. Chem., **96**, 7490-7493.
25. Gozel, P., B. Calpani and H. van den Bergh, 1984, Isrl. J. Chem., **24**, 210.
26. Graham, R. A. and H. S. Johnston, 1978, J. Phys. Chem., **82**, 254-268.
27. Graham, R. A., A. M. Winer and J. N. Pitts, Jr., 1977, Chem. Phys. Lett., **51**, 215.
28. Harwood, M. H. and R. L. Jones, 1994, J. Geophys. Res., **99**, 22995-22964.
29. Hayman, G. D. and R. A. Cox, 1989, Chem. Phys. Lett., **155**, 1-7.
30. Hjorth, J., J. Nothholt and G. Restelli, 1992, Int. J. Chem. Kinet., **24**, 51-65.
31. Horowitz, A., J. N. Crowley and G. K. Moortgat, 1994, J. Phys. Chem., **98**, 11924-11930.
32. Hynes, A. J., P. H. Wine and J. M. Nicovich, 1988, J. Phys. Chem., **92**, 3846-3852.
33. JANAF *JANAF Thermochemical Tables*, Third ed.; National Bureau of Standards, 1985.
34. Kircher, C. C., J. J. Margitan and S. P. Sander, 1984, J. Phys. Chem., **88**, 4370-4375.
35. Markwalder, B., P. Gozel and H. van den Bergh, 1992, J. Chem. Phys., **97**, 5472-5479.
36. Markwalder, B., P. Gozel and H. van den Bergh, 1993, J. Phys. Chem., **97**, 5260-5265.
37. Mauldin, R. L., III, J. B. Burkholder and A. R. Ravishankara, 1992, J. Phys. Chem., **96**, 2582-2588.
38. Murrells, T. P., E. R. Lovejoy and A. R. Ravishankara, 1990, J. Phys. Chem., **94**, 2381-2386.
39. Nickolaisen, S. L., R. R. Friedl and S. P. Sander, 1994, J. Phys. Chem., **98**, 155-169.
40. Nicovich, J. M., K. D. Kreutter, C. J. Shackelford and P. H. Wine, 1991, Chem. Phys. Lett., **179**, 367-373.
41. Nicovich, J. M., K. D. Kreutter and P. H. Wine, 1990, J. Chem. Phys., **92**, 3539-3544.
42. Orlando, J. J., G. S. Tyndall, C. A. Cantrell and J. G. Calvert, 1991, J. Chem. Soc. Far. Trans., **87**, 2345-2349.
43. Pagsberg, P. B., E. Ratajczak, A. Sillesen and J. T. Jodkowski, 1987, Chem. Phys. Lett., **141**, 88-94.
44. Perner, D., A. Schmeltekopf, R. H. Winkler, H. S. Johnston, J. G. Calvert, C. A. Cantrell and W. R. Stockwell, 1985, J. Geophys. Res., **90**, 3807-3812.
45. Prasad, S. S., 1980, Nature, **285**, 152.
46. Prasad, S. S. and T. J. Lee, 1994, J. Geophys. Res., **99**, 8225-8230.
47. Pritchard, H. O., 1994, Int. J. Chem. Kinet., **26**, 61-72.
48. Schott, G. and N. Davidson, 1958, J. Amer. Chem. Soc., **80**, 1841-1853.

49. Smith, C. A., A. R. Ravishankara and P. H. Wine, 1985, J. Phys. Chem., **89**, 1423-1427.
50. Smith, I. W. M. and G. Yarwood, 1986, Chem. Phys. Lett., **130**, 24-28.
51. Tuazon, E. C., E. Sanhueza, R. Atkinson, W. P. L. Carter, A. M. Winer and J. N. Pitts, Jr., 1984, J. Phys. Chem., **88**, 3095-3098.
52. Turnipseed, A. A., S. B. Baron and A. R. Ravishankara, 1992, J. Phys. Chem., **96**, 7502-7505.
53. Viggiano, A. A., J. A. Davidson, F. C. Fehsenfeld and E. E. Ferguson, 1981, J. Chem. Phys., **74**, 6113-6125.
54. Vosper, A. J., 1970, J. Chem. Soc. A, **1970**, 625.
55. Wangberg, I., T. Etzkorn, I. Barnes, U. Platt and K. H. Becker, 1997, J. Phys. Chem. A, **101**, 9694-9698.
56. Zabel, F., 1995, Zeitschrift fur Physikalische Chemie, **188**, 119-142.
57. Zabel, F., A. Reimer, K. H. Becker and E. H. Fink, 1989, J. Phys. Chem., **93**, 5500-5507.

SECTION 4. PHOTOCHEMICAL DATA

Table of Contents

SECTION 4. PHOTOCHEMICAL DATA 4-1
4.1 Format and Error Estimates 4-3
4.2 Halocarbon Absorption Cross Sections and Quantum Yields 4-3
4.3 References 4-102

Tables

Table 4-1. Photochemical Reactions 4-4
Table 4-2. Combined Uncertainties for Cross Sections and Quantum Yields 4-6
Table 4-3. Absorption Cross Sections of O_2 Between 205 and 240 nm 4-7
Table 4-4. Absorption Cross Sections of O_3 at 273 K 4-8
Table 4-5. Parameters for the Calculation of $O(^1D)$ Quantum Yields 4-9
Table 4-6. Absorption Cross Sections of HO_2 4-10
Table 4-7. Absorption Cross Sections of H_2O Vapor 4-11
Table 4-8. Absorption Cross Sections of H_2O_2 Vapor 4-11
Table 4-9. Mathematical Expression for Absorption Cross Sections of H_2O_2 as a Function of Temperature 4-12
Table 4-10. Absorption Cross Sections of NO_2 4-13
Table 4-11. Quantum Yields for NO_2 Photolysis 4-14
Table 4-12. Absorption Cross Sections of NO_3 at 298 K 4-16
Table 4-13. Mathematical Expression for Absorption Cross Sections of N_2O as a Function of Temperature* 4-16
Table 4-14. Absorption Cross Sections of N_2O at 298 K 4-17
Table 4-15. Absorption Cross Sections of N_2O_5 4-18
Table 4-16. Absorption Cross Sections of HONO 4-19
Table 4-17. Absorption Cross Sections and Temperature Coefficients of HNO_3 Vapor 4-20
Table 4-18. Absorption Cross Sections of HO_2NO_2 Vapor 4-20
Table 4-19. Absorption Cross Sections and Quantum Yields for Photolysis of CH_2O 4-21
Table 4-20. Absorption Cross Sections of CH_3O_2, $C_2H_5O_2$, and $CH_3C(O)O_2$ 4-22
Table 4-21. Absorption Cross Sections of CH_3OOH 4-23
Table 4-22. Absorption Cross Sections of PAN 4-25
Table 4-23. Absorption Cross Sections of FNO 4-26
Table 4-24. Absorption Cross Sections of CCl_2O, CClFO, and CF_2O at 298 K 4-27
Table 4-25. Absorption Cross Sections of Cl_2 4-28
Table 4-26. Absorption Cross Sections of ClOO 4-29
Table 4-27. Absorption Cross Sections of OClO at the Band Peaks 4-30
Table 4-28. Absorption Cross Sections of Cl_2O 4-32
Table 4-29. Absorption Cross Sections of ClOOCl at 200–250 K 4-33
Table 4-30. Absorption Cross Sections of Cl_2O_3 4-34
Table 4-31. Absorption Cross Sections of Cl_2O_4 4-34
Table 4-32. Absorption Cross Sections of Cl_2O_6 4-34
Table 4-33. Absorption Cross Sections of HCl Vapor 4-35
Table 4-34. Absorption Cross Sections of HOCl 4-36
Table 4-35. Absorption Cross Sections of ClNO 4-37
Table 4-36. Absorption Cross Sections of $ClNO_2$ 4-37
Table 4-37. Absorption Cross Sections of ClONO at 231 K 4-38
Table 4-38. Absorption Cross Sections of $ClONO_2$ 4-39
Table 4-39. Absorption Cross Sections of CCl_4 at 295–298 K 4-41
Table 4-40. Absorption Cross Sections of CH_3OCl 4-42
Table 4-41. Absorption Cross Sections of $CHCl_3$ at 295–298 K 4-43
Table 4-42. Absorption Cross Sections of CH_2Cl_2 at 295–298 K 4-44
Table 4-43. Absorption Cross Sections of CH_3Cl at 295–298 K 4-46
Table 4-44. Absorption Cross Sections of CH_3CCl_3 at 295–298 K 4-47
Table 4-45. Absorption Cross Sections of CH_3CH_2Cl at 298 K 4-47
Table 4-46. Absorption Cross Sections of $CH_3CHClCH_3$ at 295 K 4-48
Table 4-47. Absorption Cross Sections of $CFCl_3$ at 295–298 K 4-49
Table 4-48. Absorption Cross Sections of CF_2Cl_2 at 295–298 K 4-50

Table 4-49. Absorption Cross Sections of CF_3Cl at 295 K 4-51
Table 4-50. Absorption Cross Sections of $CF_2ClCFCl_2$ at 295–298 K 4-52
Table 4-51. Absorption Cross Sections of CF_2ClCF_2Cl at 295 K 4-53
Table 4-52. Absorption Cross Sections of CF_3CF_2Cl at 295–298 K 4-53
Table 4-53. Absorption Cross Sections of $CHFCl_2$ at 295–298 K 4-54
Table 4-54. Absorption Cross Sections of CHF_2Cl at 295–298 K 4-55
Table 4–55. Absorption Cross Sections of CH_2FCl at 298 K 4-55
Table 4-56. Absorption Cross Sections of CF_3CHCl_2 at 295 K 4-56
Table 4-57. Absorption Cross Sections of CF_3CHFCl at 295 K 4-57
Table 4-58. Absorption Cross Sections of CF_3CH_2Cl at 298 K 4-58
Table 4-59. Absorption Cross Sections of CH_3CFCl_2 at 295–298 K 4-59
Table 4–60. Absorption Cross Sections of CH_3CF_2Cl at 295–298 K 4-60
Table 4-61. Absorption Cross Sections of $CF_3CF_2CHCl_2$ and CF_2ClCF_2CFCl at 298 K 4-61
Table 4-62. Absorption Cross Sections at the Peak of Various Bands in the A ← X Spectrum of BrO 4-62
Table 4-63. Absorption Cross Sections of BrO 4-62
Table 4-64. Absorption Cross Sections of HOBr 4-65
Table 4-65. Absorption Cross Sections of $BrONO_2$ at 298 K 4-66
Table 4-66. Absorption Cross Sections of BrCl at 298 K 4-67
Table 4-67. Absorption Cross Sections of CH_3Br at 295–296 K 4-69
Table 4-68. Absorption Cross Sections of CH_2Br_2 at 295–298 K 4-70
Table 4-69. Absorption Cross Sections of $CHBr_3$ at 295–296 K 4-71
Table 4-70. Absorption Cross Sections of CH_2BrCH_2Br at 295 K 4-72
Table 4-71. Absorption Cross Sections of C_2H_5Br at 295 K 4-72
Table 4-72. Absorption Cross Sections of CH_2ClBr at 295 K 4-73
Table 4-73. Absorption Cross Sections of $CHClBr_2$ at 296 K 4-74
Table 4-74. Absorption Cross Sections of $CHCl_2Br$ at 298 K 4-75
Table 4-75. Absorption Cross Sections of CCl_3Br at 298 K 4-75
Table 4-76. Absorption Cross Sections of CHF_2Br at 298 K 4-76
Table 4-77. Absorption Cross Sections of CF_2Br_2 at 295–296 K 4-78
Table 4-78. Absorption Cross Sections of CF_2ClBr at 295–298 K 4-80
Table 4-79. Absorption Cross Sections of CF_3Br at 295–298 K 4-82
Table 4-80. Absorption Cross Sections of CF_3CH_2Br at 295 K 4-82
Table 4-81. Absorption Cross Sections of $CF_3CHClBr$ at 295–298 K 4-84
Table 4-82. Absorption Cross Sections of CF_3CHFBr at 295 K 4-84
Table 4-83. Absorption Cross Sections of CF_2BrCF_2Br at 296 K 4-86
Table 4-84. Absorption Cross Sections of CF_3CF_2Br at 298 K 4-87
Table 4-85. Absorption Cross Sections of CH_3I at 296–298 K and Temperature Coefficients 4-88
Table 4-86. Absorption Cross Sections of CH_2I_2 at 298 K 4-89
Table 4-87. Absorption Cross Sections of C_2H_5I at 298 K and Temperature Coefficients 4-90
Table 4-88. Absorption Cross Sections of CH_3CHI_2 at 298 K 4-91
Table 4-89. Absorption Cross Sections of C_3H_7I at 298 K and Temperature Coefficients 4-92
Table 4-90. Absorption Cross Sections of $(CH_3)_3CI$ at 298 K 4-93
Table 4-91. Absorption Cross Sections of CF_3I at 295–300 K 4-95
Table 4-92. Absorption Cross Sections of CF_2I_2 at 294 K 4-96
Table 4-93. Absorption Cross Sections of C_2F_5I at 323 K 4-96
Table 4-94. Absorption Cross Sections of 1-C_3F_7I at 295–298 K 4-97
Table 4-95. Absorption Cross Sections of CH_2ICl at 298 K and Temperature Coefficients 4-98
Table 4-96. Absorption Cross Sections of CH_2BrI at 298 K and Temperature Coefficients 4-99
Table 4-97. Absorption Cross Sections of OCS 4-100
Table 4-98. Absorption Cross Sections of NaCl Vapor at 300 K 4-101

Figures

Figure 4-1. Absorption Spectrum of NO_3 4-15
Figure 4-2. Absorption Spectrum of ClO 4-29
Figure 4-3. Absorption Spectrum of OClO 4-31
Figure 4-4. Absorption Spectrum of BrO 4-63

4.1 Format and Error Estimates

In Table 4-1 we present a list of photochemical reactions considered to be of stratospheric interest. The absorption cross sections of O_2 and O_3 largely determine the extent of penetration of solar radiation into the stratosphere and troposphere. Some comments and references to these cross sections are presented in the text, but only a sample of the data is listed here. (See, for example, WMO Report No. 11 [1]; WMO Report No. 16 [434]) The photodissociation of NO in the O_2 Schumann-Runge band spectral range is another important process requiring special treatment and is not discussed in this evaluation (see, for example, Frederick and Hudson [123]; Allen and Frederick [8]; WMO Report No. 11 [1], and Minschwaner and Siskind [259]).

For some other species having highly structured spectra, such as CS_2 and SO_2, some comments are given in the text, but the photochemical data are not presented. The species CH_2O, NO_2, NO_3, ClO, BrO, and OClO also have complicated spectra, but in view of their importance for atmospheric chemistry a sample of the data is presented in the evaluation; for more detailed information on their high-resolution spectra and temperature dependence, the reader is referred to the original literature.

Table 4-2 gives recommended reliability factors for some of the more important photochemical reactions. These factors represent the combined uncertainty in cross sections and quantum yields, taking into consideration the atmospherically important wavelength regions, and they refer to the total dissociation rate regardless of product identity. The exception is $O(^1D)$ production from photolysis of O_3: the reliability factor applies to the quantum yield at the indicated wavelengths.

The error estimates are not rigorous numbers resulting from a detailed error propagation analysis of statistical manipulations of the different sets of literature values; they merely represent a consensus among the panel members as to the reliability of the data for atmospheric photodissociation calculations, taking into account the difficulty of the measurements, the agreement among the results reported by various groups, etc.

The absorption cross sections are defined by the following expression of Beer's Law:

$$I = I_o \exp(-\sigma n l),$$

where I_o and I are the incident and transmitted light intensity, respectively; σ is the absorption cross section in cm^2 $molecule^{-1}$; n is the concentration in molecule cm^{-3}; and l is the pathlength in cm. The cross sections are room temperature values at the specific wavelengths listed in the table, and the expected photodissociation quantum yields are unity, unless otherwise stated.

4.2 Halocarbon Absorption Cross Sections and Quantum Yields

The primary process in the photodissociation of chlorinated hydrocarbons is well established: absorption of ultraviolet radiation in the lowest frequency band is interpreted as an n–σ* transition involving excitation to a repulsive electronic state (antibonding in C–Cl), which dissociates by breaking the carbon-chlorine bond (Majer and Simons [228]). As expected, the chlorofluoromethanes, which are a particular type of chlorinated hydrocarbons, behave in this fashion (Sandorfy [361]). Hence, the quantum yield for photodissociation is expected to be unity for these compounds. There are several studies that show specifically that this is the case for CF_2Cl_2, $CFCl_3$, and CCl_4. These studies, which have been reviewed in CODATA [82], also indicate that at shorter wavelengths, two halogen atoms can be released simultaneously in the primary process.

Table 4-1. Photochemical Reactions

O_x Photochemistry

A1. $O_2 + h\nu \rightarrow O + O$

A2. $O_3 + h\nu \rightarrow O_2 + O$

$O_3 + h\nu \rightarrow O_2 + O(^1D)$

HO_x Photochemistry

B1. $HO_2 + h\nu \rightarrow$ products

B2. $H_2O + h\nu \rightarrow H + OH$

B3. $H_2O_2 + h\nu \rightarrow OH + OH$

NO_x Photochemistry

C1. $NO_2 + h\nu \rightarrow NO + O$

C2. $NO_3 + h\nu \rightarrow NO_2 + O$

$NO_3 + h\nu \rightarrow NO + O_2$

C3. $N_2O + h\nu \rightarrow N_2 + O(^1D)$

C4. $N_2O_5 + h\nu \rightarrow$ products

$NH_3 + h\nu \rightarrow NH_2 + H$ (1)

C5. $HONO + h\nu \rightarrow OH + NO$

C6. $HNO_3 + h\nu \rightarrow OH + NO_2$

C7. $HO_2NO_2 + h\nu \rightarrow$ products

Organic Photochemistry

$CO + h\nu \rightarrow C + O$ (1)

$CO_2 + h\nu \rightarrow CO + O$ (1)

$CH_4 + h\nu \rightarrow$ products(2)

D1. $CH_2O \rightarrow H_2 + CO$

$CH_2O \rightarrow H + HCO$

D2. $CH_3O_2 + h\nu \rightarrow$ products

D3. $C_2H_5O_2 + h\nu \rightarrow$ products

D4. $CH_3OOH + h\nu \rightarrow$ products

D5. $HCN + h\nu \rightarrow$ products

D6. $CH_3CN + h\nu \rightarrow$ products

D7. $CH_3C(O)O_2 + h\nu \rightarrow$ products

D8. $CH_3C(O)O_2NO_2 + h\nu \rightarrow$ products

FO_x Photochemistry

E1. $HF + h\nu \rightarrow H + F$

E2. $FNO + h\nu \rightarrow F + NO$

E3. $CF_4 + h\nu \rightarrow$ products

E4. $C_2F_6 + h\nu \rightarrow$ products

E5. $CF_2O + h\nu \rightarrow$ products

E6. $CF_3OH + h\nu \rightarrow$ products

ClO_x Photochemistry

F1. $Cl_2 + h\nu \rightarrow Cl + Cl$

F2. $ClO + h\nu \rightarrow Cl + O$

F3. $ClOO + h\nu \rightarrow$ products

F4. $OClO + h\nu \rightarrow O + ClO$

F5. $ClO_3 + h\nu \rightarrow$ products

F6. $Cl_2O + h\nu \rightarrow$ products

F7. $Cl_2O_2 + h\nu \rightarrow$ products

F8. $Cl_2O_3 + h\nu \rightarrow$ products

F9. $Cl_2O_4 + h\nu \rightarrow$ products

F10. $Cl_2O_6 + h\nu \rightarrow$ products

F11. $HCl + h\nu \rightarrow H + Cl$

F12. $HOCl + h\nu \rightarrow OH + Cl$

F13. $ClNO + h\nu \rightarrow Cl + NO$

F14. $ClNO_2 + h\nu \rightarrow$ products

F15. $ClONO + h\nu \rightarrow$ products

F16. $ClONO_2 + h\nu \rightarrow$ products

F17. $CCl_4 + h\nu \rightarrow$ products

F18. $CH_3OCl + h\nu \rightarrow$ products

F19. $CHCl_3 + h\nu \rightarrow$ products

F20. $CH_2Cl_2 + h\nu \rightarrow$ products

F21. $CH_3Cl + h\nu \rightarrow$ products

F22. $CH_3CCl_3 + h\nu \rightarrow$ products

F23. $CH_3CH_2Cl + h\nu \rightarrow$ products

F24. $CH_3CHClCH_3 + h\nu \rightarrow$ products

F25. $CH_2ClCH_2Cl + h\nu \rightarrow$ products

F26. $CH_2ClCH_2CH_2Cl + h\nu \rightarrow$ products

F27. $CH_2Cl(CH_2)_2CH_2Cl + h\nu \rightarrow$ products

F28. $CCl_2O + h\nu \rightarrow$ products

F29. $CClFO + h\nu \rightarrow$ products

F30. $CFCl_3$ (CFC-11)+ $h\nu \rightarrow$ products

F31. CF_2Cl_2 (CFC-12)+ $h\nu \rightarrow$ products

F32. CF_3Cl (CFC-13)+ $h\nu \rightarrow$ products

F33. $CF_2ClCFCl_2$ (CFC-113) + $h\nu \rightarrow$ products

F34. CF_2ClCF_2Cl (CFC-114) + $h\nu \rightarrow$ products

F35. CF_3CF_2Cl (CFC-115)+ $h\nu \rightarrow$ products

F36. $CHFCl_2$ (HCFC-21) + $h\nu \rightarrow$ products

F37. CHF_2Cl (HCFC-22) + $h\nu \rightarrow$ products

F38. CH_2FCl (HCFC-31) + $h\nu \rightarrow$ products

F39. CF_3CHCl_2 (HCFC-123) + $h\nu \rightarrow$ products

F40. CF_3CHFCl (HCFC-124) + $h\nu \rightarrow$ products

F41. CF_3CH_2Cl (HCFC-133) + $h\nu \rightarrow$ products

F42. CH_3CFCl_2 (HCFC-141b) + $h\nu \rightarrow$ products

F43. CH_3CF_2Cl (HCFC-142b) + $h\nu \rightarrow$ products

F44. $CF_3CF_2CHCl_2$ (HCFC-225ca) + $h\nu \rightarrow$ products

F45. CF_2ClCF_2CHFCl (HCFC-225cb) + $h\nu \rightarrow$ products

BrO_x Photochemistry

G1. $BrO + h\nu \rightarrow$ products

G2. $HOBr + h\nu \rightarrow$ products

G3. $BrONO_2 + h\nu \rightarrow$ products

G4. $BrCl + h\nu \rightarrow Br + Cl$

G5. $CH_3Br + h\nu \rightarrow$ products

G6. $CH_2Br_2 + h\nu \rightarrow$ Products

G7. $CHBr_3 + h\nu \rightarrow$ Products

G8. $CH_2BrCH_2Br + h\nu \rightarrow$ Products

G9. $C_2H_5Br + h\nu \rightarrow$ Products

G10. CH_2ClBr (Halon-1011) + $h\nu \rightarrow$ Products

G11. $CHClBr_2$ (Halon-1012) + $h\nu \rightarrow$ Products

G12. $CHCl_2Br$ (Halon-1021) + hν → Products
G13. CCl_3Br (Halon-1031) + hν → Products
G14. CHF_2Br (Halon-1201) + hν → Products
G15. CF_2Br_2 (Halon-1202) + hν → Products
G16. CF_2ClBr (Halon-1211) + hν → Products
G17. CF_3Br (Halon-1301) + hν → Products
G18. CF_3CH_2Br (Halon-2301) + hν → Products
G19. $CF_3CHClBr$ (Halon-2311) + hν → Products
G20. CF_3CHFBr (Halon-2401) + hν → Products
G21. CF_2BrCF_2Br (Halon-2402) + hν → Products
G22. CF_3CF_2Br (Halon-2501) + hν → Products

IO_x Photochemistry

H1. $CH_3I + h\nu \rightarrow CH_3 + I(^2P_{3/2})$
H2. $CH_3I + h\nu \rightarrow CH_3 + I^*(^2P_{1/2})$
H3. $CH_2I_2 + h\nu \rightarrow CH_2I + I(^2P_{3/2})$
H4. $CH_2I_2 + h\nu \rightarrow CH_2I + I^*(^2P_{1/2})$
H5. $C_2H_5I + h\nu \rightarrow C_2H_5 + I(^2P_{3/2})$
H6. $C_2H_5I + h\nu \rightarrow C_2H_5 + I^*(^2P_{1/2})$
H7. $CH_3CHI_2 + h\nu \rightarrow$ Products
H8. $CH_3CH_2CH_2I + h\nu \rightarrow$ Products
H9. $CH_3CHICH_3 + h\nu \rightarrow$ Products
H10. $C_4H_9I + h\nu \rightarrow C_4H_9 + I(^2P_{3/2})$
H11. $C_4H_9I + h\nu \rightarrow C_4H_9 + I^*(^2P_{1/2})$
H12. $(CH_3)_2CHCH_2I + h\nu \rightarrow (CH_3)_2CCH_2 + I(^2P_{3/2})$
H13. $(CH_3)_2CHCH_2I + h\nu \rightarrow (CH_3)_2CCH_2 + I^*(^2P_{1/2})$
H14. $CH_3)_3CI + \rightarrow (CH_3)_3C + I(^2P_{3/2})$
H15. $(CH_3)_3CI + \rightarrow (CH_3)_3C + I^*(^2P_{1/2})$
H16. $C_5H_{11}I + h\nu \rightarrow C_5H_{11} + I(^2P_{3/2})$
H17. $C_5H_{11}I + h\nu \rightarrow C_5H_{11} + I^*(^2P_{1/2})$
H18. $CF_3I + h\nu \rightarrow CF_3 + I(^2P_{3/2})$
H19. $CF_3I + h\nu \rightarrow CF_3 + I^*(^2P_{1/2})$
H20. $CF_2I_2 + h\nu \rightarrow CF_2I + I(^2P_{3/2})$
H21. $CF_2I_2 + h\nu \rightarrow CF_2I + I^*(^2P_{1/2})$
H22. $CF_2I_2 + h\nu \rightarrow CF_2 + I(^2P_{3/2}) + I(^2P_{3/2})$
H23. $CF_2I_2 + h\nu \rightarrow CF_2 + I(^2P_{3/2}) + I^*(^2P_{1/2})$
H24. $C_2F_5I + h\nu \rightarrow C_2F_5 + I(^2P_{3/2})$
H25. $C_2F_5I + h\nu \rightarrow C_2F_5 + I^*(^2P_{1/2})$
H26. $C_3F_7I + h\nu \rightarrow C_3F_7 + I(^2P_{3/2})$
H27. $C_3F_7I + h\nu \rightarrow C_3F_7 + I^*(^2P_{1/2})$
H28. $C_4F_9I + h\nu \rightarrow C_4F_9 + I(^2P_{3/2})$
H29. $C_4F_9I + h\nu \rightarrow C_4F_9 + I^*(^2P_{1/2})$
H30. $C_6F_{13}I + h\nu \rightarrow C_6F_{13} + I(^2P_{3/2})$
H31. $C_6F_{13}I + h\nu \rightarrow C_6F_{13} + I^*(^2P_{1/2})$
H32. $CH_2ICl + h\nu \rightarrow CH_2Cl + I$
H33. $CH_2BrI + h\nu \rightarrow CH_2I + Br$
H34. $CH_2BrI + h\nu \rightarrow CH_2Br + I$
H35. $CF_2BrCF_2I + h\nu \rightarrow CF_2BrCF_2 + I$
H36. $CF_2BrCF_2I + h\nu \rightarrow CF_2ICF_2 + Br$

SO_x Photochemistry

I1. $SO_2 + h\nu \rightarrow SO + O$
$H_2S + h\nu \rightarrow HS + H$ (1)
I2. $CS_2 + h\nu \rightarrow CS + S$
I3. $OCS + h\nu \rightarrow CO + S$
I4. $SF_6 + h\nu \rightarrow$ products

Metal Photochemistry

J.1 $NaOH + h\nu \rightarrow Na + OH$
J2. $NaCl + h\nu \rightarrow Na + Cl$

---

(1) Hudson and Kieffer [170].
(2) Turco [405].
(3) Shaded areas indicate changes or additions since JPL 97-4/JPL 00-3.

Table 4-2. Combined Uncertainties for Cross Sections and Quantum Yields

Species	Uncertainty	Notes
O_2 (Schumann-Runge bands)	1.2	
O_2 (Continua)	1.2	
O_3 (Cross Sections Only)	1.1	
$O_3 \rightarrow O(^1D)$, λ >310 nm	1.3	
$O_3 \rightarrow O(^1D)$, 290 < λ < 310 nm	1.2	
H_2O_2	1.3	
NO_2	1.2	
NO_3	1.5	
N_2O	1.2	
N_2O_5	2.0	
HNO_3	1.3	
HO_2NO_2	2.0	
CH_2O	1.4	
CH_3OOH	1.5	
$CH_3C(O)O_2NO_2$	1.3	λ < 300 nm
$CH_3C(O)O_2NO_2$	2.0	$\lambda \geq$ 300 nm
HCl	1.1	
HOCl	1.4	
ClOOCl	1.5	λ < 300 nm
ClOOCl	3.0	$\lambda \geq$ 300 nm
Cl_2O_3	1.5	λ < 300 nm
Cl_2O_3	3.0	$\lambda \geq$ 300 nm
$ClONO_2$	1.3	
CCl_4	1.1	
CCl_3F	1.1	
CCl_2F_2	1.1	
CH_3Cl	1.1	
CF_2O	2.0	
CF_3Br	1.3	
CF_2ClBr	2.0	
CF_2Br_2	2.0	
$C_2F_4Br_2$	2.0	
HOBr	2.0	λ < 350 nm
HOBr	10	$\lambda \geq$ 350 nm
$BrONO_2$	1.4	

A1. $O_2 + h\nu \rightarrow O + O$. The photodissociation of molecular oxygen in the stratosphere is due primarily to absorption of solar radiation in the 200–220 nm wavelength region, i.e., within the Herzberg continuum. The 185–200-nm region—the O_2 Schumann-Runge band spectral range—is also very important, since solar radiation penetrates efficiently into the stratosphere at those wavelengths.

Frederick and Mentall [124] Herman and Mentall [158] and Anderson and Hall [14,15] estimated O_2 absorption cross sections from balloon measurements of solar irradiance in the stratosphere. These authors find the cross sections in the 200–210 nm range to be ~35% smaller than the smallest of the older laboratory results, which are those of Shardanand and Prasad Rao [373]. The more recent laboratory studies (Johnston et al. [190]; Cheung et al. [73,74], Jenouvrier et al. [183]) confirm the lower values obtained from solar irradiance measurements. The recommended absorption cross section values between 205 and 240 nm are listed in Table 4-3; they are taken from Yoshino et al. [438] and are based on the latter set of laboratory measurements. Amoruso et al. [11] have also carried out cross section measurements in this wavelength range (the Herzberg continuum); their values are ~15% lower than those reported by Yoshino et al.

Table 4-3. Absorption Cross Sections of O_2 Between 205 and 240 nm

λ (nm)	$10^{24}\ \sigma$ (cm^2)	λ (nm)	$10^{24}\ \sigma$ (cm^2)
205	7.35	223	3.89
206	7.13	224	3.67
207	7.05	225	3.45
208	6.86	226	3.21
209	6.68	227	2.98
210	6.51	228	2.77
211	6.24	229	2.63
212	6.05	230	2.43
213	5.89	231	2.25
214	5.72	232	2.10
215	5.59	233	1.94
216	5.35	234	1.78
217	5.13	235	1.63
218	4.88	236	1.48
219	4.64	237	1.34
220	4.46	238	1.22
221	4.26	239	1.10
222	4.09	240	1.01

The studies of the penetration of solar radiation in the atmosphere in the Schumann-Runge wavelength region were based originally on laboratory measurements of cross sections that were affected by instrumental parameters due to insufficient spectral resolution. Yoshino et al. [446] reported high resolution O_2 cross section measurements at 300 K, between 179 and 202 nm, obtaining the first set of results, which is independent of the instrument width. Additional studies at other temperatures, wavelengths, and isotopic compositions have been carried out by Yoshino et al. [439,442–445], Lewis et al. [214,215], Cheung et al. [72], and Chiu et al. [75]. More recently, Yoshino et al. [440] reported cross sections of the Schumann-Runge bands in the window region between the rotational lines for wavelengths between 180 and 195 nm; these measurements supersede their earlier ones. Minschwaner et al. [258] have fit temperature-dependent O_2 cross sections between 175 and 204 nm with polynomial expressions, providing accurate means of determining the Schumann-Runge band cross sections with a model that incorporates the most recent laboratory data. Coquart et al. [86] have reported Herzberg continuum absorption cross sections in the wavelength region 196–205 nm of the Schumann-Runge bands.

For parameterizations of the O_2 absorption in the Schumann-Runge bands used in atmospheric modeling calculations, see, e.g., the review in WMO Report No. 16 [434]. More recent work by Murtagh [285], Nicolet and Kennes, [294] and Minschwaner et al. [258] incorporates results of the later laboratory measurements into efficient schemes for computing broad-band transmission and photolysis rates. Transmission values obtained by Murtagh [285] agree well with the WMO [434] recommendations, although the high-resolution calculations of Minschwaner and Salawitch differ with the WMO values by as much as 10–20% at some wavelengths.

In view of the quality of the high-resolution laboratory measurements, the primary source of uncertainty in modeling O_2 photolysis in the Schumann-Runge bands (other than the issue of absolute solar irradiance) has shifted to the choice of broadband parameterization.

A2. $O_3 + h\nu \rightarrow O + O_2$. The O_3 absorption cross sections and their temperature dependence have been measured by several groups. An earlier review is presented in WMO Report No. 16 [434]; this reference should be consulted to obtain data for atmospheric modeling calculations. Table 4-4 lists merely a sample of the data taken from this review, namely the 273 K cross section values averaged over the wavelength intervals commonly employed in modeling calculations, except for the wavelength range 185 to 225 nm, where the present recommendation incorporates the averaged values from the work of Molina and Molina [270]; the older values were based on the work of Inn and Tanaka [179]. More recently, Daumont et al. [101] and Brion et al. [43] reported ozone absorption cross section measurements between 195 and 345 nm, in the temperature range 200–300 K; and Yoshino et al. [441] measured the cross sections in the 185 to 254 nm wavelength range at 195, 228, and 295 K; the results of these studies yield values in very good agreement with those reported by Molina and Molina [270]. Cacciani et al. [63] reported measurements of the ozone cross sections in the wavelength range from 339 to 355 nm, in reasonable agreement with the present recommendation; the same group has measured also the cross sections in the 590–610 nm region, at 230 K and at 299 K (Amoruso et al. [9]). The temperature effect on the cross sections is negligible for wavelengths shorter than ~260 nm. Recent work by Mauersberger et al. [245,246] yields a value of 1137×10^{-20} cm^2 for the cross section at 253.7 nm, the mercury line wavelength; it is about 1% smaller than the commonly accepted value of 1147×10^{-20} cm^2 reported by Hearn [156]; about 2% smaller than the value obtained by DeMore and Raper [106] and Molina and Molina [270], 1157×10^{-20} cm^2; and 0.5% larger than the value obtained by Daumont et al. [101]. The reason for the small discrepancy, which appears to be beyond experimental precision, is unclear.

Malicet et al. [229] report cross section measurements in the 195–345 nm range, at temperatures between 218 and 295 K, with a spectral bandwidth of 0.01–0.02 nm.; the results are in good agreement with the recommended values. Their data are presented in graphical form, and are also available in electronic format.

Table 4-4. Absorption Cross Sections of O_3 at 273 K

λ (nm)	$10^{20}\ \sigma$ (cm^2) average	λ (nm)	$10^{20}\ \sigma$ (cm^2) average
175.439–176.991	81.1	238.095–240.964	797
176.991–178.571	79.9	240.964–243.902	900
178.571–180.180	78.6	243.902–246.914	1000
180.180–181.818	76.3	246.914–250.000	1080
181.818–183.486	72.9	250.000–253.165	1130
183.486–185.185	68.8	253.165–256.410	1150
185.185–186.916	62.2	256.410–259.740	1120
186.916–188.679	57.6	259.740–263.158	1060
188.679–190.476	52.6	263.158–266.667	965
190.476–192.308	47.6	266.667–270.270	834
192.308–194.175	42.8	270.270–273.973	692
194.175–196.078	38.3	273.973–277.778	542
196.078–198.020	34.7	277.778–281.690	402
198.020–200.000	32.3	281.690–285.714	277
200.000–202.020	31.4	285.714–289.855	179
202.020–204.082	32.6	289.855–294.118	109
204.082–206.186	36.4	294.118–298.507	62.4
206.186–208.333	43.4	298.507–303.030	34.3
208.333–210.526	54.2	303.030–307.692	18.5
210.526–212.766	69.9	307.692–312.5	9.80
212.766–215.054	92.1	312.5–317.5	5.01
215.054–217.391	119	317.5–322.5	2.49
217.391–219.780	155	322.5–327.5	1.20
219.780–222.222	199	327.5–332.5	0.617
222.222–224.719	256	332.5–337.5	0.274
224.719–227.273	323	337.5–342.5	0.117

λ (nm)	10^{20} σ (cm^2) average	λ (nm)	10^{20} σ (cm^2) average
227.273–229.885	400	342.5–347.5	0.0588
229.885–232.558	483	347.5–352.5	0.0266
232.558–235.294	579	352.5–357.5	0.0109
235.294–238.095	686	357.5–362.5	0.00549

The recommendation for the $O(^1D)$ quantum yield from ozone photolysis as a function of wavelength and temperature is given by the expression,

$$\Phi(\lambda,T) = \left(\frac{q_1}{q_1+q_2}\right) \times A_1 \times \exp\left\{-\left(\frac{X_1-\lambda}{\omega_1}\right)^4\right\} + \left(\frac{q_2}{q_1+q_2}\right) \times A_2 \times \left(\frac{T}{300}\right)^2 \times \exp\left\{-\left(\frac{X_2-\lambda}{\omega_2}\right)^2\right\}$$
$$+ A_3 \times \left(\frac{T}{300}\right)^{1.5} \times \exp\left\{-\left(\frac{X_3-\lambda}{\omega_3}\right)^2\right\} + c$$

where $q_i = \exp\left(-\frac{\nu_i}{RT}\right)$ and X_{1-3}, A_{1-3}, ω_{1-3}, ν_{1-2} and c are best-fit parameters given in Table 4-5, λ is in nm, T is in K, and R = 0.695 (cm^{-1}/K). The parameter c is assumed to be temperature and wavelength independent. **This expression is valid only for the wavelength range 306–328 nm and temperature range 200–320 K.**

Table 4-5. Parameters for the Calculation of $O(^1D)$ Quantum Yields

Parameter	i = 1	i = 2	i = 3
X_i (nm)	304.225	314.957	310.737
ω_i (nm)	5.576	6.601	2.187
A_i	0.8036	8.9061	0.1192
ν_i (cm^{-1})	0	825.518	–
c	0.0765	–	–

At room temperature (298 K) the uncertainties of the quantum yield values calculated with the above expression are estimated to be ±10 % (1σ) for Φ(λ, 298 K) ≥ 0.4, while the uncertainties are estimated to be ±0.04 for Φ(λ, 298 K) < 0.4. At temperatures other than room temperature, the uncertainties are estimated to be ± 15 % for Φ(λ, T) ≥ 0.4 and ± 0.06 for Φ(λ, T) < 0.4.

In the wavelength range 329–340 nm we recommend the value of $\Phi(O^1D)$ = 0.08 ± 0.04, independent of temperature. For λ > 340 nm, the quantum yield may be non-zero but no recommendation is made. For λ < 306 nm. the recommended quantum yield is 0.90, independent of temperature.

The recommendation for the temperature and wavelength dependences of the quantum yield for $O(^1D)$ production, $\Phi(O^1D)$, is taken from the review of Matsumi et al. [244]. Matsumi et al. derived the recommended values using the following procedure: The measured $O(^1D)$ quantum yields at 298 K between 306 and 328 nm from eight studies (Talukdar et al. [398], Takahashi et al. [392], Ball et al. [19], Armerding et al. [16], Bauer et al. [28], Brock and Watson [44], Trolier and Wiesenfeld [403] and Smith et al. [383], were normalized using $\Phi(O^1D)$ = 0.79 at 308 nm. This value was derived from the studies listed in Table 1 of Matsumi et al. [244]. The resulting renormalized data were averaged. The wavelength dependence quantum yield data at various temperatures reported by Talukdar et al. [396,398], Takahashi et al. [392], Hancock and Hofzumahaus [149] (this includes all the data from the Oxford group), Bauer et al. [28] and Smith et al. [383] were normalized to the value at 308 nm given above. These normalized data were used to obtain the best-fit parameters for eqn. 4-1 for the wavelength range 306–328 nm and temperature range 200–320 K. Because of the large number of studies upon which the 298 K evaluation is based, the averaged 298 K data were given a larger weight in the fitting procedure than the data at other temperatures.

The major differences between this recommendation and that of JPL 00-3 [358] are: (1) inclusion of more recent data from Smith et al., Hancock and Hofzumahaus, and Bauer et al., (2) selective deletion of data from

the previous data from some of the groups, especially the use of data from Bauer et al. [28] which superseded the data of Silvente et al. [375] from the same group, (3) correcting for small differences in the absorption cross sections of ozone used by various groups, and (4) the normalization of all data to the selected value at 308 nm.

B1. $HO_2 + h\nu \rightarrow OH + H$. The absorption cross sections of the hydroperoxyl radical, HO_2, in the 190–260 nm region have been measured at room temperature by Paukert and Johnston [311], Hochanadel et al. [161], Cox and Burrows [89], McAdam et al. [250], Kurylo et al. [206], Moortgat et al. [280], Dagaut and Kurylo [99], Lightfoot and Jemi-Alade [218], who measured the cross sections up to 777 K, Crowley et al. [97], Maricq and Szente [238], Roehl et al. [342] and Sander et al. [359] at 227.5 nm. The absorption cross sections have been evaluated in earlier reviews by Lightfoot et al. [217] and Wallington et al. [426] who noted significant discrepancies in both the shapes of the spectra and the absolute magnitudes of the cross section values, particularly around 200 nm. The published ultraviolet absorption spectra have recently been reevaluated by Tyndall et al. [408]. Herein, the spectra were fitted to an analytical equation suggested by Maric et al. [237]:

$$\sigma = \frac{\sigma_{med}}{\nu(1-b)} \exp^{-a\left[\ln\left(\frac{\nu-b}{\nu_{med}-b}\right)\right]^2}$$

where $\sigma_{med} = 1.84 \times 10^{-18}$ cm^2 molecule^{-1}, a = 4.91, b = 30612 cm^{-1} and ν_{med}= 50260 cm^{-1}. Absolute cross sections were based on relative measurements of absorption cross sections of HO_2, CH_3O_2 and $C_2H_5O_2$ at 240 nm taken under identical conditions, combined with independent calibrations by Crowley et al. [97]. Table 4-6 lists the recommended cross sections, which are taken from the review by Tyndall et al. [408].

Lee [212] has detected $O(^1D)$ as a primary photodissociation product at 193 and at 248 nm, with a quantum yield that is about 15 times larger at the longer wavelength. The absolute quantum yield for $O(^1D)$ production has not been reported yet.

Photolysis of HO_2 in the stratosphere and troposphere is slow and can be neglected, but the UV absorption cross sections are important in laboratory studies of reaction kinetics.

Table 4-6. Absorption Cross Sections of HO_2

λ (nm)	$10^{20}\sigma$ (cm^2)
190	368
195	402
200	423
205	427
210	415
215	385
220	341
225	288
230	230
235	173
240	122
245	79.7
250	48.0
255	26.3
260	12.9

B2. $H_2O + h\nu \rightarrow H + OH$. Water vapor has a continuum absorption spectrum at wavelengths longer than 145 nm, with a maximum around 165 nm, the cross sections falling off rapidly toward longer wavelengths; the photodissociation threshold occurs at 246 nm. Below 69 nm the spectrum is also a continuum, and between 69 and 145 nm it consists of diffuse bands. In the atmosphere water vapor is photodissociated mainly by the solar Lyman alpha line (121.6 nm).

The absorption cross sections and the photochemistry of water vapor have been reviewed, for example, by Hudson [168,169], by Hudson and Kiefer [170], by Calvert and Pitts [65], and by Okabe [300].

The recommended absorption cross sections are taken from the review by Hudson and Kiefer [170] and are listed in Table 4-7 between 175 and 190 nm. At these wavelengths the quantum yield for production of H and

OH is unity. At shorter wavelengths H_2 and O are also formed as primary products. Stief et al. [388] report a quantum yield of 0.11 for this process between 105 and 145 nm.

Table 4-7. Absorption Cross Sections of H_2O Vapor

λ(nm)	$10^{20}\sigma$ (cm^2)
175.5	262.8
177.5	185.4
180.0	78.1
182.5	23.0
185.0	5.5
186.0	3.1
187.5	1.6
189.3	0.7

B3. $H_2O_2 + h\nu \rightarrow OH + OH$. The recommended 298 K absorption cross section values, listed in Table 4-8, are the mean of the data of Lin et al. [221], Molina and Molina [267], Nicovich and Wine [295], and Vaghjiani and Ravishankara [414]. Molina and Molina [267] supersedes the earlier results of Molina et al. [273]. Nicovich and Wine measured the cross sections at λ ± 230 relative to the values at 202.6, $\sigma = 4.32 \times 10^{-19}$ cm^2, and at 228.8 nm, $\sigma = 1.86 \times 10^{-19}$ cm^2. The values are within 2% of the recommended value.

Table 4-8. Absorption Cross Sections of H_2O_2 Vapor

λ (nm)	$10^{20}\sigma$ (cm^2)		λ (nm)	$10^{20}\sigma$ (cm^2)	
	298 K	355 K		298 K	355 K
190	67.2		270	3.3	3.5
195	56.4		275	2.6	2.8
200	47.5		280	2.0	2.2
205	40.8		285	1.5	1.6
210	35.7		290	1.2	1.3
215	30.7		295	0.90	1.0
220	25.8		300	0.68	0.79
225	21.7		305	0.51	0.58
230	18.2	18.4	310	0.39	0.46
235	15.0	15.2	315	0.29	0.36
240	12.4	12.6	320	0.22	0.27
245	10.2	10.8	325	0.16	0.21
250	8.3	8.5	330	0.13	0.17
255	6.7	6.9	335	0.10	0.13
260	5.3	5.5	340	0.07	0.10
265	4.2	4.4	345	0.05	0.06
			350	0.04	0.05

Nicovich and Wine have measured the temperature dependence of these cross sections. They expressed the measured cross sections as the sum of two components: σ_1, due to absorption from H_2O_2, which has the O–O stretch excited; and σ_0, due to absorption by ground state molecules. For atmospheric calculations the expression given in Table 4-9 may be used. The photodissociation quantum yield is believed to be unity. At and above 248 nm, the major photodissociation process is that leading to OH, i.e., the quantum yield for OH production is 2 (Vaghjiani and Ravishankara [415] and Vaghjiani et al. [416]). At 193 nm this quantum yield decreases to about 1.5 (Vaghjiani et al. [416]; Schiffman et al. [364]), and the quantum yield for O-atom production increases to about 0.16 (Vaghjiani et al. [416]).

Table 4-9. Mathematical Expression for Absorption Cross Sections of H_2O_2 as a Function of Temperature

$$10^{21}\,\sigma(\lambda,T) = \chi \sum_{n=0}^{7} A_n \lambda^n + (1-\chi) \sum_{n=0}^{4} B_n \lambda^n$$

Where T: temperature K; λ: nm; $\chi = (1 + \exp(-1265/T))^{-1}$

$A_0 = 6.4761 \times 10^4$	$B_0 = 6.8123 \times 10^3$
$A_1 = -9.2170972 \times 10^2$	$B_1 = -5.1351 \times 10^1$
$A_2 = 4.535649$	$B_2 = 1.1522 \times 10^{-1}$
$A_3 = -4.4589016 \times 10^{-3}$	$B_3 = -3.0493 \times 10^{-5}$
$A_4 = -4.035101 \times 10^{-5}$	$B_4 = -1.0924 \times 10^{-7}$
$A_5 = 1.6878206 \times 10^{-7}$	
$A_6 = -2.652014 \times 10^{-10}$	
$A_7 = 1.5534675 \times 10^{-13}$	

Range 260–350 nm; 200–400 K

C1. $NO_2 + h\nu \rightarrow NO + O$. Earlier recommendations for the absorption cross sections of nitrogen dioxide were taken from the work of Bass et al. [26]. More recent measurements have been reported by Schneider et al. [367], at 298 K, for the wavelength range from 200 to 700 nm, and by Davidson et al. [103], from 270 to 420 nm, in the 232–397 K temperature range. At room temperature the agreement between these three sets of measurements is good (within 5% between 305 and 345 nm and within 10% at the longer wavelengths). The agreement is poor below room temperature, as well as at the shorter wavelengths. A possible cause for the discrepancies is the presence of N_2O_4. The corrections needed to account for the presence of this species are largest around 200 nm, where it absorbs strongly. The corrections are also large at the lowest temperatures, because a significant fraction of the NO_2 forms N_2O_4. On the other hand, there is no error apparent in the corrections carried out by Bass et al., so that the reason for the discrepancy is not clear. Measurements of the absorption cross sections in the visible (440 to 460 nm), between 273 and 404 K, have been reported by Amoruso et al. [10], and Corcoran et al. [87] carried out high-resolution measurements at a few selected wavelength ranges between 470 and 616 nm, at 295, 573, and 673 K. Additional high-resolution studies of the cross sections, mainly aimed at improving the accuracy of atmospheric measurements, have been reported by Harwood and Jones [152], Coquart et al. [85], Mérienne et al. [257], Frost et al. [125], and Harder et al. [150].

Table 4-10 lists the recommended absorption cross sections, averaged over the wavelength intervals used for atmospheric photodissociation calculations. For the wavelength range from 200 to 274 nm the values are taken from Schneider et al. [367]; in this range the temperature effect is negligible. For the 274-to-420-nm region the temperature-dependent values are taken from Davidson et al. [103].

Table 4-10. Absorption Cross Sections of NO_2

λ (nm)	10^{20} σ, average at 25°C (cm^2 $molecule^{-1}$)	λ (nm)	10^{20} σ, average at 0°C (cm^2 $molecule^{-1}$)	10^{22} a* (cm^2 $molecule^{-1}$ $degree^{-1}$)
202.02–204.08	41.45	273.97–277.78	5.03	0.075
204.08–206.19	44.78	277.78–281.69	5.88	0.082
206.19–208.33	44.54	281.69–285.71	7.00	–0.053
208.33–210.53	46.41	285.71–289.85	8.15	–0.043
210.53–212.77	48.66	289.85–294.12	9.72	–0.031
212.77–215.06	48.18	294.12–298.51	11.54	–0.162
215.06–217.39	50.22	298.51–303.03	13.44	–0.284
217.39–219.78	44.41	303.03–307.69	15.89	–0.357
219.78–222.22	47.13	307.69–312.50	18.67	–0.536
222.22–224.72	37.72	312.5–317.5	21.53	–0.686
224.72–227.27	39.29	317.5–322.5	24.77	–0.786
227.27–229.89	27.40	322.5–327.5	28.07	–1.105
229.89–232.56	27.78	327.5–332.5	31.33	–1.355
232.56–235.29	16.89	332.5–337.5	34.25	–1.277
235.29–238.09	16.18	337.5–342.5	37.98	–1.612
238.09–240.96	8.812	342.5–347.5	40.65	–1.890
240.96–243.90	7.472	347.5–352.5	43.13	–1.219
243.90–246.91	3.909	352.5–357.5	47.17	–1.921
246.91–250.00	2.753	357.5–362.5	48.33	–1.095
250.00–253.17	2.007	362.5–367.5	51.66	–1.322
253.17–256.41	1.973	367.5–372.5	53.15	–1.102
256.41–259.74	2.111	372.5–377.5	55.08	–0.806
259.74–263.16	2.357	377.5–382.5	56.44	–0.867
263.16–266.67	2.698	382.5–387.5	57.57	–0.945
266.67–270.27	3.247	387.5–392.5	59.27	–0.923
270.27–273.97	3.785	392.5–397.5	58.45	–0.738
		397.5–402.5	60.21	–0.599
		402.5–407.5	57.81	–0.545
		407.5–412.5	59.99	–1.129
		412.5–417.5	56.51	0.001
		417.5–422.5	58.12	–1.208

* The quantity **a** is the temperature coefficient of σ as defined in the equation:

$$\sigma(t) = \sigma(0° \text{ C.}) + aT,$$

where T is in degrees Celsius.

The earlier recommendation for quantum yields was based on the work of Harker et al. [151] and of Davenport [102] for the atmospherically important 375–470 nm region. The work by Gardner et al. [129] yields values that are in much better agreement with the values reported earlier by Jones and Bayes [193]. The recommended quantum yield values, listed in Table 4-11, are in agreement with the recommendation of Gardner et al. [129]; they are based on a smooth fit to the data of Gardner et al. [129] for the wavelength range from 334 to 404 nm; Harker et al. [151] for 397–420 nm (corrected for cross sections); Davenport [102] for 400–420 nm; and Jones and Bayes [193] for 297–412 nm. Direct measurements of the solar photodissociation rate of NO_2 in the troposphere by Parrish et al. [310] and by Shetter et al. [374] agree better with theoretical estimates based on this recommendation than with the earlier one.

Table 4-11. Quantum Yields for NO_2 Photolysis

λ, nm	Φ	λ, nm	Φ
<285	1.000	393	0.953
290	0.999	394	0.950
295	0.998	395	0.942
300	0.997	396	0.922
305	0.996	397	0.870
310	0.995	398	0.820
315	0.994	399	0.760
320	0.993	400	0.695
325	0.992	401	0.635
330	0.991	402	0.560
335	0.990	403	0.485
340	0.989	404	0.425
345	0.988	405	0.350
350	0.987	406	0.290
355	0.986	407	0.225
360	0.984	408	0.185
365	0.983	409	0.153
370	0.981	410	0.130
375	0.979	411	0.110
380	0.975	412	0.094
381	0.974	413	0.083
382	0.973	414	0.070
383	0.972	415	0.059
384	0.971	416	0.048
385	0.969	417	0.039
386	0.967	418	0.030
387	0.966	419	0.023
388	0.964	420	0.018
389	0.962	421	0.012
390	0.960	422	0.008
391	0.959	423	0.004
392	0.957	424	0.000

C2. $NO_3 + h\nu \rightarrow NO + O_2$ (Φ_1)

$NO_3 + h\nu \rightarrow NO_2 + O$ (Φ_2). The absorption cross sections of the nitrate free radical, NO_3, have been studied by (1) Johnston and Graham [188], (2) Graham and Johnston [144], (3) Mitchell et al. [262], (4) Marinelli et al. [242], (5) Ravishankara and Wine [330], (6) Cox et al. [88], (7) Burrows et al. [60], (8) Ravishankara and Mauldin [327], (9) Sander [356], (10) Cantrell et al. [69], (11) Canosa-Mas et al. [67], and (12) Yokelson et al. [437]. The 1st and 4th studies required calculation of the NO_3 concentration by modeling a complex kinetic system. The other studies are more direct, and the results in terms of integrated absorption coefficients are in good agreement. The recommended value at 298 K and 662 nm, $(2.00 \pm 0.25) \times 10^{-17}$ cm^2, is the average of the results of studies (4), (5), and (7) through (11). The values in the wavelength range 600–670 nm, shown in Figure 4-1 and listed in Table 4-12, were calculated using the spectra measured in studies (8), (9), and (11), and with the 662 nm value normalized to the above average. The spectra obtained in other studies are consulted for a more extended wavelength range. The temperature dependence of the 662 nm band has been studied by Ravishankara and Mauldin, Sander, Cantrell et al., and Yokelson et al. Except for Cantrell et al., these studies all showed that the cross section at 662 nm increases with decreasing temperature. The reason for this discrepancy is not clear.

The quantum yields Φ_1 and Φ_2 have been measured by Graham and Johnston [144], and under higher resolution by Magnotta and Johnston [227], who report the product of the cross section times the quantum yield in the 400-to-630-nm range. The total quantum yield value, $\Phi_1 + \Phi_2$, computed from the results of this latter study

and the cross sections of Graham and Johnston [144], is above unity for λ <610 nm, which is, of course, impossible. Hence, there is some systematic error, and it is most likely in the primary quantum yield measurements. More recently, Orlando et al. [306] measured the photolysis quantum yields between 570 and 635 nm.

Johnston et al.[186] have recently re-analyzed the available laboratory data relevant to NO_3 photolysis, including quantum yield studies, chemiluminescence, LIF studies, and molecular-beam-scattering experiments. Their model reproduces the wavelength-dependent quantum yield data reasonably well. The new recommendation is based on the J-values calculated by Johnston et al. for overhead sun in the stratosphere:

$$J_1(NO + O_2) = 0.0201\ s^{-1}$$

$$J_2(NO_2 + O) = 0.156\ s^{-1}$$

Wavelength-specific quantum yields over the temperature range 190–298 K may be found in the tabulation by Johnston et al.

The spectroscopy of NO_3 has been reviewed by Wayne et al. [431]. The reader is referred to this work for a more detailed discussion of the cross section and quantum yield data and for estimates of the photodissociation rates as a function of zenith angle.

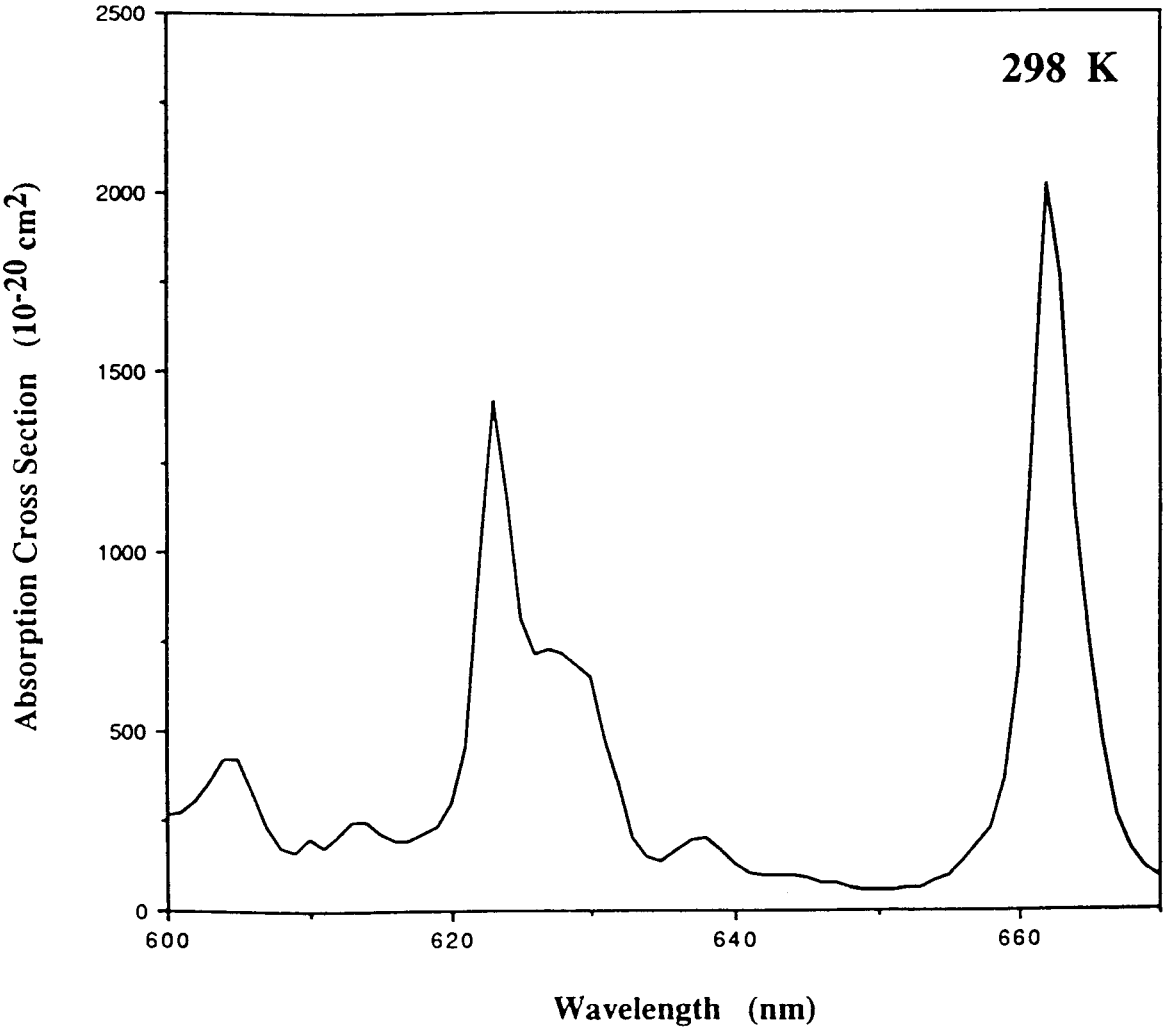

Figure 4-1. Absorption Spectrum of NO_3

Table 4-12. Absorption Cross Sections of NO_3 at 298 K

λ (nm)	$10^{20}\sigma$ (cm^2)	λ (nm)	$10^{20}\sigma$ (cm^2)	λ (nm)	$10^{20}\sigma$ (cm^2)
600	258	625	796	648	60
601	263	626	703	649	51
602	302	627	715	650	49
603	351	628	702	651	52
604	413	629	672	652	55
605	415	630	638	653	61
606	322	631	470	654	76
607	225	632	344	655	93
608	170	633	194	656	131
609	153	634	142	657	172
610	192	635	128	658	222
611	171	636	159	659	356
612	202	637	191	660	658
613	241	638	193	661	1308
614	242	639	162	662	2000
615	210	640	121	663	1742
616	190	641	99	664	1110
617	189	642	91	665	752
618	208	643	93	666	463
619	229	644	92	667	254
620	292	645	85	668	163
621	450	646	72	669	113
622	941	647	69	670	85
623	1407				
624	1139				

C3. $N_2O + h\nu \rightarrow N_2 + O(^1D)$. The recommended values are taken from the work of Selwyn et al. [371], who measured the temperature dependence of the absorption cross sections in the atmospherically relevant wavelength region. They have fitted their data with the expression shown in Table 4-13; Table 4-14 presents the room temperature data. Hubrich and Stuhl [165] remeasured the N_2O cross sections at 298 K and 208 K and Merienne et al. [256] in the range from 220 K to 296 K. The results of these two sets of measurements are in very good agreement with those of Selwyn et al. The quantum yield for photodissociation is unity, and the products are N_2 and $O(^1D)$ (Zelikoff and Aschenbrand [448], Paraskevopoulos and Cvetanovic [307], Preston and Barr [320], Simonaitis et al. [381]). The yield of $N(^4S)$ and $NO(^2\Pi)$ is less than 1% (Greenblatt and Ravishankara [147]).

Table 4-13. Mathematical Expression for Absorption Cross Sections of N_2O as a Function of Temperature*

$$\ln(\sigma(\lambda,T)) = \sum_{n=0}^{4} A_n \lambda^n + (T-300)\exp\left(\sum_{n=0}^{3} B_n \lambda^n\right)$$

Where T: temperature K; λ: nm;

$A_0 = 68.21023$ $B_0 = 123.4014$

$A_1 = -4.071805$ $B_1 = -2.116255$

$A_2 = 4.301146 \times 10^{-2}$ $B_2 = 1.111572 \times 10^{-2}$

$A_3 = -1.777846 \times 10^{-4}$ $B_3 = -1.881058 \times 10^{-5}$

$A_4 = 2.520672 \times 10^{-7}$

*Ranges of applicability: 173 nm < λ < 240 nm; 194 K < T < 320 K

Table 4-14. Absorption Cross Sections of N_2O at 298 K

λ (nm)	$10^{20}\sigma$ (cm^2)	λ (nm)	$10^{20}\sigma$ (cm^2)	λ (nm)	$10^{20}\sigma$ (cm^2)
173	11.3	196	6.82	219	0.115
175	12.6	198	5.35	221	0.0739
176	13.4	199	4.70	222	0.0588
177	14.0	200	4.09	223	0.0474
178	13.9	201	3.58	224	0.0375
179	14.4	202	3.09	225	0.0303
180	14.6	203	2.67	226	0.0239
181	14.6	204	2.30	227	0.0190
182	14.7	205	1.95	228	0.0151
183	14.6	206	1.65	229	0.0120
184	14.4	207	1.38	230	0.00955
185	14.3	208	1.16	231	0.00760
186	13.6	209	0.980	232	0.00605
187	13.1	210	0.755	233	0.00478
188	12.5	211	0.619	234	0.00360
189	11.7	212	0.518	235	0.00301
190	11.1	213	0.421	236	0.00240
191	10.4	214	0.342	237	0.00191
192	9.75	215	0.276	238	0.00152
193	8.95	216	0.223	239	0.00123
194	8.11	217	0.179	240	0.00101
195	7.57	218	0.142		

Several groups have investigated the isotopic fractionation of N_2O resulting from photolysis in the UV. Fractionation factors have been measured by several groups following photolysis at several wavelengths in the 193–213 nm range: Turatti et al. [404] employed high resolution FTIR spectroscopy; Rockmann et al. [340] used a modified isotope ratio mass spectrometric technique; and Rahn et al. [321] utilized conventional isotope ratio mass spectrometry. Zhang et al. [450] employed a low-resolution FTIR technique with N_2O photolysis at 213 nm, and Rockmann et al. [341] utilized a broadband photolysis source centered around 200 nm and simulating stratospheric actinic fluxes. The results are in reasonably good agreement, and indicate that the fractionation factors increase with photolysis wavelength from 193 to 213 nm. Furthermore, the fractionation factors show a clear dependence on the position of the ^{15}N atom, in agreement with the theoretical model of Yung and Miller [447]; however, the theoretical calculations underestimate the laboratory results by about a factor of two. Analysis of the isotopic composition of stratospheric air samples yields results that are in qualitative agreement with the laboratory results, confirming that photolysis is the predominant sink for N_2O [148,341]. On the other hand, the fractionation factors measured in the atmospheric samples are smaller than those reported from the laboratory studies, indicating the influence of atmospheric diffusion and mixing [341].

C4. $N_2O_5 + h\nu \rightarrow$ Products. The absorption cross sections of dinitrogen pentoxide, N_2O_5 have been measured at room temperature by Jones and Wulf [192] between 285 and 380 nm, by Johnston and Graham [188] between 210 and 290 nm, by Graham [143] between 205 and 380 nm, and for temperatures in the 223 to 300 K range by Yao et al. [436], between 200 and 380 nm. The agreement is good, particularly considering the difficulties in handling N_2O_5. The recommended cross section values, listed in Table 4-15, are taken from Yao et al. [436]. For wavelengths shorter than 280 nm there is little or no temperature dependence, and between 285 and 380 nm the temperature effect is best computed with the expression listed at the bottom of Table 4-15. Recent measurements of the cross sections and their temperature dependence by Harwood et al. [153] yield values in excellent agreement with this recommendation except at the longest wavelengths (380 nm) and lowest temperatures (233 K), where the new values are about 30% lower. However, the contribution to solar photodissociation from these longer wavelengths is negligible, and the differences between the predicted photolysis rates from the two sets of data are smaller than 3% (Harwood et al. [153]).

There are several studies on the primary photolysis products of N_2O_5: Swanson et al. [391] have measured the quantum yield for NO_3 production at 249 and at 350 nm, obtaining a value close to unity, which is consistent with the observations of Burrows et al. [59] for photolysis at 254 nm. Barker et al. [21] report a quantum yield

for $O(^3P)$ production at 290 nm of less than 0.1, and near unity for NO_3. For O-atom production Margitan (private communication, 1985) measured a quantum yield value of 0.35 at 266 nm, and Ravishankara et al. [331] report values of 0.72, 0.38, 0.21 and 0.15 at 248, 266, 287, and 289 nm, respectively, with a quantum yield near unity for NO_3 production at all these wavelengths. It appears, then, that NO_3 is produced with unit quantum yield while the O-atom, and hence the NO yield, increases at shorter wavelengths, with a consequent decrease in the NO_2 yield. The study of Oh et al. [299] indicates that, besides NO_3, the primary photolysis products are a wavelength-dependent mixture of NO_2, NO_2* and NO + O, where NO_2* represents one or more excited electronic states, most likely the $^2B_1$ state.

Table 4-15. Absorption Cross Sections of N_2O_5

λ (nm)	$10^{20}\sigma$ (cm^2)	λ (nm)	$10^{20}\sigma$ (cm^2)
205	820	250	40
210	560	255	32
215	370	260	26
220	220	265	20
225	144	270	16.1
230	99	275	13.0
235	77	280	11.7
240	62		

Note: For 285 nm < λ < 380 nm; 300 K > T > 225 K: $10^{20}\,\sigma = \exp(2.735 + ((4728.5 - 17.127\,\lambda)/T))$
where σ is in cm^2/molecule; λ in nm; and T in K.

C5. HONO + hν $\rightarrow$ OH + NO. The ultraviolet spectrum of HONO between 300 and 400 nm has been studied by Stockwell and Calvert [389] by examination of its equilibrium mixtures with NO, NO_2, H_2O, N_2O_3 and N_2O_4; the possible interferences by these compounds were taken into account. More recently, Vasudev [421] measured relative cross sections by monitoring the OH photodissociation product with laser-induced fluorescence; and Bongartz et al. [38] determined absolute cross section values at 0.1 nm resolution in a system containing a highly diluted mixture of NO, NO_2, H_2O, and HONO, by measuring total NO_x (NO and NO_2). There are some discrepancies between these two recent sets of results in terms of relative peak heights; however, both yield essentially the same photodissociation rate provided Vasudev's relative data are normalized to match the cross section value reported by Bongartz et al. at 354 nm. At this wavelength the value reported earlier by Stockwell and Calvert is about 20% smaller. The recommended values, listed in Table 4-16, are taken from Bongartz et al.

Table 4-16. Absorption Cross Sections of HONO

λ (nm)	$10^{20}\sigma$ (cm^2)	λ (nm)	$10^{20}\sigma$ (cm^2)	λ (nm)	$10^{20}\sigma$ (cm^2)
310	1.3	339	18.8	368	52.0
311	1.9	340	10.0	369	38.8
312	2.8	341	17.0	370	17.8
313	2.2	342	38.6	371	11.3
314	3.6	343	14.9	372	10.0
315	3.0	344	9.7	373	7.7
316	1.4	345	10.9	374	6.2
317	3.1	346	12.3	375	5.3
318	5.6	347	10.4	376	5.3
319	3.6	348	9.1	377	5.0
320	4.9	349	7.9	387	5.8
321	7.8	350	11.2	379	8.0
322	4.9	351	21.2	380	9.6
323	5.1	352	15.5	381	11.3
324	7.1	353	19.1	382	15.9
325	5.0	354	58.1	383	21.0
326	2.9	355	36.4	384	24.1
327	6.6	356	14.1	385	20.3
328	11.7	357	11.7	386	13.4
329	6.1	358	12.0	387	9.0
330	11.1	359	10.4	388	5.6
331	17.9	360	9.0	389	3.4
332	8.7	361	8.3	390	2.7
333	7.6	362	8.0	391	2.0
334	9.6	363	9.6	392	1.5
335	9.6	364	14.6	393	1.1
336	7.2	365	16.8	394	0.6
337	5.3	366	18.3	395	1.0
338	10.0	367	30.2	396	0.4

C6. $HNO_3 + h\nu \rightarrow$ products. The recommended absorption cross sections and their temperature dependency, listed in Table 4-17, are taken from the work of Burkholder et al. [56]. The temperature effect is very important for estimates of atmospheric photodissociation; the results of Burkholder et al. agree well with those of Rattigan et al. [322,323], except at 238 K, where these latter authors report significantly smaller values.

The new cross section values agree reasonably well at room temperature with the data of Molina and Molina [267], which provided the basis for the earlier recommendation. These data are also in good agreement throughout the 190–330 nm range with the values reported by Biaume [32]. They are also in very good agreement with the data of Johnston and Graham [187], except towards both ends of the wavelength range. Okabe [301] has measured the cross sections in the 110–190 nm range and his results are 20–30% lower than those of Biaume and of Johnston and Graham around 185–190 nm.

Johnston et al. [185] measured a quantum yield value of ~1 for the OH + NO_2 channel in the 200–315 nm range, using end product analysis. The quantum yield for O-atom production at 266 nm has been measured to be 0.03, and that for H-atom production less than 0.002, by Margitan and Watson [234], who looked directly for these products using atomic resonance fluorescence. Jolly et al. [191] measured a quantum yield for OH production of 0.89 ± 0.08 at 222 nm. Turnipseed et al. [407] have measured a quantum yield near unity for OH production at 248 and 222 nm. However, at 193 nm they report this quantum yield to be only ~0.33, and the quantum yield for production of O-atoms to be about 0.8. Thus, it appears that HONO is a major photolysis product at 193 nm. These results are qualitatively in agreement with those reported by Schiffman et al. [364], namely a quantum yield for OH production of 0.47 at 193 nm, and of 0.75 at 248 nm.

Table 4-17. Absorption Cross Sections and Temperature Coefficients of HNO_3 Vapor

λ (nm)	$10^{20}\sigma$ (cm^2)	10^3 B (K^{-1})	λ (nm)	$10^{20}\sigma$ (cm^2)	10^3 B (K^{-1})	λ (nm)	$10^{20}\sigma$ (cm^2)	10^3 B (K^{-1})
192	1225	0	246	2.06	1.61	300	0.263	3.10
194	1095	0	248	2.00	1.44	302	0.208	3.24
196	940	1.70	250	1.97	1.34	304	0.167	3.52
198	770	1.65	252	1.96	1.23	306	0.133	3.77
200	588	1.66	254	1.95	1.18	308	0.105	3.91
202	447	1.69	256	1.95	1.14	310	0.0814	4.23
204	328	1.74	258	1.93	1.12	312	0.0628	4.70
206	231	1.77	260	1.91	1.14	314	0.0468	5.15
208	156	1.85	262	1.87	1.14	316	0.0362	5.25
210	104	1.97	264	1.83	1.18	318	0.0271	5.74
212	67.5	2.08	266	1.77	1.22	320	0.0197	6.45
214	43.9	2.17	268	1.70	1.25	322	0.0154	6.70
216	29.2	2.17	270	1.62	1.45	324	0.0108	7.16
218	20.0	2.21	272	1.53	1.49	326	0.00820	7.55
220	14.9	2.15	274	1.44	1.56	328	0.00613	8.16
222	11.8	2.06	276	1.33	1.64	330	0.00431	9.75
224	9.61	1.96	278	1.23	1.69	332	0.00319	9.93
226	8.02	1.84	280	1.12	1.78	334	0.00243	9.60
228	6.82	1.78	282	1.01	1.87	336	0.00196	10.5
230	5.75	1.80	284	0.909	1.94	338	0.00142	10.8
232	4.87	1.86	286	0.807	2.04	340	0.00103	11.8
234	4.14	1.90	288	0.709	2.15	342	0.00086	11.8
236	3.36	1.97	290	0.615	2.27	344	0.00069	9.30
238	2.93	1.97	292	0.532	2.38	346	0.00050	12.1
240	2.58	1.97	294	0.453	2.52	348	0.00042	11.9
242	2.34	1.88	296	0.381	2.70	350	0.00042	9.30

$\sigma(\lambda, T) = \sigma(\lambda, 298) \exp(B(\lambda)(T - 298))$; T in K

C7. $HO_2NO_2 + h\nu \rightarrow$ Products. There are five studies of the UV spectrum of HO_2NO_2 vapor: Cox and Patrick [91], Morel et al. [282], Graham et al. [145], Molina and Molina [267], and Singer et al. [382]. The latter three studies are the only ones covering the gas phase spectrum in the critical wavelength range for atmospheric photodissociation ($\lambda \geq 290$ nm). The recommended values, listed in Table 4-18, are an average of the work of Molina and Molina [267] and of Singer et al. [382], which are the more direct studies. The cross sections appear to be temperature independent between 298 and 253 K (Singer et al. [382]). MacLeod et al. [226] report that photolysis at 248 nm yields one third OH and NO_3 and two thirds $HO_2 + NO_2$.

Table 4-18. Absorption Cross Sections of HO_2NO_2 Vapor

λ (nm)	$10^{20}\sigma$ (cm^2)	λ (nm)	$10^{20}\sigma$ (cm^2)
190	1010	260	28.5
195	816	265	23.0
200	563	270	18.1
205	367	275	13.4
210	239	280	9.3
215	161	285	6.2
220	118	290	3.9
225	93.5	295	2.4
230	79.2	300	1.4
235	68.2	305	0.9
240	58.1	310	0.5
245	48.9	315	0.3
250	41.2	320	0.2
255	35.0	325	0.1

D1. $CH_2O + h\nu \rightarrow H + HCO\ (\Phi_1)$

$CH_2O + h\nu \rightarrow H_2 + CO\ (\Phi_2)$. The earlier recommendation for the formaldehyde absorption cross sections was based on the work carried out by Bass et al. [25] with a resolution of 0.05 nm at 296 K and 223 K, and by Moortgat et al. [277,279] with a resolution of 0.5 nm in the 210–360 K temperature range. More recently, Cantrell et al. [68] measured the cross sections in the 300–360 nm range between 223 K and 293 K, and Rogers [345] measured the cross sections in the 235–365 nm range at 296 K, both groups using Fourier transform spectrometry at a resolution of up to 0.011 nm (1 cm^{-1}). The agreement between these two reports is very good. The recommended values are those given by Cantrell et al. as a function of temperature; the reader is referred to the original article to obtain the high-resolution data. Table 4-19 lists the low-resolution cross sections taken from that work, that are suitable for atmospheric photodissociation calculations.

The quantum yields have been reported with good agreement by Horowitz and Calvert [162], Clark et al. [79], Tang et al. [400], Moortgat and Warneck [281], and Moortgat et al. [277,279]. The recommended values listed in Table 4-19 are based on the results of these investigators, as evaluated by S. Madronich (private communication, 1991). The quantum yield for the production of H_2 and CO is pressure- and temperature-dependent for wavelengths longer than about 330 nm (Moortgat et al. [279]). Table 4-19 gives the values at atmospheric pressure and room temperature; the reader is referred to the Moortgat et al. publication for information on values at lower pressures and temperatures.

Table 4-19. Absorption Cross Sections and Quantum Yields for Photolysis of CH_2O

λ (nm)	10^{20} σ(cm^2)		T-Parameters*		Φ_1 (H + HCO)	(H_2 + CO)
	223 K	293 K	A	B		
301.25	1.38	1.36	1.37	–0.21	0.749	0.251
303.75	4.67	4.33	4.43	–4.73	0.753	0.247
306.25	3.32	3.25	3.27	–1.06	0.753	0.247
308.75	2.27	2.22	2.24	–0.724	0.748	0.252
311.25	0.758	0.931	0.882	2.48	0.739	0.261
313.75	3.65	3.40	3.47	–3.64	0.724	0.276
316.25	4.05	3.89	3.94	–2.30	0.684	0.316
318.75	1.66	1.70	1.69	0.659	0.623	0.368
321.25	1.24	1.13	1.16	–1.52	0.559	0.423
323.75	0.465	0.473	0.471	0.118	0.492	0.480
326.25	5.06	4.44	4.61	–8.86	0.420	0.550
328.75	2.44	2.29	2.34	–2.15	0.343	0.634
331.25	1.39	1.28	1.31	–1.53	0.259	0.697
333.75	0.093	0.123	0.114	0.432	0.168	0.739
336.25	0.127	0.131	0.130	0.050	0.093	0.728
338.75	3.98	3.36	3.54	–8.96	0.033	0.667
341.25	0.805	0.936	0.898	1.86	0.003	0.602
343.75	1.44	1.26	1.31	–2.64	0.001	0.535
346.25	0.004	0.071	0.052	0.957	0	0.469
348.75	0.009	0.040	0.031	0.438	0	0.405
351.25	0.169	0.235	0.216	0.948	0	0.337
353.75	1.83	1.55	1.63	–4.05	0	0.265
356.25	0.035	0.125	0.099	1.27	0	0.197

Note: The values are averaged for 2.5 nm intervals centered on the indicated wavelength.
* Cross section for –50°C < T < 20°C calculated as $\sigma(T) = A + B \times 10^{-3}\ T$; T in °C, and σ in 10^{-20} cm^2.

D2. $CH_3O_2 + h\nu \rightarrow$ Products. The absorption cross sections of the methylperoxy radical, CH_3O_2, in the 195–310-nm region have been measured at room temperature by Parkes et al. [309], Hochanadel et al. [160], Parkes [308], Anastasi et al. [12], Kan et al. [197], Cox and Tyndall [93,94] at 250 nm only; Adachi et al. [5], Sander and Watson [360] at 250 nm only; Pilling and Smith [316] at 254 nm only, Kurylo et al. [206], McAdam et al. [250], Jenkin et al. [181], Wallington et al. [425], Moortgat et al. [280], Dagaut and Kurylo [99], Simon et al. [377], Jenkin and Cox [180], Lightfoot and Jemi-Alade [218] who measured the cross sections up to 777 K., Maricq and Wallington [240], Wallington et al. [427], Roehl et al. [342], and Fahr et al.

[114]. The absorption cross sections have been evaluated in earlier reviews by Lightfoot et al. [217] and Wallington et al. [426], who noted significant discrepancies in the both the shapes of the spectra and the absolute magnitude of the cross section values. The ultraviolet absorption spectra have recently been reevaluated by Tyndall et al. [408], who fitted the absorption spectra to a semilogarithmic Gaussian distribution function suggested by Lightfoot et al. [217] and Maric et al. [237] using:

$$\sigma = \sigma_{\max} \exp^{-a\left[\ln\left(\frac{\lambda_{\max}}{\lambda}\right)\right]^2}$$

Screening of the data suggested that most spectra published before 1987 did not constrain the shape of the spectrum very well as indicated by the large relative uncertainty of the width parameter a. The shape was determined by averaging the individual fitting parameters from McAdam et al., Moortgat et al. [280], Simon et al. [377], Lightfoot and Jemi-Alade [218], Jenkin and Cox [180] and Maricq and Wallington [240], which were judged to be most reliable by Tyndall et al. [408]. Absolute cross sections were based on relative measurements of absorption cross sections of CH_3O_2 and $C_2H_5O_2$ at 240 nm taken under identical conditions (Wallington et al. [426], Maricq and Wallington [240], Fenter et al. [120] and Roehl et al. [342]), combined with independent calibrations by Dagaut and Kurylo [99], Simon et al. [377] and Lightfoot and Jemi-Alade [218]. The fitting parameters are: $\sigma_{max} = 4.26 \times 10^{-18}$ cm^2 molecule^{-1}; a = 44.4; λ_{max} = 237.3 nm. Table 4-20 lists the recommended cross sections, which are taken from the review by Tyndall et al.

Photolysis of CH_3O_2 in the stratosphere and troposphere is slow and can be neglected, but the UV absorption cross sections are important in laboratory studies of reaction kinetics.

Table 4-20. Absorption Cross Sections of CH_3O_2, $C_2H_5O_2$, and $CH_3C(O)O_2$

λ (nm)	$10^{20}\sigma$ (cm^2)		
	CH_3O_2	$C_2H_5O_2$	$CH_3C(O)O_2$
195.0			389
200.0			564
205.0	165		665
210.0	219	195	656
215.0	276	257	564
220.0	330	319	451
225.0	376	374	366
230.0	408	418	326
235.0	424	444	319
240.0	424	452	326
245.0	407	440	330
250.0	378	412	322
255.0	339	372	300
260.0	294	324	268
265.0	248	273	229
270.0	203	222	187
275.0	162	176	147
280.0	126	136	111
285.0	96.1	102	81.2
290.0	71.5	74.6	57.3
295.0	52.0	53.3	
300.0		37.3	

D3. $C_2H_5O_2 + h\nu \rightarrow$ Products. The absorption cross sections of the ethylperoxy radical, $C_2H_5O_2$, in the 200–310-nm region have been measured at room temperature by Adachi et al. [4], Anastasi et al. [13], Cattell et al. [70], Wallington et al. [426], Bauer et al. [27], Maricq and Wallington [240], Fenter et al. [120], Munk et al. [284]. The absorption cross sections have been evaluated in earlier reviews by Lightfoot et al. [217] and Wallington et al. [426], who noted significant discrepancies in the both the shapes of the spectra and the absolute magnitude of the cross section values. The ultraviolet absorption spectra have recently been reevaluated by Tyndall et al.

[408], who fitted the absorption spectra to a semilogarithmic Gaussian distribution function suggested by Lightfoot et al. and Maric et al. [237] using:

$$\sigma = \sigma_{\max} \exp^{-a\left[\ln\left(\frac{\lambda_{\max}}{\lambda}\right)\right]^2}$$

The shape was determined by averaging the individual fitting parameters from Wallington et al., Bauer et al., Maricq and Wallington and Fenter et al., which were judged to be most reliable by Tyndall et al. Absolute cross sections were based on relative measurements of absorption cross sections of CH_3O_2 and $C_2H_5O_2$ at 240 nm taken under identical conditions (Wallington et al. [426], Maricq and Wallington [240], Fenter et al. [120] and Roehl et al. [342]), combined with independent calibrations. The fitting parameters are $\sigma_{max} = 4.52 \times 10^{-18}$ cm^2 molecule^{-1}; a = 49.0; λ_{max} = 239.4 nm. Table 4-20 lists the recommended cross sections, which are taken from the review by Tyndall et al.

Photolysis of $C_2H_5O_2$ in the stratosphere and troposphere is slow and can be neglected, but the UV absorption cross sections are important in laboratory studies of reaction kinetics.

D4. $CH_3OOH + h\nu \rightarrow$ Products. Vaghjiani and Ravishankara [414] measured the cross sections of CH_3OOH by monitoring the CH_3OOH concentration via trapping and titration. These results are recommended and are listed in Table 4-21. The earlier results of Molina and Arguello [274] are consistently 40% higher than the values shown in Table 4-21; this difference is believed to be due to difficulty in trapping CH_3OOH and measuring its concentration. CH_3OOH dissociates upon light absorption to give CH_3O with unit quantum yield (Vaghjiani and Ravishankara, [415]); these authors also observed some production of H and O atoms at shorter wavelengths (i.e., 193 nm). Thelen et al. [401] report unit quantum yield for OH production at 248 and 193 nm, in agreement with the results of Vaghjiani and Ravishankara.

Table 4-21. Absorption Cross Sections of CH_3OOH

λ (nm)	$10^{20}\ \sigma$ (cm^2)	λ (nm)	$10^{20}\ \sigma$ (cm^2)
220	15.4	300	0.41
230	9.62	310	0.24
240	6.05	320	0.14
250	3.98	330	0.079
260	2.56	340	0.047
270	1.70	350	0.027
280	1.09	360	0.016

D5. $HCN + h\nu \rightarrow$ Products. Herzberg and Innes [159] have studied the spectroscopy of hydrogen cyanide, HCN, that starts absorbing weakly at $\lambda < 190$ nm.

The solar photodissociation rate for this molecule is rather small, even in the upper stratosphere; estimates of this rate would require additional studies of the absorption cross sections and quantum yields in the 200-nm region.

D6. $CH_3CN + h\nu \rightarrow$ Products. McElcheran et al. [251] have reported the spectrum of acetonitrile or methyl cyanide, CH_3CN; the first absorption band appears at $\lambda < 220$ nm. More recently, Suto and Lee [390] and Zetzsch [449] have measured the cross sections around 200 nm; solar photodissociation is unimportant compared to reaction with OH radicals.

D7 $CH_3C(O)O_2 + h\nu \rightarrow$ Products. The UV absorption spectrum of the acetylperoxy radical, $CH_3C(O)O_2$, exhibits two absorption maxima in the 185–285 nm region: a strong band near 207 nm, and a feature at 245 nm that is weaker by a factor of 2. The absorption cross sections have been measured at room temperature by Addison et al. [6], Basco and Parmer [24], Moortgat et al. [280], Maricq and Szente [239], and Roehl et al. [342]. The absorption cross sections have been evaluated in earlier reviews by Lightfoot et al. [217] and Wallington et al. [426], who noted significant discrepancies in the both the shapes of the spectra and the absolute magnitude of the cross section values. The ultraviolet absorption spectra have recently been reevaluated by Tyndall et al. [408], who fitted the absorption spectra to the sum of two Gaussian-shaped absorption bands:

$$\sigma = \sigma_{\max 1} \exp^{-a_1\left[\ln\left(\frac{\lambda_{\max 1}}{\lambda}\right)\right]^2} + \sigma_{\max 2} \exp^{-a_2\left[\ln\left(\frac{\lambda_{\max 2}}{\lambda}\right)\right]^2}$$

The shape was determined by averaging the individual fitting parameters from Maricq and Szente and Roehl et al., which were judged to be the most reliable to date; the data by Maricq and Szente were adjusted for their overcorrection for the contribution of CH_3O_2. Absolute cross sections were based on relative measurements of absorption cross sections of $C_2H_5O_2$ at 240 nm taken under identical conditions. The fitting parameters are $\sigma_{max1} = 6.29 \times 10^{-18}$ cm^2 molecule^{-1}; $\lambda_{max1} = 206.0$ nm; $a_1 = 168.0$; $\sigma_{max2} = 3.26 \times 10^{-18}$ cm^2 molecule^{-1}; $\lambda_{max2} = 246.1$ nm; $a_2 = 64.2$. Table 4-20 lists the recommended cross sections, which are taken from the review by Tyndall et al.

Photolysis of $CH_3C(O)O_2$ in the stratosphere and troposphere is slow and can be neglected, but the UV absorption cross sections are important in laboratory studies of reaction kinetics.

D8. $CH_3C(O)O_2NO_2 + h\nu \rightarrow$ Products. Absorption spectra of $CH_3C(O)O_2NO_2$ (PAN) have been measured by Senum et al. [372] over the range 200–300 nm, Libuda and Zabel [216] over the range 220–325 nm, and Talukdar et al. [395] over the spectral range 195–345 nm and temperature range 250–298 K. The three studies are in excellent agreement over their range of overlap, with the values of Senum et al. being slightly smaller (15–20%) beyond 250 nm. Libuda and Zabel carried out simultaneous infrared absorption studies that showed that the measured cross sections need to be corrected for impurities that are transparent in the ultraviolet but contribute to the sample pressure in the absorption cell. These corrections are on the order of 20%. The recommended cross sections (Table 4-22) are based on the measurements of Talukdar et al. because of the good agreement with Libuda and Zabel and the wider spectral coverage and temperature range of this study. The uncertainties in the reported cross sections are probably quite large (on the order of a factor of 2), decreasing to about 30% at shorter wavelengths. The only PAN quantum yield studies are those of Mazely et al. [248,249]. In these studies, PAN was photolyzed at 248 nm, with NO_2 and NO_3 products being observed by laser-induced fluorescence at 298 K. Quantum yields of 0.83±0.09 were obtained for the $CH_3C(O)O_2 + NO_2$ channel and 0.3±0.1 for the $CH_3C(O)O + NO_3$ channel.

Table 4-22. Absorption Cross Sections of PAN

λ (nm)	10^{20} σ(298K) (cm^2)	10^3B (K^{-1})	λ(nm)	10^{20} σ(298K) (cm^2)	10^3B (K^{-1})
196	430	2.02	274	2.4	5.55
198	400	1.73	276	2.1	5.76
200	360	1.36	278	1.7	5.98
202	320	1.07	280	1.5	6.20
204	290	0.86	282	1.2	6.43
206	260	0.75	284	1.0	6.67
208	230	0.71	286	0.81	6.90
210	200	0.75	288	0.65	7.15
212	170	0.84	290	0.54	7.39
214	140	0.97	292	0.45	7.63
216	120	1.12	294	0.37	7.86
218	100	1.29	296	0.30	8.08
220	90	1.47	298	0.24	8.27
222	78	1.64	300	0.19	8.44
224	68	1.81	302	0.15	8.61
226	59	1.98	304	0.12	8.76
228	52	2.14	306	0.10	8.87
230	46	2.30	308	0.082	9.01
232	40	2.46	310	0.067	9.13
234	35	2.63	312	0.054	9.3
236	31	2.80	314	0.046	9.46
238	28	2.96	316	0.036	9.57
240	24	3.11	318	0.030	9.75
242	21	3.25	320	0.025	10.0
244	19	3.39	322	0.020	10.2
246	17	3.52	324	0.017	10.4
248	15	3.64	326	0.014	10.6
250	13	3.76	328	0.012	10.7
252	11	3.87	330	0.011	10.9
254	10	3.98	332	0.0086	11.2
256	8.9	4.10	334	0.0068	11.5
258	7.8	4.23	336	0.0061	11.7
260	6.8	4.38	338	0.0053	11.9
262	6.0	4.53	340	0.0050	12.2
264	5.2	4.68	342	0.0036	12.4
266	4.5	4.82	344	0.0024	12.5
268	3.9	4.97	346	0.0023	
270	3.4	5.14	348	0.0025	
272	2.9	5.34	350	0.0016	

Cross sections in the temperature range 250–298 K are calculated using the equation,

$$\ln(\sigma(T)/\sigma(298K)) = B(T-298).$$

E1. $HF + h\nu \rightarrow H + F$. The ultraviolet absorption spectrum of HF has been studied by Safary et al. [354]. The onset of absorption occurs at $\lambda < 170$ nm, so that photodissociation of HF should be unimportant in the stratosphere.

E2. $FNO + h\nu \rightarrow F + NO$. The absorption cross sections have been measured by Burley et al. [58], who report their results in graphical form as well as in tabular form in 1-nm intervals, between 180 and 350 nm. The spectrum shows vibronic structure at wavelengths longer than 250 nm. The cross section values are listed in Table 4-23 in 2-nm intervals. The quantum yield for decomposition is expected to be unity (Brandon et al., [39]; Reid et al., [336]).

Table 4-23. Absorption Cross Sections of FNO

λ (nm)	$10^{20}\sigma$ (cm^2)	λ (nm)	$10^{20}\sigma$ (cm^2)	λ (nm)	$10^{20}\sigma$ (cm^2)
180	52.4	236	3.09	292	11.9
182	51.7	238	2.76	294	7.11
184	50.7	240	2.25	296	9.15
186	49.4	242	2.08	298	22.0
188	47.5	244	1.74	300	15.6
190	45.1	246	1.65	302	25.4
192	42.7	248	1.41	304	8.85
194	40.0	250	1.54	306	11.8
196	37.3	252	1.25	308	32.2
198	33.8	254	1.23	310	15.5
200	30.5	256	1.36	312	31.6
202	27.7	258	1.58	314	12.3
204	24.8	260	1.30	316	11.0
206	22.2	262	1.64	318	25.5
208	19.9	264	2.03	320	15.2
210	17.6	266	1.96	323	40.2
212	15.8	268	2.10	324	17.8
214	13.9	270	2.81	326	12.1
216	12.3	272	4.47	328	9.39
218	10.7	274	3.97	330	12.9
220	9.35	276	4.24	332	13.0
222	8.32	278	3.41	334	19.3
224	7.22	280	8.26	336	13.1
226	6.30	282	7.58	338	8.96
228	5.44	284	7.26	340	5.65
230	4.68	286	5.17	342	3.81
232	4.10	288	10.4	344	2.68
234	3.52	290	17.0	346	1.96
				348	1.48
				350	1.18

E3. $CF_4 + h\nu \rightarrow$ products. See Note E4.

E4. $C_2F_6 + h\nu \rightarrow$ products. CF_4 and C_2F_6 do not absorb in the ultraviolet at wavelengths longer than 105 and 120 nm, respectively (Sauvageau et al. [362,363]; Inn, [178]); therefore, they are not expected to photodissociate until they reach the mesosphere.

E5. $CF_2O + h\nu \rightarrow$ Products. The recommended absorption cross sections for CF_2O, CCl_2O and CClFO are listed in Table 4-24, as averages over the 500 cm^{-1} intervals commonly employed for atmospheric modeling (the wavelength given in the table is the center of the interval). The values for CCl_2O are based on the work of Gillotay et al. [139], who measured the cross sections between 170 and 320 nm at temperatures ranging from 210 to 295 K; the temperature effect is significant only at wavelengths longer than 250 nm. These cross section values are in good agreement with those recommended earlier, which were based on the data of Chou et al. [76]. For CClFO the recommended values are based on this latter work between 184 and 199 nm, and they are taken from the work of Nölle et al. [296] at the longer wavelengths. These workers measured the cross sections at temperatures ranging from 223 to 298 K; the temperature effect is not important for atmospheric photodissociation calculations, as is the case with CCl_2O. For CF_2O the cross section values are taken from Molina and Molina [268] between 184 and 199 nm, and from Nölle et al. [297] at the longer wavelengths. These authors measured the cross sections at 296 K between 200 and 230 nm.

The photodissociation quantum yield for CCl_2O is unity (Calvert and Pitts [65]); the spectrum is a continuum. Similarly, the quantum yield for CClFO is taken as unity; the spectrum shows little structure. In contrast, the CF_2O spectrum is highly structured. Nevertheless, its photodissociation quantum yield is also taken as unity, as

reported by Nölle et al. [297]. The self-reaction of the CFO photodissociation product regenerates CF_2O, and hence the apparent quantum yield is less than unity.

Table 4-24. Absorption Cross Sections of CCl_2O, CClFO, and CF_2O at 298 K

λ (nm)	10^{20} σ(cm^2)		
	CCl_2O	CClFO	CF_2O
184.4	234	–	–
186.0	186	15.6	5.5
187.8	146	14.0	4.8
189.6	116	13.4	4.2
191.4	90.3	12.9	3.7
193.2	71.5	12.7	3.1
195.1	52.4	12.5	2.6
197.0	39.3	12.4	2.1
199.0	31.2	12.3	1.6
201.0	25.2	12.5	1.3
203.0	20.9	12.0	0.95
205.1	17.9	11.5	0.74
207.3	15.8	10.8	0.52
209.4	14.3	9.9	0.40
211.6	13.3	9.0	0.28
213.9	12.6	7.9	0.20
216.2	12.3	6.8	0.12
218.6	12.2	5.8	0.08
221.0	12.2	4.8	0.049
223.5	12.4	3.8	0.035
225.7	12.7	2.9	0.024
228.6	13.1	2.2	0.018

E6. $CF_3OH + h\nu \rightarrow$ Products. An upper limit of 10^{-21} cm^2 has been determined experimentally by Molina and Molina [271] for the absorption cross sections of CF_3OH in the 190–300-nm wavelength range. This upper limit is in agreement with estimates based on similarities between CF_3OH and CH_3OH, as well as with quantum chemistry calculations, as reported by Schneider et al. [368].

F1. $Cl_2 + h\nu \rightarrow Cl + Cl$. The recommended absorption cross sections are taken from the work of Maric et al. [235]; they can be calculated at various temperatures with the expression given at the bottom of Table 4-25. For convenience, some room temperature values are also listed in the table. Ganske et al. [128] have also measured the cross sections at room temperature, and the agreement with the recommended values is excellent. These two sets of data also agree well with the earlier recommendation, which was based on the work of Seery and Britton [370], which is in turn in good agreement with the results reported by Gibson and Bayliss [131], Fergusson et al. [121], and Burkholder and Bair [51]. The estimated atmospheric photodissociation rate is only weakly affected by the temperature dependency of the cross sections.

Table 4-25. Absorption Cross Sections of Cl_2

λ (nm)	10^{20} σ, 298K (cm^2)	λ (nm)	10^{20} σ, 298K (cm^2)
260	0.20	370	8.4
270	0.82	380	5.0
280	2.6	390	2.9
290	6.2	400	1.8
300	11.9	410	1.3
310	18.5	420	0.96
320	23.7	430	0.73
330	25.5	440	0.54
340	23.5	450	0.38
350	18.8	460	0.26
360	13.2	470	0.16

$$\sigma = 10^{-20}\alpha^{0.5}\left\{27.3\exp\left(-99.0\alpha\left(\ln\left(\frac{329.5}{\lambda}\right)\right)^2\right) + 0.932\exp\left(-91.5\alpha\left(\ln\left(\frac{406.5}{\lambda}\right)\right)^2\right)\right\}$$

where α = tanh (402.7/T); λ in nm, and T in K; 300 K > T > 195 K.

F2. ClO + hν → Cl + O. The absorption cross sections of chlorine monoxide, ClO, have been reviewed by Watson [430]. There are more recent measurements yielding results in reasonable agreement with the earlier ones, (1) Mandelman and Nicholls [232] in the 250–310 nm region; (2) Wine et al. [433] around 283 nm; (3) Rigaud et al. [337], (4) Jourdain et al. [194], (5) Sander and Friedl [357], (6) Trolier et al. [402] in the 270–310-nm region, and (7) Simon et al. [378] between 240 and 310 nm. The peak cross section at the top of the continuum is 5.2×10^{-18}, based on the average of studies (4)–(7) and Johnston et al. [189]. Figure 4-2 shows a spectrum of ClO. It should be noted that the cross sections on the structured part are extremely dependent on instrument resolution, and the figure is only a guide to the line positions and approximate shapes. The cross sections of the continuum are independent of temperature (Trolier et al. [402]), while the structured part is extremely temperature dependent. The bands sharpen and grow with a decrease in temperature.

The calculations of Coxon et al. [95] and Langhoff et al. [210] indicate that photodecomposition of ClO accounts for at most 2 to 3% of the total destruction rate of ClO in the stratosphere, which occurs predominantly by reaction with oxygen atoms and nitric oxide.

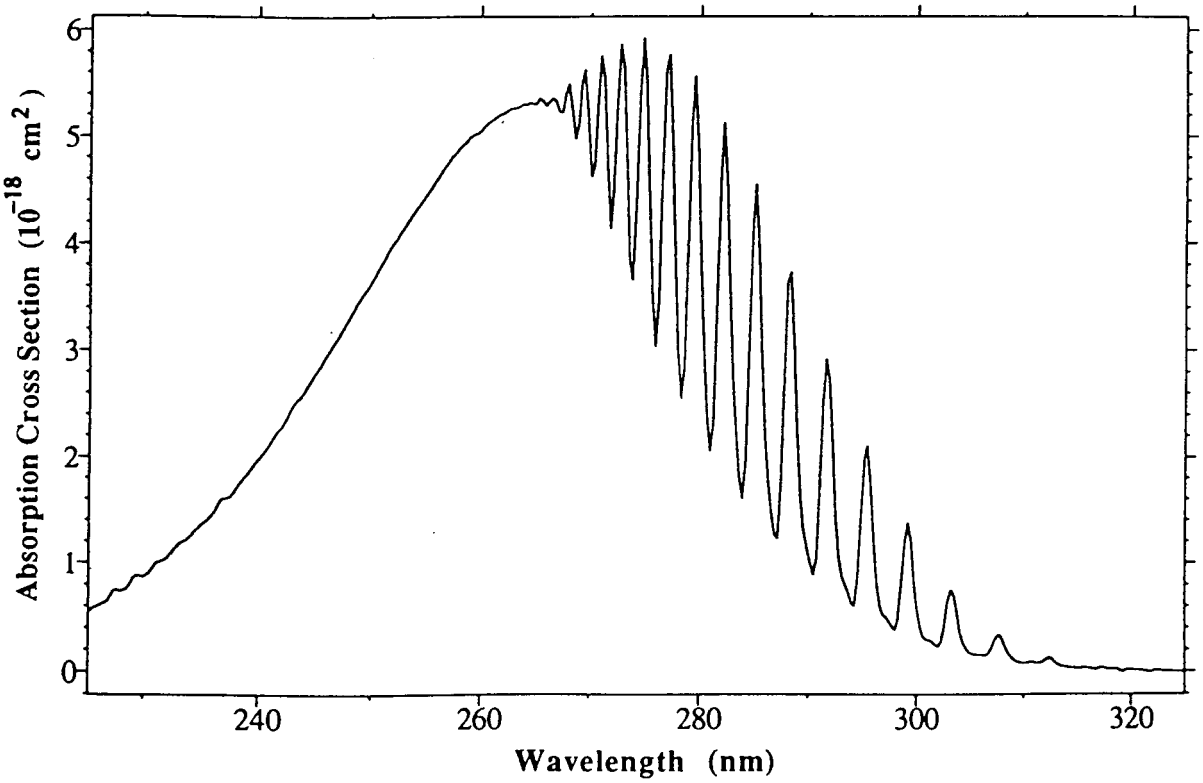

Figure 4-2. Absorption Spectrum of ClO

F3. ClOO + hν → ClO + O. Johnston et al. [189] measured the absorption cross sections of the ClOO radical using a molecular modulation technique that required interpretation of a complex kinetic scheme. More recently, Mauldin et al. [247] reported cross section measurements in the range from 220 to 280 nm, and Baer et al. [17] from 240 to 300 nm. These two studies are in very good agreement, yielding cross section values that are more than twice as large as the older Johnston et al. values. The recommended cross sections are listed in Table 4-26, and are taken from the work of Mauldin et al.

Table 4-26. Absorption Cross Sections of ClOO

λ (nm)	10^{20} σ (cm^2)	λ (nm)	10^{20} σ (cm^2)
220	611	252	2630
222	670	254	2370
224	747	256	2120
226	951	258	1890
228	1100	260	1610
230	1400	262	1370
232	1650	264	1120
234	1960	266	905
236	2240	268	725
238	2520	270	596
240	2730	272	435
242	2910	274	344
244	2960	276	282
246	2980	278	210
248	2950	280	200
250	2800		

F4. $OClO + h\nu \rightarrow O + ClO$. The spectrum of OClO is characterized by a series of well-developed progressions of bands extending from ~280 to 480 nm. The spectroscopy of this molecule has been studied extensively, and the quantum yield for photodissociation appears to be unity throughout the above wavelength range. See for example, the review by Watson [430]. Birks et al. [35] have estimated a half-life against atmospheric photodissociation of OClO of a few seconds.

The recommended absorption cross section values are those reported by Wahner et al. [424], who measured the spectra with a resolution of 0.25 nm at 204, 296, and 378 K, in the wavelength range 240 to 480 nm. Table 4-27 lists the cross section values at the peak of the bands (a(0) to a(26)). Figure 4-3, from Wahner et al., shows the OClO spectrum at 204 K and at room temperature. Hubinger and Nee [163] have extended the measurements of OClO cross sections over the spectral range 125–470 nm. Frost et al. [126] have studied the spectrum at very high spectral resolution (0.1 cm^{-1}) and at low temperature (200 K) in molecular beam expansion. In both of these studies, cross sections were measured relative to values obtained by Wahner et al.

The photochemistry of OClO is extremely complex, with several electronic excited states involved in the photodissociation dynamics. Several channels have been observed at wavelengths important in the stratosphere, including O + ClO, Cl + O_2 and isomerization to ClOO. Colussi [83] measured the quantum yield for chlorine atom production to be less than 0.01, and for oxygen atom production to be unity (within experimental error), both at 308 nm. Vaida et al. [417] and Ruhl et al. [352] reported chlorine atom production at 362 nm; and Bishenden et al. [36,37] measured the quantum yield for this process to be 0.15±0.10 around that same wavelength. In contrast, Lawrence et al. [211] report a quantum yield for Cl-atom production in the 359–368-nm region of less than 5×10^{-4}. This conclusion is supported by photofragment studies of Davis and Lee [105], who report Cl yields <0.2% below 370 nm, rising to a maximum of 4% near 404 nm. The recommendation is to use a quantum yield value of unity for the production of O-atoms. While accurate absorption cross section values are valuable for atmospheric measurements of OClO levels, the identity of the photodissociation products is only of minor importance in the context of atmospheric processes.

Table 4-27. Absorption Cross Sections of OClO at the Band Peaks

λ(nm)	10^{20} σ(cm^2)		
	204 K	296 K	378 K
475.53	–	13	–
461.15	17	17	16
446.41	94	69	57
432.81	220	166	134
420.58	393	304	250
408.83	578	479	378
397.76	821	670	547
387.37	1046	844	698
377.44	1212	992	808
368.30	1365	1136	920
359.73	1454	1219	984
351.30	1531	1275	989
343.44	1507	1230	938
336.08	1441	1139	864
329.22	1243	974	746
322.78	1009	791	628
317.21	771	618	516
311.53	542	435	390
305.99	393	312	291
300.87	256	219	216
296.42	190	160	167
291.77	138	114	130
287.80	105	86	105
283.51	089	72	90
279.64	073	60	79
275.74	059	46	–
272.93	053	33	–

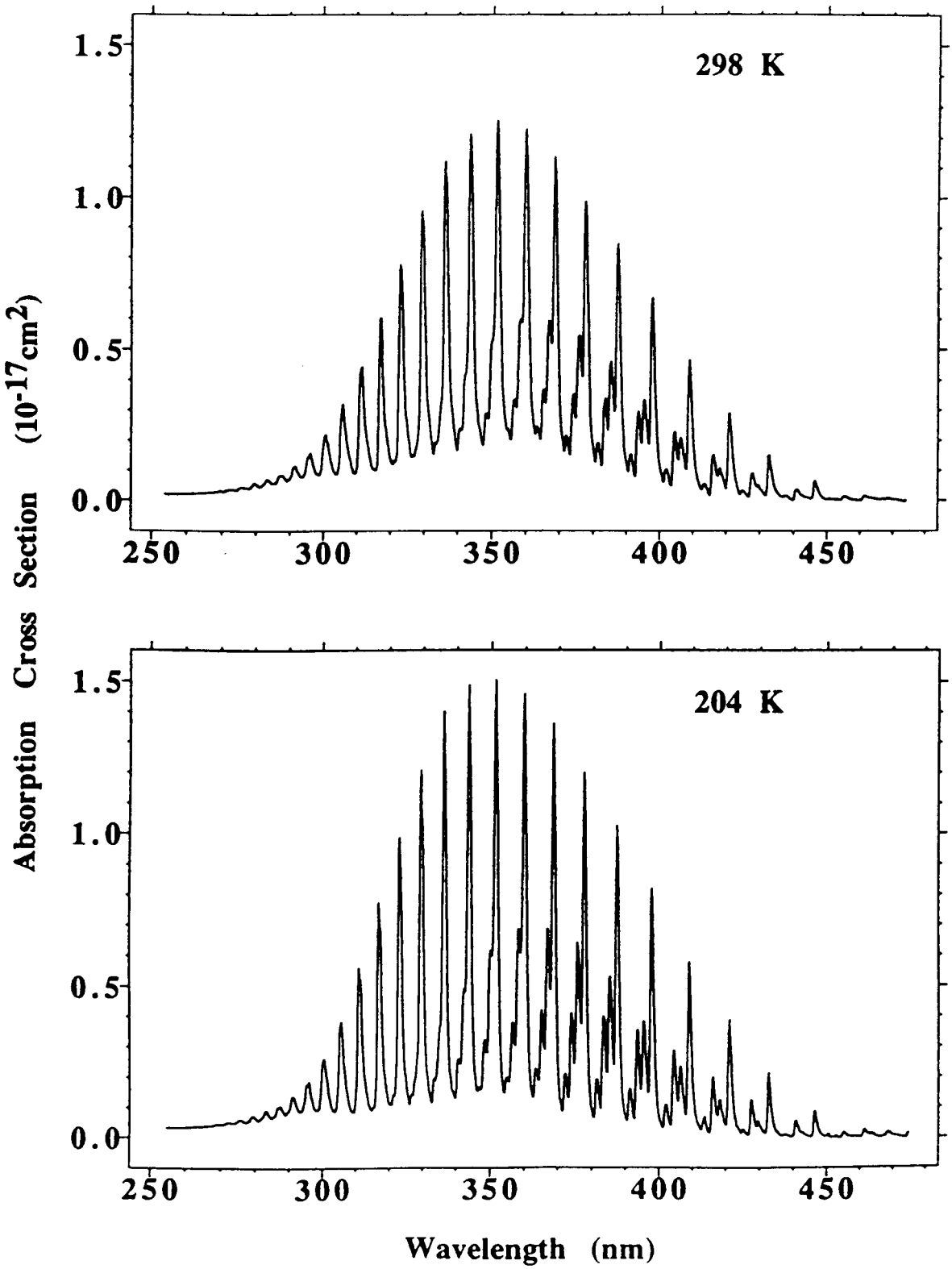

Figure 4-3. Absorption Spectrum of OClO

F5. $ClO_3 + h\nu \rightarrow$ Products. The previous recommendation for absorption cross sections was based on the work of Goodeve and Richardson [141]. Lopez and Sicre [224] have shown that the spectrum reported by Goodeve and Richardson is most likely that of Cl_2O_6. Thermochemical estimates by Colussi et al. [84] further corroborate this assignment. No recommendation is given at present for the ClO_3 cross sections.

Grothe and Willner (1994; 1995) have reported UV and IR spectra of ClO_3 trapped in a neon matrix. By monitoring the amount of ClO formed as a photolysis product, they estimated UV absorption cross sections of the order of 2×10^{-18} cm^2 around 400–450 nm.

F6. $Cl_2O + h\nu \rightarrow$ Products. The preferred absorption cross sections, listed in Table 4-28, are those reported by Knauth et al. [202] at 298 K. They are in very good agreement with the cross sections measured by Lin [220] and by Molina and Molina [265]; the discrepancy is largest at the longest wavelengths. Nee [288] has recently reported cross section measurements in the 150–200 nm wavelength region.

Sander and Friedl [357] have measured the quantum yield for production of O-atoms to be 0.25±0.05, using a broadband photolysis source extending from 180 nm to beyond 400 nm. The main photolysis products are Cl and ClO. Using a molecular beam technique, Nelson et al. [289] found Cl + ClO to be the primary photodissociation channel at 193, 248, and 308 nm. More recently, Nickolaisen et al. [292] reported that broadband photolysis at wavelengths beyond 300 nm results in pressure-dependent ClO quantum yields. Furthermore, these authors detected a transient absorption spectrum, that they assigned to a metastable triplet state of Cl_2O; the implication is that the photodecomposition quantum yield is less than unity at atmospherically relevant wavelengths, in spite of the continuous nature of the absorption spectrum. Additional experimental work is needed to corroborate this interpretation.

Table 4-28. Absorption Cross Sections of Cl_2O

λ (nm)	$10^{20}\ \sigma$ (cm^2)	λ (nm)	$10^{20}\ \sigma$ (cm^2)
200	71.0	330	8.40
210	23.8	340	3.58
220	8.6	350	1.54
230	28.1	360	0.73
240	103	370	0.40
250	191	380	0.36
260	195	390	0.51
270	151	400	0.79
280	126	420	1.26
290	103	440	1.11
300	71.0	460	0.63
310	40.3	480	0.32
320	19.5	500	0.22

F7. $ClOOCl + h\nu \rightarrow Cl + ClOO$. Recommended absorption cross sections in the wavelength range 190–450 nm for ClOOCl are listed in Table 4-29. The values for the wavelength range 200–360 nm are the average of experimental results reported by Cox and Hayman [90], DeMore and Tschuikow-Roux [107], Permien et al. [313], and Burkholder et al. [53]. For the 190–200-nm range the data are from DeMore and Tschuikow-Roux [107], these being the only data available in that range. Data at wavelengths greater than 360 nm were obtained from a linear extrapolation of the logarithm of the cross sections, using the expression $\log(10^{20}\ \sigma\ (cm^2)) = -0.01915 \times \lambda(nm) + 7.589$. For $\lambda > 360$ nm the extrapolated data are considered to be more reliable than the experimental measurements because of the very small dimer cross sections in this region.

While the results of Cox and Hayman, DeMore and Tschuikow-Roux, Permien et al., and Burkholder et al. are in good agreement at wavelengths below 250 nm, there are significant discrepancies at longer wavelengths, which may be attributed to uncertainties in the spectral subtraction of impurities such as Cl_2O, Cl_2, and Cl_2O_2. Huder and DeMore [167] measured ClOOCl cross sections over the 190–310-nm range using a method that minimized the corrections required for impurities such as Cl_2O. The cross sections from this study are significantly smaller (up to a factor of 2) than the current recommendation, particularly when extrapolated beyond 400 nm. Additional measurements are needed, particularly at the longer wavelengths, to check the results of Huder and DeMore.

These studies also indicate that only one stable species is produced in the recombination reaction of ClO with itself, and that this species is dichlorine peroxide, ClOOCl, rather than ClOClO. Using submillimeter wave spectroscopy, Birk et al. [34] have further established the structure of the recombination product to be ClOOCl. These observations are in agreement with the results of quantum mechanical calculations (McGrath et al. [254,255]; Jensen and Odershede [184]; Stanton et al. [387]).

Table 4-29. Absorption Cross Sections of ClOOCl at 200–250 K

λ (nm)	$10^{20}\sigma(cm^2)$	λ (nm)	$10^{20}\sigma(cm^2)$	λ (nm)	$10^{20}\sigma(cm^2)$	λ (nm)	$10^{20}\sigma(cm^2)$
190	565.0	256	505.4	322	23.4	388	1.4
192	526.0	258	463.1	324	21.4	390	1.3
194	489.0	260	422.0	326	19.2	392	1.2
196	450.0	262	381.4	328	17.8	394	1.1
198	413.0	264	344.6	330	16.7	396	1.0
200	383.5	266	311.6	332	15.6	398	0.92
202	352.9	268	283.3	334	14.4	400	0.85
204	325.3	270	258.4	336	13.3	402	0.78
206	298.6	272	237.3	338	13.1	404	0.71
208	274.6	274	218.3	340	12.1	406	0.65
210	251.3	276	201.6	342	11.5	408	0.60
212	231.7	278	186.4	344	10.9	410	0.54
214	217.0	280	172.5	346	10.1	412	0.50
216	207.6	282	159.6	348	9.0	414	0.46
218	206.1	284	147.3	350	8.2	416	0.42
220	212.1	286	136.1	352	7.9	418	0.38
222	227.1	288	125.2	354	6.8	420	0.35
224	249.4	290	114.6	356	6.1	422	0.32
226	280.2	292	104.6	358	5.8	424	0.29
228	319.5	294	95.4	360	5.5	426	0.27
230	365.0	296	87.1	362	4.5	428	0.25
232	415.4	298	79.0	364	4.1	430	0.23
234	467.5	300	72.2	366	3.8	432	0.21
236	517.5	302	65.8	368	3.5	434	0.19
238	563.0	304	59.9	370	3.2	436	0.17
240	600.3	306	54.1	372	2.9	438	0.16
242	625.7	308	48.6	374	2.7	440	0.15
244	639.4	310	43.3	376	2.4	442	0.13
246	642.6	312	38.5	378	2.2	444	0.12
248	631.5	314	34.6	380	2.1	446	0.11
250	609.3	316	30.7	382	1.9	448	0.10
252	580.1	318	28.0	384	1.7	450	0.09
254	544.5	320	25.6	386	1.6		

F8. $Cl_2O_3 + h\nu \rightarrow$ Products. The absorption cross sections of Cl_2O_3 have been measured by Hayman and Cox [155], Burkholder et al. [52], and Harwood et al. [154]. The results from these studies are significantly different in the spectral regions below 240 nm and in the long-wavelength tail beyond 300 nm. Table 4-30 lists the recommended values. These are derived by averaging the spectra of Burkholder et al. and Harwood et al., which are obtained by the most direct methods. Additional work is needed, particularly in the spectral region beyond 300 nm.

Table 4-30. Absorption Cross Sections of Cl_2O_3

λ (nm)	10^{20} σ (cm^2)	λ (nm)	10^{20} σ (cm^2)
220	1200	275	1470
225	1130	280	1240
230	1060	285	990
235	1010	290	760
240	1020	295	560
245	1120	300	400
250	1270	305	290
255	1450	310	210
260	1610	315	160
265	1680	320	140
270	1630		

F9. $Cl_2O_4 + h\nu \rightarrow$ Products. The absorption cross sections of Cl_2O_4 have been measured by Lopez and Sicre [223]; their results are given in Table 4-31.

Table 4-31. Absorption Cross Sections of Cl_2O_4

λ (nm)	10^{20} σ(cm^2)	λ (nm)	10^{20} σ(cm^2)
200	161	255	42
205	97	260	31
210	72	265	22
215	64	270	14
220	71	275	8.8
225	75	280	5.5
230	95	285	4.0
235	95	290	2.7
240	87	295	2.2
245	72	300	1.7
250	56	305	1.2
		310	0.7

F10. $Cl_2O_6 + h\nu \rightarrow$ Products. The absorption cross sections for Cl_2O_6 are listed in Table 4-32 and are taken from the work of Lopez and Sicre [224]. These authors show that the spectrum originally attributed to ClO_3 by Goodeve and Richardson [141] was most likely that of Cl_2O_6. The cross section values measured by Lopez and Sicre are several times larger than those reported by Goodeve and Richardson, but the shape of the spectrum is similar.

Table 4-32. Absorption Cross Sections of Cl_2O_6

λ (nm)	10^{20} σ (cm^2)	λ (nm)	10^{20} σ (cm^2)
200	1230	300	980
210	1290	310	715
220	1230	320	450
230	1080	330	285
240	1010	340	180
250	1010	350	112
260	1290	360	59
270	1440	370	28
280	1440	380	12
290	1290		

F11. $HCl + h\nu \rightarrow H + Cl$. The absorption cross sections of HCl, listed in Table 4-33, are taken from the work of Inn [177].

Table 4-33. Absorption Cross Sections of HCl Vapor

λ(nm)	10^{20} σ (cm^2)	λ (nm)	10^{20} σ (cm^2)
145	281	190	14.5
150	345	195	6.18
155	382	200	2.56
160	332	205	0.983
165	248	210	0.395
170	163	215	0.137
175	109	220	0.048
180	58.8		

F12. $HOCl + h\nu \rightarrow OH + Cl$. The absorption cross sections of HOCl vapor have been measured by several groups. Molina and Molina [265] and Knauth et al. [202] produced this species using equilibrium mixtures with Cl_2O and H_2O; their results provided the basis for the earlier recommendation. More recently, Mishalanie et al. [261] and Permien et al. [313] used a dynamic source to generate the HOCl vapor. The cross section values reported by Molina and Molina [265], Mishalanie et al. [261], and Permien et al. [313] are in reasonable agreement between 250 and 330 nm. In this wavelength range, the values reported by Knauth et al. [202] are significantly smaller, e.g., a factor of 4 at 280 nm. Beyond 340 nm, the cross sections of Mishalanie et al. are much smaller than those obtained by the other three groups. At 365 nm, the discrepancy is about an order of magnitude.

Burkholder [50] has remeasured the absorption spectrum of HOCl over the wavelength range 200 to 380 nm, following photolysis of equilibrium mixtures of Cl_2O-H_2O-HOCl. The obtained spectrum displays two absorption maxima at 242 and 304 nm, and is in excellent agreement with the work of Knauth et al. [202], but in poor agreement with the measurements of Mishalanie et al. [261] and Permien et al. [313]. The discrepancies can be attributed mostly to difficulties in correcting the measured absorptions for the presence of Cl_2 and Cl_2O. In the study by Burkholder, several control experiments were carried out in order to check the internal consistency of the data. Moreover, Barnes et al. [23] examined the near-UV spectrum of HOCl by monitoring the OH fragments resulting from photodissociation, and revealed a third weak band centered at 387 nm extending down to 480 nm. The recommended cross sections up to 420 nm, calculated from an analytical expression provided by Barnes et al. [23] and based on the values of Burkholder [50] and Barnes et al. [23], are listed in Table 4-34. The work by Jungkamp et al. [196] yields cross section values in excellent agreement with this recommendation for wavelengths shorter than 350 nm.

Molina et al. [275] observed production of OH radicals in the laser photolysis of HOCl around 310 nm, and Butler and Phillips [62] found no evidence for O-atom production at 308 nm, placing an upper limit of ~0.02 for the primary quantum yield for the HCl + O channel. Vogt and Schindler [422] used broadband photolysis in the 290–390 nm wavelength range, determining a quantum yield for OH production of >0.95.

Table 4-34. Absorption Cross Sections of HOCl

λ (nm)	10^{20} σ (cm^2)	λ (nm)	10^{20} σ (cm^2)	λ (nm)	10^{20} σ (cm^2)
200	7.18	274	5.26	348	1.55
202	6.39	276	4.94	350	1.43
204	5.81	278	4.74	352	1.33
206	5.46	280	4.64	354	1.24
208	5.37	282	4.62	356	1.17
210	5.54	284	4.68	358	1.11
212	5.98	286	4.79	360	1.06
214	6.68	288	4.95	362	1.02
216	7.63	290	5.13	364	0.985
218	8.81	292	5.33	366	0.951
220	10.2	294	5.52	368	0.919
222	11.6	296	5.71	370	0.888
224	13.2	298	5.86	372	0.855
226	14.7	300	5.99	374	0.822
228	16.2	302	6.08	376	0.786
230	17.5	304	6.12	378	0.748
232	18.7	306	6.12	380	0.708
234	19.6	308	6.07	382	0.667
236	20.2	310	5.97	384	0.624
238	20.5	312	5.84	386	0.580
240	20.6	314	5.66	388	0.535
242	20.3	316	5.45	390	0.491
244	19.8	318	5.21	392	0.447
246	19.0	320	4.95	394	0.405
248	18.1	322	4.67	396	0.364
250	17.0	324	4.38	398	0.325
252	15.8	326	4.09	400	0.288
254	14.6	328	3.79	402	0.254
256	13.3	330	3.50	404	0.222
258	12.1	332	3.21	406	0.194
260	10.9	334	2.94	406	0.168
262	9.73	336	2.68	410	0.144
264	8.68	338	2.44	412	0.124
266	7.75	340	2.22	414	0.105
268	6.94	342	2.02	416	0.089
270	6.25	344	1.84	418	0.075
272	5.69	346	1.69	420	0.063

F13. $ClNO + h\nu \rightarrow Cl + NO$. Nitrosyl chloride has a continuous absorption extending beyond 650 nm. There is good agreement between the work of Martin and Gareis [243] for the 240-to-420-nm wavelength region, of Ballash and Armstrong [20] for the 185 to 540 nm region, of Illies and Takacs [175] for the 190-to-400-nm region, and of Tyndall et al. [409] for the 190-to-350-nm region except around 230 nm, where the values of Ballash and Armstrong are larger by almost a factor of two. Roehl et al. [344] measured the absorption cross sections between 350 and 650 nm at several temperatures between 223 and 343 K. Their room temperature results agree to within 15% with those of Martin and Gareis [243], Ballash and Amstrong [20], and Tyndall et al. [409]. Table 4-35 lists the recommended cross sections: these are taken from the work of Tyndall et al. [409] between 190 and 350 nm (unchanged from the previous recommendation), and from Roehl et al. [344] beyond 350 nm.

The quantum yield for the primary photolytic process has been reviewed by Calvert and Pitts [65]. It is unity over the entire visible and near-ultraviolet bands.

Table 4-35. Absorption Cross Sections of ClNO

λ (nm)	10^{20} σ (cm^2)	λ (nm)	10^{20} σ (cm^2)	λ (nm)	10^{20} σ (cm^2)	λ (nm)	10^{20} σ (cm^2)
190	4320	246	45.2	302	10.3	370	11.0
192	5340	248	37.7	304	10.5	375	9.95
194	6150	250	31.7	306	10.8	380	8.86
196	6480	252	27.4	308	11.1	385	7.82
198	6310	254	23.7	310	11.5	390	6.86
200	5860	256	21.3	312	11.9	395	5.97
202	5250	258	19.0	314	12.2	400	5.13
204	4540	260	17.5	316	12.5	405	4.40
206	3840	262	16.5	318	13.0	410	3.83
208	3210	264	15.3	320	13.4	415	3.38
210	2630	266	14.4	322	13.6	420	2.89
212	2180	268	13.6	324	14.0	425	2.45
214	1760	270	12.9	326	14.3	430	2.21
216	1400	272	12.3	328	14.6	435	2.20
218	1110	274	11.8	330	14.7	440	2.20
220	896	276	11.3	332	14.9	445	2.07
222	707	278	10.7	334	15.1	450	1.87
224	552	280	10.6	336	15.3	455	1.79
226	436	282	10.2	338	15.3	460	1.95
228	339	284	9.99	340	15.2	465	2.25
230	266	286	9.84	342	15.3	470	2.50
232	212	288	9.71	344	15.1	475	2.61
234	164	290	9.64	346	15.1	480	2.53
236	120	292	9.63	348	14.9	485	2.33
238	101	294	9.69	350	14.2	490	2.07
240	82.5	296	9.71	355	13.6	495	1.78
242	67.2	298	9.89	360	12.9	500	1.50
244	55.2	300	10.0	365	12.0		

F14 $ClNO_2 + h\nu \rightarrow$ Products. The absorption cross sections of nitryl chloride, $ClNO_2$, have been measured between 230 and 330 nm by Martin and Gareis [243], between 185 and 400 nm by Illies and Takacs [175], and between 270 and 370 nm by Nelson and Johnston [291], and by Ganske et al. [128] between 200 and 370 nm. A major source of discrepancies in the data results from the presence of impurities. Table 4-36 lists the recommended values, which are taken from Ganske et al. Nelson and Johnston [291] report a value of one (within experimental error) for the quantum yield for production of chlorine atoms; they also report a negligible quantum yield for the production of oxygen atoms.

Table 4-36. Absorption Cross Sections of $ClNO_2$

λ (nm)	10^{20} σ (cm^2)	λ (nm)	10^{20} σ (cm^2)
190	2690	290	17.3
200	468	300	14.9
210	320	310	12.1
220	339	320	8.87
230	226	330	5.84
240	133	340	3.54
250	90.6	350	2.04
260	61.3	360	1.15
270	35.3	370	0.69
280	22.0		

F15. ClONO + hν → Products. Measurements in the near-ultraviolet of the cross sections of chlorine nitrite (ClONO) have been made by Molina and Molina [264]. Their results are listed in Table 4-37. The characteristics of the spectrum and the instability of ClONO strongly suggest that the quantum yield for decomposition is unity. The Cl–O bond strength is only about 20 kilocalories, so that chlorine atoms are likely photolysis products.

Table 4-37. Absorption Cross Sections of ClONO at 231 K

λ (nm)	10^{20} σ (cm^2)	λ (nm)	10^{20} σ (cm^2)
235	215.0	320	80.3
240	176.0	325	75.4
245	137.0	330	58.7
250	106.0	335	57.7
255	65.0	340	43.7
260	64.6	345	35.7
265	69.3	350	26.9
270	90.3	355	22.9
275	110.0	360	16.1
280	132.0	365	11.3
285	144.0	370	9.0
290	144.0	375	6.9
295	142.0	380	4.1
300	129.0	385	3.3
305	114.0	390	2.2
310	105.0	395	1.5
315	98.1	400	0.6

F16. $ClONO_2$ + hν → Products. The recommended cross sections are taken from the work of Burkholder et al. [55]; the values are listed in Table 4-38, together with the parameters needed to compute their temperature dependency. These values are in very good agreement with those reported by Molina and Molina [266], which provided the basis for the previous recommendation, and which supersedes the earlier work of Rowland, Spencer, and Molina [349].

The identity of the primary photolytic fragments has been investigated by several groups. Smith et al. [384] report O + ClONO as the most likely products, using end product analysis and steady-state photolysis. The results of Chang et al. [71], who employed the very low-pressure photolysis (VLPPh) technique, indicate that the products are Cl + NO_3. Adler-Golden and Wiesenfeld [7], using a flash photolysis atomic absorption technique, find O-atoms to be the predominant photolysis product and report a quantum yield for Cl-atom production of less than 4%. Marinelli and Johnston [241] report a quantum yield for NO_3 production at 249 nm between 0.45 and 0.85, with a most likely value of 0.55; they monitored NO_3 by tunable dye-laser absorption at 662 nm. Margitan [233] used atomic resonance fluorescence detection of O- and Cl-atoms and found the quantum yield at 266 and at 355 nm to be 0.9 ± 0.1 for Cl-atom production and ~0.1 for O-atom production, with no discernible difference at the two wavelengths. These results were confirmed by Knauth and Schindler [203], who used end-product analysis to infer the quantum yields. Burrows et al. [61] report also Cl and NO_3 as the photolysis products at 254 nm, with a quantum yield of unity within experimental error. In contrast, Nikolaisen et al. [293] report relative branching ratios of 0.44 for production of ClO and NO_2 and 0.56 for production of Cl and NO_3 at wavelengths beyond 300 nm. Minton et al. [260], Nelson et al. [290], and Moore et al. [276] measured comparable yields for these two channels at 193, 248, and 308 nm, using a molecular beam technique.

The recommended quantum yield values for production of Cl + NO_3 (ϕ_1) and ClO + NO_2 (ϕ_2) are given at the bottom of Table 4-38 and are based on the work of Nelson et al. [290], Moore et al. [276], Nickolaisen et al. [293], and Ravishankara [326]. For wavelengths shorter than 308 nm the value of ϕ_1 is 0.6, and for ϕ_2 it is 0.4. For longer wavelengths ϕ_1 increases linearly to 0.9 at 350 nm, with the corresponding decrease in ϕ_2 to 0.1. There is no evidence for production of O + ClONO in the more recent work; the production of O-atoms reported in some of the earlier studies might have resulted from decomposition of excited NO_3.

Recent work by Nickolaisen et al. [293] indicates that the photodissociation quantum yield is less than unity at wavelengths longer than about 330 nm, because of the formation of a long-lived intermediate that might be

quenched under atmospheric conditions (a situation analogous to that of Cl_2O). Additional work is needed to address these issues, which have potentially important atmospheric consequences.

Table 4-38. Absorption Cross Sections of $ClONO_2$

λ (nm)	$10^{20}\sigma(\lambda,296)$ (cm^2)	A1	A2	λ (nm)	$10^{20}\sigma(\lambda,296)$ (cm^2)	A1	A2
196	310	9.90 (–5)	–8.38 (–6)	316	1.07	5.07 (–3)	1.56 (–5)
198	294	6.72 (–5)	–8.03 (–6)	318	0.947	5.24 (–3)	1.69 (–5)
200	282	–5.34 (–6)	–7.64 (–6)	320	0.831	5.40 (–3)	1.84 (–5)
202	277	–1.19 (–4)	–7.45 (–6)	322	0.731	5.55 (–3)	2.00 (–5)
204	280	–2.60 (–4)	–7.50 (–6)	324	0.647	5.68 (–3)	2.18 (–5)
206	288	–4.12 (–4)	–7.73 (–6)	326	0.578	5.80 (–3)	2.36 (–5)
208	300	–5.62 (–4)	–8.05 (–6)	328	0.518	5.88 (–3)	2.54 (–5)
210	314	–6.96 (–4)	–8.41 (–6)	330	0.466	5.92 (–3)	2.70 (–5)
212	329	–8.04 (–4)	–8.75 (–6)	332	0.420	5.92 (–3)	2.84 (–5)
214	339	–8.74 (–4)	–9.04 (–6)	334	0.382	5.88 (–3)	2.96 (–5)
216	345	–9.03 (–4)	–9.24 (–6)	336	0.351	5.80 (–3)	3.05 (–5)
218	341	–8.86 (–4)	–9.35 (–6)	338	0.326	5.68 (–3)	3.10 (–5)
220	332	–8.28 (–4)	–9.38 (–6)	340	0.302	5.51 (–3)	3.11 (–5)
222	314	–7.31 (–4)	–9.34 (–6)	342	0.282	5.32 (–3)	3.08 (–5)
224	291	–6.04 (–4)	–9.24 (–6)	344	0.264	5.07 (–3)	2.96 (–5)
226	264	–4.53 (–4)	–9.06 (–6)	346	0.252	4.76 (–3)	2.74 (–5)
228	235	–2.88 (–4)	–8.77 (–6)	348	0.243	4.39 (–3)	2.42 (–5)
230	208	–1.13 (–4)	–8.33 (–6)	350	0.229	4.02 (–3)	2.07 (–5)
232	182	6.18 (–5)	–7.74 (–6)	352	0.218	3.68 (–3)	1.76 (–5)
234	158	2.27 (–4)	–7.10 (–6)	354	0.212	3.40 (–3)	1.50 (–5)
236	138	3.72 (–4)	–6.52 (–6)	356	0.205	3.15 (–3)	1.27 (–5)
238	120	4.91 (–4)	–6.14 (–6)	358	0.203	2.92 (–3)	1.06 (–5)
240	105	5.86 (–4)	–5.98 (–6)	360	0.200	2.70 (–3)	8.59 (–6)
242	91.9	6.64 (–4)	–6.04 (–6)	362	0.190	2.47 (–3)	6.38 (–6)
244	81.2	7.33 (–4)	–6.27 (–6)	364	0.184	2.22 (–3)	3.66 (–6)
246	71.6	8.03 (–4)	–6.51 (–6)	366	0.175	1.93 (–3)	2.42 (–7)
248	62.4	8.85 (–4)	–6.59 (–6)	368	0.166	1.62 (–3)	–3.62 (–6)
250	56.0	9.84 (–4)	–6.40 (–6)	370	0.159	1.33 (–3)	–7.40 (–6)
252	50.2	1.10 (–3)	–5.93 (–6)	372	0.151	1.07 (–3)	–1.07 (–5)
254	45.3	1.22 (–3)	–5.33 (–6)	374	0.144	8.60 (–4)	–1.33 (–5)
256	41.0	1.33 (–3)	–4.73 (–6)	376	0.138	6.73 (–4)	–1.54 (–5)
258	37.2	1.44 (–3)	–4.22 (–6)	378	0.129	5.01 (–4)	–1.74 (–5)
260	33.8	1.53 (–3)	–3.79 (–6)	380	0.121	3.53 (–4)	–1.91 (–5)
262	30.6	1.62 (–3)	–3.37 (–6)	382	0.115	2.54 (–4)	–2.05 (–5)
264	27.8	1.70 (–3)	–2.94 (–6)	384	0.108	2.25 (–4)	–2.11 (–5)
266	25.2	1.78 (–3)	–2.48 (–6)	386	0.103	2.62 (–4)	–2.11 (–5)
268	22.7	1.86 (–3)	–2.00 (–6)	388	0.0970	3.33 (–4)	–2.08 (–5)
270	20.5	1.94 (–3)	–1.50 (–6)	390	0.0909	4.10 (–4)	–2.05 (–5)
272	18.5	2.02 (–3)	–1.01 (–6)	392	0.0849	5.04 (–4)	–2.02 (–5)
274	16.6	2.11 (–3)	–4.84 (–7)	394	0.0780	6.62 (–4)	–1.94 (–5)
276	14.9	2.02 (–3)	9.02 (–8)	396	0.0740	8.95 (–4)	–1.79 (–5)
278	13.3	2.29 (–3)	6.72 (–7)	398	0.0710	1.14 (–3)	–1.61 (–5)
280	11.9	2.38 (–3)	1.21 (–6)	400	0.0638	1.38 (–3)	–1.42 (–5)
282	10.5	2.47 (–3)	1.72 (–6)	402	0.0599	1.63 (–3)	–1.20 (–5)
284	9.35	2.56 (–3)	2.21 (–6)	404	0.0568	1.96 (–3)	–8.97 (–6)
286	8.26	2.66 (–3)	2.68 (–6)	406	0.0513	2.36 (–3)	–5.15 (–6)
288	7.24	2.75 (–3)	3.09 (–6)	408	0.0481	2.84 (–3)	–6.64 (–7)
290	6.41	2.84 (–3)	3.41 (–6)	410	0.0444	3.38 (–3)	4.47 (–6)
292	5.50	2.95 (–3)	3.74 (–6)	412	0.0413	3.96 (–3)	1.00 (–5)

λ (nm)	$10^{20}\sigma(\lambda,296)$ (cm^2)	A1	A2	λ (nm)	$10^{20}\sigma(\lambda,296)$ (cm^2)	A1	A2
294	4.67	3.08 (–3)	4.27 (–6)	414	0.0373	4.56 (–3)	1.60 (–5)
296	4.09	3.25 (–3)	5.13 (–6)	416	0.0356	5.22 (–3)	2.28 (–5)
298	3.57	3.45 (–3)	6.23 (–6)	418	0.0317	5.96 (–3)	3.07 (–5)
300	3.13	3.64 (–3)	7.36 (–6)	420	0.0316	6.70 (–3)	3.87 (–5)
302	2.74	3.83 (–3)	8.38 (–6)	422	0.0275	7.30 (–3)	4.58 (–5)
304	2.39	4.01 (–3)	9.30 (–6)	424	0.0242	7.82 (–3)	5.22 (–5)
306	2.09	4.18 (–3)	1.02 (–5)	426	0.0222	8.41 (–3)	5.95 (–5)
308	1.83	4.36 (–3)	1.11 (–5)	428	0.0207	9.11 (–3)	6.79 (–5)
310	1.60	4.53 (–3)	1.20 (–5)	430	0.0189	9.72 (–3)	7.52 (–5)
312	1.40	4.71 (–3)	1.30 (–5)	432	0.0188	9.96 (–3)	7.81 (–5)
314	1.22	4.89 (–3)	1.42 (–5)				

$$\sigma(\lambda, T) = \sigma(\lambda, 296)\,(1 + A_1 (T - 296) + A_2 (T - 296)^2);\ T \text{ in K}$$

Quantum yields:

$$ClONO_2 + h\nu \rightarrow Cl + NO_3$$

$\phi_1 = 0.6$ ($\lambda < 308$ nm)

$\phi_1 = 7.143 \times 10^{-3}\,\lambda\,(\text{nm}) - 1.60$ (308 nm $< \lambda <$ 364 nm)

$\phi_1 = 1.0$ ($\lambda > 364$ nm)

$$ClONO_2 + h\nu \rightarrow ClO + NO_2$$

$\phi_2 = 1 - \phi_1$

F17. $CCl_4 + h\nu \rightarrow$ Products. The absorption cross sections of CCl_4 have been measured at room temperature and 110–200 nm by Russell et al. [353]; at 204–250 nm by Gordus and Bernstein [142]; at 186–226 nm by Rowland and Molina [347]; at 170–230 nm by Roxlo and Mandl [350]; and at 160–275 nm by Hubrich and Stuhl [165]; at 297–477 K and 250 nm by Currie et al. [98], at 279 and 296 K and 190–252 nm by Vanlaethem-Meurée et al. [418]; at 225–295 K and 174–250 nm by Simon et al. [379]; and at 220–300 K and 186–240 nm by Prahlad and Kumar [319]. The room temperature data agree within 10% between 190 and 235 nm and within 20% and 40% at 240 and 250 nm (except the value at 250 nm reported by Currie et al [98], which is lower than the half of the other values). The absorption curve based on the data (reported at 0.5-nm intervals) of Prahlad and Kumar [319] shows wiggles over the whole range 186–240 nm obviously due to experimental uncertainties. In the range 180–186 nm, the values reported by Hubrich and Stuhl [165] are higher by up to 25% than those reported by Simon et al. [379], and the value at 186 nm reported by Prahlad and Kumar [319] is lower by 18% than the value of Simon et al. [379]. In the maximum near 176 nm, the absorption cross section is 1.01×10^{-17} cm^2, as reported by Hubrich and Stuhl [165] and Simon et al. [379], whereas the plotted spectrum reported by Roxlo and Mandl [350] shows a lower value of ~7×10^{-18} cm^2. For a wavelength of 313 nm, an absorption cross section of
$\leq 3.7 \times 10^{-26}$ cm^2 was derived by Rebbert and Ausloos [332] from the C_2H_5Cl yield in the photolysis of CCl_4-C_2H_6 mixtures. The preferred absorption cross sections at room temperature, listed in Table 4-39, are the mean of the values reported by Hubrich and Stuhl [165] and Simon et al. [379] at 174–192 nm, the values of Simon et al. [379] at 194–250 nm, and the data of Hubrich and Stuhl [165] at 255–275 nm.

The temperature dependence of the absorption cross sections becomes significant at wavelengths above 205 nm, where the cross sections decrease with decreasing temperature between 300 and 210 K as observed in good agreement by Simon et al. [379] and Prahlad and Kumar [319]. Simon et al. [379] parameterized the cross sections and the temperature dependence by the polynomial expansion

$$\log_{10} \sigma(\lambda, T) = \sum A_n \lambda^n + (T - 273) \times \sum B_n \lambda^n$$

and reported smoothed values for T = 210, 230, 250, 270, and 295 K, every 2 nm, and at wavelengths corresponding to the wavenumber intervals generally used in stratospheric photodissociation calculations. The parameters A_n and B_n for the ranges T = 210–300 K and λ = 194–250 nm are as follows:

$A_0 = -37.104$ $B_0 = 1.0739$
$A_1 = -5.8218 \times 10^{-1}$ $B_1 = -1.6275 \times 10^{-2}$
$A_2 = 9.9974 \times 10^{-3}$ $B_2 = 8.8141 \times 10^{-5}$
$A_3 = -4.6765 \times 10^{-5}$ $B_3 = -1.9811 \times 10^{-7}$
$A_4 = 6.8501 \times 10^{-8}$ $B_4 = 1.5022 \times 10^{-10}$

Quantum yields ≥0.9 and ~0.75 for the photodissociative processes $CCl_4 + h\nu \rightarrow CCl_3 + Cl$ at 213.9 nm and $CCl_4 + h\nu \rightarrow CCl_2 + 2Cl$ at 163.3 nm, respectively, were derived from the gas-phase photolysis of CCl_4 in the presence of HCl, HBr, and C_2H_6 by Rebbert and Ausloos [332]. A quantum yield for $Cl^*(^2P_{1/2})$ atom formation in the broad band photolysis of CCl_4, $\Phi(Cl^*) = 0.78 \pm 0.27$, was reported by Clark and Husain [80].

Table 4-39. Absorption Cross Sections of CCl_4 at 295–298 K

λ (nm)	10^{20} σ (cm^2)	λ (nm)	10^{20} σ (cm^2)	λ (nm)	10^{20} σ (cm^2)
174	956	204	61.0	234	2.20
176	1010	206	57.0	236	1.60
178	982.5	208	52.5	238	1.16
180	806	210	46.9	240	0.830
182	647	212	41.0	242	0.590
184	478.5	214	34.5	244	0.413
186	338.5	216	27.8	246	0.290
188	227	218	22.1	248	0.210
190	145.5	220	17.5	250	0.148
192	99.6	222	13.6	255	0.0661
194	76.7	224	10.2	260	0.0253
196	69.5	226	7.60	265	0.0126
198	68.0	228	5.65	270	0.00610
200	66.0	230	4.28	275	0.00239
202	63.8	232	3.04		

Notes:

174–192 nm: mean of Hubrich and Stuhl [165] and Simon et al. [379]
194–250 nm: Simon et al. [379]
255–275 nm: Hubrich and Stuhl [165].

F18. $CH_3OCl + h\nu \rightarrow$ Products. The absorption cross sections of CH_3OCl have been determined by Crowley et al. [96] and by Jungkamp et al. [196]. The preferred cross sections, listed in Table 4-40, are the mean of the values reported by these two groups. The agreement between the two sets of measurements is excellent at wavelengths longer than 250 nm; at the maximum near 230 nm the results of Jungkamp et al. are about 15% smaller.

Table 4-40. Absorption Cross Sections of CH_3OCl

λ (nm)	10^{20} σ (cm^2)	λ (nm)	10^{20} σ (cm^2)	λ (nm)	10^{20} σ (cm^2)
230	14.9	290	1.32	350	0.662
232	15.4	292	1.34	352	0.611
234	15.7	294	1.35	354	0.574
236	15.9	296	1.37	356	0.529
238	15.8	298	1.40	358	0.482
240	15.5	300	1.43	360	0.445
242	14.9	302	1.45	362	0.411
244	14.2	304	1.47	364	0.389
246	13.2	306	1.48	366	0.356
248	12.2	308	1.49	368	0.331
250	11.1	310	1.49	370	0.298
252	9.96	312	1.48	372	0.273
254	8.86	314	1.47	374	0.246
256	7.77	316	1.46	376	0.225
258	6.80	318	1.43	378	0.209
260	5.87	320	1.41	380	0.202
262	5.05	322	1.37	382	0.186
264	4.31	324	1.33	384	0.17
266	3.69	326	1.30	386	0.16
268	3.16	328	1.24	388	0.15
270	2.71	330	1.20	390	0.13
272	2.35	332	1.14	392	0.14
274	2.06	334	1.09	394	0.13
276	1.83	336	1.04		
278	1.64	338	0.980		
280	1.53	340	0.918		
282	1.42	342	0.875		
284	1.37	344	0.822		
286	1.33	346	0.760		
288	1.32	348	0.709		

F19. $CHCl_3 + h\nu \rightarrow$ Products. The absorption cross sections of $CHCl_3$ have been measured at room temperature and in the far UV region at 113–182 nm by Lucazeau et al. [225]; at the Lyman-α line at 121.6 nm by Brownsword et al. [46]; and at 110–200 nm by Russell et al. [353]; at room temperature and 222.7 nm by Gordus and Bernstein [142]; at 160–255 nm by Hubrich and Stuhl [165]; at 279 and 296 K and 190–230 nm by Vanlaethem-Meurée et al. [418]; and at 225–295 K and 174–240 nm by Simon et al. [379]. The room temperature data of Vanlaethem- Meurée et al. [418] and Simon et al. [379] are identical at 190–210 nm and increasingly deviate up to ~15% at 212–240 nm. The data of Hubrich and Stuhl [165] and Simon et al. [379] agree within 10 % between 180 and 234 nm; however the values of Hubrich and Stuhl [165] become increasingly larger by up to~25% than those of Simon et al. [379] in the long-wavelength tail. In the region of the absorption maximum at ~176 nm, there is the largest spread: a cross sections of ~5×10^{-18} cm^2 has been measured by Simon et al. [379] in contrast to values of 3.7×10^{-18} cm^2 reported by Hubrich and Stuhl [165] and $<2 \times 10^{-18}$ cm^2 given in a plot by Lucazeau et al. [225]. We therefore recommend absorption cross sections only for the region above 180 nm. The values, listed in Table 4-41, are the mean of the values reported by Hubrich and Stuhl [165] and Simon et al. [379] for the range 180–240 nm. For the range 242–256 nm, these have been extrapolated ($\log \sigma = -1.2277 - 0.0844\ \lambda$) (in italics).

The temperature dependence of the absorption cross sections becomes significant at wavelengths above 194 nm, where the cross sections decrease with decreasing temperature between 295 and 210 K. Simon et al. [379] parameterized the cross sections and the temperature dependence by the polynomial expansion $\log_{10} \sigma(\lambda, T) = \sum A_n \lambda^n + (T - 273) \times \sum B_n \lambda^n$ and reported smoothed values for T = 210, 230, 250, 270, and 295 K, every 2 nm, and at wavelengths corresponding to the wavenumber intervals generally used in

stratospheric photodissociation calculations. The parameters A_n and B_n for the ranges T = 210–300 K and λ = 190–240 nm are as follows:

$A_0 = 269.80$ $B_0 = 3.7973$
$A_1 = -6.0908$ $B_1 = -7.0913 \times 10^{-2}$
$A_2 = 4.7830 \times 10^{-2}$ $B_2 = 4.9397 \times 10^{-4}$
$A_3 = -1.6427 \times 10^{-4}$ $B_3 = -1.5226 \times 10^{-6}$
$A_4 = 2.0682 \times 10^{-7}$ $B_4 = 1.7555 \times 10^{-9}$

Quantum yields for H atom formation have been measured in the far UV by Brownsword et al. [46], [47]: $\Phi(H) = 0.23 \pm 0.03$ and 0.13 at 121.6 and 157.6 nm, respectively, whereas H atoms could not be detected in the photolysis at 193.3 nm.

Table 4-41. Absorption Cross Sections of $CHCl_3$ at 295–298 K

λ (nm)	$10^{20}\ \sigma$ (cm^2)	λ (nm)	$10^{20}\ \sigma$ (cm^2)	λ (nm)	$10^{20}\ \sigma$ (cm^2)
180	372	206	20.7	232	0.158
182	317	208	15.1	234	0.107
184	248	210	10.7	236	0.0730
186	186	212	7.48	238	0.0503
188	144	214	5.24	240	0.0347
190	113	216	3.60	*242*	*0.0223*
192	89.9	218	2.48	*244*	*0.0151*
194	76.1	220	1.69	*246*	*0.01023*
196	64.2	222	1.13	*248*	*0.00694*
198	53.0	224	0.750	*250*	*0.00470*
200	42.6	226	0.503	*252*	*0.00319*
202	34.4	228	0.342	*254*	*0.00216*
204	27.2	230	0.234	*256*	*0.00147*

Note: 180–240 nm: mean of Hubrich and Stuhl [165] and Simon et al. [379]
242–256 nm: extrapolation of mean of Hubrich and Stuhl [165] and Simon et al. [379] data.

F20. $CH_2Cl_2 + h\nu \rightarrow$ Products. The absorption cross sections of CH_2Cl_2 have been measured at room temperature and 110–200 nm by Russell et al. [353]; at the Lyman-α line at 121.6 nm by Brownsword et al. [46]; at 213 nm by Gordus and Bernstein [142], at 160–255 nm by Hubrich and Stuhl [165]; at 279 and 296 K and 176–216 nm by Vanlaethem-Meurée et al. [418]; and at 225–295 K and 176–220 nm by Simon et al. [379]. The room temperature data of Vanlaethem-Meurée et al. [418] and Simon et al. [379] are nearly identical. The data of Hubrich and Stuhl [165] agree with those of Simon et al. [379] within 12% at 176–206 nm and become increaseingly larger at 185–220 nm by up to 50%. The preferred absorption cross sections, listed in Table 4-42, are the mean of the values reported by Hubrich and Stuhl [165] and Simon et al. [379] at 176–220 nm. For wavelengths above 220 nm, the average of their data at 200–210 nm has been extrapolated ($\log \sigma = -2.1337 - 0.08439\ \lambda$) (in italics) at wavelengths up to 256 nm. The measured values of Hubrich and Stuhl [165] are smaller by up to 7% below 230 nm and become larger by up to 50% between 235 and 255 nm than the extrapolated values.

The temperature dependence of the absorption cross sections becomes significant at wavelengths above 190 nm, where the cross sections decrease with decreasing temperature between 295 and 210 K. Simon et al. [379] parameterized the cross sections and the temperature dependence by the polynomial expansion $\log_{10} \sigma(\lambda, T) = \sum A_n \lambda^n + (T - 273) \times \sum B_n \lambda^n$ and reported smoothed values for T = 210, 230, 250, 270, and 295 K, every 2 nm, and at wavelengths corresponding to the wavenumber intervals generally used in stratospheric photodissociation calculations. The parameters A_n and B_n for the ranges T = 210–300 K and λ = 176–220 nm are as follows:

$A_0 = -1431.8$ $B_0 = -3.1171$
$A_1 = 27.395$ $B_1 = 6.7874 \times 10^{-2}$
$A_2 = -1.9807 \times 10^{-1}$ $B_2 = -5.5000 \times 10^{-4}$
$A_3 = 6.3468 \times 10^{-4}$ $B_3 = 1.9649 \times 10^{-6}$
$A_4 = -7.6298 \times 10^{-7}$ $B_4 = -2.6101 \times 10^{-9}$

Quantum yields for H atom formation have been measured in the far UV by Brownsword et al. [46], [47]: $\Phi(H) = 0.28 \pm 0.03$, 0.23, and 0.002 ± 0.001 at 121.6, 157.6, and 193.3 nm, respectively.

Table 4-42. Absorption Cross Sections of CH_2Cl_2 at 295–298 K

λ (nm)	10^{20} σ (cm^2)	λ (nm)	10^{20} σ (cm^2)	λ (nm)	10^{20} σ (cm^2)
176	186	204	4.41	*232*	*0.0194*
178	182	206	3.07	*234*	*0.0132*
180	173	208	2.13	*236*	*0.00892*
182	156	210	1.45	*238*	*0.00605*
184	135	212	0.978	*240*	*0.00410*
186	110	214	0.651	*242*	*0.00278*
188	84.2	216	0.435	*244*	*0.00188*
190	61.0	218	0.291	*246*	*0.00128*
192	43.9	220	0.190	*248*	*0.000866*
194	30.5	*222*	*0.135*	*250*	*0.000587*
196	20.6	*224*	*0.0918*	*252*	*0.000398*
198	14.1	*226*	*0.0623*	*254*	*0.000270*
200	9.48	*228*	*0.0422*	*256*	*0.000183*
202	6.40	*230*	*0.0286*		

Note: 176–220 nm: mean of Hubrich and Stuhl [165] and Simon et al. [379]
222–256 nm: extrapolation of mean of Hubrich and Stuhl [165] and Simon et al. [379] data.

F21. $CH_3Cl + h\nu \rightarrow$ Products. The absorption cross sections of CH_3Cl have been measured at room temperature and 110–200 nm by Russell et al. [353]; at the Lyman-α line at 121.6 nm by Brownsword et al. [46]; at 171.2 nm by Felps et al. [119]; and at 174–220 nm by Robbins [338]; at 208 and 298 K and 158–235 nm by Hubrich et al. [166]; at 255, 279, and 296 K and 186–216 nm by Vanlaethem-Meurée et al. [418]; and at 225–295 K and 174–216 nm by Simon et al. [379]. The room temperature data generally agree within 10% in the wavelength range 174–216 nm, those of Vanlaethem-Meurée et al. [418] and Simon et al. [379] are nearly identical. The value at 171 nm of Felps et al. [47] is smaller by ~15% than that of Hubrich et al. [166]. The preferred absorption cross sections, listed in

Table 4-43, are the mean of the values reported by Robbins [338], Hubrich et al. [166], and Simon et al. [379] at 174–184 nm, the mean of the values reported by Robbins [338], Hubrich et al. [166], Vanlaethem-Meurée et al. [418], and Simon et al. [379] at 186–216 nm, and the mean of the values reported by Robbins [338] and Hubrich et al. [166] at 218–220 nm. The values for the wavelength range 222–236 nm have been taken from an interpolation (at 2-nm intervals) of the 200–235-nm data of Hubrich et al. [166] ($\log \sigma = -0.24164 - 0.09743 \lambda$).

The temperature dependence of the absorption cross sections becomes significant at wavelengths above 194 nm, where the cross sections decrease with decreasing temperature between 295 and 210 K. There is very good agreement between the low-temperature values at 250–255 K of Vanlaethem-Meurée et al. [418] and Simon et al. [379]. The latter authors parameterized the cross sections and the temperature dependence by the polynomial expansion $\log_{10} \sigma(\lambda, T) = \Sigma A_n \lambda^n + (T - 273) \times \Sigma B_n \lambda^n$ and reported smoothed values for T = 210, 230, 250, 270, and 295 K, every 2 nm, and at wavelengths corresponding to the wavenumber intervals generally used in stratospheric photodissociation calculations. The parameters A_n and B_n for the ranges T = 210–300 K and λ = 174–216 nm are as follows:

$A_0 = -299.80$	$B_0 = -7.1727$
$A_1 = 5.1047$	$B_1 = 1.4837 \times 10^{-1}$
$A_2 = -3.3630 \times 10^{-2}$	$B_2 = -1.1463 \times 10^{-3}$
$A_3 = 95805 \times 10^{-5}$	$B_3 = 3.9188 \times 10^{-6}$
$A_4 = -1.0135 \times 10^{-7}$	$B_4 = -4.9994 \times 10^{-9}$

Quantum yields for H atom formation have been measured in the far UV by Brownsword et al. [46], [47]: $\Phi(H) = 0.53 \pm 0.05$, 0.29, 0.012 ± 0.006 at 121.6, 157.6, and 193.3 nm, respectively.

Table 4-43. Absorption Cross Sections of CH_3Cl at 295–298 K

λ (nm)	10^{20} σ (cm^2)	λ (nm)	10^{20} σ (cm^2)	λ (nm)	10^{20} σ (cm^2)
174	110	196	3.96	218	0.0345
176	93.9	198	2.68	220	0.0220
178	78.2	200	1.77	*222*	*0.0135*
180	63.6	202	1.13	*224*	*0.00859*
182	46.5	204	0.731	*226*	*0.00549*
184	35.0	206	0.482	*228*	*0.00350*
186	25.8	208	0.313	*230*	*0.00224*
188	18.4	210	0.200	*232*	*0.00143*
190	12.8	212	0.127	*234*	*0.000911*
192	8.84	214	0.0860	*236*	*0.000582*
194	5.83	216	0.0534		

Note:

174–184 nm: mean of Robbins [338], Hubrich et al. [166], and Simon et al. [379]

186–216 nm: mean of Robbins [338], Hubrich et al. [166], Vanlaethem-Meurée et al. [418] and Simon et al. [379]

218–220 nm: mean of Robbins [338] and Hubrich et al. [166]

222–236 nm: extrapolation of Hubrich et al. [166] data.

F22. $CH_3CCl_3 + h\nu \rightarrow$ Products. The absorption cross sections of CH_3CCl_3 have been measured at room temperature and 147 nm by Salomon et al. [355], and at 160–255 nm by Hubrich and Stuhl [165], who corrected (<10.7%) the absorption cross sections in the range 170–190 nm for the concentration and absorption cross sections of a 1,4-dioxane stabilizer present during the experiments. Measurements at 220–295 K and 182–240 nm were carried out by Vanlaethem-Meurée et al. [420] and at 223–333 K and 160 240 nm by Nayak et al. [287]. The latter authors also measured the absorption cross sections in the liquid phase at 235–260 nm and used a wavelength-shift procedure to convert the liquid-phase data into gas-phase data. The agreement of the room temperature data is within 20% at 165–205 nm (at 160 nm, the value reported by Nayak et al. [287] is larger by 50% than that reported by Hubrich and Stuhl [165]). Between 210 and 240 nm, the data of Vanlaethem-Meurée et al. [420] and Nayak et al. [287] are within 15%, whereas those of Hubrich and Stuhl [165] are larger by 100–150%. The preferred absorption cross sections, listed in Table 4-44, are the mean of the values reported by Hubrich and Stuhl [165] and Nayak et al. [287] at 170–180 nm, the mean of the values reported by Vanlaethem-Meurée et al. [420], Hubrich and Stuhl [165], and Nayak et al. [287] at 185–205 nm, and the mean of the values reported by Vanlaethem-Meurée et al. [420] and Nayak et al. [287] at 210–240 nm. For wavelengths above 240 nm, the average of their data at 220–240 nm has been extrapolated ($\log \sigma = -1.59792 - 0.08066\ \lambda$) at wavelengths up to 255 nm. The measured values of Hubrich and Stuhl [165] are larger by up to ~140% at 250 nm and smaller by ~80% at 255 nm than the recommended values.

The temperature dependence of the absorption cross sections becomes significant at wavelengths above 210 nm, where the cross sections decrease with decreasing temperature, as observed in good agreement at 333–223 K by Nayak et al. [287] and at 295–210 K by Vanlaethem-Meurée et al. [420]. The latter authors parameterized the cross sections and the temperature dependence by the polynomial expansion $\log_{10} \sigma(\lambda, T) = \sum A_n \lambda^n + (T - 273) \times \sum B_n \lambda^n$ and reported smoothed values for T = 210, 230, 250, 270, and 295 K, every 2 nm, and at wavelengths corresponding to the wavenumber intervals generally used in stratospheric photodissociation calculations. The parameters A_n and B_n for the ranges T = 210–300 K and λ = 182–240 nm reported by Gillotay and Simon [138] are as follows:

$A_0 = 341.085191$ $\quad B_0 = -1.660090$
$A_1 = -7.273362$ $\quad B_1 = 3.079969 \times 10^{-2}$
$A_2 = 5.498387 \times 10^{-2}$ $\quad B_2 = -2.106719 \times 10^{-4}$
$A_3 = -1.827552 \times 10^{-4}$ $\quad B_3 = 6.264984 \times 10^{-7}$
$A_4 = 2.238640 \times 10^{-7}$ $\quad B_4 = -6.781342 \times 10^{-10}$

Table 4-44. Absorption Cross Sections of CH_3CCl_3 at 295–298 K

λ (nm)	10^{20} σ (cm^2)	λ (nm)	10^{20} σ (cm^2)	λ (nm)	10^{20} σ (cm^2)
170	406	200	92.1	230	0.717
175	424	205	52.0	235	0.276
180	404	210	25.5	240	0.111
185	301	215	10.9	*245*	*0.0437*
190	212	220	4.47	*250*	*0.0173*
195	147	225	1.82	*255*	*0.00682*

Note: 170–180 nm: mean of Hubrich and Stuhl [165] and Nayak et al. [287]
185–205 nm: mean of Vanlaethem-Meurée et al. [420], Hubrich and Stuhl [165] and Nayak et al. [287]
210–240 nm: mean of Vanlaethem-Meurée et al. [420] and Nayak et al. [287]
245–255 nm: extrapolation of mean of Vanlaethem-Meurée et al. [420] and Nayak et al. [287] data.

F23. $CH_3H_2Cl + h\nu \rightarrow$ Products. The absorption cross sections of CH_3CH_2Cl have been measured at room temperature and 147 nm by Ichimura et al. [173] and at 160–240 nm by Hubrich and Stuhl [165]. The data of Hubrich and Stuhl [165] are listed in Table 4-45.

Table 4-45. Absorption Cross Sections of CH_3CH_2Cl at 298 K

λ (nm)	10^{20} σ (cm^2)	λ (nm)	10^{20} σ (cm^2)	λ (nm)	10^{20} σ (cm^2)
160	189.0	190	6.85	220	0.0127
165	110.0	195	2.56	225	0.00463
170	70.5	200	1.17	230	0.00117
175	44.4	205	0.375	235	0.000395
180	30.4	210	0.147	240	0.000156
185	13.6	215	0.0433		

Note: 160–240 nm, Hubrich and Stuhl [165].

F24. $CH_3CHClCH_3 + h\nu \rightarrow$ Products. In a compilation of ultraviolet absorption cross sections of halocarbons by Gillotay and Simon [355] results are reported for (erroneously) $CH_3CH_2ClCH_3$, which presumably should be $CH_3CHClCH_3$. The data are listed in Table 4-46.

Table 4-46. Absorption Cross Sections of $CH_3CHClCH_3$ at 295 K

λ (nm)	10^{20} σ (cm^2)	λ (nm)	10^{20} σ (cm^2)	λ (nm)	10^{20} σ (cm^2)
170	31.7	192	4.67	214	0.0965
172	27.0	194	3.49	216	0.0652
174	24.3	196	2.58	218	0.0444
176	22.1	198	1.88	220	0.0308
178	20.3	200	1.34	222	0.0212
180	18.0	202	0.954	224	0.0144
182	15.0	204	0.671	226	0.0107
184	12.2	206	0.463	228	0.00752
186	9.99	208	0.311	230	0.00580
188	7.93	210	0.214		
190	6.06	212	0.144		

Note: 170–230 nm, Gillotay and Simon [138].

F25. $CH_2ClCH_2Cl + h\nu \rightarrow$ Products.

F26. $CH_2ClCH_2CH_2Cl + h\nu \rightarrow$ Products.

F27. $CH_2Cl(CH_2)_2CH_2Cl + h\nu \rightarrow$ Products.

Absorption cross sections for these three dichloroalkanes at room temperature and 118–200 nm have been reported by Russell et al. [353].

F28. $CCl_2O + h\nu \rightarrow$ Products. See note for $CF_2O + h\nu$ (Note E5).

F29. $CClFO + h\nu \rightarrow$ Products. See note for $CF_2O + h\nu$ (Note E5).

F30. $CFCl_3$ (CFC-11) + $h\nu \rightarrow$ Products. The absorption cross sections of $CFCl_3$ have been measured at room temperature and 225 nm by Gordus and Bernstein [142], at 186–226 nm by Rowland and Molina [347], at 174–226 nm by Robbins and Stolarski [339], at 186–209 nm by Greene and Wayne [146]; at 213–296 K and 185–226 nm by Chou et al. [78]; at 208 and 298 K and 158–260 nm by Hubrich et al. [166] and Hubrich and Stuhl [165]; at 255, 279, and 296 K and 190–220 nm by Vanlaethem-Meurée et al. [419]; at 225–295 K and 174–230 nm by Simon et al. [379]; and at 220, 240, and 296 K and 200–238 nm by Mérienne et al. [256]. The room temperature data are in good agreement, generally within 10–15%. Absorption cross sections at 148–225 nm have also been derived from electron energy-loss measurements by Huebner et al. [171], which are up to 30% higher than the values obtained by optical measurements. The preferred absorption cross sections, listed in Table 4-47, are the values of Simon et al. [379] at 174–198 nm, the mean of the values reported by Simon et al. [379] and Mérienne et al. [256] at 200–230 nm, and the data of Hubrich and Stuhl [165] at 235–260 nm.

Measurements in the far UV at 60–145 nm have been reported by Gilbert et al. [132], and at 120–200 nm by Doucet et al. [110].

The temperature dependence becomes significant at wavelengths above 185 nm, where the cross sections decrease with decreasing temperature between 296 and 210 K (Hubrich et al. [166] observed such a behavior only above 200 nm). Simon et al. [379] parameterized the temperature dependence of the cross sections by the polynomial expansion $\log_{10} \sigma(\lambda, T) = \Sigma A_n \lambda^n + (T - 273) \times \Sigma B_n \lambda^n$and reported smoothed values for T = 210, 230, 250, 270, and 295 K, every 2 nm, and at wavelengths corresponding to the wavenumber intervals generally used in stratospheric photodissociation calculations. The parameters A_n and B_n for the ranges T = 210–300 K and λ = 174–230 nm are as follows:

$A_0 = -84.611$ $\quad B_0 = -5.7912$
$A_1 = 7.9551 \times 10^{-1}$ $\quad B_1 = 1.1689 \times 10^{-1}$
$A_2 = -2.0550 \times 10^{-3}$ $\quad B_2 = -8.8069 \times 10^{-4}$
$A_3 = -4.4812 \times 10^{-6}$ $\quad B_3 = 2.9335 \times 10^{-6}$
$A_4 = 1.5838 \times 10^{-8}$ $\quad B_4 = -3.6421 \times 10^{-9}$

A similar polynomial expansion, $\log_{10} \sigma(\lambda, T) = \Sigma a_n (\lambda - 200)^n + (T - 296) \times \Sigma b_n(\lambda - 200)^n$, for the ranges T = 220–296 K and λ = 200–238 nm was used by Mérienne et al. [256] with the following parameters a_n and b_n:

$a_0 = -41.925548$ $b_0 = 3.58977 \times 10^{-4}$
$a_1 = -1.142857 \times 10^{-1}$ $b_1 = 3.02973 \times 10^{-4}$
$a_2 = -3.12034 \times 10^{-3}$ $b_2 = -1.13 \times 10^{-8}$
$a_3 = 3.6699 \times 10^{-5}$

A quantum yield for $Cl^*(^2P_{1/2})$ atom formation in the broad band photolysis of $CFCl_3$, Φ (Cl*) = 0.79 ± 0.27, was reported by Clark and Husain [80].

Table 4-47. Absorption Cross Sections of $CFCl_3$ at 295–298 K

λ (nm)	$10^{20}\ \sigma$ (cm^2)	λ (nm)	$10^{20}\ \sigma$ (cm^2)	λ (nm)	$10^{20}\ \sigma$ (cm^2)
174	313.0	198	78.0	222	1.72
176	324.0	200	63.2	224	1.17
178	323.5	202	49.1	226	0.790
180	314.0	204	37.3	228	0.532
182	296.0	206	28.1	230	0.354
184	272.0	208	20.4	235	0.132
186	243.0	210	15.1	240	0.0470
188	213.0	212	10.7	245	0.0174
190	179.0	214	7.54	250	0.0066
192	154.0	216	5.25	255	0.0029
194	124.3	218	3.65	260	0.0015
196	99.1	220	2.51		

Note: 174–198 nm: Simon et al. [379]
200–230 nm: mean of Simon et al. [379] and Mérienne et al. [256]
235–260 nm: Hubrich and Stuhl [165].

F31. CF_2Cl_2 (CFC-12) + hν → Products. The absorption cross sections of CF_2Cl_2 have been measured at room temperature and 210 nm by Gordus and Bernstein [142], at 186–216 nm by Rowland and Molina [347], at 174–216 nm by Robbins and Stolarski [339], at 186–206 nm by Greene and Wayne [146]; at 234–442 K and 213.9 nm by Rebbert and Ausloos [333]; at 212, 252, and 296 K and 184–221 nm by Chou et al. [78]; at 208 and 298 K and 159–240 nm by Hubrich et al. [166]; at 255, 279, and 296 K and 190–216 nm by Vanlaethem-Meurée et al. [419]; at 225–295 K and 174–230 nm by Simon et al. [379]; and at 220, 240, and 296 K and 200–231 nm by Mérienne et al. [256]. The room temperature data are in good agreement, generally within 10–15%, except the data of Green and Wayne [146] above 195 nm and the data of Rowland and Molina [347] around 210 nm. Absorption cross sections at 148–218 nm have also been derived from electron energy-loss measurements by Huebner et al. [171], which agree within 10% with the data obtained by optical measurements around the absorption maximum and become higher than the optical data by up to 100% above 196 nm. The preferred absorption cross sections, listed in Table 4-51, are the values of Hubrich et al. [166] at 170–172 nm, the mean of the values reported by Hubrich et al. [166] and Simon et al. [379] at 174–178 nm, the values of Simon et al. [379] at 180–198 nm, the mean of the values reported by Simon et al. [379] and Mérienne et al. [256] at 200–226 nm, and the data of Mérienne et al. [256] at 228–230 nm. For the range 232–240 nm, the absorption curve above 210 nm of Mérienne et al. [256] has been extrapolated ($\log \sigma = 2.1448 - 0.1061\ \lambda$). The measured values of Hubrich et al. [166] are lower by up to ~40% at 240 nm than the extrapolated values.

High-resolution absorption cross section measurements have been carried out by Seccombe et al. [369] between 50 and 150 nm, and by Limao-Vieira et al. [219] between 113 and 225 nm using a synchrotron radiation light source. The results of Limao-Vieira et al. for the absorption band at 170–204 nm are in very good agreement with the recommendation in Table 4-48 (at wavelengths above 204 nm, noise effects become significant). The new cross section measurements for the far UV region from both recent studies significantly improve upon the earlier data of Gilbert et al. [132] for the wavelength range 60–135 nm and of Doucet et al. [110] for the wavelength range 120–200 nm.

The temperature dependence becomes significant at wavelengths above 186 nm, where the cross sections decrease with decreasing temperature between 296 and 210 K. Simon et al. [379] parameterized the temperature dependence of the cross sections by the polynomial expansion $\log_{10} \sigma(\lambda, T) = \sum A_n \lambda^n + (T - 273) \times \sum B_n \lambda^n$ and reported smoothed values for T = 210, 230, 250, 270, and 295 K, every 2 nm, and at wavelengths

corresponding to the wavenumber intervals generally used in stratospheric photodissociation calculations. The parameters A_n and B_n for the ranges T = 210–300 K and λ = 174–226 nm are as follows:

$A_0 = -711.02$ $B_0 = 6.1648$
$A_1 = 12.490$ $B_1 = -1.2093 \times 10^{-1}$
$A_2 = -8.2865 \times 10^{-2}$ $B_2 = 8.8587 \times 10^{-4}$
$A_3 = 2.4091 \times 10^{-4}$ $B_3 = -2.8743 \times 10^{-6}$
$A_4 = -2.6113 \times 10^{-7}$ $B_4 = 3.4904 \times 10^{-9}$

A similar polynomial expansion, $\log_{10} \sigma(\lambda, T) = \sum a_n (\lambda - 200)^n + (T - 296) \times \sum b_n(\lambda - 200)^n$, for the ranges T = 220–296 K and λ = 200–231 nm was used by Mérienne et al. [256] with the following parameters a_n and b_n:

$a_0 = -43.8954569$ $b_0 = 4.8438 \times 10^{-3}$
$a_1 = -2.403597 \times 10^{-1}$ $b_1 = 4.96145 \times 10^{-4}$
$a_2 = -4.2619 \times 10^{-4}$ $b_2 = -5.6953 \times 10^{-6}$
$a_3 = 9.8743 \times 10^{-6}$

A quantum yield for $Cl^*(^2P_{1/2})$ atom formation in the broad band photolysis of CF_2Cl_2, $\Phi(Cl^*) = 0.75 \pm 0.26$, was reported by Clark and Husain [80].

Table 4-48. Absorption Cross Sections of CF_2Cl_2 at 295–298 K

λ (nm)	10^{20} σ (cm^2)	λ (nm)	10^{20} σ (cm^2)	λ (nm)	10^{20} σ (cm^2)
170	124.0	194	31.5	218	0.103
172	151.0	196	21.1	220	0.0624
174	168.0	198	13.9	222	0.0381
176	185.5	200	8.71	224	0.0233
178	189.5	202	5.42	226	0.0140
180	179.0	204	3.37	228	0.0090
182	160.0	206	2.06	230	0.0057
184	134.0	208	1.26	*232*	*0.0034*
186	107.0	210	0.762	*234*	*0.0021*
188	82.8	212	0.458	*236*	*0.0013*
190	63.2	214	0.274	*238*	*0.0008*
192	45.50	216	0.163	*240*	*0.0005*

Note: 170–172 nm, Hubrich et al. [166],
174–178 nm, the mean of Hubrich et al. [166] and Simon et al. [379],
180–198 nm, Simon et al. [379],
200–230 nm, mean of Simon et al. [379] and Mérienne et al. [256],
232–240 nm, extrapolation of Mérienne et al. [256] data.

F32. CF_3Cl (CFC-13) + hν → Products. The absorption cross sections of CF_3Cl have been measured at room temperature and 184–203 nm by Chou et al. [77]; at 255, 279, and 296 K and 172–200 nm by Vanlaethem-Meurée et al. [419]; at 208 and 298 K and 160–220 nm by Hubrich and Stuhl [165]; and at 225–295 K and 172–200 nm by Simon et al. [379]. The values of Vanlaethem-Meurée et al. [419] and Simon et al. [379] are identical, the room temperature values of Hubrich and Stuhl [165] deviate from the latter by up to about ±25%, and the data of Chou et al. [77] are always larger by about 15–30% in the region 185–200 nm. The recommended absorption cross sections for CF_3Cl, presented in Table 4-49, are taken from Simon et al. [379] for the range 172–200 nm. The values at 202–220 nm are obtained by extrapolation of the absorption curve above 200 nm ($\log \sigma = -5.048 - 0.0834\ \lambda$) of Simon et al. [379].

Measurements in the far UV at 65–130 nm have been reported by Gilbert et al. [132] and at 120–160 nm by Doucet et al. [110]. Measurements at the Lyman-α line at 121.6 nm have been carried out by Ravishankara et al. [328].

Temperature effects, if any, could not be detected by Vanlaethem-Meurée et al. [419] and Simon et al. [379], whereas Hubrich and Stuhl [165] report a decrease of the absorption cross sections between 298 and 208 K by

4% at160 nm to 74% at 205 nm. Simon et al. [379] parameterized the cross sections and the temperature dependence of the absorption cross sections by the polynomial expansion

$$\log_{10} \sigma(\lambda, T) = \sum A_n \lambda^n + (T - 273) \times \sum B_n \lambda^n \text{ (with all } B_n = 0),$$

and reported smoothed values for T = 295 K, every 2 nm, and at wavelengths corresponding to the wavenumber intervals generally used in stratospheric photodissociation calculations. The parameters A_n for the ranges T = 210–300 K and λ = 172–200 nm are:

$$A_0 = -1.55.88,\ A_1 = 2.0993,\ A_2 = -1.0486 \times 10^{-2},\ A_3 = 1.6718 \times 10^{-5}.$$

A quantum yield for $Cl^*(^2P_{1/2})$ atom formation in the broad band photolysis of CF_3Cl, $\Phi(Cl^*) = 0.86 \pm 0.29$, was reported by Clark and Husain [80].

Table 4-49. Absorption Cross Sections of CF_3Cl at 295 K

λ (nm)	10^{20} σ (cm^2)	λ (nm)	10^{20} σ (cm^2)	λ (nm)	10^{20} σ (cm^2)
172	1.100	190	0.128	*206*	*0.00595*
174	0.970	192	0.0900	*208*	*0.00406*
176	0.825	194	0.0610	*210*	*0.00276*
178	0.681	196	0.0410	*212*	*0.00188*
180	0.542	198	0.0280	*214*	*0.00128*
182	0.425	200	0.0190	*216*	*0.000872*
184	0.326	200	0.0189	*218*	*0.000594*
186	0.244	202	*0.0128*	*220*	*0.000405*
188	0.175	204	*0.00874*		

Note: 172–200 nm, Simon et al. [379],
202–220 nm, extrapolation of Simon et al. [379] data.

F33. $CF_2ClCFCl_2$ (CFC-113) + hν → Products. The absorption cross sections of $CF_2ClCFCl_2$ have been measured at 298 K and 184–224 nm by Chou et al. [77]; at 208 and 298 K and 160–250 nm by Hubrich and Stuhl [165]; and at 225–295 K and 184–230 nm by Simon et al. [380]. The room temperature values agree within about 10% except in the region around 190 nm where the values of Hubrich and Stuhl [165] are smaller by up to 20 % than the other values. The preferred absorption cross sections, listed in Table 4-50, are the values of Hubrich and Stuhl [165] at 175–180 nm, a value at 184 nm interpolated between those of Hubrich and Stuhl [165] at 180 nm and Simon et al. [380] at 186 nm, and the values of Simon et al. [380] at 186–230 nm. For the range 232–250 nm, the absorption curve of Simon et al. [380] above 230 nm has been extrapolated ($\log \sigma = -0.9860 - 0.0894\ \lambda$). The measured values of Hubrich and Stuhl [165] are larger than the extrapolated values by ~20–80% at 232–250 nm.

Measurements in the far UV at 110–200 nm have been carried out by Doucet et al. [111].

The temperature dependence becomes significant at wavelengths above 194 nm and below 170 nm, where the cross sections decrease with decreasing temperature. This was observed by Simon et al. [380] at 295–225 K and by Hubrich and Stuhl [165] at 298 and 208 K. Simon et al. [380] parameterized the temperature dependence of the cross sections by the polynomial expansion $\log_{10} \sigma(\lambda, T) = \sum A_n \lambda^n + (T - 273) \times \sum B_n \lambda^n$ and reported smoothed values for T = 210, 230, 250, 270, and 295 K, every 2 nm, and at wavelengths corresponding to the wavenumber intervals generally used in stratospheric photodissociation calculations. The parameters A_n and B_n for the ranges T = 210–300 K and λ = 182–230 nm are as follows:

$A_0 = -1087.9$ $\quad B_0 = 12.493$
$A_1 = 20.004$ $\quad B_1 = -2.3937 \times 10^{-1}$
$A_2 = -1.3920 \times 10^{-1}$ $\quad B_2 = 1.7142 \times 10^{-3}$
$A_3 = 4.2828 \times 10^{-4}$ $\quad B_3 = -5.4393 \times 10^{-6}$
$A_4 = -4.9384 \times 10^{-7}$ $\quad B_4 = 6.4548 \times 10^{-8}$.

Table 4-50. Absorption Cross Sections of $CF_2ClCFCl_2$ at 295–298 K

λ (nm)	10^{20} σ (cm^2)	λ (nm)	10^{20} σ (cm^2)	λ (nm)	10^{20} σ (cm^2)
175	192	204	5.80	228	0.0410
180	155	206	4.00	230	0.0270
184	*123*	208	2.65	232	0.0188
186	104	210	1.80	234	0.0124
188	83.5	212	1.15	236	0.00824
190	64.5	214	0.760	238	0.00546
192	48.8	216	0.505	240	0.00361
194	36.0	218	0.318	242	0.00239
196	26.0	220	0.220	244	0.00159
198	18.3	222	0.145	246	0.00105
200	12.5	224	0.0950	248	0.000696
202	8.60	226	0.0630	250	0.000461

Note: 175–180 nm: Hubrich and Stuhl [165]
184 nm: interpolation: Hubrich and Stuhl (180 nm) and Simon et al. (186 nm)
186–230 nm: Simon et al. [380]
232–250 nm: extrapolation of Simon et al. [380] data.

F34. CF_2ClCF_2Cl (CFC-114) + hν → Products. The absorption cross sections of CF_2ClCF_2Cl have been measured at room temperature and 184–219 nm by Chou et al. [77]; at 208 and 298 K and 160–235 nm by Hubrich and Stuhl [165]; and at 225–295 K and 182–220 nm by Simon et al. [380]. The room temperature values of Simon et al. [380] and Chou et al. [77] agree within 5% except for a hump around 195 nm in the absorption curve reported by Chou et al. [77]. The values of Hubrich and Stuhl [165] are always larger than those of Simon et al. [380], around 190 nm by up to ~40% and between 200 and 220 nm up to ~50% with increasing wavelength. The recommended absorption cross sections, listed in Table 4-51, are the values of Simon et al. [380] at 172–220 nm. For the range 222–235 nm, the absorption curve above 200 nm of Simon et al. [380] has been extrapolated ($\log \sigma = -1.8233 - 0.00913\ \lambda$). The measured values of Hubrich et al. [165] are larger by ~40% in that range than the extrapolated values

Measurements at the Lyman-α line at 121.6 nm have been carried out by Ravishankara et al. [328]; and at 110–190 nm by Doucet et al. [111].

The temperature dependence has been observed at wavelengths above 190 nm, where Simon et al. [380] report decreasing cross sections with decreasing temperature 295–210 K. Hubrich and Stuhl [165] report for the range 160–210 nm and between 298 and 208 K a small decrease of the cross sections (generally <10%, except two data points). Simon et al. [380] parameterized the temperature dependence of the cross sections by the polynomial expansion $\log_{10} \sigma(\lambda, T) = \sum A_n \lambda^n + (T - 273) \times \sum B_n \lambda^n$ and reported smoothed values for T = 210, 230, 250, 270, and 295 K, every 2 nm, and at wavelengths corresponding to the wavenumber intervals generally used in stratospheric photodissociation calculations. The parameters A_n and B_n for the ranges T = 210–300 K,
λ = 172–220 nm are as follows:

$A_0 = -160.50$ $\quad$ $B_0 = -1.5296$
$A_1 = 2.4807$ $\quad$ $B_1 = 3.5248 \times 10^{-2}$
$A_2 = -1.5202 \times 10^{-2}$ $\quad$ $B_2 = -2.9951 \times 10^{-4}$
$A_3 = 3.8412 \times 10^{-5}$ $\quad$ $B_3 = 1.1129 \times 10^{-6}$
$A_4 = -3.4373 \times 10^{-8}$ $\quad$ $B_4 = -1.5259 \times 10^{-9}$

Table 4-51. Absorption Cross Sections of CF_2ClCF_2Cl at 295 K

λ (nm)	10^{20} σ (cm^2)	λ (nm)	10^{20} σ (cm^2)	λ (nm)	10^{20} σ (cm^2)
172	69.0	194	2.56	216	0.0290
174	55.0	196	1.75	218	0.0190
176	43.0	198	1.20	220	0.0122
178	34.0	200	0.800	*222*	*0.00809*
180	26.2	202	0.540	*224*	*0.00531*
182	19.8	204	0.370	*226*	*0.00349*
184	15.0	206	0.245	*228*	*0.00229*
186	11.0	208	0.160	*230*	*0.00151*
188	7.80	210	0.104	*232*	*0.00099*
190	5.35	212	0.0680	*234*	*0.00065*
192	3.70	214	0.0440	*235*	*0.00053*

Note: 172–220 nm: Simon et al. [380]
222–235 nm: extrapolation of Simon et al. [380] data.

F35. CF_3CF_2Cl (CFC-115) + hν → Products. The absorption cross sections of CF_3CF_2Cl have been measured at room temperature and 184–207 nm by Chou et al. [77]; at 208 and 298 K and 160–230 nm by Hubrich and Stuhl [165]; and at 225–295 K and 172–204 nm by Simon et al. [380]. The room temperature data of Simon et al. [380] and Hubrich and Stuhl [165] agree within ~20%, where Hubrich and Stuhl [165] report the larger values over the range 172–204 nm. The data of Chou et al. [77] are larger by up to more than 50% than those of Simon et al. [380]. The preferred absorption cross sections, listed in Table 4-52, are the mean of the values reported by Hubrich and Stuhl [165] and Simon et al. [380] at 172–204 nm. The mean of the values measured by Hubrich and Stuhl [165] and those obtained by extrapolating the absorption curve of Simon et al. [380] (log $\sigma = -6.2191 - 0.0756\,\lambda$) were taken for the range 205–230 nm (the extrapolated values become larger by up to nearly 50% with increasing wavelength than the measured values of Hubrich and Stuhl [165]).

Measurements at the Lyman-α line at 121.6 nm have been carried out by Ravishankara et al. [328]; and at 120–175 nm by Doucet et al. [111].

Temperature effects, if any, could not be detected for this highly fluorinated species. Simon et al. [380] parameterized the absorption cross sections by the polynomial expansion $\log_{10} \sigma(\lambda, T) = \sum A_n \lambda^n + (T - 273) \times \sum B_n \lambda^n$ (with all $B_n = 0$), and reported smoothed values for T = 295 K, every 2 nm, and at wavelengths corresponding to the wavenumber intervals generally used in stratospheric photodissociation calculations. The parameters A_n for the ranges T = 210–300 K and λ = 172–204 nm are

$$A_0 = 5.8281,\ A_1 = 2.900 \times 10^{-1},\ A_2 = 1.325 \times 10^{-3},\ A_3 = -2.6851 \times 10^{-6}.$$

Table 4-52. Absorption Cross Sections of CF_3CF_2Cl at 295–298 K

λ (nm)	10^{20} σ (cm^2)	λ (nm)	10^{20} σ (cm^2)	λ (nm)	10^{20} σ (cm^2)
172	5.50	188	0.403	204	0.0218
174	4.13	190	0.287	*205*	*0.0187*
176	3.08	192	0.203	*210*	*0.00700*
178	2.25	194	0.143	*215*	*0.00273*
180	1.58	196	0.0985	*220*	*0.00107*
182	1.13	198	0.0685	*225*	*0.00046*
184	0.790	200	0.0474	*230*	*0.00018*
186	0.563	202	0.0325		

Note: 172–204 nm: mean of Hubrich and Stuhl [165] and Simon et al. [380]
205–230 nm: mean of Hubrich and Stuhl [165] and extrapolated Simon et al. [380] data.

F36. $CHFCl_2$ (HCFC-21) + hν → Products. The absorption cross sections of $CHFCl_2$ have been measured at room temperature and 208 nm by Gordus and Bernstein [142]; at 174–222 nm by Robbins and Stolarski [339]; at 184–205 nm by and Green and Wayne [146]; and at 213.9 nm by Rebbert et al. [335]; at 208 and 298 K and 158–235 nm by Hubrich et al. [166]; and at 225–295 K and 174–222 nm by Simon et al. [379]. The results of

these groups (except those of Green and Wayne [146] which deviate strongly) are in good agreement, generally within 15%, although the data of Hubrich et al. [166] show humps around 205 and 220 nm, where the agreement is only ~40%. The preferred absorption cross sections, listed in Table 4-53, are the values of Simon et al. [379] at 174–222 nm. For the range 224–236 nm, the absorption curve above 200 nm of Simon et al. 283] has been extrapolated ($\log \sigma = 0.9806 - 0.1014\ \lambda$). The measured values of Hubrich et al. [166] deviate from the extrapolated values by up to ~–20% and +50%.

Measurements in the far UV at 60–120 nm have been reported by Gilbert et al. [132], measurements at 120–200 nm by Doucet et al. [110], and a measurement at 147 nm by Rebbert et al. [335].

The temperature dependence becomes significant at wavelengths above 190 nm, where the cross sections decrease with decreasing temperature between 296 and 210 K. Simon et al. [379] parameterized the temperature dependence of the cross sections by the polynomial expansion $\log_{10} \sigma(\lambda, T) = \sum A_n \lambda^n + (T - 273) \times \sum B_n \lambda^n$ and reported smoothed values for T = 210, 230, 250, 270, and 295 K, every 2 nm, and at wavelengths corresponding to the wavenumber intervals generally used in stratospheric photodissociation calculations. The parameters A_n and B_n for the ranges T = 210–300 K and λ = 174–222 nm are as follows:

$A_0 = -514.56$ $\quad$ $B_0 = -3.0577$
$A_1 = 8.7940$ $\quad$ $B_1 = 6.6539 \times 10^{-2}$
$A_2 = -5.6840 \times 10^{-2}$ $\quad$ $B_2 = -5.3964 \times 10^{-4}$
$A_3 = 1.5894 \times 10^{-4}$ $\quad$ $B_3 = 1.9322 \times 10^{-6}$
$A_4 = 1.6345 \times 10^{-7}$

Table 4-53. Absorption Cross Sections of $CHFCl_2$ at 295–298 K

λ (nm)	$10^{20}\ \sigma$ (cm^2)	λ (nm)	$10^{20}\ \sigma$ (cm^2)	λ (nm)	$10^{20}\ \sigma$ (cm^2)
174	166.0	198	8.10	222	0.0319
176	164.5	200	5.24	*224*	*0.0195*
178	155.0	202	3.35	*225*	*0.0154*
180	138.0	204	2.12	*226*	*0.0122*
182	116.0	206	1.34	*228*	*0.00766*
184	92.4	208	0.836	*230*	*0.00480*
186	71.5	210	0.522	*232*	*0.00301*
188	53.2	212	0.325	*234*	*0.00189*
190	38.4	214	0.203	*235*	*0.00150*
192	26.9	216	0.127	*236*	*0.00119*
194	18.4	218	0.0797		
196	12.3	220	0.0503		

Note: 174–222 nm: Simon et al. [379]
224–236 nm: extrapolation of Simon et al. [379] data.

F37. CHF_2Cl (HCFC-22) + hν → Products. The absorption cross sections of CHF_2Cl have been measured at room temperature and 174–202 nm by Robbins and Stolarski [339] and at 181–194 nm by Green and Wayne [146]; at 208 K and 298 K and 158–220 nm by Hubrich et al. [166], and at 225–295 K and 174–204 nm by Simon et al. [379]. The results of Robbins and Stolarski [339], Hubrich et al. [166], and Simon et al. [379] are in good agreement generally within 15–20%, however those of Green and Wayne [146] deviate strongly. The preferred absorption cross sections, listed in Table 4-54, are the values of Hubrich et al. [166] at 170–172 nm and the values of Simon et al. [379] at 174–204 nm. For the range 206–220 nm, the absorption curve above 190 nm of Simon et al. [379] has been extrapolated ($\log \sigma = -4.1001 - 0.0870\ \lambda$). The measured values of Hubrich et al. [166] deviate from the extrapolated values by up to 20%.

Measurements in the far UV at 60–160 nm have been reported by Gilbert et al. [132], and measurements at 120–200 nm by Doucet et al. [110].

A weak temperature dependence has been observed above 190 nm, where the cross sections decrease with decreasing temperature between 296 and 210 K. Simon et al. [379] parameterized the cross sections and the temperature dependence by the polynomial expansion $\log_{10} \sigma(\lambda, T) = \sum A_n \lambda^n + (T - 273) \times \sum B_n \lambda^n$ and reported

smoothed values for T = 210, 230, 250, 270, and 295 K, every 2 nm, and at wavelengths corresponding to the wavenumber intervals generally used in stratospheric photodissociation calculations. The parameters A_n and B_n for the ranges T = 210–300 K and λ = 174–204 nm are as follows:

$A_0 = -106.029$ $\quad B_0 = -1.3399 \times 10^{-1}$
$A_1 = 1.5038$ $\quad B_1 = 2.7405 \times 10^{-3}$
$A_2 = -8.2476 \times 10^{-3}$ $\quad B_2 = -1.8028 \times 10^{-5}$
$A_3 = 1.4206 \times 10^{-5}$ $\quad B_3 = 3.8504 \times 10^{-8}$

Table 4-54. Absorption Cross Sections of CHF_2Cl at 295–298 K

λ (nm)	10^{20} σ (cm^2)	λ (nm)	10^{20} σ (cm^2)	λ (nm)	10^{20} σ (cm^2)
170	12.9	188	0.372	*206*	*0.00842*
172	9.79	190	0.245	*208*	*0.00636*
174	5.72	192	0.156	*210*	*0.00426*
176	4.04	194	0.103	*212*	*0.00285*
178	2.76	196	0.072	*214*	*0.00191*
180	1.91	198	0.048	*216*	*0.00128*
182	1.28	200	0.032	*218*	*0.00086*
184	0.842	202	0.0220	*220*	*0.00057*
186	0.576	204	0.0142		

Note: 170–172 nm: Hubrich et al. [166]
174–204 nm: Simon et al. [379]
206–220 nm: extrapolation of Simon et al. [379] data.

F38. CH_2FCl (HCFC-31) + hν → Products. The absorption cross sections of CH_2FCl have been measured at 208 and 298 K and 160–230 nm by Hubrich and Stuhl [165]. The room temperature data at 160–230 nm are listed in Table 4–55.

Measurements in the far UV at 60–120 nm have been reported by Gilbert et al. [132], and measurements at 120–200 nm by Doucet et al. [110].

Table 4–55. Absorption Cross Sections of CH_2FCl at 298 K

λ (nm)	10^{20} σ (cm^2)	λ (nm)	10^{20} σ (cm^2)	λ (nm)	10^{20} σ (cm^2)
160	47.9	185	4.20	210	0.0188
165	55.9	190	1.95	215	0.00560
170	43.0	195	0.544	220	0.00215
175	23.3	200	0.209	225	0.00049
180	12.5	205	0.069	230	0.00026

Note: 160–230 nm: Hubrich and Stuhl [165].

F39. CF_3CHCl_2 (HCFC-123) + hν → Products. The absorption cross sections of CF_3CHCl_2 have been measured at room temperature and 185–204 nm by Green and Wayne [146]; at 225–295 K and 170–250 nm by Gillotay and Simon [136]; at 203–295 K and 190–230 nm by Orlando et al. [305]; and at 223–333 K and 160–230 nm by Nayak et al. [286]. The agreement between the results of the latter three groups is within 25% in the region below 220 nm. The results of Green and Wayne [146] are very different below 200 nm. The preferred absorption cross sections at 295 K, listed in Table 4-56, are the mean of the values reported by Gillotay and Simon [136] and Nayak et al. [286] at 170–188 nm and the mean of the values reported by Gillotay and Simon [136], Orlando et al. [305], and Nayak et al. [286] at 190–230 nm. For the range 232–250 nm, the absorption curve above 210 nm of Orlando et al. [305] has been extrapolated ($\log \sigma = -3.1097 - 0.0794\,\lambda$).

The studies of the temperature dependence show a decrease of the absorption cross sections with decreasing temperature at wavelengths above 178–180 nm and below 170 nm. Between 170–180 nm, the reverse behavior was observed by Gillotay and Simon [136] and Nayak et al. [286]. An irregular temperature dependence was reported by Orlando et al. [305] for the range 210–230 nm, where the absorption curves show wiggles.

Various parameterized fits, i.e., polynomial expansions of the logarithm of the absorption cross section, have been proposed for the temperature dependence. Gillotay and Simon [136] parameterized the cross sections and the temperature dependence by the polynomial expansion $\log_{10} \sigma(\lambda, T) = \sum A_n \lambda^n + (T - 273) \times \sum B_n \lambda^n$ and reported smoothed values for T = 210, 230, 250, 270, and 295 K, every 2 nm, and at wavelengths corresponding to the wavenumber intervals generally used in stratospheric photodissociation calculations. The parameters A_n and B_n for the ranges T = 210–300 K and λ = 182–250 nm are as follows:

$A_0 = -513.996354$ $\quad B_0 = 1.757133$

$A_1 = 9.089141$ $\quad B_1 = -3.499205 \times 10^{-2}$

$A_2 = -6.136794 \times 10^{-2}$ $\quad B_2 = 2.593563 \times 10^{-4}$

$A_3 = 1.814826 \times 10^{-4}$ $\quad B_3 = -8.489357 \times 10^{-7}$

$A_4 = -1.999514 \times 10^{-7}$ $\quad B_4 = 1.037756 \times 10^{-9}$.

Nayak et al. [286] report sixth-order polynomial coefficients for the functions $\log_{10} (\sigma_T) = \sum C_n (\lambda - 170)^n$ at T = 223, 233, 253, 273, 295, 313, and 333 K and for the range 160–230 nm. The parameters C_n are as follows:

	223 K	273 K	295 K	333 K
C_0	–17.6732	–17.6773	–17.6792	–17.6722
C_1	1.70233×10^{-2}	1.3636×10^{-2}	1.19392×10^{-2}	9.07941×10^{-3}
C_2	-7.39366×10^{-4}	-4.98553×10^{-4}	-3.71661×10^{-4}	-1.29566×10^{-4}
C_3	-1.83761×10^{-4}	-1.70566×10^{-4}	-1.61218×10^{-4}	-1.56667×10^{-4}
C_4	7.80778×10^{-6}	6.73373×10^{-6}	6.03101×10^{-6}	5.56409×10^{-6}
C_5	-1.29836×10^{-7}	-1.02726×10^{-7}	-8.76762×10^{-8}	-7.77379×10^{-8}
C_6	8.05415×10^{-10}	5.66688×10^{-10}	4.61745×10^{-10}	3.93859×10^{-10}

A double expansion in terms of twelve parameters, $\ln \sigma(\lambda, T) = \sum (\sum a_{ij} (T-245.4)^{j-1}) (\lambda - 206.214)^{i-1}$, i = 1–4, j = 1–3, T = 203–295 K, λ = 190–230 nm, was used by Orlando et al. [305]:

$a_{11} = -4.500 \times 10^{-1}$ $\quad a_{12} = 3.529 \times 10^{-3}$ $\quad a_{13} = -4.181 \times 10^{-8}$

$a_{21} = -1.985 \times 10^{-1}$ $\quad a_{22} = 6.826 \times 10^{-5}$ $\quad a_{23} = 1.555 \times 10^{-6}$

$a_{31} = -2.802 \times 10^{-4}$ $\quad a_{32} = -1.018 \times 10^{-5}$ $\quad a_{33} = 4.037 \times 10^{-8}$

$a_{41} = 6.312 \times 10^{-5}$ $\quad a_{42} = -3.055 \times 10^{-7}$ $\quad a_{43} = -2.473 \times 10^{-9}$

Table 4-56. Absorption Cross Sections of CF_3CHCl_2 at 295 K

λ (nm)	10^{20} σ (cm^2)	λ (nm)	10^{20} σ (cm^2)	λ (nm)	10^{20} σ (cm^2)
170	192	198	17.1	226	0.0880
172	207	200	11.9	228	0.0599
174	214	202	8.24	230	0.0451
176	213	204	5.70	*232*	*0.0295*
178	202	206	3.89	*234*	*0.0205*
180	184	208	2.67	*236*	*0.0142*
182	161	210	1.82	*238*	*0.0098*
184	135	212	1.23	*240*	*0.0068*
186	109	214	0.838	*242*	*0.0047*
188	85.5	216	0.573	*244*	*0.0033*
190	62.2	218	0.384	*246*	*0.0023*
192	46.4	220	0.266	*248*	*0.0016*
194	33.9	222	0.180	*250*	*0.0011*
196	24.2	224	0.124		

Note: 170–188 nm: mean of the values of Gillotay and Simon [136] and Nayak et al. [286]
190–230 nm: mean of the values of Gillotay and Simon [136], Orlando et al. [305], and Nayak et al. [286]
232–250 nm: extrapolation of Orlando et al. [305] data.

F40. CF_3CHFCl (HCFC-124) + hν → Products. The absorption cross sections of CF_3CHFCl have been measured at 203–295 K and 190–230 nm by Orlando et al. [305]; and at 210–295 K and 170–230 nm by Gillotay and Simon [137]. The agreement is better than 10 % between 190 and 220 nm, whereas above 220 nm the values of Orlando et al. [305] become increasingly larger by up to 133% than those of Gillotay and Simon [137]. The preferred room temperature values, listed in Table 4-57, are the values of Gillotay and Simon [137] at 170–188 nm and 222–230 nm and the mean of the values reported by Gillotay and Simon [137] and Orlando et al. [305] at 190–220 nm.

The temperature dependence of the cross sections has been measured by both groups and a decrease of the absorption cross sections with decreasing temperature was observed at 170–230 nm by Gillotay and Simon [137] and at 190–215 nm by Orlando et al. [305]. An irregular temperature behavior was reported by Orlando et al. [305] for the range 215–230 nm, where the absorption curves show wiggles. Parameterized fits, i.e., polynomial expansions of the logarithm of the absorption cross section, have been derived. Gillotay and Simon [137] parameterized the cross sections and the temperature dependence by the polynomial expansion $\log_{10} \sigma(\lambda, T) = \sum A_n \lambda^n + (T - 273) \times \sum B_n \lambda^n$ and reported smoothed values for T = 210, 230, 250, 270, and 295 K, every 2 nm, and at wavelengths corresponding to the wavenumber intervals generally used in stratospheric photodissociation calculations. The parameters A_n and B_n for the ranges T = 210–300 K and λ = 170–230 nm are as follows:

$$A_0 = -101.230250 \qquad B_0 = -5.795712 \times 10^{-2}$$
$$A_1 = 1.333519 \qquad B_1 = 1.053901 \times 10^{-3}$$
$$A_2 = -6.888672 \times 10^{-3} \qquad B_2 = -6.530379 \times 10^{-6}$$
$$A_3 = 1.114172 \times 10^{-5} \qquad B_3 = 1.382056 \times 10^{-8}$$

A double expansion in terms of twelve parameters, $\ln \sigma(\lambda, T) = \sum (\sum a_{ij} (T-251.7)^{j-1}) (\lambda - 206.214)^{i-1}$, i = 1–4, j = 1–3, T = 203–295 K, λ = 190–230 nm, was used by Orlando et al. [305]:

$$a_{11} = -4.967 \times 10^{-1} \qquad a_{12} = 6.562 \times 10^{-3} \qquad a_{13} = 1.735 \times 10^{-5}$$
$$a_{21} = -2.025 \times 10^{-1} \qquad a_{22} = 2.788 \times 10^{-4} \qquad a_{23} = -3.974 \times 10^{-6}$$
$$a_{31} = 6.839 \times 10^{-4} \qquad a_{32} = 5.523 \times 10^{-6} \qquad a_{33} = -3.092 \times 10^{-7}$$
$$a_{41} = 1.275 \times 10^{-4} \qquad a_{42} = -2.959 \times 10^{-7} \qquad a_{43} = -1.182 \times 10^{-8}$$

Table 4-57. Absorption Cross Sections of CF_3CHFCl at 295 K

λ (nm)	10^{20} σ (cm^2)	λ (nm)	10^{20} σ (cm^2)	λ (nm)	10^{20} σ (cm^2)
170	13.6	192	0.548	214	0.00859
172	11.1	194	0.387	216	0.00610
174	8.85	196	0.267	218	0.00431
176	6.93	198	0.185	220	0.00312
178	5.33	200	0.128	222	0.00214
180	4.03	202	0.0868	224	0.00153
182	3.00	204	0.0594	226	0.00111
184	2.20	206	0.0401	228	0.00082
186	1.60	208	0.0269	230	0.00061
188	1.14	210	0.0186		
190	0.772	212	0.0126		

Note: 170–188 nm, Gillotay and Simon [137],
190–220 nm, mean of the values of Gillotay and Simon [137] and Orlando et al. [305],
222–230 nm, Gillotay and Simon [137].

F41. CF_3CH_2Cl (HCFC-133) + hν → Products. The absorption cross sections of CF_3CH_2Cl have been measured at room temperature and 147 nm ($\sigma = 1.35 \times 10^{-17}$ cm^2) by Ichimura et al. [174], and 186–203 nm by Green and Wayne [146], and at 208 and 298 K and 160–245 nm by Hubrich and Stuhl [165]. There is no good agreement between the results at wavelengths above 180 nm. Table 4-58 gives the recommended room temperature data of Hubrich and Stuhl [165].

Table 4-58. Absorption Cross Sections of CF_3CH_2Cl at 298 K

λ (nm)	10^{20} σ (cm^2)	λ (nm)	10^{20} σ (cm^2)	λ (nm)	10^{20} σ (cm^2)
160	59.4	190	6.20	220	0.0887
165	64.6	195	2.95	225	0.0226
170	56.4	200	1.14	230	0.0147
175	37.3	205	0.598	235	0.00404
180	22.8	210	0.328	240	0.00181
185	11.6	215	0.169	245	0.00054

Note: 160–245 nm, Hubrich and Stuhl [165].

F42. CH_3CFCl_2 (HCFC-141b) + hν → Products. The absorption cross sections of CH_3CFCl_2 have been measured at 210–295 K and 170–240 nm by Gillotay and Simon [136]; at 203–295 K and 190–230 nm by Orlando et al. [305] (data of Orlando et al. reported by Gillotay and Simon [138]); at 203–295 K and 190–230 nm by Talukdar et al. [393]; and at room temperature and 190–240 nm by Fahr et al. [113], who investigated the spectrum both for the gas and liquid phases and used a wavelength-shift procedure to convert the liquid-phase data into gas-phase data. The agreement between the values reported by Gillotay and Simon [136] and Fahr et al. [113] for the 190–240-nm region is very good (1–10% up to 236 nm); the results of Orlando et al. [305] are also in good agreement with these, but only in the region 190–210 nm. The agreement of the results of Talukdar et al. [393] is not as good, their absorption cross sections become smaller below 210 nm by up to ~20% and become larger above 210 nm by up to about 70% than the above mentioned data. The preferred absorption cross sections, listed in Table 4-59, are the values of Gillotay and Simon [136] at 170–188 nm and the mean of the values reported by Gillotay and Simon [136] and Fahr et al. [113] at 190–240 nm.

A decrease of the absorption cross sections with decreasing temperature at wavelengths above 188 nm and below 172 nm and the reverse behavior between 172 and 188 nm was observed by Gillotay and Simon [136]. They parameterized the cross sections and the temperature dependence of the absorption cross sections using the polynomial expansion $\log_{10} \sigma(\lambda, T) = \sum A_n \lambda^n + (T - 273) \times \sum B_n \lambda^n$. They derived the parameters

$A_0 = -682.913042$ $B_0 = 4.04747$

$A_1 = 12.122290$ $B_1 = -8.05899 \times 10^{-2}$

$A_2 = -8.187699 \times 10^{-2}$ $B_2 = 5.946552 \times 10^{-4}$

$A_3 = 2.437244 \times 10^{-4}$ $B_3 = -1.945048 \times 10^{-6}$

$A_4 = -2.719103 \times 10^{-7}$ $B_4 = 2.380143 \times 10^{-9}$

for the ranges 210–300 K and 172–240 nm and list smoothed values for T = 210, 230, 250, 270, and 295 K at 2-nm intervals and at wavelengths corresponding to the wavenumber intervals generally used in stratospheric photodissociation calculations. A similar temperature behavior was observed by Orlando et al. [305] only between 190 and 210 nm, and by Talukdar et al. [393] only above 197 nm.

Table 4-59. Absorption Cross Sections of CH_3CFCl_2 at 295–298 K

λ (nm)	10^{20} σ (cm^2)	λ (nm)	10^{20} σ (cm^2)	λ (nm)	10^{20} σ (cm^2)
170	143.1	194	47.2	218	0.382
172	145.1	196	34.1	220	0.248
174	154.2	198	24.0	222	0.161
176	162.9	200	16.6	224	0.105
178	172.6	202	11.3	226	0.0680
180	172.3	204	7.56	228	0.0444
182	162.9	206	5.02	230	0.0290
184	146.4	208	3.30	232	0.0189
186	125.7	210	2.16	234	0.0123
188	103.6	212	1.40	236	0.00801
190	83.0	214	0.909	238	0.00518
192	63.6	216	0.589	240	0.00334

Note: 170–188 nm, Gillotay and Simon [136],
190–240 nm, mean of Gillotay and Simon [136] and Fahr et al. [113].

F43. CH_3CF_2Cl (HCFC-142b) + hν → Products. The absorption cross sections of CH_3CF_2Cl have been measured at room temperature and 120–180 nm by Doucet et al. [111]; at 184–210 nm by Green and Wayne [146]; at 298 and 208 K and 160–230 nm by Hubrich and Stuhl [165]; at 210–295 K and 170–230 nm by Gillotay and Simon [136]; at 203–295 K and 190–230 nm by Orlando et al. [305]; and at 223–333 K and 160–210 nm by Nayak et al. [286]. At wavelengths below 200 nm, the values of Hubrich and Stuhl [165] and Nayak et al. [286] are within 15%, those of Gillotay and Simon [136] and Orlando et al. [305] are lower than the latter by up to 30%. At wavelengths between 200 and 215 nm, the values of Gillotay and Simon [136], Orlando et al. [305], and Nayak et al [286] agree within 15%. Above 215 nm, the absorption curve reported by Orlando et [305] shows wiggles with deviations by up to 100% from the data of Gillotay and Simon [136]. Also the values reported for the range 205–230 nm by Hubrich and Stuhl [165] become increasingly larger by up to 600% than those of Gillotay and Simon [136] .The results of Green and Wayne [146] are very different from all other data. The preferred room temperature absorption cross sections, listed in Table 4–60, are the mean of the values reported by Hubrich and Stuhl [165], Gillotay and Simon [136], and Nayak et al. [286] at 175–185 nm, the mean of the values reported by Gillotay and Simon [136], Orlando et al. [305], and Nayak et al. [286] at 190–210 nm, and the values reported by Gillotay and Simon [136] at 212–230 nm.

A decrease of the absorption cross sections with decreasing temperature was observed by Gillotay and Simon [136] and Nayak et al. [286] over the wavelength range 160–230 nm and by Orlando et al. [305] between 190 and 200 nm. An irregular temperature behavior was reported by Orlando et al. [305] for the range 215–230 nm, where the absorption curves for the various temperatures show several crossings. Various parameterized fits for the temperature dependence of the absorption cross sections have been offered. Gillotay and Simon [136] used the polynomial expansion $\log_{10} \sigma(\lambda, T) = \sum A_n \lambda^n + (T - 273) \times \sum B_n \lambda^n$ and reported smoothed values for T = 210, 230, 250, 270, and 295 K, every 2 nm, and at wavelengths corresponding to the wavenumber intervals generally used in stratospheric photodissociation calculations. Their parameters A_n and B_n for the ranges T = 210–300 K and λ = 172–230 nm are as follows:

$A_0 = -328.092008$ $\quad B_0 = 4.289533 \times 10^{-1}$
$A_1 = 6.342799$ $\quad B_1 = -9.042817 \times 10^{-3}$
$A_2 = -4.810362 \times 10^{-2}$ $\quad B_2 = 7.018009 \times 10^{-5}$
$A_3 = 1.611991 \times 10^{-4}$ $\quad B_3 = -2.389065 \times 10^{-7}$
$A_4 = -2.042613 \times 10^{-7}$ $\quad B_4 = 3.039799 \times 10^{-10}$

Nayak et al. [286] report fourth-order polynomial coefficients $C_n(T)$ for the functions $\log_{10} (\sigma_T) = \sum C_n (\lambda - 160)^n$ at T = 223, 233, 253, 273, 295, 313, and 333 K and for the range 160–210 nm. The parameters C_n are as follows

	223 K	273 K	295 K	333 K
C_0	–18.2361	–18.2441	–18.2406	–18.1777
C_1	-1.26669×10^{-2}	-7.37889×10^{-3}	-6.48269×10^{-3}	-2.39647×10^{-2}
C_2	-2.32945×10^{-3}	-2.66537×10^{-3}	-2.80923×10^{-3}	-7.23910×10^{-4}
C_3	2.81933×10^{-5}	4.19193×10^{-5}	5.01979×10^{-5}	-1.08049×10^{-5}
C_4	-1.37963×10^{-7}	-2.88472×10^{-7}	-3.96860×10^{-7}	1.37618×10^{-7}

A double expansion in terms of twelve parameters, $\ln \sigma(\lambda, T) = \sum (\sum a_{ij} (T–245.4)^{j-1}) (\lambda – 206.214)^{i-1}$, i = 1–4, j = 1–3, T = 203–295 K, λ = 190–230 nm, was used by Orlando et al. [305]:

$a_{11} = -4.973 \times 10^{-1}$ $a_{12} = 9.077 \times 10^{-3}$ $a_{13} = -4.651 \times 10^{-5}$
$a_{21} = -2.175 \times 10^{-1}$ $a_{22} = 4.712 \times 10^{-4}$ $a_{23} = -1.005 \times 10^{-5}$
$a_{31} = 4.133 \times 10^{-4}$ $a_{32} = -6.432 \times 10^{-5}$ $a_{33} = 1.141 \times 10^{-6}$
$a_{41} = 7.145 \times 10^{-5}$ $a_{42} = -5.396 \times 10^{-6}$ $a_{43} = 1.187 \times 10^{-7}$

Quantum yields for Cl ($^2P_{3/2}$) and Cl*($^2P_{1/2}$) atom formation in the photolysis of CH_3CF_2Cl at 193.3 nm have been measured by Brownsword et al. [49] and quantum yields for H atom formation in the photolysis at 121.6 and 193.3 nm by Brownsword et al. [48]: Φ(Cl + Cl*) = 0.90 ± 0.17 with Φ(Cl) = 0.65 ± 0.12 and Φ(Cl*) = 0.25 ± 0.05 at 193.3 nm, and Φ(H) = 0.53 ± 0.12 and 0.06 ± 0.02 at 121.6 and 193.3 nm, respectively.

Table 4–60. Absorption Cross Sections of CH_3CF_2Cl at 295–298 K

λ (nm)	10^{20} σ (cm^2)	λ (nm)	10^{20} σ (cm^2)	λ (nm)	10^{20} σ (cm^2)
170	27.1	200	0.145	218	0.00243
175	14.0	202	0.0949	220	0.00145
180	6.38	204	0.0622	222	0.000845
185	2.73	206	0.0399	224	0.000484
190	1.02	208	0.0256	226	0.000271
192	0.706	210	0.0161	228	0.000148
194	0.482	212	0.0105	230	0.0000783
196	0.324	214	0.00652		
198	0.218	216	0.00401		

Note:
170–185 nm: mean of Gillotay and Simon [136], Hubrich and Stuhl [165], and Nayak et al. [286]
190–210 nm: mean of Gillotay and Simon [136], Orlando et al. [305], and Nayak et al. [286]
212–230 nm: Gillotay and Simon [136].

F44. $CF_3CF_2CHCl_2$ (HCFC-225ca) + hν → Products

F45. CF_2ClCF_2CHFCl (HCFC-225cb) + hν → Products. The absorption spectra of these compounds in the gaseous and liquid phases at 298 K have been measured by Braun et al. [40]. Table 4-61 lists the absorption cross sections for the gas phase taken from this work. The originally listed (0.5-nm intervals) absorption coefficients ε in (atm, 298 K)$^{-1}$ cm^{-1} ($\sigma = 4.06 \times 10^{-20}\ \varepsilon$) for both phases have been fitted with third-order polynomial expansions $\log_{10} \varepsilon = \sum a_n(\lambda – 160)^n$ with

$a_0 = 1.425$, $a_1 = 4.542 \times 10^{-2}$, $a_2 = -2.036 \times 10^{-3}$, $a_3 = 1.042 \times 10^{-5}$ for HCFC-225ca at 170–270 nm,

$a_0 = 1.677$, $a_1 = -2.175 \times 10^{-2}$, $a_2 = -1.484 \times 10^{-3}$, $a_3 = 1.147 \times 10^{-5}$ for HCFC-225cb at 165–250 nm.

Table 4-61. Absorption Cross Sections of $CF_3CF_2CHCl_2$ and CF_2ClCF_2CFCl at 298 K

λ (nm)	10^{20} σ (cm^2) $CF_3CF_2CHCl_2$ (HCFC-225ca)	CF_2ClCF_2CFCl (HCFC-225cb)	λ (nm)	10^{20} σ (cm^2) $CF_3CF_2CHCl_2$ (HCFC-225ca)	CF_2ClCF_2CFCl (HCFC-225cb)
160	268.7	187.9	202	11.58	0.479
162	236.8	173.3	204	8.185	0.369
164	207.6	154.8	206	5.802	0.291
166	189.0	135.1	208	4.084	0.254
168	181.4	113.2	210	2.903	0.250
170	182.7	91.35	212	2.042	
172	182.8	70.68	214	1.429	
174	189.0	54.73	216	1.05	
176	190.9	40.68	218	0.727	
178	187.9	30.04	220	0.463	
180	177.5	21.11	222	0.308	
182	161.1	14.90	224	0.209	
184	140.3	10.47	226	0.145	
186	118.3	7.308	228	0.0987	
188	96.51	5.075	230	0.0653	
190	74.30	3.492	232	0.0434	
192	57.08	2.412	234	0.0299	
194	42.83	1.661	236	0.0193	
196	31.75	1.165	238	0.0134	
198	23.22	0.873	239	0.0119	
200	16.24	0.633			

Note: HCFC-225ca, 160–239 nm, Braun et al. [40],

HCFC-225cb, 160–210 nm, Braun et al. [40].

G1. $BrO + h\nu \rightarrow Br + O$. The BrO radical has a banded spectrum in the 290–380 nm range. The strongest absorption feature is around 338 nm. The measured cross sections are both temperature- and resolution-dependent. As an example, the spectrum measured by Wahner et al. [423] is shown in Figure 4-4. The bands are due to a vibrational progression in the $A \leftarrow X$ system, and the location of the bands, along with the assignments and cross sections measured using 0.4 nm resolution, are shown in Table 4-62. BrO is expected to dissociate upon light absorption. As a guide, the cross sections averaged over 5 nm wavelength intervals are taken from the work of Cox et al. [92], and are listed in Table 4-63. These authors estimate a BrO lifetime against atmospheric photodissociation of ~20 seconds at the earth's surface, for a solar zenith angle of 30°.

The earlier BrO cross section measurements were carried out mostly around 338 nm, and these have been reviewed by CODATA ([81,82]).

Table 4-62. Absorption Cross Sections at the Peak of Various Bands in the A ← X Spectrum of BrO

ν', ν"	λ (nm)	10^{20} σ(cm^2)	
		298 K	223 K
13,0	313.5	712	938
12,0	317.0	1010	1360
11,0	320.8	1180	1570
10,0	325.0	1130	1430
9,0	329.1	1130	1390
8,0	333.5	1210	1470
7,0	338.3	1550	1950
6,0	343.7	935	1110
5,0	348.8	703	896
4,0	354.7	722	1050
3,0	360.4	264	344
2,0	367.7	145	154
1,0	374.5	90	96

Spectral resolution is 0.4 nm, fwhm.

Table 4-63. Absorption Cross Sections of BrO

λ (nm)	10^{20} σ(cm^2) average
300–305	200
305–310	259
310–315	454
315–320	391
320–325	600
325–330	753
330–335	628
335–340	589
340–345	515
345–350	399
350–355	228
355–360	172
360–365	161
365–370	92
370–375	51

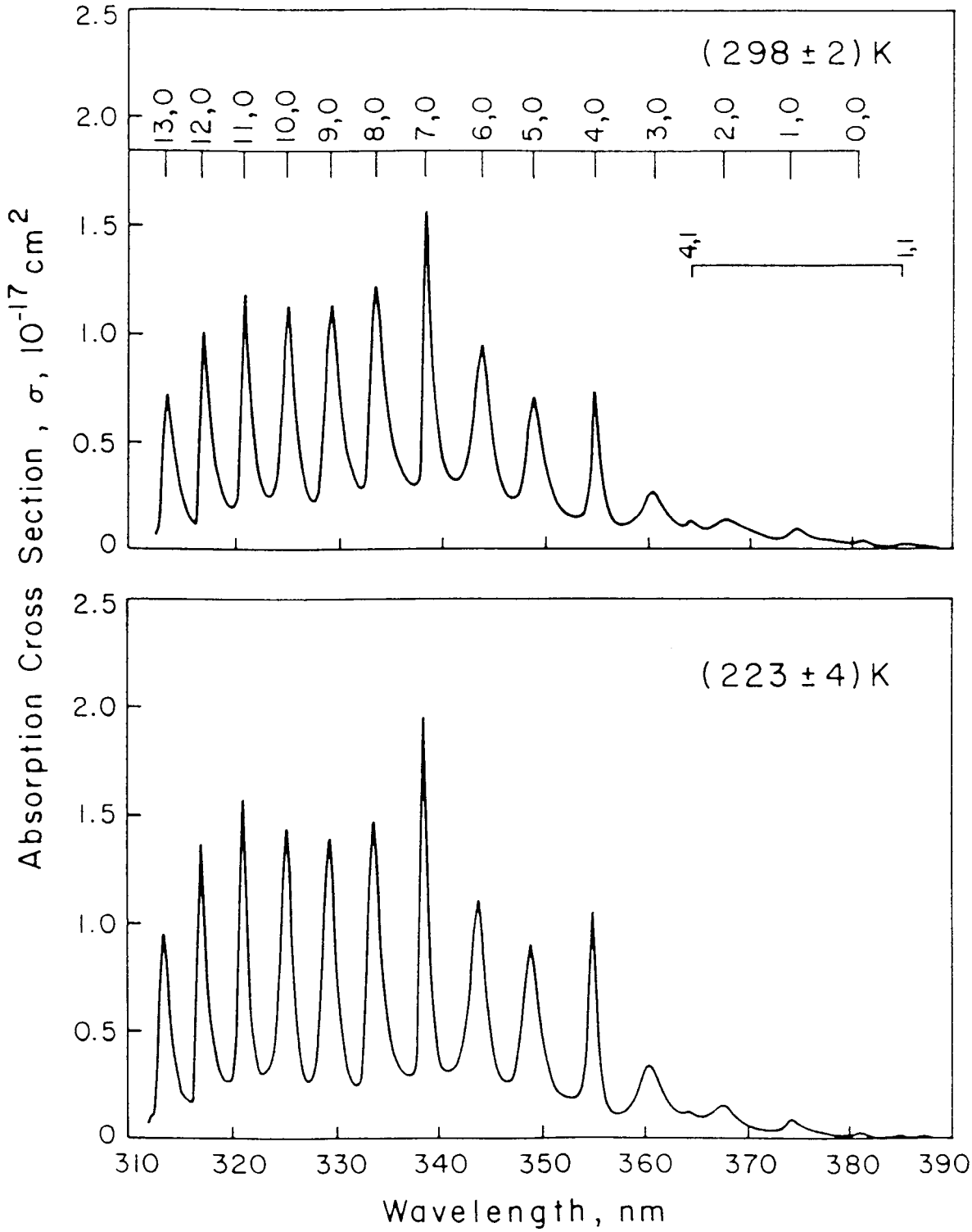

Figure 4-4. Absorption Spectrum of BrO

G2. HOBr + hν → Products. The absorption spectrum of HOBr has been measured by Orlando and Burkholder [304], Deters et al. [108], Benter et al. [31], Rattigan et al. [324], and Ingham et al. [176]. The spectra cluster has been measured in two groups. Orlando and Burkholder [304], Deters et al. [108], and Benter et al. [31] observe between 240 and 400 nm two absorption bands with maxima near 284 and 351 nm; the spectra agree reasonably well in their shape, but show a sharp decrease in cross section above 400 nm. In contrast, the cross sections reported by Rattigan et al. [324] and Ingham et al. [176] are roughly 50 % larger between 300 and 400 nm.

In addition, the spectrum obtained by Rattigan et al. shows a pronounced tail extending to 520 nm, whereas Ingham et al. observe unambiguously a third weaker absorption band ranging to 550 nm with a maximum at 457 nm. These last two studies confirm the observations of Barnes et al. [22], who showed that laser photolysis of HOBr between 440–600 nm gives rise to OH fragments. The presence of a weak band beyond 400 nm is attributable to the presence of a forbidden transition from the ground electronic to a triplet state predicted by the ab initio calculations of Francisco et al. [122]. The differences in the spectral shapes are probably attributable to impurities such as Br_2O and Br_2, and/or the use of different Br_2O cross sections. However, the presence of impurities alone cannot explain the large difference in cross sections at the peak of the absorption bands.

The recommended absorption cross sections are listed in , in the range from 250 to 550 nm; below 250 nm the data are uncertain and no recommendation is given. The cross section values in the table are based on the latest study by Ingham et al. [176]. These authors generated HOBr in situ by laser photolytic production of OH in the presence of Br_2, and determined the HOBr spectrum using a gated diode camera shortly after the pulse, circumventing the problem associated with the presence of the strong absorbing impurity Br_2O, which was encountered in previous studies. The calibration of the absorption cross sections was made relative to the established cross sections of Br_2.

The data presented in Table 4-64 are computed with the following expression taken from Ingham et al. [176], which is based on a combination of three Gaussian fits, one for each absorption band:

$$\sigma(\lambda) = 24.77\exp\left\{-109.80\left[\ln\left(\frac{284.01}{\lambda}\right)\right]^2\right\} + 12.22\exp\left\{-93.63\left[\ln\left(\frac{350.57}{\lambda}\right)\right]^2\right\} + 2.283\exp\left\{-242.40\left[\ln\left(\frac{457.38}{\lambda}\right)\right]^2\right\}$$

$\sigma(\lambda)$: 10^{-20} cm^2 molecule^{-1}; $250 < \lambda < 550$ nm.

Benter et al. [31] measured quantum yields for HOBr photolysis at 261 and 363 nm (near the peaks of the second absorption bands). The observed quantum yield for Br formation at 363 nm was greater than 0.95, and a unity quantum yield into the product channel OH + Br is recommended. The other channel O + HBr was not observed. The laser photofragment study of Barnes et al. [22] claimed that OH was the major photolysis product at wavelengths beyond 400 nm. Lock et al. [222] found that at 490 and 510 nm OH and Br fragments are in their respective vibrational and spin-orbit ground states. The assumption of unit quantum yield of OH formation should be confirmed experimentally.

Table 4-64. Absorption Cross Sections of HOBr

λ (nm)	10^{20} σ (cm^2)	λ (nm)	10^{20} σ (cm^2)	λ (nm)	10^{20} σ (cm^2)
250	4.15	355	12.1	460	2.28
255	6.19	360	11.5	465	2.14
260	10.5	365	10.5	470	1.91
265	14.6	370	9.32	475	1.62
270	18.7	375	7.99	480	1.30
275	22.1	380	6.65	485	0.993
280	24.3	385	5.38	490	0.723
285	25.0	390	4.22	495	0.502
290	24.0	395	3.23	500	0.333
295	21.9	400	2.43	505	0.212
300	19.1	405	1.80	510	0.129
305	16.2	410	1.36	515	0.076
310	13.6	415	1.08	520	0.042
315	11.8	420	0.967	525	0.023
320	10.8	425	0.998	530	0.012
325	10.5	430	1.15	535	0.0059
330	10.8	435	1.40	540	0.0029
335	11.3	440	1.68	545	0.0013
340	11.9	445	1.96	550	0.0006
345	12.3	450	2.18		
350	12.4	455	2.29		

G3. $BrONO_2 + h\nu \rightarrow$ Products. The bromine nitrate cross sections have been measured at room temperature by Spencer and Rowland [386] in the wavelength region 186–390 nm, and by Burkholder et al. [54] from 200–500 nm. The results from both studies are in excellent agreement over the range of spectral overlap. The recommended cross sections (Table 4-65) are taken from Burkholder et al.

The only study of photolysis products is that of Nickolaisen and Sander [292]. In that study, quantum yields for the Br + NO_3 and BrO + NO_2 channels were measured using broadband photolysis in quartz (λ>200 nm) and pyrex (λ>300 nm) reaction cells with the assumption that these were the only reaction pathways. The quantum yields were $\Phi_{BrO+NO_2} = 0.71$ and $\Phi_{Br+NO_3} = 0.29$.

Table 4-65. Absorption Cross Sections of $BrONO_2$ at 298 K

λ (nm)	10^{20} σ (cm^2)	λ (nm)	10^{20} σ (cm^2)	λ (nm)	10^{20} σ (cm^2)
200	680	305	16.2	410	1.81
205	520	310	14.2	415	1.66
210	361	315	12.4	420	1.50
215	293	320	11.0	425	1.38
220	258	325	9.82	430	1.30
225	231	330	8.94	435	1.20
230	205	335	8.22	440	1.11
235	174	340	7.64	445	1.04
240	139	345	7.17	450	0.930
245	106	350	6.66	455	0.834
250	79.5	355	6.21	460	0.743
255	60.1	360	5.69	465	0.652
260	47.1	365	5.17	470	0.566
265	38.9	370	4.66	475	0.461
270	33.8	375	4.16	480	0.390
275	30.5	380	3.69	485	0.275
280	27.9	385	3.23	490	0.243
285	25.6	390	2.88	495	0.214
290	23.2	395	2.53	500	0.135
295	20.7	400	2.25		
300	18.4	405	1.99		

G4. BrCl + hν → Br + Cl. The recommended absorption cross sections are given by the expression listed at the bottom of Table 4-66, which is take from the work of Maric et al. [236]. For convenience, some room temperature values are also listed in the table. Hubinger and Nee [164] have also measured the cross sections at room temperature. Their results are in excellent agreement with the recommended values.

Table 4-66. Absorption Cross Sections of BrCl at 298 K

λ (nm)	$10^{20}\sigma$ (cm^2)	λ (nm)	$10^{20}\sigma$ (cm^2)
200	2.4	390	34.7
210	4.0	400	28.2
220	5.4	410	21.9
230	6.0	420	16.9
240	5.1	430	14.2
250	3.7	440	12.4
260	2.5	450	11.1
270	1.5	460	9.6
280	1.2	470	8.0
290	0.63	480	6.8
300	0.61	490	5.0
310	1.2	500	3.8
320	2.8	510	3.1
330	7.4	520	2.3
340	14.2	530	1.5
350	22.9	540	0.96
360	33.3	550	0.76
370	38.7	560	0.31
380	38.5		

$$\sigma = 10^{-20}\alpha^{0.5}\left\{7.34\exp\left[-68.6\alpha\left(\ln\frac{227.6}{\lambda}\right)^2\right]+43.5\exp\left[-123.6\alpha\left(\ln\frac{372.5}{\lambda}\right)^2\right]+11.2\exp\left[-84.8\alpha\left(\ln\frac{442.4}{\lambda}\right)^2\right]\right\}$$

where $\alpha = \tanh\left(\frac{318.8}{T}\right)$, λ in nm and T in K, 200 nm < λ < 600 nm., 195 K < T < 300 K.

G5. $CH_3Br + h\nu \rightarrow$ Products. The absorption cross sections of CH_3Br have been measured at room temperature and 205–270 nm by Davidson [104]; at 204–260 nm by Gordus and Bernstein [142]; at 174–270 nm by Robbins [338]; at 200–260 nm by Uthman et al. [413]; at 190–290 nm by Molina et al. [272]; at 201.6 nm by Felps et al. [119]; at 180–264 nm by Man et al. [230]; and at 210–295 K and 180–280 nm by Gillotay and Simon [133]. Above 180 nm and below 270 nm, the room temperature values of Gordus and Bernstein [142], Robbins [338], Uthman et al. [413], Molina et al. [272], Gillotay and Simon [133], and the values of Davidson [104] above 210 nm are in very good agreement, i.e., generally within 10% and around the absorption maximum at 200–202 nm within 2%. The value at 202 nm of Felps et al. [119] is lower by ~10% than the rest of the data. The data of Man et al. [230], given as a plot in their paper, are lower by 20–30% over the whole absorption band than the above mentioned agreeing data sets. The preferred absorption cross sections, listed in Table 4-67, are the values of Robbins [338] at 174–178 nm; the mean of the values reported by Gillotay and Simon [133] and Robbins [338] at 180–188 nm; the mean of the values reported by Gillotay and Simon [133], Uthman et al. [413], and Robbins [338] at 190–198 nm; the mean of the values reported by Gillotay and Simon [133], Molina et al. [272], Uthman et al. [413], and Robbins [338] at 200–260 nm; the mean of the values reported by Gillotay and Simon [133], Molina et al.[272], and Robbins [338] at 262–268 nm; the mean of the values reported by Gillotay and Simon [133] and Molina et al. [272] at 270–280 nm; and the data of Molina et al. [272] at 285–290 nm.

A slight temperature dependence was observed above 220 nm, where the absorption cross sections decrease with decreasing temperature 295–210 K. Gillotay and Simon [133] parameterized the cross sections and the temperature dependence by the polynomial expansion $\log_{10} \sigma(\lambda, T) = \sum A_n \lambda^n + (T - 273) \times \sum B_n \lambda^n$ and reported smoothed values for T = 210, 230, 250, 270, and 295 K, every 2 nm, and at wavelengths corresponding to the wavenumber intervals generally used in stratospheric photodissociation calculations. The parameters A_n and B_n for the ranges T = 210–300 K and λ = 200–280 nm are as follows:

$A_0 = 46.520$	$B_0 = 9.3408 \times 10^{-1}$
$A_1 = -1.4580$	$B_1 = -1.6887 \times 10^{-2}$
$A_2 = 1.1469 \times 10^{-2}$	$B_2 = 1.1487 \times 10^{-4}$
$A_3 = -3.7627 \times 10^{-5}$	$B_3 = -3.4881 \times 10^{-7}$
$A_4 = 4.3264 \times 10^{-8}$	$B_4 = 3.9945 \times 10^{-10}$

Quantum yields for Br and H atom formation in the photodissociation of CH_3Br were measured at 298 K by Talukdar et al. [399]. The quantum yields for Br atom formation were found to be close to unity, $\Phi(Br) = 1.05 \pm 0.11$, 1.10 ± 0.20, and 1.01 ± 0.16 at 193, 222, and 248 nm, respectively; the quantum yield for H atom formation in the photolysis at 193 nm was measured to be $\Phi(H) = 0.002 \pm 0.001$, whereas H atoms could not be detected in the photolysis at 222 and 248 nm. Broad band flash photolysis of CH_3Br produced $Br^*(^2P_{1/2})$ atoms with a quantum yield $\Phi(Br^*) = 0.15 \pm 0.12$ as reported by Ebenstein et al. [112].

Table 4-67. Absorption Cross Sections of CH_3Br at 295–296 K

λ (nm)	$10^{20}\sigma$ (cm^2)	λ (nm)	$10^{20}\sigma$ (cm^2)	λ (nm)	$10^{20}\sigma$ (cm^2)
174	533	212	59.9	250	0.921
176	1010	214	54.2	252	0.683
178	1280	216	47.9	254	0.484
180	44.6	218	42.3	256	0.340
182	19.8	220	36.6	258	0.240
184	21.0	222	31.1	260	0.162
186	27.8	224	26.6	262	0.115
188	35.2	226	22.2	264	0.0795
190	44.2	228	18.1	266	0.0551
192	53.8	230	14.7	268	0.0356
194	62.6	232	11.9	270	0.0246
196	69.7	234	9.41	272	0.0172
198	76.1	236	7.38	274	0.0114
200	79.0	238	5.73	276	0.00808
202	79.2	240	4.32	278	0.00553
204	78.0	242	3.27	280	0.00382
206	75.2	244	2.37	285	0.00110
208	70.4	246	1.81	290	0.00030
210	65.5	248	1.31		

Note: 174–178 nm, Robbins [338],
180–188 nm, mean of Gillotay and Simon [133] and Robbins [338],
190–198 nm, mean of Gillotay ad Simon [133], Uthman et al. [413], and Robbins [338],
200–260 nm, mean of Gillotay and Simon [133], Molina et al. [272], Uthman et al. [413] and Robbins [338],
262–268 nm, mean of Gillotay and Simon [133], Molina et al. [272], and Robbins [338],
270–280 nm, mean of Gillotay and Simon [133] and Molina et al.[272],
285–290 nm, Molina et al. [272].

G6. $CH_2Br_2 + h\nu \rightarrow$ Products. The absorption cross sections of CH_2Br_2 have been measured at room temperature and 200–300 nm by Molina et al. [272]; at 210–295 K and 174–290 nm by Gillotay et al. [138], [135]; and at 250–348 K and 215–300 nm by Mössinger et al. [283]. The results are in good agreement, at 200–255 nm within 10% and up to 275 nm within 30%. The preferred room temperature values, listed in Table 4-68, are the values of Gillotay et al. [138], [1325] at 174–198 nm; the mean of the values reported by Molina et al. [272] and Gillotay et al. [138], [135] for the wavelength range 200–215 nm; the mean of the values reported by the three groups for the wavelength range 220–290 nm; and the values of Mössinger et al. [283] at 295–300 nm.

Both studies of the temperature dependence show a decrease of the absorption cross sections with decreasing temperature at wavelength above ~235–239 nm, and the reverse behavior around the absorption maximum down to 207 nm. At lower wavelengths, Gillotay et al. [135,138] report between 210 and 295 K a slight increase of
σ at 175–189 nm and a slight decrease around the weaker absorption maximum at 198–201 nm. The latter group parameterized the cross sections and the temperature dependence by the polynomial expansion $\log_{10} \sigma(\lambda, T) = \sum A_n \lambda^n + (T - 273) \times \sum B_n \lambda^n$ and report smoothed values for T = 210, 230, 250, 270, and 295 K, every 2 nm, and at wavelengths corresponding to the wavenumber intervals generally used in stratospheric photodissociation calculations. The parameters A_n and B_n for the ranges 210–290 nm and 210–300 K are as follows:

$A_0 = -70.211776$ $\quad B_0 = 2.899280$
$A_1 = 1.940326 \times 10^{-1}$ $\quad B_1 = -4.327724 \times 10^{-2}$
$A_2 = 2.726152 \times 10^{-3}$ $\quad B_2 = 2.391599 \times 10^{-4}$
$A_3 = -1.695472 \times 10^{-5}$ $\quad B_3 = -5.807506 \times 10^{-7}$
$A_4 = 2.500066 \times 10^{-8}$ $\quad B_4 = 5.244883 \times 10^{-10}$

Mössinger et al. [283] list the temperature coefficients B(λ) at 5-nm intervals for the ranges 215–300 nm and 250–348 K for the empirical relation $\ln \sigma(\lambda, T) = \ln \sigma(\lambda, 298K) + B(\lambda)x(T-298)$. The formulae used by

Gillotay et al. [135,138] and Mössinger et al. [283] produce cross sections which agree at 250 K within 5% in the range 215–265 nm and within 10% in the range 270–285 nm.

Table 4-68. Absorption Cross Sections of CH_2Br_2 at 295–298 K

λ (nm)	10^{20} σ (cm^2)	λ (nm)	10^{20} σ (cm^2)	10^3 B (K^{-1})	λ (nm)	10^{20} σ (cm^2)	10^3 B (K^{-1})
174	1170.9	198	226.0		255	14.10	3.91
176	662.4	200	225.6		260	6.607	5.16
178	377.2	205	215.3		265	3.037	6.33
180	241.0	210	234.5		270	1.347	7.75
182	178.4	215	263.2	–2.02	275	0.590	8.74
184	154.4	220	272.0	–1.79	280	0.255	11.6
186	153.5	225	247.4	–1.50	285	0.114	13.8
188	166.1	230	195.8	–0.96	290	0.0499	15.3
190	187.0	235	138.9	–0.04	295	0.0210	16.5
192	209.3	240	88.60	0.71	300	0.0090	21.9
194	222.5	245	51.90	1.80			
196	228.3	250	28.03	2.70			

Note: Absorption cross sections σ: 174–198 nm, Gillotay et al. [138], [135],
200–210 nm, mean of Molina et al. [272] and Gillotay et al. [138], [135],
215–290 nm, mean of Molina et al [272], Gillotay et al. [138], [135], and Mössinger et al. [283],
295–300 nm, Mössinger et al.[283].
Temperature coefficients B: 215–300 nm, Mössinger et al.[283].

G7. $CHBr_3 + h\nu \rightarrow$ Products. The absorption cross sections of $CHBr_3$ have been measured at 240–295 K and 170–310 nm by Gillotay et al. [133] and at 256–296 K and 286–362 nm by Moortgat et al. [278]; the agreement in the overlap region is excellent. The recommended cross sections at room temperature, listed in Table 4-69, are the values of Gillotay et al. [133] for the range 170–284 nm; the mean of the values reported by Gillotay et al. [133] and Moortgat et al. [278] for the range 286–310 nm; and the values of Moortgat et al. [278] at 286–362 nm.

The studies of the temperature dependence show an increase of the absorption cross sections with decreasing temperature around the three absorption maxima at 178–189 nm, 194–208 nm, and 208–234 nm, and a decrease of the absorption cross sections below 179 nm, at 189–194 nm and above 235 nm. Gillotay et al. [133] parameterized the cross sections and the temperature dependence by the polynomial expansion

$$\log_{10}(\sigma(\lambda, T)) = \sum A_n \lambda^n + (T - 273) \times \sum B_n \lambda^n$$

and report smoothed values for T = 210, 230, 250, 270, and 295 K, every 2 nm, and at wavelengths corresponding to the wavenumber intervals generally used in stratospheric photodissociation calculations. The parameters A_n and B_n for the ranges 240–310 nm and 210–300 K are given by Gillotay and Simon [135]:

$A_0 = -110.2782$ $\quad B_0 = -1.5312 \times 10^{-1}$
$A_1 = 1.0281$ $\quad B_1 = 1.6109 \times 10^{-3}$
$A_2 = -3.6626 \times 10^{-3}$ $\quad B_2 = -5.8075 \times 10^{-6}$
$A_3 = 4.1226 \times 10^{-6}$ $\quad B_3 = 7.2893 \times 10^{-9}$

For wavelengths longer than 290 nm, the atmospherically important range, Moortgat et al. [278] give the expression

$$\sigma(\lambda,T) = \exp\{(0.06183 - 0.000241\,\lambda)(273 - T) - (2.376 + 0.14757\,\lambda)\} \quad (\lambda = 290–340 \text{ nm}, T = 210–300 \text{ K})$$

These two formulae produce continuous absorption curves for the range 240–340 nm also at low temperatures

At wavelengths longer than 290 nm, the cross sections are relatively small; the presence of impurities as well as optical artifacts arising, e.g., from adsorption of $CHBr_3$ on the cell windows, complicate the measurements. Hence, additional investigations of the spectrum would be useful.

Table 4-69. Absorption Cross Sections of $CHBr_3$ at 295–296 K

λ (nm)	$10^{20}\sigma$ (cm^2)	λ (nm)	$10^{20}\sigma$ (cm^2)	λ (nm)	$10^{20}\sigma$ (cm^2)
170	1603.8	236	323.9	302	0.534
172	1173.2	238	294.7	304	0.397
174	969.6	240	272.8	306	0.297
176	872.0	242	253.3	308	0.222
178	857.6	244	233.7	310	0.165
180	831.3	246	214.4	312	0.127
182	770.3	248	193.9	314	0.0952
184	683.3	250	174.1	316	0.0712
186	570.4	252	157.7	318	0.0529
188	470.8	254	136.1	320	0.0390
190	399.1	256	116.4	322	0.0289
192	360.2	258	98.6	324	0.0215
194	351.3	260	82.8	326	0.0162
196	366.1	262	68.9	328	0.0121
198	393.6	264	56.9	330	0.00916
200	416.4	266	46.7	332	0.00690
202	433.6	268	38.0	334	0.00525
204	440.6	270	30.8	336	0.00396
206	445.0	272	24.8	338	0.00307
208	451.4	274	19.8	340	0.00240
210	468.5	276	15.8	342	0.00176
212	493.4	278	12.5	344	0.00135
214	524.2	280	9.88	346	0.00102
216	553.5	282	7.77	348	0.00080
218	573.9	284	6.10	350	0.00064
220	582.6	286	4.79	352	0.00054
222	578.0	288	3.74	354	0.00046
224	557.8	290	2.89	356	0.00032
226	527.2	292	2.20	358	0.00024
228	486.8	294	1.69	360	0.00017
230	441.2	296	1.28	362	0.00013
232	397.4	298	0.956		
234	361.8	300	0.719		

Note: 170–284 nm, Gillotay et al. [133],
286–310 nm, mean of Gillotay et al. [133] and Moortgat et al. [278],
312–362 nm, Moortgat et al. [278].

G8. $CH_2BrCH_2Br + h\nu \rightarrow$ Products. The absorption cross sections of CH_2BrCH_2Br have been measured at room temperature and 190–270 nm by Uthman et al. [413]. Their data are listed in Table 4-70.

Table 4-70. Absorption Cross Sections of CH_2BrCH_2Br at 295 K

λ (nm)	10^{20} σ (cm^2)	λ (nm)	10^{20} σ (cm^2)	λ (nm)	10^{20} σ (cm^2)
190	230	218	170	246	9.3
192	250	220	150	248	7.1
194	270	222	130	250	5.9
196	290	224	110	252	4.4
198	300	226	89	254	4.0
200	310	228	75	256	2.8
202	310	230	62	258	2.1
204	300	232	50	260	1.9
206	290	234	41	262	1.7
208	280	236	32	264	1.4
210	260	238	26	266	1.1
212	230	240	20	268	0.9
214	210	242	16	270	0.7
216	190	244	11		

Note: 190–270 nm, Uthman et al. [413].

G9. $C_2H_5Br + h\nu \rightarrow$ Products. The absorption cross sections of C_2H_5Br have been measured at 295 K and 200–260 nm by Zhang et al. [451]. This wavelength range shows part of an absorption band with a maximum of ~6×10^{-19} cm^2 at ~200 nm. Estimated values at 5-nm intervals, read from a logarithmic plot, are presented in Table 4-71.

Table 4-71. Absorption Cross Sections of C_2H_5Br at 295 K

λ (nm)	10^{20} σ (cm^2)	λ (nm)	10^{20} σ (cm^2)	λ (nm)	10^{20} σ (cm^2)
200	*60.5*	*225*	*23.7*	*250*	*1.12*
205	*59.5*	*230*	*14.9*	*255*	*0.53*
210	*53.5*	*235*	*8.30*	*260*	*0.23*
215	*44.5*	*240*	*4.30*		
220	*34.0*	*245*	*2.28*		

Note: 200–260 nm, Zhang et al. [451], estimated values read from logarithmic plot.

G10. CH_2ClBr (Halon-1011) + $h\nu \rightarrow$ Products. The absorption cross sections of CH_2ClBr have been measured at room temperature and 210–260 nm by Cadman and Simons [64], and at 187–290 nm by Orkin et al. [303]. The data of Cadman and Simons [64], which are given only on a plot in their paper, are smaller by ≤20% than the data of Orkin et al. [303]. The recommended absorption cross sections, listed in Table 4-72, are the data of Orkin et al. [303].

Quantum yields for Br ($^2P_{3/2}$) and Br*($^2P_{1/2}$) atom formation in the photolysis of CH_2ClBr at 193–242 nm and 248–268 nm have been measured by Zou et al. [452] and McGivern et al. [253], respectively. Reported values are as follows:

	193 nm	234 nm	248.5 nm	261.5 nm	266.7 nm:
Φ(Br ($^2P_{3/2}$))	0.82 ± 0.10	0.80 ± 0.10	0.86 ± 0.10	0.84 ± 0.10	0.91 ± 0.10
Φ(Br*($^2P_{1/2}$))	0.18 ± 0.10	0.20 ± 0.10	0.14 ± 0.10	0.16 ± 0.10	0.09 ± 0.10

Table 4-72. Absorption Cross Sections of CH_2ClBr at 295 K

λ (nm)	10^{20} σ (cm^2)	λ (nm)	10^{20} σ (cm^2)	λ (nm)	10^{20} σ (cm^2)
187	151.1	222	57.4	258	1.45
188	126.4	224	50.5	260	1.09
190	104.6	226	44.1	262	0.807
192	100.5	228	38.2	264	0.596
194	104.7	230	32.8	266	0.440
196	111.8	232	28.0	268	0.322
198	119.4	234	23.6	270	0.235
200	124.7	236	19.7	272	0.170
202	127.1	238	16.3	274	0.123
204	126.3	240	13.4	276	0.089
206	122.5	242	10.8	278	0.064
208	116.3	244	8.73	280	0.046
210	108.4	246	6.94	282	0.033
212	99.6	248	5.46	284	0.024
214	90.5	250	4.24	286	0.0178
216	81.5	252	3.29	288	0.0129
218	72.9	254	2.52	290	0.0098
220	64.8	256	1.92		

Note: 187–290 nm, Orkin et al. [303].

G11. $CHClBr_2$ (Halon-1012) + hν → Products. The absorption cross sections of $CHClBr_2$ have been measured at room temperature and 106–200 nm by Ibuki et al. [172]; and at 240, 261, and 296 K and 200–310 nm by Bilde et al. [33]. Two absorption bands are apparent above 200 nm, one maximizing near 210 nm and the other near 240 nm. Near the band maxima, the cross sections at 240 K are approximately higher by 10% than those at room temperature. A positive temperature dependence of the cross sections is evident in the long-wavelength tail of the spectrum, the room temperature cross section being about 15% higher at 270 nm than that obtained at 240 K. The recommended absorption cross sections, listed in Table 4-73, are the room temperature data of Bilde et al. [33] (originally listed at 1-nm intervals); values at 2-nm intervals are given for wavelengths above 212 nm, and values at 1-nm intervals are given or the region of the first absorption maximum (200–212 nm), where the absorption curve shows a somewhat irregular behavior.

Table 4-73. Absorption Cross Sections of $CHClBr_2$ at 296 K

λ (nm)	10^{20} σ (cm^2)	λ (nm)	10^{20} σ (cm^2)	λ (nm)	10^{20} σ (cm^2)
200	274.6	230	141.4	272	9.415
201	282.8	232	136.4	274	7.552
202	293.9	234	131.4	276	5.950
203	306.7	236	126.8	278	4.687
204	314.2	238	122.2	280	3.691
205	320.6	240	116.0	282	2.884
206	324.9	242	109.2	284	2.261
207	323.7	244	101.2	286	1.734
208	322.9	246	92.70	288	1.331
209	324.6	248	83.52	290	1.016
210	317.8	250	74.04	292	0.7907
211	306.2	252	64.83	294	0.6116
212	297.4	254	55.95	296	0.4583
214	279.4	256	47.67	298	0.3489
216	261.7	258	39.92	300	0.2692
218	234.9	260	33.35	302	0.2076
220	215.1	262	27.50	304	0.1588
222	199.1	264	22.50	306	0.1208
224	184.5	266	18.28	308	0.0945
226	165.3	268	14.78	310	0.0742
228	151.7	270	11.82		

Note: 200–310 nm, Bilde et al. [33]

G12. $CHCl_2Br$ (Halon-1021) + hν → Products. The absorption cross sections of $CHCl_2Br$ have been measured at room temperature and 106–200 nm by Ibuki et al. [172]; at room temperature and 201–270 nm by Cadman and Simons [64]; and at 253, 273 and 298 K and 200–320 nm by Bilde et al. [33]. The data of Cadman and Simons [64], which are given only in a plot in their paper, agree between 200 and 260 nm within ≤15% with the room temperature data of Bilde et al. [33], the absorption maximum, however, is shifted to lower wavelengths. The recommended absorption cross sections, listed in Table 4-74, are those reported by Bilde et al. [33].

A decrease of the absorption cross sections with decreasing temperature was observed between 298 and 253 K over the whole spectrum. The cross section in the absorption maximum, which has been observed at 220 nm by Bilde et al. [33], is approximately 6% lower at 253 K than at room temperature. An increasingly positive temperature dependence was observed at longer wavelengths, the room temperature cross section at 320 nm becoming about four times larger than those at 253 K.

Table 4-74. Absorption Cross Sections of $CHCl_2Br$ at 298 K

λ (nm)	10^{20} σ (cm^2)	λ (nm)	10^{20} σ (cm^2)	λ (nm)	10^{20} σ (cm^2)
200	115.0	230	58.1	276	1.63
202	93.8	232	54.6	278	1.32
204	81.1	234	50.0	280	1.07
206	73.6	236	45.8	282	0.865
208	69.0	238	41.6	284	0.694
209	69.8	240	37.3	286	0.573
210	68.8	242	33.0	288	0.454
211	67.4	244	29.3	290	0.384
212	68.4	246	25.8	292	0.317
213	70.0	248	22.2	294	0.265
214	70.1	250	19.2	296	0.217
215	70.2	252	16.5	298	0.176
216	71.1	254	13.6	300	0.146
217	71.0	256	11.5	302	0.118
218	70.7	258	9.75	304	0.0962
219	71.3	260	8.19	306	0.0761
220	71.6	262	6.82	308	0.0617
221	70.6	264	5.61	310	0.0496
222	69.3	266	4.68	312	0.0395
223	68.7	268	3.74	314	0.0317
224	68.2	270	3.01	316	0.0259
226	65.2	272	2.48	318	0.0210
228	62.2	274	2.02	320	0.0171

Note: 200–320 nm, Bilde et al. [33].

G13. CCl_3Br (Halon-1031) + hν → Products. The absorption cross sections of CCl_3Br have been measured at room temperature and 170–230 nm by Roxlo and Mandl [350] and at 207–305 nm by Cadman and Simons [64]. Both groups report their results as plots only. Estimated absorption cross sections are listed in Table 4-75, which are the results of Roxlo and Mandl [350] at 170–200 nm; the mean of the results of both groups at 205–230 nm; and the results of Cadman and Simons [64] at 235 305 nm.

Quantum yields for $Br^*(^2P_{1/2})$ atom formation in the photolysis at 234 and 265 nm, Φ(Br*) = 0.31 ± 0.01 and 0.68 ± 0.02, respectively, were reported by Jung et al. [195].

Table 4-75. Absorption Cross Sections of CCl_3Br at 298 K

λ (nm)	10^{20} σ (cm^2)	λ (nm)	10^{20} σ (cm^2)	λ (nm)	10^{20} σ (cm^2)
170	*600*	*220*	*49*	*270*	*19*
175	*600*	*225*	*46*	*275*	*11*
180	*1050*	*230*	*52*	*280*	*7.2*
185	*1100*	*235*	*50*	*285*	*5.0*
190	*850*	*240*	*50*	*290*	*3.3*
195	*530*	*245*	*49*	*295*	*2.2*
200	*230*	*250*	*48*	*300*	*1.4*
205	*140*	*255*	*46*	*305*	*1.0*
210	*90*	*260*	*42*		
215	*66*	*265*	*34*		

Note: 170–200 nm, Roxlo and Mandl [350],
205 230 nm, mean of Roxlo and Mandl [350] and Cadman and Simons [64],
235–305 nm, Cadman and Simons [64].

G14. CHF_2Br (Halon-1201) + hν → Products. The absorption cross sections of CHF_2Br have been measured at room temperature and 207–255 nm by Davidson [104]; at 190–280 nm by Talukdar et al. [394]; and at 190–280 nm by Orkin and Kasimovskaya [302]. Gillotay et al. [138] carried out measurements at 210–295 K and in the wavelength range 166–267 nm and report only smoothed values for T = 210, 230, 250, 270, and 295 K and at wavelengths corresponding to the wavenumber intervals generally used in stratospheric photodissociation calculations. The results of Davidson [104], Orkin and Kasimovskaya [302], and Gillotay et al. [138] are in excellent agreement at wavelengths below 240 nm; the values of Gillotay et al. [138] become increasingly smaller by up to about 40% at 260 nm, and those of Davidson [104] become smaller by up to about 30% at 250 nm than the values of Orkin and Kasimovskaya [302]. The results of Talukdar et al. [394], who report a plot on a logarithmic scale for measured values at 190–280 nm and extrapolated values up to 360 nm, appear to be in agreement with the results of Orkin and Kasimovskaya [302]. The preferred values, listed in Table 4-76, are the values of Gillotay et al. [138] at the centers of the 500-cm^{-1} intervals between 168 and 188 nm, and the values of Orkin and Kasimovskaya [302] at 190–280 nm.

With decreasing temperature 295–210 K, an increase of the absorption cross sections around the absorption maximum at 168–215 nm and a decrease at wavelengths above 215 nm was observed by Gillotay et al. [104] (the interpolation formula has not been reported for this molecule).

Table 4-76. Absorption Cross Sections of CHF_2Br at 298 K

λ (nm)	10^{20} σ (cm^2)	λ (nm)	10^{20} σ (cm^2)	λ (nm)	10^{20} σ (cm^2)
168.10	3.97	206	23.2	246	0.299
170.95	8.21	208	21.2	248	0.220
173.15	12.5	210	19.0	250	0.161
174.65	15.6	212	16.8	252	0.117
176.20	18.8	214	14.6	254	0.0849
177.80	21.9	216	12.6	256	0.0615
179.40	24.5	218	10.6	258	0.0444
181.00	26.6	220	8.85	260	0.0319
182.65	28.3	222	7.25	262	0.0230
184.35	29.6	224	5.88	264	0.0166
186.05	30.6	226	4.71	266	0.0121
187.80	31.4	228	3.73	268	0.0087
190	32.5	230	2.91	270	0.0063
192	32.4	232	2.24	272	0.0046
194	31.8	234	1.71	274	0.0034
196	31.0	236	1.30	276	0.0024
198	29.9	238	0.982	278	0.0018
200	28.6	240	0.735	280	0.0012
202	27.0	242	0.547		
204	25.2	244	0.405		

Note: 168–188 nm, Gillotay et al. [138],
190–280 nm, Orkin and Kasimovskaya [302].

G15. CF_2Br_2 (Halon-1202) + hν → Products. The absorption cross sections of CF_2Br_2 have been measured at room temperature and 215–290 nm by Davidson [104]; at 200–310 nm by Walton et al. [428]; at 190–340 nm by Molina et al. [272]; at 190–320 nm by Orkin and Kasimovskaya [302]; at 210–295 K and 170–304 nm by Gillotay and Simon [134]; and at 210–296 K and 190–320 nm by Burkholder et al. [57]. The room temperature data, except those of Walton [428], are in good agreement, i.e., better than 10%, over their common wavelength range from 190 to 300 nm. In the absorption maximum around 226 nm, the older data of Davidson [172] and Molina et al. [272] are the highest and lowest, respectively, and the more recent data agree within 5% (the absorption maximum reported by Walton [428] is larger by ~50%). At wavelengths above 300 nm, the values of Orkin and Kasimovskaya [302] and Burkholder et al. [57] agree within 15%, whereas those of Molina et al. [272] become increasingly larger by up to ~200% at 320 nm (and larger by up to ~660% than the extrapolated values at 340 nm, see below). The preferred absorption cross sections, listed in Table 4-77, are the values of Gillotay and Simon [134] at 170–188 nm; the mean of the values reported by Gillotay and Simon [134], Orkin and Kasimovskaya [302], and Burkholder et al. [57] for the wavelength range 190–304 nm; and the mean of the values reported by the latter two groups for the range 306–320 nm. For wavelengths 322–340 nm, the mean

of the values of Orkin and Kasimovskaya [302], and Burkholder et al.[57] for the range 306–320 nm have been extrapolated ($\log \sigma = 1.85109 - 0.07755\ \lambda$).

Measurements in the far UV were reported by Doucet et al. [109] for the wavelength range 60–220 nm and by Seccombe et al. [369] for the wavelength range 55–175 nm.

Both studies of the temperature dependence show an increase of the absorption cross sections in the two absorption bands around 190 and 226 nm with decreasing temperature 296–210 K and the reverse effect at wavelengths above 240 nm and below 177 nm. Gillotay and Simon [134] observed a regular temperature behavior, i.e., an increase of the maximum absorption cross section at ~225 nm by ~0.09×10^{-18} cm^2 $molecule^{-1}$ per 20-K temperature decrease. Burkholder et al.[57] observed a less pronounced temperature behavior below 250 K (the maximum absorption cross sections agree within 1%), so that their maximum cross section at 210 K is lower by 5% than that observed by Gillotay and Simon [134] (in contrast to the cross sections at room temperature which are nearly identical). Different parameterizations for the temperature dependence of the absorption cross section have been proposed. Gillotay and Simon [134] give the polynomial expansion $\log_{10} \sigma(\lambda, T) = \sum A_n \lambda^n + (T - 273) \times \sum B_n \lambda^n$ and report smoothed values for T = 210, 230, 250, 270, and 295 K, every 2 nm, and at wavelengths corresponding to the wavenumber intervals generally used in stratospheric photodissociation calculations. The parameters A_n and B_n for the ranges 222–304 nm and 210–300 K are as follows:

$A_0 = -206.2$	$B_0 = 1.0460 \times 10^{-1}$
$A_1 = 2.3726$	$B_1 = -1.4124 \times 10^{-3}$
$A_2 = -1.0527 \times 10^{-2}$	$B_2 = 6.9015 \times 10^{-6}$
$A_3 = 1.9239 \times 10^{-5}$	$B_3 = -1.5164 \times 10^{-8}$
$A_4 = -1.2242 \times 10^{-8}$	$B_4 = 1.3990 \times 10^{-11}$

Burkholder et al. [57] give the expansion

$$\log_{10} \sigma(\lambda, T) = (\sum A_i (\lambda - 268.7998)^I) (1 + (296-T) \sum B_i (\lambda - 268.7998)^I)$$

and report the following parameters A_i and B_i for the ranges 235–260 nm and 210–296 K:

$A_0 = -44.42756$	$B_0 = 1.481886 \times 10^{-4}$
$A_1 = -1.464955 \times 10^{-1}$	$B_1 = 6.77182 \times 10^{-6}$
$A_2 = -5.692188 \times 10^{-4}$	$B_2 = 1.154347 \times 10^{-7}$
$A_3 = 1.155366 \times 10^{-5}$	$B_3 = -2.77145 \times 10^{-11}$
$A_4 = -1.399502 \times 10^{-7}$	$B_4 = -6.619515 \times 10^{-11}$

A parameterization for extrapolated absorption cross sections up to 400 nm,

$$\log_{10} \sigma(\lambda, T) = (\sum A_i (\lambda - 301.0104)^I) + (\lambda - 260) (\sum B_i (T - 251.2)^I)$$

has also been reported by Burkholder et al. [57].

The quantum yield for formation of CF_2O and Br_2 in the photolysis of CF_2Br_2 at 206, 248, and 302 nm, in the presence of O_2 has been measured to be unity by Molina and Molina [269], independent of pressure, in contrast to an earlier report by Walton [428] that the quantum yield at 265 nm decreases from unity when the system pressure is raised to 50 torr of CO_2. Primary quantum yields for Br atom formation, $\Phi(Br) = 1.96 \pm 0.27$, 1.63 ± 0.19, and 1.01 ± 0.15, in the photodissociation of CF_2Br_2 at 193, 222, and 248 nm, respectively, were measured at 298 K by Talukdar et al. [399]. A quantum yield for CF_2 formation, $\Phi(CF_2) = 1.15 \pm 0.30$, in the 193-nm photolysis was reported by Talukdar et al. [397].

Table 4-77. Absorption Cross Sections of CF_2Br_2 at 295–296 K

λ (nm)	10^{20} σ (cm^2)	λ (nm)	10^{20} σ (cm^2)	λ (nm)	10^{20} σ (cm^2)
170	124.5	228	253.4	286	0.336
172	78.1	230	244.7	288	0.245
174	55.3	232	230.2	290	0.178
176	49.5	234	211.9	292	0.128
178	60.3	236	191.6	294	0.0926
180	75.0	238	169.3	296	0.0672
182	86.6	240	147.3	298	0.0487
184	100.9	242	125.8	300	0.0352
186	111.8	244	106.0	302	0.0253
188	118.0	246	87.8	304	0.0183
190	115.9	248	72.0	306	0.0130
192	110.3	250	58.3	308	0.00919
194	101.6	252	46.5	310	0.00650
196	91.4	254	36.8	312	0.00456
198	82.1	256	28.9	314	0.00319
200	74.9	258	22.4	316	0.00222
202	71.7	260	17.3	318	0.00157
204	73.4	262	13.1	320	0.00105
206	80.7	264	9.90	*322*	*0.000759*
208	93.0	266	7.47	*324*	*0.000531*
210	110.0	268	5.59	*326*	*0.000371*
212	131.0	270	4.17	*328*	*0.000260*
214	154.9	272	3.08	*330*	*0.000182*
216	180.4	274	2.27	*332*	*0.000127*
218	204.7	276	1.66	*334*	*0.000089*
220	226.0	278	1.21	*336*	*0.000062*
222	244.2	280	0.888	*338*	*0.000044*
224	253.3	282	0.647	*340*	*0.000030*
226	256.8	284	0.470		

Note: 170 188 nm: Gillotay and Simon [134]
190–304 nm: mean of Gillotay and Simon [134], Orkin and Kasimovskaya [302], and Burkholder et al. [57]
306–320 nm: mean of Orkin and Kasimovskaya [302] and Burkholder et al.[57]
322–340 nm: extrapolation of mean of Orkin and Kasimovskaya [302], and Burkholder et al. [57] data.

G16. CF_2ClBr (Halon-1211) + hν → Products. The absorption cross sections of CF_2ClBr have been measured at room temperature and 191–307 nm by Giolando et al. [140]; at 190–330 nm by Molina et al. [272]; at 190–304 nm by Orkin and Kasimovskaya [302]; at 210–295 K and 170–302 nm by Gillotay and Simon [134]; and at 210–296 K and 190–320 nm by Burkholder et al. [57]. The agreement between the room temperature data of Orkin and Kasimovskaya [302], Gillotay and Simon [134], and Burkholder et al. [57] is very good in the region of the absorption band, i.e., within 10% over the range 190–240 nm and within 3% in the maximum at 205–206 nm, with one exception: Gillotay and Simon [134] observed a structure near the absorption maximum, different from the other observations, which resulted in values higher by about 10% at 200–202 nm. Molina et al. [272] reported values for the range 190–240 nm which are lower by 10–20% than the above mentioned data. The few data points (at 10-nm intervals) of Giolando et al. [140] fit well to the absorption curves reported by Orkin and Kasimovskaya [302], Gillotay and Simon [134], and Burkholder et al. [57]. The deviations between the various data sets increase at longer wavelengths to ≤30% at 300 nm and up to 55% at 320 nm. The preferred absorption cross sections at 295–298 K, listed in Table 4-78, are the values of Gillotay and Simon [134] at 170–188 nm; the mean of the values reported by Molina et al. [272], Gillotay and Simon [134], Burkholder et al. [57] and Orkin and Kasimovskaya [302] at 190–302 nm; the mean of the values reported by Molina et al. [272], Burkholder et al. [57], and Orkin and Kasimovskaya [302] at 304 nm; and the mean of the values reported by Molina et al. [272] and Burkholder et al. [57] at 306–320 nm.

Measurements in the far UV at 60–220 nm were reported by Doucet et al. [109].

Both studies of the temperature dependence show an increase of the absorption cross sections in the absorption band around 204–206 nm with decreasing temperature 296–210 K and the reverse effect at wavelengths above 233 nm and below 180 nm. Gillotay and Simon [134] observed a regular temperature behavior, i.e., an increase of the maximum absorption cross section by ~0.05×10^{-18} cm^2 $molecule^{-1}$ per 20 K temperature decrease. Burkholder et al. [57] observed a less pronounced temperature behavior (the maximum absorption cross sections agree within 2.5%), so that their maximum cross section at 210 K is lower by 15% than that observed by Gillotay and Simon [134] (in contrast to the cross sections at room temperature which are within 4%). Different parameterizations for the temperature dependence of the absorption cross section have been proposed. Gillotay and Simon [134] give the polynomial expansion

$$\log_{10} \sigma(\lambda, T) = \sum A_n \lambda^n + (T - 273) \times \sum B_n \lambda^n$$

and report smoothed values for T = 210, 230, 250, 270, and 295 K, every 2 nm, and at wavelengths corresponding to the wavenumber intervals generally used in stratospheric photodissociation calculations. The parameters A_n and B_n for the ranges 200–302 nm and 210–300 K are as follows:

$A_0 = -134.80$	$B_0 = 3.3070 \times 10^{-1}$
$A_1 = 1.7084$	$B_1 = -5.0957 \times 10^{-3}$
$A_2 = -9.1540 \times 10^{-3}$	$B_2 = 2.9361 \times 10^{-5}$
$A_3 = 2.1644 \times 10^{-5}$	$B_3 = -7.6198 \times 10^{-8}$
$A_4 = -1.9863 \times 10^{-8}$	$B_4 = 7.6825 \times 10^{-11}$

Burkholder et al. [57] give the expansion

$$\log_{10} \sigma(\lambda, T) = (\sum A_i (\lambda - 259.8989)^I) (1 + (296-T) \sum B_i (\lambda - 259.8989)^I)$$

and report the following parameters A_i and B_i for the ranges 220–260 nm and 210–296 K:

$A_0 = -45.4087$	$B_0 = 1.528905 \times 10^{-4}$
$A_1 = -1.304811 \times 10^{-1}$	$B_1 = 6.024833 \times 10^{-6}$
$A_2 = -6.995443 \times 10^{-4}$	$B_2 = 1.030995 \times 10^{-7}$
$A_3 = 6.159709 \times 10^{-6}$	$B_3 = -6.387931 \times 10^{-11}$
$A_4 = -9.384074 \times 10^{-9}$	$B_4 = -3.718503 \times 10^{-11}$

A parameterization for extrapolated absorption cross sections up to 400 nm,

$$\log_{10} \sigma(\lambda, T) = (\sum A_i (\lambda - 292.2083)^I) + (\lambda - 260) (\sum B_i (T - 251.2)^I)$$

has also been reported by Burkholder et al. [57].

Quantum yields for Cl and Br atom formation in the photodissociation of CF_2ClBr at 193, 222, and 248 nm, $\Phi(Cl) = 1.03 \pm 0.14$, 0.27 ± 0.04, and 0.18 ± 003, $\Phi(Br) = 1.04 \pm 0.13$, 0.86 ± 0.11, and 0.75 ± 0.13, respectively, and a quantum yield for CF_2 formation in the 193-nm photolysis, $\Phi(CF_2) = 0.91 \pm 0.30$, were measured at 298 K by Talukdar et al. [397].

Table 4-78. Absorption Cross Sections of CF_2ClBr at 295–298 K

λ (nm)	10^{20} σ (cm^2)	λ (nm)	10^{20} σ (cm^2)	λ (nm)	10^{20} σ (cm^2)
170	323.0	222	68.3	274	0.250
172	234.2	224	60.4	276	0.184
174	176.0	226	52.7	278	0.135
176	120.9	228	45.7	280	0.0991
178	84.7	230	39.2	282	0.0724
180	58.1	232	33.8	284	0.0527
182	41.9	234	28.8	286	0.0385
184	35.0	236	24.4	288	0.0282
186	34.1	238	20.4	290	0.0205
188	38.9	240	16.9	292	0.0148
190	46.1	242	13.9	294	0.0106
192	57.0	244	11.4	296	0.00764
194	69.1	246	9.28	298	0.00544
196	81.4	248	7.50	300	0.00391
198	93.5	250	5.99	302	0.00279
200	106.0	252	4.76	304	0.00207
202	113.3	254	3.76	306	0.00161
204	117.4	256	2.94	308	0.00113
206	118.7	258	2.29	310	0.000803
208	117.7	260	1.76	312	0.000569
210	114.2	262	1.36	314	0.000403
212	108.5	264	1.03	316	0.000288
214	101.5	266	0.784	318	0.000213
216	93.6	268	0.593	320	0.000159
218	85.3	270	0.447		
220	76.8	272	0.336		

Note: 170–188 nm: Gillotay and Simon [134]
190–302 nm: mean of Molina et al. [272], Gillotay and Simon [134], Burkholder et al. [57], and Orkin and Kasimovskaya [302]
304 nm: mean of Molina et al. [272], Burkholder et al. [57], and Orkin and Kasimovskaya [302]
306–320 nm: mean of Molina et al. [272] and Burkholder et al. [57].

G17. CF_3Br (Halon-1301) + hν → Products. The absorption cross sections of CF_3Br have been measured at room temperature and 207–255 nm by Davidson [172]; at 170–230 nm by Roxlo and Mandl [350]; at 180–400 nm by Pence et al. [312]; at 190–300 nm by Molina et al. [272]; at 190–270 nm by Orkin and Kasimovskaya [302]; at 210–295 K and 168–280 nm by Gillotay and Simon [134]; and at 210–296 K and 190–285 nm by Burkholder et al. [57]. The agreement between the room temperature data is very good, i.e., 10% and better, in the region of the absorption band between 190 and 230 nm with the exception of the data of Davidson [253] below 210 nm and the whole data set of Roxlo and Mandl [350]. Pence et al. [312] report a plot of the absorbance (in arbitrary units) and give for 193 nm an absorption cross section smaller by one order of magnitude than the rest of the data for 193 nm. At wavelengths above 250 nm, Burkholder et al. [57] and Orkin and Kasimovskaya [302] measured higher values (up to ~ 35% at 270 nm) than those reported by Molina et al. [272] and Gillotay and Simon [134]. The preferred absorption cross sections at 295–298 K, listed in Table 4-79, are the values of Gillotay and Simon [134] at 168–188 nm, the mean of the values reported by Molina et al. [272], Gillotay and Simon [134], Burkholder et al. [57], and Orkin and Kasimovskaya [302] at 190–270 nm, the mean of the values reported by Molina et al. [272], Gillotay and Simon [134], and Burkholder et al. [57] at 272–280 nm, and the values of Molina et al. [272] at 295–300 nm.

Measurements in the far UV at 60–220 nm were reported by Doucet et al. [109].

Both studies of the temperature dependence show an increase of the absorption cross sections in the absorption band between 174 and 216 nm with decreasing temperature 296–210 K and the reverse effect at wavelengths above 218 nm and below 174 nm. Gillotay and Simon [134] observed a regular temperature behavior, i.e., an increase of the maximum absorption cross section by ~0.06×10^{-19} cm^2 $molecule^{-1}$ per 20 K temperature decrease. Burkholder et al. [57] observed a less pronounced temperature behavior (the maximum absorption cross sections agree within 2%), so that their maximum cross section at 210 K is lower by ~25% than that

observed by Gillotay and Simon [134] (in contrast to the cross sections at room temperature which are within 6%). Different parameterizations for the temperature dependence of the absorption cross section have been proposed. Gillotay and Simon [134] give the polynomial expansion

$$\log_{10} \sigma(\lambda, T) = \sum A_n \lambda^n + (T - 273) \times \sum B_n \lambda^n$$

and report smoothed values for T = 210, 230, 250, 270, and 295 K, every 2 nm, and at wavelengths corresponding to the wavenumber intervals generally used in stratospheric photodissociation calculations. The parameters A_n and B_n for the ranges 178–280 nm and 210–300 K are as follows:

$A_0 = 62.563$	$B_0 = -9.1755 \times 10^{-1}$
$A_1 = -2.0068$	$B_1 = 1.8575 \times 10^{-2}$
$A_2 = 1.6592 \times 10^{-2}$	$B_2 = -1.3857 \times 10^{-4}$
$A_3 = -5.6465 \times 10^{-5}$	$B_3 = 4.5066 \times 10^{-7}$
$A_4 = 6.7459 \times 10^{-8}$	$B_4 = -5.3803 \times 10^{-10}$

Burkholder et al. [57] give the expansion

$$\log_{10} \sigma(\lambda, T) = (\sum A_i (\lambda - 242.2466)^I) (1 + (296-T) \sum B_i (\lambda - 242.266)^I)$$

and report the following parameters A_i and B_i for the ranges 214–285 nm and 210–296 K:

$A_0 = -46.70542$	$B_0 = 1.694026 \times 10^{-4}$
$A_1 = -1.55047 \times 10^{-1}$	$B_1 = 8.723247 \times 10^{-6}$
$A_2 = -1.020187 \times 10^{-3}$	$B_2 = 5.953165 \times 10^{-9}$
$A_3 = 2.246169 \times 10^{-5}$	$B_3 = -3.872168 \times 10^{-9}$
$A_4 = -1.300982 \times 10^{-7}$	$B_4 = -1.803325 \times 10^{-11}$

Quantum yields for Br ($Br(^2P_{3/2} + Br^*(^2P_{1/2})$) atom formation in the photodissociation of CF_3Br at 193 and 222 nm, $\Phi(Br+Br^*) = 1.12 \pm 0.16$ and 0.92 ± 0.15, respectively, were measured at 298 K by Talukdar et al. [399]. A quantum yield for $Br^*(^2P_{1/2})$ atom formation at 193 nm, $\Phi(Br^*) = 0.56 \pm 0.05$, was reported by Pence et al. [312].

Table 4-79. Absorption Cross Sections of CF_3Br at 295–298 K

λ (nm)	10^{20} σ (cm^2)	λ (nm)	10^{20} σ (cm^2)	λ (nm)	10^{20} σ (cm^2)
168	0.517	210	12.1	252	0.107
170	0.696	212	11.4	254	0.0743
172	0.928	214	10.6	256	0.0516
174	1.22	216	9.71	258	0.0357
176	1.60	218	8.65	260	0.0248
178	2.05	220	7.56	262	0.0171
180	2.61	222	6.50	264	0.0118
182	3.26	224	5.47	266	0.00827
184	4.02	226	4.52	268	0.00580
186	4.88	228	3.69	270	0.00399
188	5.82	230	2.91	272	0.00271
190	6.56	232	2.32	274	0.00188
192	7.58	234	1.80	276	0.00129
194	8.63	236	1.39	278	0.00092
196	9.61	238	1.04	280	0.00064
198	10.5	240	0.766	285	0.00022
200	11.3	242	0.563	290	0.00008
202	11.9	244	0.414	295	0.00003
204	12.4	246	0.296	300	0.00001
206	12.5	248	0.212		
208	12.4	250	0.149		

Note: 170–188 nm: Gillotay and Simon [134]
190–270 nm: mean of Molina et al. [272], Gillotay and Simon [134], Burkholder et al. [57] and Orkin and Kasimovskaya [302]
272–280 nm: mean of Molina et al.[272] and Burkholder et al. [57]
285–300 nm: Molina et al. [272].

G18. CF_3CH_2Br (Halon-2301) + hν → Products. The absorption cross sections of CF_3CH_2Br have been measured at 295 K and 190–294 nm by Orkin and Kasimovskaya [302]. Their results are listed in Table 4-80.

Table 4-80. Absorption Cross Sections of CF_3CH_2Br at 295 K

λ (nm)	10^{20} σ (cm^2)	λ (nm)	10^{20} σ (cm^2)	λ (nm)	10^{20} σ (cm^2)
190	45.4	226	16.6	262	0.190
192	49.5	228	14.1	264	0.137
194	52.5	230	11.9	266	0.0983
196	54.4	232	9.85	268	0.0705
198	55.1	234	8.10	270	0.0504
200	54.7	236	6.58	272	0.0361
202	53.3	238	5.28	274	0.0258
204	51.2	240	4.20	276	0.0184
206	48.6	242	3.31	278	0.0132
208	45.7	244	2.58	280	0.0096
210	42.5	246	2.01	282	0.0069
212	39.1	248	1.53	284	0.0048
214	35.7	250	1.16	286	0.0034
216	32.2	252	0.876	288	0.0025
218	28.8	254	0.653	290	0.0018
220	25.5	256	0.484	292	0.0013
222	22.3	258	0.357	294	0.0011
224	19.4	260	0.261		

Note: 190–294 nm, Orkin and Kasimovskaya [302].

G19. $CF_3CHClBr$ (Halon-2311) + hν → Products. The absorption cross sections of $CF_3CHClBr$ have been measured at room temperature and 190–310 nm by Orkin and Kasimovskaya [302]; at 210–295 K and 170–290 nm by Gillotay et al. [138]; and at 223–298 K and 200–310 nm by Bilde et al. [33]. The room temperature values are in good agreement within 5–15% at wavelengths below 280 nm, where Gillotay et al. [138], [135] report the lowest, Orkin and Kasimovskaya [302] the highest values. At wavelengths above 280 nm, the data of Bilde et al. [33] become increasingly higher (up to 100% at 310 nm) than those of Orkin and Kasimovskaya [302]. The preferred absorption cross sections, listed in Table 4-81, are the values of Gillotay et al. [138] at 170–188 nm; the mean of the values reported by Gillotay et al. [138] and Orkin and Kasimovskaya [302] at 190–198 nm; the mean of the values reported by the three groups at 200–290 nm; and the mean of the values reported by Orkin and Kasimovskaya [302] and Bilde et al. [33] at 292–310 nm.

The study of the temperature dependence by Gillotay et al. [138] shows an increase of the absorption cross sections in the absorption band between 192 and 238 nm with decreasing temperature 295–210 K and the reverse effect at wavelengths above 238 nm and below 192 nm; the increase in the absorption maximum at ~202 nm is ~0.024×10^{-18} cm^2 $molecule^{-1}$ per 20 K temperature decrease, i.e., an increase by ~10% between 295 and 210 K. Bilde et al. [33] observed a less pronounced temperature behavior in the absorption band (the maximum absorption cross sections agree within 3%) and a decrease of the absorption cross sections with decreasing temperature at wavelengths above 214 nm.

Gillotay and Simon [138] parameterized the cross sections and the temperature dependence of the absorption cross section by the polynomial expansion

$$\log_{10} \sigma(\lambda, T) = \sum A_n \lambda^n + (T - 273) \times \sum B_n \lambda^n$$

and report smoothed values for T = 210, 230, 250, 270, and 295 K, every 2 nm, and at wavelengths corresponding to the wavenumber intervals generally used in stratospheric photodissociation calculations. The parameters A_n and B_n for the ranges 190–290 nm and 210–300 K are as follows:

$A_0 = -127.157358$	$B_0 = -7.959828 \times 10^{-2}$
$A_1 = 1.635435$	$B_1 = 1.978026 \times 10^{-3}$
$A_2 = -9.002683 \times 10^{-3}$	$B_2 = -1.627866 \times 10^{-5}$
$A_3 = 2.190678 \times 10^{-5}$	$B_3 = 5.480744 \times 10^{-8}$
$A_4 = 2.062651 \times 10^{-8}$	$B_4 = -6.480935 \times 10^{-11}$

Table 4-81. Absorption Cross Sections of $CF_3CHClBr$ at 295–298 K

λ (nm)	10^{20} σ (cm^2)	λ (nm)	10^{20} σ (cm^2)	λ (nm)	10^{20} σ (cm^2)
170	702.6	218	78.7	266	0.980
172	614.6	220	71.0	268	0.765
174	496.8	222	63.3	270	0.575
176	379.8	224	56.3	272	0.444
178	281.1	226	49.5	274	0.339
180	206.1	228	43.3	276	0.258
182	153.3	230	37.3	278	0.196
184	118.4	232	32.2	280	0.149
186	97.1	234	27.6	282	0.111
188	86.6	236	23.6	284	0.0818
190	93.4	238	20.0	286	0.0606
192	99.8	240	16.8	288	0.0448
194	107.1	242	14.0	290	0.0331
196	114.3	244	11.7	292	0.0263
198	119.7	246	9.51	294	0.0198
200	121.5	248	7.79	296	0.0147
202	123.0	250	6.38	298	0.0109
204	122.3	252	5.15	300	0.00808
206	119.7	254	4.13	302	0.00583
208	115.1	256	3.31	304	0.00450
210	109.0	258	2.63	306	0.00313
212	102.0	260	2.06	308	0.00235
214	94.6	262	1.61	310	0.00180
216	86.7	264	1.26		

Note: 170–188 nm, Gillotay et al. [138], [135],
190–198 nm, mean of Gillotay et al. [138][135] and Orkin and Kasimovskaya [302],
200–290 nm, mean of Gillotay et al. [138][135], Orkin and Kasimovskaya [302], and Bilde et al. [33],
292–310 nm, mean of Orkin and Kasimovskaya [302] and Bilde et al. [33].

G20. CF_3CHFBr (Halon-2401) + hν → Products. The absorption cross sections of CF_3CHFBr have been measured at 295 K and 190–280 nm by Orkin and Kasimovskaya [302]. Their results are listed in Table 4-82.

Table 4-82. Absorption Cross Sections of CF_3CHFBr at 295 K

λ (nm)	10^{20} σ (cm^2)	λ (nm)	10^{20} σ (cm^2)	λ (nm)	10^{20} σ (cm^2)
190	24.9	222	11.0	254	0.226
192	26.1	224	9.38	256	0.166
194	27.0	226	7.91	258	0.121
196	27.5	228	6.58	260	0.0873
198	27.7	230	5.42	262	0.0628
200	27.4	232	4.42	264	0.0450
202	26.9	234	3.53	266	0.0325
204	26.0	236	2.79	268	0.0235
206	24.8	238	2.19	270	0.0171
208	23.4	240	1.69	272	0.0124
210	21.9	242	1.30	274	0.0093
212	20.2	244	0.991	276	0.0069
214	18.3	246	0.736	278	0.0053
216	16.5	248	0.556	280	0.0040
218	14.6	250	0.416		
220	12.8	252	0.308		

Note: 190–280 nm, Orkin and Kasimovskaya [302].

G21. CF_2BrCF_2Br (Halon-2402) + hν → Products. The absorption cross sections of CF_2BrCF_2Br have been measured at room temperature and 195–320 nm by Molina et al. [272] and at 190–300 nm by Orkin and Kasimovskaya [302]; at 210–295 K and 170–280 nm by Gillotay et al. [138], and at 210–296 K and 190–320 nm by Burkholder et al. [57]. The room temperature data are in very good agreement, in the absorption band at 180–240 nm generally within 10%, in the absorption maximum at ~200 nm within 5%, and in the long-wavelength tail up to 310 nm within 15 %. The preferred absorption cross sections at 295–298 K, listed in Table 4-83, are the values of Gillotay et al. [138] at 170–186 nm; the mean of the values reported by Molina et al. [40], Gillotay et al. [138], Burkholder et al. [57], and Orkin and Kasimovskaya [302] at 196–280 nm; the mean of the values reported by Molina et al. [272], Burkholder et al. [57], and Orkin and Kasimovskaya [302] at 282–300 nm; and the mean of the values reported by Molina et al. [272] and Burkholder et al. [57] at 302–320 nm. In the region around 190 nm, there is some uncertainty, because there is no continuous transition between the absorption curve of Gillotay et al. [138] and that obtained by averaging the data of Gillotay et al. [138], Burkholder et al. [57], and Orkin and Kasimovskaya [302]. We therefore smoothed the absorption curve between 186 and 196 nm and give estimated values for 188, 190, 192, and 194 nm.

The results of the two temperature studies are rather controversial. A regular, but weak decrease of the absorption cross sections at 194–280 nm with decreasing temperature 295 to 210 K and the reverse effect below 194 nm was observed by Gillotay et al. [138]; the decrease in the absorption maximum at ~200 nm is ~0.010×10^{-18} cm^2 $molecule^{-1}$ per 20-K temperature decrease, i.e., a decrease by ~4% between 295 and 210 K. Burkholder et al. [57] observed a strong increase over the whole absorption band (increase of the absorption maximum by 20%) with decreasing temperature 296–210 K, and the reverse effect above 230 nm. So, low-temperature data of these two groups are not comparable Different parameterizations of the temperature dependence of the absorption cross section have been proposed. Gillotay and Simon [350] give the polynomial expansion

$$\log_{10} \sigma(\lambda, T) = \sum A_n \lambda^n + (T - 273) \times \sum B_n \lambda^n$$

and report smoothed values for T = 210, 230, 250, 270, and 295 K, every 2 nm, and at wavelengths corresponding to the wavenumber intervals generally used in stratospheric photodissociation calculations. The parameters A_n and B_n for the ranges 190–290 nm and 210–300 K are as follows:

$A_0 = 34.026000$	$B_0 = 4.010664 \times 10^{-1}$
$A_1 = -1.152616$	$B_1 = -8.358968 \times 10^{-3}$
$A_2 = 8.959798 \times 10^{-3}$	$B_2 = 6.415741 \times 10^{-5}$
$A_3 = -2.9089 \times 10^{-5}$	$B_3 = -2.157554 \times 10^{-7}$
$A_4 = 3.307212 \times 10^{-8}$	$B_4 = 2.691871 \times 10^{-10}$

Burkholder et al. [57] give the expansion

$$\log_{10} \sigma(\lambda, T) = (\sum A_i (\lambda - 242.4015)^i) (1 + (296-T) \sum B_i (\lambda - 242.4015)^i)$$

and report the following parameters A_i and B_i for the ranges 190–320 nm and 210–296 K:

$A_0 = -43.69218$	$B_0 = 3.301341 \times 10^{-5}$
$A_1 = -1.124704 \times 10^{-1}$	$B_1 = 4.695917 \times 10^{-6}$
$A_2 = -1.213301 \times 10^{-3}$	$B_2 = 6.128629 \times 10^{-8}$
$A_3 = 5.275007 \times 10^{-6}$	$B_3 = -5.443107 \times 10^{-10}$
$A_4 = 6.936195 \times 10^{-8}$	$B_4 = -1.035596 \times 10^{-11}$

Quantum yields for Br atom formation in the photodissociation of CF_2BrCF_2Br at 193, 233, and 266 nm, Φ(Br) = 1.9 ± 0.1, 1.9 ± 0.1, and 1.4 ± 0.1, respectively, were measured at room temperature by Zou et al. [453]. These values indicate bond breaking of both C–Br bonds in nearly all the CF_2BrCF_2Br molecules at 193 and 233 nm and in an appreciable fraction of the parent molecules still at 266 nm.

Table 4-83. Absorption Cross Sections of CF_2BrCF_2Br at 296 K

λ (nm)	10^{20} σ (cm^2)	λ (nm)	10^{20} σ (cm^2)	λ (nm)	10^{20} σ (cm^2)
170	50.9	222	59.6	274	0.112
172	56.4	224	52.6	276	0.0813
174	62.3	226	45.9	278	0.0592
176	68.5	228	39.7	280	0.0428
178	75.1	230	33.9	282	0.0300
180	81.8	232	28.8	284	0.0216
182	88.6	234	24.1	286	0.0152
184	95.3	236	19.9	288	0.0109
186	101.8	238	16.4	290	0.00784
188	*107.0*	240	13.2	292	0.00569
190	*112.0*	242	10.6	294	0.00410
192	*116.5*	244	8.45	296	0.00301
194	*120.0*	246	6.68	298	0.00219
196	122.3	248	5.25	300	0.00161
198	123.7	250	4.03	302	0.00124
200	124.3	252	3.12	304	0.00094
202	123.6	254	2.37	306	0.00071
204	120.3	256	1.78	308	0.00054
206	115.9	258	1.34	310	0.00042
208	110.4	260	0.973	312	0.00033
210	104.2	262	0.718	314	0.00026
212	97.4	264	0.529	316	0.00020
214	90.1	266	0.390	318	0.00016
216	82.4	268	0.287	320	0.00014
218	74.8	270	0.211		
220	67.0	272	0.154		

Note: 170–186 nm: Gillotay et al. [138]
188–194 nm: values estimated by smoothing the absorption curve
196–280 nm: mean of Molina et al. [272], Gillotay et al. [138], Burkholder et al. [57], and Orkin and Kasimovskaya [302]
282–300 nm: mean of Molina et al. [272], Burkholder et al. [57], and Orkin and Kasimovskaya [302]
302–320 nm: mean of Molina et al. [272] and Burkholder et al. [57].

G22. CF_3CF_2Br (Halon-2501) + hν → Products. Table 4-84 lists the absorption cross sections of CF_3CF_2Br measured at room temperature and reported at 5-nm intervals by Molina et al. [272]. The results of Zhang et al. [451], who report a plot on a logarithmic scale for measured values at 200–250 nm, are about 30% larger over that wavelength range than the results of Molina et al. [272]. Pence et al. [312] measured the absorption cross sections at 180–400 nm, report a plot of the absorbance (in arbitrary units) and give for 193 nm an absorption cross section smaller by ~40% than that reported by Molina et al. [272].

Broad band flash photolysis of CF_3CF_2Br produced $Br^*(^2P_{1/2})$ atoms with a quantum yield $\Phi(Br^*) = 0.48 \pm 0.02$ as reported by Ebenstein et al. [112]. A quantum yield for $Br^*(^2P_{1/2})$ atom formation at 193 nm, $\Phi(Br^*) = 0.16 \pm 0.08$, was reported by Pence et al. [312].

Table 4-84. Absorption Cross Sections of CF_3CF_2Br at 298 K

λ (nm)	10^{20} σ (cm^2)	λ (nm)	10^{20} σ (cm^2)	λ (nm)	10^{20} σ (cm^2)
190	18.1	230	3.83	270	0.0112
195	18.4	235	2.22	275	0.00505
200	18.1	240	1.20	280	0.00218
205	16.9	245	0.620	285	0.00100
210	14.8	250	0.305	290	0.00045
215	12.0	255	0.135	295	0.00020
220	8.94	260	0.0590	300	0.00009
225	6.13	265	0.0260		

Note: 190–300 nm, Molina et al. [272].

H1. $CH_3I + h\nu \rightarrow CH_3 + I(^2P_{3/2})$.

H2. $CH_3I + h\nu \rightarrow CH_3 + I^*(^2P_{1/2})$.

The absorption cross sections of CH_3I have been measured at room temperature and 147 nm by Rebbert et al. [334], at 200–360 nm by Porret and Goodeve [317], at 200–310 nm by Baughcum and Leone [29], at 180–400 nm by Pence et al. [312]; at 257.7 nm by Felps et al. [119], at 205–335 nm by Jenkin et al. [182], at 205–360 nm by Man et al. [230], and at 192–225 nm by Kwok and Phillips [208], who also measured the CH_3I spectrum in cyclohexane solution. Measurements were also carried out at 223–333 K and 160–330 nm by Fahr et al. [116]; at 243–333 K and 235–365 nm by Rattigan et al. [325]; and at 210–298 K and 200–350 nm by Roehl et al. [343]. Fahr et al. [116] also measured the absorption cross sections at 330–400 nm for the liquid phase and used a wavelength-shift procedure to convert them into gas-phase values. The room temperature data for the absorption band at 210–305 nm are in reasonable to good agreement, whereby Rattigan et al. [325] report the lowest values and Fahr et al. [116] the highest values over the whole absorption band. The agreement generally is better than 15% except for the region around the absorption maximum where the spread is ~30%: Rattigan et al. [325] and Fahr et al. [116] report values of 1.07×10^{-18} cm^2 and 1.4×10^{-18} cm^2, respectively, for the maximum at ~260 nm, and the rest of the data ranges between 1.15×10^{-18} cm^2 and 1.22×10^{-18} cm^2. At wavelengths 305–330 nm, the agreement is still within 20%. At wavelengths below 210 nm, the few data points reported by Jenkin et al. [182] and Roehl et al. [343] and the absorption curve reported by Kwok and Phillips [209] obviously fit into the strong and highly structured band system observed by Fahr et al. [116] between 160 and 205 nm. The preferred room temperature absorption cross sections for the wavelength range above 210 nm, listed in Table 4-85, are the mean of the values reported by Jenkin et al. [182], Fahr et al. [116], and Roehl et al. [343] at 210–230 nm; the mean of the values reported by Jenkin et al. [182], Fahr et al. [116], Rattigan et al. [325], and Roehl et al. [343] at 235–330 nm; the mean of the values reported by Fahr et al. [116], Rattigan et al. [325], and Roehl et al. [343] at 335–350 nm; and the values of Rattigan et al. [325] at 355–365 nm. The data of Man et al. [230] are given only as a plot in their paper and have therefore not been included in the evaluation.

The three temperature studies are in qualitative agreement. An increase of the absorption cross sections in the absorption band at 210–270 nm with decreasing temperature 333–210 K has been observed. Very small temperature effects are reported by Rattigan et al. [325] for the temperature range 243–333 K, and by Fahr et al. [116] and Roehl et al. [343] for the range between room temperature and ~240–250 K and at 313–333 K. At wavelengths above 270 nm and below 210 nm, the absorption cross sections decrease with decreasing temperature. The low temperature absorption spectra observed by the three groups differ in the same manner as their room temperature spectra, i.e., Fahr et al. [116] report the highest and Rattigan et al. [325] the lowest values for the absorption band.

A simple analytical expression for the temperature dependence,

$$\sigma(\lambda, T) = \sigma(298\ K)\ (1 + a_1(T–298) + a_2(T–298)^2)$$

and the fitting parameters $a_1(\lambda)$ and $a_2(\lambda)$ for λ = 200–350 nm and T = 210– 298 K give Roehl et al. [343]. Another simple parameterization, $\ln \sigma(\lambda, T) = \ln \sigma(\lambda, 298\ K) + B(T–298)$, and parameters $B(\lambda)$ for λ = 235–355 nm and T = 243–333 K report Rattigan et al. [325]. The parameters a_1, a_2, and B are listed also in Table 4-85.

Quantum yields for $I^*(^2P_{1/2})$ atom formation in the photolysis of CH_3I at several wavelengths between 222 and 333.5 nm have been reported: $\Phi(I^*) = 0.63 \pm 0.02$, 0.79 ± 0.02, 0.69 ± 0.02, and 0.43 ± 0.02 at 222, 266, 280,

and ~305 nm by Uma and Das [410], [411], [412]; $\Phi(I^*) = 0.72 \pm 0.08$ at 248 nm by Gedanken [412], $\Phi(I^*) = 0.81 \pm 0.03$ and ~ 0.05 at 248 and 308 nm by Pence et al. [312], $\Phi(I^*) = 0.30$ at 304 nm by Kang et al. [198]; and $\Phi(I^*) = 0.47$, 0.77, and 0.92 at 325.8, 329.4, and 333.5 nm by Ogorzalek Loo et al. [298]. The latter authors report also quantum yields for CD_3I:

$\Phi(I^*)$:	0.66	0.59	0.83	0.91	0.90	0.57	0.80	0.92	>0.95	0.61	0.84
λ, nm:	312.6	314.4	317.0	319.8	322.9	324.5	327.8	330.5	333.8	336.2	339.3 3

Brewer et al. [42] report $\Phi(I^*) = 0.75 \pm 0.02$ at 248 nm for CD_3I.

Quantum yields for $I(^2P_{3/2})$ atom formation, $\Phi(I)$, can be derived from $\Phi(I) = 1 - \Phi(I^*)$.

Table 4-85. Absorption Cross Sections of CH_3I at 296–298 K and Temperature Coefficients

λ (nm)	$10^{20}\,\sigma$ (cm^2)	$10^3\,a_1(K^{-1})$	$10^5\,a_2(K^{-2})$	$10^3\,B(K^{-1})$	λ (nm)	$10^{20}\,\sigma$ (cm^2)	$10^3\,a_1(K^{-1})$	$10^5\,a_2(K^{-2})$	$10^3\,B(K^{-1})$
210	3.62	3.07	2.42		290	8.04	6.14	2.57	4.98
215	5.08	2.61	2.28		295	4.00	7.27	2.91	6.38
220	6.90	1.06	1.22		300	2.06	7.82	3.53	6.97
225	9.11	1.74	1.96		305	1.10	7.82	3.85	6.84
230	12.6	1.47	1.67		310	0.621	7.37	3.71	6.78
235	20.5	1.91	2.04	0.67	315	0.359	6.98	3.47	6.75
240	38.1	1.74	2.06	0.61	320	0.221	7.39	3.54	6.53
245	65.6	1.52	2.15	0.34	325	0.126	7.23	2.82	6.79
250	96.3	1.20	2.11	0.08	330	0.0684	8.93	3.74	7.82
255	117.7	0.890	1.95	–0.10	335	0.0388	10.88	4.88	9.34
260	119.7	0.882	1.93	–0.12	340	0.0212	11.30	4.46	10.95
265	102.9	1.21	2.00	0.10	345	0.0114	15.68	8.44	13.58
270	75.9	1.77	2.11	0.54	350	0.00609	15.94	8.22	16.83
275	49.6	2.52	2.12	1.33	355	0.00320			18.91
280	29.2	3.62	2.24	2.43	360	0.00190			17.28
285	15.6	4.84	2.38	3.74	365	0.00090			23.63

Note: Absorption cross sections σ: 210–230 nm: mean of Jenkin et al. [182], Fahr et al. [116], and Roehl et al. [343],
235–330 nm: mean of Jenkin et al. [182], Fahr et al. [116], Rattigan et al. [325], and Roehl et al. [343],
335–350 nm: mean of Fahr et al. [116], Rattigan et al. [325], and Roehl et al. [343],
355–365 nm: Rattigan et al. [325].
Temperature coefficients a_1 and a_2: 210–298 K, Roehl et al. [343]:
$(\sigma(\lambda, T) = \sigma(298\text{ K})\,[1 + a_1(T–298) + a_2(T–298)^2])$,
Temperature coefficients B: 243–333 K, Rattigan et al. [325] ($\ln \sigma(\lambda, T) = \ln \sigma(\lambda, 298\text{ K}) + B(T–298)$).

H3. $CH_2I_2 + h\nu \rightarrow CH_2I + I(^2P_{3/2})$.

H4. $CH_2I_2 + h\nu \rightarrow CH_2I + I^*(^2P_{1/2})$.

The absorption cross sections of CH_2I_2 have been measured at room temperature and 180–400 nm by Pence et al. [312], at 220–360 nm by Schmitt and Comes [365], at 200–360 nm by Baughcum and Leone [29], at 265–341 nm by Koffend and Leone [205]; and at 220–400 nm by Kwok and Phillips [207], who measured the spectrum also in methanol and cyclohexane. Measurements at 273 and 298 K and 205–380 nm have also been carried out by Roehl et al. [343]; and at 273, 298, and 348 K and 215–385 nm by Mössinger et al. [283]. There are absorption maxima at or below 215 nm, and around 250 and 290 nm. The room temperature data of the various teams (except those of Kwok and Phillips [207], which are presented only as a plot) are in very good agreement, i.e., generally within 5–10% between 230 and 380 nm, were the older data of Schmitt and Comes [365] and Koffend and Leone [205] for the prominent absorption band around 290 nm are higher than those of Roehl et al. [343] and Mössinger et al. [283]. The values of Kwok and Phillips [207] for the prominent absorption band around 290 nm are lower by 15–20% than the rest of the data. The preferred room temperature absorption cross sections, listed in Table 4-86, are the values of Roehl et al. [343] at 205–215 nm, the mean of

the values reported by Roehl et al. [343] and Mössinger et al. [283] at 220–380 nm, which are very close, and the value of Mössinger et al. [283] at 385 nm.

Both temperature studies show, that decreasing the temperature from 298 or 348 K to 273 K causes a slight increase of the absorption cross sections between 275 and 300 nm (~2% in the maximum at 290 nm between 298 and 273 K) and a slight decrease outside this wavelength region. A simple empirical relation for the temperature dependence between 273 and 348 K, $\ln \sigma(\lambda, T) = \ln \sigma(\lambda, 298K) + B(\lambda)\cdot(T–298)$, and temperature coefficients $B(\lambda)$ for λ = 205–375 nm at 5-nm intervals are given by Mössinger et al. [283]. The temperature coefficients B are also listed in Table 4-86 (an erroneous B value at 305 nm has been corrected by Dr. Mössinger via a personal communication).

Quantum yields for $I^*(^2P_{1/2})$ atom formation in the photolysis of CH_2I_2 at 193, 248, and 308 nm, $\Phi(I^*)$ = ~0.05, 0.46 ± 0.04, and 0.25 ± 0.02, respectively, have been reported by Pence et al. [312]. Quantum yields for $I(^2P_{3/2})$ atom formation, $\Phi(I)$, can be derived from $\Phi(I) = 1 – \Phi(I^*)$.

Table 4-86. Absorption Cross Sections of CH_2I_2 at 298 K

λ (nm)	$10^{20}\ \sigma$ (cm^2)	10^3 B (K^{-1})	λ (nm)	$10^{20}\ \sigma$ (cm^2)	10^3 B (K^{-1})
205	407.0		300	357.0	–0.37
210	404.0		305	338.5	–0.16
215	366.0	0.15	310	313.5	0.07
220	260.0	0.14	315	280.0	0.15
225	197.5	0.19	320	244.0	0.27
230	133.0	0.51	325	203.0	0.27
235	109.0	0.56	330	161.5	0.51
240	122.5	0.15	335	120.5	0.55
245	150.0	0.18	340	83.3	1.36
250	157.0	0.67	345	53.7	1.99
255	139.5	1.58	350	32.6	3.19
260	120.5	2.04	355	19.2	4.09
265	130.0	1.30	360	10.9	5.39
270	178.5	0.00	365	6.05	6.77
275	255.0	–0.71	370	3.45	8.25
280	328.5	–1.24	375	1.93	11.3
285	371.5	–1.21	380	1.17	
290	380.5	–0.94	385	0.769	
295	371.5	–0.58			

Note:
Absorption cross sections σ: 205–215 nm, Roehl et al. [343], 220–380 nm, mean of Roehl et al. [343] and Mössinger et al. [283], 385 nm, Mössinger et al. [283].
Temperature coefficients B: 273–348 K, Mössinger et al. [283] ($\ln \sigma(\lambda, T) = \ln \sigma(\lambda, 298\ K) + B(T–298)$).

H5. $C_2H_5I + h\nu \rightarrow C_2H_5 + I(^2P_{3/2})$.

H6. $C_2H_5I + h\nu \rightarrow C_2H_5 + I^*(^2P_{1/2})$.

The absorption cross sections of C_2H_5I have been measured at room temperature and 147 nm ($\sigma = 1.48 \times 10^{-17}$ cm^2) by Rebbert et al. [334], at 205–360 nm by Porret and Goodeve [318]; at 223–298 K and 205–365 nm by Roehl et al. [343], at 243–333 K and 235–355 nm by Rattigan et al. [325], and at 323 K and 220–320 nm by Zhang et al. [451]. The room temperature data are in good agreement, the values of Roehl et al.[343] are higher by 5–15% at 235–325 nm and become increasingly higher up to 125% at 355 nm than the values of Rattigan et al. [325]. The latter authors found their data to agree within 10–15% with the plotted values of Porret and Goodeve [318]. The preferred absorption cross sections, listed in Table 4-87, are the mean of the values reported by Roehl et al. [343] and Rattigan et al. [325] in the common wavelength range 235–355 nm, and the data of Roehl et al. [343] at 215–230 nm.

The temperature studies of Roehl et al. [343] and Rattigan et al. [325] show, that decreasing the temperature in the range 333–223 K causes an increase of the absorption cross section in the absorption band at ~230–270 nm and a decrease at longer wavelengths. The differences between the low-temperature data of the two groups are

comparable with those between the room temperature data. The data for 323 K, reported by Zhang et al. [451] as a plot on a logarithmic scale, are larger by 10–40% around the absorption maximum and up to more than 200% in the long-wavelength tail than the data for 313 and 333 K reported by Rattigan et al. [325]. A simple analytical expression for the temperature dependence, $\sigma(\lambda, T) = \sigma(298\ K)\ [1 + a_1(T–298) + a_2(T–298)^2]$, and the fitting parameters $a_1(\lambda)$ and $a_2(\lambda)$ for λ = 205–365 nm and T = 223–298 K give Roehl et al. [343]. Another simple parameterization, $\ln \sigma(\lambda, T) = \ln \sigma(\lambda, 298\ K) + B(T–298)$, and parameters $B(\lambda)$ for λ = 235–355 nm and T = 243–333 K is reported by Rattigan et al. [325]. The parameters a_1, a_2, and B are listed also in Table 4-87.

Quantum yields for $I^*(^2P_{1/2})$ atom formation in the photolysis of C_2H_5I at a few wavelengths between 222 and 305 nm have been reported: $\Phi(I^*) = 0.57 \pm 0.02$, 0.72 (or 0.73) ± 0.02, 060 ± 0.02, and 0.39 ± 0.02 at 222, 266, 280, and ~305 nm by Uma and Das [410], [411], [412]; $\Phi(I^*) = 0.78 \pm 0.07$ at 248 nm by Gedanken [130]; $\Phi(I^*) = 0.68 \pm 0.02$ at 248 nm by Brewer et al. [42], $\Phi(I^*) = 0.22$ at 304 nm by Kang et al. [198]. Quantum yields for $I(^2P_{3/2})$ atom formation, $\Phi(I)$, can be derived from $\Phi(I) = 1 – \Phi(I^*)$.

At 147 nm, the overall process $C_2H_5I + h\nu \rightarrow C_2H_4 + H + I$ was observed with a quantum yield of 0.75 by Rebbert et al. [334].

Table 4-87. Absorption Cross Sections of C_2H_5I at 298 K and Temperature Coefficients

λ (nm)	$10^{20}\ \sigma$ (cm^2)	$10^3\ a_1(K^{-1})$	$10^5\ a_2(K^{-2})$	$10^3\ B(K^{-1})$	λ (nm)	$10^{20}\ \sigma$ (cm^2)	$10^3\ a_1(K^{-1})$	$10^5\ a_2(K^{-2})$	$10^3\ B(K^{-1})$
205	11.9	6.38	3.15		285	19.1	3.85	0.926	3.61
210	4.22	4.07	6.28		290	10.3	5.47	1.65	4.83
215	4.56	4.93	6.75		295	5.38	7.00	2.52	6.33
220	6.18	4.06	5.70		300	2.78	8.56	4.11	7.48
225	9.09	2.81	3.81		305	1.44	9.31	4.89	8.08
230	14.3	2.62	3.83		310	0.777	10.56	6.87	7.55
235	23.2	1.28	2.17	–0.27	315	0.416	10.83	6.81	7.92
240	41.7	0.876	1.96	–0.40	320	0.227	11.98	9.76	8.27
245	69.3	0.233	1.62	–0.62	325	0.127	12.98	11.3	8.81
250	99.3	–0.111	1.58	–0.79	330	0.0743	14.56	17.5	9.30
255	119.7	–1.03	0.606	–0.82	335	0.0403	18.81	24.6	10.20
260	121.8	–1.48	–0.0332	–0.75	340	0.0246	13.90	9.08	11.16
265	105.9	–1.09	1.2×10^{-6}	–0.44	345	0.0133	18.86	22.1	12.41
270	80.6	–0.538	–0.257	0.36	350	0.00840	20.19	20.1	11.28
275	54.4	0.770	0.0299	1.23	355	0.00488	–7.04	–40.5	12.20
280	33.5	2.01	0.110	2.36					

Note: Absorption cross sections σ: 205–230 nm, Roehl et al. [343],
235–355 nm, mean of Roehl et al. [343] and Rattigan et al. [325].
Temperature coefficients a_1 and a_2: 223–298 K, Roehl et al. [343]
($\sigma(\lambda, T) = \sigma(298\ K)\ [1 + a_1(T–298) + a_2(T–298)^2]$),
Temperature coefficients B: 243–333 K, Rattigan et al. [325]
($\ln \sigma(\lambda, T) = \ln \sigma(\lambda, 298\ K) + B(T–298)$).

H7. $CH_3CHI_2 + h\nu \rightarrow$ Products. The absorption cross sections of CH_3CHI_2 have been measured at 298 K and 220–360 nm by Schmitt and Comes [365]. Their data are listed in Table 4-88.

Table 4-88. Absorption Cross Sections of CH_3CHI_2 at 298 K

λ (nm)	10^{20} σ (cm^2)	λ (nm)	10^{20} σ (cm^2)	λ (nm)	10^{20} σ (cm^2)
220	304	270	183	320	222
225	240	275	243	325	201
230	181	280	304	330	175
235	144	285	352	335	138
240	138	290	374	340	107
245	151	295	366	345	75.7
250	157	300	339	350	49.3
255	143	305	305	355	31.7
260	133	310	273	360	19.1
265	145	315	247		

Note: 220–360 nm, Schmitt and Comes [365].

H8. $CH_3CH_2CH_2I + h\nu \rightarrow$ Products.

H9. $CH_3CHICH_3 + h\nu \rightarrow$ Products.

The absorption cross sections of 1-C_3H_7I have been measured at 223–298 K and 205–335 nm, those of 2-C_3H_7I at 223–298 K and 205–380 nm by Roehl et al. [343]. The absorption cross sections of 2-C_3H_7I in the gas phase and in cyclohexane solution have also been measured at room temperature and 235–305 nm by Phillips et al. [315]. The gas-phase data reported by Phillips et al. [315] and given as a plot in their paper are larger by 30–70% over the whole absorption band than the data of Roehl et al. [343]. Room temperature values at 147 nm for 1-C_3H_7I and 2-C_3H_7I have been reported by Rebbert et al. [334].].The recommended room temperature values for 1-C_3H_7I and 2-C_3H_7I, listed in Table 4-89, are taken from the paper of Roehl et al. [343].

Decreasing the temperature in the range 298–223 K causes an increase of the absorption cross sections around the absorption maximum, at 245–265 nm for 1-C_3H_7I and at 240–270 nm for 2-C_3H_7I, and a decrease in the long-wavelength tail. Decrease of the absorption cross sections with decreasing temperature generally has been observed in the short-wavelength tail of the absorption band except for slight increases between 273 and 248 K in the case of 1-C_3H_7I and between 248 and 223 K in the case of 2-C_3H_7I. At wavelengths below the minimum (~210 nm), the absorption cross sections decrease with decreasing temperature between 298 and 223 K. The temperature dependence has been parameterized by the analytical expression

$$\sigma(\lambda, T) = \sigma(298\ K)\ [1 + a_1(T–298) + a_2(T–298)^2]$$

and the fitting parameters $a_1(\lambda)$ and $a_2(\lambda)$ for T = 223–298 K and λ = 205–335 nm (1-C_3H_7I) and λ = 205–380 nm (2-C_3H_7I) are reported by Roehl et al. [343]. These are listed also in Table 4-89.

Quantum yields for $I^*(^2P_{1/2})$ atom formation in the photolysis of C_3H_7I at a few wavelengths have been reported: Φ(I*) = 0.54 ± 0.02, 0.66 ± 002, 0.56 ± 0.02, and 0.35 ± 0.02 at 222, 266, 280, and ~305 nm by Uma and Das [410], [412]; Φ(I*) = 0.60 ± 0.02 at 248 nm by Brewer et al. [42], Φ(I*) = 0.20 at 304 nm by Kang et al. [198] for 1-C_3H_7I; Φ(I*) = 0.40 ± 0.02, 0.44 ± 0.03, and 0.19 ± 0.02 at 222, 266, and ~305 nm by Uma and Das [411], and Φ(I*) = 0.26 ± 0.02 at 248 nm by Brewer et al. [42] for 2-C_3H_7I. Quantum yields for $I(^2P_{3/2})$ atom formation, Φ(I), can be derived from Φ(I) = 1 – Φ(I*).

At 147 nm, Rebbert et al. [334] observed the main overall processes 1-$C_3H_7I + h\nu \rightarrow C_3H_6 + H + I$ and

1-$C_3H_7I + h\nu \rightarrow CH_3 + C_2H_4 + I$ with quantum yields 0.38 and 0.47 and the processes

2-$C_3H_7I + h\nu \rightarrow C_3H_6 + H + I$ and 2-$C_3H_7I + h\nu \rightarrow CH_3 + C_2H_4 + I$ with quantum yields 0.80 and 0.07.

Table 4-89. Absorption Cross Sections of C_3H_7I at 298 K and Temperature Coefficients

λ (nm)	1-C_3H_7I			2-C_3H_7I		
	10^{20} σ (cm^2)	10^3 a_1 (K^{-1})	10^5 a_2 (K^{-2})	10^{20} σ (cm^2)	10^3 a_1 (K^{-1})	10^5 a_2 (K^{-2})
205	15.6	7.60	4.37	44.9	15.14	8.46
210	5.05	0.283	1.57	4.53	7.84	7.23
215	5.14	–1.49	–2.46	3.57	4.96	5.08
220	6.84	–1.59	–2.97	4.20	1.55	1.27
225	10.4	–0.891	–2.14	6.45	2.21	1.99
230	17.7	–0.375	–1.26	11.0	1.60	1.80
235	32.8	–0.311	–1.04	20.4	0.480	0.681
240	58.1	–0.611	–0.804	38.2	–0.333	0.121
245	91.9	–0.949	–0.609	66.7	–0.680	0.0947
250	124	–1.22	–0.611	102	–0.795	0.289
255	141	–1.55	–0.776	133	–0.966	0.570
260	136	–1.44	–0.867	148	–1.14	0.512
265	113	–1.02	–1.04	143	–0.589	0.824
270	82.2	–0.306	–1.16	120	–0.439,	0.281
275	53.4	0.524	–1.50	90.2	0.792	0.873
280	32.0	1.68	–1.66	61.4	1.65	0.466
285	18.1	3.08	–1.44	38.6	2.88	0.534
290	9.96	5.56	0.812	22.6	4.13	0.559
295	5.42	6.76	2.05	12.8	5.71	1.04
300	2.96	7.16	2.90,	6.94	7.20	1.93
305	1.63	6.90	3.20	3.73	8.19	2.33
310	0.945	7.10	4.01	2.04	8.75	2.81
315	0.532	5.59	2.78	1.09	8.49	2.25
320	0.301	3.68	0.0140	0.627	10.79	4.36
325	0.177	4.23	0.0238	0.348	9.54	2.76
330	0.110	11.40	12.3	0.202	10.99	5.94
335	0.0627	15.76	25.8	0.115	12.37	7.58
340				0.0688	13.69	12.2
345				0.0402	16.32	17.1
350				0.0253	18.50	24.7
355				0.0150	19.41	24.3
360				0.0105	18.61	13.9
365				0.00666	29.85	50.9
370				0.00479	37.24	76.8
375				0.00535	36.71	80.7
380				0.00530	22.00	40.0

Note: Absorption cross sections σ: 205–380 nm, Roehl et al. [343],
Temperature coefficients a_1 and a_2: 223–298 K, Roehl et al. [343]
($\sigma(\lambda, T) = \sigma(298\ K)\ [1 + a_1(T–298) + a_2(T–298)^2]$).

H10. $C_4H_9I + h\nu \rightarrow C_4H_9 + I(^2P_{3/2})$.

H11. $C_4H_9I + h\nu \rightarrow C_4H_9 + I^*(^2P_{1/2})$.

H12. $(CH_3)_2CHCH_2I + h\nu \rightarrow (CH_3)_2CCH_2 + I(^2P_{3/2})$.

H13. $(CH_3)_2CHCH_2I + h\nu \rightarrow (CH_3)_2CCH_2 + I^*(^2P_{1/2})$.

H14. $(CH_3)_3CI + \rightarrow (CH_3)_3C + I(^2P_{3/2})$.

H15. $(CH_3)_3CI + \rightarrow (CH_3)_3C + I^*(^2P_{1/2})$.

Absorption cross sections for *n*- and *iso*-C_4H_9I are not available. Absorption cross sections of *tert*-C_4H_9I have been measured at 323 K by Phillips et al. [315]. An absorptions band between 230 and 310 nm exhibits a maximum of ~2.1×10^{-18} cm^2 at ~268 nm. Estimated values at 5-nm intervals, read from a logarithmic plot, are presented in Table 4-90.

Quantum yields for $I^*(^2P_{1/2})$ atom formation in the photolysis of *n*-C_4H_9I at several wavelengths between 222 and 305 nm have been reported: $\Phi(I^*) = 0.51 \pm 0.02$, 0.64 ± 0.03, 0.50 ± 0.03, and 0.30 ± 0.02 at 222, 266, 280, and ~305 nm by Uma and Das [410], [412]; $\Phi(I^*) = 0.53 \pm 0.03$ at 248 nm by Brewer et al. [42], $\Phi(I^*) = 0.14$ at 304 nm by Kang et al. [198].

Quantum yields for $I^*(^2P_{1/2})$ atom formation in the photolysis of i*so*-C_4H_9I, $\Phi(I^*) = 0.71 \pm 0.01$, 0.56 ± 0.03, and 0.35 ± 0.02 at 266, 280, and ~305 nm, have been reported by Uma and Das [412], $\Phi(I^*) = 0.20 \pm 0.02$ at 248 nm by Brewer et al. [42].

Quantum yields for I atom formation in the photolysis of *tert*-C_4H_9I, $\Phi(I(^2P_{3/2})+I^*(^2P_{1/2})) = 0.93$ and 0.92 at 277 and 304 nm, have been reported by Kim et al. [201]. Quantum yields for $I^*(^2P_{1/2})$ atom formation, $\Phi(I^*(^2P_{1/2})) = 0.33 \pm 0.03$, 0.20 ± 0.03, and 0.12 ± 0.03, in the photolysis at 222, 266, and ~305 nm, have been reported by Uma and Das [411], $I^*(^2P_{1/2}) = 0.41 \pm 0.10$ and 0.03 ± 0.02 at 248 nm by Gedanken [412] and Brewer et al. [42], respectively.

Table 4-90. Absorption Cross Sections of $(CH_3)_3CI$ at 298 K

λ (nm)	10^{20} σ (cm^2)	λ (nm)	10^{20} σ (cm^2)	λ (nm)	10^{20} σ (cm^2)
235	*28.5*	*265*	*209*	*295*	*54.0*
240	*42.5*	*270*	*211*	*300*	*34.0*
245	*64.8*	*275*	*186*	*305*	*21.5*
250	*98.0*	*280*	*150*	*310*	*14.0*
255	*140*	*285*	*116*		
260	*180*	*290*	*83.0*		

Note: 235–310 nm, Phillips et al. [315], estimated from logarithmic plot.

H16. $C_5H_{11}I + h\nu \rightarrow C_5H_{11} + I(^2P_{3/2})$.

H17. $C_5H_{11}I + h\nu \rightarrow C_5H_{11} + I^*(^2P_{1/2})$.

Absorption cross sections for *n*-$C_5H_{11}I$ are not available. A quantum yield for $I^*(^2P_{1/2})$ atom formation in the photolysis of *n*-$C_5H_{11}I$ at 222 nm, $\Phi(I^*) = 0.50 \pm 0.03$, has been measured by Uma and Das [410].

H18. $CF_3I + h\nu \rightarrow CF_3 + I(^2P_{3/2})$

H19. $CF_3I + h\nu \rightarrow CF_3 + I^*(^2P_{1/2})$

The absorption cross sections of CF_3I have been measured at room temperature and 170–230 nm by Roxlo and Mandl [350]; at room temperature and in shock waves at 625 and 1050 K and 220–360 nm by Brouwer and Troe [45]; at 200–298 K and 216–370 nm by Solomon et al. [385]; at 218–333 K and 160–350 nm by Fahr et al. [115]; and at 243–333 K and 235–390 nm by Rattigan et al. [325]. Measurements in the long-wavelength tail of the absorption band up to 455 nm and at temperatures up to ~4000 K were also carried out with hot molecules excited by IR laser pulses by Bagratashvili et al. [18] and Abel et al. [2][3].

There is good agreement between the room temperature values above 200 nm, i.e., better than 20% around the absorption maximum at 265–270 nm and better than 15% below 255 nm and at 280–350 nm. Fahr et al. [115] report the highest absorption maximum of 7×10^{-19} cm^2, compared to 6.4×10^{-19}, 6.2×10^{-19}, and 5.9×10^{-19} cm^2 reported by Solomon et al. [385], Brouwer and Troe [45], and Rattigan et al. [325], respectively. The long-wavelength data of Solomon et al. [385] become increasingly higher by up to ~70% than those of Rattigan et al. [325]. The preferred absorption cross sections, listed in Table 4-91, are the data of Fahr et al. [115] at 180–215 nm; the mean of the values reported by Brouwer and Troe [45], Solomon et al. [385], and Fahr et al. [115] at 220–230 nm; the mean of the values reported by Brouwer and Troe [45], Solomon et al. [385], Fahr et al. [115], and Rattigan et al. [325] at 235–310 nm; the mean of the values reported by Solomon et al. [385], Fahr et al. [115], and Rattigan et al. [325] at 315–350 nm; and the values of Rattigan et al. [325] at 355–385 nm.

Fahr et al. [115] observed in the short-wavelength region a band centered at about 171 nm with cross sections up to 3.6×10^{-17} cm^2, which shows vibrational structure, and a band with a maximum approaching values of 10^{-16} cm^2 at or below 160 nm. The plotted spectrum at 170–230 nm reported by Roxlo and Mandl [350] is not in agreement with the results of Fahr et al. [115].

The temperature studies of Solomon et al. [385], Fahr et al. [115], and Rattigan et al. [325] agree in the observation, that the absorption cross sections increase in the region of the maximum (~240–280 nm) with decreasing temperature from 333 K or room temperature down to temperatures of 240–250 K; the ratios σ(298 K)/σ(~240 K) and σ(333 K)/σ(~240 K) around the maximum are ~0.9, the ratios σ(333 K)/σ(298 K) are ~1. Solomon et al. [385] observed a further increase of the cross sections down to 200 K, whereas Fahr at al. [115] observed a slight decrease between 253 and 218 K. A decrease of the absorption cross sections above 280 nm and between 333 and 200 K was observed by the three groups; the ratios σ(298 K)/σ(~240 K) increase from ~1.0 to ~1.9 at 280–340 nm, the ratios σ(333 K)/σ(298 K) are around 1.3. Thus, the temperature dependences reported by the three groups are compatible at least in the range 240–333 K.

Solomon et al. [385] and Rattigan et al. [325] fitted their spectra to the expression

$$\ln \sigma(\lambda, T) = \ln \sigma(\lambda, 298\ K) + B(T–298)$$

and report the temperature coefficients B(λ) for T = 200–298 K and λ = 216–344 nm (at 2-nm intervals) and for T = 243–333 K and λ = 235–390 nm (at 5-nm intervals), respectively. The temperature coefficients B reported by Solomon et al. [385] are nearly constantly larger by $\sim 0.8 \times 10^{-3}$ than those of Rattigan et al. [325] at 235–300 nm and become smaller by up to 1.75×10^{-3} between 315 and 345 nm. The B values reported by Rattigan et al. [325] for the ranges 235–385 nm and 243–333 K are listed also in Table 4-91.

Fahr et al. [115] gave fits for the long-wavelength tail using the expressions $\sigma(\lambda) = \sigma_0(\lambda) \exp(-L/\lambda)$ for $\lambda > 320$ nm and $\sigma(T) = \sigma_0(T) \exp(-\theta/T)$ and reported values for the parameters $\sigma_0(\lambda)$ and L at T = 218, 235, 253, 273, 295, and 333 K and for $\sigma_0(T)$ and θ at 300, 310, 320, 330, 340, and 350 nm.

In the short-wavelength region at 160–180 nm, a decrease of the absorption cross sections with decreasing temperature 333–218 K has been observed by Fahr et al. [115].

Since CF_3I serves as model system for studying the dynamics of $I^*(^2P_{1/2})$ atom production by UV photolysis, there is a great number of studies which measure $I^*(^2P_{1/2})/I(^2P_{3/2})$ branching ratios and $I^*(^2P_{1/2})$ quantum yields from CF_3I photolysis in the wavelength region of the absorption band. The following quantum yields were reported for the range between 248 and 308 nm:

$\Phi(I^*) = 0.89 \pm 0.01$, 0.87 ± 0.04, and 0.88 at 248 nm by Brewer et al. [42], Gedanken et al. [130], and Felder [117], respectively;

$\Phi(I^*) = 0.89 \pm 0.05$, 0.79 ± 0.03 and 0.63 ± 0.02 at 266, 280, and ~305 nm by Kavita and Das [199];

$\Phi(I^*) = 0.87$ at 277 nm by Kim et al. [200]; $\Phi(I^*) = 0.69$ at 304 nm by Kang et al. [198];

$\Phi(I^*) = 0.21$ at 308 nm by Felder [118], and

$\Phi(I^*)$ =	0.99 ± 0.01	0.91 ± 0.01	0.89 ± 0.01	0.84 ± 0.01	0.81 ± 0.01	0.69 ± 0.01
λ (nm)=	275	279	283	290	293	295
$\Phi(I^*)$ =	0.68 ± 0.01	0.63 ±0.02	0.61 ± 0.02	0.47 ± 0.01	0.41 ± 0.0	0.37 ± 0.01
λ (nm)=	296	297	298	300	302	303

by Furlan et al. [127].

Quantum yields for $I(^2P_{3/2})$ atom formation, $\Phi(I)$, can be derived from $\Phi(I) = 1 - \Phi(I^*)$

Table 4-91. Absorption Cross Sections of CF_3I at 295–300 K

λ (nm)	10^{20} σ (cm^2)	10^3 B (K^{-1})	λ (nm)	10^{20} σ (cm^2)	10^3 B (K^{-1})
180	3.11		285	33.4	0.55
185	0.75		290	22.7	1.65
190	0.28		295	14.3	2.98
195	0.16		300	8.60	4.22
200	0.15		305	5.06	5.61
205	0.19		310	2.82	6.84
210	0.34		315	1.62	7.68
215	0.68		320	0.905	8.27
220	1.52		325	0.485	8.74
225	2.88		330	0.262	9.25
230	5.03		335	0.142	9.92
235	8.21	0.16	340	0.0750	10.27
240	13.6	–0.16	345	0.0407	11.71
245	21.8	–0.52	350	0.0210	12.85
250	32.4	–0.86	355	0.0115	13.26
255	45.2	–1.17	360	0.0064	14.65
260	56.9	–1.37	365	0.0036	14.63
265	63.4	–1.43	370	0.002	15.49
270	63.1	–1.30	375	0.0011	17.14
275	56.1	–0.94	380	0.0007	17.66
280	45.1	–0.62	385	0.0004	19.71

Note: Absorption cross sections σ: 180–215 nm: Fahr et al. [115]
220–230 nm: mean of Brouwer and Troe [45], Solomon et al. [385], and Fahr et al.[115]
235–310 nm: mean of Brouwer and Troe [45], Solomon et al. [385], Fahr et al. [115],and Rattigan et al. [325]
315–350 nm: mean of Solomon et al. [385], Fahr et al. [115], and Rattigan et al. [325]
355–385 nm: Rattigan et al. [325].
Temperature coefficients B: 243–333 K, Rattigan et al. [325] ($\ln \sigma(\lambda, T) = \ln \sigma(\lambda, 298\ K) + B(T–298)$).

H20. $CF_2I_2 + h\nu \rightarrow CF_2I + I(^2P_{3/2})$

H21. $CF_2I_2 + h\nu \rightarrow CF_2I + I^*(^2P_{1/2})$

H22. $CF_2I_2 + h\nu \rightarrow CF_2 + I(^2P_{3/2}) + I(^2P_{3/2})$

H23. $CF_2I_2 + h\nu \rightarrow CF_2 + I(^2P_{3/2}) + I^*(^2P_{1/2})$

The photodissociation of CF_2I_2 has been studied at room temperature and wavelengths 248, 308, 337, and 351 nm by Wannenmacher et al. [429] and Baum et al. [30]. These authors report also plots of the absorption spectrum at room temperature and between 190 and 420 nm, which suggest the presence of at least two overlapping transitions corresponding to the different dissociation processes. Numerical absorption data belonging to Wannenmacher et al. and Baum et al. were obtained via personal communication by Pfister and Huber [314]. The absorption cross sections listed in Table 4-92 are normalized to a maximum value $\sigma = 2.929 \times 10^{-18}\ cm^2 \cdot molecule^{-1}$ at 300 nm, which was derived from five different spectra and has an uncertainty of ±16%.

Table 4-92. Absorption Cross Sections of CF_2I_2 at 294 K

λ (nm)	10^{20} σ (cm^2)	λ (nm)	10^{20} σ (cm^2)	λ (nm)	10^{20} σ (cm^2)
190	3163	270	203.1	350	66.24
195	4616	275	215.7	355	57.76
200	4070	280	224.3	360	49.81
205	2285	285	236.4	365	41.51
210	837.0	290	259.5	370	33.92
215	238.1	295	281.9	375	26.85
220	75.78	300	292.9	380	18.90
225	36.39	305	288.5	385	13.60
230	29.50	310	266.7	390	9.892
235	35.51	315	235.6	395	6.713
240	47.34	320	198.6	400	4.240
245	66.07	325	163.9	405	3.356
250	89.21	330	135.5	410	1.943
255	118.0	335	111.6	415	1.413
260	150.1	340	91.33	420	0.7066
265	180.5	345	78.25		

Note: 190–420 nm, Wannenmacher et al. [429], Baum et al. [30], and Pfister and Huber [314].

H24. $C_2F_5I + h\nu \rightarrow C_2F_5 + I(^2P_{3/2})$.

H25. $C_2F_5I + h\nu \rightarrow C_2F_5 + I^*(^2P_{1/2})$.

The absorption cross sections of C_2F_5I have been measured at 295 K and 268 nm ($\sigma = 6.39 \times 10^{-19}$ cm^2) by Pence et al. [312] and at 323 K and 220–320 nm by Zhang et al. [451]. The absorption band extending over the 220–320-nm range has a maximum of ~ 6.7×10^{-19} cm^2 at ~269 nm Estimated values at 5-nm intervals, read from a logarithmic plot, are presented in Table 4-93.

Quantum yields for $I^*(^2P_{1/2})$ atom formation in the photolysis of C_2F_5I at 266, 288, and ~305 nm, Φ (I*) = 0.97 ± 0.03, 0.75 ± 0.03, and 0.83 ± 0.05, respectively, have been reported by Kavita and Das [199]. Quantum yields for $I(^2P_{3/2})$ atom formation, Φ (I), can be derived from Φ (I) = 1 – Φ (I*).

Table 4-93. Absorption Cross Sections of C_2F_5I at 323 K

λ (nm)	10^{20} σ (cm^2)	λ (nm)	10^{20} σ (cm^2)	λ (nm)	10^{20} σ (cm^2)
220	*1.95*	*255*	*49.8*	*290*	*35.3*
225	*3.27*	*260*	*60.0*	*295*	*25.0*
230	*5.60*	*265*	*65.5*	*300*	*16.3*
235	*9.40*	*270*	*66.8*	*305*	*10.4*
240	*16.0*	*275*	*63.2*	*310*	*6.4*
245	*25.3*	*280*	*56.1*	*315*	*3.9*
250	*37.5*	*285*	*46.5*	*320*	*2.3*

Note: 235–310 nm, Zhang et al. [451], estimated from logarithmic plot.

H26. $C_3F_7I + h\nu \rightarrow C_3F_7 + I(^2P_{3/2})$.

H27. $C_3F_7I + h\nu \rightarrow C_3F_7 + I^*(^2P_{1/2})$.

The absorption cross sections of 1-C_3F_7I have been measured at room temperature and 265–341 nm by Koffend and Leone [205] and at 180–400 nm by Pence et al. [312]. The latter authors report a plot of the absorbance (in arbitrary units), which shows an absorption band between ~220 and 340 nm with the maximum at ~268 nm, and absorption cross sections only for 248, 268, and 308 nm. The data for 268 and 308 nm are in good agreement with the corresponding data reported by Koffend and Leone [205]. The recommended absorption cross sections of 1-C_3F_7I, listed in Table 4-94, are the value for 248 nm reported by Pence et al. [312]; the mean of the values of Pence et al. [312] and Koffend and Leone [205] at 268 nm; and, for the range 270–340 nm,

values obtained by interpolation and extrapolation at 5-nm intervals of the data reported at odd wavelength by Koffend and Leone [205].

Quantum yields for $I^*(^2P_{1/2})$ atom formation in the photolysis of C_3F_7I at 266, 288, and ~305 nm,

$\Phi(I^*) = 0.83 \pm 0.02$, 0.89 ± 0.03, and 0.90 ± 0.05 for 1-C_3F_7I and

$\Phi(I^*) = 0.83 \pm 0.01$, 0.80 ± 0.03, and 0.89 ± 0.02 for 2-C_3F_7I,

have been reported by Kavita and Das [199].

Quantum yields for $I(^2P_{3/2})$ atom formation, $\Phi(I)$, can be derived from $\Phi(I) = 1 - \Phi(I^*)$.

Table 4-94. Absorption Cross Sections of 1-C_3F_7I at 295–298 K

λ (nm)	10^{20} σ (cm^2)	λ (nm)	10^{20} σ (cm^2)	λ (nm)	10^{20} σ (cm^2)
248	31.0	*290*	*43.7*	*320*	*3.3*
268	77.3	*295*	*31.8*	*325*	*2.0*
270	*77.0*	*300*	*21.3*	*330*	*1.2*
275	*74.0*	*305*	*14.2*	*335*	*0.70*
280	*66.5*	*310*	*9.2*	*340*	*0.42*
285	*56.2*	*315*	*5.5*		

Note: 248 nm, Pence et al. [312],
268 nm, mean of Pence et al. [312] and Koffend and Leone [205]
270–340 nm, 5-nm inter- and extrapolation of Koffend and Leone [205] data.

H28. $C_4F_9I + h\nu \rightarrow C_4F_9 + I(^2P_{3/2})$.

H29. $C_4F_9I + h\nu \rightarrow C_4F_9 + I^*(^2P_{1/2})$.

H30. $C_6F_{13}I + h\nu \rightarrow C_6F_{13} + I(^2P_{3/2})$.

H31. $C_6F_{13}I + h\nu \rightarrow C_6F_{13} + I^*(^2P_{1/2})$.

Absorption cross sections are not available for these perfluoroalkyl iodides.

Quantum yields for $I^*(^2P_{1/2})$ atom formation in the photolysis of both iodides at 266, 288, and ~305 nm,

$\Phi(I^*) = 0.75 \pm 0.03$, 0.80 ± 0.03, and 0.87 ± 0.02 for *n*-C_4F_9I and

$\Phi(I^*) = 0.82 \pm 0.02$, 0.74 ± 0.03, and 0.82 ± 0.01 for *n*-$C_6F_{13}I$,
have been reported by Kavita and Das [199].

Quantum yields for $I(^2P_{3/2})$ atom formation, $\Phi(I)$, can be derived from $\Phi(I) = 1 - \Phi(I^*)$.

H32. $CH_2ICl + h\nu \rightarrow CH_2Cl + I$. The absorption cross sections of CH_2ICl have been measured at room temperature and 205–330 nm by Schmitt and Comes [366]; at 192–225 nm and 215–400 nm by Kwok and Phillips [208], [209], who also measured the CH_2ICl spectrum in cyclohexane solution. Measurements have also been carried out at 223–298 K and 205–355 nm by Roehl et al. [343] and at 243–333 K and 235–390 nm by Rattigan et al. [325]. The room temperature data of Roehl et al. [343] and Rattigan et al. [325] are in good agreement, where the values of Rattigan et al. [325] are lower by ≤10% between 240 and 345 nm. The older data of Schmitt and Comes [366] and the data of Kwok and Phillips [209] are higher with absorption maxima near 270 nm of 1.94×10^{-18} and 1.5×10^{-18} cm^2, respectively, compared to 1.35×10^{-18} and 1.21×10^{-18} cm^2 reported by the other two groups. The data of Kwok and Phillips [208] at 205 and 210 nm are lower by more than 80 % than the data of Roehl et al. [343]. The preferred absorption cross sections, listed in Table 4-95, are the data of Roehl et al. [343] at 205–230 nm; the mean of the values reported by Roehl et al. [343] and Rattigan et al. [325] at 235–355 nm; and the data of Rattigan et al. [325] at 360–390 nm. The data of Schmitt and Comes [366] and Kwok and Phillips [208], [209] are given only as a plots in their papers and have therefore not been included in the evaluation.

Both temperature studies show an increase of the absorption cross sections around the absorption maximum (~250–285 nm) with decreasing temperature between 333 and 223 K and the reverse effect above 285 nm. The absorption maxima at ~250 K reported by the two groups agree within 15%. A simple analytical expression for

the temperature dependence, $\sigma(\lambda, T) = \sigma(298\ K)\ [1 + a_1(T–298) + a_2(T–298)^2]$, and the fitting parameters $a_1(\lambda)$ and $a_2(\lambda)$ for λ = 205–355 nm and T = 223– 298 K give Roehl et al. [343]. Another simple parameterization, $\ln \sigma(\lambda, T) = \ln \sigma(\lambda, 298\ K) + B(T–298)$, and parameters $B(\lambda)$ for λ = 235–390 nm and T = 243–333 K report Rattigan et al. [325]. The temperature coefficients a_1, a_2, and B are given also in Table 4-95.

Table 4-95. Absorption Cross Sections of CH_2ICl at 298 K and Temperature Coefficients

λ (nm)	$10^{20}\ \sigma$ (cm^2)	$10^3\ a_1(K^{-1})$	$10^5\ a_2(K^{-2})$	$10^3\ B(K^{-1})$	λ (nm)	$10^{20}\ \sigma$ (cm^2)	$10^3\ a_1(K^{-1})$	$10^5\ a_2(K^{-2})$	$10^3\ B(K^{-1})$
205	132	–1.59	–3.83		300	25.9	2.38	–0.0473	2.56
210	42.1	8.47	3.76		305	16.7	3.13	0.394	3.08
215	11.1	6.12	4.30		310	10.9	3.13	0.303	3.50
220	7.50	0.232	0.129		315	7.16	2.74	–0.317	3.56
225	9.76	–0.0938	0.660		320	4.79	2.44	–0.533	3.46
230	14.9	–0.268	$-1.4 \times 10^{-}$		325	3.23	2.87	0.140	3.44
235	21.2	–0.512	–0.388	0.24	330	2.14	8.52	–4.21	3.72
240	32.1	–0.793	–0.664	0.12	335	1.40	2.02	–2.25	4.09
245	45.9	–0.929	–0.758	–0.02	340	0.906	5.20	4.54	4.87
250	63.3	–1.22	–1.13	–0.11	345	0.569	7.05	6.88	5.69
255	84.5	–1.25	–0.998	–0.28	350	0.350	9.12	11.7	6.88
260	106	–1.56	–1.14	–0.44	355	0.225	12.27	18.9	8.16
265	122	–1.05	–0.294	–0.55	360	0.133			9.01
270	128	–1.33	–0.593	–0.59	365	0.081			11.06
275	121	–1.07	–0.298	–0.47	370	0.048			11.47
280	104	–0.618	–0.309	–0.18	375	0.027			12.77
285	81.1	–0.326	–0.554	0.32	380	0.017			15.14
290	58.5	0.300	–0.711	0.99	385	0.008			19.12
295	39.9	1.55	–0.245	1.73	390	0.006			20.48

Note: Absorption cross sections σ: 205–230 nm, Roehl et al. [343],
235–355 nm, mean of Roehl et al. [343] and Rattigan et al. [325],
360–390 nm, Rattigan et al. [325].
Temperature coefficients a_1 and a_2: 223–298 K, Roehl et al. [343]
($\sigma(\lambda, T) = \sigma(298\ K)\ [1 + a_1(T–298)+ a_2(T–298)2]$).
Temperature coefficients B: 243–333 K, Rattigan et al. [325]
($\ln \sigma(\lambda, T) = \ln \sigma(\lambda, 298\ K) + B(T–298)$).

H33. $CH_2BrI + h\nu \rightarrow CH_2I + Br$.

H34. $CH_2BrI + h\nu \rightarrow CH_2Br + I$.

The absorption cross sections of CH_2BrI have been measured at room temperature and 180–360 nm by Man et al. [230]; and at 273, 298, and 348 K and 215–390 nm by Mössinger et al. [283]. The spectrum exhibits two absorption bands with maxima near 210 and 267 nm which can be assigned to electronic transitions to repulsive states antibonding in C–Br and C–I, respectively. The results of the two studies are not in quantitative agreement: Mössinger et al. [283] report room temperature absorption cross sections of 5.7×10^{-18} and 2.3×10^{-18} cm^2 at 215 and 270 nm, whereas a plot in the paper of Man et al. [230] gives the larger values of $\sim 1 \times 10^{-17}$ and 3.5×10^{-18} cm^2, respectively. We recommend the data of Mössinger et al. [283], which are listed in Table 4-96.

The absorption cross sections increase with decreasing temperature around the band maxima and decrease in their long-wavelength tails at 220–240 nm and above 290 nm. The temperature dependence was parameterized by Mössinger et al. [283] by the empirical relation $\ln \sigma(\lambda, T) = \ln \sigma(\lambda, 298\ K) + B(T–298)$. The temperature coefficients $B(\lambda)$ are listed also in Table 4-96 (an erroneous B value at 280 nm has been corrected by Dr. Mössinger via a personal communication).

Table 4-96. Absorption Cross Sections of CH_2BrI at 298 K and Temperature Coefficients

λ (nm)	10^{20} σ (cm^2)	10^3 B (K^{-1})	λ (nm)	10^{20} σ (cm^2)	10^3 B (K^{-1})	λ (nm)	10^{20} σ (cm^2)	10^3 B (K^{-1})
215	567	–2.16	275	214	–1.22	335	5.52	3.89
220	423	–0.12	280	184	–0.94	340	3.50	4.79
225	269	1.34	285	150	–0.53	345	2.24	5.74
230	155	2.06	290	110	0.10	350	1.41	6.73
235	97.9	2.05	295	82.5	0.63	355	0.817	9.47
240	80.9	1.01	300	60.6	1.03	360	0.498	11.5
245	93.7	0.00	305	42.9	1.13	365	0.303	11.6
250	125	–0.58	310	31.4	1.41	370	0.165	14.3
255	170	–1.16	315	23.1	1.52	375	0.098	17.4
260	207	–1.29	320	16.8	1.71	380	0.070	
265	228	–1.45	325	11.5	2.36	385	0.039	
270	229	–1.73	330	8.02	2.99	390	0.025	

Note: Absorption cross sections σ: 205–380 nm, Mössinger et al. [283].
Temperature coefficients B: 273–348 K, Mössinger et al. [283] (ln σ(λ, T) = ln σ(λ, 298 K) + B(T–298)).

H35. $CF_2BrCF_2I + h\nu \rightarrow CF_2BrCF_2 + I$.

H36. $CF_2BrCF_2I + h\nu \rightarrow CF_2ICF_2 + Br$.

The absorption spectrum of CF_2BrCF_2I has been measured at room temperature and 190– 350 nm by Pence et al. [312]. The spectrum, reported as a plot (with arbitrary absorbance units), exhibits an absorption band with the maximum near 268 nm corresponding to the C–I bond and part of an absorption band with the maximum at or below 193 nm corresponding to the C–Br bond. A cross section $\sigma = 2.36 \times 10^{-18}$ cm^2 and a quantum yield for $Br^*(^2P_{1/2})$ atom formation, $\Phi(Br^*) = 0.07 \pm 0.05$, at 193 nm have been reported.

I1. $SO_2 + h\nu \rightarrow$ Products

The UV absorption spectrum of SO_2 is highly structured, with a very weak absorption in the 340–390 nm region, a weak absorption in the 260–340 nm region, and a strong absorption extending from 180 to 235 nm; the threshold wavelength for photodissociation is ~220 nm. The atmospheric photochemistry of SO_2 has been reviewed by Heicklen et al. [157] and by Calvert and Stockwell [66]. Direct photo-oxidation at wavelengths longer than ~300 nm by way of the electronically excited states of SO_2 appears to be relatively unimportant.

The absorption cross sections have been measured by McGee and Burris [252] at 295 and 210 K, between 300 and 324 nm, which is the wavelength region commonly used for atmospheric monitoring of SO_2. Manatt and Lane [231] have recently compiled and evaluated the earlier cross section measurements between 106 and 403 nm.

I2. $CS_2 + h\nu \rightarrow CS + S$

The CS_2 absorption spectrum is rather complex. Its photochemistry has been reviewed by Okabe [300]. There are two distinct regions in the near UV spectrum: a strong absorption extending from 185 to 230 nm, and a weaker one in the 290–380 nm range. The threshold wavelength for photodissociation is ~280 nm. Absorption cross section measurements have been reported recently by Xu and Joens [435] between 187 and 230 nm.

The photo-oxidation of CS_2 in the atmosphere has been discussed by Wine et al. [432], who report that electronically excited CS_2 may react with O_2 to yield eventually OCS.

I3. $OCS + h\nu \rightarrow CO + S$

The absorption cross sections of OCS have been measured by Breckenridge and Taube [41], who presented their 298 K results in graphical form, between 200 and 260 nm; by Rudolph and Inn [351] between 200 and ~300 nm (see also Turco et al. [406]), at 297 and 195 K; by Leroy et al. [213] at 294 K, between 210 and 260 nm, using photographic plates; and by Molina et al. [263] between 195 and 260 nm, in the 195 K to 403 K temperature range. The results are in good agreement in the regions of overlap, except for λ > 280 nm, where the cross section values reported by Rudolph and Inn [351] are significantly larger than those reported by Molina et al. [263]. The latter authors concluded that solar photodissociation of OCS in the troposphere occurs only to a negligible extent.

The recommended cross sections, given in Table 4-97, are taken from Molina et al. [263]. (The original publication also lists a table with cross section values averaged over 1 nm intervals, between 185 and 300 nm.)

Rudolph and Inn [351] reported a quantum yield for photodissociation of 0.72, based on measurements of the quantum yield for CO production in the 220–254 nm range. Additional measurements would be useful.

Table 4-97. Absorption Cross Sections of OCS

λ (nm)	$10^{20}\sigma(cm^2)$		λ (nm)	$10^{20}\sigma(cm^2)$	
	295 K	225 K		295 K	225 K
186.1	18.9	13.0	228.6	26.8	23.7
187.8	8.33	5.63	231.2	22.1	18.8
189.6	3.75	2.50	233.9	17.1	14.0
191.4	2.21	1.61	236.7	12.5	9.72
193.2	1.79	1.53	239.5	8.54	6.24
195.1	1.94	1.84	242.5	5.61	3.89
197.0	2.48	2.44	245.4	3.51	2.29
199.0	3.30	3.30	248.5	2.11	1.29
201.0	4.48	4.50	251.6	1.21	0.679
203.1	6.12	6.17	254.6	0.674	0.353
205.1	8.19	8.27	258.1	0.361	0.178
207.3	10.8	10.9	261.4	0.193	0.0900
209.4	14.1	14.2	264.9	0.0941	0.0419
211.6	17.6	17.6	268.5	0.0486	0.0199
213.9	21.8	21.8	272.1	0.0248	0.0101
216.2	25.5	25.3	275.9	0.0119	0.0048
218.6	28.2	27.7	279.7	0.0584	0.0021
221.5	30.5	29.4	283.7	0.0264	0.0009
223.5	31.9	29.5	287.8	0.0012	0.0005
226.0	30.2	27.4	292.0	0.0005	0.0002
			296.3	0.0002	–

I4. $SF_6 + h\nu \rightarrow$ Products

The species SF_6 does not absorb at wavelengths longer than 130 nm; it is expected to have an atmospheric residence time of thousands of years (Ravishankara et al. [329]; Ko et al. [204]).

J1. $NaOH + h\nu \rightarrow Na + OH$

The spectrum of NaOH vapor is poorly characterized. Rowland and Makide [346] inferred the absorption cross section values and the average solar photodissociation rate from the flame measurements of Daidoji [100]. Additional measurements are required.

J2. $NaCl + h\nu \rightarrow Na + Cl$

There are several studies of the UV absorption spectra of NaCl vapor. For a review of the earlier work, which was carried out at high temperatures, see Rowland and Rogers [348]. The recommended cross sections, listed in Table 4-98, are taken from the work of Silver et al. [376], who measured spectra of gas phase NaCl at room temperature in the range from ~190 to 360 nm by directly monitoring the product Na atoms.

Table 4-98. Absorption Cross Sections of NaCl Vapor at 300 K

λ (nm)	$10^{20}\sigma(cm^2)$
189.7	612
193.4	556
203.1	148
205.3	90.6
205.9	89.6
210.3	73.6
216.3	151
218.7	46.3
225.2	146
230.4	512
231.2	947
234.0	1300
237.6	638
241.4	674
248.4	129
251.6	251
254.8	424
260.2	433
268.3	174
277.0	40
291.8	0.8

4.3 References

1. *The Stratosphere 1981: Theory and Measurements*; National Aeronautics and Space Administration, 1982.
2. Abel, B., B. Herzog, H. Hippler and J. Troe, 1989, J. Chem. Phys., **91**, 890-899, 900-905.
3. Abel, B., H. Hippler and J. Troe, 1992, J. Chem. Phys., **96**, 8863-8871.
4. Adachi, H., N. Basco and D. G. L. James, 1979, Int. J. Chem. Kinet., **11**, 1211-1229.
5. Adachi, H., N. Basco and D. G. L. James, 1980, Int. J. Chem. Kinet., **12**, 949.
6. Addison, M. C., J. P. Burrows, R. A. Cox and R. Patrick, 1980, Chem. Phys. Lett., **73**, 283.
7. Adler-Golden, S. M. and J. R. Wiesenfeld, 1981, Chem. Phys. Lett., **82**, 281.
8. Allen, M. and J. E. Frederick, 1982, J. Atmos. Sci., **39**, 2066-2075.
9. Amoruso, A., M. Cacciani, A. DiSarra and G. Fiocco, 1990, J. Geophys. Res., **95**, 20565.
10. Amoruso, A., L. Crescentini, G. Fiocco and M. Volpe, 1993, J. Geophys. Res., **98**, 16857-16863.
11. Amoruso, A., L. Crescentini, M. Silvia Cola and G. Fiocco, 1996, J. Quant. Spectrosc. Radiat. Transfer, **56**, 145-152.
12. Anastasi, C., I. W. M. Smith and D. A. Parkes, 1978, J. Chem. Soc. Faraday Trans. 1, **74**, 1693-1701.
13. Anastasi, C., D. J. Waddington and A. Woolley, 1983, J. Chem. Soc. Faraday Trans., **79**, 505-516.
14. Anderson, G. P. and L. A. Hall, 1983, J. Geophys. Res., **88**, 6801-6806.
15. Anderson, G. P. and L. A. Hall, 1986, J. Geophys. Res., **91**, 14509-14514.
16. Armerding, W., F. J. Comes and B. Schulke, 1995, J. Phys. Chem., **99**, 3137-3143.
17. Baer, S., H. Hippler, R. Rahn, M. Siefke, N. Seitzinger and J. Troe, 1991, J. Chem. Phys., **95**, 6463-6470.
18. Bagratashvili, V. N., S. I. Ionov, G. V. Mishakov and V. A. Semchishen, 1985, Chem. Phys. Lett., **115**, 144-148.
19. Ball, S. M., G. Hancock, S. E. Martin and J. C. Pinot de Moira, 1997, Chem. Phys. Lett., **264**, 531-538.
20. Ballash, N. M. and D. A. Armstrong, 1974, Spectrochim Acta, **30A**, 941-944.
21. Barker, J. R., L. Brouwer, R. Patrick, M. J. Rossi, P. L. Trevor and D. M. Golden, 1985, Int. J. Chem. Kinet., **17**, 991-1006.
22. Barnes, R. J., M. Lock, J. Coleman and A. Sinha, 1996, J. Phys. Chem., **100**, 453-457.
23. Barnes, R. J., A. Sinha and H. A. Michelsen, 1998, J. Phys. Chem. A, **102**, 8855-8859.
24. Basco, N. and S. S. Parmar, 1985, Int. J. Chem. Kinet., **17**, 891.
25. Bass, A. M., L. C. Glasgow, C. Miller, J. P. Jesson and S. L. Filken, 1980, Planet. Space Sci. , **28**, 675.
26. Bass, A. M., A. E. Ledford and A. H. Laufer, 1976, J. Res. NBS, **80A**, 143-166.
27. Bauer, D., J. N. Crowley and G. K. Moortgat, 1992, J. Photochem. and Photobiol., **A65**, 3530-3538.
28. Bauer, D., D. O. L. and A. J. Hynes, 2000, Phys. Chem. Chem. Phys., **2**, 1421-1424.
29. Baughum, S. L. and S. R. Leone, 1980, J. Chem. Phys., **72**, 6531-6545.
30. Baum, G. P., P. Felder and R. J. Huber, 1993, J. Chem. Phys., **98**, 1999-2010.
31. Benter, T., C. Feldmann, U. Kirchner, M. Schmidt, S. Schmidt and R. N. Schindler, 1995, Ber. Bunsenges. Phys. Chem., **99**, 1144-1147.
32. Biaume, F., 1973, J. Photochem., **2**, 139.
33. Bilde, M., T. J. Wallington, G. Ferronato, J. J. Orlando, G. S. Tyndall, E. Estupinan and S. Haberkorn, 1998, J. Phys.Chem. A, **102**, 1976-1986.
34. Birk, M., R. R. Friedl, E. A. Cohen, H. M. Pickett and S. P. Sander, 1989, J. Chem. Phys., **91**, 6588-6597.
35. Birks, J. W., B. Shoemaker, T. J. Leck, R. A. Borders and L. J. Hart, 1977, J. Chem. Phys., **66**, 4591-4599.
36. Bishenden, E., J. Haddock and D. J. Donaldson, 1991, J. Phys. Chem., **95**, 2113.
37. Bishenden, E., J. Haddock and D. J. Donaldson, 1992, J. Phys. Chem., **96**, 6513.
38. Bongartz, A., J. Kames, F. Welter and U. Schurath, 1991, J. Phys. Chem., **95**, 1076-1082.
39. Brandon, J. T., S. A. Reid, D. C. Robie and H. Reisler, 1992, J. Chem. Phys., **97**, 5246.
40. Braun, M., A. Fahr, R. Klein, M. J. Kurylo and R. E. Huie, 1991, J. Geophys. Res., **96**, 13009.
41. Breckenridge, W. and H. H. Taube, 1970, J. Chem. Phys., **52**, 1713-1715.
42. Brewer, P., P. Das, G. Ondrey and R. Bersohn, 1983, J. Chem. Phys., **79**, 720-723.
43. Brion, J., A. Chakir, D. Daumont, J. Malicet and C. Parisse, 1993, Chem. Phys. Lett., **213**, 610-612.
44. Brock, J. C. and R. T. Watson, 1980, Chem. Phys., **46**, 477-484.
45. Brouwer, L. and J. Troe, 1981, Chem. Phys. Lett., **82**, 1-4.
46. Brownsword, R. A., M. Hillenkamp, T. Laurent, R. K. Vatsa, H.-R. Volpp and J. Wolfrum, 1997, J. Chem. Phys., **106**, 1359-1366.
47. Brownsword, R. A., M. Hillenkamp, T. Laurent, R. K. Vatsa, H.-R. Volpp and J. Wolfrum, 1997, J. Phys. Chem. A, **101**, 5222-5227.

48. Brownsword, R. A., M. Hillenkamp, T. Laurent, J. Wolfrum, H.-R. Volpp, R. K. Vatsa and H.-S. Yoo, 1997, J. Chem. Phys., **107**, 779-785.
49. Brownsword, R. A., P. Schmiechen, H.-R. Volpp, H. P. Upadhyaya, Y. J. Jung and K.-H. Jung, 1999, J. Chem. Phys., **110**, 11823-11829.
50. Burkholder, J. B., 1993, J. Geophys. Res., **98**, 2963-2974.
51. Burkholder, J. B. and E. J. Bair, 1983, J. Phys. Chem., **87**, 1859-1863.
52. Burkholder, J. B., R. L. Mauldin, R. J. Yokelson, S. Solomon and A. R. Ravishankara, 1993, J. Phys. Chem., **97**, 7597-7605.
53. Burkholder, J. B., J. J. Orlando and C. J. Howard, 1990, J. Phys. Chem., **94**, 687-695.
54. Burkholder, J. B., A. R. Ravishankara and S. Solomon, 1995, J. Geophys. Res., **100**, 16793-16800.
55. Burkholder, J. B., R. K. Talukdar and A. R. Ravishankara, 1994, Geophys. Res. Lett., **21**, 585-588.
56. Burkholder, J. B., R. K. Talukdar, A. R. Ravishankara and S. Solomon, 1993, J. Geophys. Res., **98**, 22937-22948.
57. Burkholder, J. B., R. R. Wilson, T. Gierczak, R. Talukdar, S. A. McKeen, J. J. Orlando, G. L. Vaghjiani and A. R. Ravishankara, 1991, J. Geophys. Res., **96**, 5025-5043.
58. Burley, J. D., C. E. Miller and H. S. Johnston, 1993, J. Molec. Spec, **158**, 377-391.
59. Burrows, J. P., G. S. Tyndall and G. K. Moortgat. 16th Informal Conf. on Photochemistry, 1984, Boston.
60. Burrows, J. P., G. S. Tyndall and G. K. Moortgat, 1985, J. Phys. Chem., **89**, 4848-4856.
61. Burrows, J. P., G. S. Tyndall and G. K. Moortgat, 1988, J. Phys. Chem., **92**, 4340-4348.
62. Butler, P. J. D. and L. F. Phillips, 1983, J. Phys. Chem., **87**, 183-184.
63. Cacciani, M., A. D. Sarra, G. Fiocco and A. Amoruso, 1989, J. Geophys. Res., **94**, 8485-8490.
64. Cadman, P. and J. P. Simons, 1966, Trans. Faraday Soc., **62**, 631-641.
65. Calvert, J. G. and J. N. Pitts; John Wiley & Sons, Inc., pp. 230-231: New York, 1966.
66. Calvert, J. G. and W. R. Stockwell. In *Acid Precipitation: SO2, NO, NO2 Oxidation Mechanisms: Atmospheric Considerations*; Ann Arbor Sci. Publishers: Ann Arbor, Michigan, 1983.
67. Canosa-Mas, C. E., M. Fowles, P. J. Houghton and R. P. Wayne, 1987, J. Chem. Soc. Faraday Trans. 2, **83**, 1465.
68. Cantrell, C. A., J. A. Davidson, A. H. McDaniel, R. E. Shetter and J. G. Calvert, 1990, J. Phys. Chem., **94**, 3902-3908.
69. Cantrell, C. A., J. A. Davidson, R. E. Shetter, B. A. Anderson and J. G. Calvert, 1987, J. Phys. Chem., **91**, 5858-5863.
70. Cattell, F. C., J. Cavanagh, R. A. Cox and M. E. Jenkin, 1986, J. Chem. Soc. Faraday Trans. 2, **82**, 1999-2018.
71. Chang, J. S., J. R. Barker, J. E. Davenport and D. M. Golden, 1979, Chem. Phys. Lett., **60**, 385-390.
72. Cheung, A. S. C., K. Yoshino, J. R. Esmond, S. S. L. Chiu, D. E. Freeman and W. H. Parkinson, 1990, J. Chem. Phys., **92**, 842-849.
73. Cheung, A. S. C., K. Yoshino, W. H. Parkinson and D. E. Freeman, 1984, Geophys. Res. Lett., **11**, 580-582.
74. Cheung, A. S. C., K. Yoshino, W. H. Parkinson, S. L. Guberman and D. E. Freeman, 1986, Planet. Space Sci., **34**, 1007-1021.
75. Chiu, S. S. L., A. S. C. Cheung, K. Yoshino, J. R. Esmond, D. E. Freeman and W. H. Parkinson, 1990, J. Chem. Phys., **93**, 5539-5543.
76. Chou, C. C., G. Crescentini, H. Vera-Ruiz, W. S. Smith and F. S. Rowland. "Stratospheric Photochemistry of CF2O, CClFO, and CCl2O"; 173rd American Chemical Society Meeting, 1977, New Orleans, LA.
77. Chou, C. C., R. J. Milstein, W. S. Smith, H. Vera-Ruiz, M. J. Molina and F. S. Rowland, 1978, J. Phys. Chem., **82**, 1.
78. Chou, C. C., W. S. Smith, H. V. Ruiz, K. Moe, G. Crescentini, M. J. Molina and F. S. Rowland, 1977, J. Phys. Chem., **81**, 286-290.
79. Clark, J. H., C. B. Moore and N. S. Nogar, 1978, J. Chem. Phys., **68**, 1264-1271.
80. Clark, R. H. and D. Husain, 1984, J. Photochem., **24**, 103-115.
81. CODATA, 1980, J. Phys. Chem. Ref. Data, **9**, 295-471.
82. CODATA, 1982, J. Phys. Chem. Ref. Data, **11**, 327-496.
83. Colussi, A. J., 1990, J. Phys. Chem., **94**, 8922-8926.
84. Colussi, A. J., S. P. Sander and R. R. Friedl, 1992, J. Phys.Chem., **96**, 4442-4445.
85. Coquart, B., A. Jenouvier and M. F. Merienne, 1995, J. Atm. Chem, **21**, 251-261.
86. Coquart, B., M. F. Merienne and A. Jenouvrier, 1990, Planet. Space Sci., **38**, 287.
87. Corcoran, T. C., E. J. Beiting and M. O. Mitchell, 1992, J. Molecular Spectroscopy, **154**, 119-128.
88. Cox, R. A., R. A. Barton, E. Ljungstrum and D. W. Stocker, 1984, Chem. Phys. Lett., **108**, 228-232.
89. Cox, R. A. and J. P. Burrows, 1979, J. Phys. Chem., **83**, 2560-2568.
90. Cox, R. A. and G. D. Hayman, 1988, Nature, **332**, 796-800.
91. Cox, R. A. and R. Patrick, 1979, Int. J. Chem. Kinet., **11**, 635.

92. Cox, R. A., D. W. Sheppard and M. P. Stevens, 1982, J. Photochem., **19**, 189-207.
93. Cox, R. A. and G. Tyndall, 1979, Chem. Phys. Lett., **65**, 357.
94. Cox, R. A. and G. S. Tyndall, 1980, J. Chem. Soc. Faraday Trans. 2, **76**, 153.
95. Coxon, J. A., W. E. Jones and D. A. Ramsey. 12th International Symposium on Free Radicals, 1976, Laguna Beach, California.
96. Crowley, J. N., R. Helleis, R. Muller, G. K. Moortgat, P. J. Crutzen and J. J. Orlando, 1994, J. Geophys. Res., **99**, 20683-20688.
97. Crowley, J. N., F. G. Simon, J. P. Burrows, G. K. Moortgat, M. E. Jenkin and R. A. Cox, 1991, J. Photochem. and Photobiol. A: Chem., **60**, 1-10.
98. Currie, J., J. H. Sidebottom and J. Tedder, 1974, Int. J. Chem. Kinet., **6**, 481-492.
99. Dagaut, P. and M. J. Kurylo, 1990, J. Photochem. and Photobiol. A:Chem., **51**, 133.
100. Daidoji, H., 1979, Bunseki Kagaku, **28**, 77
101. Daumont, D., J. Brion, J. Charbonnier and J. Malicet, 1992, J. Atmos. Chem., **15**, 145-155.
102. Davenport, J. E. "Determination of NO2 Photolysis Parameters for Stratospheric Modeling," FAA-EQ-78-14, Federal Aviation Administration, Washington, DC. 1978.
103. Davidson, J. A., C. A. Cantrell, A. H. McDaniel, R. E. Shetter, S. Madronich and J. G. Calvert, 1988, J. Geophys. Res., **93**, 7105-7112.
104. Davidson, N., 1951, J. Am. Chem. Soc., **73**, 467-468.
105. Davis, H. F. and Y. T. Lee, 1992, J. Phys. Chem., **96**, 5681-5684.
106. DeMore, W. B. and O. Raper, 1964, J. Phys. Chem., **68**, 412-414.
107. DeMore, W. B. and E. Tschuikow-Roux, 1990, J. Phys. Chem., **94**, 5856-5860.
108. Deters, B., J. P. Burrows, S. Himmelmann and C. Blindauer, 1996, Ann. Geophysicae, **14**, 468-475.
109. Doucet, J., J. R. Gilbert, P. Sauvageau and C. Sandorfy, 1975, J. Chem. Phys., **62**, 366-369.
110. Doucet, J., P. Sauvageau and C. Sandorfy, 1973, J. Chem. Phys., **58**, 3708-3716.
111. Doucet, J., P. Sauvageau and C. Sandorfy, 1975, J. Chem. Phys., **62**, 355-359.
112. Ebenstein, W. L., J. R. Wiesenfeld and G. L. Wolk, 1978, Chem. Phys. Lett., **53**, 185-189.
113. Fahr, A., W. Braun and M. J. Kurylo, 1993, J. Geophys. Res., **98**, 20467-20472.
114. Fahr, A., A. H. Laufer, M. Kraus and R. Osman, 1997, J. Phys. Chem A, **101**, 4879-4886.
115. Fahr, A., A. K. Nayak and R. E. Huie, 1995, Chem. Phys., **199**, 275-284.
116. Fahr, A., A. K. Nayak and M. J. Kurylo, 1995, Chem. Phys., **197**, 195-203.
117. Felder, P., 1991, Chem. Phys., **155**, 435-445.
118. Felder, P., 1992, Chem. Phys. Lett., **197**, 425-432.
119. Felps, W. S., K. Rupnik and S. P. McGlynn, 1991, J. Phys. Chem., **95**, 639-656.
120. Fenter, F. F., V. Catoire, R. Lesclaux and P. D. Lightfoot, 1993, J. Phys. Chem., **97**, 3530-3538.
121. Fergusson, W. C., L. Slotin and W. G. Style, 1936, Trans. Far. Soc., **32**, 956.
122. Francisco, J. S., M. R. Hand and I. H. Williams, 1996, J. Phys. Chem., **100**, 9250-9253.
123. Frederick, J. E. and R. D. Hudson, 1979, J. Atmos. Sci., **36**, 737-745.
124. Frederick, J. E. and J. E. Mentall, 1982, Geophys. Res. Lett., **9**, 461-464.
125. Frost, G. J., L. M. Goss and V. Vaida, 1996, J. Geophys. Res, **101**, 3869-3877.
126. Frost, G. J., L. M. Goss and V. Vaida, 1996, J. Geophys. Res., **101**, 3879-3884.
127. Furlan, A., T. Gejo and R. J. Huber, 1996, J. Phys. Chem., **100**, 7956-7961.
128. Ganske, J. A., H. N. Berko and B. J. Finlayson-Pitts, 1992, J. Geophys. Res., **97**, 7651-7656.
129. Gardner, E. P., P. D. Sperry and J. G. Calvert, 1987, J. Geophys. Res., **92**, 6642-6652.
130. Gedanken, A., 1987, Chem. Phys. Lett., **137**, 462-466.
131. Gibson, G. E. and N. S. Bayliss, 1933, Phys. Rev., **44**, 188.
132. Gilbert, R., P. Sauvageau and C. Sandorfy, 1974, J. Chem. Phys., **60**, 4820-4824.
133. Gillotay, D., A. Jenouvrier, B. Coquart, M. F. Merienne and P. C. Simon, 1989, Planet. Space Sci., **37**, 1127-1140.
134. Gillotay, D. and P. C. Simon, 1989, J. Atmos. Chem., **8**, 41-62.
135. Gillotay, D. and P. C. Simon, 1990, Aeronomica Acta A, **356**, 1-173.
136. Gillotay, D. and P. C. Simon, 1991, J. Atmos. Chem., **12**, 269-285.
137. Gillotay, D. and P. C. Simon, 1991, J. Atmos. Chem., **13**, 289-299.
138. Gillotay, D., P. C. Simon and L. Dierickx, 1988, Aeronomica Acta, **A335**, 1-25.
139. Gillotay, D., P. C. Simon and L. Dierickx, 1993, Aeronomica Acta, **A368**, 1-15.
140. Giolando, D. M., G. B. Fazekas, W. D. Taylor and G. A. Takacs, 1980, J. Photochem., **14**, 335.

141. Goodeve, C. F. and F. D. Richardson, 1937, Trans. Faraday. Soc., **33**, 453-457.
142. Gordus, A. A. and R. B. Bernstein, 1954, J. Chem. Phys., **22**, 790-795.
143. Graham, R. A. Photochemistry of NO3 and the Kinetics of the N2O5-O3 System. Ph. D. Thesis, University of California, Berkeley, CA, 1975.
144. Graham, R. A. and H. S. Johnston, 1978, J. Phys. Chem., **82**, 254-268.
145. Graham, R. A., A. M. Winer and J. N. Pitts, Jr., 1978, Geophys. Res. Lett., **5**, 909.
146. Green, R. G. and R. P. Wayne, 1976/77, J. Photochem., **6**, 375-377.
147. Greenblatt, G. D. and A. R. Ravishankara, 1990, J. Geophys. Res., **95**, 3539-3547.
148. Griffith, D. W. T., G. C. Toon, B. Sen, J.-F. Blavier and R. A. Toth, 2000, Geophys. Res. Lett., **27**, 2485-2488.
149. Hancock, G. and A. Hofzumahaus "Experimental Study of the Altitude Dependence of the Tropospheric Ozone Photolysis Frequency, J(O(1D)) Between 0 and 12 km Height (ATOP)," ENV4-CT95-0158, EU R and D Programme Environment and Climate 1997.
150. Harder, J. W., J. W. Brault, P. V. Johnston and G. H. Mount, 1996, J. Geophys. Res., submitted.
151. Harker, A. B., W. Ho and J. J. Ratto, 1977, Chem. Phys. Lett., **50**, 394-397.
152. Harwood, M. H. and R. L. Jones, 1994, J. Geophys. Res., **99**, 22995-22964.
153. Harwood, M. H., R. L. Jones, R. A. Cox, E. Lutman and O. V. Rattigan, 1993, J. Photochem. Photobiol. A: Chem., **73**, 167-175.
154. Harwood, M. H., D. M. Rowley, R. A. Freshwater, R. A. Cox and R. L. Jones, 1995, J. Chem. Soc. Faraday Trans, **91**, 3027-3032.
155. Hayman, G. D. and R. A. Cox, 1989, Chem. Phys. Lett., **155**, 1-7.
156. Hearn, A. G., 1961, Proc. Phys. Soc. London, **78**, 932-940.
157. Heicklen, J., N. Kelly and K. Partymiller, 1980, Rev. Chem. Intermediates, **3**, 315-404.
158. Herman, J. R. and J. E. Mentall, 1982, J. Geophys. Res., **87**, 8967-8975.
159. Herzberg, G. and K. K. Innes, 1957, Canad. J. Phys., **35**, 842.
160. Hochanadel, C. J., J. A. Ghormley, J. W. Boyle and P. J. Ogren, 1977, J. Phys. Chem., **81**, 3.
161. Hochanadel, C. J., J. A. Ghormley and P. J. Ogren, 1972, J. Chem. Phys., **56**, 4426-4432.
162. Horowitz, A. and J. G. Calvert, 1978, Int. J. Chem. Kinet., **10**, 805.
163. Hubinger, S. and J. B. Nee, 1994, Chem. Phys., **181**, 247-257.
164. Hubinger, S. and J. B. Nee, 1995, J. Photochem. and Photobiol. A: Chem., **85**, 1-7.
165. Hubrich, C. and F. Stuhl, 1980, J. Photochem., **12**, 93-107.
166. Hubrich, C., C. Zetzsch and F. Stuhl, 1977, Ber. Bunsenges. Phys. Chem., **81**, 437-442.
167. Huder, K. J. and W. B. DeMore, 1995, J. Phys. Chem., **99**, 3905-3908.
168. Hudson, R. D., 1971, Reviews of Geophysics and Space Physics, **9**, 305-399.
169. Hudson, R. D., 1974, Canad. J. Chem., **52**, 1465-1478.
170. Hudson, R. D. and L. J. Kieffer. Absorption Cross Sections of Stratospheric Molecules. In *The Natural Stratosphere of 1974*; CIAP, 1975; Vol. Monograph 1; pp (5-156)-(5-194).
171. Huebner, R. H., J. Bushnell, D. L., R. J. Celotta, S. R. Mielczarek and C. E. Kuyatt, 1975, Nature, **257**, 376-378.
172. Ibuki, T., 1992, J. Chem. Phys., **96**, 8793-8798.
173. Ichimura, T., A. W. Kirk, G. Kramer and E. Tschuikow-Roux, 1976/1977, J. Photochem., **6**, 77-90.
174. Ichimura, T., A. W. Kirk and E. Tschuikow-Roux, 1977, J. Phys. Chem., **81**, 1153-1156.
175. Illies, A. J. and G. A. Takacs, 1976, J. Photochem., **6**, 35-42.
176. Ingham, T., D. Bauer, J. Landgraf and J. N. Crowley, 1998, J. Phys. Chem. A, **102**, 3293-3298.
177. Inn, E. C. Y., 1975, J. Atmos. Sci., **32**, 2375.
178. Inn, E. C. Y., 1980, J. Geophys. Res., **85**, 7493.
179. Inn, E. C. Y. and Y. Tanaka, 1953, J. Opt. Soc. Am., **43**, 870-873.
180. Jenkin, M. E. and R. A. Cox, 1991, J. Phys. Chem., **95**, 3229.
181. Jenkin, M. E., R. A. Cox, G. Hayman and L. J. Whyte, 1988, J. Chem. Soc. Faraday Trans. 2, **84**, 913.
182. Jenkin, M. E., T. P. Murrells, S. J. Shalliker and G. D. Hayman, 1993, J. Chem. Soc. Faraday Trans., **89**, 433-446.
183. Jenouvrier, A., B. Coquart and M. F. Merienne, 1986, J. Quant. Spectros. Radiat. Transfer **36**, 349-354.
184. Jensen, F. and J. Oddershede, 1990, J. Phys. Chem., **94**, 2235.
185. Johnston, H. S., S. Chang and G. Whitten, 1974, J. Phys. Chem., **78**, 1-7.
186. Johnston, H. S., H. F. Davis and Y. T. Lee, 1996, J. Phys. Chem., **100**, 4713-4723.
187. Johnston, H. S. and R. Graham, 1973, J. Phys. Chem., **77**, 62.
188. Johnston, H. S. and R. Graham, 1974, Canad. J. Chem., **52**, 1415-1423.

189. Johnston, H. S., E. D. Morris, Jr. and J. Van den Bogaerde, 1969, J. Am. Chem. Soc., **91**, 7712-7727.
190. Johnston, H. S., M. Paige and F. Yao, 1984, J. Geophys. Res., **89**, 661.
191. Jolly, G. S., D. L. Singleton, D. J. McKenney and G. Paraskevopoulos, 1986, J. Chem. Phys., **84**, 6662-6667.
192. Jones, E. L. and O. R. Wulf, 1937, J. Chem. Phys., **5**, 873.
193. Jones, I. T. N. and K. Bayes, 1973, J. Chem. Phys., **59**, 4836-4844.
194. Jourdain, J. L., G. Le Bras, G. Poulet, J. Combourieu, P. Rigaud and B. LeRoy, 1978, Chem. Phys. Lett., **57**, 109.
195. Jung, Y.-J., M. S. Park, Y. S. Kim, K.-H. Jung and H.-R. Volpp, 1999, J. Chem. Phys., **111**, 4005-4012.
196. Jungkamp, T. P. W., U. Kirchner, M. Schmidt and R. N. Schindler, 1995, J. Photochem. Photobiol. A: Chemistry, **99**, 1-6.
197. Kan, C. S., R. D. McQuigg, M. R. Whitbeck and J. G. Calvert, 1979, Int. J. Chem. Kinet., **11**, 921.
198. Kang, W. K., K. W. Jung, D.-C. Kim and K.-H. Jung, 1996, J. Chem. Phys., **104**, 5815-5820.
199. Kavita, K. and P. K. Das, 2000, J. Chem. Phys., **112**, 8426-8431.
200. Kim, Y. S., W. K. Kang and K.-H. Jung, 1996, J. Chem. Phys., **105**, 551-557.
201. Kim, Y. S., W. K. Kang, D.-C. Kim and K.-H. Jung, 1997, J. Phys. Chem. A, **101**, 7576-7581.
202. Knauth, H. D., H. Alberti and H. Clausen, 1979, J. Phys. Chem., **83**, 1604-1612.
203. Knauth, H. D. and R. N. Schindler, 1983, Z. Naturforsch., **38a**, 893.
204. Ko, M. K. W., D. S. Nien, W. C. Wang, G. Shia, A. Goldman, F. J. Murcray, D. G. Murcray and C. P. Rinsland, 1993, J. Geophys. Res., **98**, 10499-10507.
205. Koffend, J. B. and S. R. Leone, 1981, Chem. Phys. Lett., **81**, 136-141.
206. Kurylo, M. J., T. J. Wallington and P. A. Ouellette, 1987, J. Photochem., **39**, 201-215.
207. Kwok, W. M. and D. L. Phillips, 1996, J. Chem. Phys., **104**, 2529-2540.
208. Kwok, W. M. and D. L. Phillips, 1997, Chem. Phys. Lett., **270**, 506-516.
209. Kwok, W. M. and D. L. Phillips, 1997, Mol. Phys., **90**, 315-326.
210. Langhoff, S. R., L. Jaffe and J. O. Arnold, 1977, J. Quant. Spectrosc. Radiat. Transfer, **18**, 227.
211. Lawrence, W. G., K. C. Clemitshaw and V. A. Apkarian, 1990, J. Geophys. Res., **95**, 18591.
212. Lee, L. C., 1982, J. Chem. Phys., **76**, 4909-4915.
213. Leroy, B., G. Le Bras and P. Rigaud, 1981, Ann. Geophys., **37**, 297-302.
214. Lewis, B. R., L. Berzins and J. H. Carver, 1986, J. Quant. Spectrosc. Radiat. Transfer, **36**, 209-232.
215. Lewis, B. R., L. Berzins, J. H. Carver and S. T. Gibson, 1986, J. Quant. Spectrosc. Radiat. Transfer, **36**, 187-207.
216. Libuda, H. G. and F. Zabel, 1995, Ber. Bunsenges. Phys. Chem., **99**, 1205-1213.
217. Lightfoot, P. D., R. A. Cox, J. N. Crowley, M. Destriau, G. D. Hayman, M. E. Jenkin, G. K. Moortgat and F. Zabel, 1992, Atmos. Environ., **26A**, 1805-1961.
218. Lightfoot, P. D. and A. A. Jemi-Alade, 1991, J.Photochem. and Photobiol. A: Chem., **59**, 1-10.
219. Limao-Vieira, P., S. Eden, P. A. Kendall, N. J. Mason and S. V. Hoffmann, 2002, Chem. Phys. Lett., **364**, 535-541.
220. Lin, C. L., 1976, J. Chem. Eng. Data, **21**, 411.
221. Lin, C. L., N. K. Rohatgi and W. B. DeMore, 1978, Geophys. Res. Lett., **5**, 113-115.
222. Lock, M., R. J. Barmes and A. Sinha, 1996, J. Phys. Chem., **100**, 7972-7980.
223. Lopez, M. I. and J. E. Sicre, 1988, J. Phys. Chem., **92**, 563-564.
224. Lopez, M. I. and J. E. Sicre, 1990, J. Phys. Chem., **94**, 3860-3863.
225. Lucazeau, G. and C. Sandorfy, 1970, J. Mol. Spectrosc., **35**, 214-231.
226. MacLeod, H., G. P. Smith and D. M. Golden, 1988, J. Geophys. Res., **93**, 3813-3823.
227. Magnotta, F. and H. S. Johnston, 1980, Geophys. Res. Lett., **7**, 769-772.
228. Majer, J. R. and J. P. Simons. Photochemical Processes in Halogenated Compounds. In *Advances in Photochemistry*; Interscience, 1964; Vol. 2; pp 137-181.
229. Malicet, J., D. Daumont, J. Charbonnier, C. Parisse, A. Chakir and J. Brion, 1995, J. Atm. Chem, **21**, 263-273.
230. Man, S.-Q., W. M. Kwok, D. L. Phillips and A. E. Johnson, 1996, J. Chem. Phys., **105**, 5842-5857.
231. Manatt, S. L. and A. L. Lane, 1993, J. Quant. Spectrosc. Radiat. Transfer, **50**, 267-276.
232. Mandelman, M. and R. W. Nicholls, 1977, J. Quant. Spectrosc. Radiat. Trans., **17**, 483.
233. Margitan, J. J., 1983, J. Phys. Chem., **87**, 674-679.
234. Margitan, J. J. and R. T. Watson, 1982, J. Phys. Chem., **86**, 3819-3824.
235. Maric, D., J. P. Burrows, R. Meller and G. K. Moortgat, 1993, J. Photochem. Photobiol. A Chem., **70**, 205-214.
236. Maric, D., J. P. Burrows and G. K. Moortgat, 1994, J. Photochem. Photobiol A: Chem., **83**, 179-192.
237. Maric, D., J. N. Crowley and J. P. Burrows, 1997, J. Phys. Chem., **101**, 2561-2567.
238. Maricq, M. M. and J. J. Szente, 1994, J. Phys. Chem., **98**, 2078-2082.
239. Maricq, M. M. and J. J. Szente, 1996, J. Phys. Chem., **100**, 4507-4513.

240. Maricq, M. M. and T. J. Wallington, 1992, J. Phys. Chem., **96**, 982-986.
241. Marinelli, W. J. and H. S. Johnston, 1982, Chem. Phys. Lett., **93**, 127-132.
242. Marinelli, W. J., D. M. Swanson and H. S. Johnston, 1982, J. Chem. Phys., **76**, 2864-2870.
243. Martin, H. and R. Gareis, 1956, Z. Elektrochemie, **60**, 959-964.
244. Matsumi, Y., F. J. Comes, G. Hancock, A. Hofzumahaus, A. J. Hynes, M. Kawasaki and A. R. Ravishankara, 2002, J. Geophys. Res., **in press**.
245. Mauersberger, K., J. Barnes, D. Hanson and J. Morton, 1986, Geophys. Res. Lett., **13**, 671-673.
246. Mauersberger, K., D. Hanson, J. Barnes and J. Morton, 1987, J. Geophys. Res., **92**, 8480-8482.
247. Mauldin, R. L., III, J. B. Burkholder and A. R. Ravishankara, 1992, J. Phys. Chem., **96**, 2582-2588.
248. Mazely, T. L., R. R. Friedl and S. P. Sander, 1995, J. Phys. Chem., **99**, 8162-8169.
249. Mazely, T. L., R. R. Friedl and S. P. Sander, 1997, J. Phys. Chem., **101**, 7090-7097.
250. McAdam, K., B. Veyret and R. Lesclaux, 1987, Chem. Phys. Lett., **133**, 39-44.
251. McElcheran, D. E., M. H. J. Wijnen and E. W. R. Steacie, 1958, Can. J. Chem., **36**, 321.
252. McGee, T. J. and J. Burris, 1987, J. Quant. Spectrosc. Radiat. Trans., **37**, 165-182.
253. McGivern, W. S., R. Li, P. Zou and S. W. North, 1999, J. Chem. Phys., **111**, 5771-5779.
254. McGrath, M. P., K. C. Clemitshaw, F. S. Rowland and W. J. Hehre, 1988, Geophys. Res. Lett., **15**, 883-886.
255. McGrath, M. P., K. C. Clemitshaw, F. S. Rowland and W. J. Hehre, 1990, J. Phys. Chem., **94**, 6126-6132.
256. Merienne, M. F., B. Coquart and A. Jenouvrier, 1990, Planet. Space Sci., **38**, 617-625.
257. Merienne, M. F., A. Jenouvrier and B. Coquart, 1995, J. Atm. Chem, **20**, 281-297.
258. Minschwaner, K., G. P. Anderson, L. A. Hall and K. Yoshino, 1992, J. Geophys. Res., **97**, 10103-10108.
259. Minschwaner, K. and D. E. Siskind, 1993, J. Geophys. Res., **98**, 20401-20412.
260. Minton, T. K., C. M. Nelson, T. A. Moore and M. Okumura, 1992, Science, **258**, 1342-1345.
261. Mishalanie, E. A., J. C. Rutkowski, R. S. Hutte and J. W. Birks, 1986, J. Phys. Chem., **90**, 5578-5584.
262. Mitchell, D. N., R. P. Wayne, P. J. Allen, R. P. Harrison and R. J. Twin, 1980, J. Chem. Soc. Faraday Trans. 2, **76**, 785.
263. Molina, L. T., J. J. Lamb and M. J. Molina, 1981, Geophys. Res. Lett., **8**, 1008
264. Molina, L. T. and M. J. Molina, 1977, Geophys. Res. Lett., **4**, 83-86.
265. Molina, L. T. and M. J. Molina, 1978, J. Phys. Chem., **82**, 2410-2414.
266. Molina, L. T. and M. J. Molina, 1979, J. Photochem., **11**, 139-144.
267. Molina, L. T. and M. J. Molina, 1981, J. Photochem., **15**, 97.
268. Molina, L. T. and M. J. Molina. "Chemistry of Fluorine in the Stratosphere"; 182nd American Chemical Society National Meeting, 1982, New York.
269. Molina, L. T. and M. J. Molina, 1983, J. Phys. Chem., **87**, 1306.
270. Molina, L. T. and M. J. Molina, 1986, J. Geophys. Res., **91**, 14,501-14,508.
271. Molina, L. T. and M. J. Molina, 1996, Geophys. Res. Lett., **23**, 563-565.
272. Molina, L. T., M. J. Molina and F. S. Rowland, 1982, J. Phys. Chem., **86**, 2672-2676.
273. Molina, L. T., S. D. Schinke and M. J. Molina, 1977, Geophys. Res. Lett., **4**, 580-582.
274. Molina, M. J. and G. Arguello, 1979, Geophys. Res. Lett., **6**, 953-955.
275. Molina, M. J., T. Ishiwata and L. T. Molina, 1980, J. Phys. Chem., **84**, 821-826.
276. Moore, T. A., M. Okumura, M. Tagawa and T. K. Minton, 1995, Faraday Discuss, **100**, 295-307.
277. Moortgat, G. K., W. Klippel, K. H. Mobius, W. Seiler and P. Warneck FAA-EE-80-47, Federal Aviation Administration, Washington, DC 1980.
278. Moortgat, G. K., R. Meller and W. Schneider. Temperature dependence (256-296K) of the absorption cross-sections of bromoform in the wavelength range 285-360 nm. In *The Tropospheric Chemistry of Ozone in the Polar Regions*; Niki, H., Becker, K. H., Eds.; Springer-Verlag: Berlin, 1993; pp 359-369.
279. Moortgat, G. K., W. Seiler and P. Warneck, 1983, J. Chem. Phys., **78**, 1185-1190.
280. Moortgat, G. K., B. Veyret and R. Lesclaux, 1989, J. Phys. Chem., **93**, 2362-2368.
281. Moortgat, G. K. and P. Warneck, 1979, J. Chem. Phys., **70**, 3639-3651.
282. Morel, O., R. Simonaitis and J. Heicklen, 1980, Chem. Phys. Lett., **73**, 38.
283. Mossinger, J. C., D. E. Shallcross and R. A. Cox, 1998, J. Chem. Soc. Faraday Trans., **94**, 1391-1396.
284. Munk, J., P. Pagsberg, E. Ratajczak and A. Sillesen, 1986, J. Phys. Chem. , **90**, 2752-2757.
285. Murtagh, D. P., 1988, Planet. Space Sci., **36**, 819-828.
286. Nayak, A. K., T. J. Buckley, M. J. Kurylo and A. Fahr, 1996, J. Geophys. Res., **101**, 9055-9062.
287. Nayak, A. K., M. J. Kurylo and A. Fahr, 1995, J. Geophys. Res, **100**, 11185-11189.
288. Nee, J. B., 1991, J. Quant. Spectrosc. Radiat. Transfer, **46**, 55.

289. Nelson, C. M., T. A. Moore and M. Okumura, 1994, J. Chem. Phys., **100**, 8055-8064.
290. Nelson, C. M., T. A. Moore, M. Okumura and T. K. Minton, 1996, Chem. Phys, **2248**, 287-307.
291. Nelson, H. H. and H. S. Johnston, 1981, J. Phys. Chem., **85**, 3891.
292. Nickolaisen, S. L. and S. P. Sander, 1996, Manuscript in preparation.
293. Nickolaisen, S. L., S. P. Sander and R. R. Friedl, 1996, J. Phys. Chem., **100**, 10165.
294. Nicolet, M. and R. Kennes, 1989, Planet. Space Sci., **37**, 459-491.
295. Nicovich, J. M. and P. H. Wine, 1988, J. Geophys. Res., **93**, 2417.
296. Nolle, A., H. Heydtmann, R. Meller and G. K. Moortgat, 1993, Geophys. Res. Lett., **20**, 707-710.
297. NÖlle, A., H. Heydtmann, R. Meller, W. Schneider and G. K. Moortgat, 1992, Geophys. Res. Lett., **19**, 281-284.
298. Ogorzalek Loo, R., H.-P. Haerri, G. E. Hall and P. L. Houston, 1989, J. Chem. Phys., **90**, 4222-4236.
299. Oh, D., W. Sisk, A. Young and H. Johnston, 1986, J. Chem. Phys., **85**, 7146-7158.
300. Okabe, H. In *Photochemistry of Small Molecules*; John Wiley and Sons Inc.: New York, 1978; pp 217.
301. Okabe, H., 1980, J. Chem. Phys., **72**, 6642.
302. Orkin, V. L. and E. E. Kasimovskaya, 1995, J. Atm. Chem, **21**, 1-11.
303. Orkin, V. L., V. G. Khamaganov, A. G. Guschin, R. E. Huie and M. J. Kurylo, 1997, J. Phys. Chem. A, **101**, 174-178.
304. Orlando, J. J. and J. B. Burkholder, 1995, J. Phys. Chem., **99**, 1143-1150.
305. Orlando, J. J., J. B. Burkholder, S. A. McKeen and A. R. Ravishankara, 1991, J. Geophys. Res., **96**, 5013-5023.
306. Orlando, J. J., G. S. Tyndall, G. K. Moortgat and J. G. Calvert, 1993, J. Phys. Chem., **97**, 10996-11000.
307. Paraskevopoulos, G. and R. J. Cvetanovic, 1969, J. Am. Chem. Soc., **91**, 7572.
308. Parkes, D. A., 1977, Int. J. Chem. Kinet., **9**, 451.
309. Parkes, D. A., D. M. Paul, C. P. Quinn and R. C. Robson, 1973, Chem. Phys. Lett., **23**, 425-429.
310. Parrish, D. D., P. C. Murphy, D. L. Albritton and F. C. Fehsenfeld, 1983, Atmos. Environ., **17**, 1365.
311. Paukert, T. T. and H. S. Johnston, 1972, J. Chem. Phys., **56**, 2824-2838.
312. Pence, W., S. Baughum and S. Leone, 1981, J. Phys. Chem., **85**, 3844-3851.
313. Permien, T., R. Vogt and R. N. Schindler. Mechanisms of Gas Phase-Liquid Phase Chemical Transformations. In *Air Pollution Report #17*; Cox, R. A., Ed.; Environmental Research Program of the CEC.: Brussels, 1988.
314. Pfister, R. and R. J. Huber, 2002, personal communication.
315. Phillips, D. L., A. B. Myers and J. J. Valentini, 1992, J. Phys. Chem., **96**, 2039-2044.
316. Pilling, M. J. and M. J. C. Smith, 1985, J. Phys. Chem., **89**, 4713-4720.
317. Porret, D. and C. F. Goodeve, 1937, Trans. Faraday Soc., **33**, 690-693.
318. Porret, D. and C. F. Goodeve, 1938, Proc. Roy. Soc. London A, **165**, 31-42.
319. Prahlad, V. and V. Kumar, 1995, J. Quant. Spectrosc. Radiat. Transfer, **54**, 945-955.
320. Preston, K. F. and R. F. Barr, 1971, J. Chem. Phys., **54**, 3347-3348.
321. Rahn, T., H. Zhang, M. Wahlen and G. A. Blake, 1998, Geophys. Res. Lett., **25**, 4489-4492.
322. Rattigan, O., E. Lutman, R. L. Jones and R. A. Cox, 1992, J. Photochem. Photobiol. A: Chem., **66**, 313-326.
323. Rattigan, O., E. Lutman, R. L. Jones, R. A. Cox, K. Clemitshaw and J. Williams, 1992, J. Photochem. Photobiol. A: Chem., **69**, 125-126.
324. Rattigan, O. V., D. J. Lary, R. L. Jones and R. A. Cox, 1996, J. Geophys. Res., **101**, 23021-23033.
325. Rattigan, O. V., D. E. Shallcross and R. A. Cox, 1997, J. Chem. Soc. Soc. Faraday Trans., **93**, 2839-2846.
326. Ravishankara, A. R., 1995, Faraday Discuss, **100**, 335.
327. Ravishankara, A. R. and R. L. Mauldin, 1986, J. Geophys. Res., **91**, 8709-8712.
328. Ravishankara, A. R., S. Solomon, A. A. Turnipseed and R. F. Warren, 1993, Science, **259**, 194-199.
329. Ravishankara, A. R., S. Solomon, A. A. Turnipseed and R. F. Warren, 1993, Science, **259**, 194-199.
330. Ravishankara, A. R. and P. H. Wine, 1983, Chem. Phys. Lett., **101**, 73.
331. Ravishankara, A. R., P. H. Wine, C. A. Smith, P. E. Barbone and A. Torabi, 1986, J. Geophys. Res., **91**, 5355-5360.
332. Rebbert, R. E. and P. Ausloos, 1976/1977, J. Photochem., **6**, 265-276.
333. Rebbert, R. E. and P. J. Ausloos, 1975, J. Photochem., **4**, 419-434.
334. Rebbert, R. E., S. G. Lias and P. Ausloos, 1973, Int. J. Chem. Kinet., **5**, 893-908.
335. Rebbert, R. E., S. G. Lias and P. Ausloos, 1978, J. Photochem., **8**, 17-27.
336. Reid, S. A., J. T. Brandon and H. Reisler, 1993, J. Phys. Chem., **97**, 540.
337. Rigaud, P., B. Leroy, G. Le Bras, G. Poulet, J. L. Jourdain and J. Combourieu, 1977, Chem. Phys. Lett., **46**, 161.
338. Robbins, D. E., 1976, Geophys. Res. Lett., **3**, 213-216. See also Erratum, GRL, 1976, Vol. 3, p. 757.
339. Robbins, D. E. and R. S. Stolarski, 1976, Geophys. Rev. Lett., **3**, 603-606.

340. Rockmann, T. J., C. A. M. Brenninkmeijer, M. Wollenhaupt, J. N. Crowley and P. J. Crutzen, 2000, Geophys. Res. Lett., **27**, 1399-1402.
341. Rockmann, T. J., J. Kaiser, C. A. M. Brenninkmeijer, J. N. Crowley, R. Borchers, W. A. Brand and P. J. Crutzen, 2001, J. Geophys. Res., **106**, 10,403-10,410.
342. Roehl, C. M., D. Bauer and G. K. Moortgat, 1996, J. Phys. Chem., **100**, 4038-4047.
343. Roehl, C. M., J. B. Burkholder, G. K. Moortgat, A. R. Ravishankara and P. J. Crutzen, 1997, J. Geophys. Res., **102**, 12819-12829.
344. Roehl, C. M., J. J. Orlando and J. G. Calvert, 1992, J. Photochem. Photobiol. A: Chem., **69**, 1-5.
345. Rogers, J. D., 1990, J . Phys. Chem., **94**, 4011-4015.
346. Rowland, F. S. and Y. Makide, 1982, Geophys. Res. Lett., **9**, 473.
347. Rowland, F. S. and M. J. Molina, 1975, Rev. Geophys. Space Phys., **13**, 1-35.
348. Rowland, F. S. and P. J. Rogers, 1982, Proc. Natl. Acad. Sci. USA, **79**, 2737.
349. Rowland, F. S., J. E. Spencer and M. J. Molina, 1976, J. Phys. Chem., **80**, 2711-2713.
350. Roxlo, C. and A. Mandl, 1980, J. Appl. Phys., **51**, 2969-2972.
351. Rudolph, R. N. and E. C. Y. Inn, 1981, J. Geophys. Res., **86**, 9891.
352. Ruhl, E., A. Jefferson and V. Vaida, 1990, J. Phys. Chem., **94**, 2990.
353. Russell, B. R., L. O. Edwards and J. W. Raymonda, 1973, J. Am. Chem. Soc., **95**, 2129-2133.
354. Safary, E., J. Romand and B. Vodar, 1951, J. Chem. Phys., **19**, 379.
355. Salomon, D., A. W. Kirk and E. Tschuikow-Roux, 1977, J. Photochem., **7**, 345-353.
356. Sander, S. P., 1986, J. Phys. Chem., **90**, 4135-4142.
357. Sander, S. P. and R. R. Friedl, 1989, J. Phys. Chem., **93**, 4764-4771.
358. Sander, S. P., R. R. Friedl, W. B. DeMore, D. M. Golden, M. J. Kurylo, R. F. Hampson, R. E. Huie, G. K. Moortgat, A. R. Ravishankara, C. E. Kolb and M. J. Molina "Chemical Kinetics and Photochemical Data for Use in Stratospheric Modeling, Evaluation Number 13," JPL Publication 00-3, Jet Propulsion Laboratory, California Institute of Technology, Pasadena, CA, 2000.
359. Sander, S. P., M. Peterson, R. T. Watson and R. Patrick, 1982, J. Phys. Chem., **86**, 1236-1240.
360. Sander, S. P. and R. T. Watson, 1981, J. Phys. Chem., **85**, 2960.
361. Sandorfy, C., 1976, Atmos. Environ., **10**, 343-351.
362. Sauvageau, P., J. Doucet, R. Gilbert and C. Sandorfy, 1974, J. Chem. Phys., **61**, 391.
363. Sauvageau, P., R. Gilbert, P. P. Berlow and C. Sandorfy, 1973, J. Chem. Phys., **59**, 762.
364. Schiffman, A., D. D. Nelson, Jr. and D. J. Nesbitt, 1993, J. Chem. Phys., **98**, 6935-6946.
365. Schmitt, G. and F. J. Comes, 1980, J. Photochem., **14**, 107-123.
366. Schmitt, G. and F. J. Comes, 1987, J. Photochem. Photobiol. A, **41**, 13-30.
367. Schneider, W., G. K. Moortgat, J. P. Burrows and G. Tyndall, 1987, J. Photochem. Photobiol., **40**, 195-217.
368. Schneider, W. F., T. J. Wallington, K. Minschwaner and E. A. Stahlberg, 1995, Environ. Sci. Technol., **29**, 247.
369. Seccombe, D. P., R. Y. L. Chim, R. P. Tucket, H. W. Jochims and H. Baumgaertel, 2001, J. Chem. Phys., **114**, 4058-4073.
370. Seery, D. J. and D. Britton, 1964, J. Phys. Chem., **68**, 2263.
371. Selwyn, G., J. Podolske and H. S. Johnston, 1977, Geophys. Res. Lett., **4**, 427-430.
372. Senum, G. I., Y.-N. Lee and J. S. Gaffney, 1984, J. Phys. Chem., **88**, 1269-1270.
373. Shardanand and A. D. P. Rao, 1977, J. Quant. Spectrosc. Radiat. Transfer, **17**, 433-439.
374. Shetter, R. E., J. A. Davidson, C. A. Cantrell, N. J. Burzynski and J. G. Calvert, 1988, J. Geophys. Res., **93**, 7113-7118.
375. Silvente, E., R. C. Richter, M. Zheng, E. S. Saltzman and A. J. Hynes, 1997, Chem. Phys. Lett., **264**, 309-315.
376. Silver, J. A., D. R. Worsnop, A. Freedman and C. E. Kolb, 1986, J. Chem. Phys. , **84**, 4378-4384.
377. Simon, F.-G., W. Schneider and G. K. Moortgat, 1990, Int. J. Chem. Kinet., **22**, 791-813.
378. Simon, F. G., W. Schneider, G. K. Moortgat and J. P. Burrows, 1990, J. Photochem. Photobiol., **A55**, 1-23.
379. Simon, P. C., D. Gillotay, N. Vanlaethem-Meuree and J. Wisemberg, 1988, J. Atmos. Chem., **7**, 107-135.
380. Simon, P. C., D. Gillotay, N. Vanlaethem-Meuree and J. Wisemberg, 1988, Annales Geophysicae, **6**, 239-248.
381. Simonaitis, R., R. I. Greenberg and J. Heicklen, 1972, Int. J. Chem. Kinet., **4**, 497.
382. Singer, R. J., J. N. Crowley, J. P. Burrows, W. Schneider and G. K. Moortgat, 1989, J. Photochem. Photobiol., **48**, 17-32.
383. Smith, G. D., L. T. Molina and M. J. Molina, 2000, J. Phys.Chem. A, **104**, 8916-8921.
384. Smith, W. S., C. C. Chou and F. S. Rowland, 1977, Geophys. Res. Lett., **4**, 517-519.
385. Solomon, S., J. B. Burkholder, A. R. Ravishankara and R. R. Garcia, 1994, J. Geophys. Res., **99**, 20929-20935.
386. Spencer, J. E. and F. S. Rowland, 1978, J. Phys. Chem., **82**, 7-10.
387. Stanton, J. F., C. M. L. Rittby, R. J. Bartlett and D. W. Toohey, 1991, J. Phys. Chem., **95**, 2107-2110.

388. Stief, L. J., W. A. Payne and R. B. Klemm, 1975, J. Chem. Phys., **62**, 4000-4008.
389. Stockwell, W. R. and J. G. Calvert, 1978, J. Photochem., **8**, 193-203.
390. Suto, M. and L. C. Lee, 1985, J. Geophys. Res., **90**, 13037-13040.
391. Swanson, D., B. Kan and H. S. Johnston, 1984, J. Phys. Chem., **88**, 3115.
392. Takahashi, K., Y. Matsumi and M. Kawasaki, 1996, J. Phys. Chem., **100**, 4084-4089.
393. Talukdar, R., A. Mellouki, T. Gierczak, J. B. Burkholder, S. A. McKeen and A. R. Ravishankara, 1991, J. Phys. Chem., **95**, 5815-5821.
394. Talukdar, R., A. Mellouki, T. Gierczak, J. B. Burkholder, S. A. McKeen and A. R. Ravishankara, 1991, Science, **252**, 693-695.
395. Talukdar, R. K., J. B. Burkholder, A.-M. Schmoltner, J. M. Roberts, R. Wilson and A. R. Ravishankara, 1995, J. Geophys. Res., **100**, 14163-14173.
396. Talukdar, R. K., M. K. Gilles, F. Battin-Leclerc, A. R. Ravishankara, J.-M. Fracheboud, J. J. Orlando and G. S. Tyndall, 1997, Geophys. Res. Lett., **24**, 1091-1094.
397. Talukdar, R. K., M. Hunter, R. F. Warren, J. B. Burkholder and A. R. Ravishankara, 1996, Chem. Phys. Lett., **262**, 669-674.
398. Talukdar, R. K., C. A. Longfellow, M. K. Gilles and A. R. Ravishankara, 1998, Geophys. Res. lett., **25**, 143-146.
399. Talukdar, R. K., G. L. Vashjiani and A. R. Ravishankara, 1992, J. Chem. Phys., **96**, 8194-8201.
400. Tang, K. Y., P. W. Fairchild and E. K. C. Lee, 1979, J. Phys. Chem., **83**, 569.
401. Thelen, M.-A., P. Felder and J. R. Huber, 1993, Chem. Phys. Lett., **213**, 275-281.
402. Trolier, M., R. L. Mauldin, III and A. R. Ravishankara, 1990, J. Phys. Chem., **94**, 4896-4907.
403. Trolier, M. and J. R. Wiesenfeld, 1988, J. Geophys. Res., **93**, 7119-7124.
404. Turatti, F., D. W. T. Griffith, S. R. Wilson, M. B. Esler, T. Rahn, H. Zhang and G. A. Blake, 2000, Geophys. Res. Lett., **27**, 2489-2492.
405. Turco, R. P., 1975, Geophys. Surveys, **2**, 153-192.
406. Turco, R. P., R. J. Cicerone, E. C. Y. Inn and L. A. Capone, 1981, J. Geophys. Res., **86**, 5373.
407. Turnipseed, A. A., G. L. Vaghjiani, J. E. Thompson and A. R. Ravishankara, 1992, J. Chem. Phys., **96**, 5887.
408. Tyndall, G. S., R. A. Cox, C. Granier, R. Lesclaux, G. K. Moortgat, M. J. Pilling, A. R. Ravishankara and T. J. Wallington, 2001, J. Geophys. Res., **106**, 12157-12182.
409. Tyndall, G. S., K. M. Stedman, W. Schneider, J. P. Burrows and G. K. Moortgat, 1987, J. Photochem., **36**, 133-139.
410. Uma, S. and P. K. Das, 1994, Can. J. Chem., **72**, 865-869.
411. Uma, S. and P. K. Das, 1995, Chem. Phys. Lett., **241**, 335-338.
412. Uma, S. and P. K. Das, 1996, J. Chem. Phys., **104**, 4470-4474.
413. Uthman, A. P., P. J. Demlein, T. D. Allston, M. C. Withiam, M. J. McClements and G. A. Takacs, 1978, J. Phys. Chem., **82**, 2252-2257.
414. Vaghjiani, G. L. and A. R. Ravishankara, 1989, J. Geophys. Res., **94**, 3487-3492.
415. Vaghjiani, G. L. and A. R. Ravishankara, 1990, J. Chem. Phys., **92**, 996.
416. Vaghjiani, G. L., A. A. Turnipseed, R. F. Warren and A. R. Ravishankara, 1992, J. Chem. Phys., **96**, 5878.
417. Vaida, V., S. Solomon, E. C. Richards, E. Ruhl and A. Jefferson, 1989, Nature, **342**, 405.
418. Vanlaethem-Meuree, N., J. Wisemberg and P. C. Simon, 1978, Bull. Acad. Roy. Belgique Cl. Sci., **64**, 31.
419. Vanlaethem-Meuree, N., J. Wisemberg and P. C. Simon, 1978, Bull. Acad. Roy. Belgique Cl. Sci., **64**, 42.
420. Vanlaethem-Meuree, N., J. Wisemberg and P. C. Simon, 1979, Geophys. Res. Lett., **6**, 451-454.
421. Vasudev, R., 1990, Geophys. Res. Lett., **17**, 2153-2155.
422. Vogt, R. and R. N. Schindler, 1992, J. Photochem. Photobiol. A: Chem., **66**, 133-140.
423. Wahner, A., A. R. Ravishankara, S. P. Sander and R. R. Friedl, 1988, Chem. Phys. Lett., **152**, 507.
424. Wahner, A., G. S. Tyndall and A. R. Ravishankara, 1987, J. Phys. Chem., **91**, 2734-2738.
425. Wallington, T. J., P. Dagaut and M. J. Kurylo, 1988, J. Photochem. Photobiol. A: Chemistry, **42**, 173-185.
426. Wallington, T. J., P. Dagaut and M. J. Kurylo, 1992, Chem. Rev., **92**, 667-710.
427. Wallington, T. J., M. M. Mariq, T. Ellerman and O. J. Nielsen, 1992, J. Phys. Chem., **96**, 982-986.
428. Walton, J. C., 1972, J. Chem. Soc. Farad. Trans., **68**, 1559.
429. Wannenmacher, E. A. J., P. Felder and R. J. Huber, 1991, J. Chem. Phys., **95**, 986-997.
430. Watson, R. T., 1977, J. Phys. Chem. Ref. Data, **6**, 871-917.
431. Wayne, R. P., I. Barnes, J. P. Burrows, C. E. Canosa-Mas, J. Hjorth, G. Le Bras, G. K. Moortgat, D. Perner, G. Poulet, G. Restelli and H. Sidebottom, 1991, Atmos. Environ., **25A**, 1-203.
432. Wine, P. H., W. L. Chameides and A. R. Ravishankara, 1981, Geophys. Res. Lett., **8** 543-546.

433. Wine, P. H., A. R. Ravishankara, D. L. Philen, D. D. Davis and R. T. Watson, 1977, Chem. Phys. Lett., **50**, 101.
434. WMO *Atmospheric Ozone: 1985*; National Aeronautics and Space Administration: Geneva, 1986.
435. Xu, H. and J. A. Joens, 1993, Geophys. Res. Lett., **20**, 1035-1037.
436. Yao, F., I. Wilson and H. Johnston, 1982, J. Phys. Chem., **86**, 3611.
437. Yokelson, R. J., J. B. Burkholder, R. W. Fox, R. K. Talukdar and A. R. Ravishankara, 1994, J. Phys. Chem., **98**, 13144-13150.
438. Yoshino, K., A. S. C. Cheung, J. R. Esmond, W. H. Parkinson, D. E. Freeman, S. L. Guberman, A. Jenouvrier, B. Coquart and M. F. Merienne, 1988, Planet. Space Sci., **36**, 1469-1475.
439. Yoshino, K., J. R. Esmond, A. S. C. Cheung, D. E. Freeman and W. H. Parkinson, 1990, J. Geophys. Res., **95**, 11743.
440. Yoshino, K., J. R. Esmond, A. S.-C. Cheung, D. E. Freeman and W. H. Parkinson, 1992, Planet. Space Sci., **40**, 185-192.
441. Yoshino, K., J. R. Esmond, D. E. Freeman and W. H. Parkinson, 1993, J. Geophys. Res., **98**, 5205-5211.
442. Yoshino, K., D. E. Freeman, J. R. Esmond, R. S. Friedman and W. H. Parkinson, 1988, Planet. Space Sci., **36**, 1201-1210.
443. Yoshino, K., D. E. Freeman, J. R. Esmond, R. S. Friedman and W. H. Parkinson, 1989, Planet. Space Sci., **37**, 419-426.
444. Yoshino, K., D. E. Freeman, J. R. Esmond and W. H. Parkinson, 1987, Planet. Space Sci., **35**, 1067-1075.
445. Yoshino, K., D. E. Freeman and W. H. Parkinson, 1984, J. Phys. Chem. Ref. Data, **13**, 207-227.
446. Yoshino, K., D. F. Freeman, J. R. Esmond and W. H. Parkinson, 1983, Planet. Space Sci., **31**, 339-353
447. Yung, Y. L. and C. E. Miller, 1997, Science, **278**, 1778-1780.
448. Zelikoff, M. and L. M. Aschenbrand, 1954, J. Chem. Phys., **22** 1685-1687.
449. Zetzsch, C. In *Proceedings of the International Ozone Symposium 1988*; Bojkov, R., Fabian, P., Eds.; Deepak: Hampton, VA, 1989.
450. Zhang, H., P. O. Wennberg, V. H. Wu and G. A. Blake, 2000, Geophys. Res. Lett., **27**, 2481-2484.
451. Zhang, L., W. Fuss and K. L. Kompa, 1990, Chem. Phys., **144**, 289-297.
452. Zou, P., W. S. McGivern and S. W. North, 2000, Phys. Chem. Chem. Phys., **2**, 3785-3790.
453. Zou, P., W. S. McGivern, O. Sokhabi, A. G. Suits and S. W. North, 2000, J. Chem. Phys., **113**, 7149-7157.

SECTION 5. HETEROGENEOUS CHEMISTRY

Table of Contents

SECTION 5. HETEROGENEOUS CHEMISTRY 5-1
5.1 Introduction 5-1
5.2 Surface Types—Acid/Water, Liquids, and Solids 5-2
5.3 Surface Types—Soot and Alumina 5-2
5.4 Surface Composition and Morphology 5-3
5.5 Surface Porosity 5-4
5.6 Temperature Dependences of Parameters 5-4
5.7 Solubility Limitations 5-4
5.8 Data Organization 5-4
5.9 Parameter Definitions 5-5
5.10 Mass Accommodation Coefficients for Surfaces Other Than Soot 5-9
5.11 Notes to Table 5-1 5-10
5.12 Gas/Surface Reaction Probabilities for Surfaces Other Than Soot. 5-17
5.13 Notes to Table 5-2 5-20
5.14 Soot Surface Uptake Coefficients 5-33
5.15 Notes to Table 5-3 5-33
5.16 Henry's Law Constants for Pure Water 5-36
5.17 Notes to Table 5-4 5-37
5.18 Henry's Law Constants for Acids 5-41
5.19 Notes to Table 5-5 5-41
5.20 References 5-45

Tables

Table 5-1. Mass Accommodation Coefficients (α) for Surfaces Other Than Soot. 5-9
Table 5-2. Gas/Surface Reaction Probabilities (γ) for Surfaces Other Than Soot. 5-17
Table 5-3. Soot Surface Uptake Coefficients. 5-33
Table 5-4. Henry's Law Constants for Pure Water. 5-36
Table 5-5. Henry's Law Constants for Acids 5-41

Figures

Figure 5-1. Recommended reactive uptake coefficients as a function of temperature for key stratospheric heterogeneous processes on sulfuric acid aerosols. 5-7

5.1 Introduction

We have evaluated and tabulated the currently available information on heterogeneous stratospheric processes. In addition, because of the increasing level of interest in tropospheric processes with a direct bearing on the fluxes of reactive species into the stratosphere, such as heterogeneous loss processes for partially oxidized degradation products of hydrohalocarbons and heterogeneous contrail and cloud processing of exhaust species from aircraft, we have included kinetic data for selected heterogeneous interactions relevant to modeling cloud droplet and aqueous aerosol chemistry in the free troposphere. However, both stratospheric and tropospheric heterogeneous chemistry are relatively new and rapidly developing fields, and further results can be expected to change our quantitative and even our qualitative understanding on a regular basis. The complexity is compounded by the difficulty of characterizing the chemical and physical properties of atmospheric heterogeneous surfaces and then reproducing suitable simulations in the laboratory [227]. New and/or updated evaluations in this document have focused on uptake measurements on binary liquid sulfuric acid/water, supplemented in a few cases by data on ternary liquid sulfuric acid/water solutions, on water ice, and on "soot" (see definitions below). No updates on solid acid/ice compositions are presented in this document, although evaluations for key nitrogen oxide sequestration and/or halogen activation reactions on nitric acid trihydrate (NAT) surfaces were recently re-evaluated and presented in JPL 00-3 [306]. Uptake data on alumina, salt and aqueous salt solutions have not been updated since JPL 97-4 [102]. Henry's law solubility data for reactive upper tropospheric/stratospheric species in binary liquid sulfuric acid/water and, where available, in ternary liquid sulfuric acid/nitric acid/water solutions have also been updated and a much more extensive compilation of Henry's law parameters for pure water has been added.

5.2 Surface Types—Acid/Water, Liquids, and Solids

To a first approximation there are three major types of surfaces believed to be present at significant levels in the stratosphere. They are: (1) Type I polar stratospheric clouds (PSCs), nominally composed of nitric acid trihydrate ($HNO_3 \cdot 3H_2O$); (2) crystals of relatively pure water ice, designated as Type II PSCs because they form at lower temperatures than Type I and are believed to be nucleated by Type I (similar surfaces may form as contrails behind high-altitude aircraft under some stratospheric conditions); and (3) sulfuric acid aerosol, which is nominally a liquid phase surface generally composed of 60–80 weight percent H_2SO_4 and, concomitantly, 40–20 weight percent H_2O. While PSCs, as their name suggests, are formed primarily in the cold winter stratosphere at high latitudes, sulfuric acid aerosol is present year round at all latitudes and may influence stratospheric chemistry on a global basis, particularly after large injections of volcanic sulfur episodically increase their abundance and surface area. There is also increasing evidence that ternary $H_2SO_4/HNO_3/H_2O$ liquid solutions may play a significant role in PSC formation.

In addition to the major stratospheric surface types noted above, several other types of heterogeneous surfaces are found in the stratosphere and may play a significant role in some stratospheric processes. For instance, laboratory work has indicated that nitric acid dihydrate (NAD) may play an important role in the nucleation of Type I PSCs (Worsnop et al. [358], Fox et al. [126]) and that mixtures of solid nitric acid hydrates and sulfuric acid tetrahydrate (SAT) (Molina et al. [261], Zhang et al. [370]) and/or a more complex sulfuric acid/nitric acid hydrate (Fox et al. [126]) may also be key to understanding Type I PSC nucleation and evolution. Analyses of the range of atmospheric conditions possible in the polar stratosphere have also led to interest in solid SAT surfaces and possibly other forms of frozen sulfuric acid aerosols (Toon et al. [334], Middlebrook et al. [256]), as well as liquid sulfuric acid aerosols significantly more dilute than the 60–80 weight percent normally present at lower latitudes (Wolff and Mulvaney [356], Hofmann and Oltmans [177], Toon et al. [334]). Some modeling studies also suggest that certain types of major volcanic eruptions transport significant levels of sodium chloride into the stratosphere (Michelangeli et al. [255]), so studies of stratospheric trace species interacting with solid NaCl or similar salts, as well as salt solutions, have also been included.

In the free troposphere the heterogeneous surfaces of interest include liquid or solid water (cloud droplets, contrails), and aqueous sulfate solutions. Uptake data are compiled for liquid water for several reasons. First this surface is one asymptote of the aqueous acid aerosol continuum; second, the interactions of some trace species with liquid water and water ice (Type II PSC) surfaces are often similar, and third, the uptake of some trace species by liquid water surfaces in the troposphere can play a key role in understanding their tropospheric chemical lifetimes and thus, the fraction that may be transported into the stratosphere.

5.3 Surface Types—Soot and Alumina

Aircraft at cruise altitudes and rocket exhausts contribute small but measurable amounts of carbonaceous "soot" (Pueschel et al. [280]) and aluminized solid propellant rocket exhausts and spacecraft debris produce increasing levels of alumina (Al_2O_3) and similar metal oxide particles (Zolensky et al. [373]) in the stratosphere and upper troposphere. Soot lofted above from surface combustion sources may also be present in the upper troposphere, and to a lesser extent in the lower stratosphere. Alumina from rocket exhausts is generally emitted as liquid droplets from the rocket nozzle and deposited in the alpha or metastable gamma phases as it quickly solidifies in the exhaust plume. "Soot" refers to a material that is a combination of elemental and organic carbon, with proportions varying depending on the source material and the combustion conditions. In studies of soot directed to understanding the interaction with atmospheric gases, two types of soot have been used: carbon blacks having relatively small hydrogen and oxygen contents (e.g. Degussa FW2, Cabot Monarch 1000, ground charcoal and spark-generated soot) and organic combustion soots having higher hydrogen, oxygen and nitrogen content (e.g. soots from the combustion of n-hexane, methane, propane, decane, ethylene, acetylene, toluene, stearic candles). In the case of organic combustion soots, even different fuels used to generate the soot have been reported to affect the chemistry; for example, the yields of HONO from the reaction of NO_2 with acetylene, toluene, ethylene and decane soots were observed to vary with the fuel used [14,134].

Polycyclic aromatic hydrocarbons (PAH) and oxygenated polycyclic aromatic compounds (O-PAC) are major constituents of soots formed from the combustion of liquid fuels [10-12,63,123,139,315]. The bulk composition of soot can have varying amounts of C, H, and O. For example, Chughtai et al. [77] report that the composition (in weight %) of *n*-hexane soot varies from 87 to 92 % C, 1.2 to 1.6 % H, and 11 to 6% oxygen. Stadler and Rossi [321] showed that the elemental composition of the soot as well as its surface area depended on whether the flame was rich or lean; in the case of the rich flame giving a grey-colored soot, the composition (weight %) was 97.3% C, 0.83% H, 1.65% O, and 0.20% N while the lean flame gave a black soot comprised of 96.4% C, 0.19% H, 3.2% O, and 0.27% N.

The functional groups on the soot surface are expected to be important in terms of the uptake and reaction of gases on the surface. XPS studies of *n*-hexane soot show surface carbon and oxygen, although the specific nature of the bonding could not be determined (Akhter et al. [12]). The surface functional groups on soot vary, depending on the fuel composition, method of generation and the post-treatment of the soot. For example, Degussa FW2 carbon black, which has been used in a number of studies of uptake and reactions of gases on soots, is post-treated with NO_2 by the manufacturer and Cabot Monarch 1000 is post-treated with aqueous HNO_3. There may be sufficient NO and NO_2 concentrations generated under some conditions during the formation of soots by spark generators that these may also have been reacted with these gases prior to collection and uptake studies. Studies of a number of gases interacting with soot surfaces suggest there are at least two and likely more, types of reactive surface sites; one type reacts very rapidly, e.g. with O_3, while others react more slowly. The first type may be most relevant to the reactions of soot particles in exhaust plumes from combustion sources, while the latter is most relevant to soot diluted in air.

Fourier transform infrared (FTIR) , Raman and electron paramagentic resonance (EPR) spectroscopic studies of n-hexane soot show C–O functionalities assigned to anhydrides and aryl ethers, alkyl ketones, as well as =C–H, highly substituted aromatics and conjugated carbonyl-aromatic groups [10,315]. Kirchner et al. [220] measured the FTIR spectra of soots from the combustion of diesel fuel and *n*-hexane (described as "flame deposited") and soots collected from a commercial spark generator in Ar, from the emissions of a diesel automobile and Degussa FW2 soot (described as "filter deposited"). In all cases, absorption peaks due to –C–C–, –C=C–, –C–O, aromatic –C=O, and carboxylic –C=O groups (both aromatic and aliphatic) were observed. However, the flame-deposited soot showed bands due to substituted aromatics while the filter-collected samples did not. The filter-deposited samples had bands due to aliphatic –C–H groups that were not observed for the flame-deposited soots. Only the spark-generated soot showed bands due to both –C=C–H and to –O–H.

For soot formed from the combustion of liquid fuels, the location in the flame at which the soot is collected also changes the surface enough to alter its reactions. For example, Akhter et al. [10] showed that the functional groups as well as particle size depend on the height of collection of soot from the base of the flame. Such changes appear to also alter the reactions of soot; for example, Gerecke et al. [134] measured HONO and NO yields from the reaction of NO_2 with ethylene soot and found that the HONO yield decreased with distance from the bottom of the flame that the soot was collected from, while the yield of NO increased. Kirchner et al. [220] reported much stronger infrared absorption bands due to substituted aromatics in soot samples collected from the combustion of *n*-hexane near the bottom of the flame compared to the top; in addition, absorption bands due to the –O–H group were only observed in samples collected at the bottom of the flame.

Not only can the surface groups directly affect its interaction with gases, but they determine the hygroscopic properties of the soot surface. Chughtai et al. [84,87] have shown that the hydration of soot surfaces depends on the fuel composition (particularly sulfur and trace metal content) and combustion conditions, as well as the extent of surface oxidation. A highly hygroscopic surface holding significant amounts of water may behave differently than a "dry" surface with respect to the interaction with gases; for example, black carbon suspended in aqueous solutions with ozone and irradiated to generate OH has been shown to help assist in the initiation of bulk solution phase OH chemistry [195]. There are also free radical sites on soot surfaces whose EPR signals are strongly affected by the adsorption of paramagnetic species such as NO_2 (e.g. see Chughtai et al. [77]). These unpaired electrons in soot may contribute to the surface reactivity.

The *International Steering Committee for Black Carbon Reference Materials* (http://www.du.edu/~dwismith/bcsteer.html) has issued preliminary recommendations for representative black carbon reference materials. They recommend that soot formed from the combustion of saturated hydrocarbons, preferably *n*-hexane, be used for soot black carbon. For aerosol black carbon, they recommend the use of Urban Dust Reference Material (SRM) 1649a, which is a sample collected in Washington, D.C. in a baghouse in 1976–1977. However, for studies of the uptake and reactions of gases in the atmosphere with combustion-generated soots, organic combustion generated soots, particularly *n*-hexane soot, appear to be the most reasonable surrogate.

5.4 Surface Composition and Morphology

The detailed composition and morphology of each surface type are uncertain and probably subject to a significant range of natural variability. Certain chemical and physical properties of these surfaces, such as their ability to absorb and/or solvate HCl and HNO_3, are known to be strongly dependent on their detailed chemical composition. Moreover, most heterogeneous processes studied under laboratory conditions (and in some cases proceeding under stratospheric conditions) can change the chemical composition of the surface in ways that significantly affect the kinetic or thermodynamic processes of interest. Thus, a careful analysis of the time-dependent nature of the active surface is required in the evaluation of measured uptake kinetics experiments.

Experimental techniques which allow the measurement of mass accommodation or surface reaction kinetics with high time resolution and/or with low trace gas fluxes are often more credible in establishing that measured kinetic parameters are not seriously compromised by surface saturation or changing surface chemical composition.

The measured kinetic uptake parameters, mass accommodation coefficients, and surface reaction probabilities are separately documented for relevant atmospheric trace gas species for the major and, where available, the minor stratospheric and upper tropospheric surfaces noted above. Since these parameters can vary significantly with surface composition (e.g., the H_2SO_4/H_2O ratio for sulfate aerosol or the HNO_3/H_2O ratio for Type I PSC) the dependence of these parameters on surface composition is reviewed where sufficient data are available.

Due to its chemical and morphological complexity, uptake values for soot are documented in a separate table.

5.5 Surface Porosity

The experimental techniques utilized to measure mass accommodation, heterogeneous reaction, and other uptake coefficients generally require knowledge of the surface area under study. For solid surfaces, and most particularly for water and acid ice surfaces formed in situ, the determination of how the molecular scale ice surface differs from the geometrical surface of the supporting substrate is not easy. Keyser, Leu, and coworkers have investigated the structure of water and nitric acid ice films prepared under conditions similar to those used in their flow reactor for uptake studies [215,216,218]. They have demonstrated that ice films grown in situ from the vapor can have a considerably larger available surface than that represented by the geometry of the substrate; they have also developed a simple model to attempt to correct measured uptake rates for this effect [217,218]. This model predicts that correction factors are largest for small uptake coefficients and thick films. The application of the model to experimental uptake data remains controversial (Keyser et al. [217], Hanson and Ravishakara [162], Kolb et al. [227]). Some experimenters prefer to attempt growing ice surfaces as smooth as possible and to demonstrate that their measured uptake coefficients are only weakly dependent on surface thickness (Hanson and Ravishankara [160]). Similar issues arise for uptake experiments performed on powered, fused and single crystal salt or oxide surfaces (Fenter et al. [120]; Hanning-Lee et al. [147]).The issue of surface area available for uptake is also important for interpreting uptake measurements on soot and soot surrogate surfaces. The degree to which measured uptake parameters must be corrected for porosity effects will remain in some doubt until a method is devised for accurately determining the effective surface area for the surfaces actually used in uptake studies. Most studies evaluated in this review assume that the effective ice or salt surface area is the geometrical area.

5.6 Temperature Dependences of Parameters

A number of laboratory studies have shown that mass accommodation coefficients and, to some extent, surface reaction probabilities can be temperature dependent. While these dependencies have not been characterized for many systems of interest, temperature effects on kinetic data are noted where available. More work that fully separates heterogeneous kinetic temperature effects from temperature controlled surface composition is obviously needed.

5.7 Solubility Limitations

The uptake of certain trace gases by atmospherically relevant surfaces is usually governed by solubility limitations rather than kinetic processes. In these cases properly analyzed data can yield measurements of trace gas solubility parameters relevant to stratospheric conditions. In general, such parameters can be strongly dependent on both condensed phase composition and temperature. Such parameters may be very important in stratospheric models, since they can govern the availability of a reactant for a bimolecular heterogeneous process (e.g., the concentration of HCl available for the $HCl + ClONO_2$ reaction on sulfuric acid aerosols) or the gas/condensed phase partitioning of a heterogeneous reaction product (e.g., the HNO_3 formed by the reaction of N_2O_5 on sulfuric acid aerosols). Surface saturation limitations have also been observed in experimental uptake studies on solid surfaces, including water and water/acid ice surfaces.

5.8 Data Organization

Data for trace-gas heterogeneous interactions with relevant condensed-phase surfaces are tabulated in Tables 5-1 through 5-5. These are organized into

Table 5-1—Mass Accommodation Coefficients for Surfaces Other Than Soot.

Table 5-2—Surface Reaction Probabilities for Surfaces Other Than Soot.

Table 5-3—Soot-Surface Uptake Coefficients.

Table 5-4—Solubility Data for Pure Water.

Table 5-5—Solubility Data for Acids.

This compilation provides updated evaluations based on published literature available through 2001 for water ice, liquid sulfuric acid/nitric acid/water, and soot/soot surrogate surfaces. The evaluations for alumina, solid alkali salt, aqueous alkali salt, and liquid water (with the exception of Henry's law constants for liquid water) have not been re-evaluated since JPL Publication 97-4 [102]. Evaluations and recommendations for the latter surfaces should be used with caution since new studies have been published in some cases that would alter the recommended values or extend their range of applicability.

5.9 Parameter Definitions

Mass accommodation coefficients (α), represent the probability of reversible uptake of a gaseous species colliding with the condensed surface of interest. For liquid surfaces this process is associated with interfacial (gas-to-liquid) transport and is generally followed by bulk liquid phase solvation. Examples include: simple surface absorption, absorption followed by ionic dissociation and solvation (e.g., $HCl + nH_2O \leftrightarrow H^+(aq) + Cl^-(aq)$), and absorption followed by a reversible chemical reaction with a condensed phase substituent (e.g., $SO_2 + H_2O \leftrightarrow H^+ + HSO_3^-$ or $CH_2O + H_2O \leftrightarrow CH_2(OH)_2$).

The term "sticking coefficient" is often used for mass accommodation on solid surfaces where physisorption or chemisorption takes the place of true interfacial mass transport.

Processes involving liquid surfaces are subject to Henry's law, which limits the fractional uptake of a gas phase species into a liquid. If the gas phase species is simply solvated, a physical Henry's law constraint holds; if the gas phase species reacts with a condensed phase substituent, as in the sulfur dioxide or formaldehyde hydrolysis cases noted above, a "chemically modified" or "effective" Henry's law constraint holds (Clegg and Brimblecombe [88], Schwartz [308], Watson et al. [348]). Henry's law constants relate the equilibrium concentration of a species in the gas phase to the concentration of the same species in a liquid phase, and they have, in this report, units of
M atm^{-1}. These are tabulated for liquid surfaces in Table 5-4 and Table 5-5. Effective Henry's law constants are designated H*, while simple physical Henry's law constants are represented by H. Effective Henry's law constants are also employed to represent decreased trace gas solubilities in moderate ionic strength acid or salt solutions with the use of a Setchenow coefficient formulation which relates H* to the concentration of the acid or salt [185]. Available Henry's law constants for reactive upper tropospheric/stratospheric species in binary sulfuric acid/water solutions, and for a few cases of ternary sulfuric acid/nitric acid/water solutions, are tabulated as a function of acid weight percent and temperature. Temperature dependent Henry's law expressions for a larger set of gaseous species in pure water are presented in Table 5-4. It is presently unclear whether "surface solubility" effects govern the uptake on nominally solid water ice or HNO_3/H_2O ice surfaces in a manner analogous to bulk solubility effects for liquid substrates and no solubility parameters for these "ice" systems are presented.

For some trace species on some surfaces, experimental data suggest that mass accommodation coefficients untainted by experimental saturation limitations have been obtained. These are tabulated in Table 5-1. In other cases experimental data can be shown to be subject to Henry's law constraints, and Henry's law constants, or at least their upper limits, can be determined. Some experimental data sets are insufficient to determine if measured "uptake" coefficients are true mass accommodation coefficients or if the measurement values are lower limits compromised by saturation effects. These are currently tabulated, with suitable caveats, in Table 5-1.

Surface reaction probabilities (γ) are kinetic values for generally irreversible reactive uptake of trace gas species on condensed surfaces. The rates of such processes may not be limited by Henry's law constraints; however, the fate of the uptake reaction products may be subject to saturation limitations. For example, N_2O_5 has been shown to react with sulfuric acid aerosol surfaces. However, if the H_2SO_4/H_2O ratio is too high, the product HNO_3 will be insoluble, and a large fraction will be expelled back into the gas phase. Surface reaction probabilities for substantially irreversible processes are presented in Table 5-2. Reaction products are identified where known. .

The total experimental uptake coefficient measured in laboratory heterogeneous kinetic experiments are also often represented by the symbol γ. In those cases where surface and/or bulk reaction dominate the uptake, the total uptake coefficient (γ_{total}) and reactive uptake coefficient (γ_{rxn}) may well be identical. More formally, for cases

where bulk liquid phase reaction is facile and there are no gas phase diffusion constraints, the total uptake coefficient for aerosol or cloud droplets can be approximated in terms of γ_{rxn} and γ_{sol} as [227]:

$$\frac{1}{\gamma_{total}} = \frac{1}{\alpha} + \frac{1}{\gamma_{sol} + \gamma_{rxn}}$$

where

$$\gamma_{sol} = \frac{8HRT}{\pi^{1/2}\bar{c}}\left(\frac{D}{t}\right)^{1/2}$$

and

$$\gamma_{rxn} = \frac{4HRT}{\bar{c}}\left(Dk_{rxn}\right)^{1/2}$$

where t is the time integrated exposure of the trace gas to the liquid surface, R is the gas constant, D is the liquid phase diffusion coefficient, and $\bar{c}$ is the mean trace gas molecular speed. In the limit of low solubility or long exposure time γ_{sol} becomes negligible and

$$\frac{1}{\gamma_{total}} = \frac{1}{\alpha} + \frac{1}{\gamma_{rxn}}$$

Discussion of how to use this approach to model chemical reactions in liquid stratospheric aerosols can be found in Hanson et al. [168] and Kolb et al. [227]. Note that these formulations are approximate. In cases where separate terms are competitive, more rigorous solution of the kinetic differential equations may be appropriate.

For solid surfaces, bulk diffusion is generally too slow to allow bulk solubility or bulk kinetic processes to dominate uptake. For solids, reactive uptake is driven by chemisorption/chemical reaction at the interface, a process that can also influence trace gas uptake on liquids. For liquids, surface reaction (γ_{surf}) occurs in parallel, rather than in series with mass accommodation, thus:

$$\gamma_{total} = \gamma_{surf} + \left[\frac{1}{\alpha} + \frac{1}{\gamma_{sol} + \gamma_{rxn}}\right]^{-1}$$

Examples where this more complex situation holds for liquid surfaces can be found in Hu et al. [181] and Jayne et al. [200]. In such cases γ may be significantly larger than α.

Uptake of gases on soot may occur due to three different processes: (1) physisorption (e.g. SO_2 or HNO_3 at room temperature and low nitric acid pressures); (2) reaction with the surface (e.g. NO_2), and (3) catalytic decomposition/reactions of the gas on the surface. All three processes may occur in parallel, and the relative contributions of each of these three may vary during the course of the reaction as the surface "ages." As discussed above, there are different types of reactive sites on soot, leading in some cases to a rapid initial uptake followed by a slower uptake; these are often characterized as reactions on "fresh" and "aged" surfaces respectively. Another complexity is that in some cases the geometric surface areas were used to calculate the uptake coefficients from the experimental data while in others, the available reactive surface area was estimated and used.

Because of these complexities with soot heterogeneous chemistry, uptake coefficients for soot interactions with gases have been broken out into a separate Table 5-3 rather than being included with the other surfacesin Table 5-1 and Table 5-2. When the uncertainty is more than an order of magnitude, a recommendation is not given in Table 5-3 and the range of reported values is given in the Notes. In most cases, the available reactive surface area rather than the geometric areas have been used in obtaining the uptake coefficients; in those cases where the geometric area was used but a higher available surface area was involved in the measured uptake, the uptake coefficient is given as an upper limit. Data are most commonly available for room temperature or there are very limited data at lower temperatures characteristic of the upper troposphere.

The data in Table 5-1 and Table 5-2 for uptake on non-soot surfaces are organized by trace gas species, since some systematic variation may be expected for surface accommodation or reaction as the surface composition and/or phase is varied. Data presented for one surface may be judged for "reasonableness" by comparing with data for a "similar" surface. In some cases it is not yet clear if surface uptake is truly reversible (accommodation) or

irreversibly reactive in nature. In such cases the available uptake coefficients are generally tabulated in Table 5-1 as accommodation coefficients, a judgment that will be subject to change if more definitive data become available.

Where a specific evaluated value for an accommodation coefficient or reaction probability has been obtained, an estimated uncertainty factor is also tabulated. However, when the data evaluation yielded only a lower or upper limit, no uncertainty factor can be reliably estimated and none is presented.

Description of and reference citations to many of the laboratory techniques used to obtain the data in the following tables can be found in Kolb et al. [227].

Reactions of N_2O_5, $ClONO_2$, HOCl and $BrONO_2$ on/in sulfuric acid are generally dependent on the species' Henry's law solubility and liquid phase diffusion coefficient in the liquid acid as well as the surface and/or liquid phase reaction rate parameters. All of these processes are generally functions of the acid composition and temperature (Hanson et al. [168], Robinson et al. [293]Shi et al. [313]. Thus, these reactions' reactive uptake coefficients must be represented by a complex phenomenological or empirical models that defy simple entry into Table 5-2. The notes in Table 5-2 for these reactions discuss and present the models adopted.

To aid in visualizing the resulting reactive uptake parameters the results for several reactions have been plotted in **Figure 5-1** as a function of temperature for a background pressure of 50 mbar and background water vapor and HCl mixing ratios of 5 ppmv and 2 ppbv, respectively. These calculations are presented for monodisperse background sulfate aerosol particles with a radius of 1×10^{-5} cm (0.1 μm).

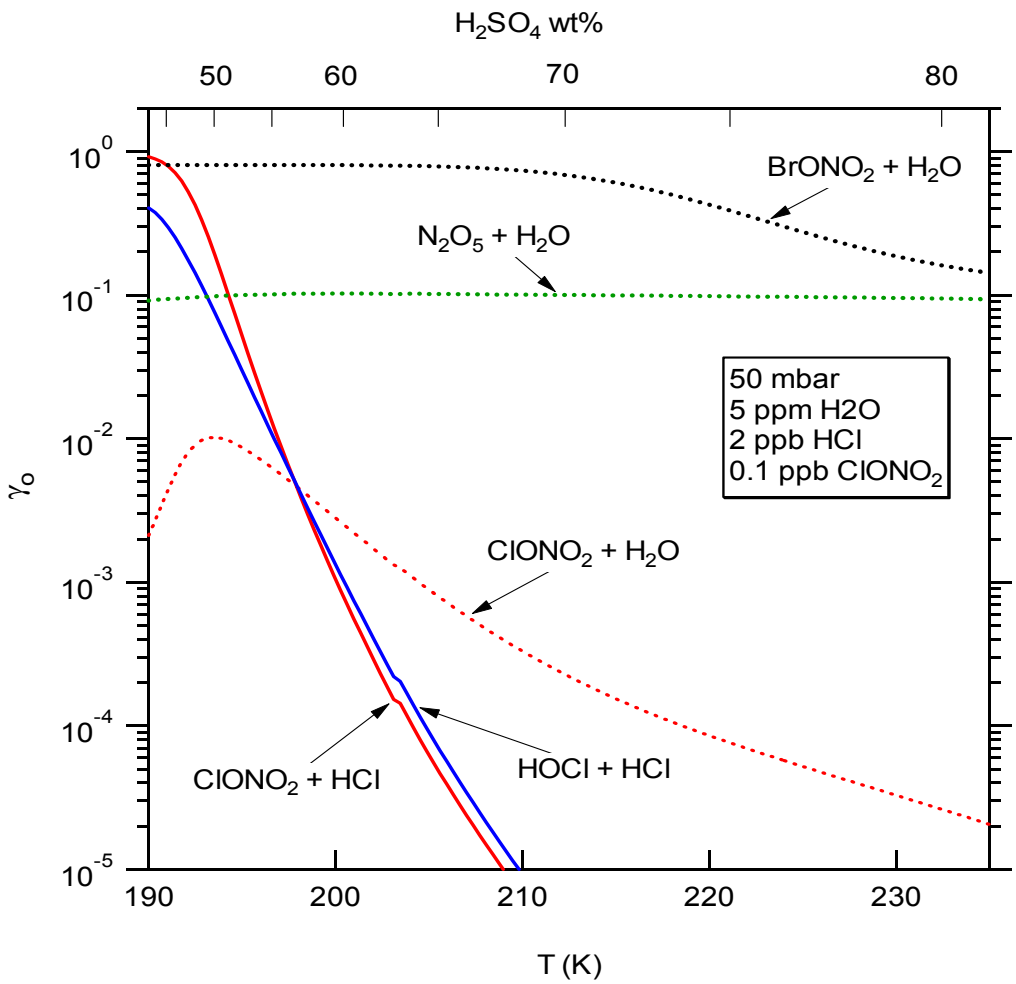

Figure 5-1. Recommended reactive uptake coefficients as a function of temperature for key stratospheric heterogeneous processes on sulfuric acid aerosols. For $ClONO_2$ and HOCl species, the aerosol radius used in the calculation is 10^{-5} cm, a typical value in the stratosphere. Because the current uptake models for N_2O_5 and $BrONO_2$ hydrolysis do not provide the information about the reacto-diffusive length (ℓ), the aerosol radius used in the

calculation is assumed to be much larger than their reacto-diffusive length (i.e. ℓ for N_2O_5 and $BrONO_2$ are set to zero.)

5.10 Mass Accommodation Coefficients for Surfaces Other Than Soot

Table 5-1. Mass Accommodation Coefficients (α) for Surfaces Other Than Soot.

Gaseous Species	Surface Type	Surface Composition	T(K)	α	Uncertainty Factor	Notes
O	Sulfuric Acid	$H_2SO_4 \cdot nH_2O(l)$ (97 wt.% H_2SO_4)	298	See Note		1
O_3	Water Ice	$H_2O(s)$	195–262	>0.04		2
	Liquid Water	$H_2O(l)$	292	$>2 \times 10^{-3}$‡		3
	Nitric Acid Ice	$HNO_3 \cdot 3H_2O(s)$	195	2.5×10^{-4}‡	3	2
	Sulfuric Acid	$H_2SO_4 \cdot nH_2O(l)$ (50–98 wt.% H_2SO_4)	193–295	See Note		4
OH	Water Ice	$H_2O(s)$	205–253	>0.1		5
	Liquid Water	$H_2O(l)$	275	$>4 \times 10^{-3}$		6
	Sulfuric Acid	$H_2SO_4 \cdot nH_2O(l)$				
		(28 wt.% H_2SO_4)	275	>0.07		7
		(97 wt.% H_2SO_4)	298	$>5 \times 10^{-4}$‡		7
	Alumina	$Al_2O_3(s)$	253–348	0.04	5	8
HO_2	Liquid Water	$H_2O(l)$	275	> 0.02		9
	Aqueous Salts	$NH_4HSO_4(aq)$ and $LiNO_3(aq)$	293	> 0.2		9
	Sodium Chloride	NaCl(s)	295	2×10^{-2}	5	10
	Potassium Chloride	KCl(s)	295	2×10^{-2}	5	10
H_2O	Water Ice	$H_2O(s)$	200	0.5	2	11
	Liquid Nitric Acid	$HNO_3 \cdot nH_2O(l)$	278	>0.3		12
	Nitric Acid Ice	$HNO_3 \cdot 3H_2O(s)$	197	See Note		13
	Sulfuric Acid	$H_2SO_4 \cdot nH_2O$ (96 wt.% H_2SO_4)	298	$> 2 \times 10^{-3}$‡		14
	Sodium Chloride	NaCl(s)	~298	See Note		
		NaCl(aq)	~299	> 0.5		15
			~298	$> 4 \times 10^{-4}$		16
H_2O_2	Liquid Water	$H_2O(l)$	273	0.18*	2	17
	Sulfuric Acid	$H_2SO_4 \cdot nH_2O(l)$ (96 wt.% H_2SO_4)	298	$> 8 \times 10^{-4}$‡		18
NO	Water Ice	$H_2O(s)$	195	See Note		19
	Sulfuric Acid	$H_2SO_4 \cdot nH_2O$		See Note		
		(70 wt.% H_2SO_4)	193–243	See Note		20
		(97 wt.% H_2SO_4)	298	See Note		20
NO_2	Water Ice	$H_2O(s)$	195	See Note		21
HONO	Water Ice	$H_2O(s)$	180–200	See Note		22
HNO_3	Water Ice	$H_2O(s)$	200	0.3	3	23
	Liquid Water	$H_2O(l)$	268	0.2*	2	24
	Nitric Acid Ice	$HNO_3 \cdot 3H_2O(s)$	191–200	0.4	2	25
	Liquid Nitric Acid	$HNO_3 \cdot nH_2O(l)$	278	0.6	2	26
	Sulfuric Acid	$H_2SO_4 \cdot nH_2O(l)$				
		(57.7 wt.% H_2SO_4)	191–200	>0.3		27
		(73 wt.% H_2SO_4)	283	0.1	2	27
		(75 wt.% H_2SO_4)	230	$>2 \times 10^{-3}$		27
		(97 wt.% H_2SO_4)	295	$>2.4 \times 10^{-3}$		27
	Sulfuric Acid Tetrahydrate	$H_2SO_4 \cdot 4\ H_2O(s)$	~192	>0.02*		27
HO_2NO_2	Water Ice	$H_2O(s)$	[a]200	0.1‡	3	28
	Sulfuric Acid	$H_2SO_4 \cdot nH_2O(l)$ (97 wt.% H_2SO_4)	298	See Note		29
NH_3	Liquid Water	$H_2O(l)$	~295	0.06*	3	30
CO_2	Liquid Water	$H_2O(l)$	293	See Note		31
CH_3OH	Liquid Water	$H_2O(l)$	260–291	0.12–0.02*	2	32
CH_3CH_2OH	Liquid Water	$H_2O(l)$	260–291	0.13–0.02*	2	33
$CH_3CH_2CH_2OH$	Liquid Water	$H_2O(l)$	260–291	0.08–0.02*	2	34
$CH_3CH(OH)CH_3$	Liquid Water	$H_2O(l)$	260–291	0.10–0.02*	2	34
$HOCH_2CH_2OH$	Liquid Water	$H_2O(l)$	260–291	0.13–0.04*	2	35
CH_2O	Liquid Water	$H_2O(l)$	260–270	0.04	3	36
	Sulfuric Acid	$H_2O \cdot mHNO_3 \cdot nH_2O(l)$	235–300	0.04	3	36
CH_3O_2	Sodium Chloride	NaCl(s)	296	$>4 \times 10^{-3}$		37
CH_3CHO	Liquid Water	$H_2O(l)$	267	>0.03*		38
$CH_3C(O)CH_3$	Liquid Water	$H_2O(l)$	260–285	0.07–0.01*	2	39
HC(O)OH	Liquid Water	$H_2O(l)$	260–291	0.10–0.02*	2	40

Gaseous Species	Surface Type	Surface Composition	T(K)	α	Uncertainty Factor	Notes
$CH_3C(O)OH$	Liquid Water	$H_2O(l)$	260–291	0.15–0.03*	2	41
Cl_2	Water Ice	$H_2O(s)$	200	See Note		42
OClO	Water Ice	$H_2O(s)$	100,189, 200	See Note		43
HCl	Water Ice	$H_2O(s)$	191– 211	0.3	3	44
	Liquid Water	$H_2O(l)$	274	0.2*	2	45
	Nitric Acid Ice	$HNO_3 \cdot 3H_2O(s)$	191– 211	0.3	3	46
	Sulfuric Acid	$H_2SO_4 \cdot nH_2O(l)$	283	0.15*	2	47
		(n≥8, ≤40 wt.% H_2SO_4)	218	>0.005*		
		(n<8, >40 wt.% H_2SO_4)	†	†	†	
	Sulfuric Acid Tetrahydrate	$H_2SO_4 \cdot 4H_2O(s)$	192–201	See Note		48
CCl_2O	Liquid Water	$H_2O(l)$	260–290	See Note		49
CCl_3CClO	Liquid Water	$H_2O(l)$	260–290	See Note		49
HBr	Water Ice	$H_2O(s)$	200	> 0.2		50
	Nitric Acid Ice	$HNO_3 \cdot 3H_2O(s)$	200	> 0.3		50
HOBr	Sulfuric Acid	$H_2O(s)$	190–239	$>10^{-3}$		51
		H_2SO_4 in $H_2O(l)$ (58 wt. % H_2SO_4)	228	>0.05‡		52
$CHBr_3$	Water Ice	$H_2O(l)$	220	See Note		53
	Sulfuric Acid	$H_2SO_4 \cdot nH_2O(l)$ (97 wt.% H_2SO_4)	220	$>3 \times 10^{-3}$‡		53
HOI	Sulfuric Acid	$H_2SO_4 \cdot nH_2O(l)$				54
		(40 wt % H_2SO_4)	195	0.07	3	
		(40 wt % H_2SO_4)	205	0.03	3	
		(40 wt % H_2SO_4)	212	0.04	3	
		(50 wt % H_2SO_4)	222–224	0.02	3	
		(70 wt % H_2SO_4)	230–232	0.02	3	
		(70 wt % H_2SO_4)	252	0.02	3	
HF	Water Ice	$H_2O(s)$	200	See Note		55
	Nitric Acid Ice	$HNO_3 \cdot 3H_2O(s)$	200	See Note		55
CF_2O	Water Ice	$H_2O(s)$	192	See Note		56
	Liquid Water	$H_2O(l)$	260–290	See Note		49
	Nitric Acid Ice	$HNO_3 \cdot 3H_2O(s)$	192	See Note		56
	Sulfuric Acid	$H_2SO_4 \cdot nH_2O(l)$	215–230			
		(40 wt.% H_2SO_4)		$>3 \times 10^{-6}$‡		56
		(60 wt.% H_2SO_4)		$>6 \times 10^{-5}$‡		56
CF_3CFO	Liquid Water	$H_2O(l)$	260–290	See Note		49
CF_3COOH	Liquid Water	$H_2O(l)$	263–288	0.2–0.1*	2	57
CF_3CClO	Liquid Water	$H_2O(l)$	260–290	See Note		49
SO_2	Liquid Water	$H_2O(l)$	260–292	0.11	2	58
	Sulfuric Acid	$H_2SO_4 \cdot nH_2O(l)$ (97 wt.% H_2SO_4)	298	See Note		59
H_2SO_4	Sulfuric Acid	$H_2SO_4 \cdot nH_2O(l)$ (50–98 wt.% H_2SO_4)	200–300	0.7	1.4	60
$CH_3S(O)CH_3$	Liquid Water	$H_2O(l)$	262–281	0.16–0.08*	2	61
$CH_3S(O_2)CH_3$	Liquid Water	$H_2O(l)$	262–281	0.27–0.08*	2	61
$CH_3S(O_2)OH$	Liquid Water	$H_2O(l)$	264–278	0.17–0.11*	2	61

* Varies with T, see Notes
† No data—all measurements; limited by HCl solubility
‡ May be affected by surface saturation

5.11 Notes to Table 5-1

1. O on $H_2SO_4 \cdot nH_2O$—Knudsen cell experiment of Baldwin and Golden [27] measured an uptake coefficient limit of $<10^{-6}$; this result probably cannot be equated with an accommodation coefficient due to surface saturation.

2. O_3 on $H_2O(s)$ and $HNO_3 \cdot nH_2O$—Undoped ice surfaces saturate too quickly for reliable measurements. When ice is doped with Na_2SO_3 to chemically remove absorbed O_3 the apparent α increases to 1×10^{-2} (0.1M) or up to 4×10^{-2} (1M) (Dlugokencky and Ravishankara [105]). Limit of $\gamma < 10^{-6}$ for undoped ice is consistent with

earlier measurement by Leu [233] of $\leq 1 \times 10^{-4}$ and with $< 6 \times 10^{-5}$ obtained by Kenner et al. [214]. Dlugokencky and Ravishankara also measured the tabulated value of an uptake coefficient for O_3 on a NAT "like" surface, but the data were difficult to reproduce and the surfaces were not well characterized. Kenner et al. also measured a lower limit for an uptake coefficient of 8×10^{-5} on NAT at 183 K, but this measurement is also certainly limited by surface saturation.

3. O_3 on $H_2O(l)$—Utter et al. [335] used a wetted wall flow tube technique with various chemical scavengers to measure a lower limit for α of 2×10^{-3}. The stopped flow measurement technique using an $SO_3^{=}$ scavenger (Tang and Lee [327]) is subject to saturation effects, so their quoted α of 5.3×10^{-4} is also taken as a lower limit.

4. O_3 on $H_2SO_4 \bullet nH_2O$—Flow tube measurements (Dlugokencky and Ravishankara [105]) of an uptake coefficient limit of $<10^{-6}$ on both 50 and 97 wt. % H_2SO_4 surfaces are consistent with earlier, but probably less quantitative, static systems measurements of Olszyna et al. [271] and aerosol chamber measurements of Harker and Ho [169], who report uptake coefficients of the order 10^{-8} or less for a variety of sulfuric acid concentrations and temperatures. In these earlier experiments, doping the H_2SO_4 with Ni^{2+}, Cr^{2+}, Al^{3+}, Fe^{3+}, and NH_4^+ (Olszyna et al. [271]) or Al_2O_3 or Fe_2O_3 (Harker and Ho [169]) did not significantly increase measured O_3 loss. An upper limit of 1×10^{-6} was also reported by Baldwin and Golden [26]for 97 wt % H_2SO_4 at 295 K. Il'in et al. [187] performed static tube reactor measurements on 98 wt. % sulfuric acid at 239, 258, 273 K measuring uptake coefficients between 1.2 and 1.75×10^{-6}. Although these measurements are slightly larger than the limits in the other studies, uptake values this small are extremely hard to quantify and these measurements are not seen to be in serious disagreement with other studies finding slightly lower upper limits. All measurements are subject to solubility limitations and probably do not reflect true limits on mass accommodation.

5. OH on $H_2O(s)$—Cooper and Abbatt[91] analyzed uptake rates in a wall-coated flow tube to determine an initial $\gamma \sim 0.1$ over the temperature range of 205 – 230 K. Uptake coefficients decreased at longer exposure times, indicating surface saturation. These data indicate that α is at least 0.1 and possibly much larger. This is confirmed by an earlier experiment using a coated insert/flow tube technique by Gershenzon et al. [136], which yielded $\alpha > 0.4$ at 253 K.

6. OH on $H_2O(l)$—see Note for HO_2 on $H_2O(l)$. The OH and HO_2 measurements of Hanson et al. [151] are subject to the same analysis issues.

7. OH on $H_2SO_4 \bullet nH_2O$—See Note for HO_2 on $H_2O(l)$ for measurement (28 wt.% H_2SO_4) by Hanson et al. [151] and Note for O on H_2SO_4 for measurement (97 wt. % H_2SO_4) by Baldwin and Golden [27].

8. OH on $Al_2O_3(s)$—Measured value is from flow tube experiment with native oxide on aluminum as the active surface. An uptake coefficient of 0.4 ± 0.2 independent of temperature over the range of 253–348 K was measured (Gershenzon et al. [136]).

9. HO_2 on $H_2O(l)$—Determination of α in liquid-wall flow tube (Hanson et al. [151]) is dependent on gas-phase diffusion corrections; measured limit ($\alpha > 0.02$) is consistent with $\alpha = 1$. In the aqueous salt aerosol measurements of Mozurkewich et al. [264], HO_2 was chemically scavenged by Cu^{++} from added $CuSO_4$ to avoid Henry's law constraints; the measured limit of >0.2 is also consistent with $\alpha = 1$.

10. HO_2 on NaCl(s) and KCl(s)—Based on measured values of $\gamma = 1.8 \times 10^{-2}$ for KCl and 1.6×10^{-2} for NaCl, both at 295 K by Gershenzon et al. [135] supplementing an earlier value of $\gamma - 8 \times 10^{-3}$ measured by Gershenzon and Purmal [137]. Results have not been calibrated with a competitive technique.

11. H_2O on $H_2O(s)$—Measurements are available from Leu [232] giving 0.3 (+0.7, –0.1) at 200 K and Haynes et al. [172] (1.06 ± 0.1 to 0.65 ± 0.08) from 20 to 185 K. Brown et al.[59] used molecular beam reflection techniques to measure a value of $\alpha = 0.99 \pm 0.03$ between 85 and 150 K and optical interference methods to obtain $\alpha = 0.97 \pm 0.10$ between 97 and 145 K.

12. H_2O on $HNO_3/H_2O(l)$—Rudolf and Wagner[302] used aerosol expansion chamber techniques to illustrate that on liquid water/nitric acid aerosols α is greater than 0.3 and is consistent with 1.0 at 278 K.

13. H_2O on $HNO_3 \bullet nH_2O(s)$—Middlebrook et al. [257] measured an uptake coefficient of .002 for water vapor co-depositing with nitric acid over NAT at 197 K.

14. H_2O on $H_2SO_4 \bullet nH_2O$—Baldwin and Golden [26] measured $\gamma \sim 2 \times 10^{-3,}$ which is almost certainly affected by surface saturation. See Note for H_2O_2 on $H_2SO_4 \bullet nH_2O$.

15. H_2O on NaCl(s)—Fenter et al. [118] used Knudsen cell/mass spectrometry methods to measure $\gamma < 2 \times 10^4$ for H_2O(g) uptake on NaCl powders, an observation confirmed by Beichert and Finlayson-Pitts [46], who found
$\gamma < 1 \times 10^{-5}$. However, Dai et al. [94] used FTIR spectroscopy on NaCl crystallite films at 240 and 296 K to determine that a water adlayer does adhere to dry salt and that a small fraction of surface sites (<1%) cause H_2O dissociation. It is likely that the measurements of Fenter et al. and Beichert and Finlayson-Pitts were affected by surface saturation.

16. H_2O on NaCl(aq)—Fung et al.[130] used Mie resonance scattering techniques to quantify aqueous NaCl droplet growth (5.8 to 7.8 μm), yielding fitted values of $\alpha > 0.5$ and consistent with 1.0.

17. H_2O_2 on H_2O(l)—Measured accommodation coefficient (Worsnop et al. [359]) has a strong negative temperature dependence over the measured range of 260–292 K, with $\alpha = 0.3$ at 260 K decreasing to 0.1 at 292 K.

18. H_2O_2 on $H_2SO_4 \bullet nH_2O$—Knudsen cell uptake measurements are subject to surface saturation, thus uptake coefficient value of 7.8×10^{-4} quoted by Baldwin and Golden [26] is almost certainly a lower limit for α. This effect is probably also responsible for the lack of measured uptake ($\gamma < 10^{-6}$) for NO, NO_2, SO_2, Cl_2, and other species reported in this reference and Baldwin and Golden [27].

19. NO on H_2O(s)—NO data (Leu [233], Saastad et al. [303]) subject to same concerns as NO_2. See Note for NO_2 on H_2O(s).

20. NO on $H_2SO_4 \bullet nH_2O$—See Notes for H_2O_2 on $H_2SO_4 \bullet nH_2SO_4$ and NO_2 on $H_2SO_4 \bullet nH_2O$. NO is subject to the same concerns as NO_2 for both reported measurements (Saastad et al. [303]; Baldwin and Golden [26]).

21. NO_2 on H_2O(s)—In the absence of a chemical sink, Leu [233] measured no sustained uptake of NO_2 on ice yielding an apparent $\alpha \leq 1 \times 10^{-4}$. Saastad et al. [303] measured a lower limit of 5×10^{-5} for temperatures between 193 and 243 K. However these values are probably influenced by surface saturation.

22. HONO on H_2O(s)—Fenter and Rossi [120] measured reversible uptake on water ice between 180 and 200 K using a Knudsen cell technique. An initial uptake coefficient of 1×10^{-3} suggests that α equals or exceeds this value. Chu et al. [73] used a cylindrical flow reactor to measure the uptake coefficient as a function of temperature, obtaining values ranging from 3.7×10^{-3} at 178 K to 6.4×10^{-4} at 200 K, in good agreement with the results of Fenter and Rossi. On the other hand, Chu et al. report significantly lower values after correction for the effects of surface porosity, i.e. 1.4×10^{-4} at 178 K and 1.3×10^{-5} at 200 K (see Keyser et al. [218]).

23. HNO_3 on H_2O(s)—Leu [232] reports 0.3 (+0.7, –0.1). Some additional uncertainty is introduced by effective ice surface area in fast-flow measurement (see Keyser et al. [218]). Hanson [148] measured an uptake coefficient of > 0.3 at 191.5 and 200 K. Aguzzi and Rossi [9] measured an uptake coefficient of 0.3 over the temperature range from 180 to 190 K, the value decreasing at T < 195 K with an exponential temperature dependence of –(3400 ± 500)/T. They attributed this change to an increasing evaporation rate, concluding that the accommodation coefficient most likely remains large. Abbatt [4] measured equilibrium uptake values at 208–248 K on the order of 1 to 3×10^{14} molecule cm^{-2}. Zondlo et al. [374] report the formation of a supercooled H_2O/HNO_3 liquid layer at 185 K, forming NAT or NAD only after decreasing the relative humidity below the ice frost point.

24. HNO_3 on H_2O(l)—Measured α has a strong negative temperature dependence varying from 0.19 ± 0.02 at 268 K to 0.07 ± 0.02 at 293 K (Van Doren et al. [338]). Ponche et al. [276] measured an accommodation coefficient of 0.05 ± 0.01 at 297 K.

25. HNO_3 on $HNO_3 \bullet nH_2O$(s)—Hanson [148] measured uptake coefficients of >0.3 and >0.2 on NAT surfaces at 191 K and 200 K, respectively. Middlebrook et al. [257] measured an uptake coefficient of 0.7 on NAT at 197 K under conditions where both nitric acid and water vapor were co-depositing.

26. HNO_3 on $HNO_3 \bullet nH_2O$(l)—Rudolf and Wagner [302] used aerosol expansion chamber techniques to deduce that α for HNO_3 on 278 K H_2O/HNO_3 droplets is > 0.3 and probably close to 1. The consistency of this value with smaller (~0.2) values measured for uptake on pure water by Van Doren et al. [338] is unclear, since the mechanism of co-condensation is unknown and the composition of the surface in the aerosol expansion chamber experiments may be kinetically controlled and has not been well determined.

27. HNO_3 on $H_2SO_4.nH_2O$ and $H_2SO_4 \cdot 4H_2O(s)$—Initial uptake at 73 wt. % H_2SO_4 allows a measurement of $\alpha = 0.11 \pm 0.01$ at 283 K (Van Doren et al. [338]). This value is expected to increase at lower temperatures, in a manner similar to $H_2O(1)$ uptake (Van Doren et al. [337]). Total HNO_3 uptake is subject to Henry's law solubility constraints, even at stratospheric temperatures (Reihs et al. [283]). Solubility limitations also affected the earlier "sticking coefficient" measurements of Tolbert et al. [332] for 75 wt % H_2SO_4 at 230 K. Hanson [148] measured an uptake coefficient of >0.3 for frozen 57.7 wt. % sulfuric acid at 191.5 and 200 K. Baldwin and Golden [26] reported a lower limit of 2.4×10^{-4} on 97 wt. % H_2SO_4 at 295 K, also reflecting solubility limits. Iraci et al. [191] monitored nitric acid trihydrate growth on sulfuric acid tetrahydrate with infrared techniques, measuring HNO_3 uptake coefficient limits of >0.03 at 192.5 K and >0.08 at 192 K. These measurements involved co-deposition of water vapor.

28. HO_2NO_2 on $H_2O(s)$—Li et al. [237] measured an uptake coefficient of 0.15 ±0.10; uptake may be limited by surface saturation.

29. HO_2NO_2 on $H_2SO_4 \bullet nH_2O(l)$—Baldwin and Golden [26] measured $\gamma = 2.7 \times 10^{-5,}$ which is probably solubility limited; see Note for H_2O_2 on $H_2SO_4 \cdot nH_2O$.

30. NH_3 on $H_2O(l)$—Ponche et al. [276] used a droplet train technique to obtain $\alpha = (9.7 \pm 0.9) \times 10^{-2}$ at 290 K, and Bongartz et al.[57] used a liquid jet technique to obtain $\alpha = 4.0\ (+3.0, -0.05) \times 10^{-2}$. Earlier levitated droplet evaporation experiments [328] on NH_4Cl obtained a larger evaporation coefficient of $\alpha = 0.29 \pm 0.03$, which is discounted because of the indirect nature of the experiment.

31. CO_2 on $H_2O(l)$—Noyes et al.[270] used a dynamic stirring technique to monitor pressure decreases in a closed cylinder. They inferred $\alpha = (5.5 \pm 0.5) \times 10^{-8}$ at 293 K. This technique is uncalibrated against more widely used procedures and probably suffers from surface saturation effects. Measured α is probably many orders of magnitude too small.

32. CH_3OH on $H_2O(l)$—Jayne et al. [197] measured uptake from 260–291 K and derived accommodation coefficients fitting $\alpha/(1-\alpha) = \exp(-\Delta G^{\ddagger}_{obs}/RT)$, where $\Delta G^{\ddagger}_{obs} = -8.0$ kcal/mol + 34.9 cal mol^{-1} K^{-1} T(K).

33. CH_3CH_2OH on $H_2O(l)$—Jayne et al. [197] measured uptake from 260–291 K and derived accommodation coefficients fitting $\alpha/(1-\alpha) = \exp(-\Delta G^{\ddagger}_{obs}/RT)$, where $\Delta G^{\ddagger}_{obs} = -11.0$ kcal/mol + 46.2 cal mol^{-1} K^{-1} T(K). Similar, but somewhat larger values were reported for chloro-, bromo-, and iodo-ethanols.

34. $CH_3CH_2CH_2OH$ and $CH_3CH(OH)CH_3$ on $H_2O(l)$—Jayne et al. [197] measured uptake coefficients between 260 and 291 K and derived accommodation coefficients fitting $\alpha/(1-\alpha) = \exp(-\Delta G^{\ddagger}_{obs}/RT)$, where $\Delta G^{\ddagger}_{obs} = -9.2$ kcal mol^{-1} + 40.9 cal mol^{-1} K^{-1} T(K) for 1-propanol and –9.1 kcal mol^{-1} + 43.0 cal mol^{-1} K^{-1} T(K) for 2-propanol. Similar data for t-butanol were also reported.

35. $HOCH_2CH_2OH$ on $H_2O(l)$—Jayne et al. [197] measured uptake coefficients for ethylene gycol between 260 and 291 K and derived accommodation coefficients fitting $\alpha/(1-\alpha) = \exp(-\Delta G^{\ddagger}_{obs}/RT)$, where $\Delta G^{\ddagger}_{obs} = -5.3$ kcal mol^{-1} + 24.5 cal mol^{-1} K^{-1} T(K).

36. $CH_2O + H_2O(l)$, $H_2SO_4 \cdot mHNO_3 \cdot nH_2O(l)$—Jayne et al.[200] report uptake measurements for 0 – 85 wt % H_2SO_4 and 0 – 54 wt% HNO_3 over a temperature range of 241–300 K. Measured uptake coefficients vary from 0.0027–0.027, increasing with H^+ activity (Jayne et al ([200]; Tolbert et al., [330]), and with increasing pH above 7 (Jayne et al., [198]). Reversible uptake is solubility limited through reactions to form $H_2C(OH)_2$ and CH_3O^+. A model of uptake kinetics (Jayne et al., [200]) is consistent with $\gamma = 0.04 \pm 0.01$ for all compositions. A chemisorbed surface complex dominates uptake at 10 – 20 wt % H_2SO_4, and CH_3O^+ formation dominates above 20 wt % (Tolbert et al., [330]; Jayne et al. [200], Iraci and Tolbert [192]). Low temperature (197–214 K) uptake studies by Iraci and Tolbert [192] confirm that uptake is solubility limited for uptake coefficients in the 10^{-3} to 10^{-2} range even at low temperatures. These chemical mechanisms allow γ to greatly exceed α for strong acidic and basic solutions. A full uptake model for acid solutions is presented in Jayne et al. [200], and for basic solutions in Jayne et al. [198]. XPS surface analysis by Fairbrother and Somorjai [114] failed to see CH_3O^+ surface species reported by Jayne et al.; however, their sensitivity of 1% of surface coverage is too poor to see the predicted amounts of the surface species.

37. CH_3O_2 + NaCl(s)—Gershenzon et al. [135] measured the uptake of CH_3O_2 on crystalline NaCl(s) in a central rod flow apparatus. They determined a value of $\gamma = (4 \pm 1) \times 10^{-3}$ at 296 K, suggesting that $\alpha \geq 4 \times 10^{-3}$.

38. CH_3CHO on $H_2O(l)$—Jayne et al. [198] measured a lower accommodation coefficient limit of > 0.03 at 267 K. Uptake can be limited by Henry's law and hydrolysis kinetics effects—see reference.

39. $CH_3C(O)CH_3$ on $H_2O(l)$—Duan et al. [108] measured uptake between 260 and 285 K, deriving $\alpha = 0.066$ at the lower temperature and 0.013 at the higher, with several values measured in between. Measured values fit $\alpha/(1-\alpha) = \exp(-\Delta G^{\ddagger}_{obs}/RT)$, where $\Delta G^{\ddagger}_{obs} = -12.7$ kcal/mol + 53.6 cal mol^{-1} K^{-1} T(K).

40. HC(O)OH on $H_2O(l)$—Jayne et al. [197] measured uptake coefficients for formic acid between 260 and 291 K and derived accommodation coefficients fitting $\alpha/(1-\alpha) = \exp(-\Delta G^{\ddagger}_{obs}/RT)$, where $\Delta G^{\ddagger}_{obs} = -7.9$ kcal mol^{-1} + 34.9 cal mol^{-1} K^{-1} T(K).

41. $CH_3C(O)OH$ on $H_2O(l)$—Jayne et al. [197] measured uptake coefficients for acetic acid between 260 and 291 K and derived an accommodation coefficient fitting $\alpha/(1-\alpha) = \exp(-\Delta G^{\ddagger}_{obs}/RT)$, where $\Delta G^{\ddagger}_{obs} = -8.1$ kcal mol^{-1} + 34.9 cal mol^{-1} K^{-1} T(K).

42. Cl_2 on $H_2O(s)$—Measurement of Leu [232] yielded a limit of $<1 \times 10^{-4}$ for Cl_2 and is subject to same concern as NO_2 (see Note) A similar limit of $<5 \times 10^{-5}$ has been measured by Kenner et al. [214], which is also probably limited by surface saturation.

43. OClO + $H_2O(s)$—Brown et al.[60] and Graham et al.[142] used complementary ultra high-vacuum (UHV) and coated-wall flow tube techniques to show sub-monolayer reversible absorption of OClO on water ice at 100 K (UHV) and 189 and 200 K (flow tube). No kinetic data are available at stratospheric temperatures but the mass accommodation coefficient for 100 K ice surfaces is near unity, with values of 0.8 ± 0.2 reported for amorphous ice and 0.6 ±0.2 for crystalline ice [142].

44. HCl on $H_2O(s)$—Leu [232] (0.4; +0.6, –0.2) and Hanson and Ravishankara, [158] ($\alpha \geq 0.3$) are in reasonable agreement at stratospheric ice temperatures. More recently, a great deal of experimental effort (Abbatt et al. [5], Koehler et al. [225], Chu et al. [75], Graham and Roberts [140], Graham and Roberts[141]; Rieley et al.[286]) has gone into understanding the uptake of HCl by ice surfaces. Rieley et al. measured $\alpha = 0.95 \pm 0.05$ at 80–120 K. Water ice at stratospheric temperatures can take up a large fraction of a monolayer even at HCl partial pressures typical of the stratosphere. Both the thermodynamic and spectroscopic properties of this absorbed HCl indicate that it has dissociated to ions, forms ionic hydrates, and is highly reactive. These experimental results contrast with initial theoretical calculations that predicted undissociated HCl hydrogen bonded to the ice surface and a very small adsorption probability at stratospheric temperatures (Kroes and Clary [228]); more recent simulations result in higher adsorption energies and theoretical accommodation coefficients of one for 190-K surfaces (Wang and Clary [346]). Recent molecular dynamics calculations by Gertner and Hynes[138] also show that ionic absorption is thermodynamically favorable by about 5 kcal/mole. At HCl partial pressures significantly above those typical of the stratosphere, a liquid surface layer forms on the ice, greatly enhancing the total amount of HCl that the surface can absorb.

45. HCl on $H_2O(1)$—Recommendation is based on Van Doren et al. [337]. Measured α's decrease from 0.18 ± 0.02 at 274 K to 0.064 ± 0.01 at 294 K, demonstrating strong negative temperature dependence. Tang and Munkelwitz [328] have measured a larger (0.45 ±0.4) HCl evaporation coefficient for an aqueous NH_4Cl droplet at 299 K.

46. HCl on $HNO_3 \bullet nH_2O$—There was previously severe disagreement between Hanson and Ravishankara [158] ($\alpha \geq 0.3$) for NAT (54 wt. % HNO_3), and Leu and coworkers (Moore et al. [262], Leu et al. [234]). However, subsequent experiments at lower HCl concentrations by Leu and coworkers (Chu et al. [75]) as well as Abbatt and Molina [6] are generally consistent with Hanson and Ravishankara. In particular, Abbatt and Molina [6] report a large uptake coefficient ($\alpha > 0.2$). The measurements of Hanson and Ravishankara are consistent with $\alpha = 1$. The experiments at stratospherically representative HCl concentrations show that HNO_3-rich NAT surfaces adsorb significantly less HCl than H_2O-rich surfaces.

47. HCl on $H_2SO_4 \bullet nH_2O$—Measurements by Watson et al. [348] at 284 K show $\alpha = 0.15 \pm 0.01$ independent of n for $n \geq 8$. Experimental uptake and, therefore, apparent α falls off for $n \leq 8$ (≥ 40 wt. % H_2SO_4). This behavior is also observed at stratospheric temperature (218 K) by Hanson and Ravishankara [158]. More recent measurements by Robinson et al. [294]extend mass accommodation measurements to lower temperatures, yielding significantly higher values. Solubility constraints also controlled earlier low temperature uptake measurements of Tolbert et al. [332]. A review of the most recent solubility data is presented in Table 5-5.

48. HCl on $H_2SO_4 \bullet 4H_2O(s)$—Uptake is a strong function of temperature and water vapor partial pressure (relative humidity) (Zhang et al. [370]), both of which affect adsorbed surface water.

49. Halocarbonyls on $H_2O(l)$—Uptake is limited by Henry's law solubility and hydrolysis rate constants (De Bruyn et al. [98,100] and Georg et al. [131,133]. See Table 5-4 and Table 5-5.

50. HBr on $H_2O(s)$ and $HNO_3 \bullet nH_2O$—Hanson and Ravishankara [159,163] have reported large uptake coefficients for HBr on 200-K ice and NAT. Lower limits of >0.3 and >0.2 for ice are reported in the two referenced publications, respectively, and a limit of >0.3 is reported for NAT. No surface saturation was observed, leading to the supposition that HBr, like HCl, dissociates to ions on ice surfaces at stratospheric temperatures. Abbatt [1] measured an uptake coefficient lower limit of >0.03 on water ice at 228 K consistent with Hanson and Ravishankara. Rieley et al. [286] measured an α of 1.0 ± 0.05 for water ice at 80–120 K. Flückiger et al. [124] report α values of ~0.2 at 210 K, increasing to ~0.3 at 190 K, while Percival et al. [274] measured an α of 0.03 ± 0.005 for water ice at T > 212 K, and α > 0.1 at T< 212 K, attributing the apparent increase in the uptake coefficient to an increase in the surface area of the ice. More definitive experiments will need to be carried out to resolve the discrepancy. Hudson et al. [183] report α = 0.61 ± 0.06 at 140 K, and
α = 0.24 ± 0.05 at 100 K, for HBr pressures ranging from 3×10^{-8} to 1.4×10^{-7} Torr. Equilibrium HBr coverages for ice are reported by Chu and Heron [74] at 188 and 195 K, and by Chu and Chu [71] at 180–220 K. The latter authors also report the formation of various solid HBr hydrates.

51. HOBr on $H_2O(s)$—Abbatt [1] measured an uptake coefficient for water ice of 2×10^{-3} at 228 K. Chu and Chu [71] report an uptake coefficient corrected for porosity effects in the range 0.11 to 0.007 at 190–218 K, with an exponential temperature dependence of (3809 ± 76)/T, and in the range 2×10^{-3} to 6×10^{-4} at 223–239 K, with an exponential temperature dependence of (4658 ± 456)/T. Chaix et al. [69] measured the uptake coefficient as a function of temperature on three different types of water-ice, obtaining values ranging from ~0.3 at 185 K to ~0.03 at 205 K, with an exponential temperature dependence of (4900 ± 500)/T. The three sets of results are in reasonable agreement with each other, and the temperature dependence is attributed predominantly to changes in the evaporation rate.

52. HOBr on $H_2SO_4 \bullet nH_2O(l)$—Abbatt [1] measured an uptake coefficient of 0.06 ± 0.02 by measuring HOBr gas phase loss at 228 K. This result may well be a lower limit due to surface saturation effects.

53. $CHBr_3$ on $H_2O(s)$ and $H_2SO_4 \bullet nH_2O(l)$—Hanson and Ravishankara [163] investigated the uptake of bromoform on ice and 58 wt.% sulfuric acid at 220 K. No uptake on ice was observed, with a measured uptake coefficient of $<6 \times 10^{-5}$. Reversible uptake by the sulfuric acid surface was observed with an initial uptake coefficient of $>3 \times 10^{-3}$; both measurements are probably limited by surface saturation.

54. HOI on $H_2SO_4 \bullet nH_2O$—Knudsen cell studies by Allanic and Rossi [18] measured uptake at several temperatures for 40, 50, and 70 acid wt. %. Time dependent studies show no sign of saturation, so uptake coefficients should correspond to mass accommodation coefficients. Some acid concentration data in the table have been averaged for similar temperatures and rounded to one significant figure. An uncertainty factor of three has been assigned due to the relatively small number of temperature/concentration points studied and a lack of confirming studies from other laboratories. The authors note evidence of HOI disproportionation to form I_2, however, this second order reaction is unlikely to occur under atmospheric conditions.

55. HF on $H_2O(s)$ and $HNO_3 \bullet nH_2O(s)$—Hanson and Ravishankara [159] attempted to measure the uptake of HF by 200 K water ice and NAT surfaces but were unable to observe measurable adsorption. They surmise that, unlike HCl and HBr, HF does not dissociate to ions on ice or NAT surfaces at 200 K. Lack of measurable uptake is probably due to surface saturation.

56. CF_2O on $H_2O(s)$, $HNO_3 \bullet nH_2O$ and $H_2SO_4 \bullet nH_2O$—Uptake coefficient measurements by Hanson and Ravishankara [156] on stratospheric surfaces are probably subject to surface and/or bulk saturation effects and may not represent accommodation coefficient measurements, particularly the lower limits of $>3 \times 10^{-6}$ reported for water and nitric acid ices.

57. CF_3COOH on $H_2O(l)$—Hu et al. [182] measured mass accommodation coefficients for five haloacetic acids, including trifluoroacetic acid (TFA); the others were mono-, di-, trichloro-, and chlorodifluoro-acetic acids. All displayed negative temperature dependence and values for α of about 0.1 at 273 K.

58. SO_2 on $H_2O(1)$—Measured α of 0.11 ± 0.02 has no significant temperature variation over a temperature range of 260–292 K (Worsnop et al. [359]). Ponche et al. [276] measured 0.13 ± 0.01 at 298 K, in agreement with the earlier measurement. Shimono and Koda [314] estimated an α of 0.2 at 293.5 K from analysis of pH-dependent uptake coefficients in a novel liquid impingement technique that has not been calibrated with

other gases. Donaldson et al. [106] have used second harmonic generation spectroscopy to detect a chemisorbed SO_2 surface species which was predicted from earlier uptake measurements by Jayne et al.[196]; this surface complex may play a role in SO_2 heterogeneous reactions on aqueous surfaces.

59. SO_2 on $H_2SO_4 \bullet nH_2O$—See Note for H_2O_2 on $H_2SO_4 \bullet nH_2O$.

60. H_2SO_4 on $H_2SO_4 \bullet nH_2O$—Poschl et al. [277] measured $0.43 < \alpha < 1.0$ for 73–98 wt. % H_2SO_4 at 303 K in a wetted wall flow tube. Lower temperatures and acid concentrations would be expected to lead to larger values of α. As discussed in Poschl et al. [277] this contradicts an indirect measurement of $0.02 < \alpha < 0.09$ at 42.5 wt. % at 298 K by Van Dingenen and Raes [336] in a photochemical aerosol reactor. The Poschl et al. [277] result is consistent with room temperature α values very near that measured for $(NH_4)_2SO_4$ particles in an aerosol flow reactor by Jefferson et al. [201].

61. $CH_3S(O)CH_3$, $CH_3S(O_2)CH_3$ and $CH_3S(O_2)OH$ on $H_2O(l)$—De Bruyn et al. [99] measured uptake over the temperature range ~262–281 K and derived accommodation coefficients fitting $\alpha / (1 - \alpha) = \exp(-\Delta G^{\ddagger}_{obs}/RT)$, where $\Delta G^{\ddagger}_{obs} =$

-0.12 kcal molecule^{-1} + 23.1 cal molecule^{-1} K^{-1} T(K) for dimethylsulfoxide

-10.7 kcal molecule^{-1} + 43.0 cal molecule^{-1} K^{-1} T(K) for dimethylsulfone

-3.50 kcal molecule^{-1} + 16.7 cal molecule^{-1} K^{-1} T(K) for methanesulfonic acid.

5.12 Gas/Surface Reaction Probabilities for Surfaces Other Than Soot.

Table 5-2. Gas/Surface Reaction Probabilities (γ) for Surfaces Other Than Soot.

Gaseous Species	Surface Type	Surface Composition	T(K)	γ	Uncertainty Factor	Notes
O_3 + Surface → Products						
O_3	Alumina	Al_2O_3(s)	210–300	See Note		1
	Sodium Chloride	NaCl(s)	300	>2 × 15^{-10}		1
OH + Surface →Products						
OH	Water Ice	H_2O(s)	205–230	>0.01		2
	Hydrochloric Acid	HCl • nH_2O(l)	220	>0.2		3
	Nitric Acid Ice	HNO_3 • 3HzO(s)	200–228	>0.2		4
	Sulfuric Acid	H_2SO_4 • nH_2O(l)	200–298	>0.2		5
	Sodium Chloride	NaCl(s)	245–339	1.2 × 10^{-5} exp 1750/T	3	6
HO_2 + Surface →Products						
	Water Ice	H_2O(s)	223	0.025	3	7
	Sulfuric Acid	H_2SO4 • nH_2O(l)				7
		(28 wt %)	275	>0.07		
		(55 wt %)	223	>0.05		
		(80–96 wt %)	243	>0.2		
$2NO_2$ + H_2O(l) →HONO + HNO_3						
NO_2	Liquid Water	H_2O(l)		See Note		8
	Sulfuric Acid	H_2SO_4 • nH_2O (40–98 wt. %)	250–325	5 × 10^{-7}	3	9
$2NO_2$ + NaCl(s) →ClNO + $NaNO_3$ $2NO_2$ + NaBr(s) →BrNO + $NaNO_3$						
NO_2	Sodium Chloride	NaCl(s)	298	See Note		10
	Sodium Bromide	NaBr(s)	298	See Note		10
NO_3 + H_2O →HNO_3 + OH						
NO_3	Water Ice	H_2O(s)	170–200	<10^{-3}		11
	Liquid Water	H_2O(l)	273	2 × 10^{-4}	20	12
N_2O_5 + H_2O →2HNO_3						
N_2O_5	Water Ice	H_2O(s)	188–195	0.02	2	13
	Liquid Water	H_2O(l)	260–295	See Note	See Note	14
	Nitric Acid Ice	HNO_3 • 3H_2O(s)	200	4 × 10^{-4}	3	15
	Sulfuric Acid	H_2SO_4 • nH_2O(l)	195–300	See Note*	See Note	16
	Sulfuric Acid Monohydrate	H_2SO_4 • H_2O(s)	200–300	See Note	3	17
	Sulfuric Acid Tetrahydrate	H_2SO_4 • 4H_2O(s)	195–207	0.006	2	18
	Ternary Acid	H_2SO_4 • nHNO_3 •nH_2O(l)	195–218	See Note		16
N_2O_5 + HCl(s) → $ClNO_2$ + HNO_3						
N_2O_5	Water Ice	H_2O(s) • HCl(s)	190–220	0.03	See Note	19
	Nitric Acid Ice	HNO_3 • 3H_2O(s) •HCl(s)	200	0.003	2	20
	Sulfuric Acid Monohydrate	H_2SO_4 • H_2O(s)	195	<1 × 10^{-4}		21
N_2O_5 + NaCl(s) → $ClNO_2$ + $NaNO_3$(s)						
N_2O_5	Sodium Chloride	NaCl(s)	–300	5 × 10^{-4}	20	22
		NaCl(aq)		>0.02		22
N_2O_5 + HBr(s) →$BrNO_2$ + HNO_3						
N_2O_5	Water Ice	H_2O	180–200	See Note		23
	Nitric Acid Ice	HNO_3 • 3H_2O(s)	200	0.005	10	24
N_2O_5 + MBr(s) →Products						
N_2O_5	Sodium Bromide	NaBr(s)	~300		See Note	25
	Potassium Bromide	KBr(s)	~300	4 × 10^{-3}	10	25
HONO + H_2O →Products						
HONO	Liquid Water	H_2O(l)	247–297	0.04	5	26
HONO + H_2SO_4 →Products						
HONO	Sulfuric Acid	H_2SO_4 • nH_2O(l)	180–200	See Note		27
HONO + HCl →ClNO + H_2O						

Gaseous Species	Surface Type	Surface Composition	T(K)	γ	Uncertainty Factor	Notes
HONO	Water Ice	$H_2O(s)$	180–200	0.05	3	28
	Sulfuric Acid	$H_2SO_4 \cdot nH_2O(l)$		See Note	See Note	29
HONO + NaCl →Products						
HONO	Sodium Chloride	NaCl(s)	~300	$<1 \times 10^{-4}$		30
HNO_3 + Na×(s) →H× + $NaNO_3$						
HNO_3	Sodium Chloride	NaCl(s)	295–298	0.02	3	31
	Sodium Bromide	NaBr(s)	~290	0.02	10	31
	Potassium Chloride	KCl(s)	~290	0.02	10	31
	Potassium Bromide	KBr(s)	~290	0.02	10	31
HO_2NO_2 + HCl → Products						
HO_2NO_2	Sulfuric Acid	$H_2SO_4 \cdot nH_2O$ (50–75 wt. %)	200–225	$<1 \times 10^{-4}$		32
$NH_3 + H_2SO_4 \rightarrow NH_4HSO_4$						
NH_3	Sulfuric Acid	$H_2SO_4 \cdot nH_2O$	288–300	0.4	2.5	33
$CH_3C(O)O_2 + H_2O \rightarrow CH_3C(O)OH + HO_2$						
$CH_3C(O)O_2$	Liquid Water	$H_2O(l)$	225	4×10^{-3}	3	34
	Sulfuric Acid	$H_2SO_4 \cdot nH_2O$				34
		(84 wt % H_2SO_4)	246	3×10^{-3}	3	
		(51 wt % H_2SO_4)	223	1×10^{-3}	3	
		(71 wt % H_2SO_4)	298	1×10^{-3}	3	
$CH_3C(O)O_2NO_2$ + HCl, Cl, ClO, and OClO → Products						
$CH_3C(O)O_2NO_2$	Sulfuric Acid	$H_2SO_4 \cdot nH_2O$ (40–70 wt. %)	200–225	$<1 \times 10^{-4}$		35
Cl + Surface →Products						
Cl	Sulfuric Acid	$H_2SO_4 \cdot nH_2O(l)$	221–296	2×10^{-4}	10	36
Cl_2 + HBr(s) →BrCl + HCl						
Cl_2	Water Ice • HBr(s)	$H_2O(s)$	200	>0.2		37
Cl_2 + KBr(s) →BrCl + KCl(s)						
Cl_2	Potassium Bromide	KBr(s)	~295	>0.1		38
Cl_2 + Na× (aq) →Cl× + NaCl (aq)						
Cl_2	Aqueous Sodium Bromide	NaBr(aq)	See Note			39
	Aqueous Sodium Iodide	NaI(aq)	See Note			39
ClO + Surface →Products						
ClO	Water Ice	$H_2O(s)$	190	See Note		40
	Nitric Acid Ice	$HNO_3 \cdot 3H_2O(s)$	183	See Note		40
	Sulfuric Acid	$H_2SO_4 \cdot nH_2O(l)$ (60 to 95 wt.% H_2SO_4)	221–296	See Note		41
HCl + HNO_3 → Products						
HCl + HNO_3	Sulfuric Acid	$H_2SO_4 \cdot mHNO_3 \cdot nH_2O(l)$		See Note	See Note	42
HOCl + HCl(s) →Cl_2 + H_2O						
HOCl	Water Ice	$H_2O(s) \cdot HCl(s)$	195–200	0.2	2	43
	Nitric Acid Ice	$HNO_3 \cdot 3H_2O(s) \cdot HCl(s)$	195–200	0.1	2	43
	Sulfuric Acid	$H_2SO_4 \cdot nH_2O(l)$	198–209	See Note	See Note	44
HOCl + HBr(s) → BrCl + H_2O						
HOCl	Water Ice	$I_2O(s)$	189–220	See Note		45
	Sulfuric Acid	$I_2SO_4 \cdot nH_2O(l)$	228	See Note	See Note	46
ClNO + NaCl(s) →Products						
ClNO	Sodium Chloride	NaCl(s)	298	$>1 \times 10^{-5}$		47
$ClNO_2$ + NaCl(s) →Products						
$ClNO_2$	Sodium Chloride	NaCl(s)	298	$<1 \times 10^{-5}$		47
$ClONO_2 + H_2O(s) \rightarrow HOCl + HNO_3$						
$ClONO_2$	Water Ice	$H_2O(s)$	180–200	0.3	3	48
	Nitric Acid Ice	$HNO_3 \cdot 3H_2O(s)$	200–202	0.004	3	49
	Sulfuric Acid	$H_2SO_4 \cdot nH_2O(l)$	200–265	See Note*	See Note	50
	Sulfuric Acid Monohydrate	$H_2SO_4 \cdot H_2O(s)$	195	$<1 \times 10^{-3}$		51
	Sulfuric Acid Tetrahydrate	$H_2SO_4 \cdot 4H_2O(s)$	196–206	See Note		51
$ClONO_2$ + HCl(s) →Cl_2 + HNO_3						

Gaseous Species	Surface Type	Surface Composition	T(K)	γ	Uncertainty Factor	Notes
$ClONO_2$	Water Ice	$H_2O(s)$	180–200	0.3	3	52
	Nitric Acid Ice	$HNO_3 \cdot 3H_2O \cdot HCl$	185–210	0.2	2	53
	Sulfuric Acid	$H_2SO_4 \cdot nH_2O(l) \cdot HCl(l)$	195–235	See Note	See Note	54
	Sulfuric Acid Monohydrate	$H_2SO_4 \cdot H_2O(s)$	195	$<1 \times 10^{-4}$		55
	Sulfuric Acid Tetrahydrate	$H_2SO_4 \cdot 4H_2O(s)$	195–206	See Note		55
	Alumina	Al_2O_3	180–200	0.3	3	56
$ClONO_2 + M{\times}(s) \rightarrow {\times}Cl + MNO_3$						
$ClONO_2$	Sodium Chloride	NaCl(s)	200–300	5×10^{-2}	10	57
	Potassium Bromide	KBr(s)	~295	5×10^{-2}	10	57
	Sodium Bromide	NaBr(s)	~295	See Note		57
$ClONO_2 + HBr(s) \rightarrow BrCl + HNO_3$						
$ClONO_2$	Water Ice	$H_2O(s) \cdot HBr(s)$	200	>0.3		58
	Nitric Acid Ice	$HNO_3 \cdot 3H_2O(s) \cdot HBr(s)$	200	>0.3		58
$ClONO_2 + HF(s) \rightarrow$ Products						
$ClONO_2$	Water Ice	$H_2O(s) \cdot HF(s)$	200	See Note		59
	Nitric Acid Ice	$H_2O(s) \cdot HNO_3(s) \cdot HF(s)$	200	See Note		59
$CF_xCl_y + Al_2O_3(s) \rightarrow$ Products						
CCl_4	Alumina	$Al_2O_3(s)$	120–300	1×10^{-5}	10	60
$CFCl_3$	Alumina	$Al_2O_3(s)$	120–300	1×10^{-5}	10	60
CF_2Cl_2	Alumina	$Al_2O_3(s)$	120–300	1×10^{-5}	10	60
CF_3Cl	Alumina	$Al_2O_3(s)$	120–300	1×10^{-5}	10	60
$BrCl + KBr(s) \rightarrow Br_2 + KCl(s)$						
BrCl	Potassium Bromide	KBr(s)	~295	>0.1		38
$Br_2 + NaI(aq) \rightarrow BrI + NaBr(aq)$						
Br_2	Aqueous Sodium Iodide	NaI(aq)	See Note			39
$2BrO \rightarrow Br_2 + O_2$						
BrO	Water Ice	$H_2O(s)$	213	See Note		61
	Sulfuric Acid	$H_2SO_4 \cdot nH_2O$				
		(60 wt% H_2SO_4)	213	See Note		61
		(70 wt % H_2SO_4)	213	See Note		61
	Aqueous Sodium Chloride	NaCl(aq) (23 wt% NaCl)	53	See Note		61
$HOBr + HCl(s) \rightarrow BrCl + H_2O$						
HOBr	Water Ice	$H_2O(s) \cdot HBr(s)$	180–228	0.3	3	62
	Sulfuric Acid	$H_2SO_4 \cdot nH_2O$ (60–69 wt% H_2SO_4)	198–218	See Note		62
$HOBr + HBr(s) \rightarrow Br_2 + H_2O$						
HOBr	Water Ice	$H_2O(s) \cdot HBr(s)$	228	0.1	3	63
	Sulfuric Acid	$H_2SO_4 \cdot nH_2O$	228	See Note		63
$BrONO_2 + H_2O \rightarrow HOBr + HNO_3$						
$BrONO_2$	Water Ice	$H_2O(s)$	190–200	>0.3	2	64
	Sulfuric Acid	$H_2SO_4 \cdot nH_2O$	210–300	See Note	See Note	65
$BrONO_2 + HCl \rightarrow BrCl + HNO_3$						
$BrONO_2/HCl$	Water Ice	$H_2O(s)$	200	See Note		64
	Sulfuric Acid	$H_2SO_4 \cdot nH_2O$	229	0.9	2	65
$CF_2Br_2 + Al_2O_3(s) \rightarrow$ Products						
CF_2Br_2	Alumina	Al_2O_3	210, 315	2×10^{-5}	10	60
$CF_3OH + H_2O \rightarrow$ Products						
CF_3OH	Water Ice	$H_2O(l)$	274	>0.01		66
	Sulfuric Acid	$H_2SO_4 \cdot nH_2O$				
		(40 wt% H_2SO_4)	210–250	0.07	3	66
		45 wt% H_2SO_4)	210–250	0.04	3	66
		(50 wt% H_2SO_4)	210–250	0.01	3	66
		(50 wt% H_2SO_4)	210–250	0.001	3	66
$SO_2 + H_2O_2$, O_3, HONO, NO_2 and $HNO_3 \rightarrow$ Products						
SO_2	Sulfuric Acid	$H_2SO_4 \cdot nH_2O$ (20–60 wt. % H_2SO_4)	293	See Note		67
$SO_3 + H_2O \rightarrow$ Products						
SO_3	Sulfuric Acid	$H_2SO_4 \cdot nH_2O$ (78–92 wt. % H_2SO_4)	300	1.0	+0.0, –0.3	68

*γ is temperature dependent

5.13 Notes to Table 5-2

1. $O_3 + Al_2O_3(s)$ and NaCl(s). Very low ozone decomposition efficiencies for reaction on coarse (3 μm dia.) and fine (0.1 μm dia., partially hydroxylated) γ-alumina and coarse (3 μm dia.) α-alumina were measured in flowing and static systems by Hanning-Lee et al.[147] at temperatures ranging between 212 and 473 K. Based on measured BET surface areas, γs ranged from 2×10^{-11} to 4×10^{-10} over the 212 to 298 K temperature range. γs for γ-alumina at lower temperatures exceeded those for α-alumina. Results are roughly consistent with earlier, unpublished flow tube data from L.F. Keyser and from fluidized bed reactor studies of Alebić-Juretić et al. [15]. Note that γs based on geometic surface particle surface areas would be significantly (10^4–10^7) larger. Alebić-Juretić et al. also studied ozone decomposition on small (<180 μm) NaCl crystals in their fluidized bed reactor and observed no effect, indicating γ for O_3 decomposition on NaCl(s) is much smaller than that for α-alumina.

2. OH + $H_2O(s)$. Cooper and Abbatt [91] measured initial irreversible OH uptake coefficients of ~ 0.1 for water ice between 205–230 K; these decayed to $\gamma = 0.03 \pm 0.02$ after repeated exposure to OH. Self-reaction to form H_2O or H_2O_2 was indicated by the lack of observable gas phase products despite observation of first-order OH loss.

3. OH + HCl • $nH_2O(l)$. Cooper and Abbatt [91] demonstrated significant enhancement of OH uptake (to $\gamma > 0.2$) after HCl doping of 220 K ice surfaces sufficient to melt the surface layer. It is unclear whether OH is lost to self-reaction or reaction with hydrated Cl^- ions.

4. OH + $HNO_3 \cdot 3H_2O$. Cooper and Abbatt [91] measured $\gamma > 0.2$ for nitric acid-doped ice surfaces under conditions suitable for NAT formation at 200 and 228 K. Increase over pure ice uptake rates is probably due to $HNO_3 + OH \rightarrow H_2O + NO_3$ reaction.

5. OH + $H_2SO_4 \cdot nH_2O$. Lower limits of 0.2 for uptake coefficients on 45–65 wt % H_2SO_4 between 220 and 230 K and for 96 wt % H_2SO_4 at 230 and 298 K by Cooper and Abbatt [91] are consistent with a lower limit of 0.07 on 28 wt % H_2SO_4 at 275 K in similar experiments by Hanson et al. [151] and a probable surface saturated value of $(4.9 \pm 0.5) \times 10^{-4}$ from Knudsen cell measurements by Baldwin and Golden [27] and an estimate of $\gamma = 1$ on ~96 wt % H_2SO_4 at 298 K by Gerhenzon et al. [136] using a coated insert flow tube technique. Uptake is probably reactive with $OH + HSO_4^- \rightarrow H_2O + SO_4^-$ the hypothesized process.

6. OH + NaCl(s). Ivanov et al. [193] used a fast flow reactor with a central salt coated rod to measure heterogeneous loss of OH between 245 and 339 K. Their fit for NaCl(s) yielded $\gamma = (1.2 \pm 0.7) \times 10^{-5} \exp[(1750 \pm 200)/T]$. Similar data for NH_4NO_3 yielded $\gamma - (1.4 \pm 0.5) \times 10^{-4} \exp[(1000 \pm 100)]$. Since uptake was irreversible, it is assumed that the loss was self-reaction.

7. HO_2 on $H_2O(s)$ and $H_2SO_4 \cdot nH_2O(l)$. Uptake of HO_2 on ice and super-cooled 55 wt % sulfuric acid at 223 K has been demonstrated to be limited by HO_2 surface saturation by Cooper and Abbatt [91]. They argue that self-reaction, presumably $2HO_2 \rightarrow H_2O_2 + O_2$ is limiting measured uptake coefficients of 0.025 ±0.005 for ice and 0.055 ±0.020 for 55 wt % H_2SO_4. However, Gershenzon et al. [135]measured $\gamma > 0.2$ for 80 and 96 wt % H_2SO_4 at 243 K and Hanson et al. [151] measured a lower limit for 28 wt % H_2SO_4 at 275 K of 0.07. However, large gas phase diffusion corrections mean this value is consistent with $\gamma = 1$.

8. $NO_2 + H_2O(1)$. Value for γ of $(6.3 \pm 0.7) \times 10^{-4}$ at 273 K (Tang and Lee, [327]) was achieved by chemical consumption of NO_2 by $SO_3^=$; their stopped-flow measurement was probably still affected by surface saturation, leading to the measurement of a lower limit. Ponche et al. [276] measured an uptake coefficient of $(1.5 \pm 0.6) \times 10^{-3}$ at 298 K, which was also probably subject to saturation limitations. Mertes and Wahner [254] used a liquid jet technique to measure a lower limit of $\gamma \geq 2 \times 10^{-4}$ at 278 K, and they observed partial conversion of the absorbed NO_2 to HONO. Msibi et al. [266] used a cylindrical/annular flow reactor to derive $g = (8.7 \pm 0.6) \times 10^{-5}$ on pH = 7 deionized water surfaces and $(4.2 \pm 0.9) \times 10^{-4}$ on pH = 9.3 wet ascorbate surfaces; it seems likely that these results are also subject to surface saturation given the gas/surface interaction times involved in the experiment. Data are consistent with an $\alpha \geq 1 \times 10^{-3}$ for 278–298 K and a liquid-phase second-order hydrolysis of NO_2 to HONO and HNO_3 which depends on temperature and pH. However, the interplay between accommodation, possible surface reaction, and bulk reaction may be complex.

9. $NO_2 + H_2SO_4 \bullet nH_2O$. Kleffman et al. [224] performed bubble tube reactor uptake measurements for 0–98 wt. % acid at 298 K and for 44.6 and 56.1 wt % from 250–325 K. At 298 K, measured uptake coefficients varied between 6 and 3×10^{-7} with a minimum near 70 wt. %. Most measurements at 44.6 and 56.1 wt. % overlapped within their error limits and showed little temperature dependence although there is evidence that uptake increases at the lowest temperatures. The data can all be captured with a recommended value of 5×10^{-7} with an uncertainty factor of three.

   This recommendation is consistent with earlier upper limits of 1×10^{-6} by Baldwin and Golden [26] for 96 wt. % at 295 K and 5×10^{-6} for 70 wt. % between 193 and 243 K by Saastad et al. [303]. Kleffman et al. [224] conclude that their uptake measurements are mass accommodation limited; however, it is not clear that their values are not influenced by bulk or surface reaction of two NO_2 with H_2O to form HONO and HNO_3 at lower acid wt. % values and the formation of nitrosyl sulfuric acid at higher acid concentrations. Kleffman et. al. [224] did perform separate static wetted wall reactor studies showing the formation of gas phase HONO at acid concentrations below 60 wt. %. It is more likely that reactive uptake is a controlling factor and the measured uptakes are solubility and/or reaction rate limited. Thus, the mass accommodation coefficient may be much larger than the recommended uptake values.

10. NO_2 + NaCl(s), NaBr(s). Vogt and Finlayson-Pitts [342,344] used diffuse reflectance infrared spectroscopy to study the reaction of NO_2 with NaCl(s) at 298 K, and Vogt et al. [341] used the same technique to study NO_2 + NaBr(s) at 298 K. Both reactions were shown to be approximately second order in NO_2. Assuming that adsorbed N_2O_4 is the reactant leads to $\gamma = (1.3 \pm 0.6) \times 10^{-4}$ for NaCl(s) and $2\ (+4, -1.3) \times 10^{-4}$ for NaBr(s). Peters and Ewing [275] measured reactive uptake for single-crystal NaCl(100) surfaces and observed both NO_3^-(c) and ClNO products. The value of $\gamma(N_2O_4)$ measured by Peters and Ewing at 298 K was only
   $(1.3 \pm 0.3) \times 10^{-6}$. They noted that small amounts of water vapor (9.5 mbar) cause γ to increase by two orders of magnitude.

11. NO_3 on H_2O(s). Fenter and Rossi [121] measured an upper limit for γ of 10^{-3} over the range from 170 to 200 K.

12. $NO_3 + H_2O$(l). Rudich et al. [300,301] used wetted-wall flow tube techniques to measure uptake coefficients for NO_3 on pure water and aqueous NaCl, NaBr, NaI, and $NaNO_2$ solutions. These studies were extended to other aqueous solutions by Imamura et al. [189]. Uptake on pure water was consistent with reaction of NO_3 to produce HNO_3 and OH. Uptake coefficients with solutions containing I^-, Cl^-, Br^-, NO_2^- and other anions were larger and scaled with anion concentration, indicating electon transfer reactions to produce NO_3^-. The γ of $(2.0 \pm 1.0 \times 10^{-4})$ at 273 K determined for pure water by Rudich et al. is significantly lower than the lower limit of 2.5×10^{-3} quoted by Mihelcic et al. [258]. A detailed analysis of uptake coefficients for KI aqueous solutions indicated that the NO_3 mass accommodation coefficient is >0.04 [301].

13. $N_2O_5 + H_2O$(s). Leu [232] and Hanson and Ravishankara [157] measured nearly identical values of 0.028 (±0.011) and 0.024 (±30%) in the 195–202 K range on relatively thick ice films in coated wall flow tubes. Quinlan et al. [281] measured a maximum value for γ on ice surfaces at 188 K of 0.03 in a Knudsen cell reactor. The average of these three studies is 0.027 with a standard deviation of 0.003. Hanson and Ravishankara [158,160] presented new and re-analyzed data as a function of ice thickness, with a value of ~0.008 for the thinnest ice sample, rising to 0.024 for the thickest. From these data there would appear to be no strong dependence on temperature, at least over the 188–195 K range. It is unclear whether the measured dependence on ice film thickness is due to added porosity surface area in the thicker films or decreased ice film integrity in thinner films. The error estimate in the table is driven by the possible systematic error due to unresolved film thickness effects rather than the small statistical error among the "thick film" values from the three groups.

    Zondlo et al. [374] report the formation of a supercooled H_2O/HNO_3 liquid layer at 185 K as a reaction product, forming NAT or NAD only after decreasing the relative humidity below the ice frost point. This effect is similar to that resulting from the interaction of gaseous HNO_3 or $ClONO_2$ with the ice surface. These authors measured $\gamma = (7 \pm 3) \times 10^{-4}$ at 185 K for the reaction of N_2O_5 with this supercooled liquid layer.

14. $N_2O_5 + H_2O$(l). Reaction on liquid water has a negative temperature dependence. Van Doren et al. [337] measured γs of 0.057 ± 0.003 at 271 K and 0.036 ± 0.004 at 282 K using a droplet train uptake technique. George et al. [132] also used a droplet train technique to measure γs of $(3.0 \pm 0.2) \times 10^{-2}$ (262 K), $(2.9 \pm 1.2) \times 10^{-2}$ (267 K), $(2.0 \pm 0.2) \times 10^{-2}$ (273 K), $(1.6 \pm 0.8) \times 10^{-2}$ (276 K), and $(1.3 \pm 0.8) \times 10^{-2}$ (277 K) on pure water, while Schweitzer et al. [310] used the same approach for pure water

and salt solutions between 262 and 278 K, obtaining similar results. Mozurkewich and Calvert [263] studied uptake on $NH_3/H_2SO_4/H_2O$ aerosols in a flow reactor. For their most water-rich aerosols (RH = 76%) they measured γs of 0.10 ±0.02 at 274 and 0.039 ±0.012 at 293 K. However, similar studies by Hu and Abbatt [180] on $(NH_3)_2SO_4$ aerosols at 297 K showed that uptake rises with decreasing relative humidity (RH); their 94% RH results agree very well with the temperature trend measured by Van Doren et al. Msibi et al.[265] measured a smaller γ of 2.5×10^{-3} for water adsorbed on a denuder flow tube well under 66–96% relative humidity conditions at room temperature. The higher γ values of Van Doren et al., Mozurkewhich and Calvert, and Hu and Abbatt are quite consistent when temperature and RH effects are factored in. The lower values from the Louis Pasteur (George et al.; Schweitzer et al.) and Birmingham (Msibi et al.) groups appear to have much less pronounced temperature dependence and are inconsistent with the other measurements. The same function used to fit the N_2O_5 uptake on sulfuric acid as a function of temperature and concentration, discussed in note 17 below, has been extended to the Van Doren et al. and Hu and Abbatt data for pure water and very high RH aerosols. See note 17 for the functional fit and its error discussion.

15. $N_2O_5 + HNO_3 \bullet 3H_2O(s)$. Hanson and Ravishankara [155] have measured γ = 0.0006 (± 30%) near 200 K. They presented re-analyzed and additional data as a function of ice thickness (Hanson and Ravishankara [158,160]), deriving a value of 3×10^{-4} for the thinnest NAT covered ice layer, with values up to three times higher for thicker NAT-covered ice layers. As in the case of uptake on water ice this may be due to increased surface area from porosity in the thicker films, or less integrity in the thinner films. The uncertainty listed in Table A-1 is driven by this observed effect. All of the Hanson et al. data are in very poor agreement with the γ = 0.015 (±0.006) reported by Quinlan et al. [281] from their Knudsen cell measurements; this measurement may have been biased by formation of a super-cooled aqueous nitric acid surface and is judged to be unreliable.

16. $N_2O_5 + H_2SO_4 \bullet nH_2O(l)$. This reaction has been intensively studied between 195 and 296 K for a wide range of H_2SO_4 wt. % values using four complementary experimental techniques. Data are available from aerosol flow tube studies (Fried et al. [129], Hanson and Lovejoy [152], Hu and Abbatt [180], and Hallquist et al. [145]), coated wall flow tube studies (Hanson and Ravishankara [155], Zhang et al. [365]), a stirred Knudsen cell (Manion et al. [249]) and droplet train studies (Van Doren et al. [337], Robinson et al. [293]). All studies have yielded γs between ~0.05 and 0.20 with modest dependence on surface H_2SO_4 wt. % and temperature. The Knudsen cell studies, aerosol flow tube studies at higher N_2O_5 exposure and the ternary $H_2SO_4/HNO_3/H_2O$ studies of Zhang et al. [365] all illustrate that significant levels of HNO_3 in the H_2SO_4/H_2O solutions will reduce γ measurably; this fact explains some of the scatter in aerosol flow tube studies and the surface saturation evident in the Knudsen cell studies. The effect of 5.0×10^{-7} Torr HNO_3 on γ as a function of temperature at two water vapor concentrations are plotted in Zhang et al. [365]; the decrease in γ is greatest at low temperatures, approaching a factor of 2–5 between 200 and 195 K.

Experimental data on sulfuric acid surfaces between 40 and 80 wt. % sulfuric acid deemed to be free of saturation effects, plus the pure water uptake data of Van Doren et al. [337] and high relative humidity ammonium sulfate aerosol uptake data of Hu and Abbatt [180] were all fit to a polynomial expression to yield a single model describing γ for N_2O_5 uptake valid between 0 and 80 wt. % H_2SO_4 and 180 to 300 K (Robinson et al. [293]). The form of this function is: $\gamma_o = \exp(k_o + k_1/T + k_2/T^2)$, where T is the temperature in K. The parameters k_o, k_1, and k_2 obtained from the best-fit are:

$$k_o = -25.5265 - 0.133188wt + 0.00930846wt^2 - 9.0194\times10^{-5}wt^3$$

$$k_1 = 9283.76 + 115.345wt - 5.19258wt^2 + 0.0483464wt^3$$

$$k_2 = -851801 - 22191.2wt + 766.916\,wt^2 - 6.85427wt^3$$

where wt is the weight percentage of H_2SO_4.

The overall error of applying the uptake function provided here consists of two components. One is the standard deviation of the model-calculated value with respect to measured data, σ_m, which is given by

$$\sigma_m = \sqrt{\frac{\sum_{i=1}^{N}\left(1 - \frac{\gamma_i}{\gamma_{\text{model}}}\right)^2}{N-1}}\,.$$

The other is the standard deviation of relative experimental measurement error from the mean, σ_d, which is given by

$$\sigma_d = \sqrt{\frac{\sum_{i=l}^{N}\left(\frac{\Delta\gamma_i}{\gamma_i}\right)^2}{N(N-1)}} .$$

The overall error is

$$\sigma = \sqrt{\sigma_m^2 + \sigma_d^2} .$$

(These formulations are also applied below in the error estimation for the $ClONO_2 + H_2O$ and HCl, $BrONO_2 + H_2O$, and HOCl + HCl reaction system. For N_2O_5, the error is estimated to be 15% (one sigma), with σ_m=14.7% and σ_d=2.9%).

17. $N_2O_5 + H_2SO_4 \bullet H_2O(s)$. Zhang et al. [366] used coated flow tube techniques to measure the uptake of N_2O_5 on solid sulfuric acid monohydrate over a temperature range of 200 to 225 K. The measurement values of γ were significantly higher at 200 K ($\gamma \sim 1 \times 10^{-3}$) than at 225 K ($\gamma \sim 10^{-4}$) and were well fit by $\log \gamma = [4.78 - 0.0386T(K)]$. Acid-rich $H_2SO_4 \bullet H_2O$ surfaces had a lower γ than water rich surfaces ($\log \gamma = [0.162 - 0.789 \times \log p_{H2O}]$ where p_{H2O} is their experimental water vapor partial pressure).

18. N_2O_5 on $H_2SO_4 \bullet 4H_2O(s)$. Hanson and Ravishankara [162] studied N_2O_5 uptake by frozen 57.5 and 60 wt % H_2SO_4 as a function of temperature and relative humidity. The 57.5 wt % surface was not sensitive to relative humidity and was slightly more reactive (γ = 0.008 vs 0.005) at 205 K than at 195 K. Reaction probabilities on the 60 wt % surface dropped off with temperature and relative humidity.

19. N_2O_5 + HCl on $H_2O(s)$. Leu [233] measured γ = 0.028 (±0.011) at 195 K, while Tolbert et al. [331] measured a lower limit of 1×10^{-3} at 185 K. These experiments were done at high HCl levels probably leading to a liquid water/acid surface solution (Abbatt et al. [5]). Seisel et al. [311] measured $\gamma \sim 0.03$ at 200 K using a Knudsen flow reactor with a range of HCl flows. The uptake coefficient at low HCl flows is only slightly enhanced compared to the uptake on a pure ice surface.

20. N_2O_5 + HCl on $HNO_3 \bullet 3H_2O(s)$. Hanson and Ravishankara [155] measured γ = 0.0032 (±30%) near 200 K.

21. N_2O_5 + HCl on $H_2SO_4 \bullet H_2O(s)$. Zhang et al. [366] saw no increase in N_2O_5 uptake on sulfuric acid monohydrate at 195 K upon exposure to HCl, setting $\gamma < 10^{-4}$.

22. N_2O_5 + NaCl (s,aq). Using FTIR analysis, Livingston and Finlayson-Pitts [241] have demonstrated that N_2O_5 reacts with crystalline NaCl to form $NaNO_3(s)$, and they report $\gamma > 2.5 \times 10^{-3}$ at 298 K. However, Leu et al.[235] used flow tube/mass spectrometric techniques to obtain $\gamma < 1 \times 10^{-4}$ for dry salt at 223 and 296 K; they also noted that exposing salt surfaces to small amounts of H_2O vapor increased γ significantly. Fenter et al.[119] measured $\gamma = (5.0 \pm 0.2) \times 10^{-4}$ on fused salt surfaces at room temperature, assuming the geometrical surface area is the only surface accessed. Msibi et al. [265] measured NO_3^- deposition on an annular flow reactor to determine $\gamma = 1 \times 10^{-3}$ for salt surfaces between 45 and 96% relative humidity at room temperature, rising to $\gamma = 1.5 \times 10^{-2}$ at 96–97% relative humidity, but they argue that most of the uptake is due to reaction with H_2O. On aqeous NaCl solutions, Zetzsch, Behnke, and co-workers [43,44,362] have studied the reaction of N_2O_5 with aqueous NaCl aerosols in an aerosol chamber. The relative yields of $ClNO_2$ and HNO_3 rise with the NaCl concentration. A reaction probability of ~0.03 is measured with a 50% $ClNO_2$ yield at the deliquescence point (Zetsch and Behnke). This picture is confirmed by droplet uptake studies on 1 M NaCl solutions reported by George et al. [132] which confirm that uptake on salt solutions in the 263–278 K temperature range is larger than that on pure water droplets.

23. N_2O_5 + HBr on $H_2O(s)$. Seisel et al. [311] report γ values ranging from $\sim 3 \times 10^{-3}$ to 0.1, depending on the HBr concentrations employed; the measurements were conducted at 180 and 200 K. These authors report Br_2 and HONO in 80% yield as products with respect to N_2O_5 taken up, generated presumably by the secondary reaction of the primary product $BrNO_2$ with HBr.

24. N_2O_5 + HBr on $HNO_3 \bullet 3H_2O(s)$. This reaction, yielding γ ~0.005, was investigated on NAT surfaces near 200 K by Hanson and Ravishankara [159]. Under some conditions a much higher reaction coefficient of ~0.04 was observed.

25. N_2O_5 + MBr. Finlayson-Pitts et al. [122] used FTIR techniques to demonstrate that $BrNO_2$(ads) is a major product of the $N_2O_5(g)$ + NaBr(s) reaction. However, Fenter et al. [119] failed to measure gas-phase evolution of $BrNO_2$ using Knudsen cell/mass spectrometry techniques, detecting $Br_2(g)$ instead. They propose that $BrNO_2$ reacts with KBr(s) to yield $KNO_2(s) + Br_2(g)$. A γ of $(4.0 \pm 2.0) \times 10^{-3}$ at room temperature was determined for fused KBr surfaces with well-defined surface areas.

26. HONO + $H_2O(l)$. Bongartz et al. [56] present uptake measurements by two independent techniques, the liquid jet technique of Schurath and co-workers and the droplet train/flow tube technique of Mirabel and co-workers (Ponche et al. [276]). With a surface temperature of ~245 K the droplet train techniques yielded $0.045<\gamma<0.09$, while the liquid jet operating with a surface temperature of 297 K obtained $0.03 < \gamma < 0.15$. Mertes and Wahner used a liquid jet technique to measure $4 \times 10^{-3} < \gamma < 4 \times 10^{-2}$ at 278 K. Since HONO uptake by liquid water probably involved hydrolysis, an increase in Henry's law solubility with decreasing temperature may be offset by a decreasing hydrolysis rate constant, leaving the uptake coefficient's temperature trend uncertain. Measured uptake coefficients will not correspond to the mass accommodation coefficient.

27. HONO + $H_2SO_4 \bullet nH_2O(l)$. Zhang et al. [368] measured uptake coefficients for HONO on sulfuric acid that increased from $(1.6 \pm 0.1) \times 10^{-2}$ for 65.3 wt. % H_2SO_4 (214 K) to $(9.1 \pm 1.6) \times 10^{-2}$ for 73 wt. % H_2SO_4 (226 K). Fenter and Rossi [120] measured uptake coefficients rising from 1.8×10^{-4} for 55 wt. % H_2SO_4 (220 K) to 3.1×10^{-1} for 95 wt. % H_2SO_4 (220 K and 273 K). Baker et al. [24] measured much smaller uptake coefficients for 60 wt. % at 298 K. In general, the values measured by Zhang et al. [368] are a factor of 2 to 5 higher than those of Fenter et al. [120] for comparable acid concentrations. Since the reaction probably depends on both temperature and acid concentration and since the data scatter is high in both experiments, further independent data will be required to define γ as a function of acid concentration and temperature. These data are generally consistent with the effective Henry' law constant measurements of Becker et al. [42] who illustrate that HONO solubility decreases exponentially with H_2SO_4 concentration until ~53 wt %, at which point reaction to form nitrosyl sulfuric acid increases H* dramatically as H_2SO_4 concentration increases. Baker et al. [24] invoke surface decomposition of HONO to explain their room temperature data, since they separately determine that the bulk second-order disproportionation rate for HONO is too slow to account for even their small uptake coefficients. It is possible that surface formation of nitrosyl sulfuric acid and not HONO disproportionation is responsible for much of their measured uptake. The Zhang et al. [368] and Fenter and Rossi [120] data have been combined and fit with a four-term polynomial as a function of acid wt. % (these data did not show an obvious temperature dependence):

$$\ln \gamma = a + b\ wt + c\ wt^2 + d\ wt^3$$

where wt is the H_2SO_4 wt. %, and

$$a = -155.7 \pm 29.7$$

$$b = 5.663 \pm 1.232$$

$$c = -0.07061 \pm 0.01679$$

$$d = 0.000297 \pm 0.000076$$

This parameterization should be used only within the 55–95-wt.-%-H_2SO_4 range and the 214-to-273-K temperature range.

28. HONO + HCl + $H_2O(s)$. Knudsen cell uptake studies for HONO/HCl co-deposited on ice (180–200 K) and for HONO on 0.1 to 10 m HCl frozen solutions (~190 K) by Fenter and Rossi [120] showed HONO uptake coefficients in the 0.02 to 0.12 range as long as surface HCl concentrations significantly exceed HONO concentrations. ClNO was evolved quantitatively with HONO consumption.

29. HONO + HCl on $H_2SO_4 \bullet nH_2O(l)$. Fenter and Rossi [120] saw no reaction for acid wt. % > 65. They measured $\gamma = 2.0 \pm 0.7 \times 10^{-3}$ for 60 wt. % acid saturated with HONO at 230 K. Zhang et al. [368] also measured the uptake of HCl after exposure to HONO, they observed HCl uptake with γs between 0.01–0.02 over an acid wt. % range of 60.8–71.3 (T = 207.9–222.6 K). The reaction was also studied by Longfellow et al. [242] using both HCl doped and HONO doped sulfuric acid aerosols. Their uptake measurements

confirmed reaction at higher acid wt. %, but by using lower HONO partial pressures they measured smaller γs. The reverse reaction, ClNO hydrolysis, was also studied in a wetted wall flow reactor and in the aerosol flow reactor by Longfellow et al. [242] and in a Knudsen cell reactor by Fenter and Rossi [120]. Data show clear evidence of both surface and bulk kinetics for the forward reaction. Longfellow et al. [242] report k^{II} values for the bulk reaction (in units of 10^4 $M^{-1}s^{-1}$) for 50 wt. %: 81 at 250 K and 15 at 205 K; for 60 wt. %: 9.4 at 250 K, 6.9 at 230 K and 5.0 at 219 K; for 67 wt. %: 3.9 at 250 K; and for 70 wt. %: 5.8 at 269 K and 0.35 at 215 K. The reaction is clearly complex and will require a comprehensive model of both the surface and bulk processes to arrive at an appropriate parameterization for γ.

30. HONO + NaCl(s). Diffuse reflectance experiments by Vogt and Finlayson-Pitt [343] on room temperature NaCl(s) and Knudsen cell uptake experiments by Fenter and Rossi on room temperature NaCl(s) and frozen 0.1 M NaCl aqueous solutions, all failed to show HONO uptake. The latter results yield $\gamma < 1 \times 10^{-4}$.

31. HNO_3 + NaX(s)/KX(s). Vogt and Finlayson-Pitts [342,344] used diffuse infrared reflectance spectroscopy to characterize the process. There was absorption of HNO_3, but no reaction was observed on completely dry NaCl(s); however, $NaNO_3$ forms in the presence of very low (well below the deliquescence point) levels of H_2O(g). Using XPS spectroscopy to identify surface products and a dry HNO_3 source, Laux et al. [230] (also see Vogt et al.) measured $\gamma = (4 \pm 2) \times 10^{-4}$ at 298 K. Fenter et al. [118] measured the room temperature uptake of HNO_3 on solid powders of NaCl, NaBr, KCl, KBr, and $NaNO_3$, using Knudsen cell/mass spectrometry techniques. They saw similar uptake for all surfaces, including unreactive $NaNO_3$, and recommend $\gamma = (2.8 \pm 0.3) \times 10^{-2}$ for all salts. HCl or HBr was produced with ~100% yield from the halide surfaces. There is some concern about the effective surface area of the powders used by Fenter et al. (see Leu et al.[235]). Fenter et al. report new HNO_3 data to support their argument that "sticky" gases such as HNO_3 cannot penetrate below the top surface layer of the powders used in their experiments. Leu et al. [235] used flow tube/mass spectrometry techniques to measure $\gamma = (1.3 \pm 0.4) \times 10^{-2}$ at 296 K and $\gamma > 8 \times 10^{-3}$ at 223 K, both in the presence of low levels of H_2O(g). They determined that uptake at 296 K was reactive, producing HCl but that at 223 K reaction was suppressed and uptake was largely absorptive. Beichert and Finlayson-Pitts [46] measured $\gamma = (1.4 \pm 0.6) \times 10^{-2}$ at 298 K with a Knudsen cell technique, and, using D_2O, demonstrated that chemisorbed water, presumably retained on defect sites, was crucial for $NaNO_3$ formation. This suggests that low levels of defect-retained water are responsible for the small uptake values measured by Laux et al.

32. HO_2NO_2 + HCl on $H_2SO_4 \bullet nH_2O$(l). Zhang et al. [369] performed wetted-wall flow-reactor studies with HCl and HO_2NO_2 partial pressures in the 10^{-6} to 10^{-7} Torr range. Using chemical ionization mass spectrometry (CIMS) to detect expected reaction products, no Cl_2 (using SF_4^- as an analyte ion) or HOCl (using F^-) was detected over a temperature range of 200–225 K and an acid concentration range of 50–70 wt. % H_2SO_4. An upper limit for the reactive uptake coefficient for HO_2NO_2 reacting with HCl of $\gamma < 1 \times 10^{-4}$ was deduced.

33. NH_3 + $H_2SO_4 \bullet nH_2O$. Robbins and Cadle [289], Huntzicker et al. [184], McMurry et al. [253], and Daumer et al. [97] all studied NH_3 uptake by sulfuric acid aerosols in near room temperature flow reactors (T = 281–300 K). Uptake coefficients varied between 0.1 and 0.5. Rubel and Gentry [299] used levitated H_3PO_4 acid droplets to show that heterogeneous reaction does control the initial NH_3 uptake on strong acid solutions. Both Rubel and Gentry and Däumer et al. also explored the effect of organic surface coatings.

34. $CH_3C(O)O_2$ + H_2O(l) and $H_2SO_4 \bullet nH_2O$. Villalta et al. [339] used wetted-wall flow tube techniques to measure $\gamma = 4.3\ (+2.4\ /-1.5) \times 10^{-3}$ for water at 274 ± 3K. They also measured uptake for 34 wt % H_2SO_4 at 246 K ($\gamma = (2.7 \pm 1.5) \times 10^{-3}$), 51 wt % at 273 K ($\gamma = (0.9 \pm 0.5) \times 10^{-3}$), and 71 wt % at 298 K ($\gamma = (1.4 \pm 0.7) \times 10^{-3}$). They suggest that products subsequent to hydrolysis are HO_2 and $CH_3C(O)OH$.

35. $CH_3C(O)O_2NO_2$ + HCl, Cl, ClO, and OClO on $H_2SO_4 \bullet nH_2O$(l). Zhang and Leu [364] performed wetted wall flow reactor studies with Cl species partial pressures in the 10^{-6} to 10^{-7} Torr range and $CH_3C(O)O_2NO_2$ at 3×10^{-6} Torr after equilibrating the acid surfaces (42, 51, and 69 wt. % at 202 and 224 K) with $CH_3C(O)O_2NO_2$. Also uptake studies with 5×10^{-7} Torr $CH_3C(O)O_2NO_2$ were performed after exposing the acid surface to the Cl species. No Cl species or $CH_3C(O)O_2NO_2$ uptake enhancements were observed under either condition and an upper limit for the reactive uptake coefficient of $\gamma < 1 \times 10^{-4}$ of $CH_3C(O)O_2NO_2$ was deduced. No gas phase reaction products were observed using CIMS after 42 wt. % H_2SO_4at 210 K was exposed to $CH_3C(O)O_2NO_2$ and each Cl species for 20 minutes.

36. Cl + $H_2SO_4 \bullet nH_2O$(l). Measured reaction probability (Martin et al. [250]) varies between 3×10^{-5} and 7×10^{-4} as H_2O and T co-vary. Reaction product is claimed to be HCl.

37. Cl_2+HBr + H_2O(s). Hanson and Ravishankara [159] measured a reaction probability of > 0.2 on water ice near 200 K. BrCl was not detected, presumably due to rapid reaction with excess HBr.

38. Cl_2 and BrCl + KBr(s). Caloz et al. [64] measured $\gamma > 0.1$ for reactive uptake of Cl_2 and BrCl on KBr(s) in a room temperature Knudsen cell experiment.

39. Cl_2 and Br_2 + NaBr(aq) and NaI(aq). Hu et al. [181] measured large uptake coefficients for Cl_2 on dilute aqueous droplets of NaBr and NaI solutions and Br_2 on NaI solutions using a droplet train technique. Reaction was demonstrated to proceed through both a chemisorbed surface complex and normal bulk solution second-order kinetics. Second-order bulk reaction rate constants near the diffusion limit and consistent with bulk-phase kinetic measurements were obtained between 263 and 293 K.

40. ClO + H_2O(s) and $HNO_3 \bullet nH_2O$(s). Proposed reaction (Leu [233]) is 2 ClO → Cl_2 + O_2; reactive uptake may depend on ClO surface coverage, which in turn may depend on gas phase ClO concentrations. Kenner et al. [214] measured reaction probabilities of $(8 \pm 2) \times 10^{-5}$ for ice at 183 K which is far lower than the limit of $>1 \times 10^{-3}$ obtained by Leu [233]. Abbatt [3], using nearly the same low levels of ClO as Kenner et al., obtained $\gamma < 1 \times 10^{-5}$ at 213 K. The difference may lie in the level of ClO or other adsorbable reactive species present. The lower value of Abbatt is probably closer to the expected reactivity under stratospheric conditions. Kenner et al. also measured a reaction probability limit of $< (8 \pm 4) \times 10^{-5}$ for NAT at 183 K.

41. ClO + $H_2SO_4 \bullet nH_2O$. Measured reaction probability (Martin et al. [250]) varies between 2×10^{-5} and 2×10^{-4} as H_2O content is varied by changing wall temperature. Reaction product is claimed to be HCl, not Cl_2. Abbatt [3] measured $\gamma < 1 \times 10^{-5}$ for 60 and 70 wt % H_2SO_4 at 213 K.

42. HCl + HNO_3 on $H_2SO_4 \bullet$ m $HNO_3 \bullet nH_2O$(l). Two studies have noted HCl activation in concentrated ternary $H_2SO_4/HNO_3/H_2O$ solutions or ice slurries. Luick et al. [246] saw only gas phase HCl in 64.6 wt. % H_2SO_4/ 4.8 wt. % HNO_3 at 200 K, but saw a vapor phase Cl partitioning of 50% HCl and 50% ClNO/$ClNO_2$ for a 76.6/20.1 wt. % solution (an ice slurry) at 200 K. Cappa et al. [65] saw substantial yields of ClNO, $ClNO_2$, and Cl_2 at 273 K for a range of solution compositions; e.g. 32.6%, 9.8% and 44.4% respectively for a total HCl conversion of 86.9% in a 35% H_2SO_4 /45% HNO_3 solution and 20.2%, 6.9%, 27.9% for a 60/25 wt. % solution. While no kinetic coefficients or detailed mechanisms are available, these studies do show the potential for HCl activation in strong $H_2SO_4/HNO_3/H_2O$ solutions.

43. HOCl + HCl + H_2O(s) and $HNO_3 \bullet 3H_2O$(s). Hanson and Ravishankara [158] and Abbatt and Molina [6] have investigated the HOCl + HCl reaction on water ice and NAT-like surfaces, and Chu et al. [76][72] studied the reaction on water ice. Product yield measurements support the identification of Cl_2 and H_2O as the sole products. The measured yield of product Cl_2 is 0.87 ±0.20 and was stated to be similar on both surfaces according to Abbatt and Molina. Within the accuracy of the experiments, the reaction probability does not depend on the gas phase HCl and HOCl densities. Only Abbatt and Molina investigated at more than one temperature, their data indicates that γ increases at lower temperatures. A plot of data from the three studies does show a weak temperature trend, with γ increasing about a factor of two as the temperature drops from 202 to 188 K. However, the data are too sparse to assign a definitive temperature dependence. The average of all three studies yields $\gamma = 0.26 \pm 0.08$ for data based on the geometrical area of the flow tube surfaces. Chu et al. [72] indicate that a porosity correction for their data would reduce their value bya factor of 3 to 4. The real uncertainty would appear to be dominated by systematic uncertainties in porosity corrections and a potential temperature dependence. Given the fact that any porosity correction must reduce the value, a central value of 0.2 is adopted with an uncertainty factor of 2. The high reaction probabilities measured for water ice indicate that this reaction may play a significant role in release of reactive chlorine from the HCl reservoir.

    Two studies (Hanson and Ravishankara [158]; Abbatt and Molina [6]) have measured the reaction probability of HOCl + HCl on NAT surfaces. These data show γ increases as the ambient water pressure increases and then reaches a plateau. At relatively high water pressure, the two studies averaged $\gamma = 0.135 \pm 0.049$, with no porosity correction. The reaction probability on water poor NAT-like surfaces falls off dramatically (a factor of 10). A recommendation of 0.1 with an uncertainty factor of 2 is shown in Table 5-2. Carslaw and Peter [67] have published a model of this reaction and its dependence on HCl uptake.

44. HOCl + HCl + $H_2SO_4 \bullet nH_2O$(l). This process has been studied in coated flow tubes over ~200–260 K by Zhang et al. [363], Hanson and Ravishankara [161], Donaldson et al. [107], and Hanson and Lovejoy [154]. Hanson and Lovejoy also made measurements in an aerosol flow tube from 251 to 276 K. A model of this and related sulfuric acid aerosol reactions tailored to stratospheric conditions has been published by Hanson et al. [168]. Zhang et al. held the water vapor partial pressure at 3.8×10^{-4} Torr and showed γ increased by a

factor of 50 as the temperature was lowered from 209 to 198 K, showing that the reaction rate is strongly dependent on water activity.

A detailed kinetic uptake model has been developed to fit the experimental data [313]. The formulation for γ is given as:

$$\frac{1}{\gamma} = \frac{1}{\alpha} + \frac{1}{\Gamma_{HOCl}^{rxn}}$$

where

$$\Gamma_{HOCl}^{rxn} = \frac{4H_{HOCl}RT}{\bar{c}}\left(D_{HOCl}k_{HOCl_HCl}\right)^{1/2}$$

At the low temperatures of interest, α for HOCl was assumed to be unity consistent with the value for HCl measured at 240 K and below (Robinson et al. [294]). The individual formulations for H_{HOCl}, D_{HOCl} and $k_{HOCl\text{-}HCl}$ are given in Table A-4 in Shi et al. [313]. Reaction of HOCl with HCl is considered to be acid catalyzed. It is known that the reaction rate for HOCl + HCl in pure water is low (Donaldson et al. [107]). Experimental data noted above indicated that the reaction rate of HOCl + HCl increases with acidicity of H_2SO_4 solution. The data from the experimental studies noted above were fit to the model without bias. Using the same error analysis discussed in the note for N_2O_5 uptake on sulfuric acid, a detailed kinetic model yields a 33.4% error (one sigma fit to the available data set, with σ_m=33.3% and σ_d=3.0%).

In the cold stratosphere where T<190 K, the reaction of $ClONO_2$ + HCl is so fast that HCl is depleted which slows down the reaction of HOCl + HCl. As shown in Table A-4 in Shi et al., the effect of HCl depletion on the HOCl reactive uptake coefficient (due to reaction with $ClONO_2$ inside/on the surface of particles) is taken into account via the factor F_{HCl} (also see the note on chlorine nitrate/hydrochloric acid reactive uptake on sulfuric acid surfaces).

45. HOCl + HBr on H_2O(s). Chu and Chu [72] measured γ at 189 K to be in the range from 0.06 to 0.38 for HBr partial pressures ranging from 1.1×10^{-7} to 6.6×10^{-5} Torr. At 220 K they measured γ in the range from 0.01 to 0.07 for HBr partial pressures in the range from 7.2×10^{-7} to 1.3×10^{-5} Torr. These γ values were estimated assuming the area of the ice surface to be equal to the geometric area of the cylindrical flow reactor; corrections for surface porosity effects range from a factor of 3 to 10 lower.

46. HOCl + HBr on $H_2SO_4 \cdot nH_2O$(l). Abbatt and Nowak [8] measured uptake of HOCl in the presence of excess HBr on a 69.3 wt. % sulfuric acid solution in a wetted wall flow reactor at 228 K. A second order bulk reaction rate constant, k^{II}, of 2×10^6 $M^{-1}s^{-1}$ was derived; this is a factor of ~10 faster than HOBr + HCl under the same conditions. Since HOCl and HBr have similar solubilities under stratospheric conditions, characterizing this reaction with a simple uptake coefficient is not appropriate. A full reaction/solubility/liquid phase diffusion model will require further data.

47. ClNO and $ClNO_2$ + NaCl(s). Using a Knudsen cell technique Beichart and Finlayson-Pitts set upper limits of $\gamma < \sim 10^{-5}$ for reactive uptake of ClNO and $ClNO_2$ on NaCl(s) powders at 298 K.

48. $ClONO_2$ + H_2O(s). Measurement of γ = 0.3 (+0.7, –0.1) (Hanson and Ravishankara [155]) significantly exceeds previous measurements of Molina et al. [260], Tolbert et al. [333], Leu [232] and Moore et al. [262] but agrees reasonably well with subsequent measurements by Chu et al. [76] and Zhang et al. [365] when geometrical surface areas are assumed for analysis. Previous measurements were probably complicated by NAT formation on the surface (Hanson and Ravishankara [158]; Chu et al. [76]). Lower levels of $ClONO_2$ (g) used by Hanson and Ravishankara [155] minimized this surface saturation problem. Also, using lower $ClONO_2$ concentrations, Zhang et al. obtained a reaction probability of 0.08 ± 0.02 at 195 K, in fair agreement with the range of 0.03 to 0.13 measured by Chu et al. Subsequent Knudsen cell measurements at 180 and 200 K by Oppliger et al. [272] showed initial uptake γs in the 0.2 to 0.4 range. Measured reaction products were HNO_3 and HOCl. All of the HNO_3 and much of the HOCl is retained on the surface under polar stratospheric conditions (Hanson and Ravishankara [155,158]). Hanson [149] deposited $ClONO_2$ on $H_2{}^{18}O$ enriched ice and detected $H^{18}OCl$ showing the Cl–ONO2 bond is broken at 191 K.

Data plots confirm a trend showing that at a high density of $ClONO_2$, the product HNO_3 covers the ice surface preventing the further reaction of $ClONO_2$ with H_2O molecules on the surface. Therefore, data obtained at high $ClONO_2$ densities (>10^{14} molecules/cm^3) are excluded from further evaluation. An experiment (Berland et al. [53]) using a laser-induced thermal desorption technique yielded a much lower value of $ClONO_2$ reaction probability at 190 K (about 3 orders of magnitude lower) after extrapolating the

results obtained at temperatures of 140 K and below. We also exclude this point in the averaging of data since the physical characteristics of ice surfaces at these very low temperatures may not be very representative of those found at stratospheric temperatures. Selected data show no temperature dependence between T=180 and 200 K and averaged γ_o= 0.28 ± 0.25. Again, within the experimental accuracy, the Hanson and Ravishankara [158,160] and Chu et al. [76] data show that uptake measurements are nearly independent of ice substrate thickness. See Henson et al. [173,174] for discussion of a model which accounts for the effect of HNO_3 on the reaction $ClONO_2$ on water and nitric acid ice surfaces.

Zondlo et al. [374] report the formation of a supercooled H_2O/HNO_3 liquid layer at 185 K as a reaction product, forming NAT or NAD only after decreasing the relative humidity below the ice frost point. This effect is similar to that resulting from the interaction of gaseous HNO_3 or N_2O_5 with the ice surface. These authors measured $\gamma = (3 \pm 2) \times 10^{-3}$ at 185 K for the reaction of $ClONO_2$ with this supercooled liquid layer.

49. $ClONO_2 + HNO_3 \bullet nH_2O(s)$. Hanson and Ravishankara [155] report a γ value of 0.006 at 201 K for the $ClONO_2$ reaction with the water on NAT ($HNO_3 \bullet nH_2O$). However, these authors present re-analyzed and additional data with $\gamma \approx 0.001$ at 191 K in Hanson and Ravishankara [158,160]. Similar experiments (Moore et al. [262], Leu et al. [234]) report a larger value of 0.02 ±0.01 which falls very rapidly as slight excesses of H_2O above the 3/1 H_2O/HNO_3 ratio for NAT are removed. They measure γ of less than 1×10^{-6} for slightly water poor NAT surfaces. The inconsistency between Hanson and Ravishankara and the JPL group (Moore et al. [262]; Leu et al., [234]) has not been resolved. Abbatt and Molina [7] report γ values reaching 0.002 at 202 K and high RH. Hanson and Ravishankara [158] reported that γ for this reaction increases by a factor of 4 as the surface temperature increases from 191 to 211 K. However, Knudsen cell measurements at 185 K by Barone et al. [30] reported γ = 0.004 at a relative humidity (RH) of 100%, rising to 0.007 near RH = 120%, indicating a possible mild negative temperature dependence when high RH values from this and other studies are compared. Excluding the JPL data, the other data obtained at high RH (~90%) were averaged, assuming no temperature dependence, to yield γ = 0.0043 ±0.0021. The strong dependence on RH and the possible temperature dependence suggest that systematic error probably exceeds the calculated statistical error. Within the experimental accuracy, the data of Hanson and Ravishankara [158,160] show that measured uptake coefficients are independent of ice substrate thickness. Barone et al. report very similar uptake coefficients for nitric acid dihydrate (NAD) as for NAT as a function of RH at 202 K. See Henson et al. [173,174] for discussion of a model which accounts for the effect of HNO_3 on the reaction of $ClONO_2$ on water and nitric acid ice surfaces.

50. $ClONO_2 + H_2SO_4 \bullet nH_2O(l)$. Results from wetted-wall flow tube (Hanson and Ravishankara [165]) Knudsen cell reactor (Manion et al. [249]), aerosol flow tube (Hanson and Lovejoy [153]), and droplet train uptake (Robinson et al. [293]) experiments supplement older wetted-wall flow tube (Hanson and Ravishankara, [157]) and Knudsen cell measurements (Rossi et al. [298]), (Tolbert et al [332]). Although earlier Knudsen cell measurements probably suffered from surface saturation, more recent results compare well with those from other techniques. Saturation free results, available over a temperature range of 200–265 K and a H_2SO_4 concentration range of 39 to 75 wt. %, were fit to a phenomenological model developed by Robinson et al. [293]. Measured γ values depend strongly on H_2SO_4 concentration and vary modestly with temperature, with a trend to somewhat higher values for the 210–220 K temperature range. The temperature-dependent uptake model takes into account the temperature and composition dependence of the effective Henry's Law constant, liquid phase diffusion coefficient, and the liquid phase hydrolysis rate constant. The hydrolysis reaction was treated by modeling two reaction channels, a direct hydrolysis process dominating reaction at low H_2SO_4 concentrations with a reaction rate proportional to water activity and a proton-catalyzed reaction with a rate proportional to H^+ activity, which dominates at higher acid concentrations.

The data fit to the original Robinson et al. model have been supplemented by additional wetted-wall flow tube and aerosol flow tube data from Hanson [150] and aerosol flow tube data from Ball et al. [28]. A revised kinetic model (Shi et al. [313]) incorporating these data has been developed that is based on the earlier work of Robinson et al. [293].In this model, γ is calculated using the expression

$$\frac{1}{\gamma} = \frac{1}{\alpha} + \frac{1}{\Gamma_b^{H_2O}}$$

where,

$$\Gamma_b^{H_2O} = \frac{4H_{ClONO_2}RT}{\bar{c}}\left(D_{ClONO_2}k_{hydr}\right)^{1/2}$$

The detailed parameterizations for H_{ClONO_2}, D_{ClONO_2}, and k_{hydr} are given in the Appendix in Shi et al. [313] As was the case for N_2O_5 hydrolysis k_{hydr} is seen to have a direct and an acid catalyzed channel. Using the same error analysis approach as in the note on N_2O_5 uptake, the model error is about 32.4% (one sigma), with σ_m=32.2% and σ_d=4.0%.

In the calculation of the chlorine activation (Cl_2 production) rate under stratospheric conditions, one needs to take into account the competition between the reactions of $ClONO_2 + H_2O$ and $ClONO_2 + HCl$. The presence of HCl will depress the reaction probability of $ClONO_2$ with H_2O (see note 49).

51. $ClONO_2 + H_2SO_4 \bullet H_2O(s)$ and $H_2SO_4 \bullet 4H_2O(s)$. Measurements by Hanson and Ravishankara [162] and Zhang et al. [363] demonstrate that the reaction probability on the tetrahydrate is a strong function of both temperature and relative humidity, both of which affect the level of adsorbed H_2O. Both groups covered the temperature range of 192–205 K. The reaction is slowest at higher temperatures and lower relative humidities. Zhang et al. [363] have parameterized their data in the form of $\log \gamma = a_1 + a_2 \log x + a_3 \log^2 x$; for 195 K and x = water partial pressure in Torr: $a_1 = 10.12$, $a_2 = 5.75$ and $a_3 = 0.62$; for a water partial pressure of
3.4×10^{-4} Torr and x = T(K) between 182 and 206: $a_1 = 318.67$, $a_2 = -3.13$ and $a_3 = 0.0076$. Zhang et al.[367] have also measured a low value of $\gamma \sim 2 \times 10^{-4}$ on sulfuric acid monohydrate at 195 K.

52. $ClONO_2 + HCl + H_2O(s)$. Reaction probabilities of 0.27 (+0.73, –0.13) (Leu [232]) and 0.05 to 0.1 (Molina et al. [260]) were reported at 195 and 185 K, respectively. Abbatt and Molina [7] and Hanson and Ravishankara [157] report that a portion of the reaction may be due to $HOCl + HCl \rightarrow Cl_2 + H_2O$, with HOCl formed from $ClONO_2 + H_2O(s) \rightarrow HOCl + HNO_3(s)$. Hanson and Ravishankara [155] saw no enhancement of the $ClONO_2$ reaction probability when $H_2O(s)$ is doped with HCl. Their preferred value at 192 K is γ = 0.3, but this is consistent with $\gamma = 1$. Chu et al. [76] also report a value of 0.27 (±0.19) at 188 K, assuming no correction for porosity, but suggest the true value is 0.10 (±0.08). Using a Knudsen cell technique and looking at initial uptake, Oppliger et al. [272] measured $\gamma = 0.7$ at 180 K and 0.2 at 200 K with HCl in excess. Eliminating the Molina et al. points, which were taken at much higher $ClONO_2$ concentrations than the others, plots of the remaining data show no obvious bias when plotted as a function of reactant concentration or temperature (180–200 K). Their average value $\gamma = 0.26 \pm 0.06$. The Oppliger et al. data were presented for two HCl concentrations, differing by a factor of three. All points from both HCl concentrations were included since all the data were generally consistent with previous measurements, although the higher HCl concentrations did tend to produce modestly higher uptake coefficients. Until a fuller model is available, a single temperature independent value with a moderate uncertainty due to surface porosity seems appropriate.

53. $ClONO_2 + HCl + HNO_3 \bullet 3H_2O$. Measurements by Hanson and Ravishankara [155,158], Leu and co-workers in Moore et al. [262] and Leu et al. [234], and Abbatt and Molina [7] all report high γ values (>0.1) on NAT for temperatures between 192 and 202 K. Hanson and Ravishankara indicate that reaction probabilities on NAD are similar to those on NAT. The most recent NAT studies (Abbatt and Molina [7]) show a strong fall-off with relative humidity from $\gamma > 0.2$ at 90% RH to 0.002 at 20% RH, indicating the necessity of sufficient water to solvate reactants. Within the limited measurements, data plots show no indication that the reaction probability of $ClONO_2 + HCl$ depends on HCl and $ClONO_2$ gas phase concentrations or temperature between 191 and 202 K. Averaged data yield is $\gamma = 0.23 \pm 0.10$. Carslaw and Peter [67] have published a model of this reaction and its dependence on HCl uptake.

54. $ClONO_2 + HCl + H_2SO_4 \bullet nH_2O(l)$. Early work by Tolbert et al. [332] and Hanson and Ravishankara [157] indicated that the presence of HCl had little effect on the reaction of $ClONO_2$ with concentrated sulfuric acid (>65 wt.% H_2SO_4). Subsequent realization that HCl would be more soluble, and therefore a more potent reactant, in the colder, more dilute sulfuric acid aerosols characteristic of the polar stratosphere led to additional investigations by Hanson and Ravishankara [165], Zhang et al. [363], Elrod et al. [113] and Hanson [150]. All these measurements show a strong dependence of reactivity on HCl solubility, which in turn depends on water activity. The solubility of HCl in a wide range of sulfuric acid solutions has been experimentally determined by a range of techniques that agree well with current thermodynamic models. See Robinson et al. [294] for a review. Hanson and Lovejoy [153] measured a reacto-diffusive length, ℓ, of only 0.009±0.005 μm for 60 wt.% H_2SO_4 in an aerosol flow reactor. (See Hanson et al. [168] for a definition of ℓ.) This is a factor of four lower than the value for the hydrolysis reaction of $ClONO_2$ showing the significant enhancement of $ClONO_2$ uptake due to HCl.

The $ClONO_2$ + HCl reaction on sulfuric acid has been modeled in Shi et al. [313] using the same phenomenological model for $ClONO_2$ hydrolysis driven uptake by sulfuric acid. Since the effect of HCl on the $ClONO_2$ uptake is to increase the $ClONO_2$ pseudo-first-order reaction rate, the model of $ClONO_2$ uptake (see note on $ClONO_2$ uptake on sulfuric acid) should include the pseudo first order reaction rate, k_{HCl}. The formulation of k_{HCl} is found in the Appendix in Shi et al. [313].. It is likely that the $ClONO_2$ reaction with HCl, like the $ClONO_2$ hydrolysis reaction, is acid catalyzed via protonated $HClONO_2^+$, where Cl^+ is activated as in the case of HOCl + HCl. For the $ClONO_2$ + HCl reaction, there is also a surface reaction (Hanson [150]). Hanson proposed that Γ_s is linearly proportional to water activity; however, the calculated value of γ_o at 250 K and 60 wt% H_2SO_4 using his formulation is 0.02 (here $\gamma_o \sim \Gamma_s$), which is contradictory to his aerosol flow reactor result, which yielded γ_o=0.0079 (here $\gamma_o \sim \Gamma_b$) (Hanson and Lovejoy [153]). In the model presented in the Shi et al. appendix, it is assumed that that Γ_s is linearly proportional to Henry's law constant of $ClONO_2$, rather than the water activity. The temperature dependence of Γ_s is determined, based on two measured values of Γ_s at 203 K (Hanson, [150]) and 250 K (Hanson and Lovejoy, [153]). The model yields a value of $\gamma_o \sim 0.011$ (here $\gamma_o \sim \Gamma_s$), which is close to the measured value.

In the stratosphere, when the reaction rate of $ClONO_2$ with HCl exceeds the flux of HCl to the particle surface, HCl is depleted. This, in turn, will depress the rate of both the $ClONO_2$ and HOCl + HCl reactions, and increase the $ClONO_2$ hydrolysis rate. Shi et al. [313] have proposed a model in which this effect is taken into account by including a factor F_{HCl} (see Table A–3 in Shi et al.). The formulation of F_{HCl} is based on scaling HCl reaction and accommodation fluxes. This flux correction is not exact (i.e. it does not rigorously calculate the HCl surface or bulk concentration) but provides a good approximation to the expected reduction in HCl + $ClONO_2$/HOCl reactivity and, just as importantly, the effective increase in $ClONO_2$ + H_2O reactivity when $p_{ClONO_2} > p_{HCl}$. This is particularly relevant during cold Cl activation events when HCl can be removed almost completely (i.e., see Jaegle et al. [194]).

Using the same error analysis approach as in the note on N_2O_5 uptake by sulfuric acid, the error of using the model in the Appendix is about 40.0% (one sigma), with σ_m=39.8% and σ_d=4.0%

55. $ClONO_2$+HCl + $H_2SO_4 \bullet H_2O$(s) and $H_2SO_4 \bullet 4H_2O$(s). This reaction has been studied by Hanson and Ravishankara [162] and Zhang et al. [363]. The reaction probability is strongly dependent on the thermodynamic state of the SAT surface, which is controlled by the temperature and the water vapor partial pressure. At a water vapor pressure of 5.6×10^{-4} Torr the measured γ drops by over two orders of magnitude as the SAT surface temperature rises from 195 to 206 K. The results from the two groups are in qualitative agreement, but sample different H_2O and HCl partial pressures. Zhang et al. have parameterized their data as a function of water partial pressure (at 195 K) and temperature (both at an HCl partial pressure of 4 to 8×10^{-7} Torr) in the form $\log \gamma = a_1 + a_2 \log x + a_3 (\log x)^2$. For H_2O partial pressure, $a_1 = 5.25$, $a_2 = 1.91$, and $a_3 = 0.0$; for T(K), $a_1 = 175.74$, $a_2 = -1.59$, and $a_3 = 0.0035$. Care must be taken in extrapolating either data set to lower HCl concentrations. Zhang et al. [367] measured no enhancement of $ClONO_2$ uptake on sulfuric acid monohydrate at 195 K with $(2–8) \times 10^{-7}$ Torr of HCl present, implying $\gamma < 1 \times 10^{-4}$.

56. $ClONO_2$ + HCl + Al_2O_3(s). Molina et al. [259] used flow tube techniques to measure $\gamma = 0.020 \pm 0.005$ on α–alumina at 195–230 K with stratospheric (5 ppmV) water vapor levels. Measured γ was independent of T and was affected very little by 5 ppbv HNO_3 vapor. The same γ was measured for a Pyrex surface, indicating the absorbed water and not the inorganic substrate hosted the reaction.

57. $ClONO_2$ + MX(s). Finlayson-Pitts and co-workers have shown that $ClONO_2$ reacts with crystalline NaCl (Finlayson-Pitts et al. [122]) and NaBr (Berko et al. [52]) to produce Cl_2 and BrCl, respectively. Timonen et al. [329] have measured the reaction rate for $ClONO_2$ with dry and slightly wet (water vapor pressure 5×10^{-5} to 3×10^{-4} Torr) NaCl at temperatures of 225 and 296 K. Reaction probabilities were analyzed as $\gamma = 4–7 \times 10^{-3}$ and were independent of temperature and water vapor pressure within experimental error. The Cl_2 yield on dry NaCl was 1.0 ± 0.2. Caloz et al. [64] used a room temperature Knudsen cell technique to measure $\gamma = 0.23 \pm 0.06$ for NaCl(s) and $\gamma = 0.35 \pm 0.06$ for KBr(s). They argue that the surface corrections imposed by Timonen et al. were too large. Caloz et al. measured quantitative yields of Cl_2 and BrCl products.

58. $ClONO_2$+HBr + H_2O(s) and $HNO_3 \bullet nH_2O$(s). This reaction was studied by Hanson and Ravishankara [159] on water ice and NAT near 200 K. A diffusion-limited reaction probability of >0.3 was observed. Allanic et al. [17] measured $\gamma = 0.56 \pm 0.11$ at 200 K on water ice, observing Cl_2 and Br_2 to be formed in yields of 100% and 66 to 80%, respectively, in the range 180 to 200 K.

59. $ClONO_2$ + HF + H_2O(s) and $HNO_3 \bullet nH_2O$(s). Hanson and Ravishankara [159] were not able to observe this reaction on water ice and NAT surfaces near 200 K.

60. $CF_xCl_{(4-x)}$ (x=0–3) and CF_2Br_2 + Al_2O_3(s). Robinson et al. [291] reported dissociative uptake of CF_2Cl_2 and CF_2Br_2 on α-alumina surfaces at 210 and 315 K. Reaction probabilities of about 1×10^{-3} at 210 K were measured by monitoring the amounts of surface species bonded to the Al_2O_3 substrate. A re-analysis (Robinson et al. [292]) lowered this value by about a factor of 50. Moderate surface dosage with water vapor did not quench the reaction. In addition, Dai et al. [95] and Robinson et al. [290] studied dissociative chemisorption of CF_3Cl, CF_2Cl_2, $CFCl_3$, and CCl_4 on dehydroxylated γ-alumina powders. The obtained reactive uptake probabilities ranging from 0.4×10^{-5} for $CFCl_3$ to 1.0×10^{-5} for $CFCl_3$ over a temperature range of 120 to 300 K. HCl and halomethyl radicals were observed as desorption products. Loss of these products may point to somewhat higher γs, since they were measured by integrating halogen bound to Al_2O_3 substrates.

61. BrO + H_2O(s) and $H_2SO_4 \bullet nH_2O$(l) and NaCl(aq). Abbatt [3] used a coated flow tube technique to measure heterogeneous uptake on water ice, 60 and 70 wt % H_2SO_4 at 213 K, and 23 wt % aqueous NaCl at 253 K. He obtained γ(ice) = $(1.0 \pm 0.4) \times 10^{-3}$, γ (60 wt % H_2SO_4) = $(7 \pm 2) \times 10^{-4}$, γ (70 wt % H_2SO_4) = $(5 \pm 2) \times 10^{-4}$ and γ (23 wt % NaCl) < 3×10^{-3}. He observed product Br_2, indicating BrO self-reaction on both water ice and sulfuric acid solutions. Since reaction rate will depend on BrO concentrations, no recommendation is made for an atmospheric rate.

62. HOBr + HCl(s). Abbatt [1] measured γ = 0.25 (+0.10/–0.05) for this reaction on ice at 228 K. The BrCl product was observed by mass spectrometry. No data on NAT surfaces are currently available.

For the sulfuric acid reaction, Abbatt [2] measured γs of ~ 0.1 to 0.2 for [HCl] > 1×10^{12} cm^{-3} over 68.8 wt. % H_2SO_4 at 228 K; yielding an estimated $k^{II}_{HCl+HOBr} = 1.4 \times 10^5$ M^{-1} s^{-1} with a factor of 2 uncertainty. Hanson and Ravishankara [166] also measured γ = 0.2 [+0.2, – 0.1] for 60 wt. % H_2SO_4 at 210 K. However, both of these measurements were based on significant underestimation of the solubility of HOBr in the relevant sulfuric acid solutions. More recent measurements by Waschewsky and Abbatt [347] indicate that H for HOBr varies slightly with acidity between 60 to 70 wt.% H_2SO_4 and more strongly with temperature between 208 and 238 K. (For 59.7 wt.% H_2SO_4, H (M atm^{-1}) = 1.2×10^6 at 208 K and and 2.2×10^5 at 228 K.) The HOBr + HCl second order liquid phase rate constant, $k^{II}_{HCl+HOBr}$, varies between 2×10^5 and
3×10^8 ($M^{-1}s^{-1}$) between 213 and 238 K over the same composition range (60–70 wt.% H_2SO_4). Such a strong dependence on acid composition for the reaction rate of HOBr + HCl and the very small acid composition dependence for HOBr solubility in H_2SO_4 solution might be partially due to the formation of H_2OBr^+ in the acidic solution as discussed in their paper. However, this acid catalyzed reaction, i.e. H_2OBr^+ + HCl, alone does not completely account for measured reaction rates over the acid composition range studied.

Using the Henry's Law data for HOBr reported by Waschewsky and Abbatt [347], the limiting reagent will vary depending on atmospheric temperature (H_2SO_4 wt.%) and the concentrations of HOBr and HCl. For stratospheric conditions where [HOBr] is 10 pptv and [HCl] 1ppbv, they predict dissolved HOBr will be in excess above 204 K and HCl in excess below 204 K for a H_2O vapor partial pressure of 3×10^{-7} atm. From their coated wall flow reactor uptake measurements, Waschewsky and Abbatt [347] derived expressions for $k^{II}_{HCl+HOBr}$ and predicted uptake coefficients. For temperature between 204 and 218 K where HOBr is likely to be in excess, they calculated HCl uptake coefficients, γ_{HCl}, which range between 7×10^{-5} and 9×10^{-5}. For temperatures in the 202–198 K range, where dissolved HCl is likely to be excess, the calculated uptake coefficients for HOBr, γ_{HOBr}, of ~1×10^{-2}. Clearly, the HOBr + HCl reaction will be difficult to parameterize in a simple manner. Potential inconsistencies in their $k^{II}_{HCl+HOBr}$ values, as discussed by Waschewsky and Abbatt, indicate that further measurements will be required before this reaction can be definitively modeled.

63. HOBr + HBr + H_2O(s) and $H_2SO_4 \bullet nH_2O$. Abbatt [1] measured γ = 0.12 ± (0.03) on ice at 228 K. The Br_2 product was observed by mass spectrometry. Abbatt [2] measured γ = 0.25 for [HBr] = 1×10^{12} cm^{-3} over 68.8 wt % H_2SO_4 at 228 K; yielding an estimated $k_{II} > 5 \times 10^4$ M^{-1} s^{-1}.

64. $BrONO_2$ + H_2O(s). Hanson and Ravishankara [160] investigated these reactions in an ice-coated flow reactor at 200 (± 10) K. The reaction of $BrONO_2$ with H_2O(s) proceeded at a rate indistinguishable from the gas phase diffusion limit, implying that the reaction probability may be as high as one; the product BrNO(g) was observed. Allanic et al [16] used a Knudsen cell reactor to measure $BrONO_2$ uptake between 190–200 K. Values of initial γs in the 0.2–0.3 range were observed. An average γ = 0.26 ± 0.05 was obtained from all of the appropriate data from both experiments.

65. $BrONO_2$ + $H_2SO_4 \bullet nH_2O$(l). Hanson and co-workers used both coated flow tube and aerosol flow tube techniques to show that the reaction of $BrONO_2$ with 45–70 wt. % H_2SO_4 is extremely facile at temperatures

from 210 to 298 K. Hanson and Ravishankara [166] measured γs of 0.5 (+0.5, –0.25) (45 wt. % H_2SO_4, 210 K, 0.4 (+0.6, –0.2) (60 wt. %, 210 K) , and 0.3 (+0.7, –0.1) (70 wt. %, 220 K) in a coated-wall flow tube experiment. Hanson et al. [167] measured γ ~ 0.8 (20 to 40% error) for submicron aerosols at temperatures between 249 and 298 K and H_2SO_4 concentrations of 45 to 70 wt. %; they did observe a sharp fall off in γ for H_2SO_4 concentrations between 73 and 83 wt. %. Hanson has analyzed these combined data sets, the data indicated that γ is a function of sulfuric acid concentration, but independent of temperature. He has fit an empirical expression for γ for $BrONO_2 + H_2O$ of: γ = exp(a+b*wt.)+c [Hanson, priv. comm.]. The data have been fitted to the formulation $1/\gamma=1/\alpha+1/\gamma_{rxn}$, yielding α=0.805, and a=29.24, b=–0.396, c=0.114. Additional unpublished measurements using both techniques at higher temperatures performed by Hanson [priv. comm.] also fit this functional form. Using the same approach as detailed in the note for N_2O_5 uptake on sulfuric acid, the error for $BrONO_2$+ H_2O is 27.3% (one sigma), with σ_m=26.6% and σ_d=6.3%.

66. $CF_3OH + H_2O + H_2O(l)$ and $H_2SO_4 \bullet nH_2O(l)$. Lovejoy et al. [245] used both wetted-wall and aerosol flow tube techniques to measure reactive uptake of CF_3OH on water at 274 K and 39–60 wt % H_2SO_4 at various temperatures between 206 and 250 K. γ's showed a strong dependence on water activity. Aerosol uptake studies yielded reacto-diffusive lengths of > 0.4 µm for 40 wt % H_2SO_4 and 1.0 µm for 50 wt % H_2SO_4, both at 250 K. Recommended γ's were estimated by averaging bulk uptake measurements at similar H_2SO_4 concentrations and ignoring temperature effects on water activity.

67. $SO_2 + H_2O_2$, O_3, HONO, NO_2, HNO_3 on $H_2SO_4 \bullet nH_2O(l)$. Rattigan et al. [282] used a bubble train reactor to measure the uptake of SO_2 in the presence of solvated oxidants at 293 K. For H_2O_2 the second order rate constant at 1 wt. % H_2SO_4 agreed well with previous bulk kinetics measurements and with previous droplet train/flow reactor measurements. Measurements at 20, 40, and 60 wt. % H_2SO_4 are the first reported for concentrated acid. Reaction rate data were fit to a two term (acid catalyzed and water catalyzed) bulk second order rate expression, which, in the limit of high acid activity ($a_{H^+} = \alpha_{H+}[H^+]$, where α_{H+} is the H^+ activity coefficient) reduces to: $k^{II}_{H_2O_2}= 8.3 \times 10^4 (\alpha_{H_2O}/ a_{H^+})$, where α_{H_2O} is the water activity coefficient. Both α_{H+} and α_{H_2O} can be obtained from the sulfuric acid thermodynamic model of Carslaw et al. [66]. The high a_{H^+} approximation for $k^{II}_{H_2O_2}$ should be accurate to a factor of two between 40 and 70 wt %.

Uptake of SO_2 in the presence of solvated O_3 was measured for 1–70 wt. % acid; the Henry's law expression for O_3 was determined in separate experiments. Measured second order rates agree reasonably well with previous results measured below 18 wt. %. A three term fit for reaction with $SO_2(aq)$, HSO_3^-, and $SO_4^=$ was fit to the data: $k^{ii}_{O_3} = 6.6 \times 10^3 [SO_2(aq)] + 3.2 \times 10^5 [HSO_3^-] + 1 \times 10^9 [SO_4^=]$. This expression should be accurate to a factor of two between 20 and 70 wt. %.

The HONO reaction was studied by adding nitrosyl sulfuric acid to 20, 40, 60, and 70 wt. % acid. Measured second order rate constants were moderately consistent with previous measurements below 10 wt. %. A $k^{ii}_{HONO} = 142[H^+]$ was fit to the full data set; it should be accurate to a factor of two for acid concentrations between 10 and 70 wt. %.

No enhanced SO_2 uptake was observed with added gas phase NO, NO_2, or with 20 wt. % HNO_3 added to 50–60 wt. % sulfuric acid.

68. SO_3 on $H_2SO_4 \bullet nH_2O(l)$. Jayne et al. [199] measured the uptake coefficient in a wetted wall-flow reactor at 300 K over a composition range of 78–92 H_2SO_4 wt. %. The measured γ was indistinguishable from 1.0. Higher water concentrations and lower temperatures probably tend to increase γ, so a value near 1.0 probably holds for all atmospheric conditions.

5.14 Soot Surface Uptake Coefficients

Table 5-3. Soot Surface Uptake Coefficients.

Gaseous Species	Uptake Coefficient (γ)	Notes
SO_2	See Note	1, 2
NH_3	0, See Note	1, 3
O_3	See Note	1, 4
HNO_3	See Note	1, 5
N_2O_5	See Note	1, 6
NO_2	See Note	1, 7
NO_3	See Note	1, 8
HO_2	See Note	1, 9
HO_2NO_2	See Note	1, 10
H_2O	See Note	1, 11

5.15 Notes to Table 5-3

1. See also the sections on soot under "Surface Types" and "Parameter Definitions" for a description of some of the factors affecting the uptake and reaction of gases on soot surfaces. In most cases, the available reactive surface area rather than the geometric areas have been used in obtaining the uptake coefficients; in those cases where the geometric area was used but a higher available surface area was involved in the measured uptake, the uptake coefficient is given as an upper limit. Most data are available at room temperature or there are very limited data at lower temperatures characteristic of the upper troposphere.

2. SO_2 + soot. $\gamma \leq 3 \times 10^{-3}$ measured using Degussa FW2 carbon black by Rogaski et al. [295]. This is an upper limit since it is based on the geometric surface area. Koehler et al. [226] measured an average value of $(2 \pm 1) \times 10^{-3}$ over the first 10–30 s on n-hexane soot at –100° C (the initial uptake may be larger), but indicate that taking into account surface roughness would reduce this value. A number of studies [25,77,78,90,226,238,295] suggest that uptake is primarily due to physisorption on the surface; oxidation occurs in the presence of water, oxidants and metals.

3. NH_3 + soot. Chughtai et al. [77] and Muenter and Koehler [267] measured the uptake of NH_3 on soot. Based on Muenter and Koehler [267] where conditions are closest to atmospheric, NH_3 is not taken up by soot particles at temperatures above 173 K.

4. O_3 + soot. Many studies report a rapid, initial loss of O_3 followed by a slower loss that also occurs on aged soot or soot pre-exposed to ozone [81,87,104,115,117,187,210,244,295,316,319,323]. Initial, rapid O_3 loss may be most applicable for soot as it comes out of aircraft exhaust, with $\gamma^{init} \sim 10^{-3}$ from most studies using both carbon black and organic combustion soots [115,117,187,295,323]. The second stage of the reaction is probably more applicable to soot dispersed in air; $\gamma^{aged} \sim 10^{-4}$–$10^{-6}$ using both carbon black and organic combustion soots [115,117,187,210,244,278,323], but in the range of 10^{-4} to 10^{-5} based on organic combustion soot data alone [187,244]. A few studies have been carried out at temperatures below room temperature [81,187,210,244]; given the wide ranges measured even at room temperature, these values generally fall in the same range. Il'in et al. [187] report a temperature dependence for the initial uptake on fresh soot of $\gamma^{fresh} = 1.9 \times 10^{-3}(\exp{-780/T})$ and for aged soots, $\gamma^{aged} = 1.8\times10^{-4}(\exp{-1000/T})$. Both physisorption and reaction of ozone with the surface appear to take place. The studies of Fendel et al. [115] suggest that lower particle growth in size below 40 ppb O_3 is due to less than a monolayer of O_3 on the surface. Stephens et al. [323] proposed a Langmuir-type reversible adsorption of O_3, followed by a slower reaction with the surface. Pöschl et al. [278] proposed a similar scheme for uptake of ozone on spark-generated graphite soot coated with benzo[*a*]pyrene. Initial reversible physisorption occurred with $\gamma \sim 10^{-3}$, and "apparent reaction probabilities" for O_3 with BaP on soot of $\gamma \sim 10^{-5}$–10^{-6} were reported. The presence of water inhibited the reaction, which was postulated to be due to competitive adsorption between water and ozone on the surface; this is in contrast to the report of Chughtai et al. [82] in which the rate of ozone loss increased with RH. Pöschl et al. [278] report Langmuir adsorption equilibrium constants for O_3 and H_2O, and a second order surface reaction rate constant for the O_3-BaP reaction of $(2.6 \pm 0.8) \times 10^{-17}$ cm^{-2} s^{-1}. Three possible paths have been proposed: (1) chemisorption of O_3; (2) catalytic decomposition of O_3: $2O_3 \rightarrow 3O_2$; (3) surface oxidation and formation of gas-phase carbon oxides. The studies of Fendel et al. [116] suggest that lower particle growth in size below 40 ppb O_3 is due to less than a monolayer of O_3. Studies of Smith et

al. [319] and Smith and Chughtai [316] suggest that catalytic decomposition occurs to some extent over the entire reaction sequence. CO_2 and H_2O are the major gas phase and surface oxidized functional groups on the surface such as carboxylic acids are observed [82-84,104,115,210,252,316-318,323].

5. HNO_3 + soot. Studies of the uptake of HNO_3 on soot have been carried out over a range of nitric acid pressures [70,92,103,220,244,295,297,304,305]. Measured values of γ at room temperature are typically in the range 10^{-1}–10^{-5}, with smaller uptake coefficients measured at longer reaction times. Saatthoff et al. [304] report an upper limit of 3×10^{-7} as a time-averaged value over two days. At lower concentrations characteristic of the atmosphere, uptake appears to be primarily due to physisorption while at higher concentrations, $> 2 \times 10^{12}$ molecule cm^{-3}, a surface reaction occurs. At 220 K, $\gamma \sim 0.1$ with irreversible uptake attributed to reaction with surface groups [70]. Reaction of HNO_3 at concentrations from $(1–9) \times 10^{12}$ molecule cm^{-3} with "grey" soot from a rich flame using hexane has been reported [305] to generate HONO as the major gaseous product with initial and steady-state reaction probabilities of $\gamma_o = 4.6 \times 10^{-3}$ and $\gamma_{ss} = 5.2 \times 10^{-4}$ respectively; reaction with "black" soot from a lean flame gave NO as the major gaseous product, with initial and steady-state reaction probabilities of $\gamma_o = 2.0 \times 10^{-2}$ and $\gamma_{ss} = 4.6 \times 10^{-3}$ respectively (based on geometric surface area of sample holder). The NO was hypothesized to result from secondary reactions of an initial HONO product.

6. N_2O_5 + soot. Brouwer et al. [58], Longfellow et al. [244] and Saathoff et al. [304]studied the uptake of N_2O_5 at room temperature on a ground charcoal (carbon black) sample, on propane soot and on spark-generated graphite soot, respectively. Brouwer et al. and Longfellow et al. report uptake coefficients based on the geometric sample surface area, and therefore give upper limits. An upper limit of $\gamma \leq 0.02$ can be derived based on the larger value of 0.016 reported by Longfellow et al. As discussed below, much smaller values are reported by Saathoff et al.: 4×10^{-5} under dry conditions and 2×10^{-4} at 50% RH. Three possible reactions may occur: (1) Decomposition of N_2O_5 on the surface to generate $NO_2 + NO_3$; (2) reaction of N_2O_5 with the soot; (3) hydrolysis of N_2O_5 with water on the surface to generate HNO_3. The studies of Longfellow et al. support the decomposition reaction, with yields of NO_2 within experimental error of 100%; the generation of NO_3 on the surface followed by its decomposition to NO_2, may contribute to the observed production of NO_2. The studies of Brouwer et al. suggest that a redox reaction with the soot surface to generate NO occurs in parallel with hydrolysis of N_2O_5 to generate HNO_3. Saathoff et al. propose two independent, parallel reactions: (1) hydrolysis generating HNO_3, N_2O_5 + soot $\rightarrow$ 2 HNO_3 with $\gamma = (4 \pm 2) \times 10^{-5}$ under dry conditions (< 10 ppm H_2O) which increases to $(2 \pm 1) \times 10^{-4}$ at 50% RH. (2) decomposition to NO and NO_2: N_2O_5 + soot $\rightarrow$ NO + NO_2 + products, with $\gamma = (4 \pm 2) \times 10^{-6}$ under dry conditions.

7. NO_2 + soot. A fast initial uptake of NO_2 is observed on fresh soots [13,14,21,77,80,85,86,134,205,220,243,295,321,325,326] with the initial uptake coefficient in studies involving both carbon blacks and organic combustion soots in the range of $\gamma^{init} \cong 10^{-1}$ to 10^{-4}. For longer reaction times on carbon black soots, $\gamma^{aged} \sim 10^{-4}$ based on studies by Kalberer et al. [206] and Ammann et al. [21,22]. However, Kleffmann et al. [223] report a lower uptake coefficient of $\sim 10^{-7}$ on carbon black over the first 5 minutes of reaction and and Saathoff et al. [304] report an upper limit of $< 4 \times 10^{-8}$ averaged over 5 days under dry conditions (< 10 ppm H_2O) on spark-generated graphite. On organic combustion soots, γ^{aged} has been reported to be in the range of $\sim 10^{-4}$–10^{-6} [13,22,23,243,321][305]. All studies were done at room temperature except those of Longfellow et al. [243] which were carried out at 262 K. The surface deactivates on continued exposure to NO_2, suggesting a maximum amount of HONO that can be formed per cm^2 of soot area or mg of soot; this has been reported to be in the range of 10^{16} to 10^{18} HONO per mg of soot [23,134,204,205,223,321]. However, reactivation on heating of the surface, exposure to water vapor and/or with time after the exposure is stopped has been observed [134,243,321,325,326]. A small portion (~10-20%) of the NO_2 taken up appears to be chemisorbed to the surface [13,23,80,204,205,220,223,321,325,326]. Infrared studies [13,220,318] show that surface C–ONO, C–N–NO_2, and C–NO_2 groups are formed. The remainder of NO_2 reacted appears as gaseous HONO and NO; Salgado and Rossi [305] report HONO as the major product for hexane soot from a flame at near stoichiometric ratio but NO as the major product for soot from an extremely lean flame. In addition, N_2O, CO, and CO_2 have been observed as products at higher temperatures [34,35]. At lower NO_2 concentrations, the HONO yield can approach 100%; production of NO may be due to the bimolecular reaction of HONO on the surface at higher concentrations to give NO + NO_2 + H_2O. The HONO yield at 262 K appears to be smaller than at room temperature [243]. Formation of HONO is due to reaction with a reduced surface site and not to NO_2 surface-catalyzed hydrolysis. The formation of HONO from the reaction of NO_2 with unspecified semi-volatile organics in

diesel exhaust has been reported [143] and proposed to be a much larger source of HONO than the reaction with the soot itself.

8. NO_3 + soot. Saathoff et al. [304] report an upper limit of $\gamma < 3 \times 10^{-4}$ on dry soot (< 10 ppm H_2O) and $\leq 10^{-3}$ at 50% RH based on measurements of NO_3 and N_2O_5.

9. HO_2 + soot. Saathoff et al. [304] report an upper limit of $\gamma < 10^{-2}$ on dry soot (<10 ppm H_2O) based on the decay of HO_2NO_2 (in equilibrium with HO_2 and NO_2) in the presence and absence of soot.

10. HO_2NO_2 + soot. Saathoff et al. [304] report an upper limit of $\gamma < 10^{-5}$ on dry soot (<10 ppm H_2O) based on the decay of HO_2NO_2 in the presence and absence of soot.

11. H_2O + soot. Alcala–Jornod et al. [14] report an upper limit to the initial uptake coefficient of $\gamma < 2 \times 10^{-3}$, consistent with the earlier measurements of Rogaski et al. [295]. The uptake is most likely a reversible physisorption [14,277] although based on water uptake isotherms, Chughtai et al. [77,79,84,87] propose that at low relative humidities (< 25%) chemisorption occurs. While prior exposure of Degussa FW-2 to NO_2 and SO_2 was not found to increase the uptake coefficient for water, treatment with HNO_3 increased the measured uptake coefficient by a factor of 28 and with H_2SO_4 by a factor of 68 [295]. Water adsorption isotherms on soot have been measured in a number of studies, e.g. [77,79,82,84,87] and the amount of water taken up found to increase with the air/fuel ratio used to generate the soot, with the sulfur content, with aging and oxidation of the surface (e.g. by O_3) and with the presence of metals [77,79,82,84,87,350].

5.16 Henry's Law Constants for Pure Water

Table 5-4. Henry's Law Constants for Pure Water.

Substance	Temperature Range, K	H (298 K)[a]	*A*	*B*	*C*	Uncertainty Range[b]	Note
O_2	273–348	1.27×10^{-3}	–161.6	8160	22.39	A	1
O_3	273–333	1.03×10^{-2}	–14.08	2830		C	2
HO_2	298	1000				D	3
H_2O_2	278–303	7.73×10^{4}	–13.27	7310		C	4
N_2	273–348	6.52×10^{-4}	–177.1	8640	24.71	A	5
NH_3	273–348	60.2	–9.84	4160		C	6
NO	273–358	1.92×10^{-3}	–157.1	7950	21.298	B	7
NO_2	298	1×10^{-2}				E	8
N_2O	273–313	2.42×10^{-2}	–148.1	8610	20.266	A	9
CO	278–323	9.81×10^{-4}	–178.0	8750	24.875	A	10
CO_2	273–353	3.38×10^{-2}	–145.1	8350	19.960	A	11
CH_4	273–328	1.41×10^{-3}	–194.7	9750	27.274	A	12
C_2H_6	273–323	1.88×10^{-3}	–240.2	12420	33.744	A	13
C_3H_8	273–348	1.51×10^{-3}	–281.1	14510	39.652	A	14
n–C_4H_{10}	273–348	1.24×10^{-3}	–269.9	14330	37.734	A	15
$CH_3CH(CH_3)CH_3$	278–318	9.18×10^{-4}	–360.6	18020	51.444	B	16
C_2H_4	288–348	5.96×10^{-3}	–154.6	8540	21.202	B	17
C_2H_2	273–343	4.14×10^{-2}	–145.8	7880	20.384	B	18
CH_3OH	273–298	220	–12.08	5210		C	19
CH_3CH_2OH	273–298	200	–16.98	6630		C	20
n–C_3H_5OH	273–298	130	–20.16	7470		D	21
iso–C_3H_5OH	273–298	130	–20.15	7450		D	21
n–C_4H_9OH	273–298	127	–19.34	7210		D	21
iso–C_4H_9OH	298	102				D	21
sec–C_4H_9OH	273–298	110	–19.65	7260		D	21
tert–C_4H_9OH	273–298	70	–23.63	8310		D	21
CH_3OOH	277–293	300	–11.99	5280		D	22
$HOCH_2OOH$	278–293	1.7×10^{6}	–18.79	9870		E	23
HCHO	288–318	3.23×10^{3}	–15.73	7100		D	H* 24
CH_3CHO	273–313	12.9	–17.19	5890		D	H* 25
C_2H_5CHO	273–313	10.0	–12.20	4330		E	26
C_3H_7CHO	283–318	9.6	–18.59	6220		E	27
CH_3COCH_3	273–311	28.1	–13.62	5050		D	28
$C_2H_5COCH_3$	273–298	18	–16.40	5740		D	29
HC(O)OH	275–308	8.9×10^{3}	–11.40	6100		D	30
$CH_3C(O)OH$	275–308	4.1×10^{3}	–12.50	6200		D	31
CH_3CN	273–303	52.8	–9.35	3970		C	32
CH_3NO_2	293–323	34.6	–9.92	4010		D	33
$C_2H_5NO_2$	293–323	21.7	–11.80	4430		D	33
$C_3H_7NO_2$	293–323	13.1	–13.22	4710		D	33
$CH_3CH(NO_2)CH_3$	293–323	8.42	–13.02	4520		D	33
CH_3ONO_2	273–298	2.0	–15.20	4740		D	34
$C_2H_5ONO_2$	273–298	1.59	–17.50	5360		D	34
1–$C_3H_7ONO_2$	273–298	1.10	–18.31	5490		D	34
2–$C_3H_7ONO_2$	273–298	0.791	–18.20	5360		D	34
1–$C_4H_9ONO_2$	273–298	1.01	–19.40	5790		D	34
2–$C_4H_9ONO_2$	273–298	0.648	–18.59	5410		D	34
$CH_3C(O)O_2NO_2$	274–297	2.8	–18.15	5730		D	35
$O_2NOC_2H_4ONO_2$	293	640				D	36
$HOC_2H_4ONO_2$	293	3.99×10^{4}				D	36
$HOCH_2CH(ONO_2)CH_3$	293	7.3×10^{3}				D	36
$CH_3CH(OH)CH_2ONO_2$	293	6.7×10^{3}				D	36
$CH_3CH(ONO_2)CH_2ONO_2$	293	175				D	36
$CH_3C(O)CH_2ONO_2$	293	1.01×10^{3}				D	36
Cl_2	283–383	9.29×10^{-2}	–134.4	7590	18.702	B	37
Cl_2O	273–293	17	–3.23	1810		D	38

Substance	Temperature Range, K	H (298 K)[a]	*A*	*B*	*C*	Uncertainty Range[b]	Note
ClO_2	383–333	1.01	–11.65	3470		B	39
HOCl		660	–13.2	5880		D	40
Br_2	273–308	0.725	–15.05	4390		B	41
BrCl	279–299	0.98	–18.9	5630		C	42
SO_2	278–383	1.36	–39.72	4250	4.525	B	43
	278–298		–9.53	2930			
H_2S	273–323	0.102	–145.2	8120	20.296	C	44
CS_2	274–305	0.062	–17.05	4250		D	45
COS	273–288	2.02×10^{-2}	–15.68	3510		D	46
CH_3SH	298–368	0.39	–12.42	3420		E	47
C_2H_5SH	298–368	0.28	–13.82	3740		E	48
CH_3SCH_3	272–305	0.54	–12.19	3460		E	49
$CH_3S(O)CH_3$	298	9.9×10^{4}				E	50

a. $\ln H = A + B/T + C \ln(T)$ [M atm^{-1}]

b. Uncertainty Classes:

A—Better than 10%
B—10% to 50%
C—50% to 100%
D—Factor of 2 to factor of 10
E—Factor of 10 to factor of 100
F—Greater than a factor of 100

5.17 Notes to Table 5-4

Many of the data sets required various transformations to convert them to the units (mol L^{-1} atm^{-1}) and form (solubility instead of volatility) used in this Table. The transformations often involve either the mass or molar density of water, which in all cases was taken from [231].

1. O_2. The recommendation was taken from the studies of Benson [51] and Rettich [285]. The data show clear curvature in a plot of ln (K_h) v. 1/T. A two parameter fit gives A = –13.26 and B = 1950 K for the temperature range 273–285 K.

2. O_3. The recommendation of Rischbieter [288] was accepted and refitted.

3. HO_2. The recommendation was based on a calculation by Schwartz [307]. Thermodynamic values were updated to those in our Thermodynamic tables.

4. H_2O_2. The data of Lind and Kok [239,240], Hwang and Dasgupta [186], Yoshizumi et al. [361], and O'Sullivan et al. [273] are all in good agreement. The recommendation is from a two-parameter fit to all the results.

5. N_2. The recommendation of Battino [34] was accepted and refitted to three-parameter equations. A two parameter fit gives A = 12.81 and B = 1625 K for the temperature range 273–293 K.

6. NH_3. Based on the recommendation by Edwards et al. [111], refit to a two-parameter equation. Over the temperature range 273–348 K, there appears to be little curvature in the data. The more recent work of Dasgupta and Dong [96] are in quite good agreement with this recommendation, whereas the results of Hales and Drewes [144] are somewhat higher and those of Shi and Davidovits [312] (an uptake study) are significantly lower. The Hales and Drewes paper also included studies of the effect of dissolved CO_2 on the solubility of NH_3. The solubility of NH_3 in solutions containing a wide variety of ions is discussed by Clegg and Brimblecombe [89].

7. NO. Three-parameter refit from the recommendation of Battino [32]. Two-parameter fit gives A = –12.27 and B = 1790 K for the temperature range 273–293 K.

8. NO_2. From analysis of studies of reactive dissolution of NO_2 by Schwartz and White [309].

9. N_2O. Three-parameter refit to the recommendation of Battino [31]. Two parameter fit gives A = 13.40 and B = 2880 K for the temperature range 273–293 K.

10. CO. The recommendation is based on smoothed data from Rettich et al. [284] and refit to three-parameter equation. A two parameter fit gives A = –12.72 and B = 1720 K for the temperature range 273–293 K.

11. CO_2. Refit to three- parameter equation from the recommendation of Wilhelm et al. [352]. Two parameter fit gives A = 12.49 and B = 2710 K for the temperature range 273–293 K.

12. CH_4. The recommendation is a three-parameter fit to the smoothed recommendation of Battino [41]. There is very good agreement with the more recent data of Ben-Naim and Battino [50]. A two parameter fit gives A = –13.45 and B = 2040 K for the temperature range 273–293 K.

13. C_2H_6. The recommendation is a three-parameter fit to the smoothed recommendation of Battino [33]. There is very good agreement with the more recent data of Ben-Naim and Battino [50]. Two parameter fit gives A = –15.95 and B = 2875 K for the temperature range 273–293 K.

14. C_3H_8. The recommendation is from a three-parameter fit to the smoothed recommendation of [40]. There is very good agreement with the more recent data of Ben-Naim and Battino [50]. A two parameter fit gives A = 17.52 and B = 3275 K for the temperature range 273–293 K.

15. n-C_4H_{10}. The recommendation is from a three-parameter fit to the smoothed recommendation of Battino [39]. There is very good agreement with the more recent data of Ben-Naim and Battino [50]. A two parameter fit gives A = –19.28 and B = 3740 K for the temperature range 273–288 K.

16. $CH_3CH(CH_3)CH_3$. The recommendation is from a three-parameter fit to the smoothed recommendation of Battino [38]. A two parameter fit gives A = 18.22 and B = 3340 K for the temperature range 278–293 K.

17. C_2H_4. The recommendation is from a three-parameter fit to the smoothed recommendation of Wilhelm [352]. A two parameter fit gives A = –12.40 and B = 2170 K for the temperature range 288–313 K.

18. C_2H_2. The recommendation is from a three-parameter fit to the smoothed recommendation of Wilhelm [352]. The recommendation of Yaws et al. [360] generates identical results. A two parameter fit gives A = –10.12 and B = 2065 K for the temperature range 273–298 K.

19. CH_3OH. The recommendation is based on the two data points of Snider and Dawson [320]. The 298 K result of Butler et al. [62] and a calculation based on the NBS Thermodynamic tables, [345], are in very good agreement. The 298 K result of Altschuh et al. [20] is about 40% lower.

20. C_2H_5OH. The recommendation is based on the two data points of Snider and Dawson [320]. The 298 K results of [62] and [296], and a calculation based on the NBS Thermodynamic tables, [345], are in very good agreement. The 298 K result of Altschuh [20] is about 50% lower.

21. All of the recommendations for the C3–C4 alcohols are based on two data points each from Snider and Dawson [320]. Room temperature data from other studies ([61],[62], and [20]) typically support these results.

22. CH_3OOH. The data of Lind and Kok [239,240] and O'Sullivan et al. [273] are in excellent agreement and were fit to a two-parameter expression.

23. $HOCH_2OOH$. The results of O'Sullivan [273] and Staffelback and Kok [322] are very close and were fit to obtain the recommended values. The results of Zhou and Lee [371] are much lower and were not included.

24. HCHO. The recommended value is the apparent Henry's law constant and includes a contribution due to hydrolysis $H^* = H(1 + K_{hyd})$. Data from Betterton and Hoffmann [54] and Zhou and Mopper [372] are in substantial agreement and were fit to a two-parameter expression. Betterton and Hoffmann have calculated $K_H = 2.5$ M atm^{-1} at 298 K for the physical solubility.

25. CH_3CHO. The recommended value is the apparent Henry's law constant and includes a contribution due to hydrolysis $H^* = H(1 + K_{hyd})$. The results of Snider and Dawson [320], Benkelberg et al. [49], and Betterton and Hoffmann [54] are in excellent agreement and have been fit to a two-parameter expression for the recommendation. The results of Zhou and Mopper [372] curve off at higher temperatures and were not included in the fit. (Note the similar situation for acetone.) Betterton and Hoffmann have calculated $K_H = 4.8$ M atm^{-1} at 298 K for the physical solubility.

26. C_2H_5CHO. Results of Zhou and Mopper [372] and Snider and Dawson [320] agree only to within about a factor of two. The two points from the former were weighted by 3 and combined with the five points of the latter to generate the recommendation.

27. C_3H_7CHO. The only results are from Zhou and Mopper [372], which have been fit to a two-parameter expression.

28. CH_3COCH_3. The recommendation is from a fit to the data of Snider and Dawson [320] and Benkelberg et al. [49]. Room temperature data points of Hoff et al. [176], Burnett [61] and Vitenberg et al. [340] are in very good agreement. Results of Zhou and Mopper [372] are somewhat higher, particularly at room temperature and above. The situation is similar for acetaldehyde.

29. $C_2H_5COCH_3$. The recommendation is from the two points of Snider and Dawson [320]. The room temperature points of Vitenberg et al. [340] and Rohrschneider [296] are in good agreement. The higher temperature data of Zhou and Mopper [372] are somewhat higher and the those of Friant and Suffet [128] are lower than the recommendation.

30. HC(O)OH. The results of Johnson et al. [203] are accepted. The 298 K result of Khan et al. [219] are about 75% lower. Bob, did you consider the results of Servant et al. (quoted in 97-4)?

31. $CH_3C(O)OH$. The results of Johnson et al. [203] are accepted. A value calculated from the NBS Thermodynamic tables [345] is about a factor of two higher. Bob, did you consider the results of Servant et al. (quoted in 97-4)?

32. CH_3CN. The values reported by Benkelberg [49], Snider and Dawson [320], Hamm et al. [146] are all in good agreement and have been fit to a two-parameter expression for the recommendation. The Hamm et al. paper includes a measurement with artificial seawater at 293 K.

33. Nitroalkanes (CH_3NO_2, $C_2H_5NO_2$, $C_3H_7NO_2$, and $CH_3CH(NO_2)CH_3$). The recommended values are all taken from the work of Benes and Dohnal [47]. For nitromethane, the 298 K value from Rohrschneider [296] is about 30% higher.

34. Alkyl nitrates (CH_3ONO_2, $C_2H_5ONO_2$, 1-$C_3H_7ONO_2$, 2-$C_3H_7ONO_2$, 1-$C_4H_9ONO_2$, 2-$C_4H_9ONO_2$). The recommended values are all taken from the work of Kames and Schurath [208]. The results of Luke et al. [247] are in very good agreement for 1-butyl and 2- butyl nitrates, but the values reported by Hauff [170] for 1- and 2-propyl and butyl nitrates by head-space chromatography are significantly (~50%) lower.

35. $CH_3C(O)O_2NO_2$. The results of Kames and Schurath [208] and Frenzel et al. [127] are close, but somewhat higher (~60%) than the single temperature point of Holdren et al. [178]. The recommendation is a fit to the data of Kames and Schurath, and Frenzel et al. Frenzel et al., Kames and Schurath, and Holdren et al. also measured hydrolysis rate constants and Kames and Schurath measured solubility in artificial sea water.

36. Bifunctional alkyl nitrates. The recommended values (at 293 K) are taken from the work of Kames and Schurath [207].

37. Cl_2. Three-parameter refit to the recommendation of Battino [36]. Two parameter fit gives A = 9.38 and B = 2090 K for the temperature range 283–313 K.

38. Cl_2O. Fit to recommendation of Wilhelm et al. [351]. Data appear somewhat uncertain.

39. ClO_2. Two-parameter fit to the recommendation of Battino [35].

40. HOCl. Huthwelker et al. [185] analyzed the limited data for pure water from Blatchley et al. [55] and Holzwarth et al. [179] along with the more extensive data for uptake by sulfuric acid from Hanson and Ravishankara [164], along with thermodynamic information, and obtained a consistent expression for the solubility of HOCl.

41. Br_2. The results of Kelley and Tartar [213] and Jenkins and King [202] agree well below about 313 K, and with the 298 K point of Hill et al. [175]. Recommendation based on a two-parameter fit to all data at and below 308 K.

42. BrCl. The recommendation is from the work of Barlett and Margerum [29].

43. SO_2. Two- and three-parameter fits to the recommendation of Battino [37]. The earlier recommendation of Edwards et al. [111] is slightly lower.

44. H_2S. In the recommendation of Fogg [125], two expressions were given, representing the results above and below 283 K. The predicted values from these expressions were calculated, with the points at 283 K averaged, converted to the desired units, and then fit with the two- and three-parameter expressions. These are the recommended values. More recent results of Rinker and Sandall [287] and Munder et al. [268] are slightly lower; in these studies, the physical solubility of H_2S was determined through measurements involving aqueous solutions of glycols or amines, neutralized with HCl. The reported values of De Bruyn et al. [101] are significantly (~30%) lower. The earlier recommendation of Edwards et al. [111] is very close to

the recommendation of Fogg [125] as is the recommendation of Yaws et al. [360]. The room temperature point calculated from the NBS Thermodynamic tables Wagman et al. [345] is also slightly lower. The work of De Bruyn et al. [101] covered also a wide range of NaCl and $(NH_4)_2SO_4$ concentration and of pH.

45. CS_2. The recommendation is from a fit to data of Elliott [112], who also present data in 0.5 mol L^{-1} NaCl. The results of De Bruyn et al. [101] are significantly (50%) lower. The work of DeBruyn et al. covered also a wide range of NaCl and $(NH_4)_2SO_4$ concentration and of pH.

46. COS. The reviews by Wilhelm et al. [352] and Yaws et al. [360] result in identical results over the low temperature range (<303 K) and are combined to generate the recommendation. The results of De Bruyn et al. [101] are somewhat (~25%) lower at the lower temperature range. The work of De Bruyn et al. covered also a wide range of NaCl and $(NH_4)_2SO_4$ concentration and of pH.

47. CH_3SH. The recommendation is based on the data of Przyjazny et al. [279]. Results of De Bruyn et al. [101] are about half the recommended value at 298 K. Similar low values were observed for other compounds in the work of De Bruyn et al. The work of De Bruyn et al. covered a wide range of pH and NaCl and $(NH_4)_2SO_4$ concentrations.

48. C_2H_5SH. The recommendation is based on the data of Przyjazny et al. [279]. The results of Vitenberg [340] are slightly lower than the extrapolated value at 293 K.

49. CH_3SCH_3. The recommendation is based on the values of Dacey et al. [93]. The single temperature point of Wong and Wang [357] and the higher temperature results of Przyjazny et al. [279] are in good agreement. The results of De Bruyn et al. [101] are about 30% lower. The studies of Dacey et al. [93] and Wong and Wang [357] were also carried out with seawater. The work of De Bruyn et al. [101] covered also a wide range of NaCl and $(NH_4)_2SO_4$ concentration and of pH.

50. $CH_3S(O)CH_3$. The recommendation is from Watts and Brimblecombe [349], cited by Allen et al. [19].

5.18 Henry's Law Constants for Acids

Table 5-5. Henry's Law Constants for Acids

	T(K)	Wt. % H_2SO_4	H or H* (M/atm)	Notes
O_3 in $H_2SO_4 \cdot nH_2O(l)$	293	1–70	$Ln(H_o/H) = (4.08 \pm 0.2) \times 10^{-3} \times wt$ $H_o = 0.012$ M atm^{-1} wt is the H_2SO_4 wt. %	1
NO_2 in $H_2SO_4 \cdot nH_2O(l)$	203–343	39–68	See Note	2
HONO in $H_2SO_4 \cdot nH_2O(l)$	248–298	>60	$\ln H^* = a_1 + a_2 wt + a_3 wt^2 + (b_1 + b_2 wt)/T$ $a_1 = 26.1 \pm 9.4$, $a_2 = -1.095 \pm 0.21$, $a_3 = 0.00732 \pm 0.00121$ $b_1 = -5792 \pm 1610$, $b_2 = 181.3 \pm 24$	3
HNO_3 in $H_2SO_4 \cdot nH_2O(l)$	~195–300	0–80	See Note	4
HNO_3 and HCl in $H_2SO_4 \cdot nHNO_3 \cdot mH_2O(l)$	~195–300	0–80	See Note	4
HO_2NO_2 in $H_2SO_4 \cdot nH_2O(l)$	201–230	50–75	$\ln H = 3.69 - mH_2SO_4 \times (-0.25 + 65/T) - 8400 \times (1/T_o - 1/T)$ mH_2SO_4 is the molality of the H_2SO_4 solution, $T_o = 298.15$ K	5
CH_2O in $H_2SO_4 \cdot mHNO_3 \cdot nH_2O(l)$	240–300	10–85 also 8–40 wt. % HNO_3	See Note	6
CH_3OH in $H_2SO_4 \cdot nH_2O(l)$	197–223		See Note	7
$CH_3C(O)CH_3$ in $H_2SO_4 \cdot nH_2O(l)$	198–298	10–80	$\ln H^* = a_1 + a_2 wt + a_3 wt^2 + (b_1 + b_2 wt + b_3 wt^2)/T$ wt is the H_2SO_4 wt. %, $a_1 = -21.438 \pm 4.31$, $a_2 = -0.32163 \pm 0.207$, $a_3 = 0.0072935 \pm 0.00235$ $b_1 = 7292 \pm 1220$, $b_2 = 33.524 \pm 53.42$, $b_3 = -0.975 \pm 0.571$	8
$CH_3C(O)O_2NO_2$ in $H_2O(l)$, $H_2SO_4 \cdot nH_2O(l)$	199–295	0–75	$\ln H^* = 1.07 - mH_2SO_4 \times (0.69 - 152/T) - 5810 \times (1/T_o - 1/T)$, mH_2SO_4 = molality of the H_2SO_4 solution $T_o = 298.15$ K	9
CF_2O in $H_2SO_4 \cdot nH_2O(l)$	215–230	60	< 5	10
CF_3OH in $H_2SO_4 \cdot nH_2O(l)$	250	40 50	> 240 210	11
HOCl in $H_2SO_4 \cdot nH_2O(l)$	200–300	46–80	$H_{HOCl} = 1.91 \times 10^{-6} \times \exp(5862.4/T) \times \exp(-S_{HOCl} M_{H2SO4})$ M atm^{-1} where: $S_{HOCl} = 0.0776 + 59.18/T$ M^{-1}, $M_{H2SO4} = H_2SO_4$ molar conc	12
$ClONO_2$ in $H_2SO_4 \cdot nH_2O(l)$	200–265	40–75	$H_{ClONO2} = 1.6 \times 10^{-6} \times \exp(4710/T) \times \exp(-S_{HOCl} M_{H2SO4})$ M atm^{-1} where: $S_{ClONO2} = 0.306 + 24.0/T$ M^{-1}, $M_{H2SO4} = H_2SO_4$ molar conc.	13
HBr in $H_2SO_4 \cdot nH_2O \cdot H_2O(l)$ and $H_2SO_4 \cdot nHNO_3 \cdot mH_2O(l)$	200–240	40–72	$\ln H^* = a_1 + (b_1 + b_2 wt)/T$ $a_1 = -11.695 \pm 0.537$, $b_1 = 11{,}101 \pm 163$, $b_2 = -90.7 \pm 1.2$	14
SO_2 in H_2O (l), $H_2SO_4 \cdot nH_2O(l)$	193–242	0–97	$\ln H^* = a_1 + a_2 wt + a_3 wt^2 + (b_1 + b_2 wt + b_3 wt^2)/T$, where: wt is the H_2SO_4 wt. %, $a_1 = -10.778 \pm 2.07$, $a_2 = -0.11541 \pm 0.0827$, $a_3 = 0.0012506 \pm 0.000811$ $b_1 = 3310 \pm 578$, $b_2 = 30.581 \pm 22.2$, $b_3 = -0.35469 \pm 0.209$	15

5.19 Notes to Table 5-5

1. O_3 in $H_2SO_4 \cdot nH_2O(l)$—Bubble train uptake measurements where performed by Rattigan et al. [282] at 293 K for 1–70 wt. % H_2SO_4. Recommended expression is a Setchenow coefficient formulation where $H_o = 0.012$ M atm^{-1} is the 293 K value of H for pure water fom Wilhelm et al. [351]. In the measurement, account was taken of the loss of O_3 due to reaction with H^+.

2. NO_2 in $H_2SO_4 \cdot nH_2O(l)$—Langenberg et al. [229] present novel capillary gas chromatography measurements for 39, 59, and 68 wt. % H_2SO_4 over the temperature range of 203 to 243 K. However, NO_2 solubility must be derived from chromatographic waveforms which are contorted by much higher N_2O4 solubility. The resulting values for H_{NO2} are in the 1 to 10^2range, but show inconsistent trends with temperature and concentration, indicating possibly large systematic error.

3. HONO in $H_2SO_4 \cdot nH_2O(l)$—Becker et al. [42] measured HONO partial pressue, P_{HONO}, over bulk solutions in a temperature range of 248–298 K and a H_2SO_4 concentration range of 0–67 wt. %. Longfellow et al. [242] measured P_{HONO} in a wetted wall flow reactor over a temperature range of 218–295 K and an acid concentration range of 60–83 wt. %. Agreement between these two data sets is excellent. H* decreases from

0 wt. % to 53 wt. % due to physical solubility, then increases above 53 wt. % due to protonation and/or association with H_2SO_4 to make nitrosyl sulfuric acid. Becker et al. parameterize their data as a function of sulfuric acid wt. % and temperature. However, the Becker et al. parameterization is not able to fit the combined sets of Becker et al. [42] and Longfellow et al. [242] data, particularly at the lower temperatures and higher wt. % most relevant to the stratosphere. Therefore, the recommended functional form was used to fit the data for >60 wt. %. This function fits both sets of data very well It is important to note that this function is only valid for H_2SO_4 concentrations near 60 wt% and above. The parameterization in Becker et al. [42] should be used to calculate H for H_2SO_4 concentrations <60 wt %. (Note that the units for H are mol/kg-bar in Becker et al. [42]. The density parameterization of Myhre et al. [269] was used to convert to M/atm units.)

4. HNO_3 and HCl in $H_2SO_4 \bullet nH_2O(l)$ and $H_2SO_4 \bullet nHNO_3 \bullet mH_2O(l)$—Effective Henry''s law coefficients, H^*, for HNO_3, and HCl in binary H_2SO_4/H_2O and ternary $H_2SO_4/HNO_3/H_2O$ solutions over the temperature range 195 to 300 K are required to model the composition and heterogeneous chemistry of stratospheric and upper tropospheric aerosols. Solubility data can be obtained from analysis of heterogeneous uptake experiments with the liquid phase diffusion coefficient estimated from acid solution viscosity (Williams and Long [355]) Solubilities can also be obtained from equilibrium or from vapor pressure data.

   Experimental solubility data for HNO_3 is provided by Van Doren et al. [338], Reihs et al. [283] and Zhang et al. [370]. Data for HCl solubility is provided by Watson et al. [348], Hanson and Ravishankara [158,161], Zhang et al. [370], Williams and Golden [353], Abbatt [2], Elrod et al.[113] and Robinson et al. [294].

   These studies all show that trace species solubility in H_2SO_4/H_2O and $H_2SO_4/HNO_3/H_2O$ solutions is a strong function of water activity, which, in turn, depends on both temperature and acid concentrations. Prediction of HNO_3 and HCl H^* values for atmospheric compositions requires a sophisticated model. Comprehensive thermodynamic models of acid solutions for a range of atmospheric conditions have been published by Carslaw et al. [66], Tabazadeh et al. [324] and Luo et al. [248] and reviewed by Carslaw and Peter [68]. These models do an excellent job of reproducing the available experimental data, even for ternary $H_2SO_4/HNO_3/H_2O$ solutions (Elrod et al. [113]). These models and the Carslaw review should be consulted for plots/predictions of H^* for HNO_3 and HCl in strong acid solutions over the atmospheric temperature range. The most widely used model of Carslaw et al. [66] was revised in Massucci et al. [251].

5. HO_2NO_2 in $H_2SO_4 \bullet nH_2O(l)$—Zhang et al. [369] performed wetted wall flow reactor studies using CIMS to detect HO_2NO_2 uptake over a temperature range of 201–230 K and an acid concentration range of 52.9–74 wt. % H_2SO_4. $HD_l^{1/2}$ values where determined for 52.9, 58.3/59.1, 66.4 and 73.8/74 wt. %, with 5 to 15 data points per temperature or temperature pair. All uptake appeared to be reversible with the variation in H strongly temperature dependent, but only moderately dependent on H_2SO_4 wt. %. D_l values were calculated from a cubic cell model to derive H. Uncertainties in measured H values were estimated by authors to be 25% for $H < 1 \times 10^6$ M atm^{-1} and 50% for $H > 1 \times 10^6$ M atm^{-1}. These data were parameterized by Leu and Zhang [236] in the Setchenow coefficient form adopted by Huthwelker for HOCl [185], and their formulation is recommended.

6. CH_2O in $H_2SO_4 \bullet mHNO_3 \bullet nH_2O(l)$—The recommended Henry's Law relationship is:

$$H^* = H\left(1 + K_2 a_{H_2O} + K_3 a_{H^+}\right)$$

   where: $H = 3.4 \times 10^{-5} \exp -[(-0.0456 + 55.5/T)\,(0.46\, m_{H_2SO_4} + 0.13\, m_{HNO_3})]$ M atm^{-1}, T is the temperature in K, and $m_{H_2SO_4}$ and m_{HNO_3} are the respective acid molalities; $K_2 = \exp(4020/T - 5.83)$ M^{-1}, $K_3 = 0.56 \exp[8.84 - (T - 260/T)]$ M^{-1}, and a_{H_2O} and a_{H+} are the water and H^+ activities which are obtained from a thermodynamic model of the solution, e.g. Carslaw et al. [66] Valid for 10–85 wt. % H_2SO_4, 8–40 wt % HNO_3, T = 240–300 K.

   Knudsen cell studies by Tolbert et al. [330] and Iraci and Tolbert [192] and droplet train/flow reactor studies by Jayne et al. [200] all yield data showing that CH_2O is strongly absorbed by sulfuric acid solutions, and Jayne et al. also provide data for ternary acid solutions. The Jayne et al. [200] studies included H_2SO_4 concentrations from 10 to 85 wt. % and HNO_3 concentration between 8 and 40 wt. % with temperature variations from 241 to 300 K. These data were parameterized with three terms, representing physical CH_2O solubility, reversible hydrolysis to $CH_2(OH)_2$, important in more dilute solutions, and reversible formation of CH_3O^+, dominant at high acidities. The Jayne et al. [200] parameterization is recommended above. The H* data from Iraci and Tolbert [192] cover 49 to 95 wt. % H_2SO_4 and a temperature range of 197 to 214.5 K and are in fair agreement with extrapolation of H* expression from Jayne et al. [200] for concentrations below

~75 wt. %. However, the Iraci and Tolbert data are taken on such thin acid films that initial uptake slopes are difficult to determine accurately and the data scatter is large. While the Iraci and Tolbert data do indicate significantly larger H* values for H_2SO_4 concentrations above 75 wt. %, the data do not compel a reformulation of the Jayne et al. parameterization.

7. CH_3OH in $H_2SO_4 \cdot nH_2O(l)$—H* data from Kane and Leu [211], taken over 40–85 wt. % H_2SO_4 and from 210–235 K, indicate soluble uptake below 65 wt. % and predominately reactive uptake to form methanesulfonic acid and dimethysulfate above 65 wt. %. Uptake decreased slightly with temperature below 65 wt. % and increases slightly with temperature above. Data yield $H^*k^{1/2}$ at high acid concentrations. Weakly temperature dependent γs of ~0.15 were measured for 65, 75, and 80 wt. %. However, Knudsen cell studies by Iraci et al. [190] at 45, 61 and 72 wt. % over a 197–223 K temperature range show only well behaved reversible uptake. They argue that low vapor pressures explain the lack of CH_3OH recovery for the short observation times used by Kane and Leu. They also cite three older literature studies on the reaction of methanol and ethanol at room temperature in sulfuric acid which report reaction rate constants much lower than those deduced by Kane and Leu [190]. Iraci et al. present the following parameterization of their data plus data for water:

$$\log H^* = A + 1000B/T$$

where $A = 7.00 + \log M_{H2O}$, $B = 0.000619\ m^2 + 0.00544\ m + 2.267$, M_{H2O} is the molarity of water in the solution (mol L^{-1}) and m is the molality of the H_2SO_4 (moles H_2SO_4 per kg H_2O).

Note that this parameterization is based only on the Iraci et al. data. A reanalysis of the Kane and Leu [211] results to provide additional data in the 40–72 wt. % range, and H^* values for higher wt. % should be undertaken to validate and extend the Iraci et al. data.

8. $CH_3C(O)CH_3$ in $H_2SO_4 \cdot nH_2O(l)$—Duncan et al. [109,110] used IR spectra of thin sulfuric acid films to establish that acetone is absorbed as the protonated species. Above 70 wt. % protonated acetone undergoes a self-condensation/dehydration reaction to form protonated mesityl oxide, which, in turn, reacts with an additional protonated acetone to form trimethyl benzene. Duncan et al. [110] measured reversible uptake and derived Henry's law constants for 70 wt. % H_2SO_4 at 180, 187 and 195 K and a value at 201 K for 76 wt. %. Kane et al. [212] measured uptake in a wetted wall flow reactor and derived H* parameters for 40, 50, 65, and 75 wt. % over a much wider temperature range than Duncan et al. [110]. Their data diverge above 80 wt. % which they attribute to reactive uptake a la Duncan et al. [109,110]. Klassen et al. [221] provide Knudsen cell uptake derived data for 48.7 to 78.3 H_2SO_4 wt % between 210 and 240 K that are generally consistent with that of Kane et al. [212]. Imamura and Akiyoshi [188] report wetted wall flow reactor H* measurements at 230 K for 50 and 60 wt. %, 250 K for 60, 69 and 76 wt. %, and 270 K for 76 and 79 wt. %; their data diverges a factor of 2 to 4 from that of Kane et al. [212] and Klassen et al. [221].

Equally weighted data sets from Kane et al. [212] and Klassen et al. [221] were combined and fit to generate the recommended parameterization. Two points for the solubility of acetone in water at 298 K and 273 K (Benkelberg et al. [48]) were included to improve the extrapolation to low wt. % solutions.

The data points from Imamura and Akiyoshi [188] were not included because they were inconsistent with the other data and have a very different temperature dependence. The few data points from Duncan et al. [109,110] are also inconsistent with the other data and were not included in the parameterization.

9. $CH_3C(O)O_2NO_2$ in H_2O and $H_2SO_4 \cdot nH_2O(l)$—Zhang and Leu [364] performed wetted wall flow reactor studies using CIMS to detect $CH_3C(O)O_2NO_2$ uptake over a temperature range of 199 to 226 K. Uptake studies were performed at 46, 54, 59, and 72 wt. % H_2SO_4 to yield $H^*D_l^{1/2}$ values. D_l values were calculated from a cubic cell model to derive H*. Leu and Zhang [236] fit their data from Zhang and Leu [364], including water data from Kames and Schurath [208] and Kames et al. [209], using the Setchenow coefficient form adopted by Huthwelker for HOCl [185]. This formulation is recommended for both water and sulfuric acid solutions.

10. CF_2O in $H_2SO_4 \bullet nH_2O(l)$—Hanson and Ravishankara [156] calculate an upper limit for H of CF_2O based on assumed solubility limit resulting in lack of measurable uptake into 60 wt% H_2SO_4.

11. CF_3OH in $H_2SO_4 \bullet nH_2O(l)$—Lovejoy et al. [245] determined reacto-diffusive lengths of > 0.4 µm and 1.0 µm for CF_3OH uptake at 250 K on 40 and 50 wt % H_2SO_4 aerosols, respectively. This leads to H^* estimates of >240 and 210 M atm^{-1}, respectively.

12. HOCl in $H_2SO_4 \bullet nH_2O(l)$—Recommendation is from the model of Shi et al. [313] which is based on wetted wall flow tube data from Hanson and Ravishankara [162] and Hanson and Lovejoy [154], and uptake by stirred and static solutions by Donaldson et al. [107]. This model incorporates newer, higher temperature data and replaces earlier recommended formulation by Huthwelker et al. [185].

13. $ClONO_2$ in $H_2SO_4 \bullet nH_2O(l)$—Recommendation is from the model of Shi et al. [313] who used a measurement of the hydrolysis reaction's reacto-diffusive length by Hanson and Lovejoy [153] on 60 wt. % H_2SO_4 at 250 K to derive the hydrolysis rate constant, k_{hyd}, and constrain H_{ClONO2} at 250 K. Shi et al. fit the $Hk^{1/2}$ dependence of the $ClONO_2$ uptake coefficients for a variety of $ClONO_2$ hydrolysis and $ClONO_2$ + HCl data to derive a parameterization for H as a function of wt. % and T.

14. HBr in $H_2SO_4 \bullet mHNO_3 \bullet nH_2O(l)$—Experimental data for HBr solubility is provided by Williams et al. [354], Abbatt [2], Abbatt and Nowak [8], Kleffman et al. [222], and Behr et al. [45]. Data from time-dependent uptake measurements and from vapor pressure measurements is in good agreement after correcting for the fact that for some of the vapor pressure measurements the HBr concentration in solution was high enough to increase the acidity and thereby decrease the HBr solubility. By comparing pairs of data points with different HBr concentrations (from the same experiment), an average correction factor was obtained. The correction factor was used to correct the vapor pressure data of Williams et al. [354], Abbatt and Nowak [8] and Kleffmann et al. to zero effective HBr concentration. (This is different than the approach taken in Kleffmann et al. of using a "corrected" H_2SO_4 wt. %. However, the resulting parameterization is very similar to the one in Kleffmann et al. [222].) The time-dependent uptake data of Williams et al. [354] and Abbatt [2], and the molecular beam uptake data of Behr et al. [45] did not require correction. All of the experimental data have been fit to obtain the recommended parameterization as a function of H_2SO_4 wt. % and temperature.

    Agreement between this parameterization and the updated activity coefficient model of Massucci et al. [251] (and http://www.hpc1.uea.ac.uk/~e770/aim.html) is good for > 60 wt. %, but not very good at lower H_2SO_4 wt. %, particularly at low temperatures. Therefore, this parameterization is recommended for calculating HBr Henry's law solubilities.

    The only data for HBr solubilities in ternary solutions is from Kleffmann et al. [222]. The data do not agree well with the updated activity coefficient in Massucci et al. [222] or with the older activity coefficient model in Luo et al. [248]. Until further information becomes available, the recommendation is to use the parameterization for ternary solutions given in Kleffmann et al. [222].

15. SO_2 in $H_2SO_4 \bullet nH_2O(l)$—Room temperature vapor pressure measurements reviewed by Hayduk et al. [171] and bubble train reactor uptake measurements by Rattigan et al. [282] for 0–70 wt. % H_2SO_4 agree very well. Langenberg et al. [229]] used a novel capillary gas chromatography technique to deduce H* values for 41–83 wt. % H_2SO_4 over a temperature range of 193–242 K. The recommended parameterization is a fair fit to the Rattigan et al. and Langenberg et al. data sets and allows reasonable extrapolation over the full range of atmospheric temperatures. Note that the Langenberg et al. [229] data is in mol/kg-bar units and was converted to mole/l units using the density parameterization of Myhre et al. [269].

5.20 References

1. Abbatt, J. P. D., 1994, Geophys. Res. Lett., **21**, 665-668.
2. Abbatt, J. P. D., 1995, J. Geophys. Res., **100**, 14009-14017.
3. Abbatt, J. P. D., 1996, Geophys. Res. Lett., **23**, 1681-1684.
4. Abbatt, J. P. D., 1997, Geophys. Res. Lett., **24**, 1479-1482.
5. Abbatt, J. P. D., K. D. Beyer, A. F. Fucaloro, J. R. McMahon, P. J. Wooldridge, R. Zhong and M. J. Molina, 1992, J. Geophys. Res., **97**, 15819-15826.
6. Abbatt, J. P. D. and M. J. Molina, 1992, Geophys. Res. Lett., **19**, 461-464.
7. Abbatt, J. P. D. and M. J. Molina, 1992, J. Phys. Chem., **96**, 7674-7679.
8. Abbatt, J. P. D. and J. B. Nowak, 1997, J. Phys. Chem. A, **101**, 2131-2137.
9. Aguzzi, A. and M. J. Rossi, 2001, Phys. Chem. Chem. Phys., **3**, 3707-3716.
10. Akhter, M. S., A. R. Chughtai and D. M. Smith, 1985, Appl. Spectrosc., **39**, 143-153.
11. Akhter, M. S., A. R. Chughtai and D. M. Smith, 1985, Appl. Spectrosc., **39**, 154-167.
12. Akhter, M. S., A. R. Chughtai and D. M. Smith, 1991, Appl. Spectrosc., **45**, 653-665.
13. Al-Abadleh, H. A. and V. H. Grassian, 2000, J. Phys. Chem. A, **104**, 11926-11933.
14. Alcala-Jornod, C., H. Van den Bergh and M. J. Rossi, 2000, Phys. Chem. Chem. Phys., **2**, 5584-5593.
15. Alebic'-Juretic', A., T. Cuitas and L. Klasine, 1992, Ber. Bunsenges Phys. Chem., **96**, 493-495.
16. Allanic, A., R. Oppliger and M. Rossi, 1997, J. Geophys. Res., **102**, 23529-23541.
17. Allanic, A., R. Oppliger, H. Van den Bergh and M. J. Rossi, 2000, Zeitschrift fur Physikalische Chemie, **214**, 11, 1479-1500.
18. Allanic, A. and M. J. Rossi, 1999, J. Geophys. Res., **104**, 18,689-18,696.
19. Allen, H. C., D. E. Gragson and G. L. Richmond, 1999, J. Phys. Chem. B, **103**, 660-666.
20. Altschuh, J., R. Bruggemann, H. Santl, G. Eichinger and O. G. Piringer, 1999, Chemosphere, **39**, 1871-1887.
21. Ammann, M., M. Kalberer, D. T. Jost, L. Tobler, E. Rossler, D. Piguet, H. W. Gaggeler and U. Baltensperger, 1998, Nature, **395**, 157-160.
22. Ammann, M., M. Kalberer, K. Tabor, K. Tobler, C. Zellweger, E. Weingartner, S. Nyeki, Y. Parrat, F. Li, D. Piguet, E. Rossler, D. T. Jost, H. W. Gaggeler and U. Baltensperger. "Proc. 7th Euro. Symp. on Physico-Chem. Behav. of Atmos. Poll.", 1996.
23. Arens, F., L. Gutzwiller, U. Baltensperger, H. Gaggeler and M. Ammann, 2001, Environ. Sci. Technol., **35**, 2191-2199.
24. Baker, J., S. F. M. Ashbourn and R. A. Cox, 1999, Phys. Chem. Chem. Phys., **1**, 683-690.
25. Baldwin, A. C., 1982, Int. J. Chem. Kin., **14**, 269-277.
26. Baldwin, A. C. and D. M. Golden, 1979, Science, **206**, 562.
27. Baldwin, A. C. and D. M. Golden, 1980, J. Geophys. Res., **85**, 2888-2889.
28. Ball, S. M., A. Fried, B. E. Henry and M. Mozurkewich, 1998, Geophys. Res. Lett., **25**, 3339-3342.
29. Barlett, W. P. and D. W. Margerum, 1999, Environ. Sce. Technol., **33**, 3410-3414.
30. Barone, S. B., M. A. Zondlo and M. A. Tolbert, 1997, J. Phys. Chem. A, **101**, 8643-8652.
31. Battino, R. Nitrous oxide in water. In *Oxides of Nitrogen*; Young, C. L., Ed.; Pergamon: Oxford, 1981; Vol. 8; pp 1-22.
32. Battino, R. Oxygen in water. In *Oxygen and Ozone*; Battino, R., Ed.; Pergamon: Oxford, 1981; Vol. 7; pp 1-5.
33. Battino, R. Ethane in water. In *Ethane*; Hayduk, W., Ed.; Pergamon: Oxford, 1982; Vol. 9; pp 1-26.
34. Battino, R. Nitrogen in water. In *Nitrogen and Air*; Battino, R., Ed.; Pergamon: Oxford, 1982; Vol. 10; pp 1-29.
35. Battino, R. Chlorine dioxide in water. In *Sulfur Dioxide, Chlorine, Fluorine and Chlorine Oxides*; Young, C. L., Ed.; Pergamon: Oxford, 1983; Vol. 12; pp 454-456.
36. Battino, R. Chlorine in water. In *Sulfur Dioxide, Chlorine, Fluorine and Chlorine Oxides*; Young, C. L., Ed.; Pergamon: Oxford, 1983; Vol. 12; pp 333-347.
37. Battino, R. Sulfur dioxide in water. In *Sulfur Dioxide, Chlorine, Fluorine and Chlorine Oxides*; Young, C. L., Ed.; Pergamon: Oxford, 1983; Vol. 12; pp 3-33.
38. Battino, R. 2-Methylpropane in water. In *Propane, Butane and 2-Methylpropane*; Hayduk, W., Ed.; Pergamon: Oxford, 1986; Vol. 24; pp 34-37.
39. Battino, R. Butane in water. In *Propane, Butane and 2-Methylpropane*; Hayduk, W., Ed.; Pergamon: Oxford, 1986; Vol. 24; pp 16-32.
40. Battino, R. Propane in water. In *Propane, Butane and 2-Methylpropane*; Hayduk, W., Ed.; Pergamon: Oxford, 1986; Vol. 24; pp 1-15.

41. Battino, R. Methane in water. In *Methane*; Clever, H. L., Young, C. L., Eds.; Pergamon: Oxford, 1987; Vol. 27/28; pp 1-44.
42. Becker, K. H., J. Kleffman, R. Kurtenbach and P. Wiesen, 1996, J. Phys. Chem., **100**, 14,984-14,990.
43. Behnke, W., H.-U. Kruger, V. Scheer and C. Zetzsch, 1992, J. Aerosol Sci., **23**, S923-S936.
44. Behnke, W., V. Scheer and C. Zetzsch, 1993, J. Aerosol Sci., **24**, S115-S116.
45. Behr, P., J. R. Morris, M. D. Antman, B. R. Ringeisen, J. Splan and G. M. Nathanson, 2001, Geophys. Res. Lett., **28**, 1961-1964.
46. Beichert, P. and B. J. Finlayson-Pitts, 1996, J. Phys. Chem., **100**, 15,218-15,228.
47. Benes, M. and V. Dohnal, 1999, J. Chem. Eng. Data, **44**, 1097-1102.
48. Benkelberg, H. J., S. Hamm and P. Warneck, 1995, J. Atmos. Chem., **20**, 17-34.
49. Benkelberg, H. J., S. Hamm and P. Warneck, 1995, J. Atmos. Chem., **20**, 17-34.
50. Ben-Naim, A. and R. Battino, 1985, J. Sol. Chem., **14**, 245-253.
51. Benson, B. B., D. Krause and M. A. Peterson, 1979, J. Sol. Chem., **8**, 655-690.
52. Berko, H. N., P. C. McCaslin and B. J. Finlayson-Pitts, 1991, J. Phys. Chem., **95**, 6951-6958.
53. Berland, B. S., M. A. Tolbert and S. M. George, 1997, J. Phys. Chem. A, **101**, 9954-9963.
54. Betterton, E. A. and M. R. Hoffmann, 1988, Environ. Sci. Technol., **22**, 1415-1418.
55. Blatchley, E. R., R. W. Johnson, , J. E. Alleman and W. F. McCoy, 1991, Wat. Res., **26**, 99-106.
56. Bongartz, A., J. Kames, U. Schurath, C. George, P. Mirabel and J. L. Ponche, 1994, J. Atm. Chem., **18**, 149-160.
57. Bongartz, A., S. Schweighoefer, C. Roose and U. Schurath, 1995, J. Atmos. Chem., **20**, 35-58.
58. Brouwer, L., M. J. Rossi and D. M. Golden, 1986, J. Phys. Chem., **90**, 4599-4603.
59. Brown, D. E., S. M. George, C. Huang, E. K. L. Wong, K. B. Rider, R. S. Smith and B. D. Kay, 1996, J. Phys. Chem., **100**, 4988-4995.
60. Brown, L. A., V. Vaida, D. R. Hanson, J. D. Graham and J. T. Roberts, 1996, J. Phys. Chem., **100**, 3121-3125.
61. Burnett, M. G., 1963, Anal. Chem., **35**, 1567-1570.
62. Butler, J. V. A., C. N. Ramchandani and D. W. Thomson, 1935, J. Chem. Soc., 280285.
63. Cachier, H. Carbonaceous Combustion Aerosols. In *Atmospheric Particles*; Harrison, R. M., VanGrieken, R., Eds.; Wiley: New York, 1998.
64. Caloz, F., F. F. Fentner and M. J. Rossi, 1996, J. Phys. Chem., **100**, 7494-7501.
65. Cappa, C. D., S. E. Kuipers, J. M. Roberts, A. S. Gilbert and M. J. Elrod, 2000, J. Phys. Chem. A, **104**, 4449-4457.
66. Carslaw, K. S., S. L. Clegg and P. Brimblecombe, 1995, J. Phys. Chem., **99**, 11,557-11,574.
67. Carslaw, K. S. and T. Peter, 1997, Geophys. Res. Lett., **24**, 1743-1746.
68. Carslaw, K. S., T. Peter and S. L. Clegg, 1997, Rev. Geophys., **35**, 125-154.
69. Chaix, L., A. Allanic and M. J. Rossi, 2000, J. Phys. Chem. A, **104**, 7268-7277.
70. Choi, W. and M. T. Leu, 1998, J. Phys. Chem A, **102**, 7618-7630.
71. Chu, L. and L. T. Chu, 1999, J. Phys. Chem. A, **103**, 8640-8649.
72. Chu, L. and L. T. Chu, 1999, J. Phys. Chem. A, **103**, 691-699.
73. Chu, L., G. Diao and L. T. Chu, 2000, J. Phys. Chem. A, **104**, 3150-3158.
74. Chu, L. T. and J. W. Heron, 1995, Geophys. Res. Lett., **22**, 3211-3214.
75. Chu, L. T., M.-T. Leu and L. F. Keyser, 1993, J. Phys. Chem., **97**, 7779-7785.
76. Chu, L. T., M.-T. Leu and L. F. Keyser, 1993, J. Phys. Chem., **97**, 12798-12804.
77. Chughtai, A. R., M. M. O. Atteya, J. Kim, B. K. Konowalchuck and D. M. Smith, 1998, Carbon, **36**, 1573-1589.
78. Chughtai, A. R., M. E. Brooks and D. M. Smith, 1993, Aer. Sci. Tech., **19**, 121-132.
79. Chughtai, A. R., M. E. Brooks and D. M. Smith, 1996, J. Geophys. Res., **101**, 19505-19514.
80. Chughtai, A. R., S. A. Gordon and D. M. Smith, 1994, Carbon, **32**, 405-416.
81. Chughtai, A. R., J. Kim and D. M. Smith, 2001, Croatica Chem. Acta, **in press**.
82. Chughtai, A. R., J. M. Kim and D. M. Smith, 2002, J. Atmos. Chem., **43**, 21-43.
83. Chughtai, A. R., J. M. Kim and D. M. Smith, 2002, J. Atmos. Chem., **in press.**
84. Chughtai, A. R., N. J. Miller, D. M. Smith and J. R. Pitts, 1999, J. Atmos. Chem., **34**, 259-279.
85. Chughtai, A. R., W. F. Welch, M. S. Akhter and D. M. Smith, 1990, Appl. Spectrosc., **44**, 294-298.
86. Chughtai, A. R., W. F. Welch and D. M. Smith, 1990, Carbon, **28**, 411-421.
87. Chughtai, A. R., G. R. Williams, M. M. O. Atteya, N. J. Miller and D. M. Smith, 1999, Atmos. Environ., **33**, 2679-2687.
88. Clegg, S. L. and P. Brimblecombe, 1986, Atmos. Environ., **20**, 2483.
89. Clegg, S. L. and P. Brimblecombe, 1989, J. Phys. Chem., **93**, 7237-7248.

90. Cofer, W. R., D. R. Schryer and R. S. Rogowski, 1981, Atm. Environ., **15**, 1281-1286.
91. Cooper, P. L. and J. P. D. Abbatt, 1996, J. Phys. Chem., **100**, 2249-2254.
92. Cowin, J. P., personal comm.
93. Dacey, J. W. H., S. G. Wakeham and B. L. Howes, 1984, Geophys. Res. Lett., **11**, 991-994.
94. Dai, D. J., S. J. Peters and G. E. Ewing, 1995, J. Phys. Chem., **99**, 10,299-10,304.
95. Dai, Q., G. N. Robinson and A. Freedman, 1996, J. Phys. Chem., submitted.
96. Dasgupta, P. K. and S. Dong, 1986, Atmos. Environ., **20**, 565-570.
97. Daumer, R. Nissner and D. Klockow, J. Aerosol Sci., **23**, 315-325.
98. De Bruyn, W. J., S. X. Duan, X. Q. Shi, P. Davidovits, D. R. Worsnop, M. S. Zahniser and C. E. Kolb, 1992, Geophys. Res. Lett., **19**, 1939-1942.
99. De Bruyn, W. J., J. A. Shorter, P. Davidovits, D. R. Worsnop, M. S. Zahniser and C. E. Kolb, 1994, J. Geophys. Res., **99**, 16927-16932.
100. De Bruyn, W. J., J. A. Shorter, P. Davidovits, D. R. Worsnop, M. S. Zahniser and C. E. Kolb, 1995, Environ. Sci Technol., **29**, 1179-1185.
101. De Bruyn, W. J., E. Swartz, J. H. Hu, J. A. Shorter, P. Davidovits, D. R. Worsnop and M. S. Zahniser, 1995, J. Geophys. Res., **100**, 7245-7251.
102. DeMore, W. B., S. P. Sander, D. M. Golden, R. F. Hampson, M. J. Kurylo, C. J. Howard, A. R. Ravishankara, C. E. Kolb and M. J. Molina "Chemical Kinetics and Photochemical Data for Use in Stratospheric Modeling, Evaluation Number 12," JPL Publication 97-4, Jet Propulsion Laboratory, California Institute of Technology, Pasadena, CA, 1997.
103. Disselkamp, R. S., M. A. Carpenter and J. P. Cowin, 2000, J. Atmos. Chem., **37**, 113-123.
104. Disselkamp, R. S., M. A. Carpenter, J. P. Cowin, C. M. Berkowitz, E. G. Chapman, R. A. Zaveri and N. S. Laulainen, 2000, J. Geophys. Res., **105**, 9767-9771.
105. Dlugokencky, E. J. and A. R. Ravishankara, 1992, Geophys. Res. Lett., **19**, 41-44.
106. Donaldson, D. J., J. A. Guest and M. C. Goh, 1995, J. Phys. Chem., **99**, 9313-9315.
107. Donaldson, D. J., A. R. Ravishankara and D. R. Hanson, 1997, J. Phys. Chem. A, **101**, 4717-4725.
108. Duan, S. X., J. T. Jayne, P. Davidovits, D. R. Worsnop, M. S. Zahniser and C. E. Kolb, 1993, J. Phys. Chem., **97**, 2284-2288.
109. Duncan, J. L., L. R. Schindler and J. T. Roberts, 1998, Geophys. Res. Lett., **25**, 631-634.
110. Duncan, J. L., L. R. Schindler and J. T. Roberts, 1999, J. Phys. Chem. B, **103**, 7247-7259.
111. Edwards, T. J., G. Maurer, J. Newman and J. M. Prausnitz, 1978, AIChE Journal, **24**, -.
112. Elliott, S., 1989, Atmos. Environ., **23**, 1977-1980.
113. Elrod, M. J., R. E. Koch, J. E. Kim and M. S. Molina, 1995, Faraday Discuss, **100**, 269-278.
114. Fairbrother, D. H. and G. Somorjai, 2000, J. Phys. Chem. B, **104**, 4649-4652.
115. Fendel, W., D. Matter, H. Burtscher and A. Schimdt - Ott, 1995, Atmos. Environ, **29**, 967-973.
116. Fendel, W., D. Matter, H. Burtscher and A. Schmidt-Ott, 1995, Atmos. Environ., **29**, 967-973.
117. Fendel, W. and A. S. Ott, 1993, J. Aerosol Sci., **24**, S317-S318.
118. Fenter, F. F., F. Caloz and M. J. Rossi, 1994, J. Phys. Chem., **98**, 9801-9810.
119. Fenter, F. F., F. Caloz and M. J. Rossi, 1996, J. Phys. Chem., **100**, 1008-1019.
120. Fenter, F. F. and M. J. Rossi, 1996, J. Phys. Chem., **100**, 13765-13775.
121. Fenter, F. F. and M. J. Rossi, 1997, J. Phys. Chem. A, **101**, 4110-4113.
122. Finlayson-Pitts, B. J., M. J. Ezell and J. N. Pitts, Jr., 1989, Nature, **337**, 241-244.
123. Finlayson-Pitts, B. J. and J. N. Pitts *Chemistry of the Upper and Lower Atmosphere: Theory, Experiments and Applications*; Academic: San Diego, 2000.
124. Fluckiger, B., A. Thielmann, L. Gutzwiller and M. J. Rossi, 1998, Ber. Bunsenges. Phys. Chem., **102**, 915-928.
125. Fogg, P. G. T. Hydrogen sulfide in water. In *Hydrogen Sulfide, Deuterium Sulfide and Hydrogen Selenide*; Fogg, P. G. T., Young, C. L., Eds.; Pergamon: Oxford, 1988; Vol. 32; pp 1-19.
126. Fox, L. E., D. R. Worsnop, M. S. Zahniser and S. C. Wofsy, 1994, Science, **267**, 351-355.
127. Frenzel, A., S. Kutsuna, K. Takeuchi and T. Ibusuki, 2000, Atmos. Environ., **34**, 3641-3544.
128. Friant, S. L. and I. H. Suffet, 1979, Anal. Chem., **51**, 21672176.
129. Fried, A., B. E. Henry, J. G. Calvert and M. Mozukewich, 1994, J. Geophys. Res., **99**, 3517-3532.
130. Fung, K. N., I. N. Tang and H. R. Munkelwitz, 1987, Appl. Optics, **26**, 1282-1287.
131. George, C., J. Lagrange, P. Lagrange, P. Mirabel, C. Pallares and J. L. Ponche, 1994, J. Geophys. Res., **99**, 1255-1262.
132. George, C., J. L. Ponche, P. Mirabel, W. Behnke, V. Sheer and C. Zetzsch, 1994, J. Phys. Chem., **98**, 8780-8784.
133. George, C., J. Y. Saison, J. L. Ponche and P. Mirabel, 1994, J. Phys. Chem., **98**, 10857-10862.

134. Gerecke, A., A. Thielmann, L. Gutzwiller and M. J. Rossi, 1998, Geophys. Res. Lett., **25**, 2453-2456.
135. Gershenzon, V. M., V. M. Grigorieva, A. V. Ivanov and R. G. Remorov, 1995, Faraday Discuss, **100**, 83-100.
136. Gershenzon, Y. M., A. V. Ivanov, S. I. Kucheryavyi and V. B. Rozenshtein, 1986, Kinet. Katal., **27**, 1069-1074.
137. Gershenzon, Y. M. and A. P. Purmal, 1990, Russ. Chem. Rev., **59**, 1007-1023.
138. Gertner, B. J. and J. T. Hynes, 1996, Science, **271**, 1563-1566.
139. Goldberg, E. D. *Black Carbon in the Environment*; Wiley: New York, 1985.
140. Graham, J. D. and J. T. Roberts, 1994, J. Phys. Chem., **98**, 5974-5983.
141. Graham, J. D. and J. T. Roberts, 1995, Geophys. Res. Lett., **22**, 251-254.
142. Graham, J. D., J. T. Roberts, L. A. Brown and V. Vaida, 1996, J. Phys. Chem., **100**, 3115-3120.
143. Gutzwiller, L., F. Arens, U. Baltensperger, H. W. Gäggeler and M. Ammann, 2002, Environ. Sci. Technol., **36**, 677-682.
144. Hales, J. M. and D. R. Drewes, 1979, Atmos. Environ., **13**, 1133-1147.
145. Hallquist, M., D. J. Stewart, J. Baker and R. A. Cox, 2000, J. Phys. Chem. A, **104**, 3984.
146. Hamm, S., J. Hahn, G. Helas and P. Warneck, 1984, Geophys. Res. Let., **11**, 1207-1210.
147. Hanning-Lee, M. A., B. B. Brady, L. R. Martin and J. A. Syage, 1996, Geophys. Res. Lett., **23**, 1961-1964.
148. Hanson, D. R., 1992, Geophys. Res. Lett., **19**, 2063-2066.
149. Hanson, D. R., 1995, J. Phys. Chem., **99**, 13,059-13,061.
150. Hanson, D. R., 1998, J. Phys. Chem. A, **102**, 4794-4807.
151. Hanson, D. R., J. B. Burkholder, C. J. Howard and A. R. Ravishankara, 1992, J. Phys. Chem., **96**, 4979-4985.
152. Hanson, D. R. and E. R. Lovejoy, 1994, Geophys. Res. Lett., **21**, 2401-2404.
153. Hanson, D. R. and E. R. Lovejoy, 1995, Science, **267**, 1326-1329.
154. Hanson, D. R. and E. R. Lovejoy, 1996, J. Phys. Chem., **100**, 6397-6405.
155. Hanson, D. R. and A. R. Ravishankara, 1991, J. Geophys. Res., **96**, 5081-5090.
156. Hanson, D. R. and A. R. Ravishankara, 1991, Geophys. Res. Lett., **18**, 1699-1701.
157. Hanson, D. R. and A. R. Ravishankara, 1991, J. Geophys. Res., **96**, 17307-17314.
158. Hanson, D. R. and A. R. Ravishankara, 1992, J. Phys. Chem., **96**, 2682-2691.
159. Hanson, D. R. and A. R. Ravishankara, 1992, J. Phys. Chem., **96**, 9441-9446.
160. Hanson, D. R. and A. R. Ravishankara, 1993, J. Phys. Chem., **97**, 2802-2803.
161. Hanson, D. R. and A. R. Ravishankara, 1993, J. Phys. Chem., **97**, 12309-12319.
162. Hanson, D. R. and A. R. Ravishankara, 1993, J. Geophys. Res., **98**, 22931-22936.
163. Hanson, D. R. and A. R. Ravishankara. In *The Tropospheric Chemistry of Ozone in the Polar Regions*; Niki, H., Becker, K. H., Eds.; NATO, 1993; pp 17281-17290.
164. Hanson, D. R. and A. R. Ravishankara, 1993, J. Phys. Chem., **97**, 12309-12319.
165. Hanson, D. R. and A. R. Ravishankara, 1994, J. Phys. Chem., **98**, 5728-5735.
166. Hanson, D. R. and A. R. Ravishankara, 1995, Geophys. Res. Lett., **22**, 385-388.
167. Hanson, D. R., A. R. Ravishankara and E. R. Lovejoy, 1996, J. Geophys. Res., **101**, 9063-9069.
168. Hanson, D. R., A. R. Ravishankara and S. Solomon, 1994, J. Geophys. Res., **99**, 3615-3629.
169. Harker, A. B. and W. W. Ho, 1979, Atmos. Environ., **13**, 1005-1010.
170. Hauff, K., R. G. Fischer and K. Ballschmiter, 1998, Chemosphere, **37**, 2599-2615.
171. Hayduk, W., H. Asatani and B. C. Y. Lu, 1988, J. Chem. Eng. Data, **33**, 506-509.
172. Haynes, D. R., N. J. Tro and S. M. George, 1992, J. Phys. Chem., **96**, 8502-8509.
173. Henson, B. F., K. R. Wilson and J. M. Robinson, 1996, Geophys. Res. Lett., **23**, 1021-1024.
174. Henson, B. F., K. R. Wilson and J. M. Robinson, 1999, submitted to J. Phys. Chem. A.
175. Hill, J. O., I. G. Worsley and L. G. Helper, 1968, J. Phys. Chem., **72**, 3695-3697.
176. Hoff, J. T., D. Mackay, R. Gillham and W. Y. Shiu, 1993, Environ. Sci. Tehcnol., **27**, 2174-2180.
177. Hofmann, D. J. and S. J. Oltmans, 1992, Geophys. Res. Lett., **22**, 2211-2214.
178. Holdren, M. W., C. W. Spicer and J. M. Hales, 1984, Atmos. Environ., **18**, 1171-1173.
179. Holzwarth, G., R. G. Balmer and L. Soni, 1984, Water Res., **18**, 1421-1427.
180. Hu, J. H. and J. P. D. Abbatt, 1997, J. Phys. Chem. A, **101**, 871-878.
181. Hu, J. H., Q. Shi, P. Davidovits, D. R. Worsnop, M. S. Zahniser and C. E. Kolb, 1995, J. Phys. Chem., **99**, 8768-8776.
182. Hu, J. H., J. A. Shorter, P. Davidovits, D. R. Worsnop, M. S. Zahniser and C. E. Kolb, 1993, J. Phys. Chem., **97**, 11037-11042.
183. Hudson, P. K., K. L. Foster, M. A. Tolbert, S. M. George, S. R. Carlo and V. H. Grassian, 2001, J. Phys. Chem. A, **105**, 694-702.

184. Huntzicker, J. J., R. A. Cary and C.-S. Ling, 1980, Environ. Sci. Technol., **14**, 819-824.
185. Huthwelker, T., T. Peter, B. P. Juo, S. L. Clegg, K. S. Carshlaw and P. Brimblecombe, 1995, J. Atmos. Chem., **21**, 81-95.
186. Hwang, H. and P. K. Dasgupta, 1985, Environ. Sci. Technol., **19**, 255-258.
187. Il'in, S. D., V. V. Selikhonovich, Y. M. Gershenson and V. B. Rozenshtein, 1991, Sov. J. Chem. Phys., **8**, 1858-1880.
188. Imamura, T. and H. Akiyoshi, 2000, Geophys. Res. Lett., **27**, 1419-1422.
189. Imamura, T., Y. Rudich, R. K. Talukdar, R. W. Fox and A. R. Ravishankara, 1997, J. Phys. Chem., **101**, 2316-2322.
190. Iraci, L. T., A. M. Essin and D. M. Golden, 2002, J. Phys. Chem. A, **106**, 4054-4060.
191. Iraci, L. T., A. M. Middlebrook, M. A. Wilson and M. A. Tolbert, 1994, Geophys. Res. Lett., **21**, 867-870.
192. Iraci, L. T. and M. A. Tolbert, 1997, J. Geophys. Res., **102**, 16,099-16,107.
193. Ivanov, A. V., Y. M. Gersherzon, F. Gratpanche, P. Devolder and J.-P. Saverysyn, 1996, Am. Geophys., **14**, 659-664.
194. Jaegle, L., C. R. Webster, R. D. May, D. C. Scott, R. M. Stimpfle, D. W. Kohn, P. O. Wennberg, T. F. Hansico, R. C. Cohen, M. H. Proffitt, K. K. Kelly, J. Elkins, D. Baumgardner, J. E. Dye, J. C. Wilson, R. F. Pueschel, K. R. Chan, R. J. Salawitch, A. F. Tuck, S. J. Hovde and Y. L. Yung, 1997, J. Geophys. Res., **102**, 13,235-13,253.
195. Jans, U. and J. Hoigne, 2000, Atmos. Environ., **34**, 1069-1085.
196. Jayne, J. T., P. Davidovits, D. R. Worsnop, M. S. Zahniser and C. E. Kolb, 1990, J. Phys. Chem., **94**, 6041-6048.
197. Jayne, J. T., S. X. Duan, P. Davidovits, D. R. Worsnop, M. S. Zahniser and C. E. Kolb, 1991, J. Phys. Chem., **95**, 6329-6336.
198. Jayne, J. T., S. X. Duan, P. Davidovits, D. R. Worsnop, M. S. Zahniser and C. E. Kolb, 1992, J. Phys. Chem., **96**, 5452-5460.
199. Jayne, J. T., U. Poschl, Y. Chen, D. Dai, L. T. Molina, D. R. Worsnop, C. E. Kolb and M. J. Molina, 1997, J. Phys. Chem. A, **101**, 10,000-10,011.
200. Jayne, J. T., D. R. Worsnop, C. E. Kolb, E. Swartz and P. Davidovits, 1996, J. Phys. Chem., **100**, 8015-8022.
201. Jefferson, A., F. L. Eisele, P. J. Zieman, R. J. Weber, J. J. Marti and P. H. McMurry, 1997, J. Geophys. Res., **102**, 19,021-19,028.
202. Jenkins, J. and M. B. King, 1965, Chem. Engin. Sci., **20**, 921-922.
203. Johnson, B. J., E. A. Betterton and D. Craig, 1996, J. Atmos. Chem., **24**, 113-119.
204. Kalberer, M., M. Ammann, F. Arens, H. W. Gaggeler and U. Baltensperger, 1999, J. Geophys. Res., **104**, 13825-13832.
205. Kalberer, M., M. Ammann, H. W. Gaggeler and U. Baltensperger, 1999, Atmos. Environ., **33**, 2815-2822.
206. Kalberer, M., K. Tabor, M. Ammann, Y. Parrat, E. Weingartner, D. Piguet, E. Rossler, D. T. Jost, A. Turler, H. W. Gaggeler and U. Baltensperger, 1996, J. Phys. Chem., **100**, 15487-15493.
207. Kames, J. and U. Schurath, 1992, J. Atmos. Chem., **15**, 79-95.
208. Kames, J. and U. Schurath, 1995, J. Atmos. Chem., **21**, 151-164.
209. Kames, J., S. Schweighoefer and U. Schurath, 1991, J. Atmos. Chem., **12**, 169-180.
210. Kamm, S., O. Mohler, K.-H. Naumann, H. Saathoff and U. Schurath, 1999, Atmos. Environ., **33**, 4651-4661.
211. Kane, S. M. and M.-T. Leu, 2001, J. Phys. Chem. A, **105**, 1411-1415.
212. Kane, S. M., R. S. Timonen and M.-T. Leu, 1999, J. Phys. Chem. A, **103**, 9259-9265.
213. Kelley, C. M. and H. V. Tartar, 1956, J. Amer. Chem. Soc., **78**, 5752-5756.
214. Kenner, R. D., I. C. Plumb and K. R. Ryan, 1993, Geophys. Res. Lett., **20**, 193-196.
215. Keyser, L. F. and M.-T. Leu, 1993, Micros. Res. Technol., **25**, 434-438.
216. Keyser, L. F. and M.-T. Leu, 1993, J. Colloid Interface Sci., **155**, 137-145.
217. Keyser, L. F., M.-T. Leu and S. B. Moore, 1993, J. Phys. Chem., **97**, 2800-2801.
218. Keyser, L. F., S. B. Moore and M. T. Leu, 1991, J. Phys. Chem., **95**, 5496-5502.
219. Khan, I., P. Brimblecombe and S. L. Clegg, 1995, J. Atmos. Chem., **22**, 285-302.
220. Kirchner, U., V. Scheer and R. Vogt, 2000, J. Phys. Chem. A, **104**, 8908-8915.
221. Klassen, J. K., J. Lynton, D. M. Golden and L. R. Williams, 1999, J. Geophys. Res., **104**, 26,355-26,361.
222. Kleffman, J., K. H. Becker, R. Broske, D. Rothe and P. Wiesen, 2000, J. Phys. Chem. A, **104**, 8489-8495.
223. Kleffman, J., K. H. Becker, M. Lackhoff and P. Wiesen, 1999, Phys. Chem. Chem. Phys., **1**, 5443-5450.
224. Kleffman, J., K. H. Becker and P. Wiesen, 1998, Atmos. Environ., **32**, 3129-3137.

225. Koehler, B. G., L. S. McNeill, A. M. Middlebrook and M. A. Tolbert, 1993, J. Geophys. Res., **98**, 10563-10571.
226. Koehler, B. G., V. T. Nicholson, H. G. Roe and E. S. Whitney, 1999, J. Geophys. Res., **104**, 5507-5514.
227. Kolb, C. E., D. R. Worsnop, M. S. Zahniser, P. Davidovits, L. F. Keyser, M.-T. Leu, M. J. Molina, D. R. Hanson, A. R. Ravishankara, L. R. Williams and M. A. Tolbert. Progress and Problems in Atmospheric Chemistry. In *Adv. Phys. Chem. Series, 3*; Barker, J. R., Ed., 1994; pp 771-875.
228. Kroes, G.-J. and D. C. Clary, 1992, J. Phys. Chem., **96**, 7079-7088.
229. Langenberg, S., V. Proksch and U. Schurath, 1998, Atm. Environ., **32**, 3129-3137.
230. Laux, J. M., J. C. Hemminger and B. J. Finlayson-Pitts, 1994, Geophys. Res. Lett., **21**, 1623-1626.
231. Lemmon, E. W., M. O. McLinden and D. G. Friend. Thermophysical properties of fluid systems. In *NIST Chemistry WebBook*; Number 69 ed.; Mallard, W. G., linstrom, P. J., Eds.; National Institute of Standards and Technology: Gaithersburg, MD, 2000.
232. Leu, M. T., 1988, Geophys. Res. Lett., **15**, 17-20.
233. Leu, M.-T., 1988, Geophys. Res. Lett., **15**, 851-854.
234. Leu, M. T., S. B. Moore and L. F. Keyser, 1991, J. Phys. Chem., **95**, 7763-7771.
235. Leu, M.-T., R. S. Timonen, L. F. Keyser and Y. L. Yung, 1995, J. Phys. Chem., **99**, 13,203-13,212.
236. Leu, M.-T. and R. Zhang, 1999, Geophys. Res. Lett., **26**, 1129-1132.
237. Li, Z., R. R. Friedl, S. B. Moore and S. P. Sander, 1996, J. Geophys. Res., **101**, 6795-6802.
238. Liberti, A., D. Brocco and M. Possanzini, 1978, Atmos. Environ., **12**, 255-261.
239. Lind, J. A. and G. L. Kok, 1986, J. Goephys. Res., **91**, 7889-7895.
240. Lind, J. A. and G. L. Kok, 1994, J. Geophys. Res., **99**, 21119.
241. Livingston, F. E. and B. J. Finlayson-Pitts, 1991, Geophys. Res. Lett., **18**, 17-20.
242. Longfellow, C. A., T. Imamura, A. R. Ravishankara and D. R. Hanson, 1998, J. Phys. Chem. A, **102**, 3323-3332.
243. Longfellow, C. A., A. R. Ravishankara and D. R. Hanson, 1999, J. Geophys. Res., **104**, 13833.
244. Longfellow, C. A., A. R. Ravishankara and D. R. Hanson, 2000, J. Geophys. Res., **105**, 24,345-24,350.
245. Lovejoy, E. R., L. G. Huey and D. R. Hanson, 1995, J. Geophys. Res., **100**, 18,775-18,780.
246. Luick, T. J., R. W. Heckbert, K. Schultz and R. S. Disselkamp, 1999, J. Atmos. Chem., **32**, 315-325.
247. Luke, W. T., R. R. Dickerson and L. J. Nunnermacker, 1989, J. Geophys. Res., **94**, 14905-14921.
248. Luo, B., K. S. Carslaw, T. Peter and S. L. Clegg, 1995, Geophys. Res. Lett., **22**, 247-250.
249. Manion, J. A., C. M. Fittschen, D. M. Golden, L. R. Williams and M. A. Tolbert, 1994, Israel J. Chem., **34**, 355-363.
250. Martin, L. R., H. S. Judeikis and M. Wun, 1980, J. Geophys. Res., **85**, 5511-5518.
251. Massucci, M., S. L. Clegg and P. Brimblecombe, 1999, J. Phys. Chem. A, **103**, 4209-4226.
252. Mawhinney, D. B. and J. J. T. Yates, 2001, Carbon, **39**, 1167-1173.
253. McMurry, P. H., H. Takano and G. R. Anderson, 1983, Environ. Sci. Technol., **17**, 347-357.
254. Mertes, S. and A. Wahner, 1995, J. Phys. Chem., **99**, 14,000-14,006.
255. Michelangeli, D. V., M. Allen and Y. L. Yung, 1991, Geophys. Res. Lett., **18**, 673-676.
256. Middlebrook, A. M., L. T. Iraci, L. S. McNeil, B. G. Koehler, M. A. Wilson, O. W. Saastad and M. A. Tolbert, 1993, J. Geophys. Res., **98**, 20473-20481.
257. Middlebrook, A. M., B. G. Koehler, L. S. McNeill and M. A. Tolbert, 1992, Geophys. Res. Lett., **19**, 2417-2420.
258. Mihelcic, D., D. Klemp, P. Msgen, H. W. Ptz and A. Volz-Thomas, 1993, J. Atmos. Chem., **16**, 313-335.
259. Molina, M. J., R. F. Meads, D. D. Spencer and L. T. Molina, 1996, Geophys. Res. Lett., submitted.
260. Molina, M. J., T. L. Tso, L. T. Molina and F. C. Wang, 1987, Science, **238**, 1253-1259.
261. Molina, M. J., R. Zhang, P. J. Woolridge, J. R. McMahon, J. E. Kim, H. Y. Chang and K. D. Beyer, 1993, Science, **261**, 1418-1423.
262. Moore, S. B., L. F. Keyser, M. T. Leu, R. P. Turco and R. H. Smith, 1990, Nature, **345**, 333-335.
263. Mozurkewich, M. and J. Calvert, 1988, J. Geophys. Res., **93**, 15882-15896.
264. Mozurkewich, M., P. H. McMurray, A. Gupta and J. G. Calvert, 1987, J. Geophys. Res., **92**, 4163-4170.
265. Msibi, I. M., Y. Li, J. P. Shi and R. M. Harrison, 1994, J. Atmos. Chem., **18**, 291-300.
266. Msibi, I. M., J. P. Shi and R. M. Harrison, 1993, J. Atmos. Chem., 17,339-17,351.
267. Muenter, A. H. and B. G. Koehler, 2000, J. Phys. Chem. A, **104**, 8527-8534.
268. Munder, B., H. Lidal and O. C. Sandall, 2000, J. Chem. Eng. Data, **45**, 1201-1204.
269. Myhre, C. E. L., C. J. Nielsen and O. W. Saastad, 1998, J. Chem. Eng. Data, **43**, 617-622.
270. Noyes, R. M., M. B. Rubin and P. G. Bowers, 1996, J. Phys. Chem., **100**, 4167-4172.
271. Olszyna, K., R. D. Cadle and R. G. dePena, 1979, J. Geophys. Res., **84**, 1771-1775.
272. Oppliger, R., A. Allanic and M. J. Rossi, 1997, J. Phys. Chem. A, **101**, 1903-1911.

273. O'Sullivan, D. W., M. Lee, B. C. Noone and B. G. Heikes, 1996, J. Phys. Chem., **100**, 3241-3247.
274. Percival, C. J., J. C. Mossinger and R. A. Cox, 1999, Phys. Chem. Chem. Phys., **1**, 4565-4570.
275. Peters, S. J. and G. E. Ewing, 1996, J. Phys. Chem., **100**, 14,093-14,102.
276. Ponche, J. L., C. George and P. Mirabel, 1993, J. Atmos. Chem., **16**, 1-21.
277. Poschl, U., M. Canagaratna, J. T. Jayne, L. T. Molina, D. R. Worsnop, C. E. Kolb and M. J. Molina, 1998, J. Phys. Chem. A, **102**, 10,082-10,089.
278. Pöschl, U., T. Letzel, C. Schauer and R. Niessner, 2001, J. Phys. Chem. A, **105**, 4029-4041.
279. Przyjazny, A., W. Janicki, W. Chrzanowski and R. Staszewski, 1984, J. Chromatogr., **280**, 249-260.
280. Pueschel, R. F., D. F. Blake, A. G. Suetsinger, A. D. A. Hansen, S. Verma and K. Kato, 1992, Geophys. Res. Lett., **19**, 1659-1662.
281. Quinlan, M. A., C. M. Reihs, D. M. Golden and M. A. Tolbert, 1990, J. Phys. Chem., **94**, 3255-3260.
282. Rattigan, O. V., J. Boniface, E. Swartz, P. Davidovits, J. T. Jayne, C. E. Kolb and D. R. Worsnop, 2000, J. Geophys. Res., **105**, 29,065-29,078.
283. Reihs, C. M., D. M. Golden and M. A. Tolbert, 1990, J. Geophys. Res., **95**, 16,545-16,550.
284. Rettich, T. R., R. Battino and E. Wilhelm, 1982, Ber. Bunsen. Phys. Chem., **86**, 1128-1132.
285. Rettich, T. R., R. Battino and E. Wilhelm, 2000, J. Chem. Themo., **32**, 1145-1156.
286. Rieley, H., H. D. Aslin and S. Haq, 1995, J. Chem. Soc. Faraday Trans., **91**, 2349-2351.
287. Rinker, E. B. and O. C. Sandall, 2000, Can. J. Chem. Eng., **78**, 232-236.
288. Rischbieter, E., H. Stein and A. Schumpe, 2000, J. Chem. Eng. Data, **45**, 338-340.
289. Robbins, R. C. and R. D. Cadle, 1958, J. Phys. Chem., **62**, 469-471.
290. Robinson, G. N., Q. Dai and A. Freedman, 1996, J. Phys. Chem., submitted.
291. Robinson, G. N., A. Freedman, C. E. Kolb and D. R. Worsnop, 1994, Geophys. Res. Lett., **21**, 377-380.
292. Robinson, G. N., A. Freedman, C. E. Kolb and D. R. Worsnop, 1996, Geophys. Res. Lett., **23**, 317.
293. Robinson, G. N., D. R. Worsnop, J. T. Jayne, C. E. Kolb and P. Davidovits, 1997, J. Geophys. Res., **102**, 3583-3601.
294. Robinson, G. N., D. R. Worsnop, J. T. Jayne, C. E. Kolb, E. Swartz and P. Davidovits, 1998, J. Geophys. Res., **103**, 25371-25381.
295. Rogaski, C. A., D. M. Golden and L. R. Williams, 1997, Geophys. Res. Lett., **24**, 381-384.
296. Rohrschneider, L., 1973, Anal. Chem., **45**, 1241-1247.
297. Rossi, M. J., F. F. Fenter, K. Tabor, F. Caloz and L. Gutzwiller. Heterogeneous Reactions of Nitrogen Oxides (NO_2, N_2O_5, HNO_3, $C1ONO_2$) with Surfaces Representative of Atmospheric Aerosol. In *Heterogeneous and Liquid Phase Processes. Transport and Chemical Transformation of Pollutants in the Troposphere*; Warneck, P., Ed.; Springer-Verlag: Berlin, 1996; pp 213-220.
298. Rossi, M. J., R. Malhotra and D. M. Golden, 1987, Geophys. Res. Lett., **14**, 127-130.
299. Rubel, G. O. and J. W. Gentry, 1984, J. Aerosol Sci., **15**, 661-671.
300. Rudich, Y., R. K. Talukdar, R. W. Fox and A. R. Ravishankara, 1996, J. Geophys. Res., **101**, 21,023-21,031.
301. Rudich, Y., R. K. Talukdar, T. Imamura, R. W. Fox and A. R. Ravishankara, 1996, Chem. Phys. Lett., **261**, 467-473.
302. Rudolf, R. and P. E. Wagner, 1994, J. Aerosol Sci., **25**, 597-598.
303. Saastad, O. W., T. Ellerman and C. J. Nielson, 1993, Geophys. Res. Lett., **20**, 1191-1193.
304. Saathoff, H., K.-H. Naumann, N. Riemer, S. Kamm, O. Möhler, U. Schurath, H. Vogel and B. Vogel, 2001, Geophys. Res. Lett., **28**, 1957-1960.
305. Salgado-Muñoz, M. S. and M. J. Rossi, 2002, Phys. Chem. Chem. Phys., **4**, 5110-5118.
306. Sander, S. P., R. R. Friedl, W. B. DeMore, D. M. Golden, M. J. Kurylo, R. F. Hampson, R. E. Huie, G. K. Moortgat, A. R. Ravishankara, C. E. Kolb and M. J. Molina "Chemical Kinetics and Photochemical Data for Use in Stratospheric Modeling, Evaluation Number 13," JPL Publication 00-3, Jet Propulsion Laboratory, California Institute of Technology, Pasadena, CA, 2000.
307. Schwartz, S. E., 1984, J. Geophys. Res., **89**, 11589-11598.
308. Schwartz, S. E., 1988, Atmos. Environ., **22**, 2331.
309. Schwartz, S. E. and W. H. White. Kinetics of reactive dissolution of nitrogen oxides into aqueous solution. In *Trace Atmospheric Species. Properties, Transformations and Fates*; Schwartz, S. E., Ed.; John Wiley & Sons: New York, 1983; Vol. 12; pp 1-116.
310. Schweitzer, F., P. Mirabel and C. George, 1998, J. Phys. Chem. A, **102**, 3942-3952.
311. Seisel, S., B. Fluckiger and M. J. Rossi, 1998, Ber. Bunsenges. Phys. Chem., **102**, 811-820.
312. Shi, Q. and P. Davidovits, 1999, J. Phys. Chem. A, 8812-8823.
313. Shi, Q., P. Davidovits, J. T. Jayne, C. E. Kolb and D. R. Worsnop, 2001, J. Geophys. Res., **106**, 24259-24274.

314. Shimono, A. and S. Koda, 1996, J. Phys. Chem., **100**, 10,269-10,276.
315. Smith, D. M. and A. R. Chughtai, 1995, Colloids and Surfaces, **105**, 47-77.
316. Smith, D. M. and A. R. Chughtai, 1996, J. Geophys. Res., **101**, 19607-19620.
317. Smith, D. M. and A. R. Chughtai, 1997, J. Atmos. Chem., **26**, 77-91.
318. Smith, D. M., W. F. Welch, S. M. Graham, A. R. Chughtai, B. G. Wicke and K. A. Grady, 1988, Appl. Spectrosc., **42**, 674-680.
319. Smith, D. M., W. F. Welch, J. A. Jassim, A. R. Chughtai and D. H. Stedman, 1988, Appl. Spectros., **42**, 1473-1482.
320. Snider, J. R. and G. A. Dawson, 1985, J. Geophys. Res., **90**, 3797-3805.
321. Stadler, D. and M. J. Rossi, 2000, Phys. Chem. Chem. Phys., **2**, 5420-5429.
322. Staffelbach, T. A. and G. L. Kok, 1993, J. Geophys. Res., **98**, 12713-12717.
323. Stephens, S., M. J. Rossi and D. M. Golden, 1986, Int. J. Chem. Kinetics, **18**, 1133-1149.
324. Tabazadeh, A., R. P. Turco and M. Z. Jacobson, 1994, J. Geophys. Res., **99**, 12,897-12,914.
325. Tabor, K., L. Gutzwiller and M. J. Rossi, 1993, Geophys. Res. Lett., **20**, 1431-1434.
326. Tabor, K., L. Gutzwiller and M. J. Rossi, 1994, J. Phys. Chem., **98**, 6172-7186.
327. Tang, I. N. and J. H. Lee. In *The Chemistry of Acid Rain*; Gordon, G. E., Johnson, R. W., Eds.; Am. Chem. Soc. Symp. Series, 1987; pp 109-117.
328. Tang, I. N. and H. R. Munkelwitz, 1989, J. Colloid Interface Sci., **128**, 289-295.
329. Timonen, R. S., L. T. Chu, M.-T. Leu and L. F. Keyser, 1994, J. Phys. Chem., **98**, 9509-9517.
330. Tolbert, M. A., J. Praff, I. Jayaweera and M. J. Prather, 1993, J. Geophys. Res., **98**, 2957-2962.
331. Tolbert, M. A., M. J. Rossi and D. M. Golden, 1988, Science, **240**, 1018-1021.
332. Tolbert, M. A., M. J. Rossi and D. M. Golden, 1988, Geophys. Res. Lett., **15**, 847-850.
333. Tolbert, M. A., M. J. Rossi, R. Malhotra and D. M. Golden, 1987, Science, **238**, 1258-1260.
334. Toon, O., E. Browell, B. Gray, L. Lait, J. Livingston, P. Newman, R. P. P. Russell, M. Schoeberl, G. Toon, W. Traub, F. P. J. Valero, H. Selkirk and J. Jordan, 1993, Science, **261**, 1136-1140.
335. Utter, R. G., J. B. Burkholder, C. J. Howard and A. R. Ravishankara, 1992, J. Phys. Chem., **96**, 4973-4978.
336. Van Dingenen, R. and F. Raes, 1991, Aerosol Sci. Technol., **15**, 93-106.
337. Van Doren, J. M., L. R. Watson, P. Davidovits, D. R. Worsnop, M. S. Zahniser and C. E. Kolb, 1990, J. Phys. Chem., **94**, 3265-3269.
338. Van Doren, J. M., L. R. Watson, P. Davidovits, D. R. Worsnop, M. S. Zahniser and C. E. Kolb, 1991, J. Phys. Chem., **95**, 1684-1689.
339. Villalta, P. W., E. R. Lovejoy and D. R. Hanson, 1996, Geophys. Res. Lett., **23**, 1765-1768.
340. Vitenberg, A. G., B. V. Ioffe, Z. S. Dimitrova and I. L. Butaeva, 1975, J. Chromatog., **112**, 319-327.
341. Vogt, R., Elliott, C., Allen, H.C., Laux, J.M., J. C. Hemminger and B. J. Finlayson-Pitts, 1996, Atmos. Environ, **30**, 1729-1737.
342. Vogt, R. and B. Finlayson-Pitts, 1994, J. Phys. Chem., **98**, 3747-3755.
343. Vogt, R. and B. F. Finlayson-Pitts, 1994, Geophys. Res. Lett., **21**, 2291-2294.
344. Vogt, R. and B. J. Finlayson-Pitts, 1995, J. Phys. Chem., **99**, 13,052.
345. Wagman, D. D., W. H. Evans, V. B. Parker, R. H. Schumm, I. Halow, S. M. Bailey, K. L. Churney and R. L. Nutall, 1982, J. Phys. Chem. Ref. Data, **11**, 392 pp.
346. Wang, L. and D. C. Clary, 1996, J. Chem. Phys., **104**, 5663-5673.
347. Waschewsky, G. C. G. and J. P. D. Abbatt, 1999, J. Phys. Chem. A, **103**, 5312-5320.
348. Watson, L. R., J. M. V. Doren, P. Davidovits, D. R. Worsnop, M. S. Zahniser and C. E. Kolb, 1990, J. Geophys. Res., **95**, 5631-5638.
349. Watts, S. F. and P. Brimblecombe, 1987, Environ. Technol. Lett., **8**, 483-486.
350. Weingartner, E., H. Burtscher and U. Baltensperger, 1997, Atmos. Environ., **31**, 2311-2327.
351. Wilhelm, E., R. Battino and R. J. Wilcock, 1977, Chem. Rev., **77**, 219-262.
352. Wilhelm, E., R. Battino and R. J. Wilcock, 1977, Chem. Rev., **77**, 219-262.
353. Williams, L. R. and D. M. Golden, 1993, Geophys. Res. Lett., **20**, 2227-2230.
354. Williams, L. R., D. M. Golden and D. L. Huestis, 1995, J. Geophys. Res., **100**, 7329-7335.
355. Williams, L. R. and F. S. Long, 1995, J. Phys. Chem., **99**, 3748-3751.
356. Wolff, E. W. and R. Mulvaney, 1991, Geophys. Res. Lett., **18**, 1007-1010.
357. Wong, P. K. and Y. H. Wang, 1997, Chemosphere, **35**, 535-544.
358. Worsnop, D. R., L. E. Fox, M. S. Zahniser and S. C. Wofsy, 1993, Science, **259**, 71-74.
359. Worsnop, D. R., M. S. Zahniser, C. E. Kolb, J. A. Gardner, L. R. Watson, J. M. V. Doren, J. T. Jayne and P. Davidovits, 1989, J. Phys. Chem., **93**, 1159-1172.
360. Yaws, C. L., J. R. Hopper, X. Wang and A. K. Rathinsamy, 1999, Chem. Eng., 102-105.

361. Yoshizumi, K., K. Aoki, I. Nouchi, T. Okita, T. Kobayashi, S. Kamakura and M. Tajima, 1984, Atmos. Environ., **18**, 395-401.
362. Zetzsch, C. and W. Behnke, 1992, Ber. Bunsenges. Phys. Chem., **96**, 488-493.
363. Zhang, R., J. T. Jayne and M. J. Molina, 1994, J. Phys. Chem., **98**, 867-874.
364. Zhang, R. and M.-T. Leu, 1997, J. Geophys. Res., **102**, 8837-8843.
365. Zhang, R., M.-T. Leu and L. F. Keyser, 1994, J. Phys. Chem., **98**, 13,563-13,574.
366. Zhang, R., M.-T. Leu and L. F. Keyser, 1995, Geophys. Res. Lett., **22**, 1493-1496.
367. Zhang, R., M.-T. Leu and L. F. Keyser, 1995, J. Geophys. Res., **100**, 18,845-18,854.
368. Zhang, R., M.-T. Leu and L. F. Keyser, 1996, J. Phys. Chem., **100**, 339-345.
369. Zhang, R., M.-T. Leu and L. F. Keyser, 1997, J. Phys. Chem. A, **101**, 3324-3330.
370. Zhang, R., P. J. Wooldridge and M. J. Molina, 1993, J. Phys. Chem., **97**, 8541-8548.
371. Zhou, X. and Y. N. Lee, 1992, J. Phys. Chem., **96**, 265-272.
372. Zhou, X. and K. Mopper, 1990, Environ. Sci. Technol., **24**, 1864-1869.
373. Zolensky, M. E., D. S. McKay and L. A. Kaczor, 1989, J. Geophys. Res., **94**, 1047-1056.
374. Zondlo, M. A., S. B. Barone and M. A. Tolbert, 1998, J. Phys. Chem. A, **102**, 5735-5748.

APPENDIX A. THERMODYNAMIC PARAMETERS

Table of Contents

APPENDIX A. THERMODYNAMIC PARAMETERS A-1
A.1 Gas-phase entropy and enthalpy values.....A-1
A.1 References A-8

Tables

Table A-1. Gas-phase entropy and enthalpy values for selected species at 298.15 K and 100 kPa. A-1

A.1 Gas-phase entropy and enthalpy values

Table A-1 lists selected entropy and enthalpy of formation values at 298 K for a number of atmospheric species. As much as possible, the values were taken from primary evaluations, that is, evaluations that develop a recommended value from the original studies. Otherwise, the values were selected from the original literature, which is referenced in the table. Often, the enthalpy of formation and the entropy values are taken from different sources, usually due to a more recent value for the enthalpy of formation. The cited error limits are from the original references and therefore reflect often widely varying criteria. Some enthalpy values were corrected slightly to reflect the value of a reference compound selected for this table; these are indicated. Values that are calculated or estimated are also indicated in the table.

Table A-1. Gas-phase entropy and enthalpy values for selected species at 298.15 K and 100 kPa.

SPECIES	ΔH_f(298 K) kJ mol^{-1}	ΔH_f(298 K) kcal mol^{-1}	S(298 K) J K^{-1} mol^{-1}	S(298 K) cal K^{-1} mol^{-1}	Reference[a, b, c]
H	217.998±0.006	52.103±.001	114.717±0.002	27.418±.0.001	[28]
H_2	0.00	0.00	130.680±0.003	31.233±0.001	[28]
O(^{3}P)	249.18±0.10	59.56±0.02	161.059±0.003	38.194±0.001	[28]
O(^{1}D)	438.05±0.1	104.70±0.03			[70]
O_2	0.00	0.00	205.152±0.005	49.033±0.001	[28]
$O_2(^1\Delta_g)$	94.29±0.01	22.54±0.01			[36]
$O_2(^1\Sigma_g^+)$	156.96±0.01	37.51±0.01			[36]
O_3	141.8±2	33.9±0.5	239.01	57.12	[33]
OH	37.20±0.38	8.89±0.09	183.74	43.91	[33,87]
HO_2	13.8±3.3	3.3±0.8	229.1	54.76	[35,58]
H_2O	–241.826±0.040	–57.798±0.010	188.835±0.010	45.133±.002	[28]
H_2O_2	–135.88±0.22	–32.48±0.05	234.52	56.05	[33]
N(^{4}S)	472.68±0.40	112.973±0.10	153.301±0.003	36.640±0.001	[28]
N_2	0.00	0.00	191.609±0.004	45.796±0.001	[28]
NH	357±1	85.3±0.3	181.25±0.04	43.32±0.01	[4]
NH_2	186±1	44.5±0.3	194.71±0.05	46.54±0.01	[4]
NH_3	–45.94±0.35	–10.98±0.08	192.77±0.05	46.07±0.01	[28]
NH_2OH	–40.2±9.2	–9.6±2.2	236.18	56.45	[5]
NH_2NO_2	–26±10	–6.2±3	268.54	64.18	[33]
NO	91.29±0.17	21.82±0.04	210.76	50.37	[5,22]
N_2O	81.6±0.5	19.50±0.12	220.01	52.58	[33]
NO_2	34.19±0.5	8.17±0.1	240.17	57.40	[33]
NO_3	73.7±1.4	17.6±0.3	258.4±1.0	61.76±0.24	[1,29]
N_2O_3	86.6±1	20.7±0.3	314.74	75.22	[33]
N_2O_4	11.1±1	2.65±0.25	340.45	81.37	[33]
N_2O_5	13.3±1.5	3.18±0.36	355.7±7	85.01±2	[33]
HNO	107.1±2.5	25.6±0.6			[5]

SPECIES	ΔH_f(298 K) kJ mol^{-1}	ΔH_f(298 K) kcal mol^{-1}	S(298 K) J K^{-1} mol^{-1}	S(298 K) cal K^{-1} mol^{-1}	Reference[a, b, c]
HONO	–78.45±0.8	–18.75±0.2	254.07	60.72	[33]
$HONO_2$	–133.9±0.6	–32.0±0.1	266.88	63.78	[33]
HO_2NO	–23.8	–5.7	274	65.6	[61], calc.
HO_2NO_2	–53.1±2.5	–12.7±0.6	294±3	70.3±0.7	[84]
C	716.68±0.45	171.29±0.11	158.100±0.001	37.787±0.001	[28]
CH	597.37±1.3	142.77±0.3	183.04	43.75	[33]
$CH_2(^3B_1)$	390.4±0.8	93.31±0.2	194.90	46.58	[88]
$CH_2(^1A_1)$	428.0±0.8	102.3±0.2			[39]
CH_3	146.65±0.29	35.05±0.07	193.96	46.36	[33,88]
CH_4	–74.48±0.41	–17.80±0.10	186.38	44.55	[31,82]
CN	440±5	105±1	202.64	48.43	[33]
HCN	132±4	31.5±1	201.82	48.24	[33]
C_2N_2	309.1±0.8	73.9±0.2	242.20	57.89	[33]
CH_2NH_2	149±8	35.6±2			[62], corr.
CH_3NH_2	–23.4±1.0	–5.6±0.3	242.89	58.05	[31,79]
CH_2NO	157±4	37.5±1			[96], calc.
NH_2CO	–15.1±4	–3.6±1			[96], calc.
NCO	151±14	36±3	232.38	55.54	[75], corr., [33]
HNCO	–104±12	– 24.8±2.8	237.97±0.8	56.9±0.2	[97], corr.,[102]
CO	–110.53±0.17	–26.42±0.04	197.660±0.004	47.242±0.001	[28]
CO_2	–393.51±0.13	–94.05±0.03	213.785±0.010	51.096±0.002	[28]
HCO	44.15±0.43	10.55±0.10	224.34	53.62	[8], corr., [33]
CH_2O	–108.7±0.05	–25.98±0.01	218.76	52.28	[33]
HCOO	127	30	244.7	58.5	[106], calc.
C(O)OH	–193	–45	251.6	60.1	[106]
HC(O)OH	–378.8±0.5	–90.54±0.1	248.87	59.48	[33,106]
CH_3O	17.15±3.8	4.1±0.9	232.86	55.655	[11,33]
CH_3O_2	9.0±5.1	2.15±1.2			[46]
CH_2OH	–11.5±1.3	–2.75±0.31	244.170±0.018	58.358±0.004	[41]
CH_3OH	–201.0±0.6	–48.04±0.14	239.865	57.329	[33]
CH_3OOH	–139.0±8.1	–33.2±1.9			[46]
CH_2NO_2	147.3	35.2	272.48	65.12	[31]
CH_3NO_2	–74.3±0.6	–17.8±0.2	275.2	65.8	[31,79]
CH_3ONO	–64.0	–15.3	284.3	67.95	[98]
CH_3ONO_2	–122.2±4.3	–29.2±1.1	301.9	72.15	[79,98]
C_2H	565.3±2.9	135.1±0.7	209.73	50.13	[11,33]
C_2H_2	227.4±0.8	54.35±0.2	200.93	48.02	[33]
C_2H_2OH	121±11	28.9±2.6			[32]
C_2H_3	299±5	71.5±.1			[99]
C_2H_4	52.4±0.5	12.52±0.12	219.316	52.418	[33]
C_2H_5	120.9±1.7	28.9±0.4	250.52	59.88	[11,33]
C_2H_6	–83.85±0.29	–20.04±0.07	229.162	54.771	[33,82]
CH_2CN	252.6±4	60.4±1.0			[52]
CH_3CN	74.04±0.37	17.70±0.09	245.12±0.8	58.59±0.2	[2,102]
CH_2CO	–49.58±0.88	–11.85±0.21			[88]
CH_3CO	–10.0±1.2	–2.4±0.3			[11]
CH_2CHO	10.5±9.2	2.5±2.2			[11]
CH_3CHO	–166.1±0.5	39.7±0.1	263.95	63.09	[31,79]
CH_3CH_2O	–15.5±3.3	–3.7±0.8			[11]
$(CHO)_2$	–212±0.8	–50.7±0.2			[30]

SPECIES	ΔH_f(298 K) kJ mol^{-1}	ΔH_f(298 K) kcal mol^{-1}	S(298 K) J K^{-1} mol^{-1}	S(298 K) cal K^{-1} mol^{-1}	Reference[a, b, c]
C_2H_5O	–17.2	–4.1			[62]
$C_2H_5O_2$	–27.4±9.9	–6.6±2.4			[46]
C_2H_5OOH	–175.4±12.9	–41.9±3.1			[46]
CH_2CH_2OH	–31±7	–7.5±1.7			[32]
CH_3CHOH	–63.7±4	–15.2±1			[62]
C_2H_5OH	–234.8±0.5	–56.12±0.12	281.622	67.309	[33]
CH_3COO	–190	–45	284.9	68.1	[106], calc.
$CH_2C(O)OH$	–243	58	238.4	57.0	[106]
$CH_3C(O)O$	–192.5	–46.0			[63], calc.
$CH_3C(O)OH$	–432.8±0.5	–103.4±0.1	332.67	79.51	[18,79]
$CH_3C(O)O_2$	–154.4	–36.9			[63], calc.
$CH_3C(O)O_2NO_2$	–240.1	–57.4			[63], calc.
$HOCH_2COOH$	–583±10	–139±3	318.6±5.0	76.1±1.2	[30]
CH_3OCH_2	–13.0±4	–3.1±1			[62], corr.
CH_3OCH_3	–184.1±0.5	–44.0±0.1	267.34	63.90	[31,79]
$CH_2(OH)CH_2OH$	–392.2±4.0	93.7±1.0	303.81	72.61	[31,79]
CH_3OOCH_3	–125.5±5.0	–30.0±1.2			[30]
$(HOCO)_2$	–731.8±2.0	–174.9±0.5	320.6±5.0	76.6±1.2	[30]
C_3H_5	166.1±4.3	39.7±1.0	248±15	59.3±3.6	[94]
C_3H_6	20.0±0.7	4.78±0.2	266.6	63.72	[17,79]
n–C_3H_7	100±2	24±0.5			[99]
i–C_3H_7	86.6±2.0	20.7±0.5	281±5	67.2±1.2	[95]
i–$C_3H_7O_2$	–65.4±11.3	–15.6±2.7			[46]
C_3H_8	–104.68±0.50	–25.02±0.12	270.20	64.58	[16,82]
C_2H_5CHO	–185.6±0.8	44.4±0.2	304.51		[31,79]
CH_3COCH_3	–217.1±0.7	51.9±0.2	295.46	70.62	[31,79]
n-C_4H_{10}	-125.65±0.67	-30.03±0.16	309.91	74.07	[31,82]
$(CH_3COO)_2$	–500±10	–120±3	390.7±6.0	93.4±1.4	[30]
F	79.38±0.30	18.94±0.07	158.751±0.004	37.942±0.001	[28]
F_2	0.00	0.00	202.791±0.005	48.468±0.001	[28]
HF	–273.30±0.70	–65.32±0.17	173.799±0.003	41.539±0.001	[28]
HOF	–98.3±4.2	–23.5±1.0	226.77±0.21	54.20±0.05	[22]
FO	109±10	26±3	216.40±0.3	51.72±0.07	[21]
FOF	24.5±2	5.86±0.5	247.46±0.4	59.14±0.1	[21]
OFO	380±20	90.8±5	251±1	60.0±0.3	[21], calc.
FOO	25.4±2	6.07±0.5	259.5±0.2	62.02±0.05	[21]
FOOF	19.2±2.0	4.59±0.5	277.2±0.2	66.25±0.05	[21]
FONO	67	16			[6], est
FNO	–65.7	–15.70	248.0	59.27	[98]
FNO_2	–79	–19.0	277.1	66.24	[98]
$FONO_2$	10±2	2.5±0.5	290	70	[22], est.
CF	244.1±10	58.3±2.4	213.03±0.04	50.92±0.01	[22,33]
CHF	143.1±12	34.2±3.0	234.87	56.14	[33,83]
CF_2	–184±8	–44.0±2	240.83±0.04	57.56±0.01	[22,83]
CF_3	–465.7±2.1	–111.3±0.5	264.56	63.23	[33,89]
CF_4	–933.20±0.75	–223.04±0.18	261.454	62.49	[28]
CHF_3	–692.9±2.1	–165.6±0.5	259.67	62.06	[33,89]
CHF_2	–239±4	–57.1±1.0	258.50	61.78	[81]
CH_2F_2	–452.7±0.8	–108.2±0.2	246.59	58.94	[85]
CH_2F	–32±8	–7.6±2	236.52	56.53	[81]

SPECIES	ΔH_f(298 K) kJ mol^{-1}	ΔH_f(298 K) kcal mol^{-1}	S(298 K) J K^{-1} mol^{-1}	S(298 K) cal K^{-1} mol^{-1}	Reference[a, b, c]
CH_3F	–238±8	–56.8±2	222.78	53.246	[85], H est.
FCO	–161.2±8.1	–38.5±2.0			[44]
CHFO	–383±7	–91.6±1.7	246.82	58.99	[91],calc., [33]
CF_2O	–607.9±7.1	–145.3±1.7	258.97	61.89	[91],calc., [33]
CF_3O	–624±8	–149±2			[91], calc.
CF_2O_2	–427±6	–102±1.5			[48], calc.
CF_3O_2	-612.5±15.4	146±4			[56]
CF_3OH	–911±8	–218±2			[91]
CF_3OOCF_3	–1434±11	–343±3			[91]
CF_3OF	–724±8	–173±2			[91]
CH_2CH_2F	59.4±8	–14.2±2	279.7	66.86	[66],[25], calc.
CH_3CHF	–70.3±8	–16.8±2	274.0	65.48	[66], [26], calc.
CH_3CH_2F	–277.4±4.2	–66.3±1	265.1	63.4	[59], est. [33]
CH_2FCH_2F	–432±25	–103.2±6			[42]
CH_2FCHF	235.5	56.28	293.3	70.11	[27]
CH_2FCHF_2	–665±4	–158.9±1			[51], corr.
CHF_2CHF_2	–860±24	–205.6±5.7	320.3	76.6	[64], corr. [31]
CH_2CF_3	–517.1±5	–123.6±1.2	306.8	73.32	[25,104]
CH_3CF_3	–745.6±1.7	–178.2±0.4	287.3	68.67	[23]
CHF_2CH_2	–277	–66.3	297.8	71.17	[25], calc.
CH_3CF_2	–302.5±8.4	–72.3±2	290.3	69.39	[80], [26], S calc
CH_3CHF_2	–500.1±6.3	–119.7±1.5	282.4	67.50	[23]
$CHFCF_3$	–697	–166.5	326.2	77.97	[27], H corr.
CH_2FCF_3	–896±8	–214.1±2	316.2	75.58	[23], H est.
CF_2CF_3	–891±5	–213±1.3			[105]
CHF_2CF_3	–1105±5	–264±1.1	333.7	79.76	[23]
C_2F_6	–1344.3±3.4	–321.3±0.8	331.8	79.30	[23,89]
Cl	121.301±0.008	28.992±0.002	165.190±0.004	39.481±0.001	[28]
Cl_2	0.00	0.00	223.081±0.010	53.318±0.002	[28]
HCl	–92.31±0.10	–22.06±0.02	186.902±0.005	44.671±0.001	[28]
ClO	101.63v0.1	24.29±0.03	225.07±0.5	53.79±0.12	[22]
ClOO	98.0v4	23.4±1	269.32±0.5	64.37±0.1	[22]
OClO	94.6v1.2	22.6±0.3	256.84±0.1	61.39±0.03	[22,72]
ClO_3	194±12	46±3	270.75±0.5	64.71±0.1	[22]
ClClO	90±30	22±7	278.8±2.0	66.6±0.5	[22]
ClOCl	81.3±1.8	19.4±0.4			[34]
ClOOCl	127.6±2.9	30.5±0.7	301.0±5.0	71.9±1.2	[22,72]
$ClClO_2$	154.2	36.9	294±2	70.3±0.5	[55],calc., [22]
ClOClO	175.5	41.9	309±2	73.9±0.5	[55],calc., [22]
Cl_2O_3	150±6	35.8±1.5	390±20	94±5	[14]
HOCl	–74.8±1.2	–17.9±0.3	236.50±0.42	56.52±0.10	[22,34]
ClNO	52.7±0.5	12.6±0.1	261.58	62.52	[33]
$ClNO_2$	12.5±1.0	3.0±0.3	272.23	65.06	[33]
cis–ClONO	–64.4±6.3	15.4±1.5			[54], calc.
trans–ClONO	75.3±6.3	18.0±1.5			[54], calc.
ClO_2NO	102	24.3	316	75.5	[61], calc.
$ClONO_2$	22.9±2.0	5.5±0.5	302.38	72.27	[3]
FCl	–55.70±0.31	13.31±0.07	217.94	52.09	[33]
CHCl	326±8	78.0±2.0	234.88	56.85	[33,83]
CCl_2	230±8	55.0±2.0	265.03	63.34	[33,83]

SPECIES	ΔH_f(298 K) kJ mol^{-1}	ΔH_f(298 K) kcal mol^{-1}	S(298 K) J K^{-1} mol^{-1}	S(298 K) cal K^{-1} mol^{-1}	Reference[a, b, c]
CCl_3	71.1±2.5	17.0±0.6	303.24	72.47	[37]
CCl_3OH	–293±20	–70.0±5			[90], calc.
CCl_3O	–43.5±20	–10.4±5			[90], calc
CCl_3O_2	–20.9±8.9	–5.0±2.1			[46]
CCl_4	–95.6±2.5	–22.8±0.6	309.90	74.069	[38,85][60]
$CHCl_3$	–102.9±2.5	–24.6±0.6	295.51	70.63	[60,85]
$CHCl_2$	89.0±3.0	21.3±0.7	280±7	66.9±2	[92]
$CHCl_2O_2$	–17±7	–4!2			[92]
CH_2Cl	117.3±3.1	28.0±0.7	271±7	64.5±2	[92]
CH_2ClO_2	–4v11	–1±3			[92]
CH_2Cl_2	–95.1±2.5	–22.8±0.6	270.31	64.606	[60,85]
CH_3Cl	–81.9±0.6	–19.6±0.2	227.15	54.290	[60,85]
ClCO	–24.9±4.2	–5.9±1.0	266.0	63.6	[22,57]
CHClO	–164±20	–38±5	259.07	61.92	[33], H est,
CCl_2O	–220.9	–52.8	283.8	67.82	[98]
CHFCl	–61±10	–14.5±2.4			[100]
CH_2FCl	–264±8	–63.2±2	264.3	63.17	[24,100], H est.
CFCl	31v13	7.4±3.2	259.032	61.91	[33,83]
$CFCl_2$	–89.1±10.0	–21.3±2.4			[100]
$CFCl_3$	–285.3	–68.2	309.9	74.06	[24], corr.
CF_2Cl_2	–494.1	–118.1	300.7	71.87	[24], corr.
CF_3Cl	–709.2±2.9	–169.5±0.7	285.2	68.16	[24,89]
$CHFCl_2$	–285±9	–68.1±2.1	293.0	70.04	[24], H est.
CHF_2Cl	–484.8	–115.6	280.8	67.11	[24], H est.
CF_2Cl	–279±8	–66.7±2			[68]
CFClO	–429±20	–103±5	276.70	66.13	[33]
$CH_2ClCOOH$	–427.6±1.0	–102.2±0.2	325.9±5.0	77.9±1.2	[30]
C_2H_3Cl	22±3	5.3±0.7			[60]
CH_3CHFCl	–313.4±2.6	–74.9±0.6			[47]
CH_2CF_2Cl	–318	–75.9	322.08	76.98	[77]
CH_3CF_2Cl	–536.2±5.2	–128.2±1.2	307.1	73.41	[47,77]
C_2Cl_4	–18.8±4	–4.5±1	341.03	81.51	[33,38]
1,1–$C_2H_2Cl_2$	2.4±2.0	0.6±0.5			[60]
Z–1,2–$C_2H_2Cl_2$	–3±2	–0.7±0.5			[60]
E–1,2–$C_2H_2Cl_2$	–0.5±2.0	–0.1±0.5			[60]
C_2HCl_3	–19.1±3.0	–.6±0.7	325.20	77.72	[31,78]
CH_2CCl_3	71.5±8	17.1±2			[86]
1,1,1–$C_2H_3Cl_3$	–144.6±2.0	–34.6±0.5	320.03	76.488	[15,47,60]
1,1,2–$C_2H_3Cl_3$	–148.0±4.0	–35.4±0.9			[60]
1,1,1,2–$C_2H_2Cl_4$	–152.3±2.4	–36.4±0.6			[60]
1,1,2,2–$C_2H_2Cl_4$	–156.7±3.5	–37.5±0.8			[60]
C_2HCl_5	–155.9±4.3	–37.3±1.0			[60]
CH_3CCl_2	42.5±1.7	10.2±0.4	288±5	68.8±1.1	[92]
$CH_3CCl_2O_2$	–69.7±4	–16.7±1			[45], corr.
CH_3CHCl_2	–130.6±3.0	–31.2±0.7	305.05	72.908	[15,47]
CH_2CH_2Cl	93.0±2.4	22.2±0.6	271±7	64.8±2	[93]
CH_3CHCl	76.5±1.6	18.2±0.4	279±6	66.7±1.4	[92]
CH_3CH_2Cl	–112.1±0.7	–26.8±0.2	275.78	65.913	[15,60]
C_2Cl_6	–142±4	–34.0±1	398.62	95.27	[33,38]
Br	111.870±12	26.74±0.03	175.018±0.004	41.830±0.001	[28]

SPECIES	ΔH_f(298 K) kJ mol^{-1}	ΔH_f(298 K) kcal mol^{-1}	S(298 K) J K^{-1} mol^{-1}	S(298 K) cal K^{-1} mol^{-1}	Reference[a, b, c]
Br_2(g)	30.91±0.11	7.39±0.03	245.468±0.005	58.668±0.001	[28]
HBr	–36.29±0.16	–8.67±0.04	198.700±0.004	47.490±0.001	[28]
Br_2O	106.2±2.5	25.4±0.6			[34]
HOBr	–60.5±1.1	–14.5±0.3			[34]
BrO	126.2±1.7	30.2±0.4	232.97±0.1	55.681±0.023	[19,103]
OBrO	163.9±4.4	39.2±1.1	271±2	64.8±0.5	[19,43], est.
BrOO	108±40	26±10	289±3	69.1±0.7	[19]
BrO_3	221±50	53±12	285±2	68.1±0.5	[19], est.
BrOBr	107.6±3.5	25.7±0.8	290.8±2	69.50±0.48	[19]
BrBrO	168±20	40±5	313±2	74.8±0.5	[19], est.
BrNO	82.17±0.8	19.64±0.2	273.66±0.8	65.41±0.2	[102]
Z–BrONO	71.9	17.19			[53], calc.
E–BrONO	88.3	21.1			[53], calc.
$BrNO_2$	45.2	10.8			[53], calc.
$BrONO_2$	42.3±6.3	10.1±1.5			[76]
BrF	–58.9±1.0	–14.08±0.3	228.985	54.729	[33]
BrCl	14.79±0.16	3.53±0.04	240.046	57.372	[33]
CH_2Br	169±4	40.4±1.0			[100]
$CHBr_3$	23.8±4.5	5.7±1.1	330.67	79.03	[13]calc.,[33]
$CHBr_2$	188.9	45.0±2.2			[100]
CBr_3	235±25	56±6	334.57	80.0	[33]
CH_2Br_2	–11.1±5.0	–2.7±1.2	294	70.23	[13], calc.
CH_3Br	–37.7±1.5	–9.02±0.36	245.85±0.25	58.76±0.06	[49]
CH_2CH_2Br	135.6±6.7	32.4±1.6			[10]
CH_3CHBr	127±4	30.4±1			[67] corr.
CH_3CH_2Br	–61.5±1.0	–14.7±0.3	287.3±0.4	68.66±0.09	[47,50]
CH_3CBr_2	140.2±5.4	33.5±1.3			[69]
CH_3CBr_2H	26.7±1.9	6.4±0.5			[47]
CF_3Br	–641.4±2.3	–153.3±0.5			[89]
CBr_4	83.9±3.4	20.0±0.8	358.06	85.6	[13,33]
$CH_2BrCOOH$	–383.5±3.1	–91.7±0.7	337.0±5.0	80.5±1.2	[30]
I	106.76±0.04	25.52±0.01	180.787±0.004	43.209±0.001	[28]
I_2	62.42±0.08	14.92±0.02	260.687±0.005	62.306±0.001	[28]
HI	26.50±0.10	6.33±0.03	206.590±0.004	49.376±0.001	[28]
HOI	–69.6±5.4	–16.6±1.3	255.0±0.1	60.95±0.03	[12,34]
IO	115.9±5.0	27.7±1.2	239.6±0.1	57.27±0.03	[9,34]
OIO	77±15	18±4	279.9	66.9	[65], calc.
IOO	96.6±15	23±4	308.4	73.7	[65], calc.
IO_3	242±50	58±12	293±4	70.0±1.0	[20], est.
IOI	92.4±15	22.1±4	306.5	73.3	[65]
IIO	134.1±15	32.1±4	317.8	76.0	[65]
IOOI	156.8±15	37.5±4	337.0	80.5	[65], calc.
IIOO	103.0±15	24.6v4	339.9	81.2	[65], calc.
IOIO	124.2±15	29.7±4	349.7	83.6	[65], calc.
OIIO	224.0±15	53.5±4	356.3	85.2	[65], calc.
INO	121±4	29.0±1	282.8±4	67.6±1	[101]

SPECIES	ΔH_f(298 K) kJ mol^{-1}	ΔH_f(298 K) kcal mol^{-1}	S(298 K) J K^{-1} mol^{-1}	S(298 K) cal K^{-1} mol^{-1}	Reference[a, b, c]
INO_2	60.2±4	14.4±1	294±6	70.3±1.5	[101]
ICl	17.506±0.105	4.184±0.025	427.567	102.191	[22]
IBr	40.88±0.08	9.77±0.02	258.95	61.89	[22]
CH_3I	13.76±0.12	3.29±0.03	253.70±0.25	60.635±0.06	[49]
CH_2I_2	118.4±0.1	28.30±0.03	309.41±1.34	73.95±0.32	[49]
CF_3I	–586.2±2.1	–140.1±0.5	307.78	73.56	[33,89]
CH_3CH_2I	–7.5±0.9	–1.79±0.2	295.52±0.42	70.63±0.10	[47,50]
S	277.17±0.15	66.25±0.04	167.829±0.006	40.112±0.002	[28]
S_2	128.6±0.3	30.74±.07	228.167±0.010	54.533±0.003	[28]
HS	142.80±2.85	34.13±0.68	195.55	46.74	[74], corr., [33]
H_2S	–20.6±0.5	–4.92±0.12	205.81±0.05	49.19±0.01	[28]
SO	4.78±0.25	1.14±0.06	221.94	53.04	[33]
SO_2	–296.81±0.20	–70.94±0.05	248.223±0.050	59.327±0.012	[28]
SO_3	–395.9±0.7	–94.62±0.17	256.541	61.315	[33]
HSO	–6.1±2.9	–1.5±0.7			[7]
H_2SO_4	–733±2	–175.2±0.5	299.282	71.530	[33]
CS	279.775±0.75	66.87±0.18	210.55	50.32	[33]
CS_2	116.7±1.0	27.9±0.2	237.882	56.855	[33]
CS_2OH	110.5±4.6	26.4±1.1	321±20	77±5	[71]
CH_3S	125.0±1.8	29.87±0.44			[73], corr.
CH_3SH	–22.9±0.7	–5.47±0.17	255.14	60.98	[31,79]
CH_2SCH_3	136.8±5.9	32.7±1.4			[40]
CH_3SCH_3	–37.4±0.6	–8.94±0.2	285.96	68.35	[31,79]
CH_3SSCH_3	–24.7±1.0	–5.9±0.3	336.80	80.50	[31,79]
OCS	–141.7±2	–33.9±0.5	231.644	55.36	[33]

Notes:

a. Error limits are estimates from the original references.

b. If two references are given for a substance, the first refers to the enthalpy value while the second to the entropy.

c. The terms “calc” and “est” indicate that the value is calculated or estimated. The term “corr” indicates that an enthalpy value has been adjusted to reflect the value chosen in this table for a reference substance.

References

1. Abramowitz, S. and M. W. Chase, 1991, Pure App. Chem., **63**, 1449-1454.
2. An, X. W. and M. Mansson, 1983, J. Chem. Thermo., **15**, 287-293.
3. Anderson, L. C. and D. W. Fahey, 1990, J. Phys. Chem., **94**, 644-652.
4. Anderson, W. R., 1989, J. Phys. Chem., **93**, 530-536.
5. Anderson, W. R., 1999, Comb. Flame, **117**, 394-403.
6. Atkinson, R., D. L. Baulch, R. A. Cox, R. F. Hampson, J. A. Kerr, M. J. Rossi and J. Troe, 1997, J. Phys. Chem. Ref. Data, **26**, 521-1011.
7. Balucani, N., P. Casavecchia, D. Stranges and G. G. Volpi, 1993, Chem. Phys. Lett., **211**, 469-472.
8. Becerra, R., I. W. Carpenter and R. Walsh, 1997, J. Phys. Chem., **101**, 4185-4190.
9. Bedjanian, Y., G. Le Bras and G. Poulet, 1997, J. Phys. Chem. A, **101**, 4088-4096.
10. Bedjanian, Y., G. Poulet and G. Le Bras, 1999, J. Phys. Chem. A, **103**, 4026-4033.
11. Berkowitz, J., G. B. Ellison and D. Gutman, 1994, J. Phys. Chem., **98**, 2744-2765.
12. Berry, R., J. Yuan, A. Misra and P. Marshall, 1998, J. Phys. Chem. A, **102**, 5182-5188.
13. Bickerton, J., M. E. M. da Piedade and G. Pilcher, 1984, J. Chem. Thermo., **16**, 661-668.
14. Burkholder, J. B., R. K. Talukdar, A. R. Ravishankara and S. Solomon, 1993, J. Geophys. Res., **98**, 22937-22948.
15. Chao, J., A. S. Rodgers, R. C. Wilhoit and B. J. Zwolinski, 1974, J. Phys. Chem. Ref. Data, **3**, 141-162.
16. Chao, J., R. C. Wilhoit and B. J. Zwolinski, 1973, J. Phys. Chem. Ref. Data, **2**, 427-437.
17. Chao, J. and B. J. Zwolinski, 1975, J. Phys. Chem. Ref. Data, **4**, 251-261.
18. Chao, J. and B. J. Zwolinski, 1978, J. Phys. Chem. Ref. Data, **7**, 363-377.
19. Chase, M. W., 1996, J. Phys. Chem. Ref. Data, **25**, 1069-1111.
20. Chase, M. W., 1996, J. Phys. Chem. Ref. Data, **25**, 1297-1340.
21. Chase, M. W., 1996, J. Phys. Chem. Ref. Data, **25**, 551-603.
22. Chase, M. W., 1998, J. Phys. Chem. Ref. Data, **Monograph 9**.
23. Chen, S. S., A. S. Rodgers, J. Chao, R. C. Wilhoit and B. J. Zwolinski, 1975, J. Phys. Chem. Ref. Data, **4**, 441-456.
24. Chen, S. S., R. C. Wilhoit and B. J. Zwolinski, 1976, J. Phys. Chem. Ref. Data, **5**, 571-580.
25. Chen, Y., A. Rauk and E. Tschuikow-Roux, 1990, J. Chem. Phys., **93**, 6620-6629.
26. Chen, Y., A. Rauk and E. Tschuikow-Roux, 1990, J. Chem. Phys., **93**, 1187-1195.
27. Chen, Y., A. Rauk and E. Tschuikow-Roux, 1991, J. Chem. Phys., **94**, 7299-7310.
28. Cox, J. D., D. D. Wagman and V. A. Medvedev *CODATA Key Values for Thermodynamics*; Hemisphere Publishing Corp.: New York, 1989.
29. Davis, H. F., B. Kim, H. S. Johnston and Y. T. Lee, 1993, J. Phys. Chem., **97**, 2172-2180.
30. Dorofeeva, O., V. P. Novikov and D. B. Neumann, 2001, J. Phys. Chem. Ref. Data, **30**, 475-513.
31. Frenkel, M., G. J. Kabo, K. N. Marsh, G. N. Roganov and R. C. Wilhoit *Thermodynamics of organic compounds in the gas state*; Thermodynamics Research Center: College Station, TX, 1994; Vol. I.
32. Fulle, D., H. F. Hamann, H. Hippler and C. P. Jänsch, 1997, Ber. Bunsenges. Phys. Chem., **101**, 1433-1442.
33. Gurvich, L. V., I. V. Veyts and C. B. Alcock *Thermodynamic Properties of Individual Substances,*, Fourth ed.; Hemisphere Publishing Corp.: New York, 1991; Vol. 2.
34. Hassanzadeh, P. and K. K. Irikura, 1997, J. Phys. Chem. A, **101**, 1580-1587.
35. Hills, A. J. and C. J. Howard, 1984, J. Chem. Phys., **81**, 4458-4465.
36. *Constants of Diatomic Molecules*; Huber, K. P. and G. Herzberg, Eds.; National Institute of Standards and Technology, 1998.
37. Hudgens, J. W., R. D. Johnson, R. S. Timonen, J. A. Seetula and D. Gutman, 1991, J. Phys. Chem., **95**, 4400-4405.
38. Huybrechts, G., M. Marmon and B. Van Mele, 1996, Int. J. Chem. Kinet., **28**, 27-36.
39. Jacox, M. E. *Vibrational and Electronic Energy Levels of Polyatomic Transient Molecules*; National Institute of Standards and Technology, 1998.
40. Jefferson, A., J. M. Nicovich and P. H. Wine, 1994, J. Phys. Chem., **98**, 7128-7135.

41. Johnson, R. D. and J. W. Hudgens, 1996, J. Phys. Chem., **100**, 19874-19890.
42. Kerr, J. A. and D. M. Timlin, 1971, Int. J. Chem. Kinet., **3**, 427-441.
43. Klemm, R. B., R. P. Thorn, L. J. Stief, T. J. Buckley and R. D. Johnson, 2001, J. Phys. Chem. A, **105**, 1638-1642.
44. Knyazev, V. D., A. Bencsura and I. R. Slagle, 1997, J. Phys. Chem. A, **101**, 849-852.
45. Knyazev, V. D., A. Bencsura and I. R. Slagle, 1998, J. Phys. Chem. A, **102**, 1760-1769.
46. Knyazev, V. D. and I. R. Slagle, 1998, J. Phys. Chem. A, **102**, 1770-1778.
47. Kolesov, V. P. and T. S. Papina, 1983, Russ. Chem. Rev., **52**, 425-439.
48. Kraka, E., Z. Konkoli, D. Cremer, J. Fowler and H. F. Schaefer, 1996, J. Amer. Chem. Soc., **118**, 10595-10608.
49. Kudchadker, S. A. and A. P. Kudchadker, 1975, J. Chem. Phys. Ref. Data, **4**, 457-470.
50. Kudchadker, S. A. and A. P. Kudchadker, 1979, J. Phys. Chem. Ref. Data, **8**, 519-526.
51. Lacher, J. R. and H. A. Skinner, 1968, J. Chem. Soc. A, 1034-1038.
52. Lafleur, R. D., B. Szatary and T. Baer, 2000, J. Phys. Chem. A, **104**, 1450-1455.
53. Lee, J. H., R. B. Timmons and L. J. Stief, 1976, J. Chem. Phys., **64**, 300-305.
54. Lee, T. J., 1994, J. Phys. Chem., **98**, 111-115.
55. Li, W. K. and C. Y. Ng, 1997, J. Phys. Chem. A, **101**, 113-115.
56. Lightfoot, P. D., R. A. Cox, J. N. Crowley, M. Destriau, G. D. Hayman, M. E. Jenkin, G. K. Moortgat and F. Zabel, 1992, Atmos. Environ., **26A**, 1805-1961.
57. Lim, K. P. and J. V. Michael, 1994, J. Phys. Chem., **98**, 211-215.
58. Litorja, M. and B. Ruscic, 1998, J. Electron.Spec. Rel. Phenom., **97**, 131-146.
59. Luo, Y. R. and S. W. Benson, 1997, J. Phys. Chem. A, **101**, 3042-3044.
60. Manion, J. A., 2002, J. Phys. Chem. Ref. Data, **31**, 123-172.
61. McGrath, M. P. and F. S. Rowland, 1994, J. Phys. Chem., **98**, 1060-1067.
62. McMillen, D. F. and D. M. Golden, 1982, Ann. Rev. Phys. Chem., **33**, 493-532.
63. Miller, C. E., J. I. Lynton, D. M. Keevil and J. S. Franscisco, 1999, J. Phys. Chem. A, **103**, 11451-11459.
64. Millward, G. E., R. Hartig and E. Tschuikow-Roux, 1971, J. Phys. Chem., **75**, 3195-3201.
65. Misra, A. and P. Marshall, 1998, J. Phys. Chem. A, **102**, 9056-9060.
66. Miyokawa, K., S. Ozaki and T. Yano, 1996, Bull. Chem. Soc. Jpn., **69**, 869-873.
67. Miyokawa, K. and E. Tschuikow-Roux, 1990, J. Phys. Chem., **94**, 715-717.
68. Miyokawa, K. and E. Tschuikow-Roux, 1992, J. Phys. Chem., **96**, 7328-7331.
69. Miyokawa, K. and E. Tschuikow-Roux, 1999, Bull. Chem. Soc. Jpn., **72**, 1-5.
70. Moore, C. E. *Atomic Energy Levels*; NSRDS: Washington. DC, 1971; Vol. 1.
71. Murrells, T. P., E. R. Lovejoy and A. R. Ravishankara, 1990, J. Phys. Chem., **94**, 2381-2386.
72. Nickolaisen, S. L., R. R. Friedl and S. P. Sander, 1994, J. Phys. Chem., **98**, 155-169.
73. Nicovich, J. M., K. D. Kreutter, C. A. van Dijk and P. H. Wine, 1992, J. Phys. Chem., **96**, 2518-2528.
74. Nicovich, J. M., K. D. Kreutter, C. A. van Dijk and P. H. Wine, 1992, J. Phys. Chem., **96**, 2518-2528.
75. Okabe, H., 1970, J. Chem. Phys., **53**, 3507-3515.
76. Orlando, J. J. and G. S. Tyndall, 1996, J. Phys. Chem., **100**, 19398-19405.
77. Paddison, S. J., Y. H. Chen and E. Tschuikow-Roux, 1994, Can. J. Chem., **72**, 561-567.
78. Papina, T. S. and V. P. Kolesov, 1985, Russ. J. Phys. Chem., **59**, 1289-1292.
79. Pedley, J. B. *Thermochemicsl Data and Structures of Organic Compounds*; Thermodynamics Data Center: College Station, TX, 1994.
80. Pickard, J. M. and A. S. Rodgers, 1977, J. Amer. Chem. Soc., **99**, 691-694.
81. Pickard, J. M. and A. S. Rodgers, 1983, Int. J. Chem. Kinet., **15**, 569-577.
82. Pittam, D. A. and G. Pilcher, 1972, J. Chem. Soc. Farad. Trans 1, **68**, 2224-2229.
83. Poutsma, J. C., J. A. Paulino and R. R. Squires, 1997, J. Phys. Chem. A, **101**, 5327-5336.
84. Regimbal, J. M. and M. Mozurkewich, 1997, J. Phys. Chem. A, **101**, 8822-8820.
85. Rodgers, A. S., J. Chao, R. C. Wilhoit and B. J. Zwolinski, 1974, J. Phys. Chem. Ref. Data, **3**, 117-140.
86. Rodgers, A. S. and P. Jerus, 1988, Int. J. Chem. Kinet., **20**, 565-575.
87. Ruscic, B., D. Feller, D. A. Dixon, K. A. Peterson, L. B. Harding, R. L. Asher and A. F. Wagner, 2001, J. Phys. Chem A, **105**, 1-4.

88. Ruscic, B., M. Litorja and R. L. Asher, 1999, J. Phys. Chem. A, **103**, 8625-8633.
89. Ruscic, B., J. V. Michael, P. C. Redfern, L. A. Curtiss and K. Raghavachri, 1998, J. Phys. Chem. A, **102**, 10889-10899.
90. Schneider, W. F., B. I. Nance and T. J. Wallington, 1995, J. Amer. Chem. Soc., **117**, 478-485.
91. Schneider, W. F. and T. J. Wallington, 1994, J. Phys. Chem., **98**, 7448-7451.
92. Seetula, J. A., 1996, J. Chem. Soc. Faraday Trans., **92**, 3069-3078.
93. Seetula, J. A., 1998, J. Chem. Soc. Faraday Trans., **94**, 891-898.
94. Seetula, J. A., 1999, Phys. Chem. Chem. Phys., **1**, 4727-4731.
95. Seetula, J. A. and I. R. Slagel, 1997, J. Chem. Soc. Faraday Trans., **93**, 1709-1719.
96. Shapley, W. A. and G. B. Bacskay, 1999, J. Phys. Chem. A, **103**, 4505-4513.
97. Spiglanin, T. A., R. A. Pery and D. W. Chandler, 1986, J. Phys. Chem., **90**, 6184-6189.
98. Stull, D. R., E. F. Westrum and G. C. Sinke *The Chemical Thermodynamics of Organic Compounds*; John Wiley & Sons: New York, 1969.
99. Tsang, W. Heats of formation of organic free radicals by kinetic methods. In *Energetics of Free Radicals*; Simoes, J. A. M., Greenberg, A., Liebman, J. F., Eds.; Blackie Academic & Professional: London, 1996; pp 22-58.
100. Tschuikow-Roux, E. and S. Paddison, 1987, Int. J. Chem. Kinet., **19**, 15-24.
101. van den Bergh, H. and J. Troe, 1976, J. Chem. Phys., **64**, 736-742.
102. Wagman, D. D., W. H. Evans, V. B. Parker, R. H. Schumm, I. Halow, S. M. Bailey, K. L. Churney and R. L. Nutall, 1982, J. Phys. Chem. Ref. Data, **11**, 392 pp.
103. Wilmouth, D. M., T. F. Hanisco, N. M. Donahue and J. G. Anderson, 1999, J. Phys. Chem A, **103**, 8935-8945.
104. Wu, E. C. and A. S. Rodgers, 1974, J. Phys. Chem., **78**, 2315-2317.
105. Wu, E. C. and A. S. Rodgers, 1976, J. Amer. Chem. Soc., **98**, 6112-6115.
106. Yu, D., A. Rauk and D. A. Armstrong, 1994, J. Chem. Soc. Perkin Trans 2, 2207-2215.